METHODOLOGY FOR UPDATING NUMERICAL PREDICTIONS OF EXCAVATION PERFORMANCE

by

Gonzalo Andrés Corral Jofré

B.Sc. in Civil Engineering (2000)
Structural Engineer (2001)
Pontificia Universidad Católica de Chile

M.Sc. in Geotechnical Engineering (2008)
Universidad de Chile

Civil Engineer (2010)
Massachusetts Institute of Technology

Submitted to the Department of Civil & Environmental Engineering
In Partial Fulfillment of the Requirements for the Degree of

DOCTOR OF SCIENCE IN GEOTECHNICAL ENGINEERING

at the

Massachusetts Institute of Technology

June 2013

Signature of Author.....
Department of Civil & Environmental Engineering
March 18, 2013

Certified by.....
Andrew J. Whittle
Professor of Civil and Environmental Engineering
Thesis Supervisor

Accepted by.....
Heidi M. Nepf
Chair, Departmental Committee for Graduate Students

METHODOLOGY FOR UPDATING NUMERICAL PREDICTIONS OF EXCAVATION PERFORMANCE

by

Gonzalo Andrés Corral Jofré

Submitted to the Department of Civil and Environmental Engineering
on March 18, 2013 in Partial Fulfillment of the Requirements for the Degree of
Doctor of Science in the Field of Geotechnical Engineering

ABSTRACT

Due to the usual limitations in site investigations and measurements of soil properties, simplified constitutive models are routinely used in geotechnical analyses for the design of excavation support systems. However, monitoring data provides additional information on the performance of these support systems during construction. This thesis proposes a rational framework for updating constitutive model input parameters in finite element predictions of soil-structure interaction based on the monitoring data. The goal of this methodology is to provide an objective procedure that can be used during construction to update the instrument pre-set trigger levels that are used to control construction. In this way, the methodology aims to preserve safety by increasing confidence in the parameters controlling performance, and to mitigate impacts of unnecessary work stoppages. The proposed methodology is designed to handle diverse designs, ground conditions, and sources of information during construction to operate within existing construction project management procedures (based on trigger levels for individual field measurements). The framework comprises three key components: 1) rational sensitivity analyses (exploring full realistic search spaces for model parameters); 2) error structures of field measurements (maximum likelihood approach); and 3) inverse analyses based on heuristic optimization methods (genetic algorithms).

The proposed methodology is evaluated for a well-instrumented excavation project in South Boston (MBTA Courthouse Station, South Piers Transitway project) comprising a floating diaphragm wall, underlain by soft, normally consolidated Boston Blue Clay and supported by five levels of cross-lot bracing. This project has a very low margin of safety against basal instability, but was completed successfully in 2003. Numerical analyses using a conventional linearly-elastic perfectly-plastic (Mohr-Coulomb; MC) soil model are updated using a combination of wall deflection, ground movement, pore pressure and strut load data through the full depth of the excavation. While the proposed procedure produces improved agreement between predictions and measurements, based on reasonable updating of individual input parameters, MC model limitations clearly produce compromises among the measured parameters. The results have been compared with predictions from a more complex elasto-plastic soil model, MIT-E3. In this case, the model input parameters are derived from an extensive laboratory test program (Ladd et al. 1999) and principal uncertainties relate to the in-situ stress history profile. Results from the MIT-E3 model show more consistent agreement with the field measurements and achieve comparable accuracy to the more approximate MC model (with parameter updating).

The results show the effectiveness of the proposed updating procedure, but also highlight the challenge of updating predictions using simplified models of soil behavior. The study also confirms the value of using more advanced constitutive models calibrated using high quality laboratory tests. Further studies are now needed to evaluate how the proposed updating procedure can mitigate cases where the measured performance deviates from prior predictions and causes interruption of the construction process.

Thesis Supervisor: Prof. Andrew J. Whittle
Title: Professor of Civil and Environmental Engineering

ACKNOWLEDGEMENTS

This thesis would not have been possible without the help of several individuals who in one way or another contributed to the completion of this study.

First and foremost, I would like to express my most sincere gratitude to my thesis supervisor Prof. Andrew J. Whittle. I must say that it has been an outstanding learning process. I will always be grateful for his continuous encouragement, support, and guidance during this research work. Thank you very much!

Second, I would like to thank my doctoral committee members, Prof. Herbert H. Einstein and Dr. John T. Germaine, for their great advice and recommendations throughout this process.

Third, I would like to thank Dr. Paul Bonnier for continuously helping me out with the Plaxis MIT-GA development.

I am very grateful to Prof. Eduardo Kausel for his kindness and support during my MIT experience.

I would like to thank Dr. Lucy Jen, Richard O'Brien, and Robert Rawnsley for kindly providing the material needed to develop the Transitway case study.

Also, I would like to thank the MIT CEE headquarters: Kris, Mira, Jeanette, and Andre – for all the help provided.

I will always be very grateful to Prof. Ramón Verdugo, my former advisor at Universidad de Chile, for strongly encouraging me to come to MIT.

I would like also to thank my MIT friends for helping me in many different ways: Nina, Despina, Jay, Alejandro, Antonios, Maria, Amy, Eva, Alberto, Yvonne, Sinan, Jérémie, Naeem, Zhandos, Yixing, Rita, Jana, and Ray.

Finally, I would like to thank my parents – Elisa and Eduardo – for their continuous love, inspiration, and motivation.

Last but not least, I would like to thank my wife – Natalia – for her unconditional love, joy, help, and support throughout this unforgettable journey.

TABLE OF CONTENTS

LIST OF FIGURES

LIST OF TABLES

1 INTRODUCTION

Numerical analyses are widely used to predict excavation performance and to design lateral earth support systems. Current finite element programs enable complex 3D simulations (e.g., basement of Stata Center on MIT campus; Orazalin, 2012) due to advances in computational algorithms (e.g., iterative solvers, embedded elements, etc.). However, despite the enormous progress in FE analyses, users are still faced with: 1) uncertainties in how best to use programs (e.g., appropriate assumptions in material model properties and boundary conditions), 2) uncertainties in site investigation, soil properties, and spatial variability (e.g., associated with improvement techniques), and 3) ill-defined sources of ground movements and stress changes (e.g., associated with wall installation, pile removal, etc.).

Excavation support systems are monitored continuously during construction. In principle, these data provide valuable information that can used to update input parameters used in the FE model, reduce uncertainties in predictions for subsequent phases of construction and hence, reduce risks. Ideally the updating procedure should be done in an objective automated procedure that can be integrated in engineering practice. The main challenge is to develop a general strategy that can handle diverse designs, ground conditions, and sources of information during construction. Well documented case studies with high quality site investigation data, detailed construction records, and reliable monitoring data play a key role in the development and validation of updating procedures.

1.1 Organization

The thesis chapters have been organized as follows:

Chapter 2 describes two case studies of numerical predictions of excavation performance in Boston and Singapore: 1) Transitway Project: Courthouse Station for South Boston Piers*, a case study that compares class A, B, and C predictions for a deep, wide excavation, supported by a diaphragm wall and five pre-loaded strut levels in Boston; 2) Nicoll Highway collapse (Whittle and Davies, 2006), the well-documented failure of a 30 m deep braced excavation in Singapore (Circle Line Phase 1) in underconsolidated marine clay. These projects are analyzed using an advanced effective stress soil model (MIT-E3; Whittle, 1987; Whittle and Kavvadas, 1994). Although there are several sources of uncertainty in both case studies, the analyses based on information available prior to construction, combined with detailed monitoring of construction activities and performance of the support system are sufficient to achieve high fidelity predictions of soil deformations, pore pressures, as well as stresses and deformations of the structural support systems.

Chapter 3 presents an overview of literature on the updating of predictions from measurements of field performance varying from the Observational Method to inverse analysis of FE predictions in geotechnical problems. The description of the inverse problem is subdivided into two parts: 1) identification criteria (i.e., selection of objective function), and 2) optimization

* Currently known as the Massachusetts Bay Transportation Authority (MBTA) Silver Line

algorithms. We focus on inverse analyses for finite element predictions of geotechnical problems, including a comprehensive grouping of literature published in the last 30 years.

Chapter 4 proposes a rational methodology for updating finite element predictions of excavation performance based on the maximum likelihood approach. Initially, a simplified version of this methodology is introduced and the main parts of the framework are described. This is followed by a description of the covariance matrices for field measurements and the error structures for some typical instruments used to monitor excavations. The proposed methodology uses sensitivity analyses to filter and select input parameters for the inverse analyses. The chapter also presents a more detailed framework for using the updating approach in the project management through integration with alert or trigger criteria. Finally, some comments are provided on the application of the methodology in 2-D and 3-D numerical analyses.

Chapter 5 presents an application of the proposed methodology for updating finite element predictions of excavation performance for the Transitway case study. This project involves a 17.3 m deep excavation for the MBTA Silver Line Courthouse Station. The excavation and support system diaphragm walls with 5 levels of cross-lot bracing are well represented by a 2D finite element model (Platform section) of the half-section (i.e., full model symmetry). This chapter describes the finite element model, identification of essential improvement parameters at each stage of construction through sensitivity analyses. The chapter gives full details of the inverse analyses and updating of parameters using simplified Mohr-Coulomb (MC) models of soil behavior. The results show how model updating would be applied and how these analyses assist in reducing uncertainties through the course of the construction.

The final section compares these results with predictions using a more complex soil model (MIT-E3) that were presented in Chapter 2.

Finally, Chapter 6 presents the summary, conclusions, and recommendations for future research.

1.2 References

Orazalin, Z. (2010). "Three-Dimensional Finite Element Analysis of a Complex Excavation on the MIT Campus." *S.M. Thesis, Department of Civil and Environmental Engineering, Cambridge, MIT.* 143p.

Whittle, A.J. (1987) "A Constitutive Model for Overconsolidated Clays with Application to the Cyclic Loading". *Sc.D Thesis. Department of Civil and Environmental Engineering, Cambridge, MIT.* 641p.

Whittle, A.J., Hashash, Y.M.A., and Whitman, R.V. (1993). "Analysis of Deep Excavation in Boston." *ASCE Journal of Geotechnical Engineering* 119(1): 69-90.

Whittle, A.J. and Kavvadas, M. J. (1994). "Formulation of MIT-E3 Constitutive Model for Overconsolidated Clays." *ASCE Journal of Geotechnical Engineering* 120(1): 173-198.

Whittle, A.J., & Davies, R.V. (2006). "Nicoll Highway Collapse: Evaluation of Geotechnical Factors Affecting Design of Excavation Support System." *Proc. Int. Conf. on Deep Excavations*, Singapore, June 2006.

2 TWO CASE STUDIES ON EXCAVATION PERFORMANCE

2.1 Introduction

There are many factors affecting excavation performance including those directly and indirectly related to the excavation and support system (e.g. Peck, 1969b; Lambe, 1970; O'Rourke, 1981; Clough and O'Rourke, 1990). Direct factors include soil types and in situ stress conditions, support system stiffness, preloading of bracing or tieback elements, construction sequencing (berms, over excavation, etc.), workmanship, minor construction details, and auxiliary activities. Indirect factors affecting ground movements include dewatering, removal of utilities, wall installation, etc.

Nowadays, numerical analyses are widely used to predict excavation performance and design lateral earth support system. Currently, available commercial FE programs are capable of modeling coupled flow-deformation (including partially saturated soils), and are equipped with a range of soil models of varying complexity. It is possible to analyze very complex systems such as the support systems for the basement of the Stata Center on MIT campus (Orazalin, 2012). However, despite the enormous progress in the development capabilities, there remain uncertainties in how best to use these programs (e.g., assumptions regarding soil models, input parameters, and boundary conditions), uncertainties in site investigation, soil properties, and spatial variability (e.g., effects of ground improvement), and factors beyond our immediate knowledge (e.g., effects of concrete shrinkage; Whittle et al., 1993).

In order to understand the relative importance of factors affecting predictions from numerical analyses, it is crucial to learn from well-documented case studies where predictions are compared with quality field measurements. One key question that needs to be resolved from the case studies is the importance of the constitutive models used to represent soil behavior and the selection of input parameters for those models. More complex models are able to achieve more reliable description of soil behavior (observed in lab tests), but require more and higher quality data in order to select appropriate input parameters. This chapter presents two case studies that evaluate numerical predictions of braced excavation performance.

1. **Transitway Project**: this project has provided a unique opportunity to compare class A, B and C predictions for deep excavation in South Boston, supported by a diaphragm wall and five levels of pre-loaded struts. The numerical analyses use coupled flow and soil deformation to simulate construction activities and an advanced constitutive soil model (MIT-E3; Whittle and Kavvadas, 1994) that has been previously calibrated for BBC (Whittle et al., 1994). The use of information available prior to construction and real-time records of site activities makes it possible to build an accurate numerical representation of the project. Direct comparisons of measured and predicted lateral wall and soil displacements, surface settlements, excavation heave, pore pressures, and strut forces allow a detailed evaluation of prediction capabilities.
2. **Nicoll Highway Collapse (Corral, 2010; Corral and Whittle, 2010)**: the well-documented failure of a 30 m deep braced excavation in underconsolidated marine clay is re-analyzed using an advanced effective stress soil model (MIT-E3). The collapse of the Nicoll Highway during construction of cut-and cover tunnels for the new Circle Line in

Singapore has been extensively investigated and documented. All prior analyses of the collapse (e.g., Whittle and Davies, 2006; GIM, 2001) have relied on simplified soil models with undrained strength parameters based on empirical correlations and piezocone penetration data. The current analysis use results from high quality consolidation and undrained triaxial shear tests that were only available after completion of the public inquiry into the collapse (COI, May 2005).

2.2 Transitway Project

2.2.1 Project Description

The South Boston Piers Transitway Project was an extension to MBTA public transit network in Boston comprising a one-mile long, two-lane subway tunnel with three underground stations connecting South Station to the new Federal Courthouse (Figure 2-1), and World Trade Center in South Boston. The cut-and-cover tunnel and station sections were designed in order to accommodate electric buses (Silver Line service to Logan Airport) with provisions for future conversion to light rail. The Transitway Project was located within generally level land that was reclaimed during the period prior to 1916. Figure 2-2 shows the instrumentation location plan at the central area of the Courthouse Station, referred to as the "Platform section". There are a series of low rise buildings located 50-60 m to the South of the section and one small structure (Seaman's Chapel) to the North. These existing buildings are generally brick construction with heights up to 6 stories. The original design of the excavation support system was submitted in 1998 (PB, 1998) and later revised by the contractor. The actual construction (i.e., excavation

work) began in November 2000 and reached final grade level in August 2001 (Figure 2-3). Platform section involved an approximate excavation area of 2475 m^2 (75 x 33 m), 33 m wide with a final excavation depth of 17.3 m (formation at El. +16.5m; Fig. 2.4). The excavation support system consisted of a 1.22 m thick reinforced concrete, diaphragm wall panels, extending to a depth of 26.2 m. The wall was internally braced with 5 levels of pre-loaded steel struts.

From a geological point of view, the project site is located within the Boston Basin, which is an East-Northeast trending structural and topographic depression. Based on a generalized bedrock geologic map of the area (Kaye, 1976), the site is underlain by Cambridge Argillite. The Cambridge Argillite is described as a gray, very thinly bedded, and fine grained sedimentary rock (Kaye, 1976), containing varying amounts of very fine-grained sericite[†] and chlorite with very low-grade metamorphism. The surficial geology is dominated by repeated retreats and re-advances of glaciers during the Wisconsin Period and by centuries of land reclamation during the expansion and urbanization of Boston. Glacial soils such as basal tills, ablation tills, and outwash deposits, are generally found directly above the bedrock. Above the glacial deposits is a deep deposit of marine clay, locally known as the Boston Blue Clay (BBC). This layer was formed as clay, silt, and fine sand settled out in the quiet brackish water during glacial retreats. Above the BBC are the more recent tidal marsh organic deposits and man-made fills (PB, 1998).

[†] A white, fine-grained potassium mica, usually muscovite in composition, having a silky luster and found as small flakes in various metamorphic rocks.

PB (1998) carried out subsurface exploration program for the Transitway Project in two phases, June to August 1994, and June to August 1995. The exploration program included 15 geotechnical test borings (advanced with standard penetration tests); 43 "undisturbed" tube samples of cohesive soils; 48 field vane tests; and rock coring in the vicinity of the proposed station. Laboratory testing of undisturbed soil samples included unconsolidated, undrained (UU) triaxial compression tests and 1-D consolidation tests. The principal source of data on the stress history and undrained shear strength properties of the BBC at the Transitway site is from an extensive program of laboratory tests performed for the CA/T[‡] project at the South Boston Special Test Site (SBSTS - H&A, 1993; Ladd et al., 1999). The SBSTS is located 300 m approximately from the Platform Section of the Courthouse Station, as shown in Figure 2-1.

Ground elevations[§] typically range from El. +33.5 m to El. +34.1 m, with an average value of El. +33.8 m. The PB (1998) site investigation report describes the typical soil profile comprising five soil strata overlying bedrock (Figure 2.5b). A general description of soil profiles based principally on SPT measurements, from top to bottom, is as follows:

1. **Granular Fill**: in general, clean sand with a thickness ranging from 1.2 to 2.9 m, with $\bar{N}$=38 ± 28 bpf (n=13).

[‡] Central Artery / Third Harbor Tunnel project

[§] The Transitway Project elevations are referenced to the Central Artery / Third Harbor Tunnel (CA/THT) datum which is 30.48m below the National Geodetic Vertical Datum of 1929 (NGVD 1929). Therefore, El. +30.48m Transitway Project Datum = El. 0.0 NGVD.

2. **Cohesive Fill**: typically very soft hydraulic fill and/or very soft to medium stiff organic silt with occasional layers of gray silty sand. The combined thickness ranges from 4 to 7.6 m, with $\bar{N}$=4 ± 4 bpf (n=49).
3. **Silty Sand**: thickness ranges from 0.9 to 6.4 m, and N_{SPT} values range from 10 to 70, with $\bar{N}$=29 ± 13 bpf (n=40)**. Samples from this stratum had a tendency to liquefy when the split spoon was opened and the sample shaken.
4. **Boston Blue Clay (BBC)**: this stratum ranges in thickness from 22.9 to 37.1 m. Data from laboratory consolidation tests indicate that approximately the top 15-20 m of the clay stratum is lightly overconsolidated, with maximum $\sigma'_p \approx$ 670 kPa (OCR=4-5) at the top of the unit (Ladd et al., 1999). The lower portion of the BBC layer (i.e., below El. +7.6 m) is effectively normally consolidated. The plasticity index, I_P ranges from approximately 20 to 35%, and the natural water content, w_n varies from 30 to 45% approximately (Ladd et al., 1999).
5. **Glacial Till**: thickness ranging from 0 to 12.5 m. The till is generally granular with $\bar{N}$=104 ± 53 bpf (n=44). Boulders and cobbles were encountered at several locations and occasional layers of cohesive till.
6. **Bedrock**: soft weathered to hard fractured Cambridge Argillite. Core recovery ranged from 46 to 100% with the Rock Quality Designation, average $\overline{RQD}$ = 20%.

PB (1998) installed thirteen observation wells at the project site. The groundwater table varies seasonally in the range El. +29.9 to +31.1 m. Piezometric measurements in the lower

** Corresponding to an approximate average relative density $\overline{Dr} \approx 50 \pm 15\%$ (Skempton, 1986).

glacial till are 1.8 to 3.0 m below the groundwater table, implying a small head loss through the BBC layer.

2.2.2 Numerical Analysis

The main objective of the current analysis is to evaluate capabilities of finite element models through direct comparisons of measured and predicted lateral wall displacements, lateral soil movements, surface settlements, excavation heave, pore pressures, and strut forces. Lambe (1973) proposed a classification system for predictions: 1) class A predictions correspond to those made before the event; 2) class B predictions to those made during the event; and 3) class C predictions to those made after the event.

Jen (1998) carried out a series of class A predictions (12 numerical simulations at four different sections of the Transitway Project), including 6 cases for the Platform section. These analyses examined carefully the impact of changes in the wall embedment, vertical strut spacing, partial drainage conditions in the clay, and uncertainties in the shear strength profile. The section geometry, soil profile, boundary conditions, strut system and excavation levels assumed in these class A predictions are summarized in Fig. 2-5a. The contractor ultimately decided to modify the excavation support system (both the diaphragm wall thickness and the strut sections; Table 2-3 and Figure 2-3) prior to construction. As a result, the current analyses (class A, B, and C) differ from results presented by Jen (1998), as they use the updated support system. Figure 2-5a shows that the class A model assumes horizontal soil layers and excavated grade conditions such that

symmetry is preserved through the construction and hence a half section model is used. It is also important to highlight that no strut pre-loads forces were used in the original class A analyses.

In contrast, class B and C predictions (Corral et al., 2013) include information available prior to construction regarding the local site stratigraphy and groundwater conditions. The simulation of the construction sequence is derived from actual record of site activities. Class B and C use same initial conditions but different model geometries. Class B is based on the North side of the class C model, shown in Fig. 2-5b, and uses horizontal layers without including the glacial till and the bedrock as well as 2-D plane strain symmetric assumptions (see Figure 2-7). From Fig. 2-5b, it can be noted that, in class C, non-horizontal soil/rock layers were selected and 2-D plane strain conditions were assumed. Actual strut pre-loads measurements were used in the class B and C predictions.

Apart from the minor difference in excavation elevations, strut vertical spacing, and soil layer thicknesses (see Figure 2-5), the most important differences between class A, B, and C model assumptions are the strut pre-loads (Table 2-4). The following paragraphs describe details of finite element models, soil models, and constructions sequences of class A, B, and C predictions.

2.2.2.1 Finite Element Model

Class A, B, and C finite element analyses for the Platform Section have been carried out using the commercial finite element code, Plaxis^{TM} (Brinkgreve et al., 2008). The class A and C model geometries are shown in Figures 2-5a and 2-5b. The FE models for class A, B, and C (mesh and

boundary conditions) are shown in Figures 2-6, 2-7 and 2-8, respectively. Coupled analyses of fluid flow and deformations in the soil are performed using 15-3 mixed interpolation solid triangular finite elements to describe the soil, bedrock and diaphragm wall. Figure 2-3 shows the plans and typical section of the strutting system. The cross lot bracing is simulated using node-to-node anchors (elastic spring elements with constant axial stiffness) with average horizontal strut spacing of 6.45 m (Figure 2-3). Properties of the wall and struts are listed in Table 2.3.

The initial ground-water level assumed corresponds to El. +32.3 m for class A, and to El. +31.1 m for class B and C (see Fig. 2-5). Measured data of piezometric heads at the glacial till and bedrock show a constant value, El. +29 m, approximately. Both models assumed a linear head loss through the BBC layer. Class A assumes constant head value at the bottom of the BBC of 30.5 m (Fig. 2-6), while class B and C a constant head value of 28.2 m (Figures 2-7 and 2-8).

2.2.2.2 Constitutive Soil Models

The constitutive modeling of soil behavior and selection of input parameters represents a major source of uncertainty in finite element analyses (Whittle et al., 1993). The lack of lab tests on high quality samples in the granular fill, cohesive fill, silty sand, glacial till and bedrock limits current capabilities to describe these units. The only available data are standard penetration tests (SPT). Empirical correlations between N_{SPT} and friction angle and Young's modulus are available (e.g., Skempton, 1986; Stroud, 1989) but carrying a high uncertainty. For this reason,

the simple linearly elasto-perfectly plastic constitutive model Mohr-Coulomb[††] (MC) was selected for the three upper soil layers (granular fill, cohesive fill, and silty sand layers) and for the glacial till and bedrock (used in class C). This very-well-known model requires only five parameters[‡‡]: 1) Young's modulus: E'; 2) Poisson's ratio: ν'; 3) apparent cohesion: c; 4) internal friction angle: ϕ'; and the 5) initial effective stress ratio: K_0. Table 2-1 presents the engineering properties and model parameters for these specific layers for the three classes of predictions. It is important to highlight that material properties for the three upper layers used in class A were the ones assumed by Jen (1998). In class B and C, the three upper layers, the glacial till, and the bedrock were modeled as drained material in Plaxis (i.e., no excess pore pressures develop in these layers). Due to the lack of lab tests on the upper layers, the hydraulic conductivities for the upper layers were assumed to be 0.31 m/day (in class B and C); however, material properties for the glacial till and bedrock were estimated from Einstein et al. (1983), and Whittle et al. (1993).

In contrast, the BBC has been extensively studied in the past 50 years, especially at MIT. Therefore the generalized effective stress soil model MIT-E3[§§], developed by Whittle (1987) and fully described by Whittle and Kavvadas (1994), was selected to describe the behavior of this unit.

MIT-E3 is a generalized effective stress soil model for normally and moderately overconsolidated clays. The model describes a number of important aspects of soil behavior

[††] Although the correct name of this constitutive law is Coulomb model; the Mohr-Coulomb (MC) nomenclature follows the Plaxis user manual.

[‡‡] We assume zero dilation (ψ=0°) for all layers in order to assume zero volume strain conditions at failure.

[§§] The MIT-E3 model has recently been integrated within the kernel of Plaxis (Akl, Bonnier; pers. comm., 2008).

which have been observed in laboratory tests on K_0-consolidated clays including: (1) small strain non-linearity following a reversal of load direction; (2) hysteretic behavior during unload-reload cycles of loading; (3) anisotropic stress-strain-strength properties associated with 1-D consolidation history and subsequent straining; (4) post-peak, strain softening in undrained shear tests in certain modes of shearing on normally and lightly overconsolidated clays; and (5) occurrence of irrecoverable plastic strains during cyclic loading and shearing of overconsolidated clays. The model also has a number of key restrictions: (a) It uses a rate-independent formulation and hence, does not describe creep, relaxation or other strain rate dependent properties; and (b) it assumes normalized soil properties (e.g., the strength and stiffness are proportional to the confining pressure at a given overconsolidation ratio, OCR) and hence, does not describe complex aspects of soil behavior associated with cementation.

Another very important reason for selecting MIT-E3 to represent the BBC behavior is because it has been already calibrated for the BBC and extensively tested in excavation problems by several authors (e.g., Whittle & Hashash, 1993; Whittle et al., 1994; Hashash & Whittle, 1996; Jen, 1998). Table 2-2 presents the MIT-E3 input model parameters selected for BBC.

The selection of the OCR profile in the MIT-E3 model is critical for defining the profile of undrained shear strength of the clay. Figure 2-9 shows the stress history form 1-D consolidation tests at SBSTS (after Ladd. et al., 1999). Jen (1998) noted that when used in conjunction with the best estimate of σ'_p (mean profile shown in Figure 2-9), the MIT-E3 model overestimates the laboratory strengths by 15 to 25%. Therefore, a different σ'_p profile was assumed to be used in MIT-E3, as shown in Figure 2-9 (referred to as revised profile; Jen, 1998).

Figure 2-10a compares the predicted MIT-E3 undrained shear strength profiles with the SHANSEP strength profiles (Ladd et al., 1999). It can be seen that there is a good agreement between the predicted MIT-E3 s_u profiles (DSS and TC[***] modes of shearing) and the measured data (there was no data in the extension shear mode). Figure 2-10b shows the assumed isotropic (i.e., $k_x=k_y$) hydraulic conductivity profile for the BBC unit and also shows measured data from constant rate of strain consolidation tests (after Whelan, 1995). Figure 2-11 shows the initial conditions used in class A, B, and C: (a) initial effective stress and pore pressures; (b) initial effective stress ratio, K_0; and (c) the s_{uDSS} profile compared with field vane data. From Figure 2-11c, it can be seen a large scatter of the measured field vane undrained shear strength, especially at the lower clay (L-BBC). It is very important to highlight that class A, B, and C analyses use the same MIT-E3 properties (i.e., input parameters and state variables – stress history).

2.2.2.3 Simulation of Construction Sequences

Table 2-4 summarizes the sequence of events used in 2-D non-linear finite element simulation for the Platform section which involves partial drainage (i.e., consolidation). Since non-horizontal soil layers are considered in the class C model, it is necessary to use an additional initial phase in order to fully reach drained equilibrium of initial stresses. The duration of each excavation step in the class B and C predictions is based on a detailed interpretation of the as-built construction records and differs (modestly) from the timeline considered prior to construction. Existing buildings on the South side are mainly supported by shallow foundations

[***] DDS: direct simple shear; TC: triaxial compression; TE: triaxial extension

(mats and footings). Their effect was approximated in the class C analyses as a surcharge load of 25 kPa acting on the silty sand layer, as shown in Figure 2-8.

Each excavation stage was simulated with partial drainage (i.e., using consolidation phases). The excavation work started in 01/Nov/2000 (referred to as excavation level 1). Then each corresponding strut was installed and, for class B and C, also pre-loaded, at its corresponding level (Table 2-1). The last excavation stage (referred to as excavation level 6) reaches a final formation level at El. +16.5 m which corresponds to the final phase on the simulation (7/Aug/2001). The total time assumed to reach formation level was 279 days for class B and C predictions.

2.2.3 Comparison of Measurements and Predictions

Figure 2-2 shows the scope of instrumentation used to monitor the excavation performance for the Platform section. This includes: 1) lateral movements of the diaphragm wall, measured by five inclinometers cast within the wall; three in the North wall (I-05N1, I-06N1, and I-07N1) and two in the South wall (I-06S1, I-07S1); 2) lateral soil displacements by two in-soil inclinometers (I-06N2 and I-06S2) located approximately 40 m behind each wall; 3) surface settlements by sixteen deflection monitoring points (denoted by DMP); 4) excavation heave by one multi-point heave gage (HV-6C) located at the center of the excavation; 5) piezometric head measurements from one vibrating wire piezometer inside the excavation (PZ-06 C); and 6) strut forces measured by twenty strain gauges distributed at different strut lines and elevation in the Platform section. Figure 2-3 shows plans and typical sections for the strutting system at the

Platform section. The first three strut levels use single struts while the last two strut levels use double struts.

2.2.3.1 Lateral Wall Displacements

Figure 2-12 compares the computed and measured horizontal wall and soil displacements for the last three excavation levels, 4 (El. +21.6 m), 5 (El. +18.9 m) and 6 (El. +16.5 m) reached in March/April 2001, May 2001, and August 2001, respectively. The results show the following:

The measured data (which include both wall and underlying soil movements) show a very good agreement with class B and C predictions for both North and South sides at each excavation level. The maximum measured horizontal wall displacements occur at the toe of the wall and are comparable in magnitudes for both sides (32-52 mm North and 50 mm South in August 2001), confirming the initial assumption of symmetric loading conditions.

The class A analyses overestimate the measured lateral wall/soil movements at excavation levels 4, 5, and 6. The analyses show larger inward movements below the excavated grade. Although class A predictions involve larger symmetric movements, they show reasonable agreement in the mode shape of wall deflections, but overestimate toe deflections for the last phase of excavation. It should be noted that the class A predictions played a very important role in the final design of the Transitway project as the design of the excavation support system does not include any ground improvements to control the deflections of the diaphragm wall.

2.2.3.2 Lateral Soil Displacements

Figure 2-13 compares the horizontal soil displacements measured in the retained soil (35-40 m from the diaphragm wall; see Figure 2-2) with class A, B, and C numerical predictions. The measured data were only available at the final excavation grade (CD 286-288). The data show maximum inward movements at the ground surface (26-28 mm). The class B and C analyses tend to underestimate inward movements in the upper soil units, while the class A results are in surprisingly good agreement over the over the full soil profile.

2.2.3.3 Surface Settlements

Figure 2-14 summarized the measured and computed (class A, B, and C) surface settlements in the retained soil for the last three excavation levels 4, 5 and 6. Throughout these periods (March-August, 2001), the measured data show higher settlements behind the South wall reaching maximum magnitudes of 16, 26, 33 mm, respectively (compared to maximum values of 11, 14, 24 mm at the North side). At formation level, the maximum surface settlements occur at 28 m and 42 m behind the North and South wall, respectively. Higher measured surface settlements on the South side are attributed to the presence of the buildings.

The predictions are generally in good agreement with the measured settlements especially on the North side. Class A generates higher settlements close to the walls due to larger inward wall deflections, while the building surcharge in the class C analyses partially explains larger settlements on the South side of the excavation. Other effects such as local lowering of the

groundwater table are also expected to contribute to the results, but were not well documented (or sufficient to include in the class B and C analyses).

2.2.3.4 Excavation Heave

In excavation problems, it is very difficult to obtain measurements of soil heave because most of the time construction activities inside the excavation cause severe damage to instrumentation. Figure 2-15 shows measurements versus predictions of excavation heave from excavation level 4 to excavation level 6. Measurements of heave were obtained using a multi-point heave gage (with 5 elevation points). The deepest point (not shown) is used as a reference datum installed in the till/bedrock, so the others correspond to the elevations shown in Figure 2.4 (installed in the BBC layer). The results show very good agreement between predictions and measurements throughout these periods (March-August, 2001). The maximum measured value is 70 mm at El. +13.1 m (the uppermost point). It is important to highlight that the integrations of the units of glacial till and bedrock plays an important role in predicting heave (main difference between class B and C).

2.2.3.5 Pore Pressures

Figure 2-16 shows measured time responses from two vibrating wire piezometers (PZ-06C at El. +13.7 m and El. +7.6m) installed within the lower BBC at the center of the excavation with predictions over the time period of the excavation. The class B and C predictions are in a very good agreement with the measured piezometric heads at both sensor levels. This result confirms the time sequence of excavations assumed in the class B and C models. Class A predictions are

offset from the measurements due to assumptions on the time frame of construction activities. The class A model also appears to overestimate the initial and long term pore pressures in the clay (also highlighted in Figure 2-11a).

2.2.3.6 Strut Loads

Measurements of strut forces were achieved by averaging data from the twenty strain gauges installed at different strut lines. The data were properly compensated for temperature effects. Average values of the measured pre-loads were included in the class B and C finite element simulations with values ranging from 41 to 613 kN/m, as shown in Figure 2-17. This figure also compares the maximum measured and predicted forces at each strut level (together with standard deviations in the magnitudes of measured data). The class B and C are generally in reasonable agreement with the measured data, but tend to overestimate loads, especially at strut level 5. Class A predictions (no-pre-loads) underestimate significantly the measured forces at strut levels 3 and 4. The measured strut loads are typically less than 50% of the ultimate capacity of each strut level.

2.2.4 Conclusions

In this study, the Transitway Project and site stratigraphy of South Boston have been briefly described. The upper soil layers (granular fill, cohesive fill, and silty sand) and the lower layers (glacial till and bedrock) have been modeled by a simple elasto-plastic model due to lack of field and lab test data that prevents calibration of a more advanced soil model. However, the key unit of Boston Blue Clay (BBC), was modeled using a generalized effective stress soil model (MIT-

E3) that describes very well the stress-strain-strength properties measured in lab test. The main conclusions of these numerical analyses are the following:

1. Class A predictions, using an advanced effective stress soil model that is well calibrated using high quantity lab test data, can achieve realistic and consistent predictions of performance for a braced excavation system including wall deflections, ground movements, and pore pressures. The strut loads can also be well predicted but this requires advance knowledge or design of pre-load forces.
2. Class A predictions performed previously by Jen (1998), which considered several parametric numerical analyses, were extremely useful and relevant for the final geotechnical design. In fact, they enabled construction of the project without resort to expensive ground improvement techniques.
3. Class B and C predictions that use available information prior to construction together with real-time records of site activities are able to show modest improvement on the class A predictions.
4. The assumed stress history profile of the clay in the MIT-E3 model was the same used in class A, B, and C predictions. This plays a very important role in predictions of wall movements, soil deformations, surface settlements, excavation heave, pore pressure and strut forces.
5. The modeling differences between class B and C are the integration of the non-horizontal glacial till and bedrock units, the building surcharge, and the symmetric conditions. While most predictions are extremely similar, the integration of these soil/rock units plays an important role in predicting accurately excavation heave.

2.3 Nicoll Highway Collapse

2.3.1 Description

The collapse of the Nicoll Highway during excavations for the cut-and-cover tunnels for the new Circle Line in Singapore (Phase 1 contract C824) has been extensively documented in a Committee of Inquiry report (COI, 2005). Many local and international experts contributed to this report and have subsequently published detailed interpretations of the failure (e.g., Yong et al., 2006; Endicott, 2006; Davies et al., 2006). One key aspect was the under-design of the temporary lateral earth support system. Figure 2-15 shows the design for the (intended) 33.3 m deep excavation comprising 0.8 m thick diaphragm wall panels that extend through deep layers of Estuarine and Marine clays (Kallang formation) and are embedded a minimum of 3m within the underlying Old Alluvium (layer SW-2). The walls were to be supported by a total of ten levels of pre-loaded, cross-lot bracing struts and by two relatively thin rafts of continuous Jet Grout Piles (JGP). The Upper JGP raft was a sacrificial layer that was excavated after installation of the 9th level of struts. Collapse occurred on April 20th 2004 following excavation of the Upper JGP (to an elevation of approximately 72.3 m RL[†††], Fig. 2-15).

The design of the temporary lateral earth support system was based on a table of geotechnical design parameters (GIM, August 2001). These parameters were the unit weights, K_0 coefficients, hydraulic conductivities, k, elastic moduli, E, and both the Mohr-Coulomb (drained) effective stress strength parameters (c', ϕ') and undrained shear strength profiles, $s_u(z)$

[†††] RL – reduced level. Mean sea level is at 100m RL

for all of the main soil units and JGP layers. Many of these parameters were based on prior local experience (e.g., Bo et al., 2003; Tan et al., 2003; Chiam et al., 2003; Li & Wong, 2001).

Piezocone penetration data were the only reliable site-specific information on undrained shear strengths available at the time of design. Figure 2-16 compares the undrained shear strength profile specified in the GIM table with results from 4 piezocone tests interpreted using a cone factor N_{kT} = 14. The results show good agreement between the GIM and piezocone strengths in the Upper unit of the Marine Clay (UMC). However, the piezocone results also suggest that the Lower Marine Clay (below 75 m RL) is weaker than the design strength profile. Whittle and Davies (2006) have attributed this to that the Lower Marine Clay is underconsolidated locally (i.e., has not fully consolidated under the 5m fill placed in the 1970's). This explanation assumes that the underlying units of Old Alluvium have low bulk permeability and/or low recharge potential.

The design of the lateral earth support system was based on finite element analyses of soil-structure interaction using an elastic-perfectly plastic Mohr-Coulomb (MC) model for the soil behavior. The analyses simulated undrained shear behavior of the clay layers using drained effective stress, strength parameters (c', ϕ'). This approach, referred to as Method A (COI, 2005), led to gross overestimation of the undrained shear strength in the analyses (Fig. 2-16). As a result, the designers underestimated the wall deflections and bending moments and under-designed the bending capacity of the diaphragm wall and thickness of the two JGP layers.

Ironically, most of the experts involved in the investigations of the collapse used the same finite element program and MC constitutive model to diagnose the failure mechanism. These experts used total stress strength parameters (s_u = c', ϕ' = 0°) to represent directly the expected undrained strength profiles, referred to as Method B in Figure 2-16 (e.g., GIM, 2001; Whittle & Davies, 2006). These Method B analyses were able to describe, to a reasonable first order approximation, the measured lateral wall deflections and strut loads. They also provided the basis for explaining the collapse mechanism in which the brittle failure of the 9th level strut-waler connections led to a redistribution of lateral earth pressures that could not be supported by the bracing system and led to catastrophic failure (COI, 2005).

Extensive post-failure site investigation programs were carried out to resolve uncertainties associated with the complex stratigraphy (which includes a deep relic channel through the Old Alluvium). A detailed program of high quality laboratory consolidation and shear strength testing on high quality samples of marine clay was also performed (Kiso-Jiban, 2004). None of these data were analyzed in detail at the time of the inquiry but were included in a revised design manual (Amberg, 2005). This section presents a re-analysis of the excavation performance based on the post-failure laboratory test program. The behavior of the Upper (UMC) and Lower (LMC) Marine Clay units is represented by the MIT-E3 model (Whittle and Kavvadas, 1994) which is able to simulate the anisotropic effective stress-strain-strength properties measured in the tests.

2.3.2 Calibration of MIT-E3 Model for Singapore Marine Clays

Calibration of the model for UMC and LMC clays follows the general procedure proposed by Whittle et al. (1994). Table 2-5 summarizes these input parameters, their physical meanings within the model formulation and laboratory tests from which they can be obtained, together with parameters selected for UMC and LMC units. The parameters have been derived principally from a set of 1-D consolidation tests (Fig. 2-20) and K_0-consolidated undrained triaxial shear tests (Fig. 2-21) on specimens reconsolidated to the in situ stress conditions.

The compressibilities of the normally consolidated UMC and LMC units are well-characterized virgin consolidation lines with $\lambda = 0.37 - 0.38$, Figure 2-17a. The upper marine clay generally has higher in situ void ratio ($e = 1.7 - 1.9$) than the lower unit ($e = 1.5 - 1.6$). The marine clays show significant elastic rebound when unloaded. Figure 2-17b shows that recoverable axial strains, $\Delta\varepsilon_a$ = 10-12% when the effective stress is reduced by one order of magnitude (ξ_v = OCR = 10). This behavior is consistent with laboratory measurements of the maximum shear modulus, G_{max}, (from bender elements), reported by Tan et al. (2003). The Authors have used these data to estimate the model input parameter, κ_0, and then selected input values of C, n (Table 2-5) from the swelling data as shown in Figure 2-20.

A series of CAU normally consolidated triaxial compression and extension tests were performed on specimens from 4 depths within the UMC and LMC units, Figure 2-21. All of the specimens were consolidated to a common lateral stress ratio, $K_0 = 0.52$ prior to shearing. The measured data show a significant difference in the average undrained triaxial compression

strength ratios measured in these tests, s_{uTC}/σ'_{vc} = 0.30 vs 0.27 for the UMC and LMC units, respectively. The data also show that UMC specimens mobilize higher friction angles when sheared to large strains (in both compression and extension), ϕ' = 32.4° -33.8° vs 27.0° - 27.1° for UMC and LMC, respectively. The UMC exhibits higher undrained strength anisotropy (s_{uTE}/s_{uTC} = 0.60 – 0.66) compared to LMC (0.80 – 0.88) and both exhibit relatively modest post-peak softening in compression shear modes for $\varepsilon_a > 2\%$.

Details of the measured effective stress paths and shear stress-strain properties are well characterized by MIT-E3 through model input parameters c, S_t, ϕ'_{TC}, ϕ'_{TE}, ω and γ (Table 2-5). The remaining parameters in Table 1 have been estimated from prior studies on similar clays.

2.3.3 Finite Element Model

The numerical simulations of excavation performance have been carried out focusing on one specific cross-section (within the collapse zone) corresponding to the location of the instrumented strut line S335, Figure 2-22. Loads in each of the nine levels of struts installed at S335 were measured through sets of three strain gauges. These data have been extensively validated by each of the expert witnesses for the public inquiry (e.g., Davies et al., 2006). Measurements of the lateral wall movements at this section are obtained from inclinometer I-65 (installed through the North diaphragm wall panel) and I-104 located in the soil mass 1.5 – 2.0m outside the South wall.

Figure 2-23 shows the cross-sectional geometry for section S335 based on data from both pre-tender and post-failure site investigations: The section is notably more complex than the design section indicated in Figures 2-18 and 2-19. The base of the LMC dips notably to the South. This is part of a relic channel in the underlying Old Alluvium that was highlighted by Whittle and Davies (2006). On the South side, the LMC directly overlies the Old Alluvium, while units of fluvial sand, F1, and estuarine clay (E) separate the Marine Clay and OA on the North side. The post-failure investigations have established that the OA has relatively low bulk hydraulic conductivity, while the F1 layer has relatively limited extent with no ready source of recharge (although there is a hydraulic connection across the wall due to the absence of a diaphragm wall panel between S336 – S337 in Fig. 2-22). These details were critical in establishing that failure of the excavation was not caused by hydraulic uplift (Whittle and Davies, 2006). The lateral earth support design includes two layers of continuous jet grout pile (JGP) rafts that were intended to provide additional passive resistance below the formation. At section S335 it is unlikely that the lower JGP raft is continuous within the Old Alluvium, as installation jetting parameters for the jet grout columns were based on parameters calibrated to marine clay conditions. Hence, the section shows a truncation of the lower JGP raft at the North wall.

Section S335 has been modeled using the Plaxis™ program[‡‡‡]. Following Whittle and Davies (2006), the current numerical simulations assume that the groundwater table in the Fill is at 100.5m RL and that there is a small excess pressure in the underlying LMC and OA units

[‡‡‡] The MIT-E3 model has recently been integrated within the kernel of Plaxis (Akl, Bonnier; pers. comm., 2008).

(piezometric head, H = 103m). The UMC and LMC units[§§§] are modeled using the MIT-E3 model with parameters listed in Table 2-5, while engineering properties of all other soils and JGP rafts are simulated using the Mohr-Coulomb (MC) model with parameters reported in the prior studies (COI, 2005), as shown in Table 2.6.

In order to apply the MIT-E3 effective stress soil model it is essential to specify carefully the boundary and initial conditions. Figure 2-21a shows the in-situ stresses and stress history profile, where the stress history shown corresponds to a post-failure investigation performed by Kiso-Jiban (2004). The current analyses assume $\sigma'_p/\sigma'_{v0} = 1.0$ (i.e. OCR=1.0) in both UMC and LMC units (Figure 2-21a). When combined with the assumed pore pressure conditions, this implies that the marine clays are slightly under-consolidated. The in-situ stresses also deviate from K_0-conditions due to the inclined stratigraphy. This is modeled using a standard drained relaxation stress procedure within Plaxis.

Figure 2-24b summarizes the anisotropic undrained shear strength profiles (corresponding to a South section behind the South wall) within the marine clays obtained using the MIT-E3 model for three standard modes of plane strain shearing. The undrained plane strain active and passive strengths bound the best estimate profile recommended by Whittle and Davies (2006), based on their interpretation of piezocone tests (this assumes $s_{uDSS}/\sigma'_{v0} = 0.21$ for normally consolidated Singapore marine clay, after Tan et al., 2003). It is interesting to note that the undrained shear strength predicted by MIT-E3 in the DSS mode is 5-7kPa lower than the best estimate used in the prior MC analyses within the LMC. The figure compares the profiles

[§§§] The lower Estuarine clay (E, Fig. 2.18) is assumed to have the same properties and behavior as the LMC

obtained using the MC model (with parameters listed in Table 5-6) with results obtained while MIT-E3 model is used to represent the UMC and LMC units (and Estuarine layers). The following points should be noted:

1. The MC model generally describes higher strengths in the Upper Marine Clay than MIT-E3, but is closer to the average of the anisotropic strength in the Lower Marine Clay.
2. The MIT-E3 model predicts very similar shear strengths in the simple shear and passive (extension) modes in both UMC and LMC units.

All other parameters for the lateral earth support system including the as-built diaphragm wall embedment, capacity of the critical strut-waler connections and pre-load of the struts are based on prior interpretation of the construction records (Bell & Chiew, 2006).

2.3.4 Results

Figures 2.25-2.27 compare predictions of lateral wall deflections from the current analyses with measured data from the two inclinometers (I-104, I-65) and with results of prior analyses (marked as MC) performed by Whittle & Davies (2006). The results are shown at 6 excavation stages (during the period February - April 2004). The current analyses predict very well the maximum lateral wall deflection on the South side of the excavation including the large deflections associated with removal of the upper JGP layer (April 17-20, Figure 2-24). At this stage, a plastic hinge formed in the South wall (at a depth of 32 m) and there is very large rotation of the toe. The current analyses also describe very well the maximum lateral wall deflection on the North side through March. The analyses tend to overestimate inward

movements of both walls within the upper 10-15 m of the bracing system. This may be attributed to the assumption that the UMC is normally consolidated, while the pre-consolidation data show a small OCR in this layer (Fig. 2-21a). The analysis predicts significant lateral displacements at the toe of the North wall in April 2004 (70mm at time of failure on April 17-20). In contrast, inclinometer I-65 suggests that the North diaphragm wall panel remains well anchored. The net effect is that the analysis underestimates the deflections and flexure in the lower part of the North wall during April. This result is largely related to the complex stratigraphy and assumed truncation of the lower JGP at the North wall.

The current analyses using MIT-E3 predict larger inward wall deflections than the prior MC analyses and are in rather better agreement with the measured data. This result is encouraging as the current analyses are based on calibration of a complex constitutive model using laboratory test data (rather than a best estimate of a design strength line). However, it is clear that certain features of the measured data such as the toe fixity on the North wall are difficult to interpret and are not controlled by the properties of the marine clay. Similarly, the current analyses do require additional judgment in the selection of the OCR profile.

It is generally agreed that collapse of the Nicoll Highway initiated when the 9th level strutting failed due to sway buckling of the strut-waler connections. Overloading of the strut-waler connections occurred due to the absence of splays that had been designed for all struts (see Fig. 2-22). The strut-waler connections exhibited a brittle post-peak load response due to a mechanism of 'sway buckling' that was associated with the use of C-channel stiffeners at the strut-waler connections in levels 7-9 of the bracing system (this was a revised design used during

construction; Bell & Chiew, 2006). Collapse occurred as the bracing system was unable to transfer loads upward through the bracing system.

Figure 2-28 summarizes predictions of the strut loads at levels 7-9 on prior to collapse (April 20, 2004). The results show very reasonable agreement between the computed and measured loads in strut levels 7 and 8. The current analyses are also in close agreement with loads obtained by Whittle and Davies (2006) using the MC model. Both sets of analyses predict that the capacity of the 9th level strut-waler connection is fully mobilized at this stage of excavation (30.6m deep) immediately following the removal of the upper JGP raft (since the elevation of that excavation stage was deeper than the upper JGP raft). However, the measurement of the 9th level strut load is much smaller. This is an inconsistency noted by all the experts to the public inquiry (COI, 2005). Hence, it can be concluded that the current analyses with MIT-E3 are able to predict the onset of collapse consistent with prior MC analyses, but they do not shed any insight to explain the measured loads at level 9.

2.3.5 Conclusions

Corral (2010) and Corral and Whittle (2010) have re-analyzed the performance of the lateral earth support system for a critical instrumented section, S335, of the cut-and-cover excavations at the site where the Nicoll Highway collapsed in 2004. Engineering properties of the key Upper and Lower marine clay units have been modeled using the generalized effective stress soil model, MIT-E3, with input parameters calibrated using laboratory test data obtained as part of the post-failure site investigation. The model predictions are evaluated through comparisons

with monitoring data and through comparisons with results of prior analyses using the Mohr-Coulomb (MC) model (Whittle & Davies, 2006). The MIT-E3 analyses provide a modest improvement in predictions of the measured wall deflections compared to prior MC calculations and give a consistent explanation of the bending failure in the South diaphragm wall and the overloading of the strut-waler connection at the 9th level of strutting. The current analyses do not resolve uncertainties associated with performance of the JGP rafts, movements at the toe of the North-side diaphragm wall or discrepancies with the measured strut loads at level 9. However, they represent a significant advance in predicting excavation performance based directly on results of laboratory tests compared to prior analyses that used generic (i.e., non site-specific) design isotropic strength profiles.

2.4 References

Amberg & TTI (2004). Final geotechnical interpretative report CCL824 – Reconstruction of Braced Excavation System, Project document.

Bell, B.C. & Chiew, S.P. (2006). "Nicoll Highway collapse: Some structural observations. Part 2: Soil retention system." *Proc. Int. Conf. on Deep Excavations*, Singapore, June 2006.

Bo, M.W., Choa, V. & Hong, K.H. (2003) "Material characterization of Singapore Marine Clay at Changi," *Quarterly Journal of Engineering Geology and Hydrogeology*, 36, 305-319.

Brinkgreve, R.B.J., Broere, W., and Waterman, D. (2008) "PLAXIS: Finite Element Code for Soil and Rock Analyses.", Version 9.0, Balkema.

Chiam, S.L., Wong, K.S., Tan, T.S., Ni, Q., Khoo, K.S. & Chu, J. (2003) "The Old Alluvium," *Proc. Underground Singapore*, 2003, 408-427.

Clough, W. and Hansen, L. (1981). "Clay Anisotropy and Braced Wall Behavior." *ASCE Journal of the Geotechnical Division*, 107(7):893-913.

Clough, W. and O'Rourke, T. (1990). "Construction Induced Movements of In-situ Walls." *Proc. ASCE Conference Design and Performance of Earth Retaining Structures*: 439-470.

COI (2005). Report of the Committee of Inquiry into the Incident at the MRT Circle Line Worksite that Led to the Collapse of Nicoll Highway 20 April 2004. Report Submitted to the Minister of Manpower.

Corral, G. (2010). "Re-analysis of Deep Excavation Collapse Using Generalized Effective Stress Soil Model." *CE Thesis, Department of Civil and Environmental Engineering, Cambridge, MIT.* 138p.

Corral, G. and Whittle A.J. (2010). "Re-analysis of Deep Excavation Collapse Using Generalized Effective Stress Soil Model." *Proceedings of the 2010 Earth Retention Conference (ER2010)*, ASCE GSP (208): 720:731

Davies, R.V., Fok, P., Norrish, A. & Poh, S.T. (2006). "Nicoll Highway Collapse: Field Measurements and Observations." *Proc. Int. Conf. on Deep Excavations*, Singapore, June, 2006.

Endicott, L.J. (2006). "Nicoll Highway lessons learnt," *Proc. Int. Conf. on Deep Excavations*, Singapore, June 2006.

Finno, R., Harahap I., and Sabatini, P. (1991). "Analysis of Braced Excavations with Coupled Finite Element Formulations." *Computers and Geotechnics* 12: 91-114.

Finno, R., Blackburn. J.T., and Roboski, J.F. (2007). "Three-Dimensional Effects for Supported Excavations in Clay." *Journal of Geotechnical and Geoenvironmental Engineering, ASCE* 133(1): 30-36.

GEI Consultants, Inc. (1996), "Geotechnical Data Report, MBTA South Boston Piers Transitway, Section CC09, MBTA Contract SOPS08, Boston, Massachusetts.", submitted to *Frederic R. Harris, Inc.*, August.

GEI Consultants, Inc. (1996), "Geotechnical Data Report, MBTA South Boston Piers Transitway, Sections CC03A and CC05, MBTA Contract SOPS08, Boston, Massachusetts.", submitted to *Frederic R. Harris, Inc.*

GIM (2001). Geotechnical Interpretative Memorandum C824/DES/DM/002A, Project Document.

Kiso-Jiban (2004). Factual reports on soil investigation at Nicoll Highway, 3 Vols., Project Documents.

Haley & Aldrich, Inc. (1992), "Geotechnical Data Report, New United States Courthouse, Boston, Massachusetts, Contract No. GS-02P91CUC0031 (NEG).", submitted to *Pei Cobb Freed &Partners and Jun/Brannen Associates*, March.

Haley &Aldrich, Inc. (1993), "Final Geotechnical Engineering Report, Central Artery (I-93) / Tunnel (I-90) Project, Design Sections D001A and 0001 B, Boston, Massachusetts.", submitted to *Massachusetts Highway Department*, File NO.1 036071, June.

Hashash, Y.M.A. and Whittle, A.J. (1996). "Ground Movement Prediction for Deep Excavations in Soft Clay." *ASCE Journal of Geotechnical Engineering,* 122(6): 474-486.

Jen, L. C. (1998), "The design and performance of deep excavations in clay." *PhD Thesis. Department of Civil and Environmental Engineering, Cambridge, MIT*, 698p.

Kaye, C.A (1976), "The Geology and Early History of the Boston Area of Massachusetts: A Bicentennial Approach." *U.S. Geological Survey*, Bulletin 1476: U.S. Geological Survey, Denver, CO, 77 p.

Ladd, C.C., Young, G.A., Kraemer, S.R. and Burke, D.M. (1999). "Engineering properties of Boston Blue Clay from Special Testing Program." *Proceedings, Special Geotechnical Testing: Central Artery/Tunnel Project in Boston, Massachusetts*, ASCE GSP 91, GeoCongress '98, National Convention, Boston, 1-24.

Lambe, T. W. (1970), "Braced Excavations." *ASCE Specialty Conference on Lateral Stresses in Ground and Design of Earth-Retaining Structures,* Ithaca, NY: 149-218.

Lambe, T.W. (1973), "Predictions in Soil Engineering." *Géotechnique*, 23(2), 149-202.

Li, W.W. & Wong, K.S. (2001) "Geotechnical properties of Old Alluvium in Singapore," *Proc. Journal of the Institution of Engineers*, Singapore, 41(3), 10-20.

Orazalin, Z. (2010). "Three-Dimensional Finite Element Analysis of a Complex Excavation on the MIT Campus." *S.M. Thesis, Department of Civil and Environmental Engineering, Cambridge, MIT.* 143p.

O'Rourke, T. (1981). "Ground Movements Caused by Braced Excavations." *ASCE Journal of Geotechnical Engineering Division* 107(9): 1159-1178.

O'Rourke, T. D. and C. J. O'Donnell (1997). "Deep Rotational Stability of Tieback Excavation in Clay." *ASCE Journal of Geotechnical and Geoenvironmental Engineering* 123(6), 516–524.

Parsons Brinckerhoff Quade & Douglas, Inc. (1994), "Geotechnical Data Report, Preliminary Design Phase, MBTA South Boston Piers I Fort Point Channel Underground Transitway, Boston, Massachusetts", submitted to *Stone & Webster Civil and Transportation Services Inc.*, October.

Parsons Brinckerhoff Quade &Douglas, Inc. (1995), "South Boston Piers Transitway Project, Geotechnical Data Report, Sleeper Street to New Congress Street", submitted to *Stone & Webster Civil and Transportation Services, Inc.*, September.

Parsons Brinckerhoff (1998), "Final Design Geotechnical Report, South Boston Piers Transitway Project, MBTA Contract E02CN14, Courthouse Station and Tunnel Construction, contracts CC07, CC08 & CC10. " submitted to *MBTA and STV Inc.*

Peck, R. B. (1969b). "Advantages and Limitations of the Observational Method in Applied Soil Mechanics.", *Géotechnique* 19(2): 171-187.

Skempton, A. W. (1986), "Standard Penetration Test Procedures and the Effects in Sands of Overburden Pressure, Relative Density, Particle Size, Ageing and Overconsolidation." *Géotechnique*, 36(2): 425-447.

Stroud, M. A. (1989), "The Standard Penetration Test – its Applications and Interpretations." *Penetration Testing in the UK, Thomas Telford, London*, 29-49.

Tan, T.S., Phoon, K.K., Lee, F.H., Tanaka, H., Locat, J. & Chong, P.T. (2003) "A characterization study of Singapore Lower Marine Clay," *Proc. Conf. On Characterization and Engineering Properties of Natural Soils*, Eds. Tan et al., Swets & Zeitlinger, 1, 429-454.

Whelan, M.P. (1995), "Performance of deep excavations in Boston." SM Thesis. Department of Civil and Environmental Engineering, Cambridge, MIT, 356p.

Whittle, A.J. (1987) "A Constitutive Model for Overconsolidated Clays with Application to the Cyclic Loading". *Sc.D Thesis. Department of Civil and Environmental Engineering, Cambridge, MIT.* 641p.

Whittle, A.J., Hashash, Y.M.A., Whitman, R.V. (1993). "Analysis of Deep Excavation in Boston." *ASCE Journal of Geotechnical Engineering* 119(1): 69-90.

Whittle, A.J. and Kavvadas, M.J. (1994). "Formulation of MIT-E3 Constitutive Model for Overconsolidated Clays." *ASCE Journal of Geotechnical Engineering* 120(1): 173-198.

Whittle, A.J., DeGroot, D.J., Ladd, C.C. & Seah, T-H. (1994). "Model prediction of the anisotropic behavior of Boston Blue Clay." *ASCE Journal of Geotechnical Engineering* 120(1): 199-225.

Whittle, A.J., & Davies, R.V. (2006). "Nicoll Highway Collapse: Evaluation of Geotechnical Factors Affecting Design of Excavation Support System." *Proc. Int. Conf. on Deep Excavations*, Singapore, June 2006.

Yong, K.Y., Teh, H.S. & Wong, K.S. (2006). "System failure of temporary earth retaining structure leading to collapse of Nicoll Highway." *Proc. Int. Conf. on Deep Excavations*, Singapore, June 2006.

Table 2-1: Soil material properties used in class A, B, and C finite element models

Material: Soil/Rock Layer								
	Granular Fill		**Cohesive Fill**		**Silty Sand**		**Glacial Till**	**[a] Bedrock**
Class	A	B/C	A	B/C	A	B/C	C	C
[1] Mat. Type	U	D	U	D	U	D	D	D
Const. Model	Mohr-Coulomb							
γ (kN/m^3)	18.9		18.1		18.9		18.9	21.8
k (m/day)	4.34	0.31	8.8×10^{-3}	0.31	8.8×10^{-3}	0.31	9.1×10^{-2}	8.6×10^{-3}
[2] E'^{ref} (MPa)	1×10^{-3}	1.68	0.77	1.77	9.3	10.6	93	5100
ΔE'/Δz (MPa/m)	1.71	-	0.43	-	0.82	-	37	190
ν'	0.3							
[2] c'^{ref} or s_u (kPa)	0		7.2 12.4 17.2		0		0	6.8×10^{5}
Δc'/Δz (kPa/m)	-							2.6×10^{4}
ϕ' (°)	0	30	0	15		35	43	32
K_0	0.5		0.75		0.5		1.0	1.0
[2] Ref. Elev., z_0 (m)	34.1	-	32.0	-	25.6	-	-0.8	-6.2

Notes:

[a] Properties estimated from Einstein et al. (1983) and Whittle el al. (1993).

[1] D: Drained (no excess pore pressures develop in these layers); U: Undrained

[2] $E' = E'^{ref} + \frac{\Delta E'}{\Delta z}(z - z_0)$; $c' = c'^{ref} + \frac{\Delta c'}{\Delta z}(z - z_0)$

Table 2-2: MIT-E3 model input parameters for resedimented Boston Blue Clay used in Class A, B, and C finite element models

Test Type	Parameter / Symbol	Physical contribution/meaning	Boston Blue Clay (BBC)
1-D Consolidation (Oedometer, CRS, etc.)	e_o	Void ratio at reference stress on virgin consolidation line	0.988
	λ	Compressibility of virgin normally consolidated clay	0.184
	C	Non-linear volumetric swelling behavior	22.0
	n		1.6
	h	Irrecoverable plastic strain	0.2
K_0-Oedometer or K_0-Triaxial	K_{0NC}	K_0 for virgin normally consolidated clay	0.53
	2G/K	Ratio of elastic shear to bulk modulus (Poisson's ratio for initial unload)	1.05
Undrained Triaxial Shear Tests: OCR=1; CKoUC OCR=1; CKoUE OCR=2, CKoUC	ϕ'_{TC}	Critical state friction angles in triaxial compression and extension (large strain failure criterion)	33.4°
	ϕ'_{TE}		45.9°
	c	Undrained shear strength (geometry of bounding surface)	0.866
	S_t	Amount of post-peak strain softening in undrained triaxial compression	4.5
	ω	Non-linearity at small strains in undrained shear	0.07
	γ	Shear induced pore pressure for OC clay	0.5
Shear wave velocity	κ_0	Small strain compressibility at load reversal	0.001
Drained Triaxial	ψ_0	Rate of evolution of anisotropy (rotation of bounding surface)	100

Note:
Boston Blue Clay (BBC): γ=18.1 kN/m3 and k=4.32×10^{-5} m/day (see Figures 2-9, 2-10, and 2-11)

Table 2-3: Material properties of excavation support system used in Class A, B, and C finite element models

[1] Diaph. Wall	Thickness (m)	E (MPa)	ν	Unit Weight, γ (kN/m^3)
Concrete	1.22	2.26×10^4	0.15	22.8

[1] D. Wall modeled as an elastic non-porous material.

[2] Strut Level	Section	E (MPa)	A (cm^2)	EA (kN)	EA/$\bar{s}$ [3] (kN/m)	Ultimate Axial Capacity (kN/m)
1	24"ϕ x 5/8"	2.0×10^5	296.1	5.9×10^6	9.2×10^5	609
2	36"ϕ x 5/8"		448.1	9.0×10^6	1.4×10^6	810
3	36"ϕ x 1"		709.4	1.4×10^7	2.2×10^6	1223
4	2-W36 x 135		512.3	1.0×10^7	1.6×10^6	1328
5	2-W36 x 230		872.3	1.7×10^7	2.7×10^6	1977

[2] Struts modeled as elasto-plastic anchors with null tensile strength.
[3] Average horizontal spacing, $\bar{s}$=6.45m.

Table 2-4: Construction Sequences used in Class A, B, and C predictions

Activity					Class	
					A	B / C
Description				† FE Anlys. Type	CD (days)	
Initial Phase				P	-	-
Drained Equilibrium and Building q=25 kPa				PD	NA	NA / -
D. Wall Installation (1.22m thick)				P	-	-
(zero displacements)	Elevation (m) Class A	Elevation (m) Class B / C	*Pre-loads (kN/m) B / C	-		
Exc. Level 1	32.0		-	C	45	51
Strut Level 1	32.6	33.2	41	P	-	-
Exc. Level 2	29.0	27.4	-	C	90	84
Strut Level 2	29.6	28.7	110	P	-	-
Exc. Level 3	25.9	25.0	-	C	135	111
Strut Level 3	26.5		429	P	-	-
Exc. Level 4	22.9	21.6	-	C	180	153
Strut Level 4	23.5	23.2	501	P	-	-
Exc. Level 5	19.8	18.9	-	C	225	185
Strut Level 5	20.4	19.5	613	P	-	-
Exc. Level 6	16.5		-	C	360	279

† P: Plastic; PD: Plastic Drained; C: Consolidation (EPP)
* No pre-loads in Class A

Table 2-5: Input parameters for MIT-E3 constitutive soil model: Upper Marine Clay (UMC) and Lower Marine Clay (LMC)

Test Type	Parameter/ Symbol	Physical contribution/meaning	Upper Marine Clay (UMC)	Lower Marine Clay (LMC)
1-D Consolidation (Oedometer, CRS, etc.)	e_o	Void ratio at reference stress on virgin consolidation line	1.80	1.60
	λ	Compressibility of virgin normally consolidated clay	0.380	0.370
	C	Non-linear volumetric swelling behavior	10.0	9.0
	n		1.5	1.5
	h	Irrecoverable plastic strain	0.2	0.2
K_0-Oedometer or K_0-Triaxial	K_{0NC}	K_0 for virgin normally consolidated clay	0.52	0.52
	2G/K	Ratio of elastic shear to bulk modulus (Poisson's ratio for initial unload)	0.94	0.94
Undrained Triaxial Shear Tests: OCR=1; CKoUC OCR=1; CKoUE OCR=2, CKoUC	ϕ'_{TC}	Critical state friction angles in triaxial compression and extension (large strain failure criterion)	32.4°	27.0°
	ϕ'_{TE}		33.8°	27.1°
	c	Undrained shear strength (geometry of bounding surface)	0.96	0.96
	S_t	Amount of post-peak strain softening in undrained triaxial compression	3.0	5.0
	ω	Non-linearity at small strains in undrained shear	0.40	0.40
	γ	Shear induced pore pressure for OC clay	0.5	0.5
Shear wave velocity	κ_0	Small strain compressibility at load reversal	0.0094	0.0094
Drained Triaxial	ψ_0	Rate of evolution of anisotropy (rotation of bounding surface)	100	100

Table 2-6: MC model parameters for soil layers at S335 model.

ID	Layer	* Material Type	Reference Elevation RL, m	$k_x=k_y$ (m/day)	γ_t (kN/m3)	Strength Parameters: s_u [c'] (kPa)	† $\Delta s_u/\Delta z$ (kPa/m)	ϕ' (°)	ψ' (°)	Elastic Properties: E' (kPa)	† E'/Δz (kPa/m)	ν'	K_{0NC}
1	Fill	D	-	8.64×10^{-2}	19.0	[0]	-	30	0	10000	-	0.25	0.50
2	Upper MC	UD	98.2	8.64×10^{-5}	16.0	20	0.397	0	0	6913	137	0.25	0.52
3	F2 Clay	UD	-	8.64×10^{-5}	19.0	88	-	0	0	29250	-	0.25	0.70
4	Lower MC	UD	83.4	8.64×10^{-5}	16.8	31	0.79	0	0	10310	346	0.25	0.52
5	F2-2 Clay	UD	-	8.64×10^{-5}	20.0	88	-	0	0	29250	-	0.25	0.70
6	F1-Sand	UD	-	8.64×10^{-5}	19.0	[0]	-	30	0	10000	-	0.25	0.50
7	OA-weathered	UD	61.6	8.64×10^{-4}	20.0	100	52	0	0	33250	13600	0.25	1.00
8	OA-competent	UD	-	8.64×10^{-5}	20.0	500	-	0	0	167500	-	0.25	1.00
9	JGP	UD	-	8.64×10^{-5}	16.0	300	-	0	0	250000	-	0.15	-

* D: Drained (no excess of pore pressures develop in this layer); UD: Undrained

† Linear variations with depth in stiffness and shear strength within soil layers starting at reference elevation (constant values above)

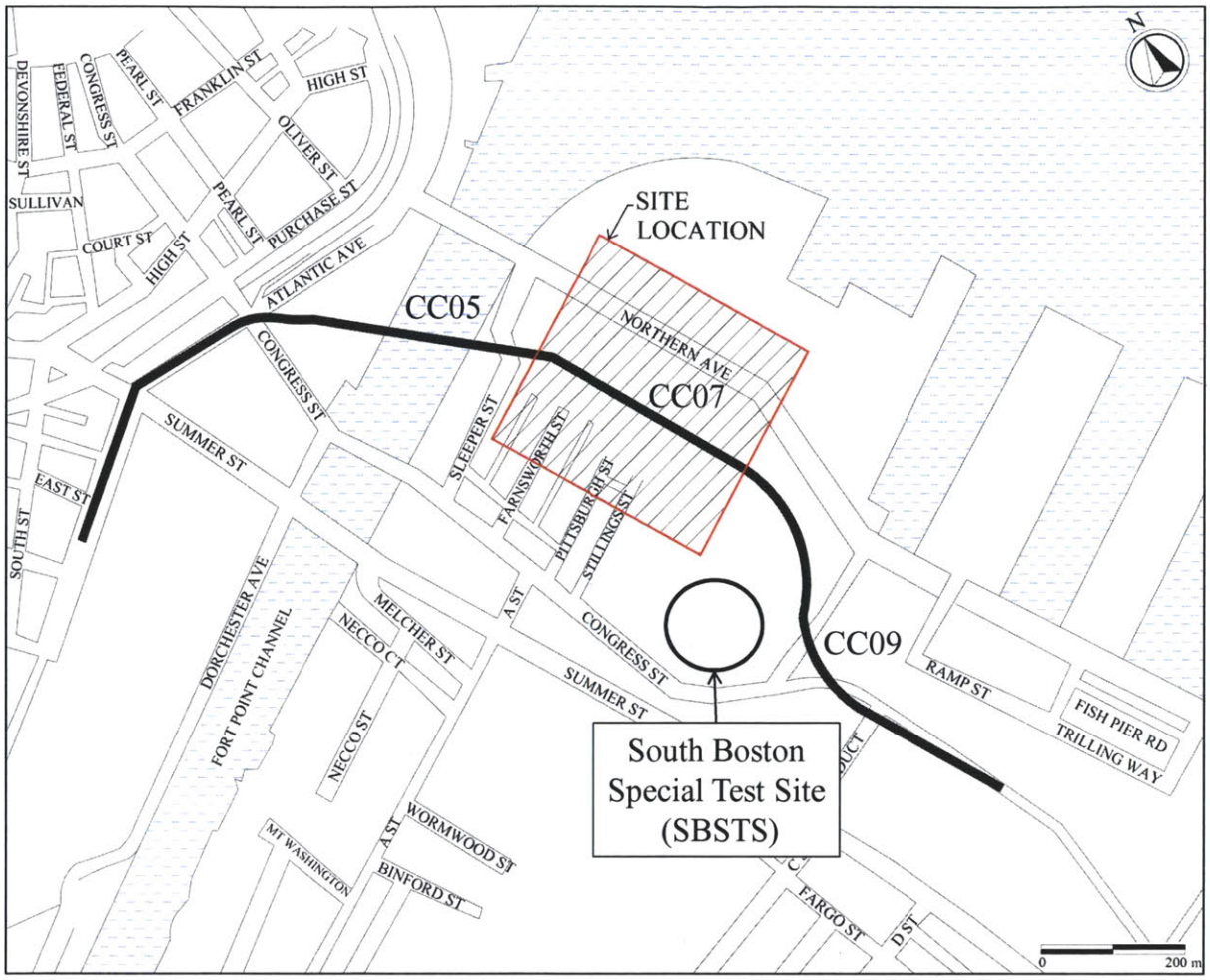

Figure 2-1: Site location of Courthouse Station of Transitway Project in South Boston (MBTA Contract E02CN14, Courthouse Station and Tunnel; after PB, 1998) and approximate location of SBSTS (after Ladd et al., 1999)

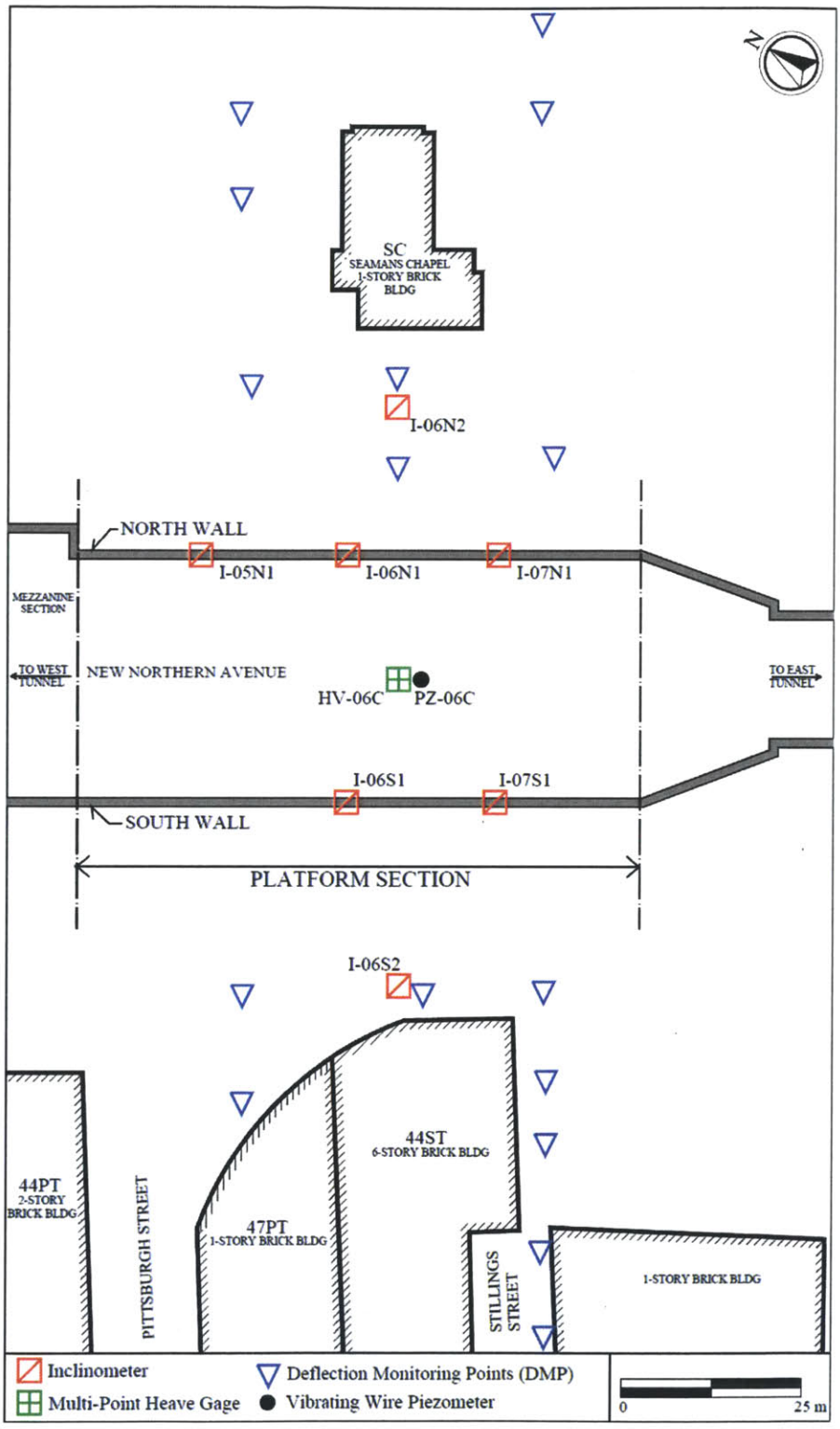

Figure 2-2: Instrumentation location plan of Platform section of Courthouse Station (after PB, 1998)

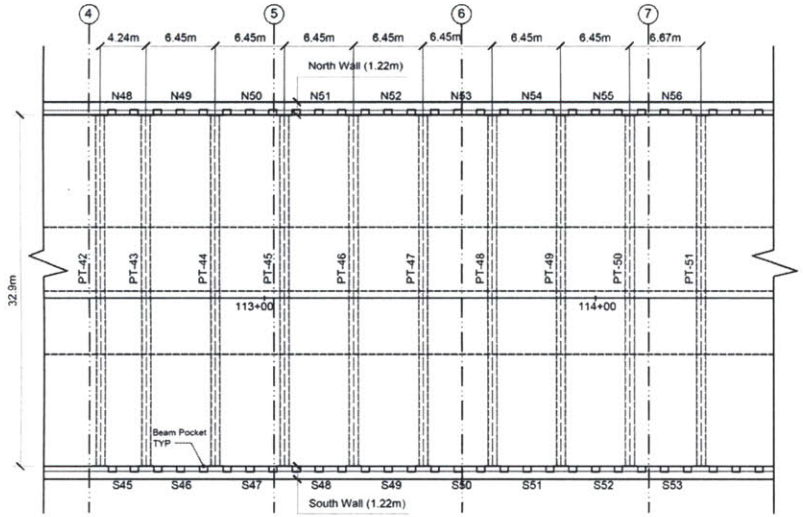

Strut Level	Typical Section
1	24"ϕ x 5/8"
2	36"ϕ x 5/8"
3	36"ϕ x 1"

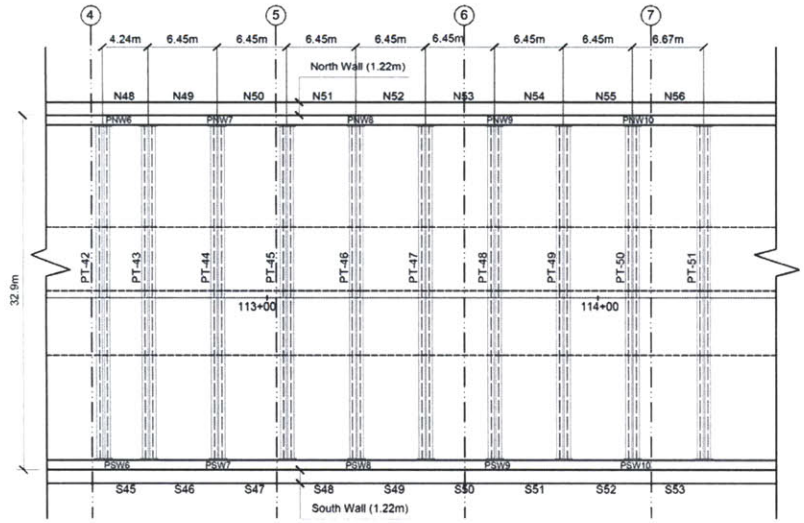

Strut Level	Typical Section
4	2-W36 x 135
5	2-W36 x 230

Figure 2-3: Plans and sections for strutting system at Platform section (after PB, 1998)

Figure 2-4: Courthouse Station photo taken in September 2001

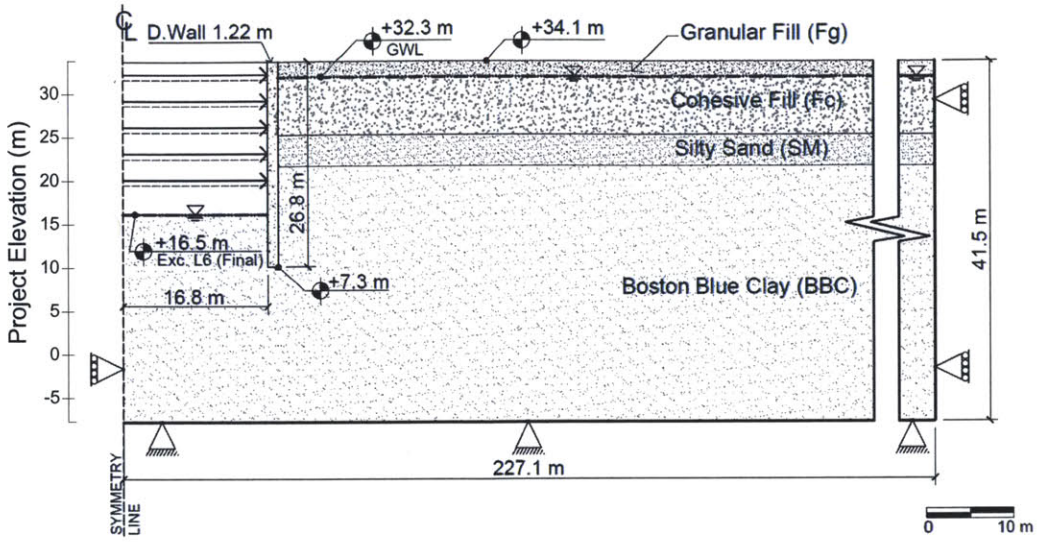

(a) Geometry assumed in Class A predictions (after Jen, 1998)

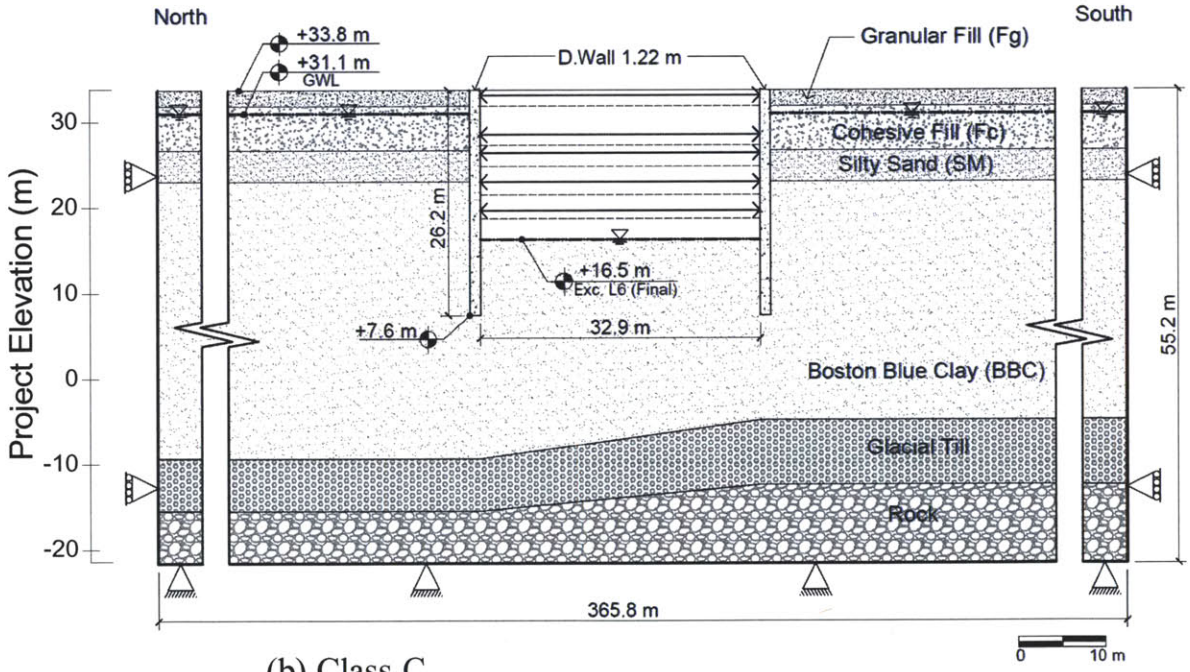

(b) Class C

Figure 2-5: Platform section geometries, boundary conditions, and strut and excavation levels used in (a) Class A; (b) Class C Predictions

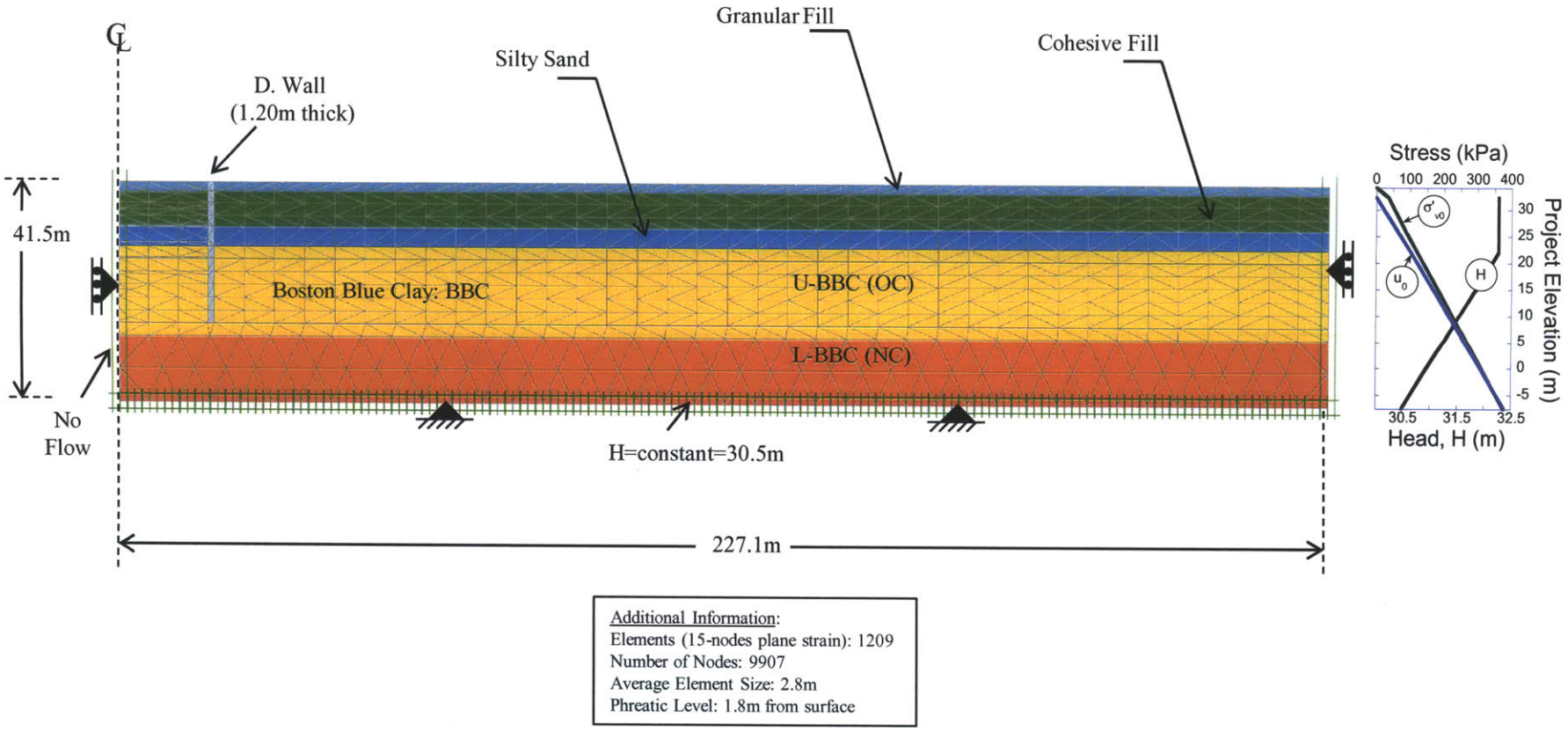

Figure 2-6: Finite element model and mesh used in Class A predictions

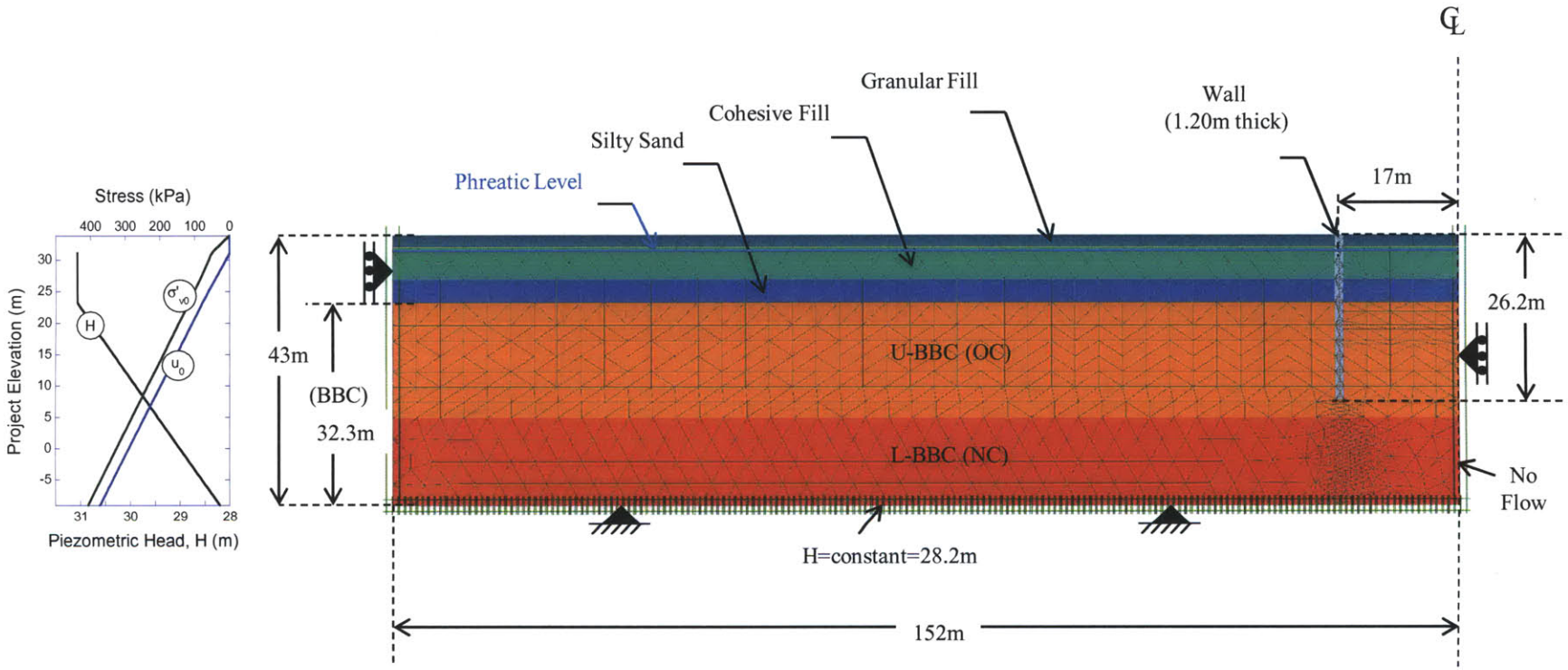

Note:
BBC: Boston Blue Clay
U-BBC: Upper BBC
L-BBC: Lower BBC

Additional Information:
Elements (15-nodes plane strain): 1857
Number of Nodes: 15119
Average Element Size: 1.8m
Phreatic Level: 2.7m from surface

Figure 2-7: Finite element model and mesh used in Class B predictions

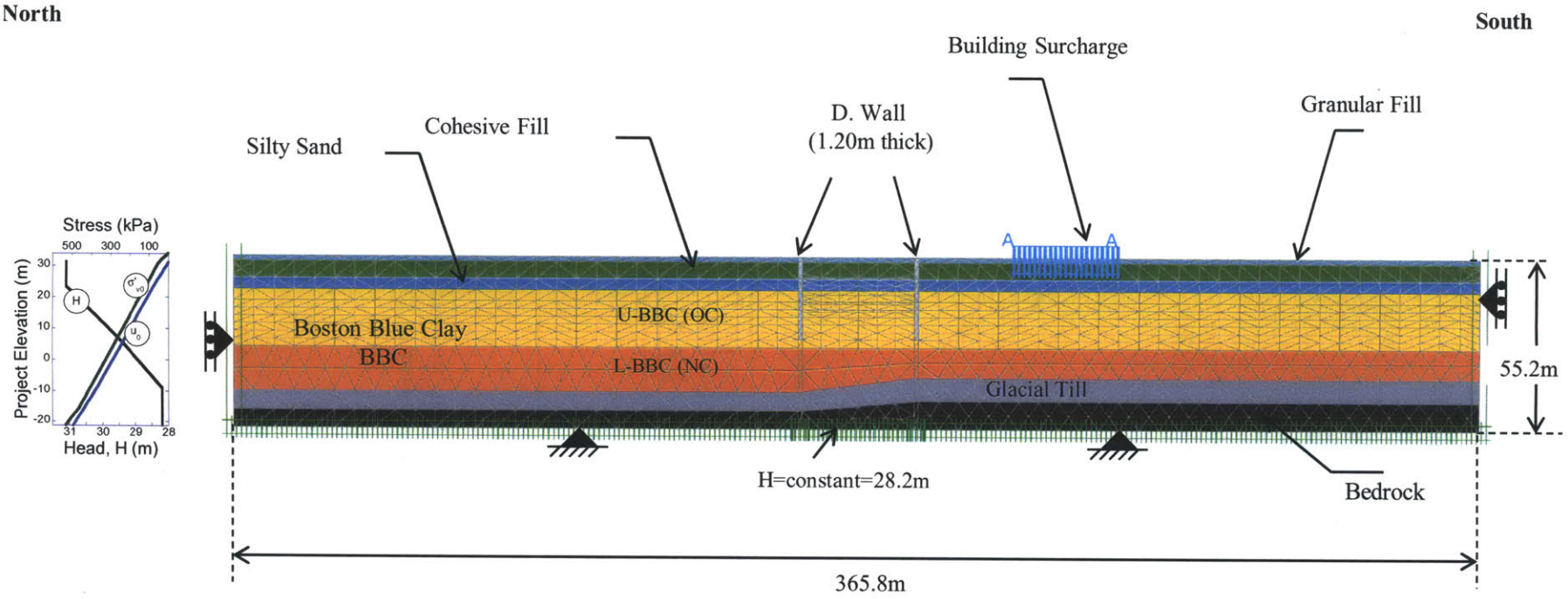

Figure 2-8: Finite element model and mesh used in Class C predictions

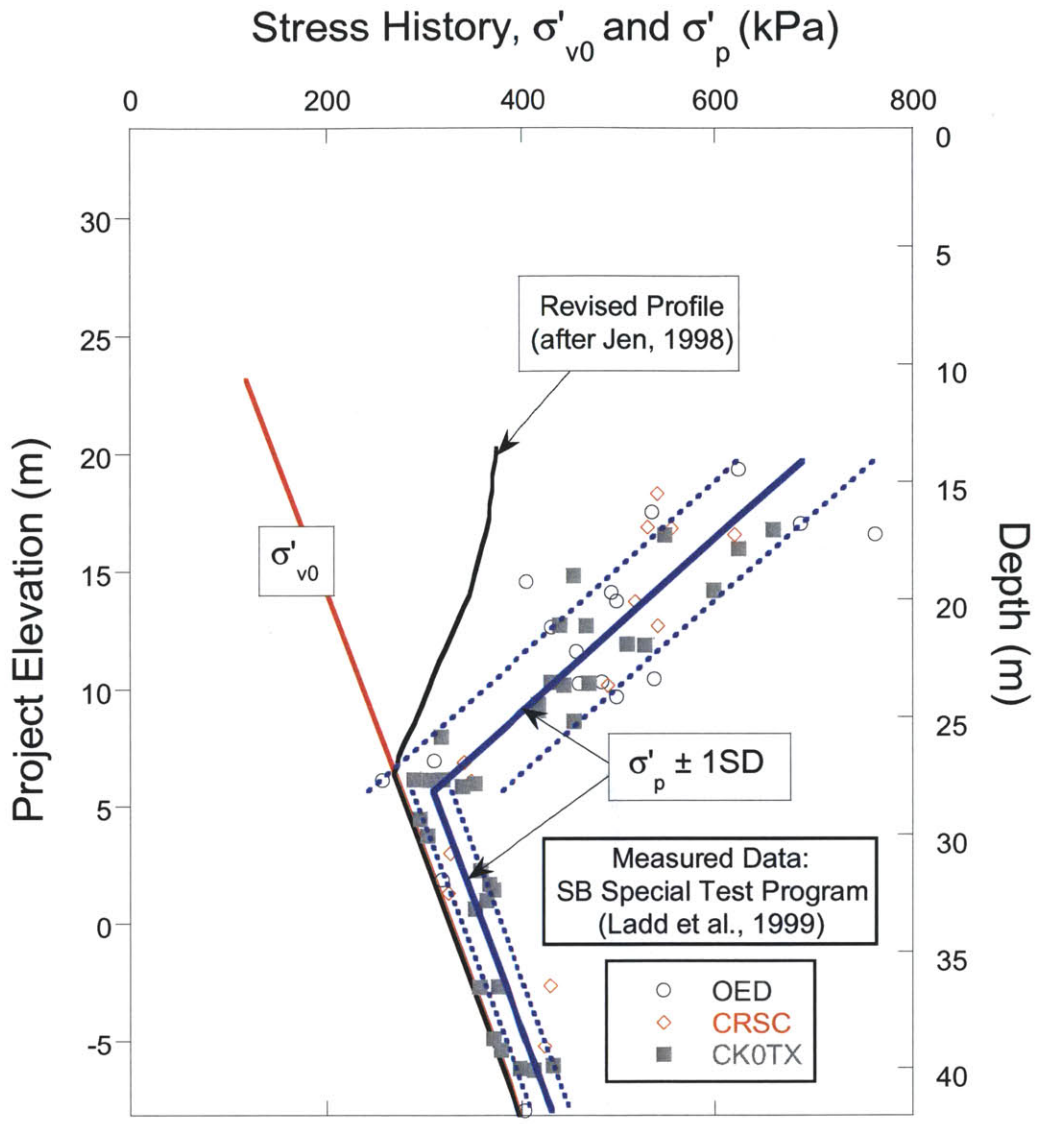

Figure 2-9: Stress history from 1-D consolidation tests at South Boston Special Test Site - SBSTS (after Ladd et al., 1999), and assumed stress history profile in MIT-E3 (after Jen, 1998)

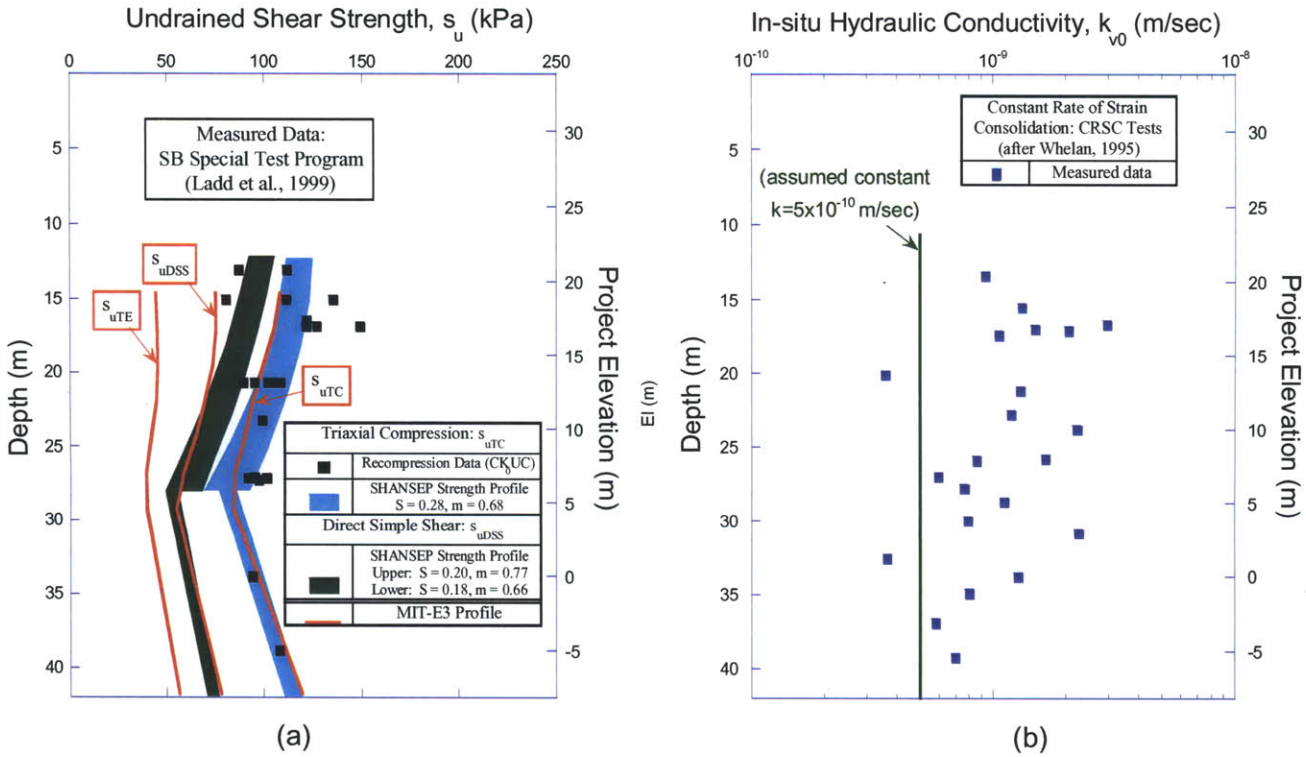

Figure 2-10: (a) Comparison of revised MIT-E3 and SHANSEP undrained strength profiles; (b) assumed hydraulic conductivity profile

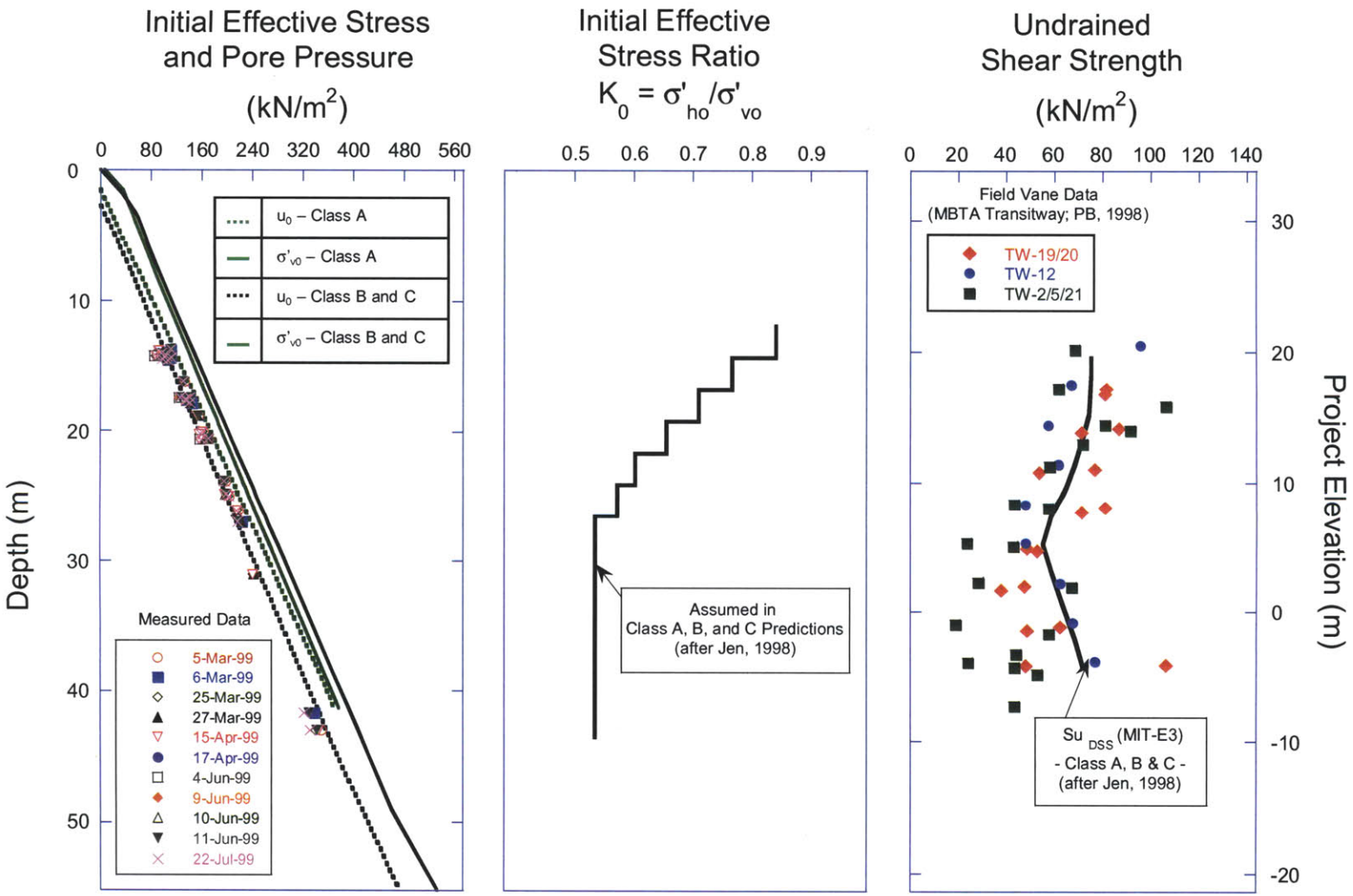

Figure 2-11: Initial conditions assumed in Class A (after Jen, 1998), Class B, and Class C predictions

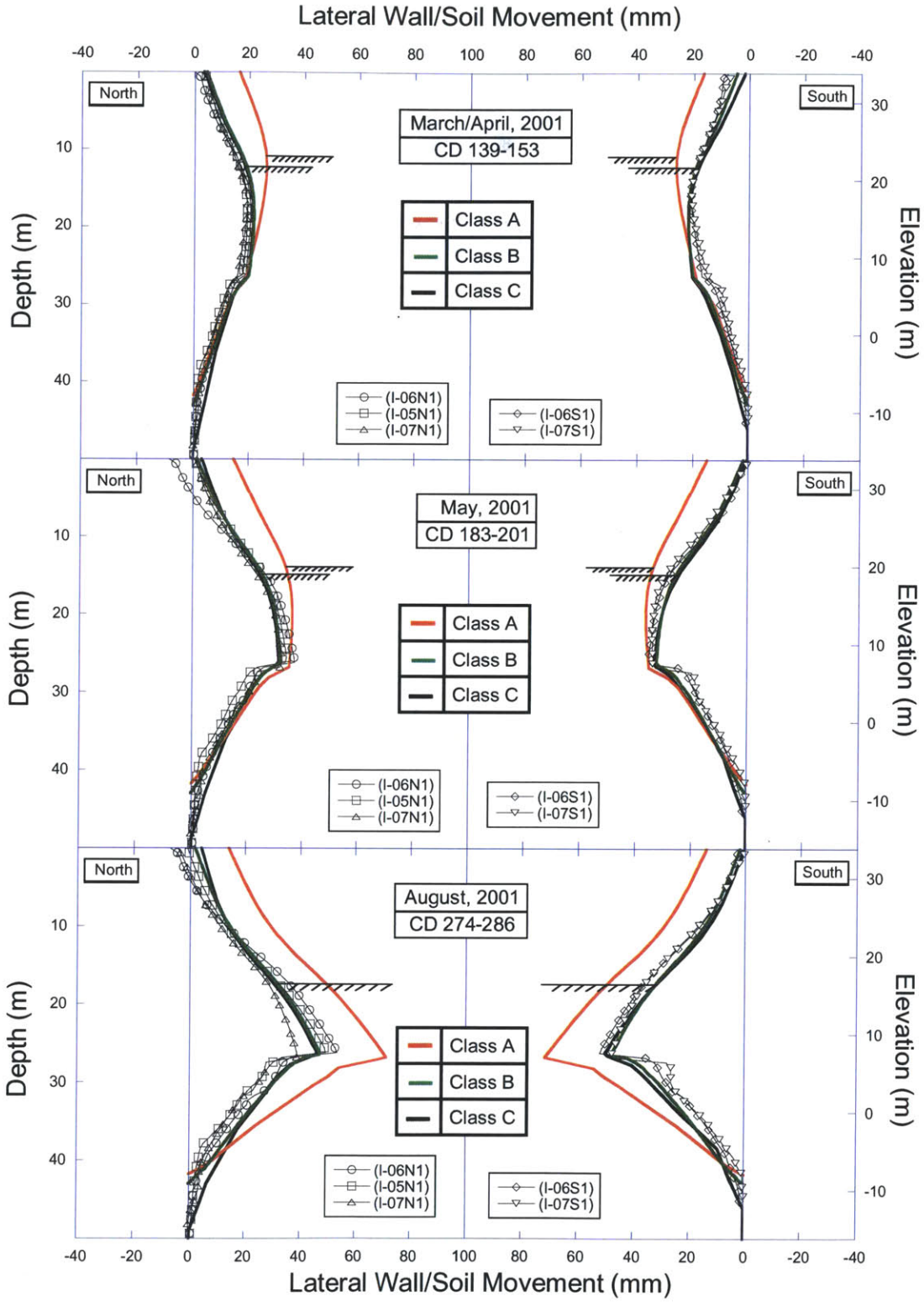

Figure 2-12: Measurements versus class A, B, and C predictions of lateral wall/soil displacements for excavation levels 4, 5 and 6

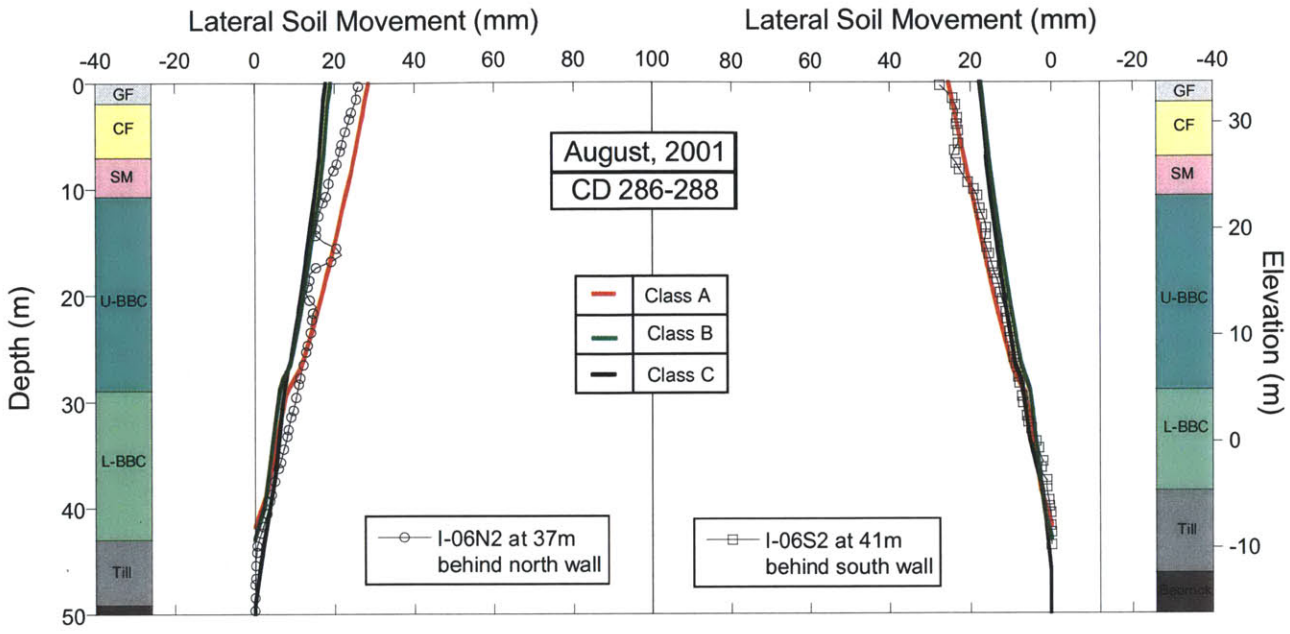

Figure 2-13: Measurements versus class A, B, and C predictions of horizontal soil movements at similar distances behind diaphragm walls for excavation level 6

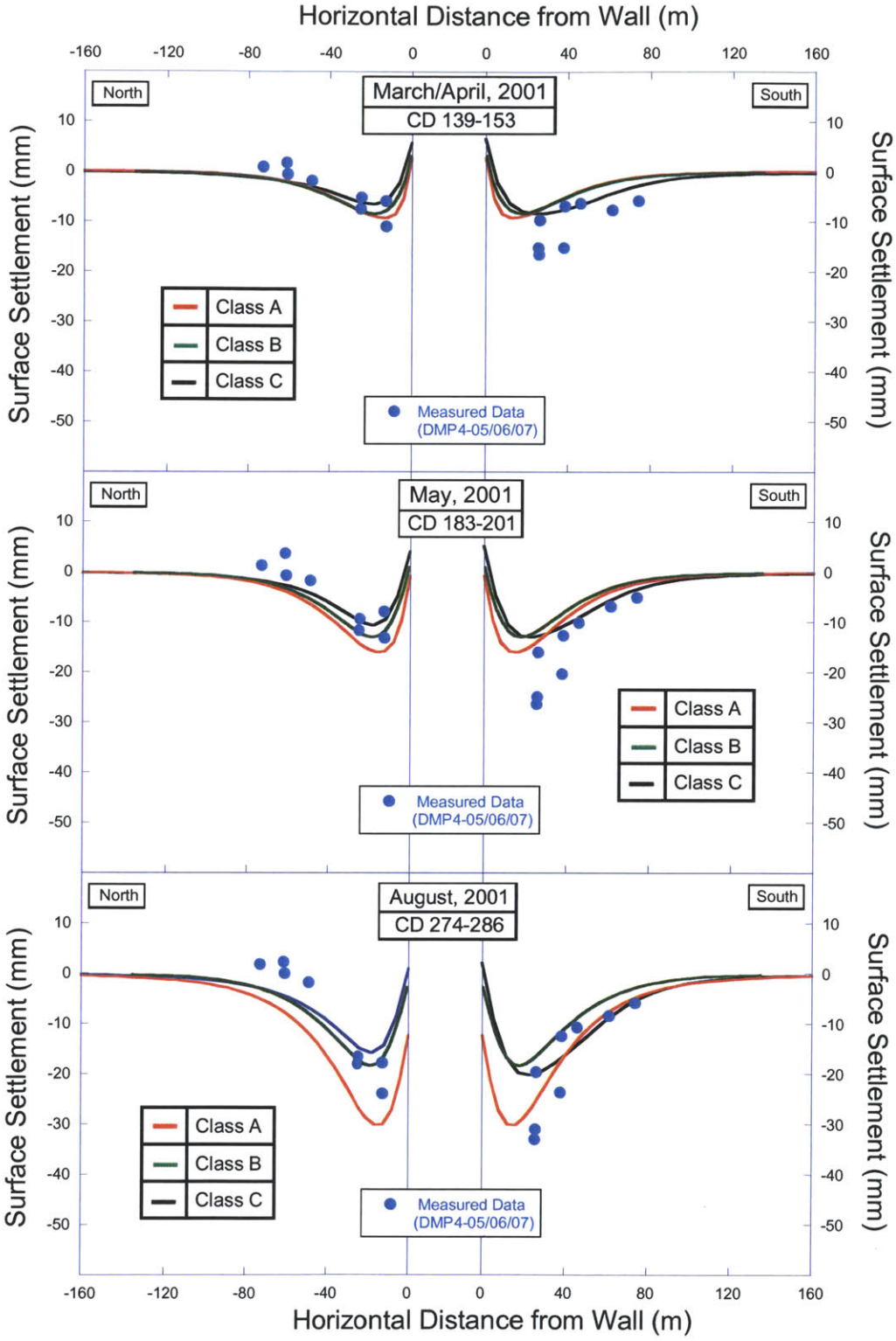

Figure 2-14: Measurements versus class A, B, and C predictions of surface settlements for excavation levels 4, 5 and 6

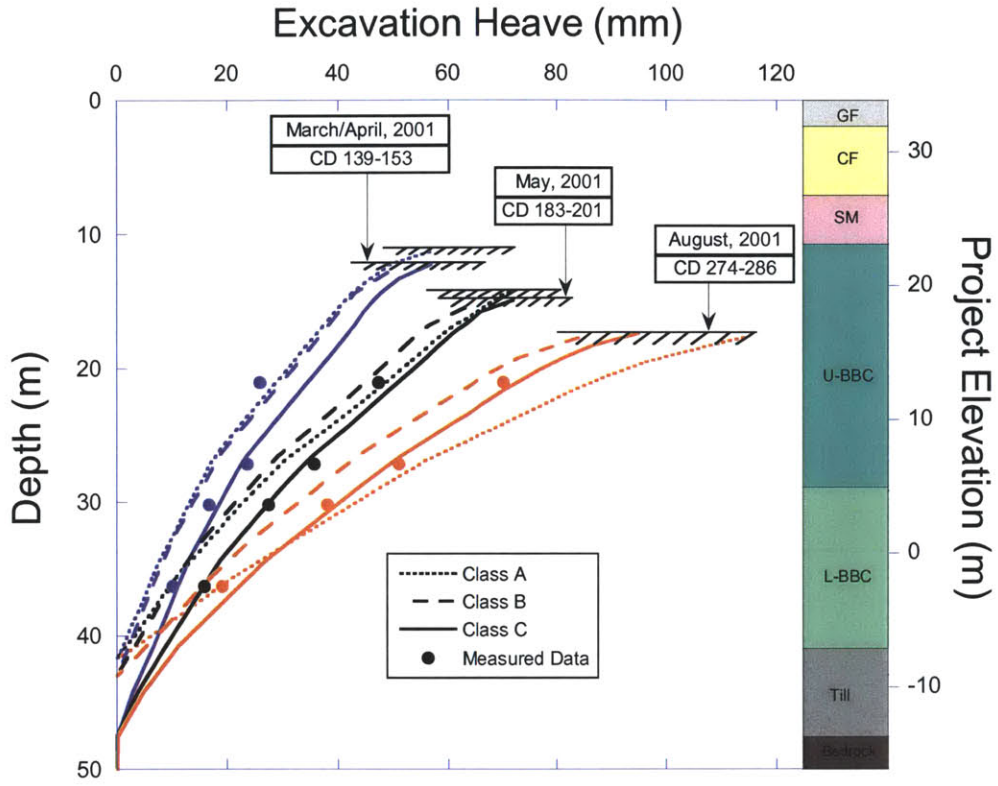

Figure 2-15: Measurements versus class A, B, and C predictions of excavation heave at center line for excavation levels 4, 5, and 6

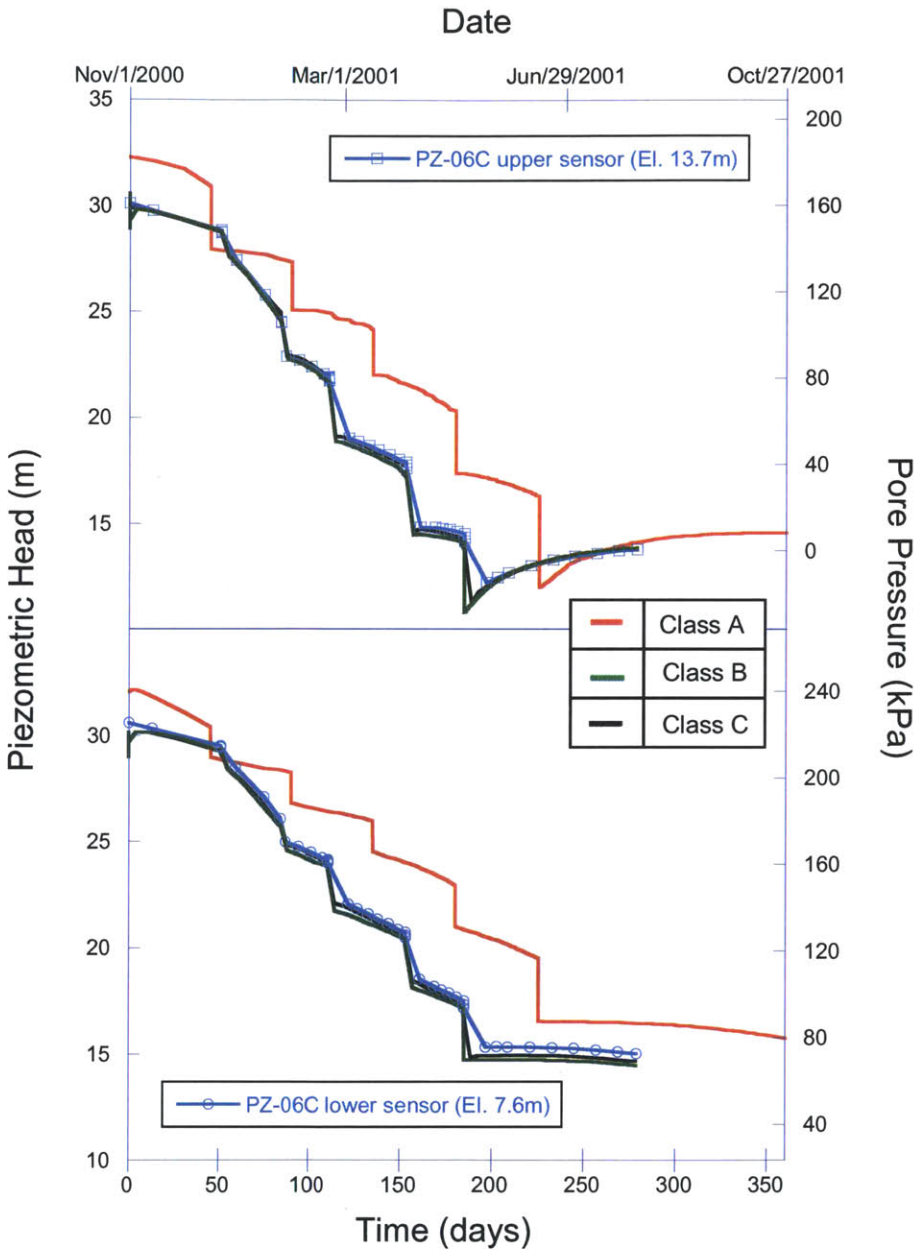

Figure 2-16: Measurements versus class A, B, and C predictions of piezometric heads and pore pressures at center line of excavation

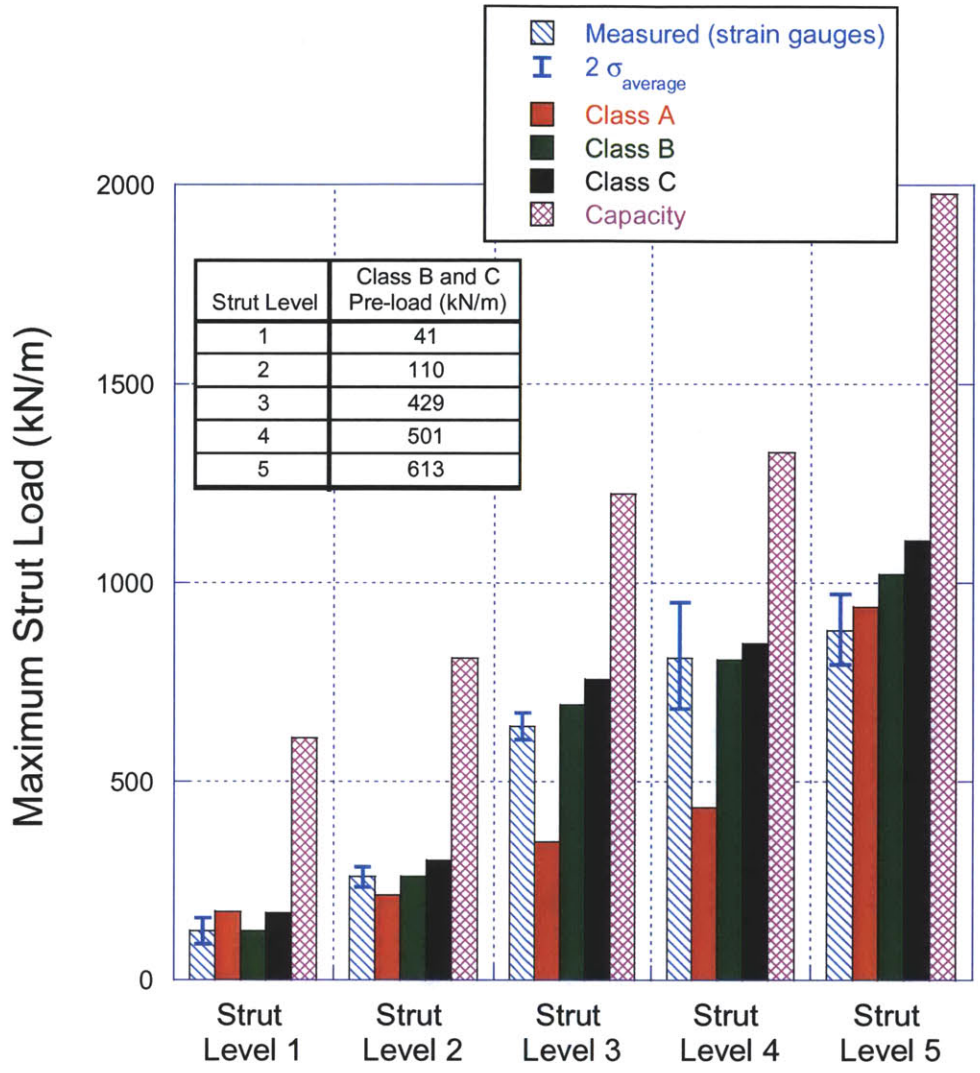

Figure 2-17: Measurements versus class A, B, and C predictions of maximum strut forces

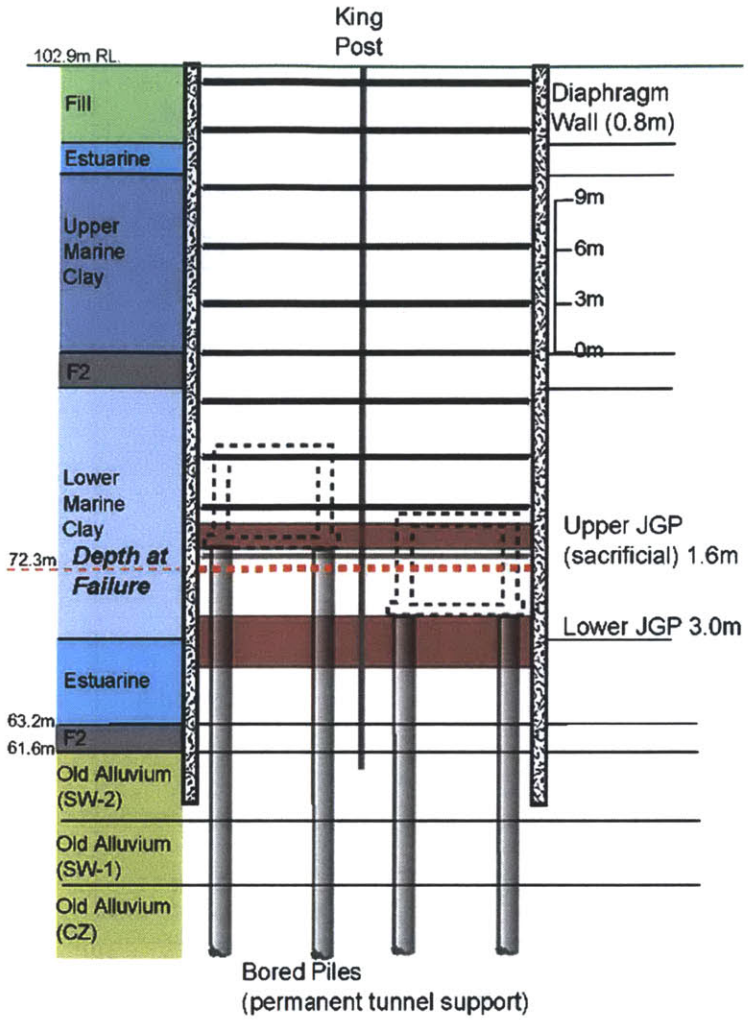

Figure 2-18: M3 typical design cross-section of excavation support system (Whittle and Davies, 2006)

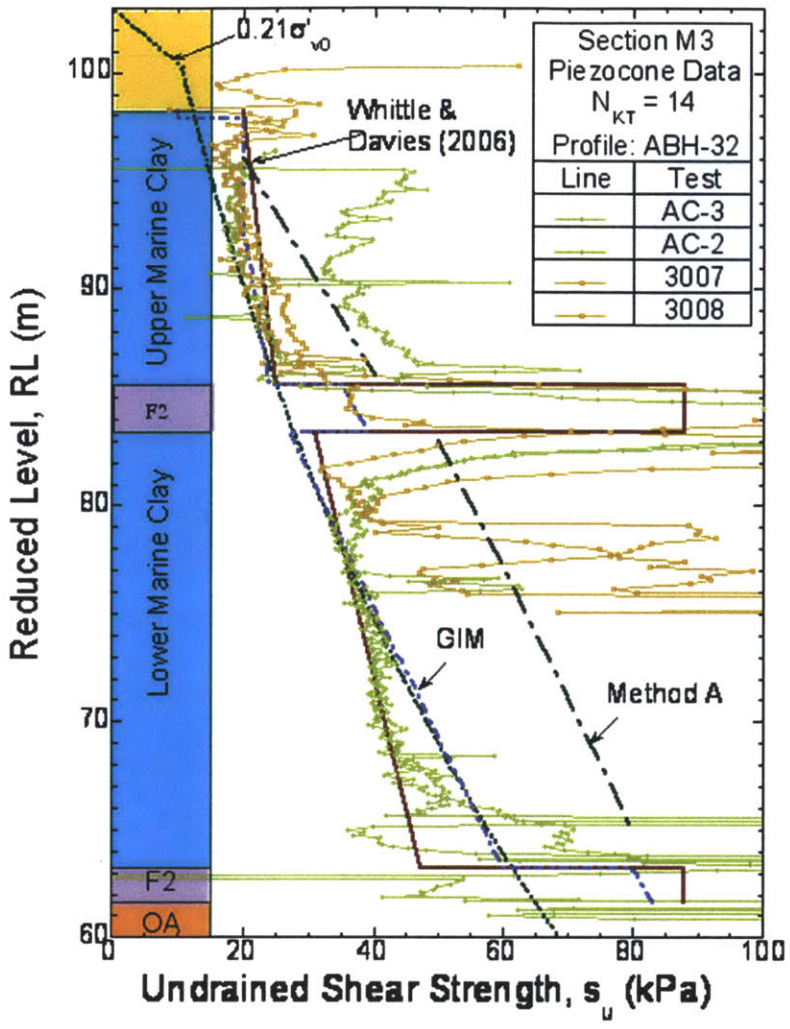

Figure 2-19: Undrained shear strength profiles (Corral & Whittle, 2010)

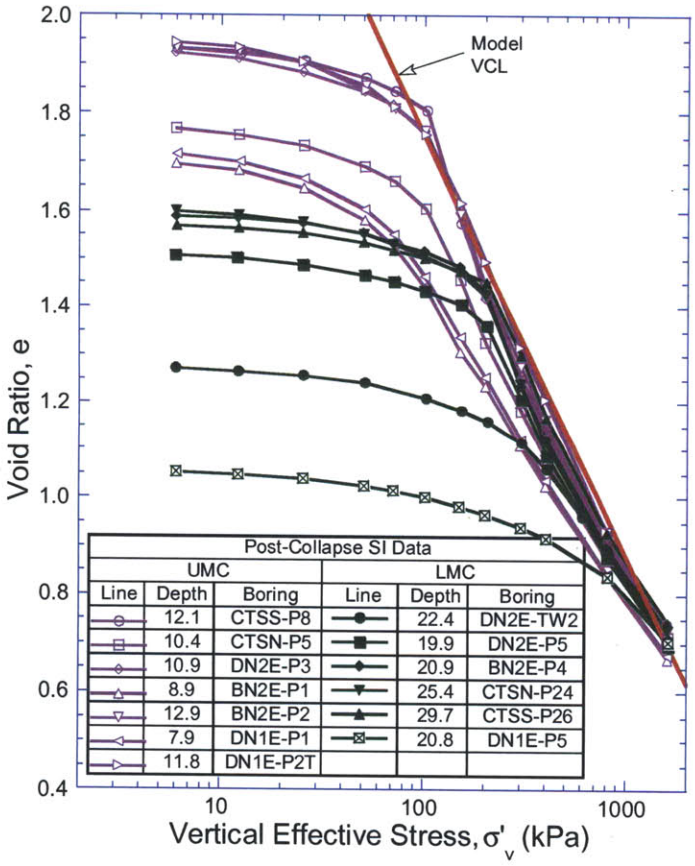

a) Compression behavior

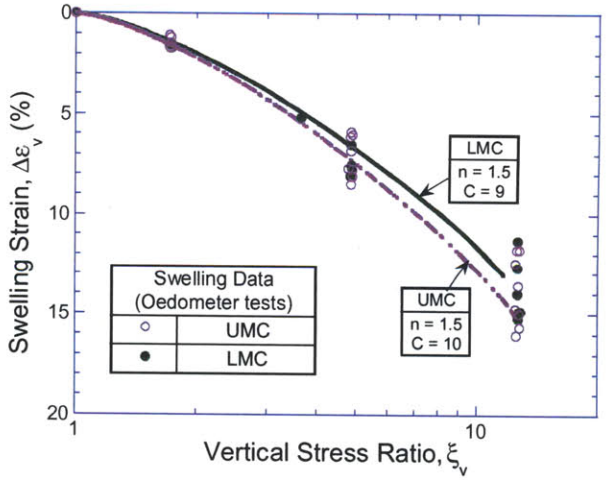

b) Swelling behavior

Figure 2-20: Compression and swelling properties of the Upper and Lower Marine Clays

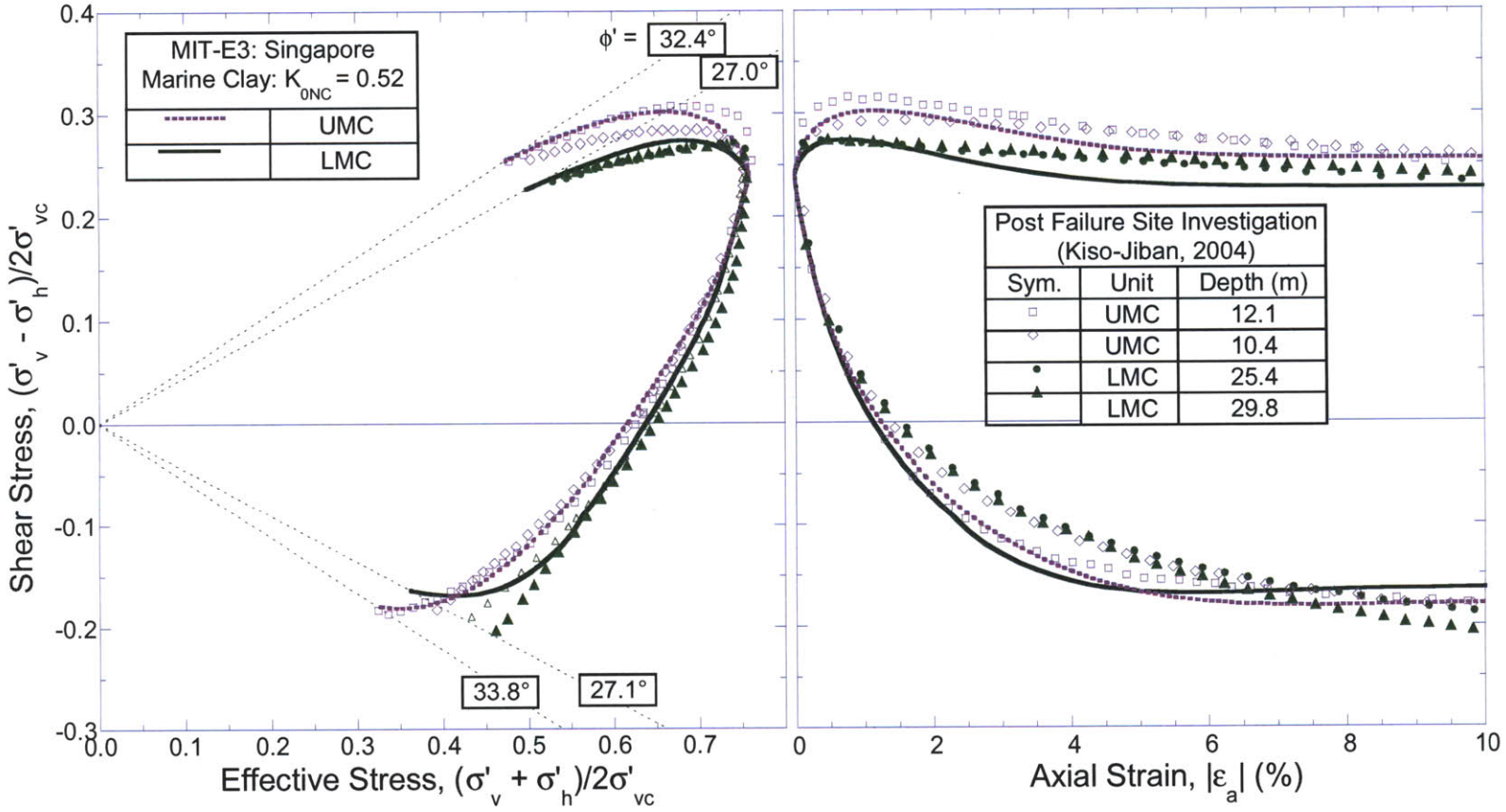

a) Effective Stress Paths

b) Shear strain-stress behavior

Figure 2-21: Comparison of measured undrained shear behavior from laboratory CAU compression and extension tests on normally consolidated UMC and LMC specimens with numerical simulations using the MIT-E3 model

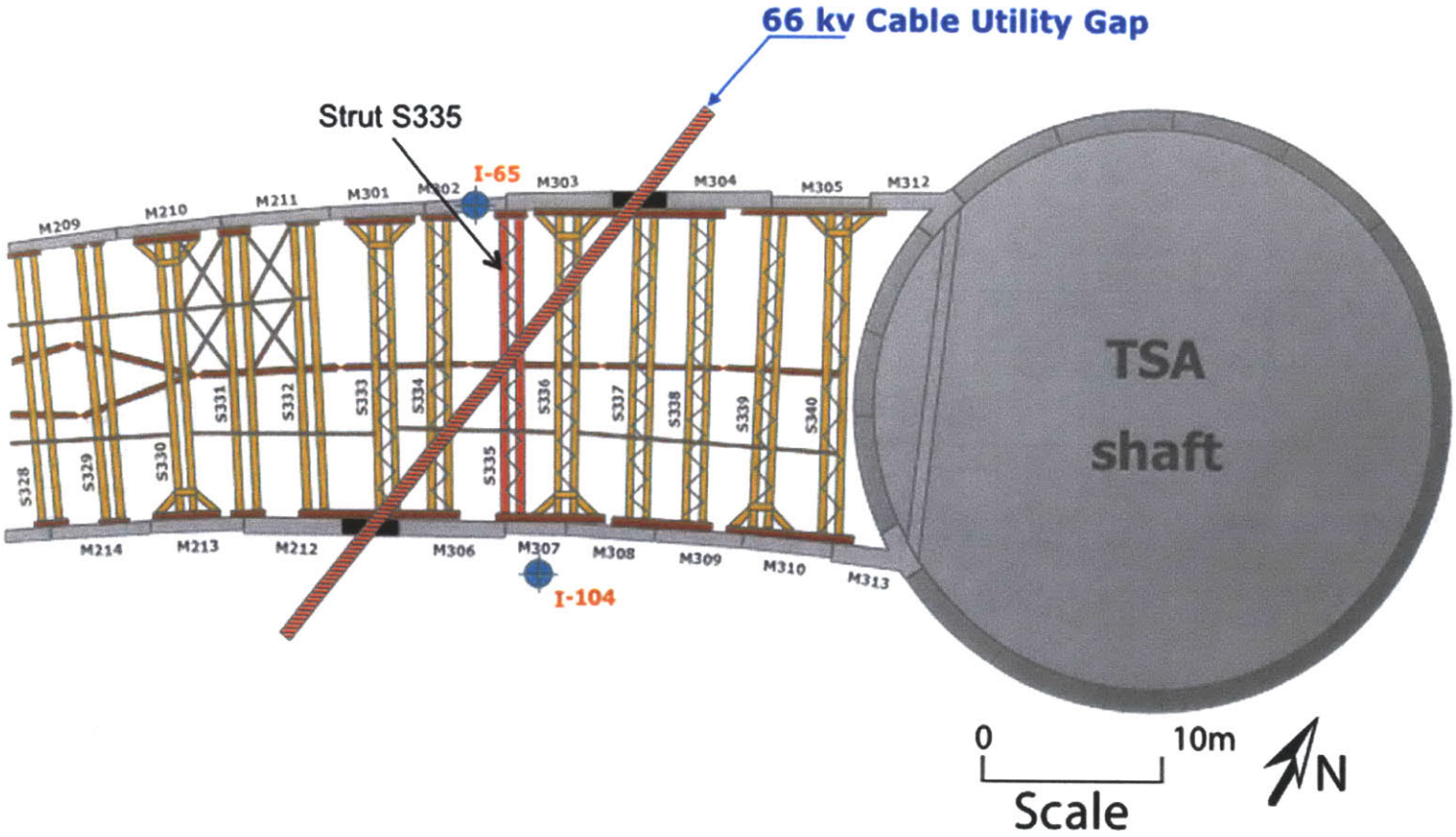

Figure 2-22: Plan showing the structural support system and 9th level strutting and monitoring instrumentation (Corral & Whittle, 2010)

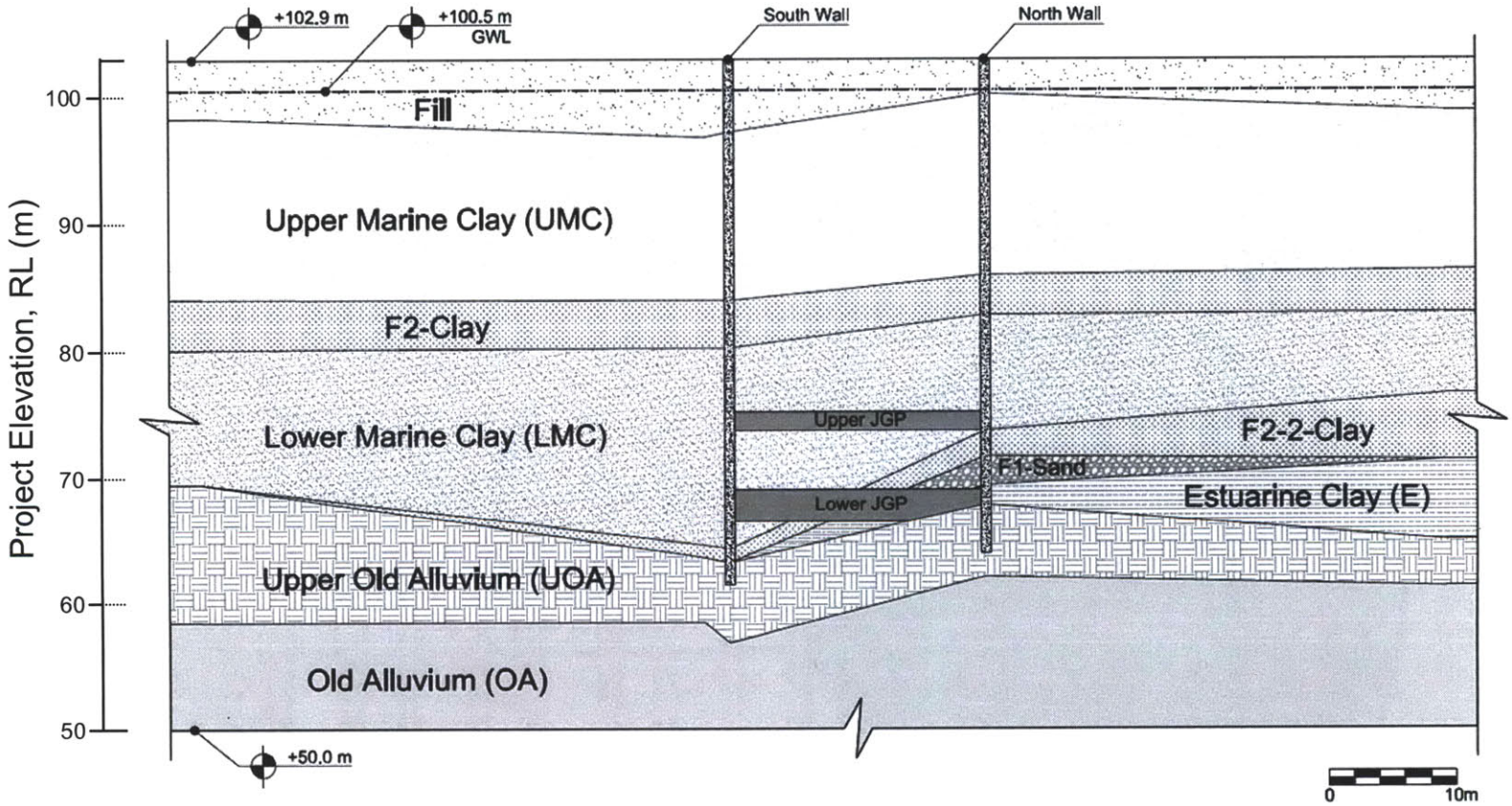

Figure 2-23: S335 Section geometry used in FE model (Corral and Whittle, 2010)

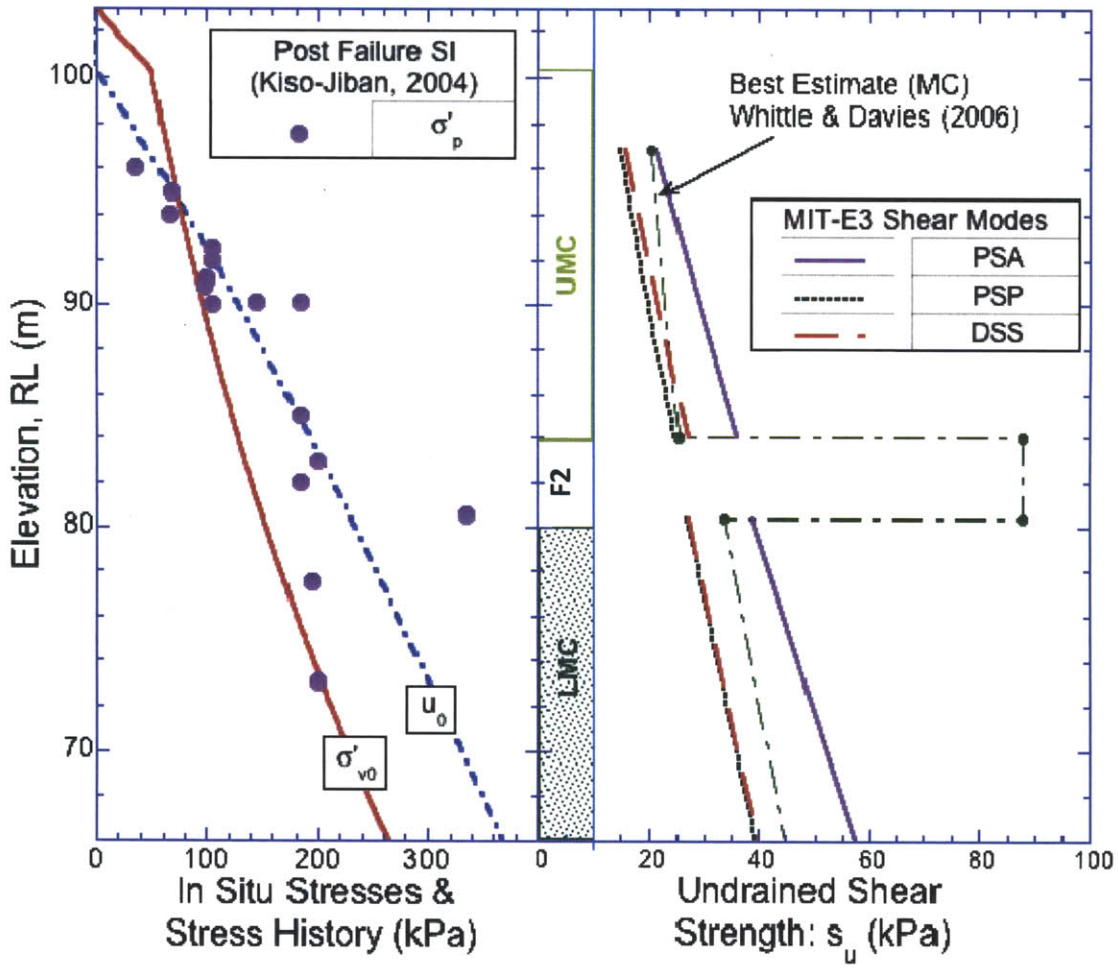

Figure 2-24: Comparison of in situ stresses and undrained strengths of marine clay used in FE model (Corral & Whittle, 2010)

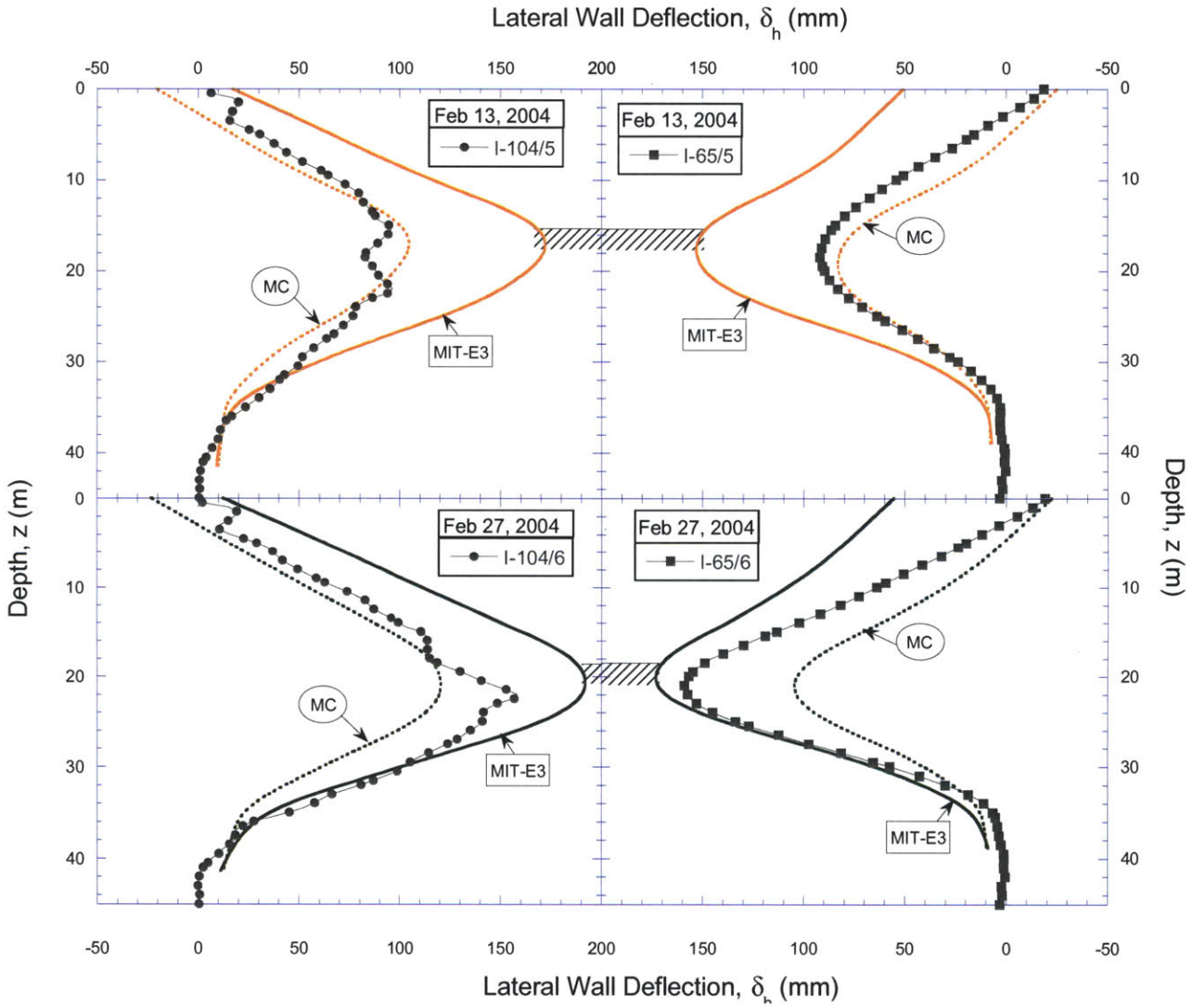

Figure 2-25: Measured and predicted wall deflections for excavation levels 5 and 6

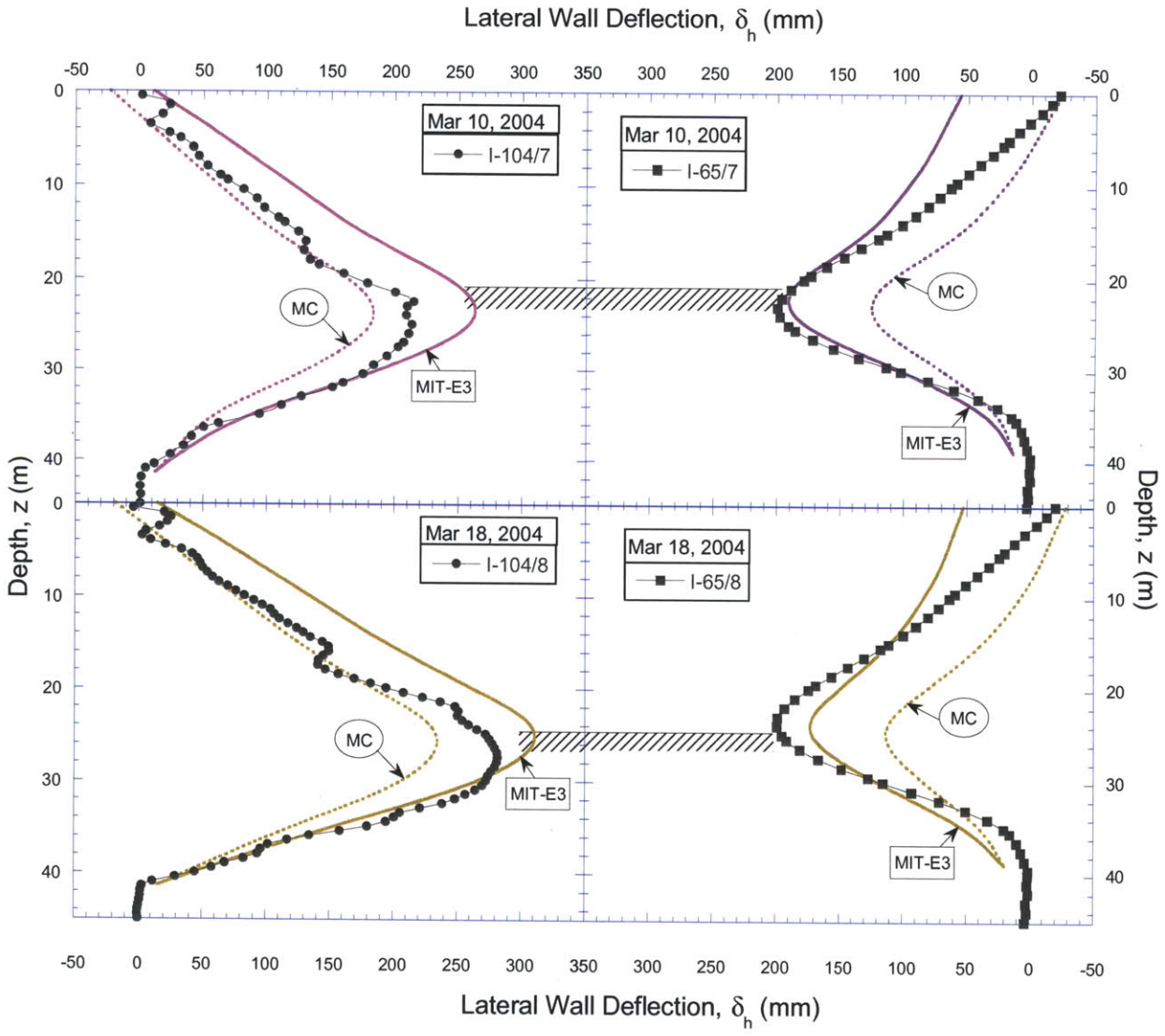

Figure 2-26: Measured and predicted wall deflections for excavation levels 7 and 8

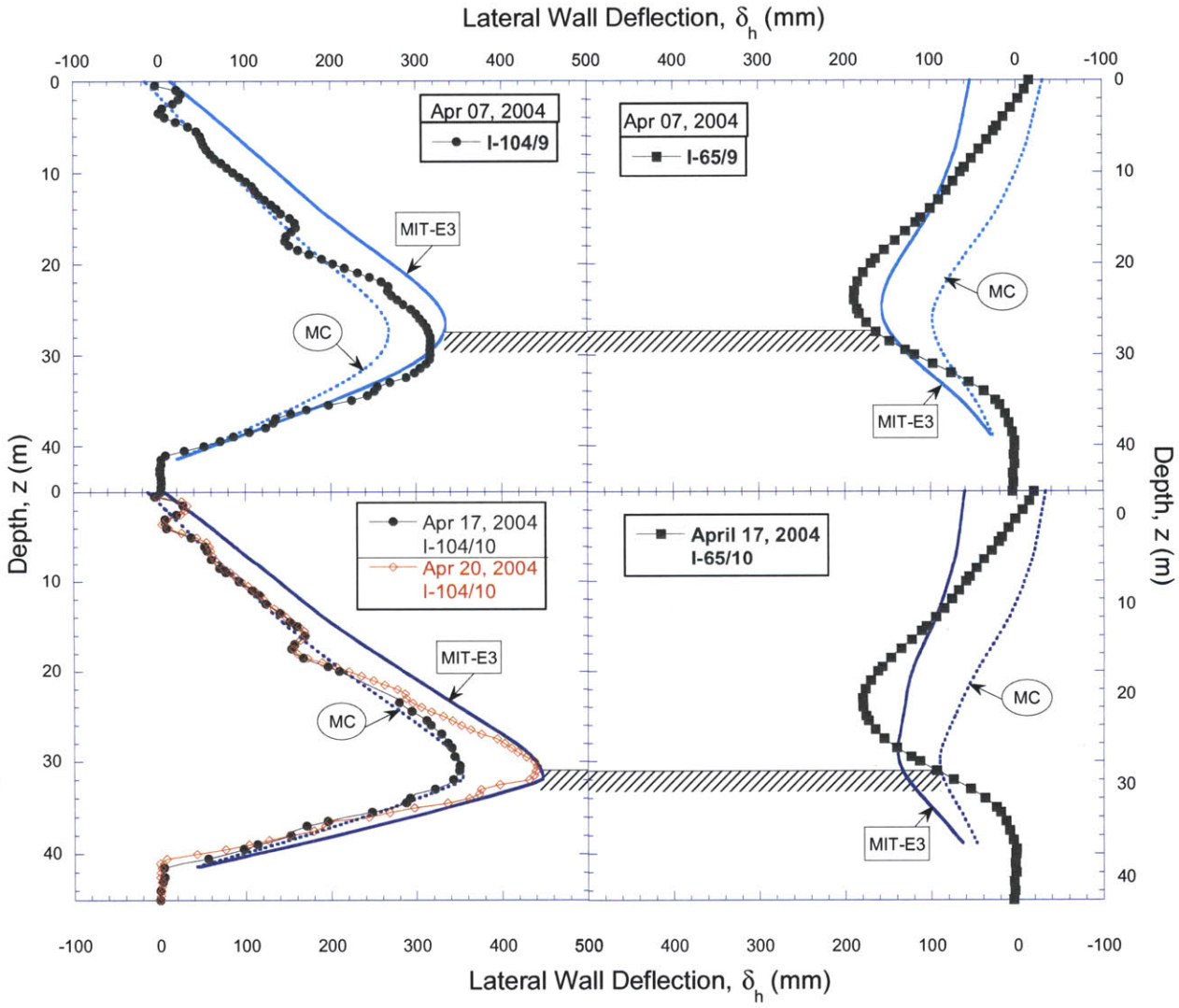

Figure 2-27: Measured and predicted wall deflections for excavation levels 9 and 10

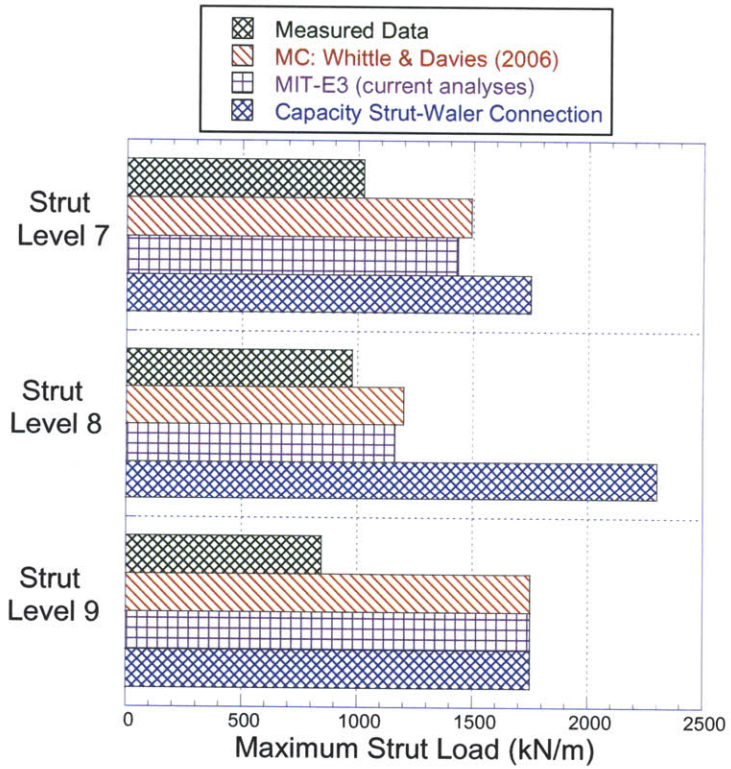

Figure 2-28: Comparison of computed and measured strut loads for excavation to 30.6m (April 17-20, 2004)

3 LITERATURE REVIEW

3.1 Introduction

The purpose of this chapter is to review existing methods for updating predictions of excavation performance using monitoring data. This works has its origins in the observational method first formally proposed by Peck (1969). The chapter gives a brief history of the observational method and then proceeds to methods involving numerical predictions of performance. Section 3.3 introduces the inverse problem formally, and Section 3.4 describes applications of inverse analysis in geotechnical engineering.

3.2 Observational Method

The term observational method/procedure was first introduced by Terzaghi (1961):

"*Satisfactory solutions of earthwork engineering problems can be obtained on the basis of our knowledge of the fundamental principles of soil mechanics supplemented by a moderate amount of boring and testing. However, there are others in which the geological conditions preclude the possibility of securing in advance of construction all the essential information required for adequate design. If this condition prevails, sound engineering calls for design on the basis of the most unfavorable assumptions compatible with the results of the subsoil exploration. This rather uneconomical procedure can be avoided only on the condition that the project permits modification in the design during or after construction in accordance with the results of significant observational data which are secured after construction is started. This can be called an "Observational Procedure*".

Einstein (1991) describes the path which led Terzaghi from Observation to Quantification to Judgement and culminated in the integration of those three components in his concept of engineering geology and, specifically, in the Observational Method (OM).

Subsequently, Peck (1969) defined a formal framework for the application of the observation method (OM) that involves the following steps:

a. *Exploration sufficient to establish at least the general nature, pattern and properties of the deposits, but not necessarily in detail.*
b. *Assessment of the most probable conditions and the most unfavorable conceivable deviations from these conditions. In this assessment geology often plays a major role.*
c. *Establishment of the design based on a working hypothesis of behavior anticipated under the most probable conditions.*
d. *Selection of quantities to be observed as construction proceeds and calculation of their anticipated values on the basis of the working hypothesis.*
e. *Calculation of values of the same quantities under the most unfavorable conditions compatible with the available data concerning the subsurface conditions.*
f. *Selection in advance of a course of action or modification of design for every foreseeable significant deviation of the observational findings from those predicted on the basis of the working hypothesis.*
g. *Measurement of quantities to be observed and evaluation of actual conditions.*
h. *Modification of design to suit actual conditions.*

More recently, Nicholson et al. (1999) defined the Observational Method in ground engineering: "*is a continuous, managed, integrated, process of design, construction control, monitoring and review that enables previously defined modifications to be incorporated during or after construction as appropriate. All these aspects have to be demonstrably robust. The objective is to achieve greater overall economy without compromising safety. The Method can be adopted from the inception of a project or later if benefits are identified. However, the Method*

should not be used where there is insufficient time to implement fully and safely complete the planned modification or emergency plans."

Table 3.1 presents a summary of the development of the Observational Method (OM). Traditionally engineers relied exclusively on observations to do their work, because they did not have design theories to guide them. As such, structures were designed mostly on a trial-and-error method, even though they were monitored during construction so that engineers could develop an empirical understanding of soil-structure interaction. Between 1912 and 1922, the observational procedure was used for the first time by the administration of the Swedish State Railroads, for a large-scale earthwork engineering, in connection with an investigation of the stability of slopes on glacial deposits (Terzaghi, 1961).

Terzaghi and Peck (1948) pointed out that design based on the "most unfavorable assumptions" is uneconomical, if gaps in the available information can be filled by observations during construction and the design can be modified (safely) during construction. Casagrande (1965) reviewed the role of the "calculated risk" in earthwork and foundation engineering, with particular reference to the application of the observational method for the Great Salt Lake railroad fill.

In his Rankine Lecture, Peck (1969) described two OM approaches: 1) **Ab Initio** where the observation method is adopted from the inception of the project; and 2) **Best Way Out** approach when construction has already started and some unexpected development has occurred, or whenever a failure or accident threatens or has already taken place.

Requirements for the use of the observational method were formally adopted within design codes in final draft of Eurocode 7, EC7, in Table 3.2, and subsequently been adopted by retaining wall design by Hong Kong Geotechnical Control Office (GCO, 1993).

Cases presented on the GeoTechNet site (www.geotechnet.org) give examples of both the "Ab Initio" and "Best Way Out" OM approaches. Nicholson et al. (2006) describe a structural framework on how the "best way out" approach to OM could be used for recovery of deep, multistage excavation projects when problems occur during construction using as example the Nicoll Highway collapse in Singapore (2004).

Concerning the differences between Peck (1969) and CIRIA (1999) approaches to the OM, it is important to highlight that Peck adopted the "most probable" design and then reduced the design to "moderately conservative" soil parameters, when triggers were exceeded. In contrast, CIRIA considers a "safer" approach to design by adopting a "progressive modification" of the design starting with the design based on moderately conservative parameters, and then reverting to most probable conditions through field observations (e.g., Powderham and Nicholson, 1996). Figure 3.1 shows the elements of the CIRIA OM approach (Patel et al., 2007). The OM offers the potential savings of time or money, and the monitoring provides the needed assurance of safety. Several possible benefits of using OM are shown in Figure 3.2 (Patel et al., 2007). It is important to note that cost savings can be allocated to all the parties, such as the client, designer and the constructors. This method, however, should not be applied for when there is insufficient time to fully monitor performance and finish the contingency and emergency plans.

3.3 Inverse Problem

3.3.1 Definition

To understand certain complex geotechnical problems such as soil-structure interaction for excavation support systems, we generally use numerical modeling tools (e.g., FEM, FDM). The goal of these analyses is to obtain realistic predictions based on a set of assumptions regarding the stratigraphy, groundwater conditions, and constitutive properties of the soil/rock layers. For saturated soils constitutive laws are needed to describe the effective stress-strain-strength and hydraulic conductivity properties. The construction sequences and boundary conditions are also extremely important in these analyses.

Einstein and Baecher (1982) emphasized that probably the most distinctive characteristic of engineering geology compared to any other engineering fields is the uncertainty about geologic conditions and geotechnical parameters. They pointed out the sources and consequences of uncertainty in engineering geology. The three main sources of uncertainty described correspond to: 1) spatial variability (i.e., geological subsurface conditions are spatially variable); 2) measurement errors (i.e., there are uncertainties in measuring and estimating engineering properties); and 3) model uncertainty (i.e., models are simplifications of reality and thus introduce modelling errors). Einstein and Baecher (1982) also pointed out that, in addition to those three uncertainty sources, there is uncertainty due to omissions (i.e., it is not possible to know what has been left out of an analysis).

Assuming that the fundamental physics of a certain problem are well understood (i.e., including all possible variables required for the analysis) and considering that a certain numerical model depends only on the model parameters, it is possible to write the following expression:

$$G(\boldsymbol{\Theta}) = \boldsymbol{p} \tag{3.1}$$

where

$G(\,)$: function or operator that represents a numerical model (e.g., FE model)

$\boldsymbol{\Theta}$: vector of model parameters

$\boldsymbol{p}$: vector of predictions

Equation 3.1 states that for a given numerical model and model parameters, it is possible to find certain predictions of interest (e.g., ground movements, pore pressures, etc.). Assuming that there are no uncertainties associated with spatial variability, omissions, modeling, or measurements. It is similarly possible to define a vector of field measurements, $\boldsymbol{m}$ (associated with a vector of predictions, $\boldsymbol{p}$), that defines the "forward problem":

$$G(\boldsymbol{\Theta}) = \boldsymbol{m} \tag{3.2}$$

The inverse problem (also referred to as the "parameter estimation" problem) is to find $\boldsymbol{\Theta}$ given G and $\boldsymbol{m}$.

Jurina et al. (1977) illustrated a scheme of parametric estimation. Figure 3.3 shows that once both the measured and calculated responses (i.e., predictions) are available from the actual system and the mathematical model, an error criterion function (also referred to as identification

criterion) should be defined to model the error (i.e., the model uncertainty). Through parameter adjustment algorithms, a new vector of parameters is established and therefore used in the mathematical model to update the predictions or calculated response and so on. Similarly, Rechea (2006), in her doctoral thesis, illustrated a flowchart of the inverse problem, Figure 3-4, highlighting explicitly the error coming from different systems and/or steps.

Errors in field measurements and model uncertainty are always present. Therefore, Equation (3.2) must be corrected and re-written as follows:

$$\boldsymbol{m} = G(\boldsymbol{\Theta}) + \boldsymbol{r} \tag{3.3}$$

where $\boldsymbol{r}$ is the vector of residuals.

Combining Equations 3.1 and 3.3, the residual can be expressed as the difference between the vectors of measurements and predictions:

$$\boldsymbol{r} = \boldsymbol{m} - \boldsymbol{p} \tag{3.4}$$

According to Aster et al. (2005), solving an inverse problem is usually a difficult task due to three main issues: 1) solution existence, 2) solution uniqueness, and 3) instability of the solution process.

Figure 3-5 illustrates two very common inverse problems in geophysics and earthquake engineering. The determination of an earthquake hypocenter (in space and time) for given certain

information captured by a seismic network of sensors, is illustrated in Figure 3-5a, while, the determination of material properties (generally based on behavior of an elastic medium) for given a certain input source, is exemplified in Fig. 3-5b.

The process of solving the inverse problem comprises two main parts: 1) selection of an identification criterion (i.e., specify an error function or objective function for optimization); and 2) selection of an algorithm to solve the optimization problem.

3.3.2 Identification Criteria

3.3.2.1 Residual Norm Criteria

Using the residual vector, expressed in Equation (3.4), certain residual norms can be defined. A generalized set of n-order norms (e.g., Santamarina and Fratta, 2005) can be expressed as follows:

$$L_n = \left(\sum_i |r_i|^n \right)^{\frac{1}{n}} \tag{3.5}$$

where r_i is the residual of the i-th measurement.

The three most important criteria are those that minimize the residual norms corresponding to n=1, n=2, and n=∞:

a. Minimum Total Absolute Value criterion (n=1):

$$min\{L_1\} = min\left\{\sum_i |r_i|\right\} \tag{3.6}$$

b. Least Squares criterion (n=2):

$$\min\{L_2\} = min\left\{\sqrt{\sum_i |r_i|^2}\right\} \tag{3.7}$$

c. Minimax criterion (n=∞):

$$min\{L_\infty\} = min\left\{\max_i |r_i|\right\} \tag{3.8}$$

In order to visualize these criteria, an illustrative example, showing the minimization of the three residual norm criteria is presented in Figure 3.6 (Ledesma, 1987). From this figure, it can be seen that the Minimax criterion gives much more importance to the point which is below the line L_∞ (i.e., value with higher dispersion comparing with all others). In addition, there are more reasons why the Least Squares criterion has become the traditional one, especially, for non-linear problems.

Santamarina and Fratta (2005) give the example of fitting data points with a linear regression $y = a + b \cdot t$. Figure 3.7 shows the residual surfaces computed for the three norms. It can be seen that the minimum in the L_∞ norm surface is not a point (as is the case for L_1 and L_2),

but a contour implying that the solution is non-unique. Figure 3.7c shows different calibrations of (a,b) that have the same minimum L_∞. It is clear, from these Figures 3.6 and 3.7 that the Minimax criterion is not appropriate for some problems.

In geotechnical engineering and, also in excavation problems, the most commonly used criterion is Least Squares (L_2 norm). Therefore, this can be re-written in vector notation as follows:

$$min\{J\} = min\{\boldsymbol{r}^T\boldsymbol{r}\} \tag{3.9}$$

where J is the objective function (scalar) .

When using different measurement types (i.e., different physical quantities with different units), normalization is definitely required. The most common criterion corresponds to the Weighted Least Squares criterion (e.g., Calvello, 2002; Rechea, 2006; Levasseur, 2007), also sometimes referred to as Markov criterion (e.g., Ledesma, 1987). It is very important to note that these weights represent the relative importance of certain measurements. A generalized expression for the square objective function, expressed in Equation 3.9, under the Weighted Least Squares Criterion, is:

$$min\{J\} = min\{\boldsymbol{r}^T\boldsymbol{W}\boldsymbol{r}\} \tag{3.10}$$

where $\boldsymbol{r}$ is the residual vector, and $\boldsymbol{W}$ the diagonal weight matrix

Combining with Equation 3.4, Equation 3.10 can be expressed, in terms of measurements and predictions, as follows:

$$min\{J\} = min\{(\boldsymbol{m}-\boldsymbol{p})^T \boldsymbol{W} (\boldsymbol{m}-\boldsymbol{p})\} \quad (3.11)$$

In principle, the diagonal weight matrix, $\boldsymbol{W}$ should include the inverse of the measurement variances as diagonal elements of the matrix. Calvello (2002), Rechea (2006), and Finno (2007) associate this diagonal weight matrix with the accuracy of individual instruments (i.e., not with actual measurements) based on the manufacturer's specification, shown in Table 3-3. This represents a good option when the actual measurement variances are not available (i.e., there is a lack of measurements); however, it does not consider measurement errors.

The main drawback of the Weighted Least Squares criterion is that it does not take into consideration the covariance of measurements (i.e., coupling effect of residuals), that is extremely useful for linewise types of instrumentations such as inclinometers. This is described in detail in Chapter 4.

3.3.2.2 Maximum Likelihood Approach

The maximum likelihood estimation is a general method that can be applied to any estimation problem where a joint probability density function can be assigned to the measurements (Aster

et. al, 2005). Based on the formulation by Edwards (1972) and summarized by Ledesma et al. (1996), the maximum likelihood approach can be described as follows:

$$L(\boldsymbol{\Theta} \mid \boldsymbol{m}) = k \cdot P(\boldsymbol{m} \mid \boldsymbol{\Theta}) \tag{3.12}$$

where $L(\boldsymbol{\Theta} \mid \boldsymbol{m})$ is the likelihood of the model parameters $\boldsymbol{\Theta}$ given measurements $\boldsymbol{m}$; k is an arbitrary constant of proportionality; and $P(\boldsymbol{m} \mid \boldsymbol{\Theta})$ the conditional probability of measurements $\boldsymbol{m}$ given $\boldsymbol{\Theta}$ (and a probabilistic model).

Assuming that the numerical modeling is correct (i.e. no errors in the numerical results), and the difference between the measurements and predictions are attributed only to measurements, the probability of measuring $\boldsymbol{m}$ given $\boldsymbol{\Theta}$, corresponds to the probability of reproducing the residuals $\boldsymbol{r}$ of measurements (Ledesma et al. 1996). In fact, using Equations 3.3 and 3.4, it can be shown that $P(\boldsymbol{m} \mid \boldsymbol{\Theta}) = P(\boldsymbol{m} - G(\boldsymbol{\Theta})) = P(\boldsymbol{r}) = P(\boldsymbol{m} - \boldsymbol{p})$. Therefore, assuming a multivariate normal probability distribution, it possible to express that probability as follows:

$$P(\boldsymbol{m} - \boldsymbol{p}) = \frac{1}{\sqrt{(2\pi)^n |\boldsymbol{C_m}|}} exp\{-1/2 \cdot (\boldsymbol{m} - \boldsymbol{p})^T \boldsymbol{C_m}^{-1} (\boldsymbol{m} - \boldsymbol{p})\} \tag{3.13}$$

where n is the number of measurements; C_m is the covariance matrix of the measurements $\boldsymbol{m}$; and $(\boldsymbol{m} - \boldsymbol{p}) = \boldsymbol{r}$ is the vector of residuals (Equation 3.4)

The identification criterion establishes the maximum likelihood of the model parameters $\boldsymbol{\Theta}$ given measurements $\boldsymbol{m}$:

$$\max\{ L(\boldsymbol{\Theta} \mid \boldsymbol{m})\} = \max\{ k \cdot P(\boldsymbol{m} - \boldsymbol{p}) \} \tag{3.14}$$

Edwards (1972) defined a "support function" S, as the natural logarithm of the likelihood function:

$$S = -2 \ln\{ L(\boldsymbol{\Theta}/\boldsymbol{m})\} \tag{3.15}$$

$$S = -2 \ln \left\{ \frac{\mathrm{k}}{\sqrt{(2\pi)^n |\boldsymbol{C_m}|}} exp\{-1/2 \cdot (\boldsymbol{m} - \boldsymbol{p})^T \boldsymbol{C_m}^{-1} (\boldsymbol{m} - \boldsymbol{p})\} \right\}$$

Using the basic properties of logarithm, it follows:

$$S = (\boldsymbol{m} - \boldsymbol{p})^T \boldsymbol{C_m}^{-1} (\boldsymbol{m} - \boldsymbol{p}) + ln|\boldsymbol{C_m}| + n \ln(2\pi) - 2 \ln(k) \tag{3.16}$$

It is logical to think that the covariance of the measurement is constant at a given time (e.g., at a certain excavation stage in FE analysis); thus, the maximum likelihood approach (using Eq. 3.16) is reduced to the following minimization problem*:

$$\min\{ S \} = \min\{ J \} = \min\{(\boldsymbol{m} - \boldsymbol{p})^T \boldsymbol{C_m}^{-1} (\boldsymbol{m} - \boldsymbol{p})\} \tag{3.17a}$$

* The natural logarithm is a monotonically increasing function. Hence the conversion of L to S (Eq. 3.15) enables the mapping of $\max\{L\}$ to $\min\{S\}$

Using Equation 3.4, this can be expressed as:

$$\min\{J\} = \min\{\boldsymbol{r}^T \boldsymbol{C_m}^{-1} \boldsymbol{r}\} \tag{3.17b}$$

The maximum likelihood approach, under all the assumptions mentioned, corresponds to a more general form of the Weighted Least Squares criterion. This is because, the covariance matrix is not a diagonal matrix, since it has terms that are correlated – covariance terms (see Chapter 4). If this matrix is diagonal only (i.e., independent measurements), the maximum likelihood approach will particularly correspond to the Weighted Least Squares criterion shown in Equation 3.11. Moreover, in the particular case that this covariance matrix is the identity matrix, the problem reproduces the simplest expression of the Least Squares criterion presented in Equation 3.9.

Assuming that there are t independent instruments that can read $\boldsymbol{m}$ measurements, the function J of Equation 3.17b can be written in terms of individual covariance matrices:

$$J = \sum_{j}^{t} \boldsymbol{r_j^T} \boldsymbol{C_{m_j}}^{-1} \boldsymbol{r_j} \tag{3.18}$$

Following the work by Ledesma et al. (1996), the most remarkable advantage of using the maximum likelihood is that the covariance matrix can be expressed as:

$$\boldsymbol{C}_{m_j} = \sigma_j^2 \cdot \boldsymbol{E}_{m_j} \tag{3.19}$$

where $\boldsymbol{C}_{m_j}$ is the covariance matrix of the j-instrument; σ_j^2 is the scale factor which represents the global variance of the measurements by the j-instrument; and $\boldsymbol{E}_{m_j}$ is the error structure of the j-instrument which depends on the device itself.

The use and definition of error structure matrices will be treated and discussed later in Chapter 4.

3.3.3 Genetic Algorithms as Optimization Method

Even though that there are several optimization methods available in the literature, the heuristic method called Genetic Algorithms (GA's) was considered because it can adequately find the global minima of highly non-linear problems, being also able to tackle to three main issues that inverse problems have been suffered (Aster et al., 2005): 1) solution existence, 2) solution uniqueness, and 3) instability of the solution process. Therefore, for the purpose of this thesis, genetic algorithms were selected as the optimization method to solve the inverse problem.

The concept of genetic algorithms was developed by Holland and his colleagues in the 1960s and 1970s (Holland, 1975). Genetic algorithms (GA's) are methods for solving both constrained and unconstrained optimization problems that are based on natural selection, the process that drives biological evolution. GA's repeatedly modify a population of individual solutions. At each step, GA's select individuals at random from the current population to be parents and use them to produce the children for the next generation. Over successive

generations, the population "evolves" toward an optimal solution or a set of optimal solutions. GA's can be applied to solve a variety of optimization problems that are not well suited for standard optimization algorithms, including problems in which the objective function is discontinuous, non-differentiable, stochastic, or highly nonlinear. Procedures of generic GA's can be found in the classical book by Goldberg (1989).

It is very important to highlight that GA's use three main types of rules at each step to create the next generation from the current population: 1) **Selection rules**: select the individuals, called parents that contribute to the population in the next generation; 2) **Crossover rules**: combine two parents to form children for the next generation; and 3) **Mutation rules**: apply random changes to individual parents to form children.

Also, it is important to note that GA's are different from more normal optimization and search procedures in three ways: 1) they search from a population of points, rather than a single point; 2) they use payoff (objective function) information, rather than derivatives or other auxiliary knowledge; 3) they use probabilistic transition rules, rather than deterministic rules.

Figure 3.8 shows a flowchart that describes the main steps in GA's.

Figure 3.9 shows an example of the Rastrigin's function (in 3D and contour levels) which presents many local minima. Genetic algorithms have the capabilities to easily find the global minima of that function; even though, when the initial population starts at a different region (see Figure 3.10). GA's take only few seconds to reach the Iteration 100 shown (Figure 3-10).

3.4 Inverse FE Analyses in Geotechnical Engineering

Table 3-4 summarizes the published literature on geotechnical engineering applications[†] of inverse analyses. Much of the pioneering development can be attributed to researchers in Italy (e.g., Gioda and Maier, 1980; Cividini et al., 1981; 1983), and Japan (e.g., Sakurai and Takeuchi, 1983; Arai et al. 1984; 1986; 1987; Asaoka and Matsuo, 1984). The following paragraphs provide a chronological assessment of these and other papers.

Gioda and Maier (1980) described the formulation of a direct search solution for an inverse problem in elastoplasticity. The numerical model simulates a very simple in-situ pressure tunnel test carried out in a deep rock formation, assuming an elastic-perfectly plastic Mohr-Coulomb constitutive law and a homogeneous isotropic initial stress state. The updated model parameters correspond to the cohesion and friction angle as well as the in-situ initial stress[‡]. The identification criterion (i.e., objective function) corresponded to the Least Squares criterion in terms of displacements, measuring the difference between theoretical and experimental relationships (pressure vs. average diameter increase) only, for a standard pressure tunnel test carried out well into the nonlinear range of behavior. They applied two different optimization methods: 1) the Nelder-Mead algorithm or modified simplex method (Nelder and Mead, 1965); and 2) the Rosenbrock algorithm or the alternating variable strategy (Rosenbrock, 1960). The concluded that the identification process can be carried out by "search techniques", such as

[†] Several other published papers relate to calibration of laboratory tests (e.g. Anandarajah et al., 1991; Ghaboussi and Sidarta, 1998; Calvello, 2002; Cekerevac et al., 2006; Fu and Hashash, 2007; Navarro et al. 2007), or field tests (e.g. Gioda and Maier, 1980; Cividini et al., 1981; 1983; Levasseur et al. 2009a; 2009b).

[‡] Surprisingly, they assumed a constant elastic modulus.

Nelder-Mead flexible polyhedron method, with a reasonable computational effort and beyond the accuracy level of practical interest, although, they also suggested that the use of other search techniques might provide computational gains.

Cividini et al. (1981) discussed different aspects of parameter identification problems in the field of geomechanics. Inverse and direct procedures are discussed for the solution of characterization problems with reference to linear elastic material behaviour only. The direct procedure is then applied to the determination of geometry, material and load parameters, on the basis of the displacements obtained from a hypothetical in-situ load test. The authors also discussed the influence of the number of input data (and of the experimental errors affecting them) on the results of characterization problems. As far as the identification criterion is concerned, they used the Least Square approach. They specified the objective functions in terms of displacements. They offered two main conclusions: 1) the determination of distributed load values appears to be more affected by the experimental errors than the elastic modulus; and 2) the determination of distributed load values is strongly influenced by the locations where the in-situ measurements are performed.

Two years later, Cividini et al. (1893) studied the estimation of parameters defining local elastic properties and/or geometrical aspects on the basis of experimental data concerning displacements under given static loads. The same hypothetical in-situ load test problem was used as a numerical model, which assumed linear-elastic behaviour. But in this case, apart from the generalized least squares, the Bayesian approach was also included; thus two identification criteria were used. The objective function was minimized by the simplex method or Nelder-

Mead algorithm (Nelder and Mead, 1965). They concluded that computation effort of Bayesian approach required was significantly higher than the Least Square method.

Sakurai and Takeuchi (1983) proposed a method of inverse analysis to be used for the interpretation of field measurements in monitoring the deformations in the rock mass around a tunnel cavity. They used the indirect method, proposed by Cividini et al (1981) using a finite element model for a tunnel in a linear, isotropic, and elastic rock mass. They analyzed two cases: 1) an unlined tunnel and 2) a lined tunnel. Assuming Poisson's ratio and initial vertical stress as deterministic values, they estimated the complete initial state of stress (σ_{xx}, σ_{yy}, and τ_{xy}) and Young's modulus from a set of relative displacements measured between adjacent measuring points. A case study for a lined tunnel converged in a small number of iterations while a single calculation was sufficient for the unlined tunnel. Figure 3-11 shows the comparison between the measurement and the updated displacements from extensometers (satisfied using internal convergence measurements). The figure shows that there are significant discrepancies between measurements and predictions, and hence, the method is not that effective.

Arai et al. (1984) presented a numerical procedure in which the soil parameters affecting the two dimensional consolidation are back-calculated from the data monitored in the field. Finite element models were carried out for five different hypothetical case studies of embankments and two actual test/trial embankments in order to validate their formulation. Linear-elastic constitutive soil models were assumed, such that (E', ν', and k) were obtained for multiple soil layers by a Least Squares method using an objective function defined in terms of displacements and pore pressures. No details were provided on the normalization of the different

physical quantities. Optimization was carried out using the gradient method. The authors concluded that the method proposed reasonable estimates the soil parameters. Arai et al. (1986) investigated the practical use of the back-analysis technique applied to four different trial embankment projects in Japan and England (6 cases in total were analyzed). In this case only displacements were included in the objective function. Later, Arai et al. (1987) proposed a numerical procedure to estimate the nonlinear constitutive parameters and permeability from the monitored movements of subsoil under two-dimensional consolidation. In this later publication, a simplified hyperbolic model (Duncan and Chang, 1970) was used to represent soil behavior. Both hypothetical and actual test embankments were used to validate the procedure. The authors concluded that the proposed procedure provides a good agreement between calculated and measured deformations; but also noted the difficulty in estimating non-linear soil model parameters.

Asaoka and Matsuo (1984) presented an inverse approach to the prediction of multi-dimensional consolidation behavior using examples and a case study of in-situ test embankment. This approach is based on Biot's equations. A linear elastic soil model was used in the numerical models. Deformations (settlements) and/or pore pressures were used as observations. The updated parameters correspond to Young's moduli, Poison's ratios, and hydraulic conductivities. They concluded the examples and case studies shows high accuracy of the proposed prediction procedure; however further research should be performed using more realistic soil constitutive models.

Gioda and Sakurai (1987) presented a survey of recent developments of the numerical techniques for back-analysis in the field of geomechanics, with particular reference to tunneling problems. The authors summarized both deterministic and probabilistic viewpoints used in the literature, and illustrated some applications to practical problems. They report the two rail highway tunnels excavated in relatively homogeneous weathered granite, Figure 3-12. Displacement measurements were conducted during the tunnel construction of a trial ("work") tunnel, excavated in advance of the main tunnels and almost parallel to them. Ground movements were measured using sliding micrometers and inclinometers, installed from the ground surface. The positions of these instruments and the directions chosen for some convergence measurements are shown in Figure 3.13. These displacements were adopted as input data in a back analysis of the elastic modulus of the rock mass, in which suitable values for the vertical in situ stress and Poisson's ratio of the rock were assumed, and the shotcrete lining was neglected because of its small thickness. From Figure 3.13a, it can be noted that it is difficult to update predictions under this inverse approach and under all assumptions made in this study (as seen in the comparisons for instruments 3 and 4; Fig. 3-13b).

Shoji et al. (1990) described a backanalysis framework for a set of two-dimensional elastic consolidation problems including three embankments and a retaining wall structure. The retaining wall structure was constructed for the basement of a building in Tokyo that was 22m deep with 6 levels of struts. The soil profile includes 3 layers (Figure 3-14). They used sensitivity analyses for locating the monitoring instruments, and the Least Squares approach as an identification criterion (objective function). They included both lateral displacements and strut loads as measurements in order to estimate values of Young's Moduli, Poisson's ratios, and

permeabilities for each layer. The optimization method selected was the quasi-Newton method using the BFGS (Broyden–Fletcher–Goldfarb–Shanno) formula. The authors concluded that: 1) sensitivity analysis is an efficient tool for choosing the location of measuring points; 2) the use of the quasi-Newton method and its finite element program can quickly and precisely predict deformation. However, they pointed out that is very difficult to predict the soil behavior when the anisotropy of soil is important and measurement errors are prominent. Figure 3-14 shows the predicted and measured lateral movements in the retaining wall structure for 3 stages (out of 7). They included initial predictions, updated predictions, and the measurements. At least for those stages, it seems that this approach accomplished reasonable results.

Honjo et al. (1994) proposed a new type of indirect inverse analysis based on the extended Bayesian method. This method combines the objective information (i.e., measurements) with the subjective information (i.e., prior information). They presented a case study of an embankment on soft clay (at Muar Flat, Malaysia) and compared measured and predicted settlements. The authors estimated Young's moduli (E') and horizontal hydraulic conductivities (k_h). The optimization methods selected were the Fletcher-Davidson (F-D) and Davidson-Fletcher-Powell (D-F-P). They concluded that more detailed studies on inverse analysis based on the proposal method should be carried out.

Ou and Tang (1994) described a procedure of back analysis to determine soil parameters in excavation performance using non-linear optimization techniques. They assumed that soil behavior can be described by the hyperbolic model (Duncan and Chang, 1970). Both hypothetical and actual cases are presented. The actual case study, for the Chi-Ching project in

Taipei, comprised an externally braced excavation 13 m deep supported by 70 cm thick and 28 m deep diaphragm wall. The soil profile comprised four different layers (sand and clay). Among the nine (or seven for the simplified version) input parameters of the hyperbolic model, only the stiffness, K, was assumed to be unknown; thus, four parameters were estimated (i.e., one for each of four soil layers). The identification criterion used was the Least Squares expressed in terms of the horizontal wall movements. The conjugate gradient method (Fletcher and Reeves, 1964) and Powell's quadratic interpolation method were adopted as optimization methods. Although the results matched the maximum values of wall displacements at four excavation stages, the method did not achieve good fit to the deformed mode shape of the wall (i.e., curvature and bending of wall). It is important to note that the authors did not present initial predictions of wall movements, making difficult the validation and/or evaluation of the proposed procedure.

Ledesma et al. (1996) described a probabilistic formulation for the backanalysis problem based on the Maximum Likelihood approach applied to a tunnel excavation problem. In order to validate this probabilistic approach, both hypothetical and actual problems of a tunnel excavation problem were introduced. The maximum likelihood approach involves the evaluation of the measurement covariance matrices, which the authors derived for some geotechnical instruments used in field instrumentation. The effect of the number of measurements and their error structures was also discussed (see Chapter 4). The case study application was presented by Gens et al. (1996) and corresponds to a 200 m long tunnel in tertiary clay in Terrassa (Barcelona, Spain). The soil profile consisted of three layers, and was analyzed using a 2D plane strain finite element model with linear elastic soil behavior. The authors compared Least Squares and

Maximum Likelihood approaches. The objective functions integrated only displacements captured by both extensometer and inclinometer measurements. The elastic moduli of the layers (E_1, E_2, and E_3) and the K_0 values of the overconsolidated clay layer only were estimated (i.e., 4 parameters considered). They also compared the well-known Gauss-Newton and Marquardt algorithms and included reliability analyses of the estimated parameters. Figures 3-15 and 3-16 show the soil profiles and instrumentation as well as comparisons of measured and computed (backanalyzed) displacements for two different tunnel sections (referred to as section B and C). Each section included two inclinometers and two extensometers. They compared results for DCM (diagonal covariance matrix in the least squares approach) and FCM (full covariance matrix for the maximum likelihood). Figure 3-15b shows small differences between DCM and FCM results and measurements from inclinometers only (labeled I3 and I4 at section B). The measurements of extensometer E3 show fair agreement between the measured and computed DCM (i.e., Least Squares). On the other hand, Figure 3-16b depicts comparisons of both approaches and measurements of two inclinometers and two extensometers at section C. In general, there is a little difference in the two inverse methods with the exception of inclinometer I5 that is described better by the Maximum Likelihood approach (FCM), since it involves the error structure of inclinometer measurements. The authors did not present initial predictions (including initial parameter values from site investigation and/or laboratory tests) making it difficult to evaluate the improvement achieved by the backanalysis approach.

Gioda and Locatelli (1999) presented a backanalysis of a railroad tunnel (Monteolimpino 2) connecting Milan to Chiasso. They assumed linear elastic behavior for six different sandy soils described (i.e., with 6 elastic moduli estimated). They used the Least Squares approach as

an identification criterion of the objective function and a direct search algorithm as an optimization method. Figure 3-17a shows the results of their initial backanalysis which was based only on displacement measurements (of three instruments) corresponding to phase A (top heading only). Due to poor results for an initial FE mesh (Figure 3-17a), they modified the mesh adding a potentially softer region above the shoulder of the tunnel and included an additional stiffness parameter in this region (from the shoulder of the tunnel up to the surface). This led to much better results (as shown in Figure 3-17b); but does not reflect direct knowledge of degraded soil properties near to the lining.

Lecampion et al. (2002) considered the estimation of viscoplastic parameters for synthetic unlined and lined tunnel problems. The numerical modeling was performed using finite element methods with an elasto-viscoplastic constitutive law of Perzyna class (with a Norton-Hoff law to correlate friction angle with the stress levels). Four parameters were estimated corresponding to the Young's modulus (E), the yield limit (σ_y), the viscoplastic exponent (N), and the viscosity coefficient (K). The identification criterion adopted was the least squares approach where the objective function was in terms of displacements and pressures of lining and rock mass interface. The optimization technique employed used the Levenberg–Marquardt algorithm. Although, the authors claimed that the proposed inverse method can be applied successfully in tunneling problems, they admitted that further research should focus on including covariance matrices of measurements of actual tunnel excavations.

Calvello (2002), Calvello and Finno (2004), and Finno and Calvello (2005) present an inverse analysis procedure for a 12 m supported excavation (Chicago-State subway renovation)

through Chicago glacial clays. Figure 3-18 shows the section view of the excavation support system as well as the construction sequences assumed in the finite element analyses. The model includes eight different soil layers, one level of cross-lot bracing and two levels of tieback anchors. The numerical modeling was performed by the finite element software Plaxis^{TM} using the hardening soil (HS) model (Schanz et al. 1999) to represent the behavior of the clayey layers, and the Mohr-Coulomb model for the uppermost layer of sand and fill (Fig. 3-18). Calvello and Finno (2004) assumed material properties for the two upper layers (sand/fill and clay crust) as deterministic (i.e., constant values) and performed sensitivity analyses by coupling Plaxis^{TM} with UCODE (e.g., Hill and Tiedeman, 2007; Poeter and Hill, 2008), for the rest of the soil layers, focusing on three HS model parameters (E_{50}^{ref} , $\emptyset$, and m). Under some assumptions, they concluded that only the stiffness parameter E_{50}^{ref} needed to be updated. The other stiffnesses of the model (E_{oed}^{ref} *and* E_{ur}^{ref}) are correlated with E_{50}^{ref} following default recommendations of Plaxis. Finno and Calvello (2005) estimated the E_{50}^{ref} for three clayey soil layers only (3 parameter optimization), but updated fifteen input parameters in total. The identification criterion adopted was the Least Squares approach with the objective function in terms of displacements. The optimization technique corresponded to the Modified Gauss-Newton method. Figure 3-19 shows the initial predictions versus measurements captured by two inclinometers (five stages for the East and three stages for the West inclinometer). The analyses overestimate the measured lateral wall movements using model parameters based on triaxial shear tests. Figure 3-20 shows the updated predictions from stage 1 only and the measured data. In general, it can be observed that predictions for subsequent stages were improved significantly. When measurements of all stages were used to update parameters at each stage, the predictions improved remarkably with

some details of the shape of wall deflections (shown in Figure 3-21). Although this procedure is effective for the case study presented (lateral wall movements only), it may be limited for other case studies as: 1) the sensitivity analysis included only a small perturbation of each parameter (rather than a full exploration of the search space); 2) the optimization method used (gradient method or Gauss-Newton method) depends highly on the initial value assumed; 3) when combining different type of measurements, the results depend on the number of measured points used; and 4) the identification criterion employed (i.e. Least Squares) is incapable of capturing the error structure of inclinometers (as there is no account of the coupling effect on inclinometer residuals). In fact, when both lateral wall deflections and settlements were used as measurements under the same technique, the wall deflections are over-predicted while settlements are significantly under-predicted (specifically those close to the wall), as shown in Figure 3-22.

Rechea (2006) and Finno & Rechea (2006) studied the effect of different observation types in an inverse analysis for a synthetic braced excavation. Figure 3-23 shows the location of "field" observations in the synthetic example as well as the finite element model (Rechea, 2006). Their simulations were carried out with the Mohr-Coulomb model and the Hardening Soil (HS) model. For the HS model, the stiffness parameter E_{50}^{ref} was estimated for the two soil layers, under the same inverse procedure and assumptions (i.e. identification criterion, sensitivity analysis, and optimization method) described by Calvello (2002) and Finno and Calvello (2005). Four types of observations (horizontal displacements, settlements, pore pressures, and strut forces) were used and different combinations were analyzed. Finno and Rechea (2006) concluded that the effect of including strut forces in either horizontal movements or settlements resulted in an important increment of composite scaled sensitivities (Calvello, 2002), suggesting

the benefits of using these observation together. However, they also claimed that: "*to use strut forces in a 2D analysis, they have to be converted to an average value per unit length, so the field measurements cannot be employed directly in the inverse analysis.*" In addition, Rechea (2006) backanalyzed two braced excavation case studies through Chicago glacial clays: and 1) Ford Center, and 2) Lurie Research Center. The finite element models and construction sequences are shows in Figures 3-24 and 3-26, respectively. The HS model was used to represent soil behavior and was based on Finno and Calvello (2002). Figure 3-25 shows inclinometer measurements versus updated predictions for the Ford Center case study. The results correspond to two excavation stages (phases 9 and 11) and for three cases of updated predictions. The computed results do not describe particularly well the measured data, suggesting other sources of error in the model. Figure 3-27a shows the plan view of Lurie Research Center excavation site and instrumentation. Measurements of horizontal soil movements and updated predictions for the Lurie Center show reasonable fitting to maximum wall deflections at stage 6, but miss some aspects of behavior at stage 4 (Figure 3-27b). These limitations might be attributed to tieback prestress magnitudes and/or to assumed properties of the fill and sand layers.

Levasseur (2007) and Levasseur et al. (2007) described a soil parameter estimation procedure based on genetic algorithms, specifically, for the identification of parameters of the Mohr–Coulomb constitutive model from two in situ geotechnical tests: 1) a pressuremeter curve, and 2) the horizontal displacements of a sheet pile wall retaining an excavation. They compared two types of optimization algorithms: 1) gradient method, and 2) genetic algorithms, concluding that genetic algorithms are more suitable to solve inverse geotechnical problems, and that the gradient method is efficient only when the objective functions are relatively smooth and/or when

the initial parameter value is very close to the solution. Levasseur (2007) also applied the genetic algorithm procedure to the Lurie Research Center excavation project in Chicago. Parameter updating again focused on E_{50}^{ref} for the two clay layers. The main difference was the optimization method selected (genetic algorithms). Rechea et al. (2008) presented the horizontal movement prediction comparison and measurements for both gradient method and genetic algorithms for the last excavation stage only, as shown in Figure-3.28. From the figure, it can be observed that some observations were removed (upper part of measurements) in the inverse analyses and that there is no difference between the optimization method used. If the upper part of the measurements is not included, the inverse analysis problem will basically rely on material properties of clay layers. Levasseur et al. (2009) also presented a statistical inverse analysis using GA together with a principal component analysis (PCA) for the Lurie Research Center case study. Figure 3-29 compares measured and computed wall deflections and surface settlements for the last excavation stage of the Lurie Center, while surface settlements are very well predicted behind the inclinometer LR8, they underestimated the measured settlements behind LR6.

Hashash et al. (2003), Hashash et al. (2006), and Hashash et al. (2010) proposed an inverse approach that extracts material behavior referred to as self-learning simulation concept (SelfSim). This approach was implemented and extended from an algorithm to extract material constitutive behavior introduced by Ghaboussi and Sidarta (1998), and Ghaboussi et al. (1998). Figure 3-30 shows the application of the SelfSim learning simulations to deep excavation problems which basically consists of three different steps: 1) obtain field measurements (usually wall deflections and settlements), 2) iteration of SelfSim learning FEM which extract stresses

from simulating the construction sequences and extract strains from applying measurements allowing stress-strain pairs training of a neural network (NN) constitutive soil model, and 3) forward FEM analysis with trained NN material model. Figure 3-31 shows the construction sequence reported for the Lurie Research Center by Hashash et al. (2010)[§]. Figure 3-32 presents a comparison of measurements versus SelfSim computed lateral wall deflections and surface settlements for all excavation levels at Lurie Center. The SelfSim analyses underestimate measured wall deflections at the final formation level (but overestimate at earlier stages), while they match well the surface settlements at final formation.

Hashash et al. (2010) also compared measurements, versus lateral wall deflections and settlements computed by optimal parameters obtained from genetic algorithms and by SelfSim procedure, shown in Figure 3.33. This figure suggests that based-genetic algorithms (GA) results predict better the elevation of the maximum movement. However, both methods tend to under-predict the maximum lateral wall movement. The difference of the maximum elevation might be attributed to some differences between the Abaqus (SelfSim) and Plaxis (GA) modeling. On the other hand, surface settlements are under-predicted by the least squares and GA inverse approach. The constitutive model chosen for Plaxis simulations was the Hardening Soil (HS) Model. The authors claimed that the HS model selection is probably the cause of under-prediction of surface settlements. Osouli & Hashash (2010) and Osouli et al. (2010) have recently applied the same inverse technique with SelfSim excavation projects in Texas, Shanghai, and Taipei.

[§] The construction sequence differs from previously presented and described by Rechea (2006) and Levasseur (2007).

3.5 Comments

Most researchers have been using the Least Squares criterion to describe the objective function together with non-heuristic optimization methods. The most common identification criterion (i.e., Least Squares) is incapable of capturing the error structure of inclinometers, as there is no account of the coupling effect on linewise instruments (e.g., inclinometers). It is very important to highlight that the use of the Least Squares method depends highly on the number of data points used, and therefore presents an important limitation when different types of measurements are to be combined.

Also, the most common optimization methods used (e.g., gradient method, Gauss-Newton method, etc.) depend on the initial values of the paremeters assumed which presents a clear drawback for non-linear inverse problems, as soil-structure interaction problems are often highly non-linear. Levasseur and co-workers used genetic algorithms as optimization methods which present a clear advantage to deal with complex and non-linear functions; however, the identification criterion adopted by them corresponds to the Least Squares.

In general, the authors do not include sensitivity analyses to understand and select which parameters are important. Although Finno and co-workers presents sensitivity analysis, this procedure includes only a small perturbation of each parameter. Unfortunately, this method fails in exploring full realistic search spaces which must be based on soil behavior knowledge, and therefore it does not select properly the parameters to update.

In engineering practice, engineers use "back-analyses" of FE analyses where model parameters are varied based on engineering judgement and sometimes even randomly (i.e., without any rational methodology) to achieve better agreements between predictions and field measurements. A great example of this is the Nicoll Highway collapse occurred in April 20th 2004 (see Section 2.3).

Figure 3-34 compares predicted and measured maximum wall deflections. The measured values are shown by vertical bars and correspond to two different inclinometers (referred to as I-104 and I-65). The predictions of maximum wall deflections from initial design, first back-analysis, and second back-analysis are shown with continuous lines. The first back-analysis occurred on March 5th 2004 and included the following parameter modifications at different excavation stages: 1) 50% reduction of wall stiffness; 2) 20% reduction of strength and elastic modulus on the JGP (Jet Grouting Pile) unit; 3) 20% reduction of strength and elastic modulus on the upper marine clay unit; and 4) 50% reduction of strength and elastic modulus on the lower marine clay unit. The second back-analysis occurred on April 19th 2004 and included the following parameter modifications at different excavation stages: 1) 55-70% reduction of wall stiffness; 2) 20-40% reduction of strength and elastic modulus on the JGP (Jet Grouting Pile) unit; 3) 30% reduction of strength and elastic modulus on the upper marine clay unit; 4) 65-75% reduction of strength and elastic modulus on the lower marine clay unit; 5) 30-40% reduction of the strength and modulus on the fluvial clay unit (referred to as F2); 6) 45% reduction of strength and elastic modulus. Although several other technical and administrative problems led to the collapse (April 20th 2004), the most relevant aspects correspond to the two back-analyses

performed by NLJV (COI, 2005) where the updated parameters do not explain the prior history but simply match the current state, lacking objectivity as modifications of material properties.

Therefore, a rational methodology for updating FE predictions that can handle diverse designs, ground conditions, and sources of information during construction is urgently needed. In principle, this should integrate: 1) rational sensitivity analyses; 2) error structures of field measurements; and 3) heuristic optimization methods.

3.6 References

Anandarajah, A. and Agarwal D. (1991). "Computer-aided Calibration of a Soil Plasticity Model." *Int. Journal for Num. and Analytical Methods in Geomechanics* 15(12):835-856.

Arai, K., H. Ohta, and Yasui, T. (1983). "Simple Optimization Techniques for Evaluating Deformation Moduli from Field Measurements." *Soils and Foundations* 23(1): 107-113.

Arai, K., Ohta, H., and Kojima, K. (1984). "Estimation of Soil Parameters Based on Monitored Movement of Subsoil Under Consolidation." *Soils and Foundations* 24(4): 65-108.

Arai, K., Ohta, H., Kojima, K., and Wakasugi, M. (1986). "Application of Back-Analysis to Several Test Embankments on Soft Clays." *Soils and Foundations* 26(2): 60-72.

Arai, K., Ohta, H., and Kojima, K. (1987). "Estimation of Nonlinear Constitutive Parameters based on Monitored Movement of Subsoil under Consolidation." *Soils and Foundations* 27(1): 35-49.

Asaoka, A. and Matsuo, M. (1980). "An Inverse Problem Approach to Settlement Prediction." *Soils and Foundations* 20(4): 53-66.

Asaoka, A. and Matsuo, M. (1984). "An Inverse Problem Approach to the Prediction of Multi-Dimensional Consolidation Behavior." *Soils and Foundations* 24(1): 49-62.

Aster, R., Borchers, B., Thurber, C.H. (2005). "Parameter Estimation of Inverse Problems." International Geophysics Series. Elsevier Academic Press.

Baroth, J. and Malecot, Y. (2010). "Probabilistic Analysis of the Inverse Analysis of an Excavation Problem." *Computers and Geotechnics* 37(3): 391-398.

Brown, S. M., Lincoln, D. R. and Wallace, W. A. (1990) "Application of Observational Method to hazardous waste engineering." *ASCE Journal of Management in Engineering* 6(4): 479-500.

Calvello, M. (2002). "Inverse Analysis of a Supported Excavation through Chicago Glacial Clays." *PhD Thesis in Civil Engineering. Northwestern University, Evanston, Illinois.*

Calvello, M. and Finno, R. J. (2004). "Selecting Parameters to Optimize in Model Calibration by Inverse Analysis." *Computers and Geotechnics* 31(5): 411-425.

Cekerevac, C., Girardin, S., Klubertanz, G., and Laloui, L. (2006). "Calibration of an Elasto-Plastic Constitutive Model by a Constrained Optimisation Procedure." *Computers and Geotechnics* 33(8): 432-443.

Charles, .J. A. (1993). "Embankment dams and their foundations: safety evaluation for static loading." *International workshop on dam safety evaluation, Grindelwald* 4:47-75.

Cividini, A., Jurina, L., and Gioda, G. (1981). "Some Aspects of 'Characterization' Problems in Geomechanics." *Int. J. Rock Mech. Min. Sci. & Geomech* 18(6): 487-503.

Cividini, A., Maeir, G., Nappi, A. (1983). "Parameter Estimation of a Static Geotechnical Model Using a Bayes' Approach." *Int. J. Rock Mech. Min. Sci. & Geomech* 20(5): 215-226.

Cividini, A. and Gioda G. (1993). "Numerical back analysis techniques for rock engineering." *Assessment and Prevention of Failure Phenomena in Rock Engineering*, Balkema, Rotterdam: 11-21.

COI (2005). Report of the Committee of Inquiry into the Incident at the MRT Circle Line Worksite that Led to the Collapse of Nicoll Highway 20 April 2004. Report Submitted to the Minister of Manpower.

D'Appolonia, E. (1990). "Monitored decisions." *ASCE J. of Geotech. Engineering* 116 (1): 4-34.

De Mello, V.F.B. (1977) "Reflections on design decisions of practical significance to embankment dams." *Géotechnique*, 27 (3): 279-355

Deng, J. H. and Lee, C. F. (2001). "Displacement Back Analysis for a Steep Slope at the Three Gorges Project Site." *Int. Journal of Rock Mechanics & Mining Sciences* 38(2): 259-268.

Ding, W. Q., Wang, X. X., Cheng, Y., Zhu, H.H., and Xie, D.W. (2006). "Optimal Analysis of Construction Schemes for Twin Tunnel based on Back Analysis." *Underground Contruction and Ground Movement ASCE*, GSP 155, p.112-119.

Duncan, J. M. and Chang, C.Y., (1970). "Nonlinear analysis of stress and strain in soils." *ASCE Journal of Soil Mechanics and Foundation Division* 96(5): 1629-1653.

Eclaircy-Caudron, S., Dias, D., Kastner, R., Miranda, T., Gomes Correia, A., and Ribeiro e Sousa, L. (2007). "Inverse Analysis on two Geotechnical Works: a Tunnel and a Cavern." *CEC - GEO - Comunicações a Conferências Internacionais.*

Edwards, A.W.F. (1972). "Likelihood" (1st edition). Cambridge: Cambridge University Press.

Einstein, H. H. (1991), "Observation, Quantification, and Judgment: Terzaghi and Engineering Geology." *ASCE Journal of Geotechnical Engineering* 117 (11): 1772-1778.

Einstein, H. H. and Baecher, G. B. (1982). "Probabilistic and Statistical Methods in Engineering Geology. I. Problem Statement and Introduction to Solution." *Rock Mechanics*, Suppl. 12: 47-61.

Eurocode 7 (BS EN 1997-1:2004) "Geotechnical design - Part 1: General rules."

Finno, R., Harahap, I. (1991). "Analysis of Braced Excavations with Coupled Finite Element Formulations." *Computers and Geotechnics* 12(1991): 91-114.

Finno, R.J. and Calvello, M. (2005). "Supported Excavations: Observational Method and Inverse Modeling." *ASCE Journal of Geotechnical and Geoenvironmental Engineering* 131(7): 826.

Finno, R.J. and Hashash, Y.M. (2006). "Integrating Tools to Predict, Monitor and Control Deformation due to Excavations." *ASCE GeoCongress 2006: Geotechnical Engineering in the Information Technology Age.* Atlanta, USA. February 15.

Finno, R. and Rechea C. (2006). "Use of lateral movements and strut loads in inverse analysis of supported excavations." *ASCE GeoCongress 2006: Geotechnical Engineering in the Information Technology Age.* Atlanta, USA. February 15.

Finno, R. (2007). "Use of Monitoring Data to Update Performance Predictions of Supported Excavations." *ASCE FMGM 2007: Seventh International Symposium on Field Measurements in Geomechanics.* GSP 175. Boston.

Finno, R. (2010). "Recent Trends in Supported Excavation Practice." *Proceedings of the 2010 Earth Retention Conference (ER2010)*, ASCE GSP (208): 1:18

Fu, Q., Hashash, Y. M, Jung, S., and Ghaboussi, J. (2007). "Integration of Laboratory Testing and Constitutive Modeling of Soils." *Computers and Geotechnics* 34(5): 330-345.

Gens, A., Ledesma A., and Alonso, E. (1996). "Estimation of Parameters in Geotechnical Backanalysis - II. Application to a Tunnel Excavation Problem." *Computers and Geotechnics* 18(1): 29-46.

GeoTechNet Project GTC2-2000-33033, WP3: Innovation Design Tools in Geotechnics – Observational Method and Finite Element Method, editor Noel Huybrechts, BBRI. (reference also http://www.geotechnet.org/)

Geotechnical_Engineering_Office (1990). "Review of Design Methods for Excavations." Civil Engineering Department. G. P. No.1/90. The Government of the Hong Kong, Special Administrative Region.

Ghaboussi, J., Pecknold, D., Zhang, M., and Haj-Ali, R.M. (1998). "Autoprogressive training of neural network constituttive models." *International Journal for Numerical Methods in Engineering* 42(1): 105-126.

Ghaboussi, J. and Sidarta D.E. (1998). "New Nested Adaptive Neural Networks (NANN) for Constitutive Modeling." *Computers and Geotechnics* 22(1): 29-52.

Gioda, G. and De Donato, O. (1979). "Elastic-Plastic Analysis of Geotechnical Problems by Mathematical Programming." *International Journal for Numerical and Analytical Methods in Geomechanics* 3(4): 381-401.

Gioda, G. and Maier, G. (1980). "Direct Search Solution of an Inverse Problem in Elastoplasticity: Identification of Cohesion, Friction Angle & In-Situ Stress by Pressure Tunnel Tests." *Inter. Journal for Numerical Methods in Engineering* 15(12): 1823-1848.

Gioda, G., Jurina, L. (1981). "Numerical Identification of Soil-Structure Interaction Pressures." *Int. Journal for Numerical and Analytical Methods in Geomechanics* 5(1): 33-56.

Gioda, G. and Sakurai, S. (1987). "Back Analysis Procedures for the Interpretation of Field Measurements in Geotechnics." *International Journal for Numerical and Analytical Methods in Geomechanics* 11(6): 555-583.

Gioda, G. and Locatelli, L. (1999). "Back Analysis of the Measurements performed during the excavation of a Shallow tunnel in Sand." *International Journal for Numerical and Analytical Methods in Geomechanics* 23: 1407-1425.

Goldberg, D.E. (1989), "Genetic Algorithms in Search, Optimization and Machine Learning." Crawfordsville, Indiana, Addison-Wesley.

Hashash, Y.M.A. and Whittle, A.J. (1996). "Ground Movement Prediction for Deep Excavations in Soft Clay." *ASCE Journal of Geotechnical Engineering* 122(6): 474:486.

Hashash, Y. M., Marulanda, C., Ghaboussi, J., and Jung, S. (2003). "Systematic Update of a Deep Excavation Model using Field Performance Data." *Computers and Geotechnics* 30(6): 477-488.

Hashash, Y. M., Marulanda, C., Ghaboussi, J., and Jung, S., (2006). "Novel Approach to Integration of Numerical Modeling and Field Observations for Deep Excavations." *ASCE Journal of Geotechnical and Geoenvironmental Engineering* 132(8): 1019.

Hashash, Y. M. (2007). "Special Issue on Biologically Inspired and other Novel Computing Techniques in Geomechanics." *Computers and Geotechnics* 34(5): 329.

Hashash, Y. M. and Finno, R. (2008). "Development of New Integrated Tools for Predicting, Monitoring, and Controlling Ground Movements due to Excavations." *Practice Periodical on Structural Design and Construction* 13(1): 4.

Hashash, Y. M., Levasseur, S., Osouli, A., Finno, R., and Malecot, Y. (2010). "Comparison of two Inverse Analysis Techniques for Learning Deep Excavation Response." *Computers and Geotechnics* 37(3): 323-333.

Hill, M.C. and Tiedeman, C.R. (2007). "Effective Groundwater Model Calibration with Analysis of Data, Sensitivities, Predictions, and Uncertainty." John Wiley & Sons.

Holland, J. H. (1975). "Adaption in Natural and Artificial Systems." Ann Arbor: The University of Michigan Press.

Honjo, Y., L. Wen-Tsung, L., and Guha, S. (1994). "Inverse Analysis of an Embankment on Soft Clay by Extended Bayesian Method." *International Journal for Numerical and Analytical Methods in Geomechanics* 18(10): 709-734.

Health and Safety Commission (1996). "Guidance on the use of rockbolts to support roadways in coal mines." HSE Books, Suffolk, England.

Hu, B. (2006). "Inteligent Back Analysis of Rheology parameters of Left Bank High Slope Rock Masses at Longtan Hydropower Station in China." *Advances in Earth Structures: Research to Practice ASCE*, GSP 151: 90-97

Ikuta, Y., Maruoka, M., Aoki, M., and Sato, E. (1994). "Application of the observational method to a deep basement excavation." *Géotechnique* 44(4): 655-664.

Institution of Civil Engineers (1996a). "Sprayed concrete linings (NATM) for tunnels in soft ground". Thomas Telford, London

Institution of Civil Engineers (1996b). "Creating value in engineering." Thomas Telford, London

Institution of Civil Engineers (1996c). "The Observational Method in Geotechnical Engineering" Thomas Telford, London

Institution of Civil Engineers (2001). "Managing Geotechnical Risk: Improving Productivity in the UK Building and Construction." Thomas Telford, London

Jeon, Y. S. and Yang, H. S. (2004). "Development of a Back Analysis Algorithm using FLAC." *Int. Journal of Rock Mechanics and Mining Sciences* 41 (Supplement 1): 447-453.

Jurina, L., Maier, G., Podolak, K. (1977). "On Model Identification Problems in Rock Mechanics." *Associazione Geotecnica Italiana – The Geotechnics of Structurally Complex Formations* .

Kim, W. S. and Borden, R. H. (2007). "Lessons Learned in Use of Instrumented Soldier Pile Wall for Inverse Analysis of Material Properties." *ASCE Seventh International Symposium on Field Measurements in Geomechanics* (FMGM 2007). GSP 175. Boston.

Lecampion, B., Constantinescu, A., and Nguyen Minh, D. et al. (2002). "Parameter Identification for Lined Tunnels in a Viscoplastic Medium." *International Journal for Numerical and Analytical Methods in Geomechanics* 26: 1191-1211.

Ledesma, A. (1987). "Identificación de Parámetros en Geotecnia. Aplicación a la Excavación de Túneles." *PhD Thesis - Escuela Técnica Superior de Ingenieros de Caminos, Canales y Puertos de Barcelona.*

Ledesma, A., Gens, A., and Alonso, E. (1996). "Estimation of Parameters in Geotechnical Backanalysis - I. Maximum Likelihood App." *Computers and Geotechnics* 18(1):1-27.

Levausser, S. (2007). "Inverse Analysis in Geotechnics (in French)". *Grenoble I, Universite Joseph Fourier PhD*, 240p.

Levasseur, S., Malecot, Y., Boulon, M., Flavigny, E.. (2008). "Soil Parameter Identification Using a Genetic Algorithm." *International Journal for Numerical and Analytical Methods in Geomechanics* 32(2): 189-213.

Levasseur, S., Malecot, Y., Boulon, M., Flavigny, E. (2009a). "Statistical Inverse Analysis based on Genetic Algorithm and Principal Component Analysis: Method and Developments using Synthetic Data." *International Journal for Numerical and Analytical Methods in Geomechanics* 33(12): 1485-1511.

Levasseur, S., Malecot, Y., Boulon, M., Flavigny, E. (2009b). "Statistical inverse analysis based on genetic algorithm and principal component analysis: Applications to excavation problems and pressuremeter tests." *International Journal for Numerical and Analytical Methods in Geomechanics* 34(5): 471-491.

MATLAB (2004-2009). "Genetic Algorithm and Direct Search Toolbox TM 2 - User's Guide." The MathWorks, INC.

Meir, J., Schaedler, W. , Borgatti, L., Corsini, A., and Schanz, T. (2008). "Inverse Parameter Identification Technique Using PSO Algorithm Applied to Geotechnical Modeling." *Journal of Artificial Evolution and Applications* (Article ID 574613): 14 p.

Michalewicz, Z. (2011). "Genetic Algorithms+Data Structures = Evolution Programs." Springer.

Morgenstern, N.R. (1994). "The Observational Method in environmental geotechnics." Proceedings of 1st Int. Conf. on Environmental / Geotechnics, Alberta, Canada, 965-976.

Muir Wood, A. (1987). "To NATM or not to NATM." Felsbau, 5(1): 26-30

Muir Wood, A. (1990). "The observational Method revisited". *Proceedings of 10th Southeast Asian Geotechnical Conference*". April 1990, Taipei, 2: 37-42.

Navarro, V., Candel, M., Barencam A., Yustres, A., and García, B. et al. (2007). "Optimisation Procedure for Choosing Cam Clay Parameters." *Computers and Geotechnics* 34:524-531.

Nicholson, D., Tse, C. and Penny, C. (1999). "The Observational Method in ground engineering – principles and applications." Report 185, CIRIA, London

Nicholson, D., Dew C.E., and Grose W.J. (2006) "A systematic "Best Way Out" approach using backanalysis and the Principles of the Observational Method." *International Conference on Deep Excavations*, 28-30 June, Singapore. 22p.

Osouli, A. and Hashash, Y.M. (2010). "Case studies of prediction of excavation response using learned excavation performance." *Int. Journal of Geoeng. Case Histories* 1(4): 340.

Osouli, A., Hashash, Y., and Song, H. (2010). "Interplay between Field Measurements and Soil Behavior for Capturing Supported Excavation Response." *ASCE Journal of Geotechnical and Geoenvironmental Engineering*: 131(1): 69-84.

Ou, C. Y. and Y. G. Tang (1994). "Soil parameter determination for deep excavation analysis by optimization." *Journal of the Chinese Institute of Engineers* 17(5): 671-688.

Patel, D., Nicholson, D., Huybrechts, N., and Maertens, J. (2007). "The Observational Method in Geotechnics." Proceedings of XIV European Conference on Soil Mechanics and Geotechnical Engineering: Geotech. Eng. in urban environments, Madrid, 2:10

Peck, R.B. (1969). "Advantages and Limitations of the Observational Method in Applied Soil Mechanics." *Géotechnique - Ninth Rankine Lecture* 19(2): 171-187.

Poeter, E., Hill, M., Banta, E., Mehl, S., and Christensen, S. (2008). "UCODE 2005 - Code for Universal Sensitivity Analysis, Calibration, and Uncertainty Evaluation." R. U.S. Geological Survey, Virginia.

Powderham, A.J. and Rutty, P.C. (1994) "The Observational Method in value engineering." *Proc. of 5th int. Conference on Piling and Deep Foundations*, Bruges, (5.7):1-12.

Powderham, A.J. (1994). "An Overview of the Observational Method: Development in Cut and Cover and Bored Tunnelling Projects." *Géotechnique* 44(4): 619-634.

Powderham, A.J. and Nicholson, D.P. (1996) "The Observational method in geotechnical engineering" ICE, Thomas Telford, London

Rechea, C. (2006). "Inverse Analysis of Excavations in Urban Environments." *PhD Thesis in Civil & Environmetal Engineering. Evanston, Illinois, Northwestern University*, 259p.

Rechea, C., Levasseur, S., and Finno, R. (2008). "Inverse Analysis Techniques for Parameter Identification in Simulation of Excavation Support Systems." *Computers and Geotechnics* 35(3): 331-345.

Sakurai, S. and K. Takeuchi (1983). "Back Analysis of Measured Displacements of Tunnels." *Rock Mechanics and Rock Engineering* 16(3): 173-180.

Sakurai, S. (1998). "Lessons Learned from Field Measurements in Tunnelling." *Tunnelling and Underground Space Technology* 12(4): 453-460.

Sakurai, S., Akutagawa, S., Takeuchi, K., Shinji, M., and Shimizu, N. (2003). "Back analysis for tunnel engineering as a modern observational method." *Tunnelling and Underground Space Technology* 18(2): 185-196.

Santamarina, J.C. and Fratta, D. (2005). "Discrete Signals and Inverse Problems: An Introduction for Engineers and Scientists. " John Wiley & Sons.

Shanz, T., Vermeer, P.A., and Bonnier, P. (1999). "The Hardening Soil Model: Formulation and Verification." Beyond 2000 in Computational Geotechnics, Balkema, Rotterdam.

Shoji, M., Ohta, H., Arai, K., Matsumoto, T., and Takahashi, T. (1990). "Two-Dimensional Consolidation Back-Analysis. " *Soils and Foundations* 30(2): 60-78.

Tang, Y.G. and Kung, T.C. (2009). "Application of Nonlinear Optimization Technique to Back Analyses of Deep Excavation. " *Computers and Geotechnics* 36(1-2): 276-290.

Tang, Y.G. and Kung, G. (2010). "Investigating the Effect of Soil Models on Deformations caused by Braced Excavations through an Inverse-Analysis Technique. " *Computers and Geotechnics* 37(6): 769-780.

Terzaghi, K. (1961). "Past and Future of Applied Soil Mechanics." *Journal of Boston Society of Civil Engineers*. April: 110-139.

Terzaghi, K and Peck, R (1948). "Soil Mechanics in Engineering Practice." 1st Edition. John Wiley & Sons, New York.

Wakita, E. and Matsuo, M. (1994). "Observational design method for earth structures constructed on soft ground. " *Géotechnique* 44(4): 747-755.

Whitman, R. V. (1984). "Evaluating calculated risk in geotechnical engineering." *ASCE Journal of Geotechnical Engineering* 110 (2): 143-188.

Table 3-1: Summary of the development of the Observational Method

Year	Name	Event
1912-1922	Statens Järvägars	Between 1912 and 1922, the observational procedure was used for the first time by the administration of the Swedish State Railroads for an investigation on the stability of slopes on glacial deposits (Terzaghi, 1961).
1929	Terzaghi	First use of the observational procedure in 1926 in Granville Dam near Westfield, Massachusetts (Terzaghi, 1961).
1958	Terzaghi and Leps	Design of the Vermilion Dam in Southern California in 1950's (Terzaghi, 1961).
1965	Casagrande	The Second Terzaghi Lecture held in New York in 1964, where Casagrande talked about the role of the "calculated risk" in earthwork and foundation engineering. A great example of an application of the observational method was described referred to as "The Great Salt Lake railroad fill".
1969	Peck	In the ninth Rankine Lecture, Peck listed requirements and limitations for application of the OM.
1977	De Mello	Recommended the OM as a design principle for embankment dams.
1984	Whitman	Recognized the use of the OM for managing risks in geotechnical engineering.
1987	Muir Wood	A six-step OM was proposed for use in tunneling.
1987	Eurocode 7 - EC7	Draft set out requirements for the use of the OM.
1993	Hong Kong GCO	*Guide to retaining wall design.*
1995	EC7	The final draft of EC7 was published including the requirements for the OM.
1999	CIRIA	"The Observational Method in ground engineering: principles and applications." (CIRIA, Report 185)

Table 3-2: Comparison of the predefined design process and the Observational Method (Patel et al., 2007)

Traditional Design or Predefined Design Process	**The OM Process**
• Permanent works • One set of parameters • One design / predictions • Outline of construction method • Contractors temporary works design /method statement • Monitoring checks predictions not exceeded • If checks are exceeded, consider (a) Best Way out approach to design; or (b) redefine the predefined design approach reassessing the geotechnical uncertainties in the ground • Emergency plan	• Temporary works • Two sets of parameters • Two designs and predictions • Integrated design and construction methods • Methods relate to triggers • Comprehensive and robust monitoring system • Review and modify process – Contingency plan – Improvement plan • Emergency Plan

Table 3-3: Typical Weights of Observations used in Braced Excavations (Finno, 2007)

Instrumentation	Range (full scale)	Accuracy	95% standard deviation, σ	Weight
Lateral movements with inclinometers	±53° from vertical	± 0.25 mm/m $\frac{0.25}{1000} \cdot d$	$\frac{0.25}{1000} \cdot \frac{d}{1.96} = 0.0001 \cdot d$ (m)	$\frac{1}{(0.0001 \cdot d)^2}$
		where d is distance (m) from bottom of casing		
Ground surface settlement with optical survey		± 0.01 ft ± 0.003 m	$\frac{0.003}{1.96} = 0.00155$ (m)	$\frac{1}{(0.00155)^2}$
vibrating wire piezometer	3.5 bar/50 psi 344.8 Pa	± 0.1% FS ± 0.34 Pa	$\frac{0.34}{1.96} = 0.173$ (Pa)	$\frac{1}{(0.173)^2}$
Strut force with spot-weldable strain gauge	2,500 microstrain	± 0.1%FS =± 2.5 microstrain	$\frac{E \cdot A \cdot Accuracy}{1.96}$ (kN)	$\frac{1}{(6.19)^2}$ (1)

(1) value shown is for a steel brace with A = 0.024 m^2

Table 3-4: Summary of Literature Review of Inverse FE Analyses in Tunnel and Excavation Problems

Reference	Problem Type Tunnel/Excavation	Constitutive Law	Soil/Rock Parameters (#of parameters)	Identification Criterion	Optimization Method
Gioda and Maier (1980)	Hypothetical In-situ Pressure Tunnel Test	Mohr-Coulomb	c, ϕ, initial stress (3)	Least Squares	Nelder-Mead flexible polyhedron; Rosenbrock Algorithm
Sakurai and Takeuchi (1983)	Unlined/Lined Tunnels	Isotropic Linear-Elastic	$[\sigma_{xx}, \sigma_{yy}, \tau_{xy}]^T$; E (4)	Least Squares	Proposed Inverse Problem Approach
Gioda and Sakurai (1987)	Work Tunnel	Linear-Elastic	E; σ' (2)	Least Squares	-
Shoji et al. (1990)	Retaining Wall structure (Tokyo)	Isotropic Linear-Elastic	E', ν', k (3)	Least Squares	Quasi-Newton Method
Ou and Tang (1994)	Synthetic/Actual Excavation	Hyperbolic (Duncan-Chang)	Stiffness: K (4)	Least Squares	Conjugate Gradient; Powell's Quadratic Interpolation Method
Ledesma et al. (1996), Gens et al. (1996)	Synthetic Tunnel/ Actual tunnel (Barcelona, Spain)	Linear-Elastic	E and K_0 (2) E_1, E_2, E_3 and K_0 (4)	Least Squares and Maximum Likelihood	Gauss-Newton and Marquardt Algorithms
Gioda and Locatelli (1999)	Actual Railroad Tunnel: (Switzerland)	Linear-Elastic & Elasto-Plastic	E (4)	Least Squares	Direct Search Method
Lecampion et al. (2002)	Synthetic Lined Tunnels	Elasto-viscoplastic constitutive law	K, σ_y, E, N (4)	Least Squares	Levenberg-Marquardt Algorithm

Table 3-4: Summary of Literature Review of Inverse FE Analyses in Tunnel and Excavation Problems (con't)

Reference	Problem Type Tunnel/Excavation	Constitutive Law	Soil/Rock Parameters (# of parameters)	Identification Criterion	Optimization Method
Calvello and Finno (2004), Finno and Calvello (2005)	Chicago- State Excavation Project	Hardening Soil Model	E_{50}^{ref} (3)	Least Squares	Modified Gauss–Newton Method
Rechea (2006) and Finno & Rechea (2006)	Synthetic Excavation Actual excavations (Ford Center & Lurie Research Center	Mohr-Coulomb & Hardening Soil Model	Synthetic Exc.: E^{ref}, E^{inc} (2) E_{50}^{ref}, E_u^{ref} (2) Actual Exc.: E_{50}^{ref} (2)	Least Squares	Gradient Method
Rechea et al. (2008)	Synthetic Excavation Actual Excavation (Lurie Research Center)	Hardening Soil Model	Synthetic Exc.: E_{50}^{ref}, E_u^{ref} (2) Actual Exc.: E_{50}^{ref} (2)	Least Squares	Gradient Method & Genetic Algorithms
Levasseur (2007); Levasseur et al. (2007) Levasseur et al. (2009)	Actual Excavation and Pressuremeter Test	Mohr-Coulomb	ϕ,G (2); ϕ, G, ψ or K_0 (3)	Least Squares	Genetic Algorithms (GA) & Principal Component Analysis (PCA)
Hashash et al. (2003), Hashash et al. (2006), and Hashash et al. (2010); Osouli and Hashash (2010)	Actual Excavation (Lurie Research Center) Actual Excavations (Texas, Shanghai and Taipei)	Hardening Soil Model (for GA)	E_{50}^{ref} (3) – for GA Extract Soil Behavior (SelfSim)	Least Squares	Genetic Algorithms (GA) & Principal Component Analysis (PCA) SelfSim (ANN)

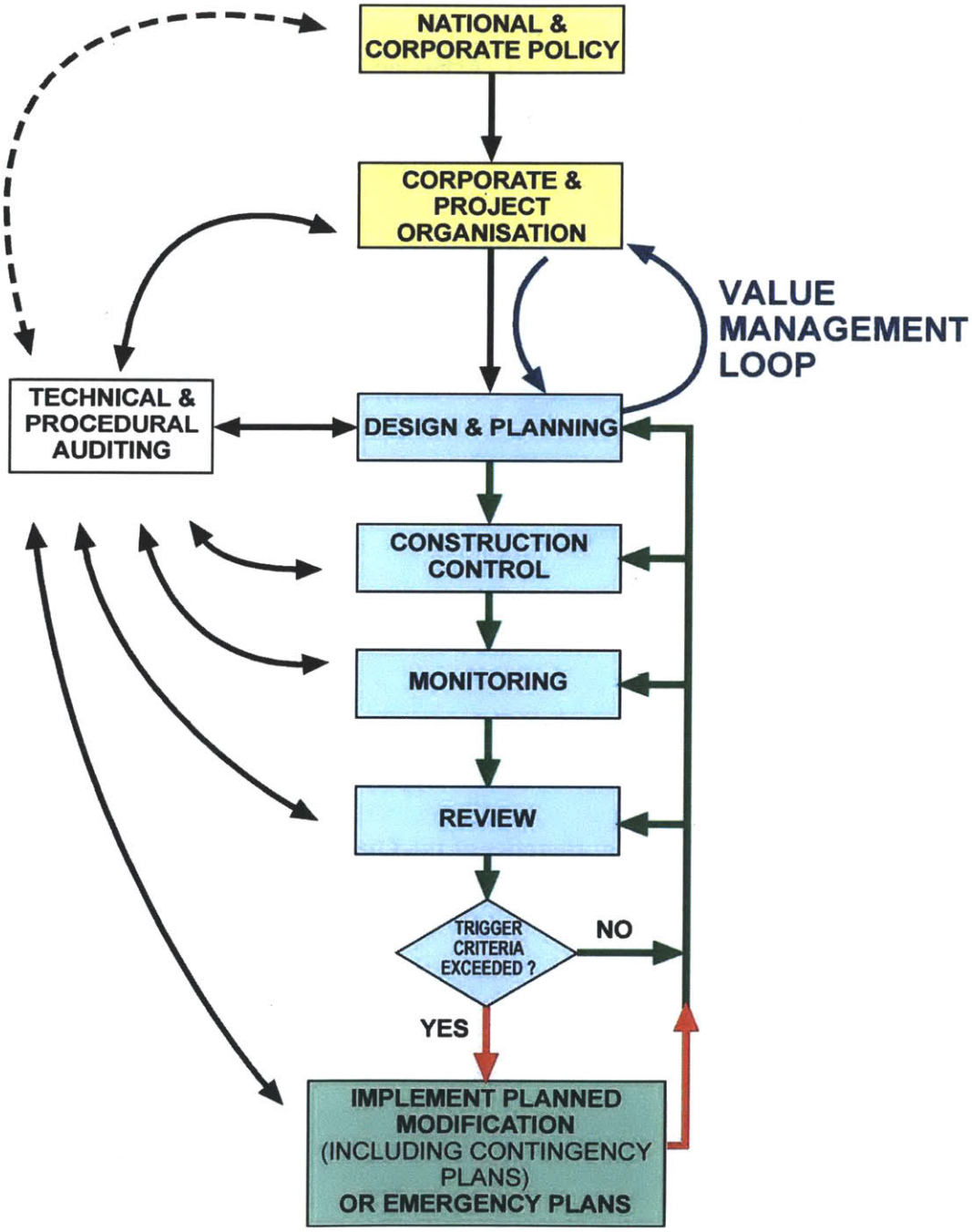

Figure 3-1: The CIRIA Observational Method (Patel et al., 2007)

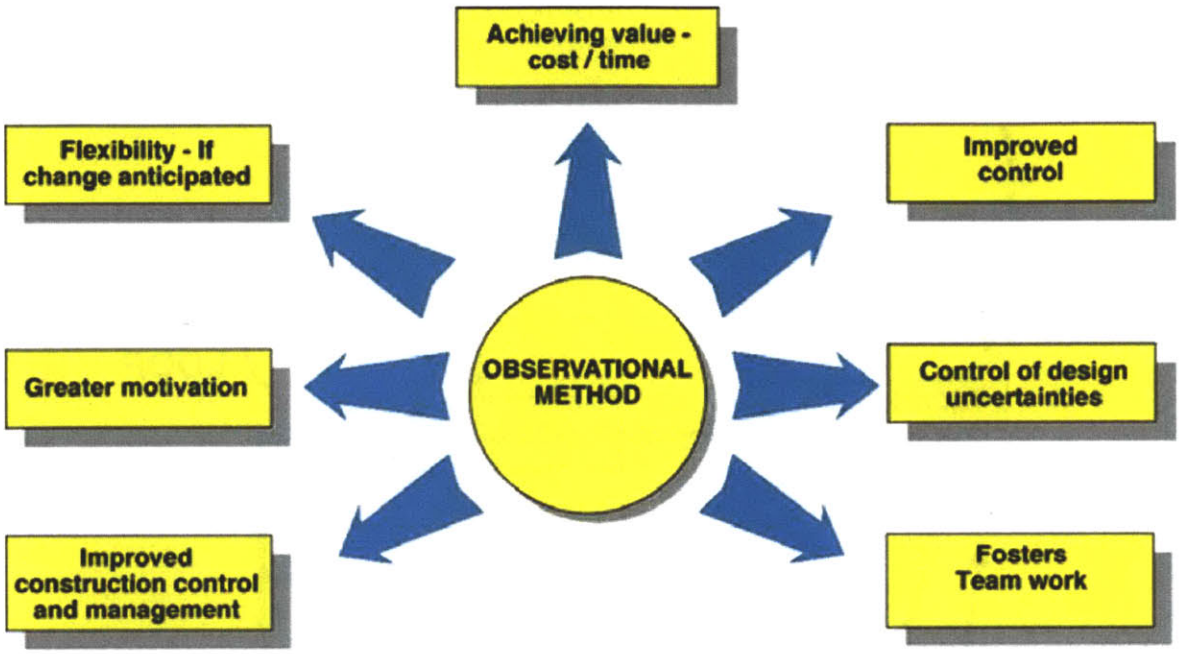

Figure 3-2: Some Potential Benefits of the Observational Method (Patel et al. 1996)

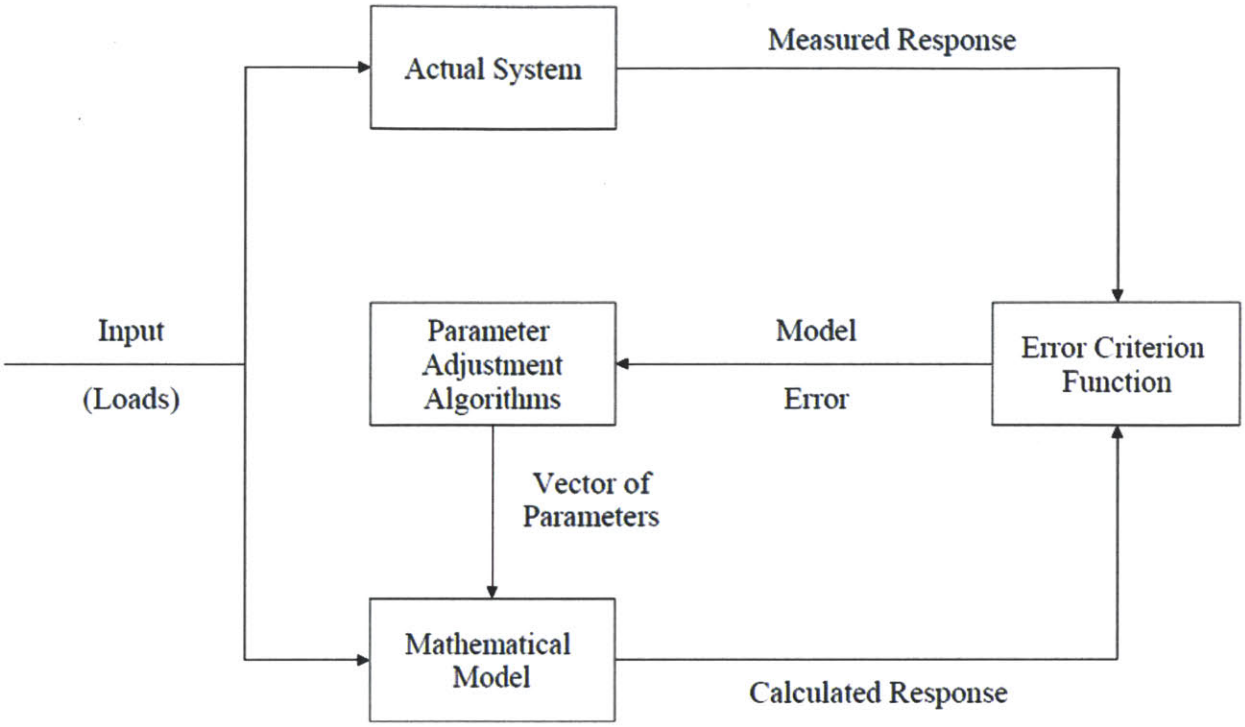

Figure 3-3: Illustrative Scheme of Parametric Estimation (after Jurina et al. 1977)

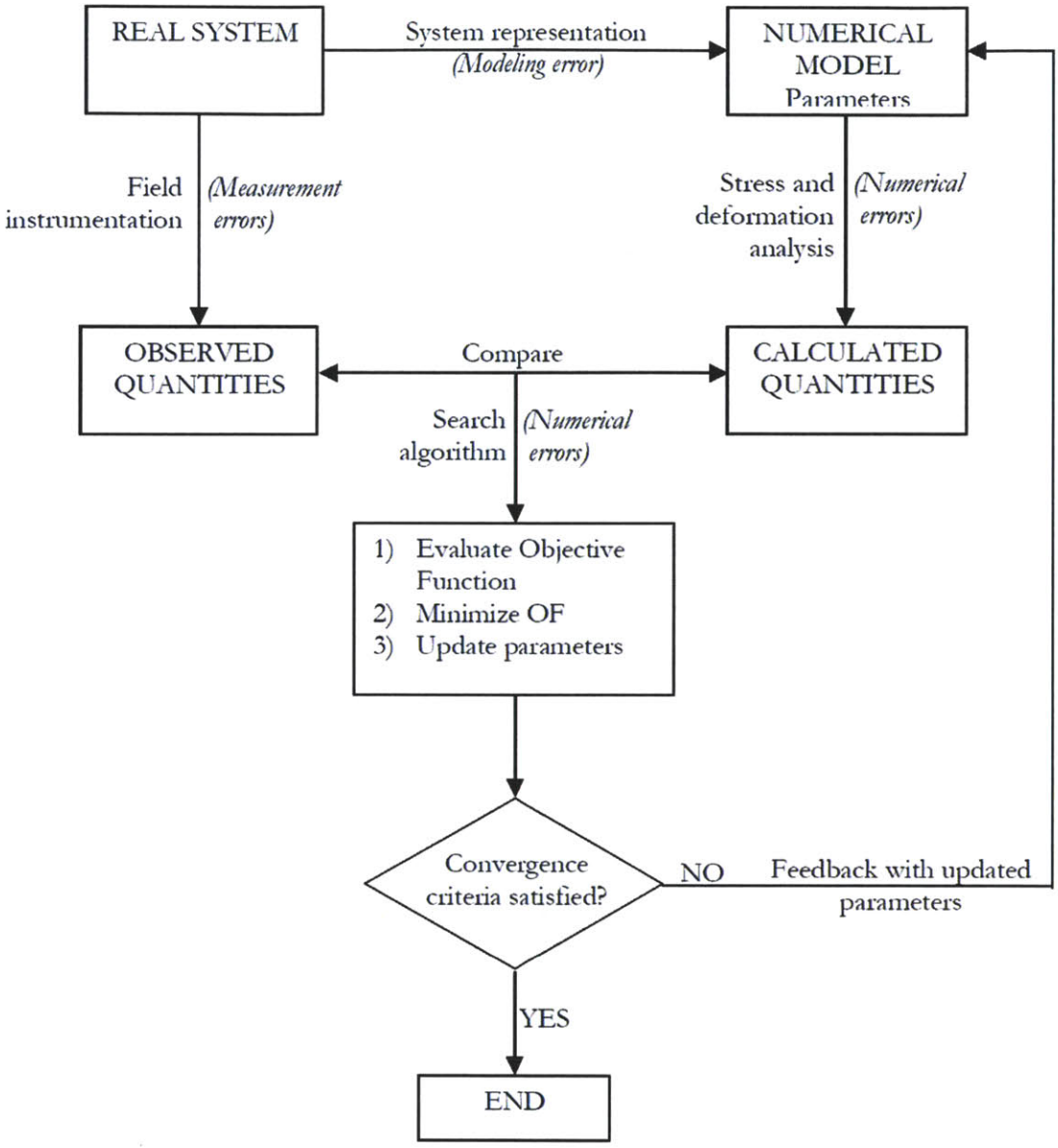

Figure 3-4: Flowchart of the Inverse Problem (Rechea, 2006)

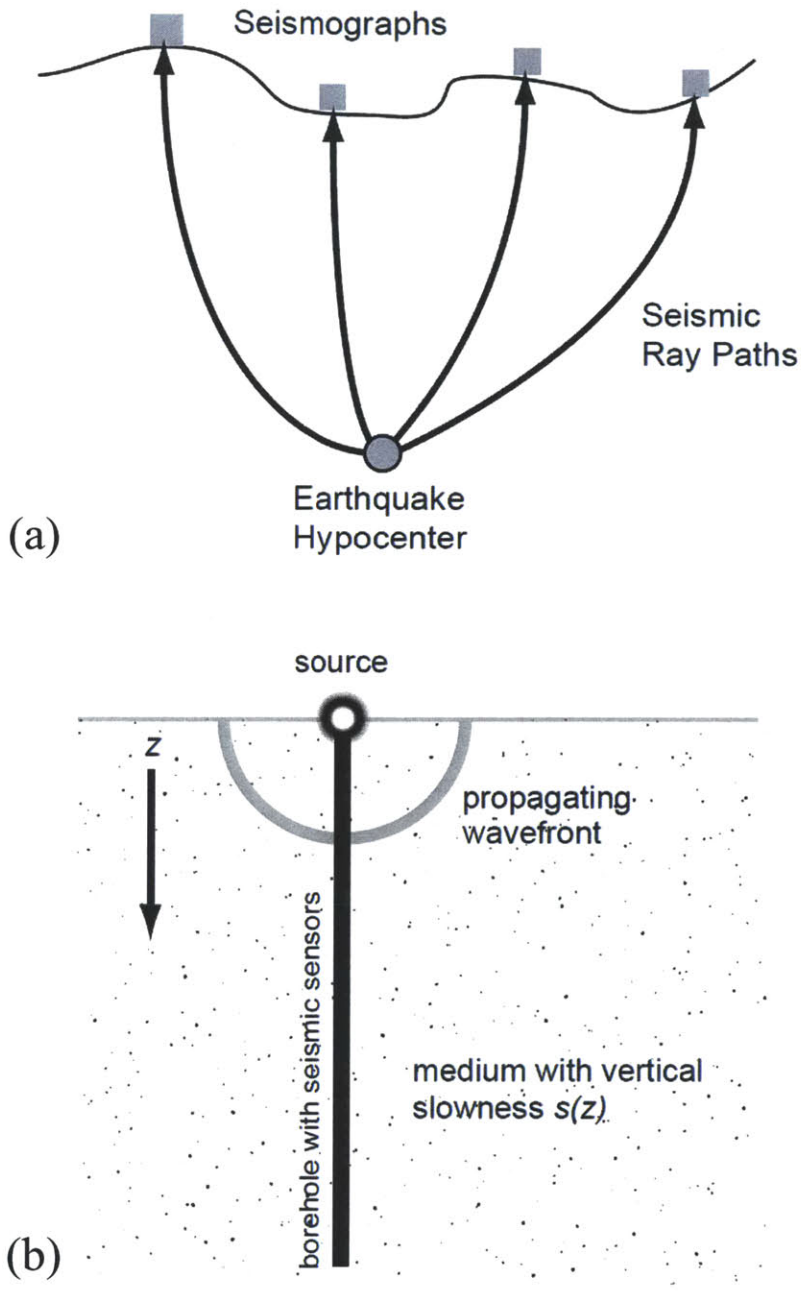

Figure 3-5: Inverse Problem Examples: (a) Determination of an Earthquake Hypocenter, (b) Determination of Wave Velocities or Material Properties (Aster et al., 2005)

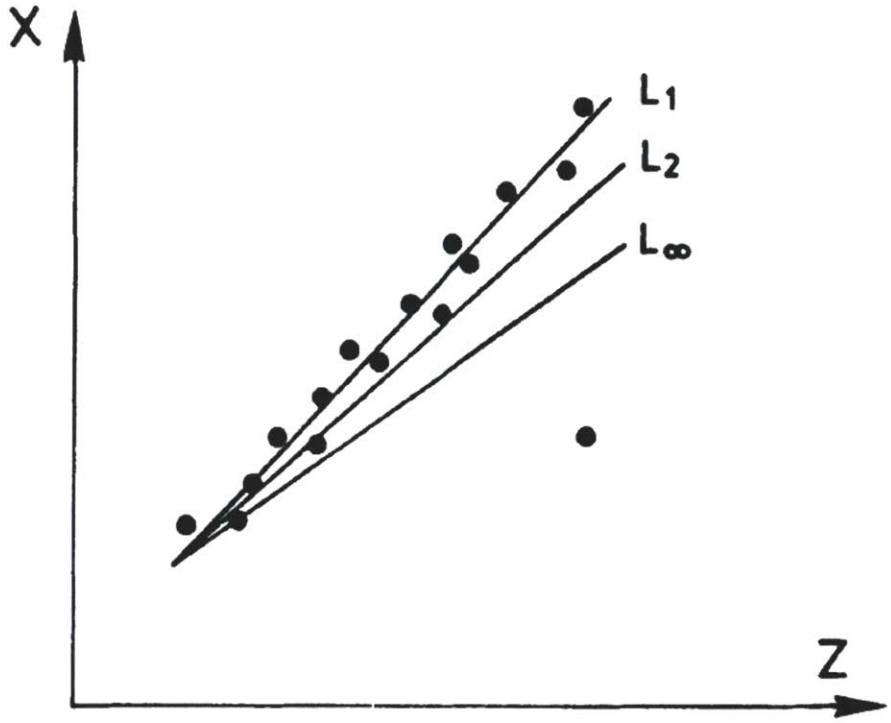

Figure 3-6: Illustrative Example of Residual Norms L_1, L_2, and L_∞ (Ledesma, 1987)

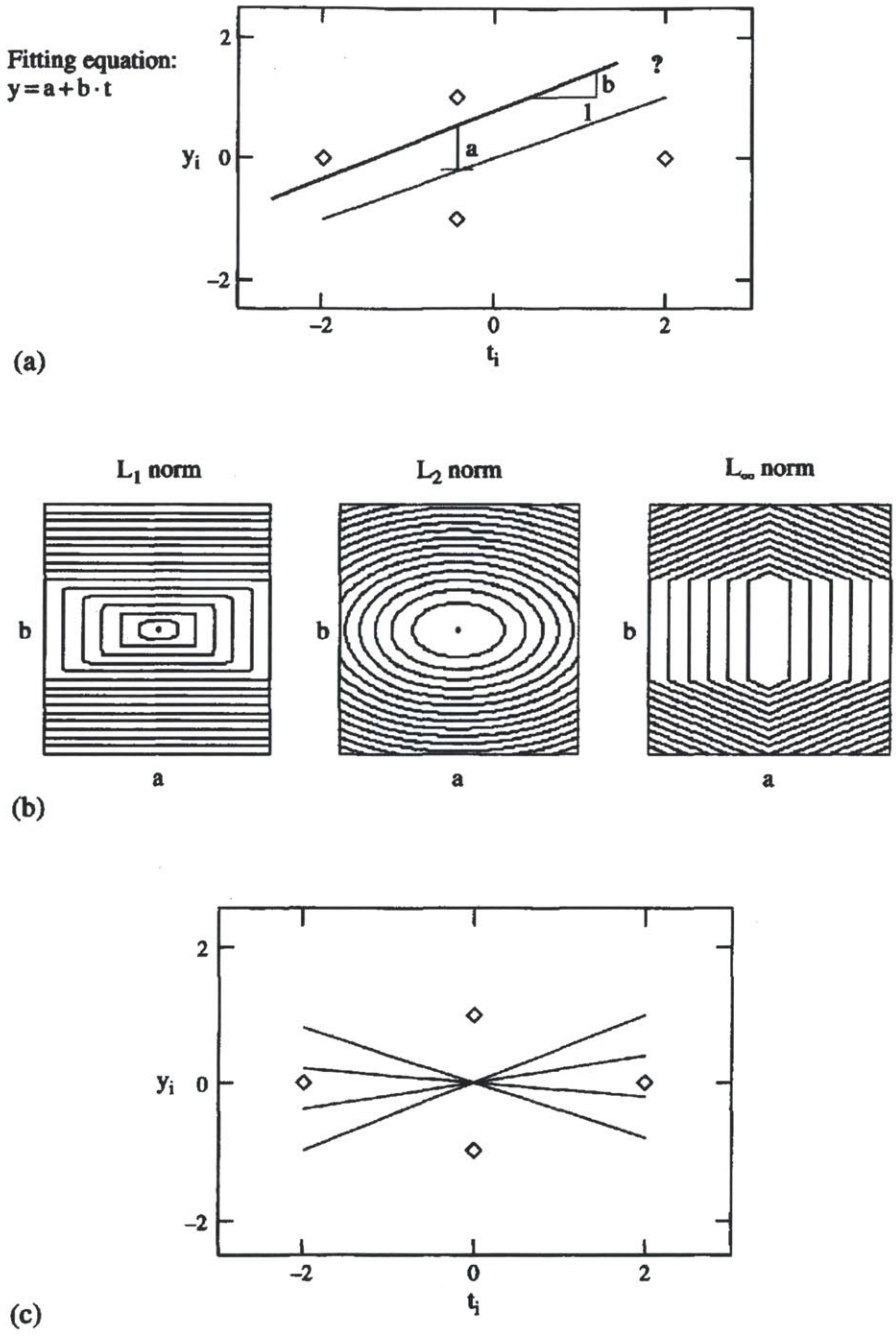

Figure 3-7: Illustrative Example of (a) four data points to be fitted with a straight line; (b) contours of residual surfaces; and (c) different lines with same minimum value in L_∞ (Santamarina and Fratta, 2005)

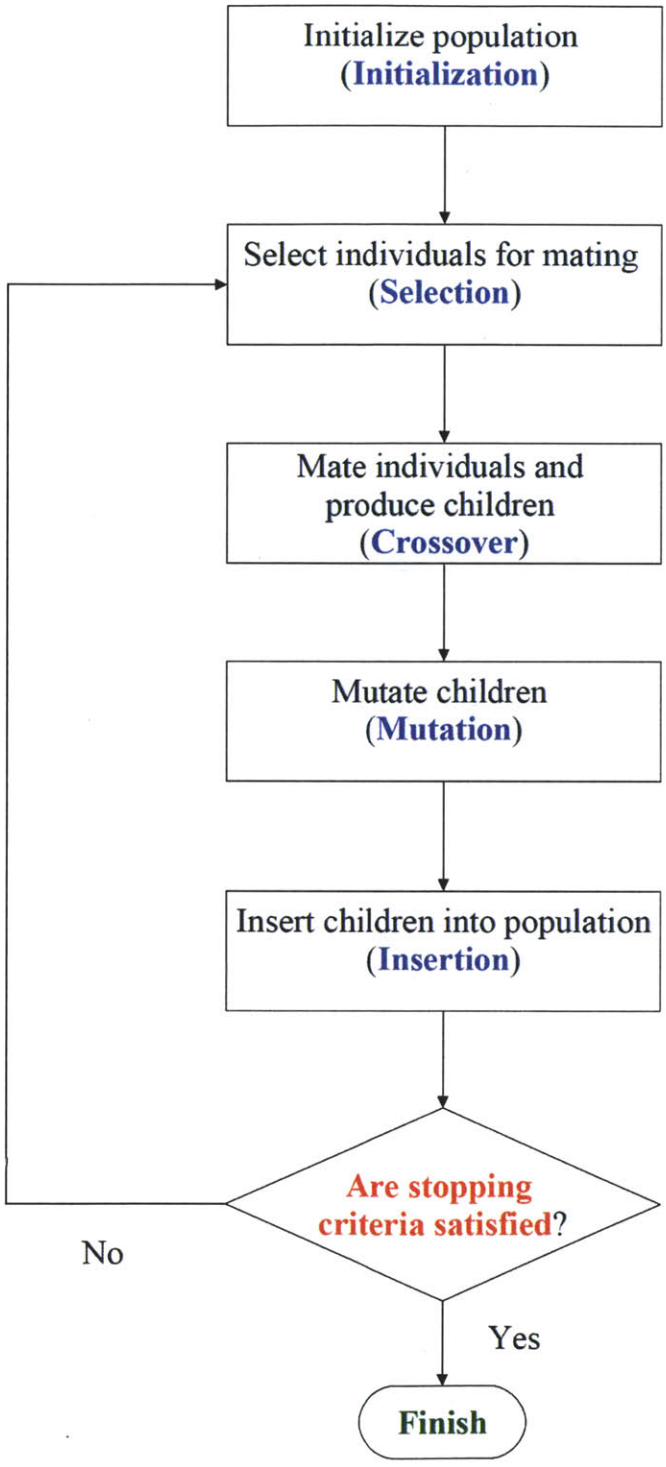

Figure 3-8: Typical Genetic Algorithm Flowchart (after Goldberg, 1989; after Michalewicz, 2011)

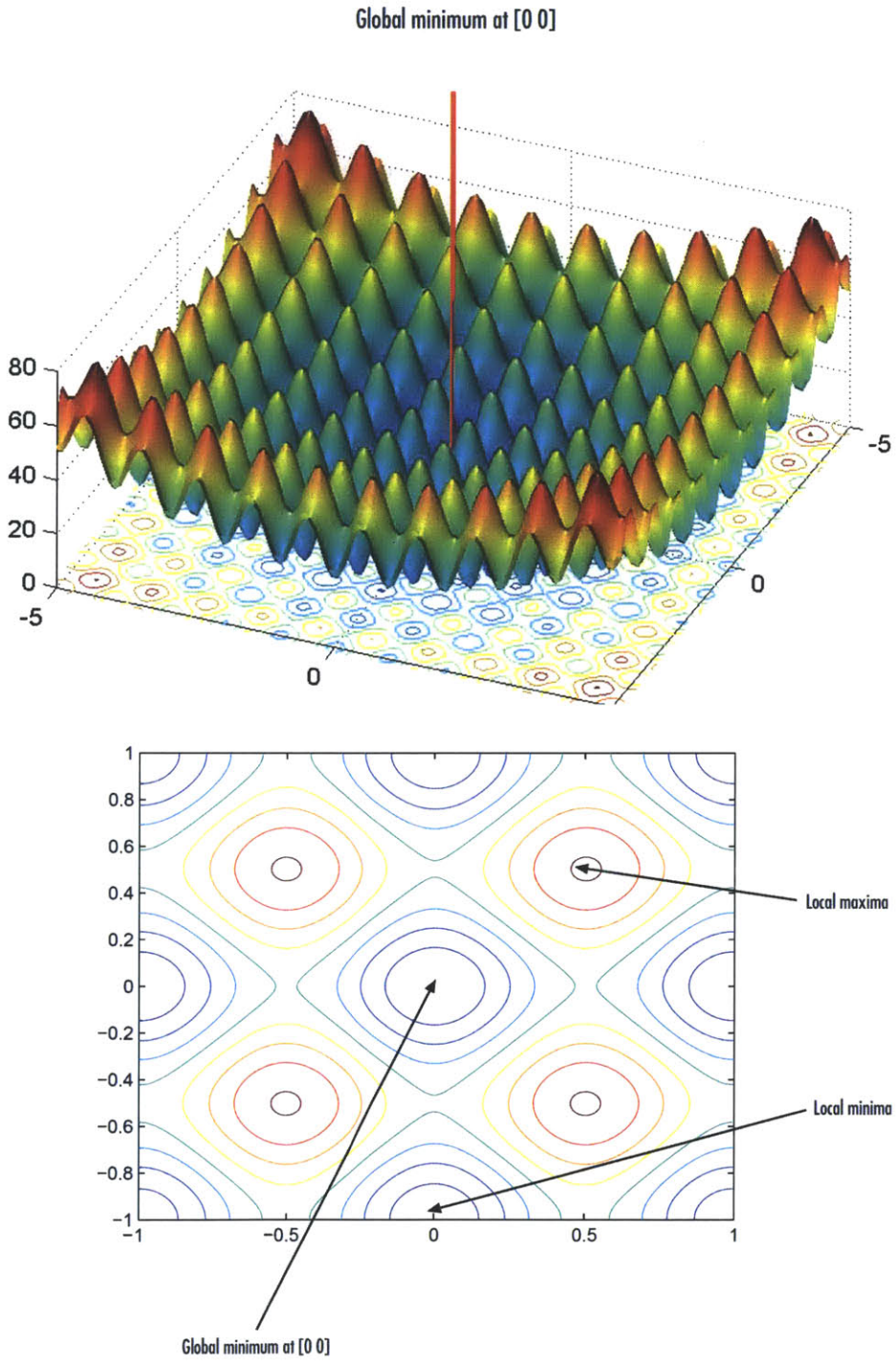

Figure 3-9: Example of Rastrigin's function which has many local minima (after MATLAB, 2004-2009)

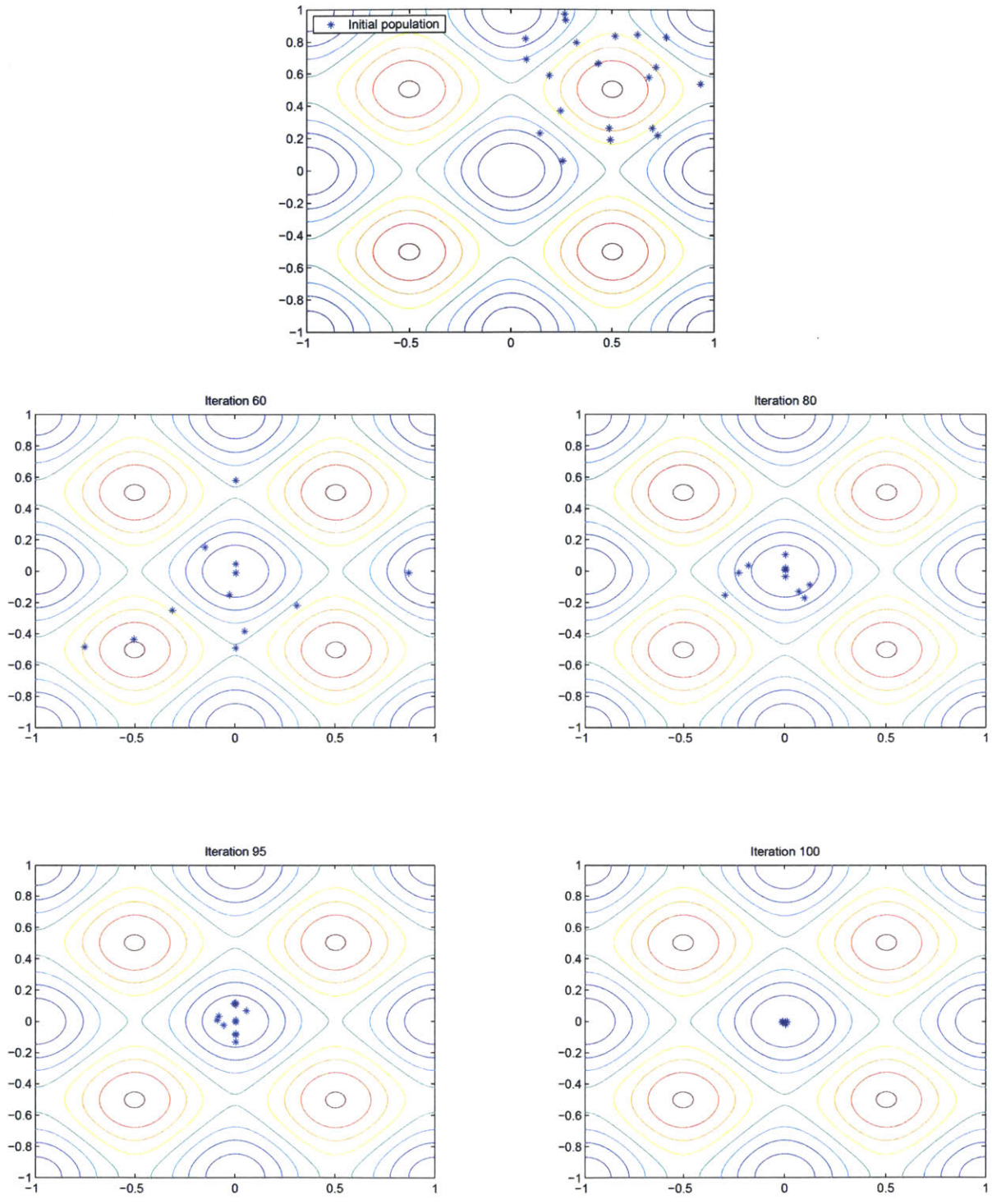

Figure 3-10: Genetic Algorithm capabilities to find global minimum of the Rastrigin's function (after MATLAB, 2004-2009)

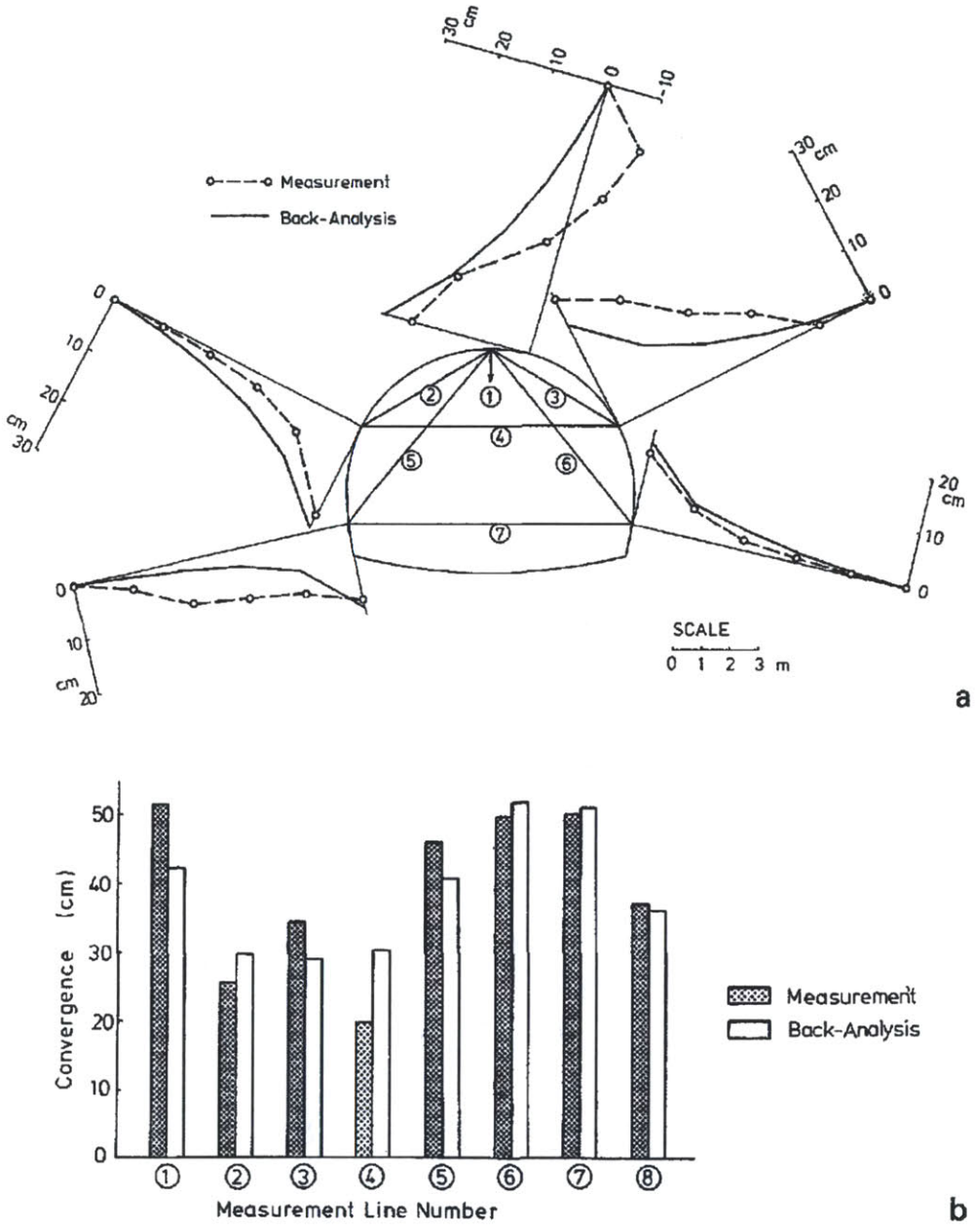

Figure 3-11: Comparison between measurements and updated predictions: (a) Extensometer measurements, and (b) Convergence measurements (Sakurai and Takeuchi, 1983)

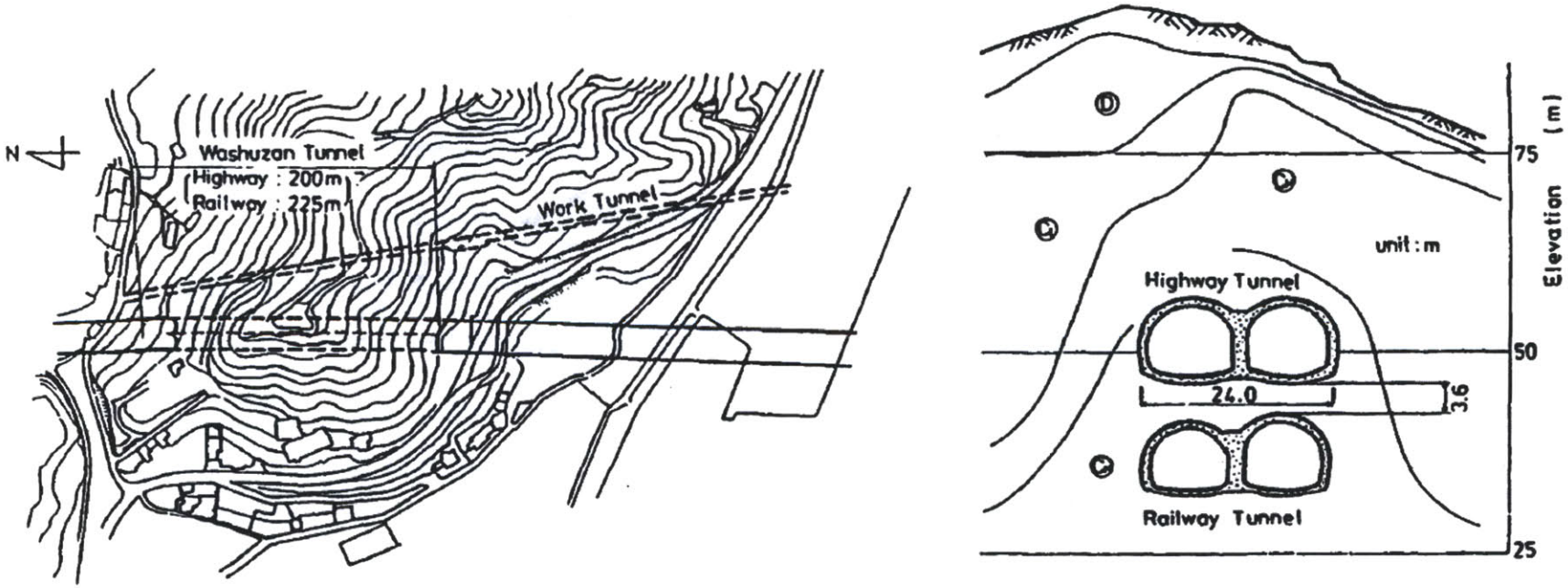

Figure 3-12: Plan view of tunnel construction site and tunnel cross-section (Gioda and Sakurai, 1987)

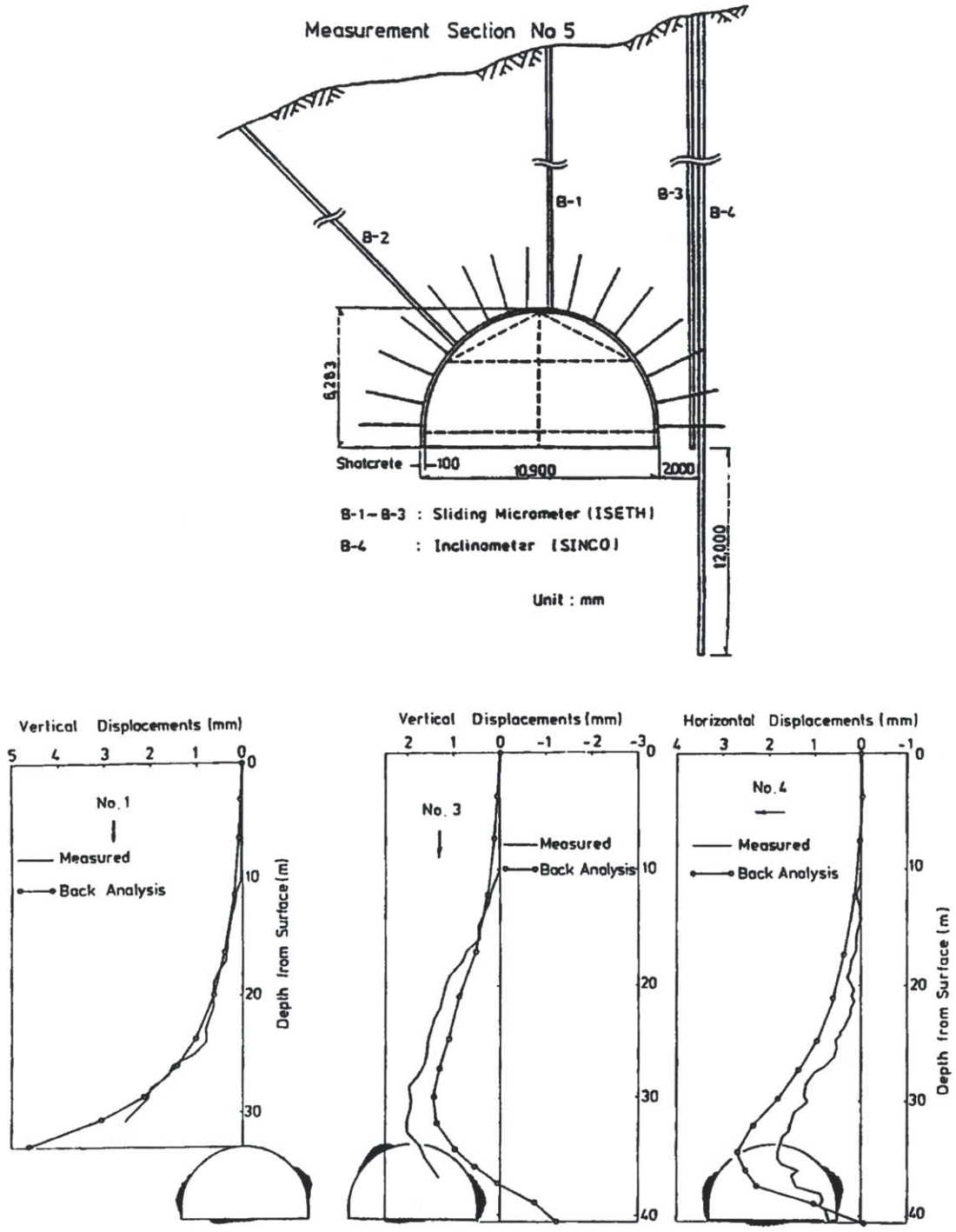

Figure 3-13: (a) Positions of the boreholes for inclinometers and micrometers (B1..B4) and the directions of the convergence measurements; (b) Comparison of back analyzed displacements with measured values (Gioda and Sakuria, 1987)

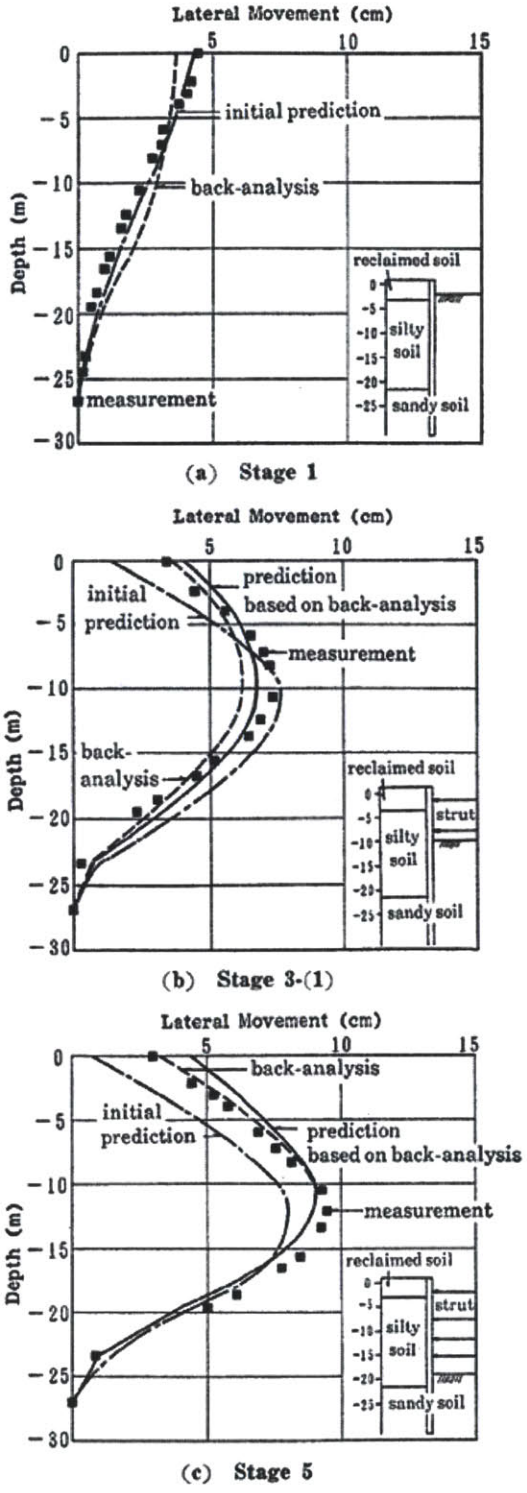

Figure 3-14: Calculated and measured lateral movements in the retaining wall structure (Shoji et al. 1990)

(a)

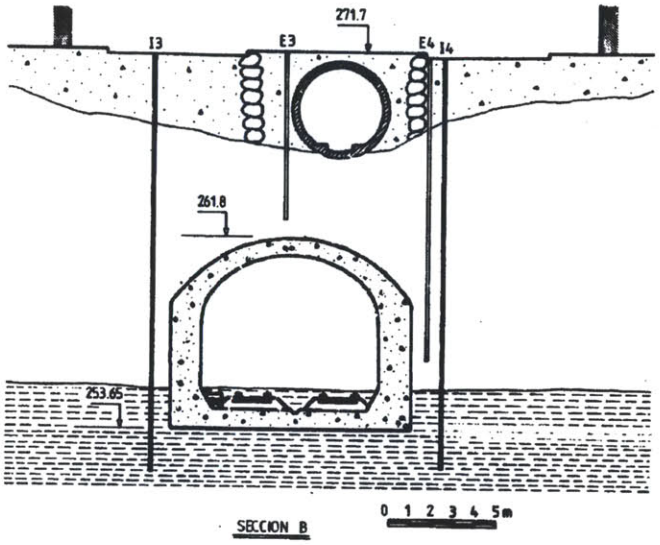

(b)

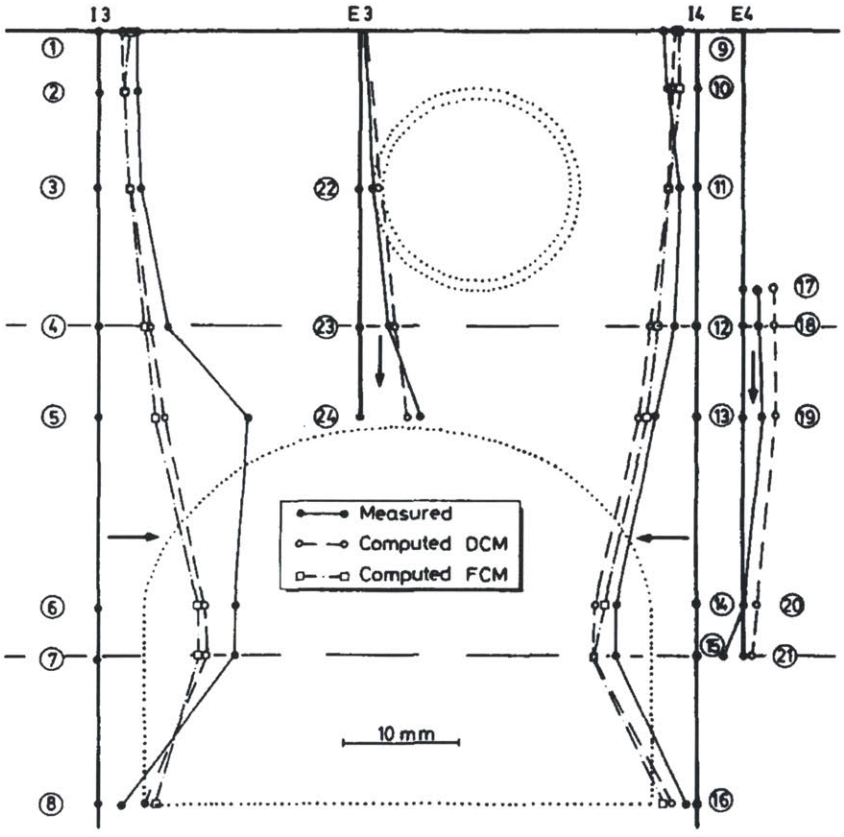

Figure 3-15: (a) Soil profile and instrumentation of tunnel section B (Ledesma, 1987); (b) Comparison of measured and computed displacements in section B using Least Squares: DCM and Maximum Likelihood approach: FCM (Gens at al., 1986)

(a)

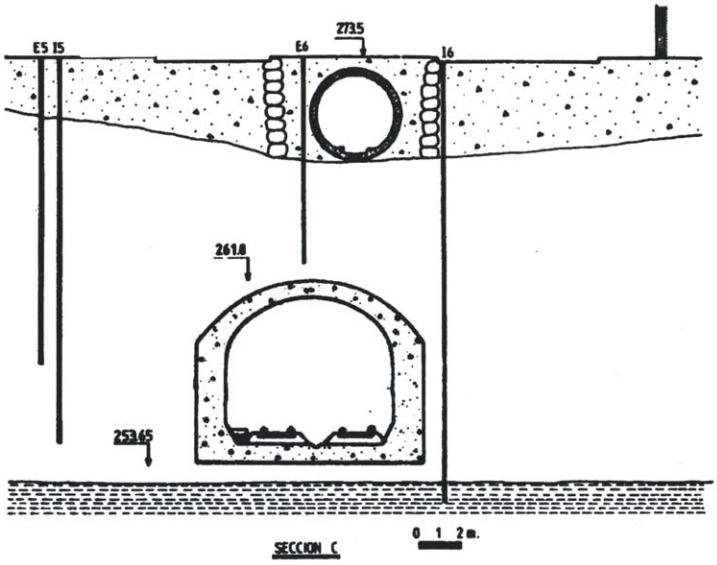

(b)

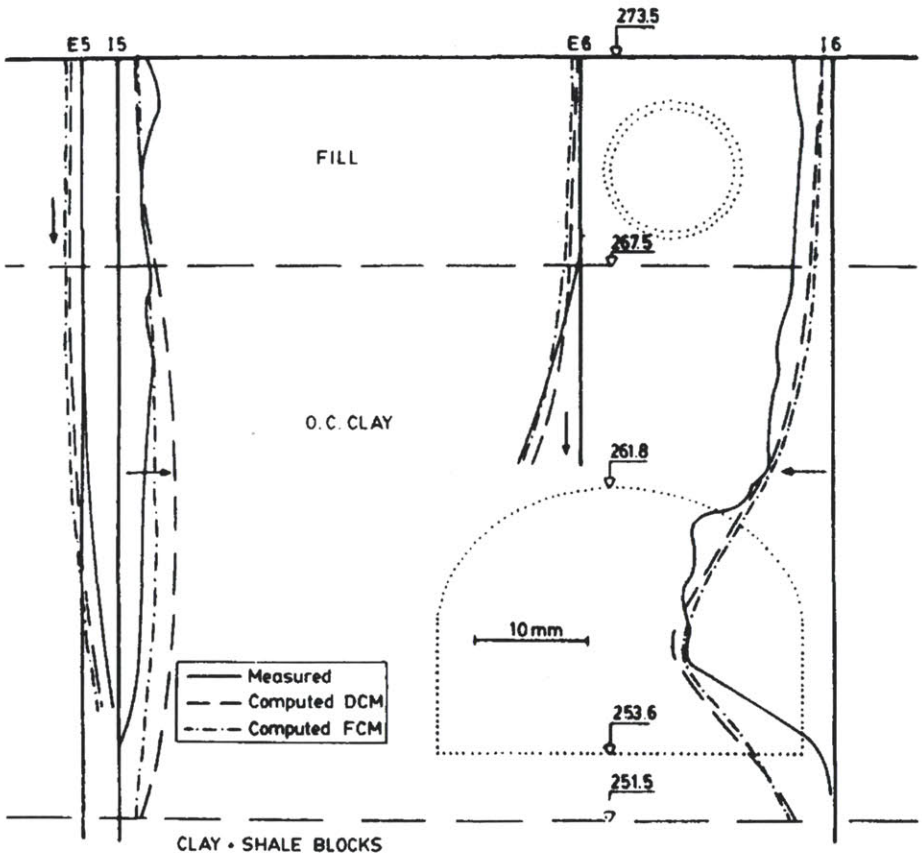

Figure 3-16: (a) Soil profile and instrumentation of tunnel section C (Ledesma, 1987); (b) Comparison of measured and computed displacements in section C using Least Squares: DCM and Maximum Likelihood approach: FCM (Gens at al., 1986)

(a)

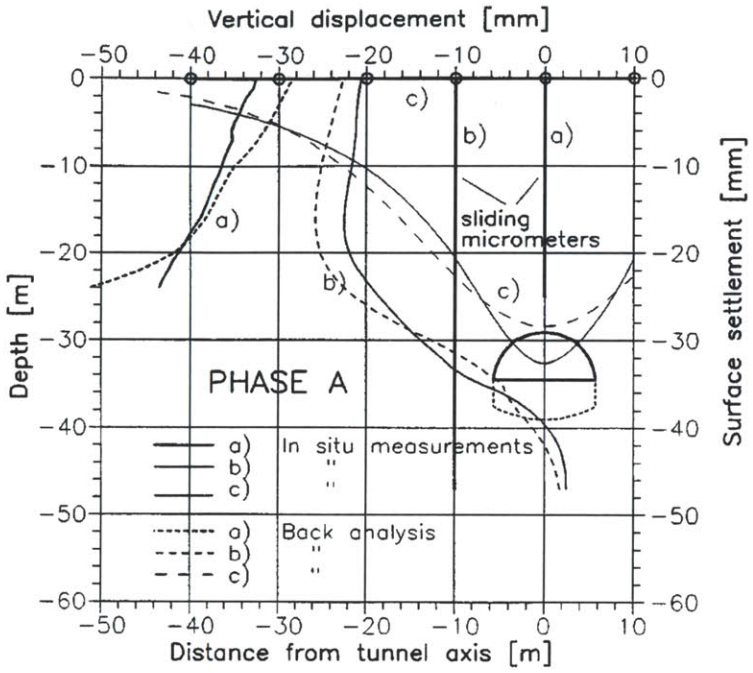

(b)

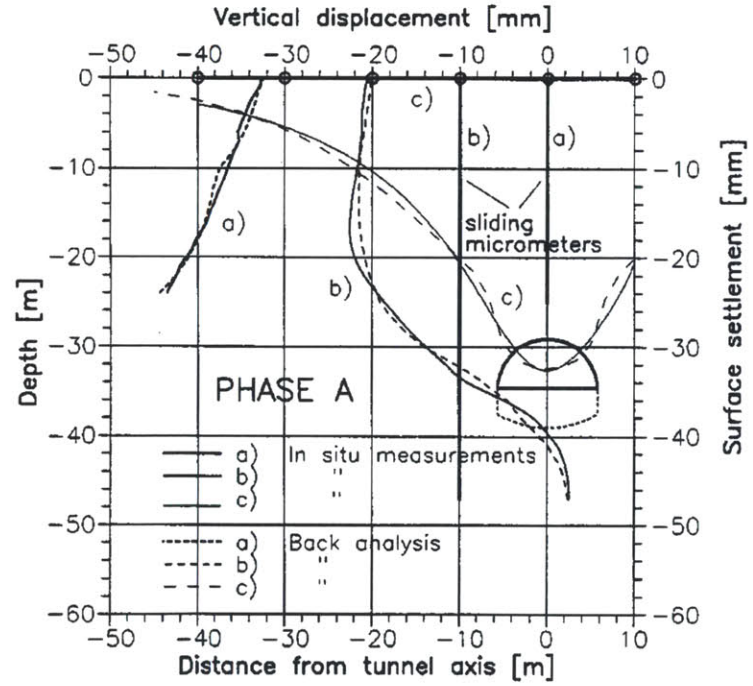

Figure 3-17: Comparison of measurements and backanalyzed predictions of upper part of excavation of a tunnel simulation corresponding to: (a) initial FE mesh, and (b) modified FE mesh (Gioda and Locatelli, 1999)

(a)

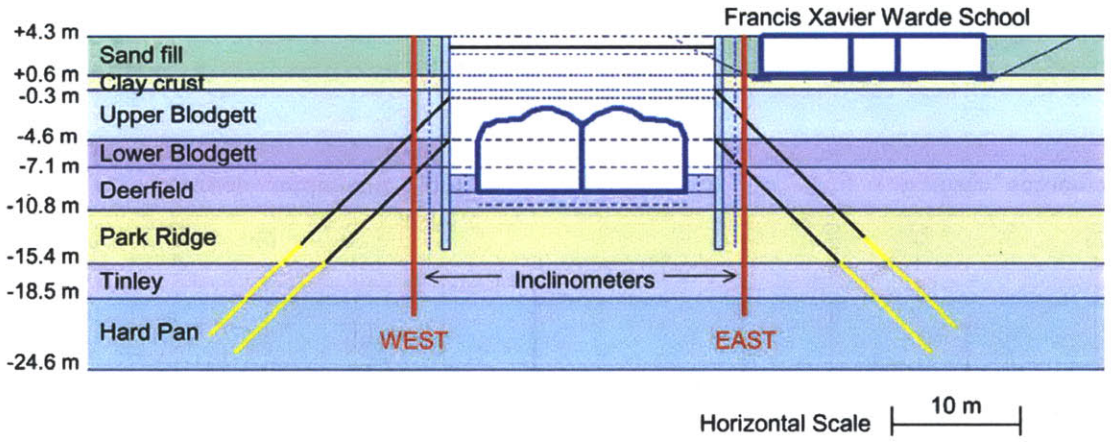

(b)

	Calculation phase	Construction stage
	0	Initial conditions
	1 to 4	Tunnel construction (1940)
	5	Consolidation stage
	6 to 10	School construction (1960)
	11	Consolidation stage
Wall	12	Reset displacements
installation	13	Drill secant pile wall (1999)
	14	Pour concrete in piles—Stage 1
	15	Consolidation stage (20 days)
Excavation	16	Excavate (+2.75 m) and install strut—Stage 2
	17	Excavate (−0.9 m)
	18	Prestress first tiebacks—Stage 3
	19	Excavate (−4.6 m)
	20	Prestress second tiebacks—Stage 4
	21	Excavate (−7.9 m)—Stage 5

Figure 3-18: Chicago-State case study: (a) Schematic section view of excavation support system (Calvello and Finno, 2004) (b) Construction sequences considered in finite element analysis (Finno and Calvello, 2005)

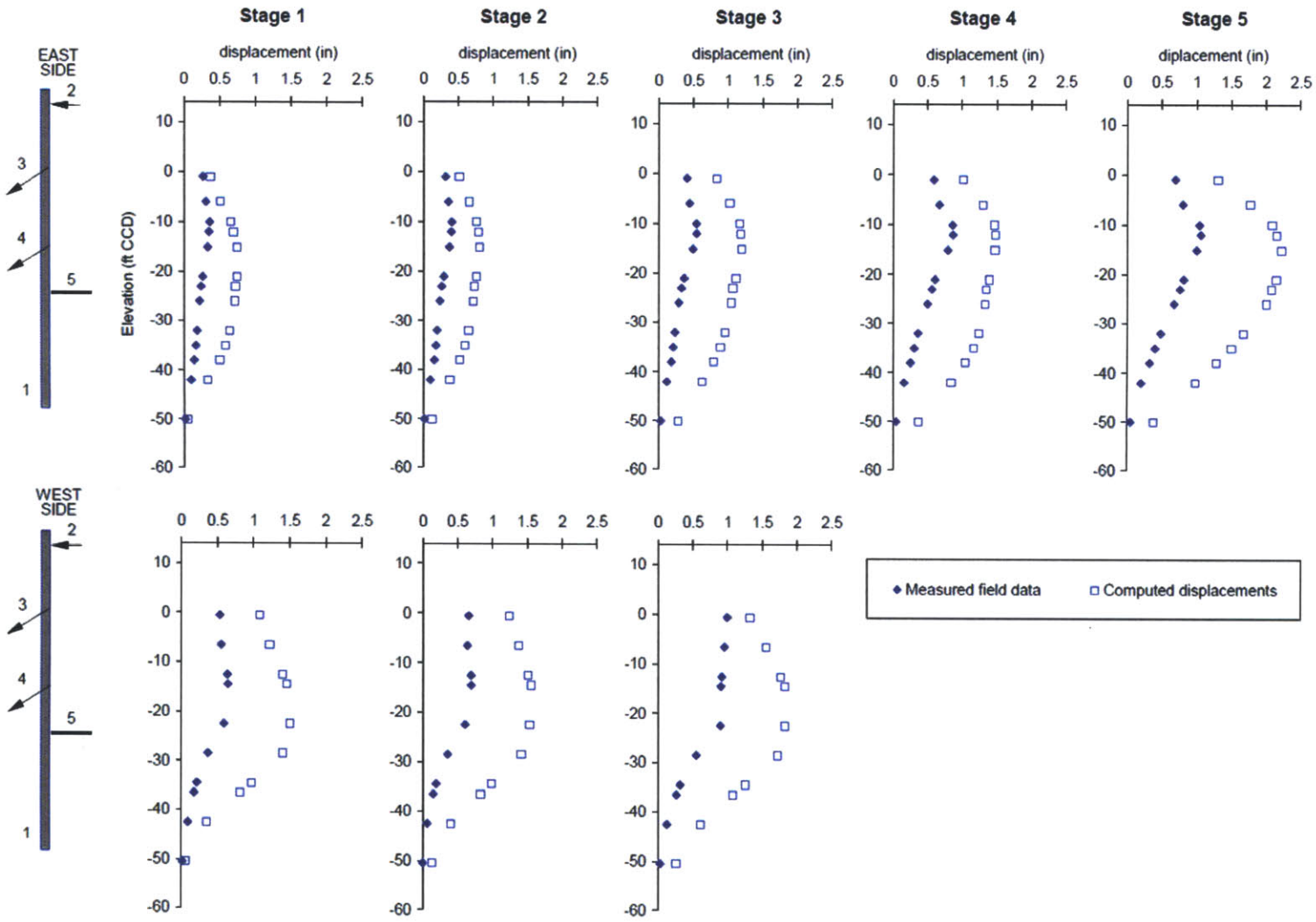

Figure 3-19: Measurements and initial predictions of horizontal wall displacements (Finno and Calvello, 2005)

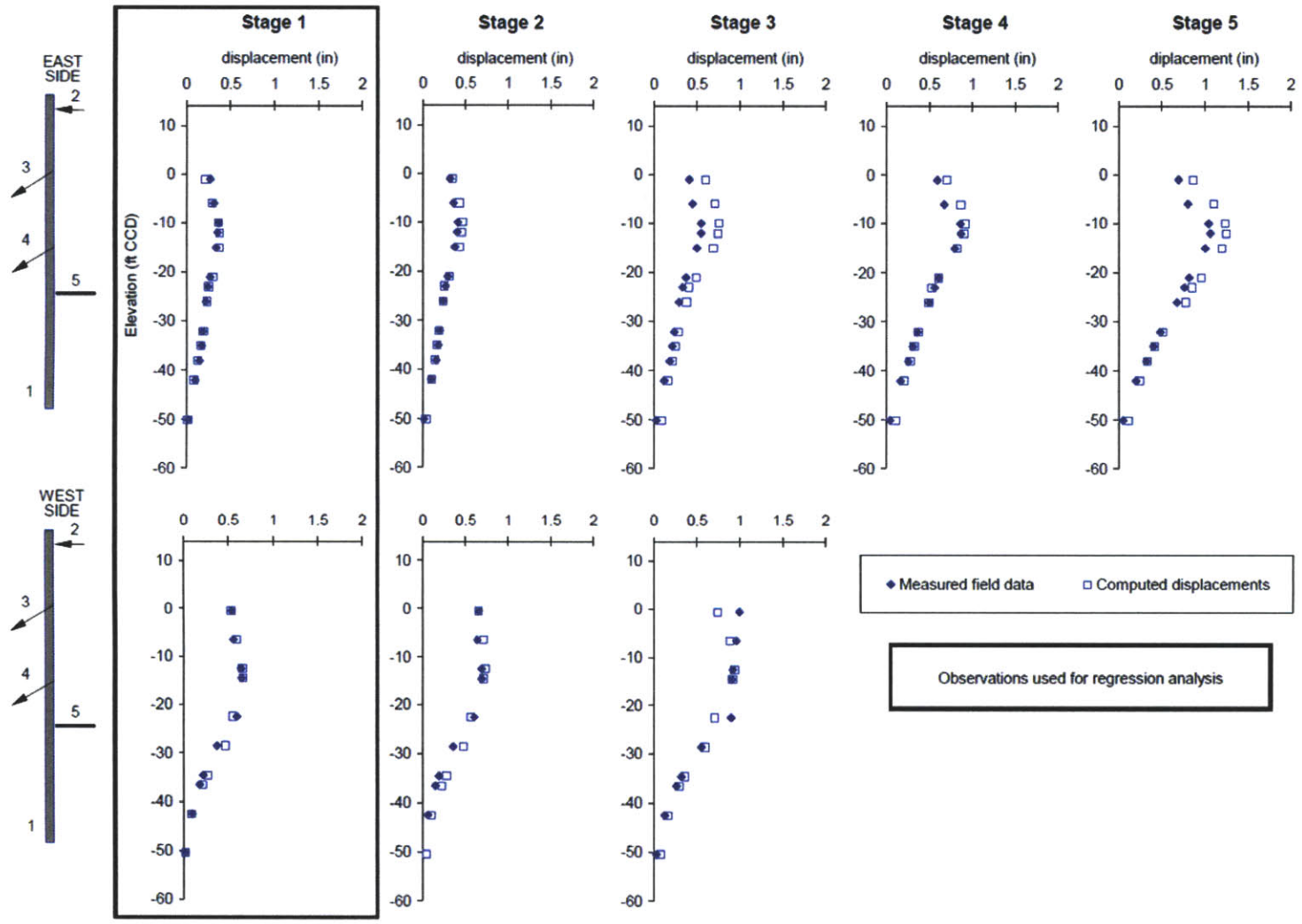

Figure 3-20: Measurements versus updated predictions (updated after stage 1) of horizontal wall displacements (Finno and Calvello, 2005)

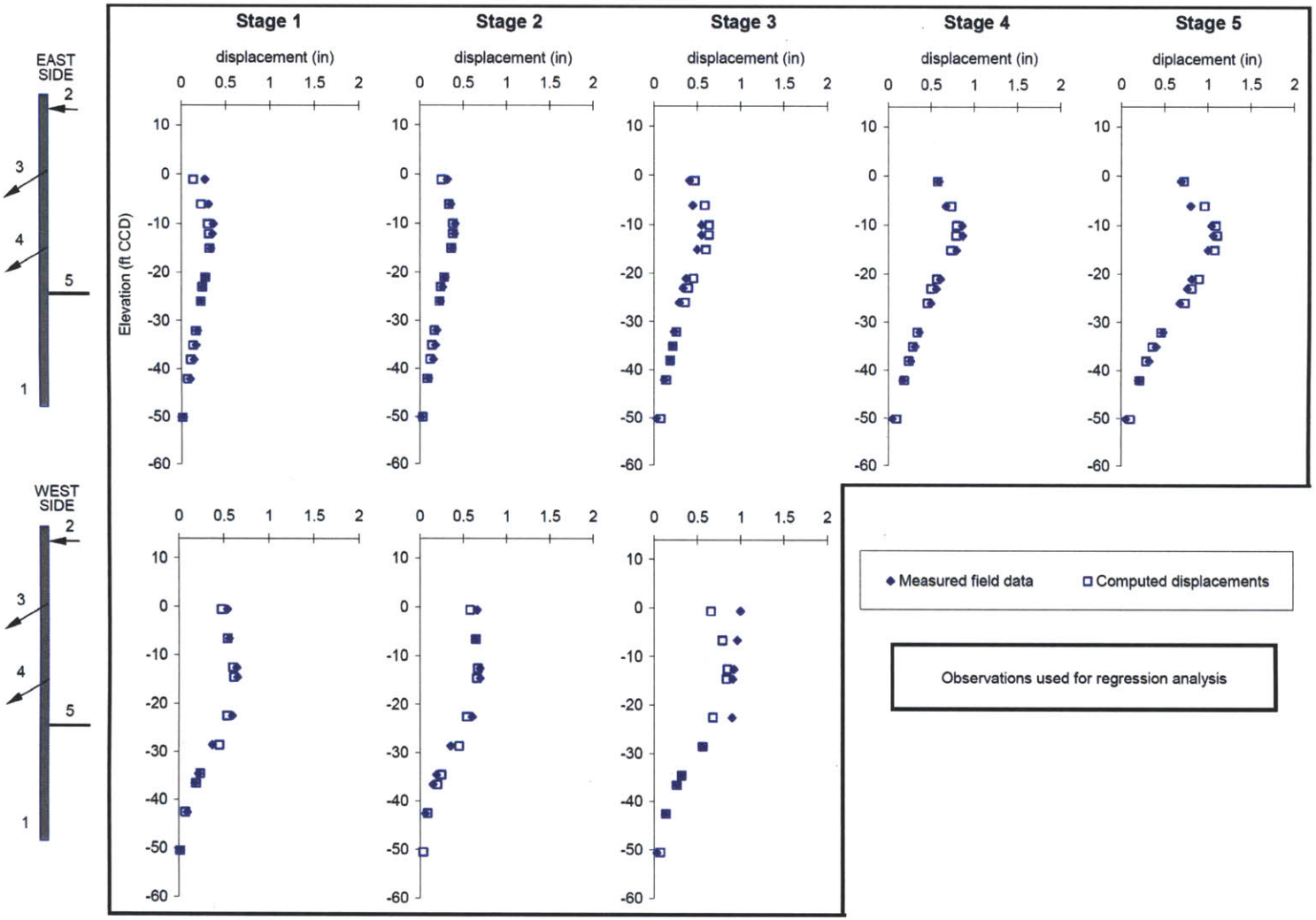

Figure 3-21: Measurements versus updated predictions (updated using data from all stages) of horizontal wall displacements (Finno and Calvello, 2005)

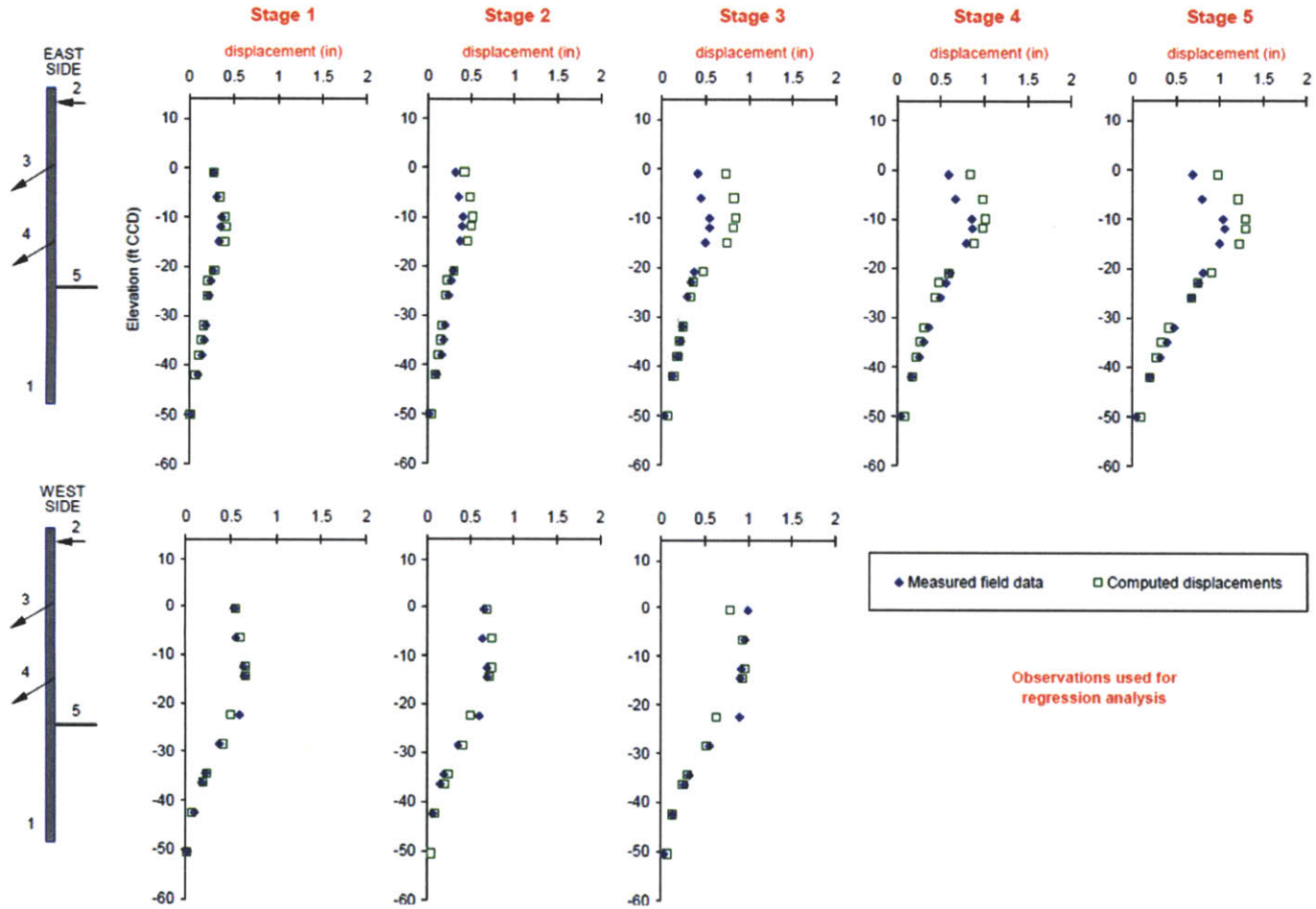

Figure 3-22a: Measurements versus updated predictions for all stages using horizontal wall displacements (Calvello, 2002)

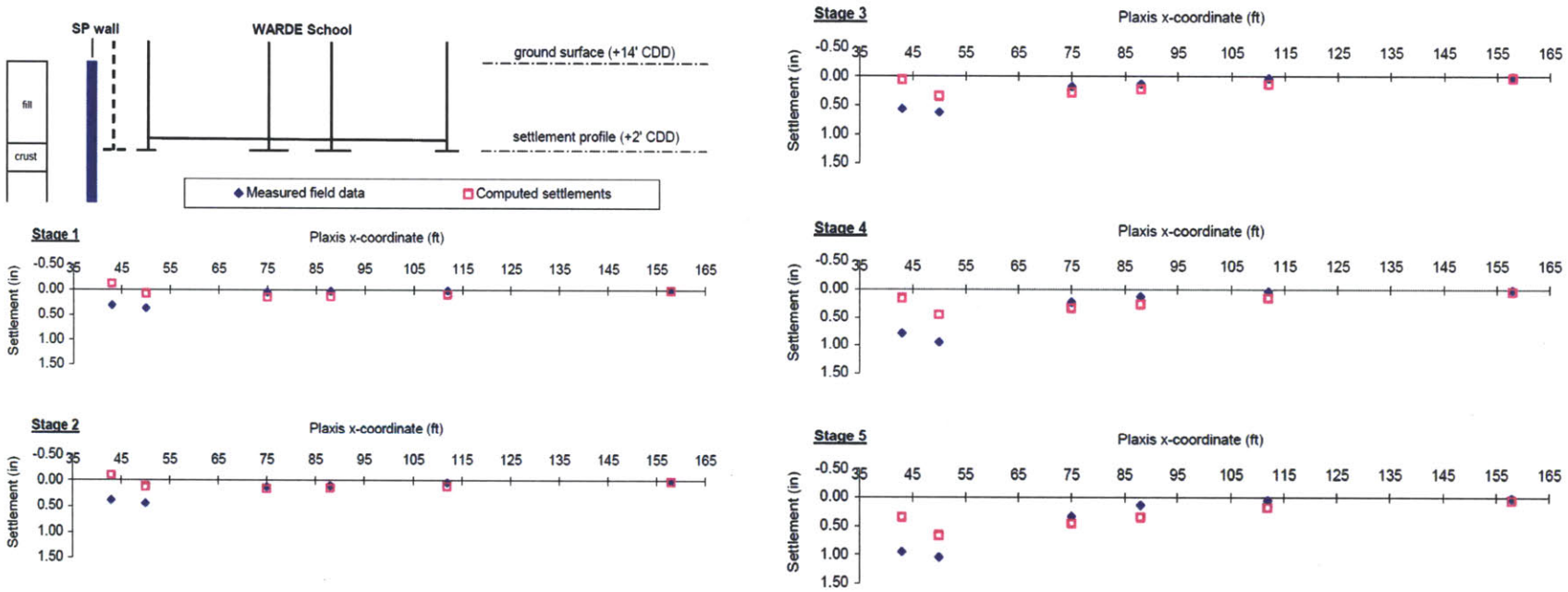

Figure 3-22b: Measurements versus updated predictions for all stages using vertical settlements (Calvello, 2002)

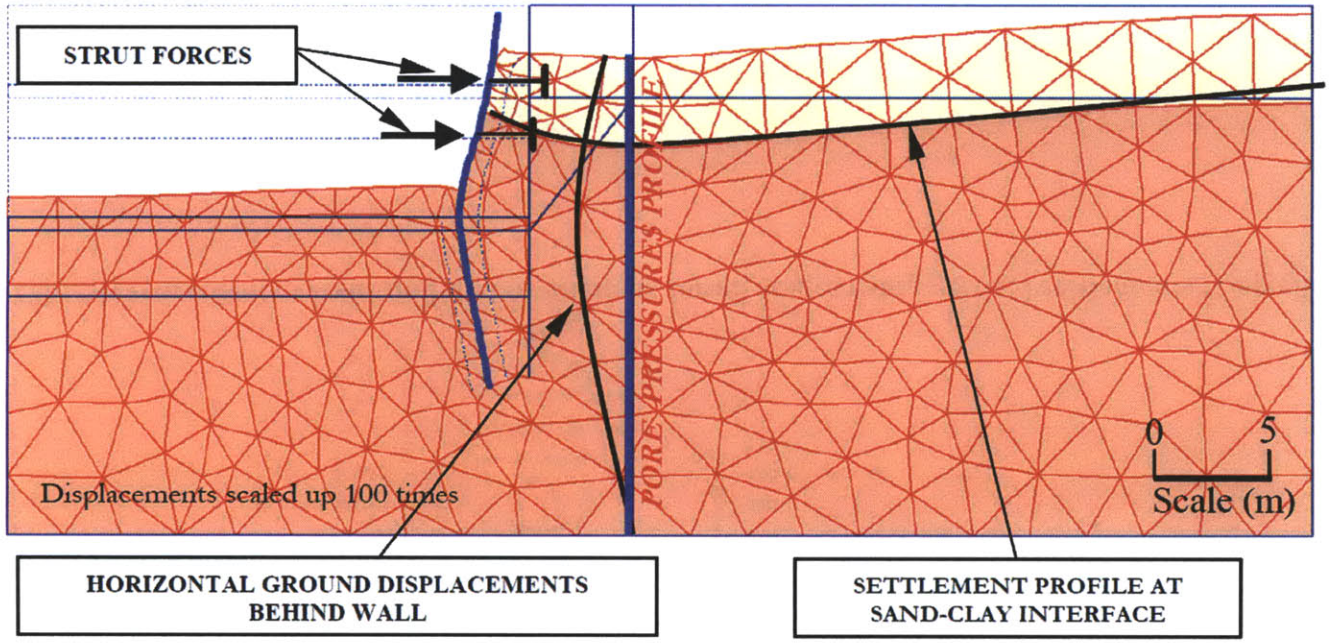

Figure 3-23: Location of synthetic field observations (Rechea, 2006)

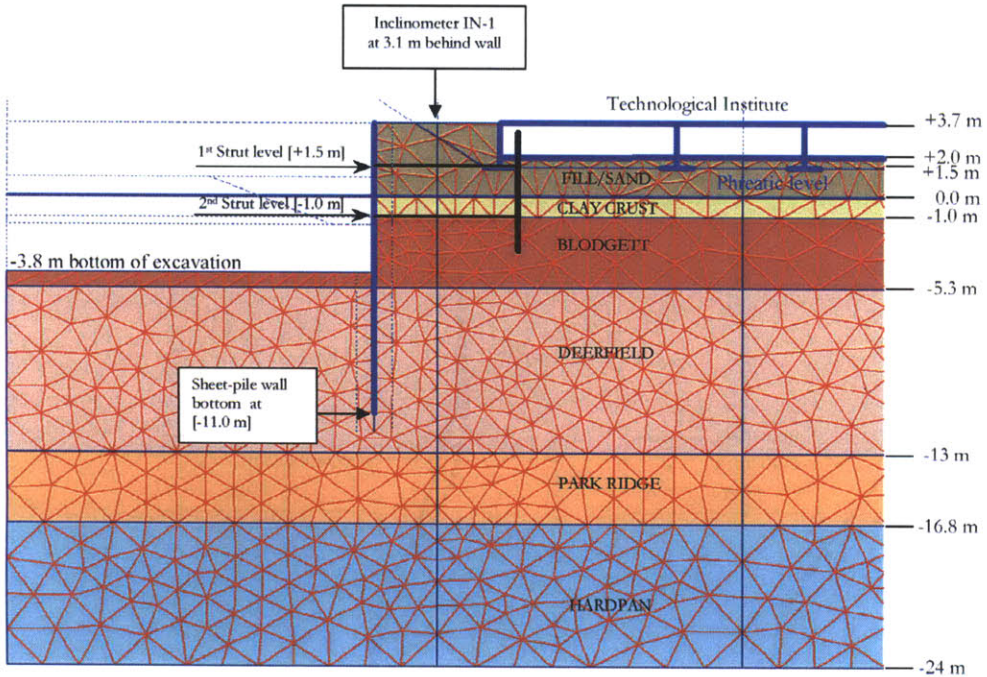

(a)

PLAXIS phase #	Description
0	Geostatic conditions
1	Reset displacements to zero at beginning of calculations Excavate for Tech building
2	Built structure of Tech
3	Apply loads of Tech on foundations
4	Consolidate for 60 years
5	Reset displacements to zero at beginning of calculations Level Ford site [+3.7 m ECD]
6	Install sheet pile wall
7	Reset displacements to zero at beginning of calculations Excavate [+1 m ECD]
8	Install upper strut level at [+1.5 m ECD]
9	Excavate berm close to wall to [-1.5 m ECD] Remove soil and water inside excavation. Keep general phreatic level to ensure undrained conditions
10	Remove berm completely and Install lower strut level at [-1.0 m ECD] Remove soil and water inside excavation. Keep general phreatic level to ensure undrained conditions
11	End excavation [-3.8 m ECD] Remove soil and water inside excavation. Keep general phreatic level to ensure undrained conditions

(b)

Figure 3-24: Ford Center: (a) finite element model for the North side, and (b) FE simulation of construction sequences (after Rechea, 2006)

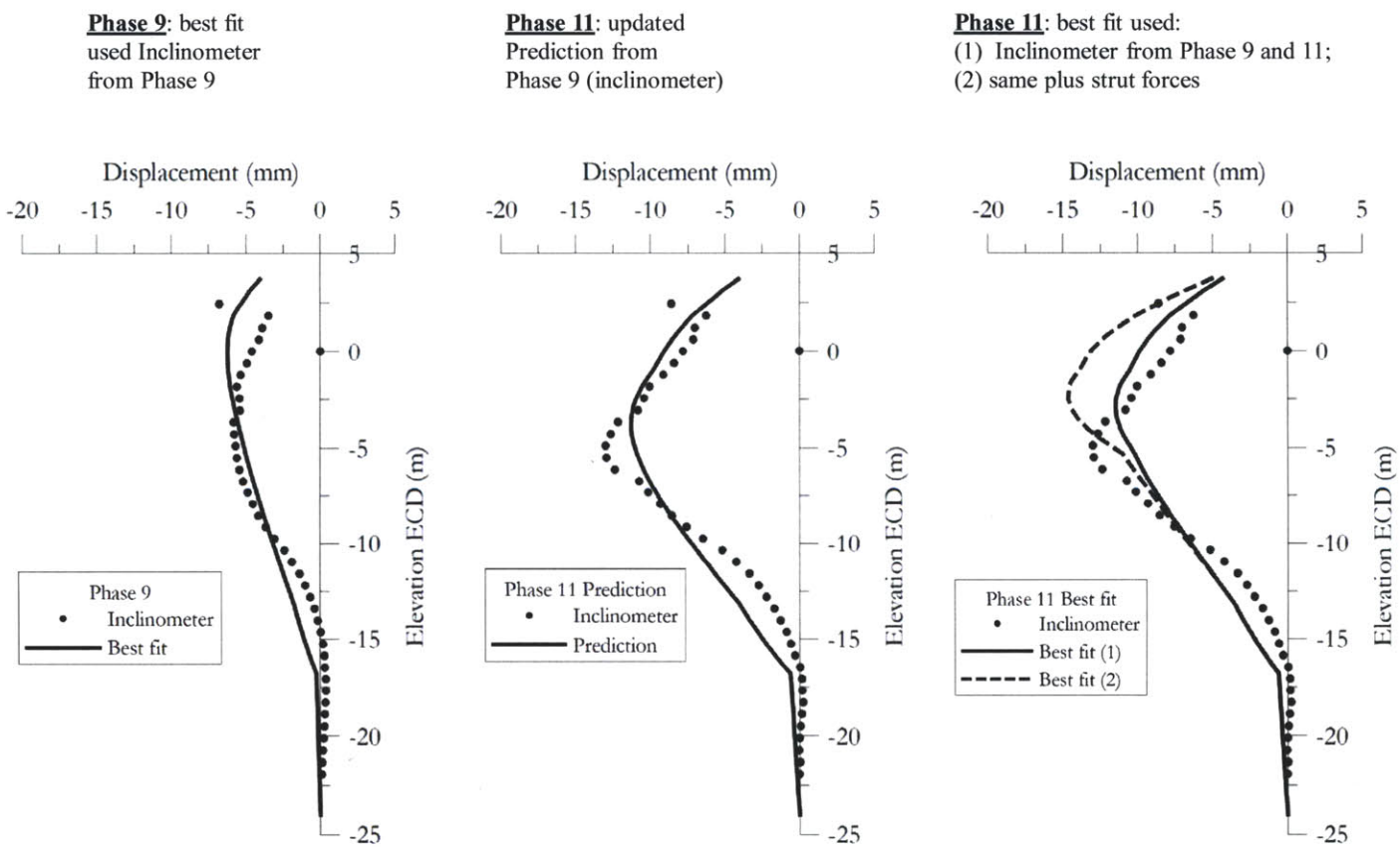

Figure 3-25: Ford Center measurements versus updated predictions at two stages (after Rechea, 2006)

(a)

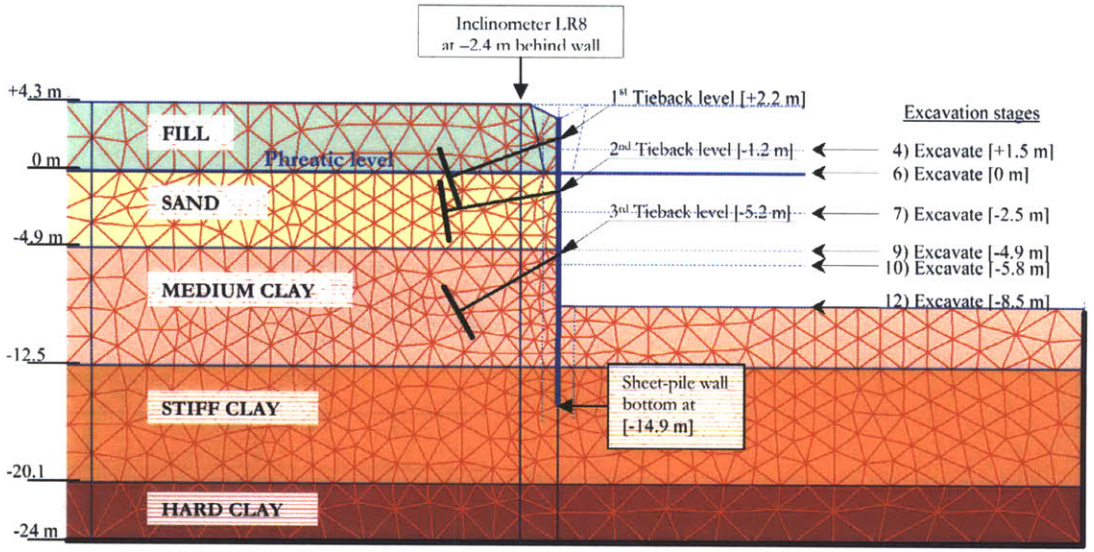

(b)

Stage number	Activity
1	Potholing and sheet-pile wall installation
2	Excavate to +1.52 m CCD and install and prestress first level of ground anchors at +2.13 m CCD
3	Construct caissons from working grade of +1.52 m CCD
4	Excavate to -2.44 m CCD and install and prestress second level of ground anchors at -1.22 m CCD
5	Excavate to -5.79 m CCD and install and prestress third level of ground anchors at -5.18 m CCD
6	Excavate to –8.53 m CCD and pour grade beams
7	Construct basement walls, pour slab and backfill

Figure 3-26: Lurie Research Center: (a) finite element model for the South side, and (b) construction sequences of excavation stages (after Rechea, 2006)

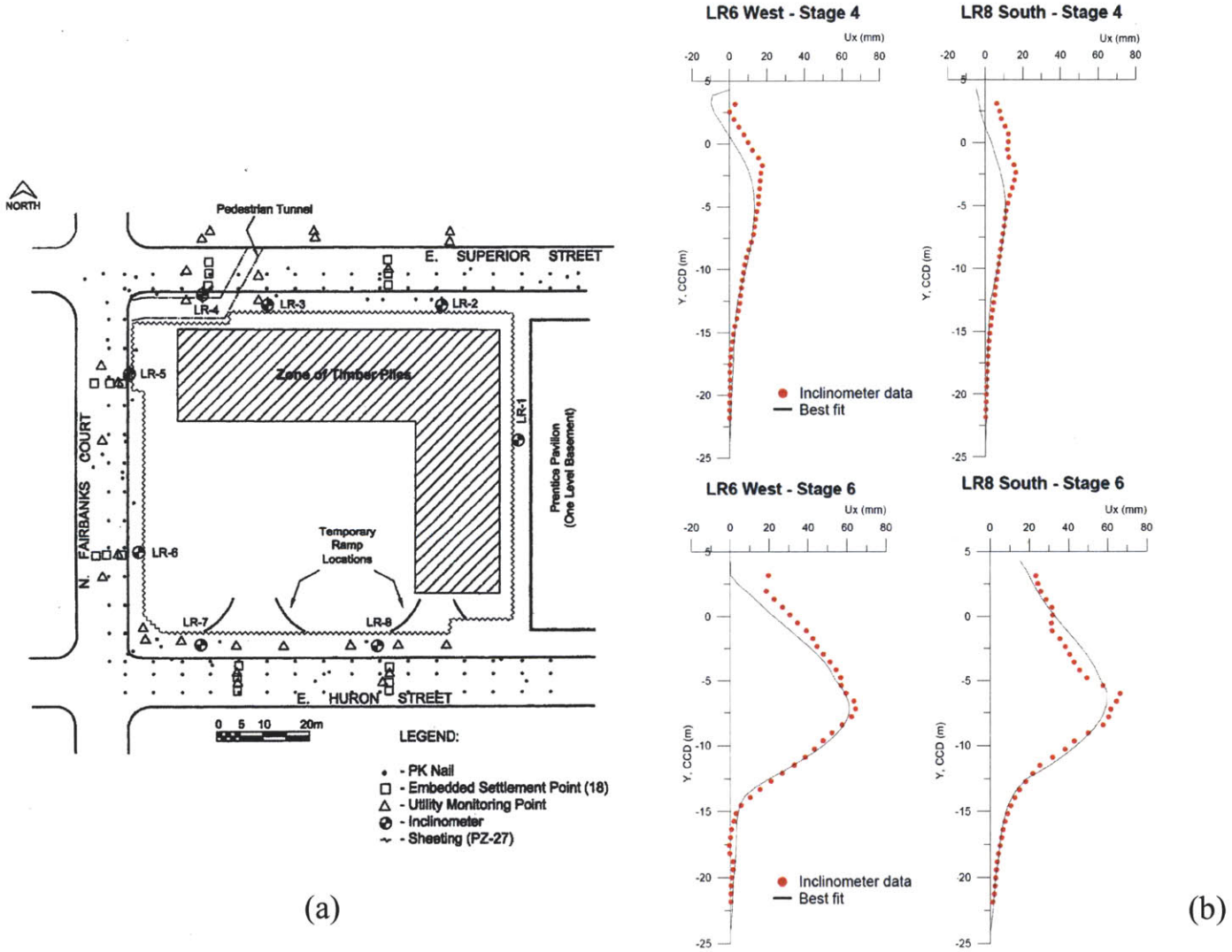

Figure 3-27: Lurie Research Center: (a) plan view of excavation site and instrumentation; (b) two inclinometer measurements vs. updated predictions for two excavation stages (after Rechea, 2006)

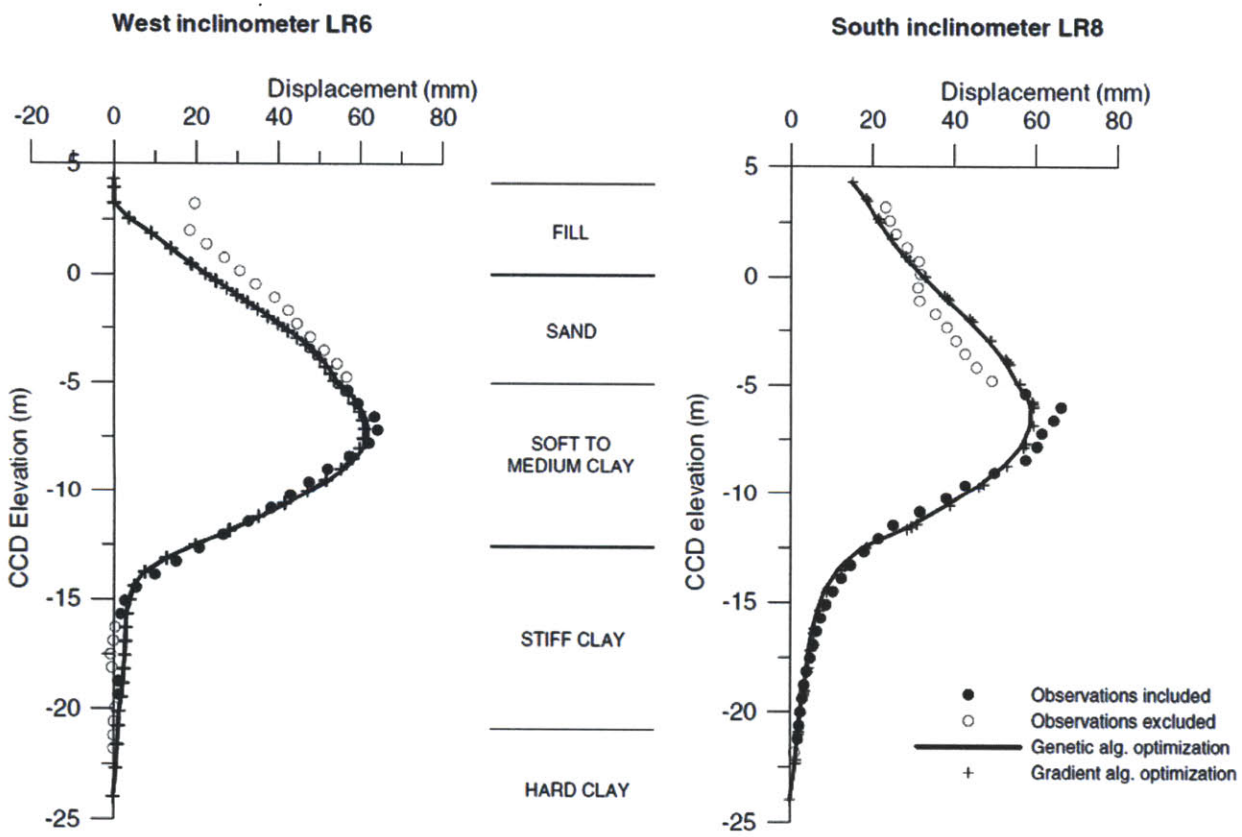

Figure 3-28: Comparison of measurements and updated predictions using genetic algorithms and the gradient method (after Rechea et al., 2008)

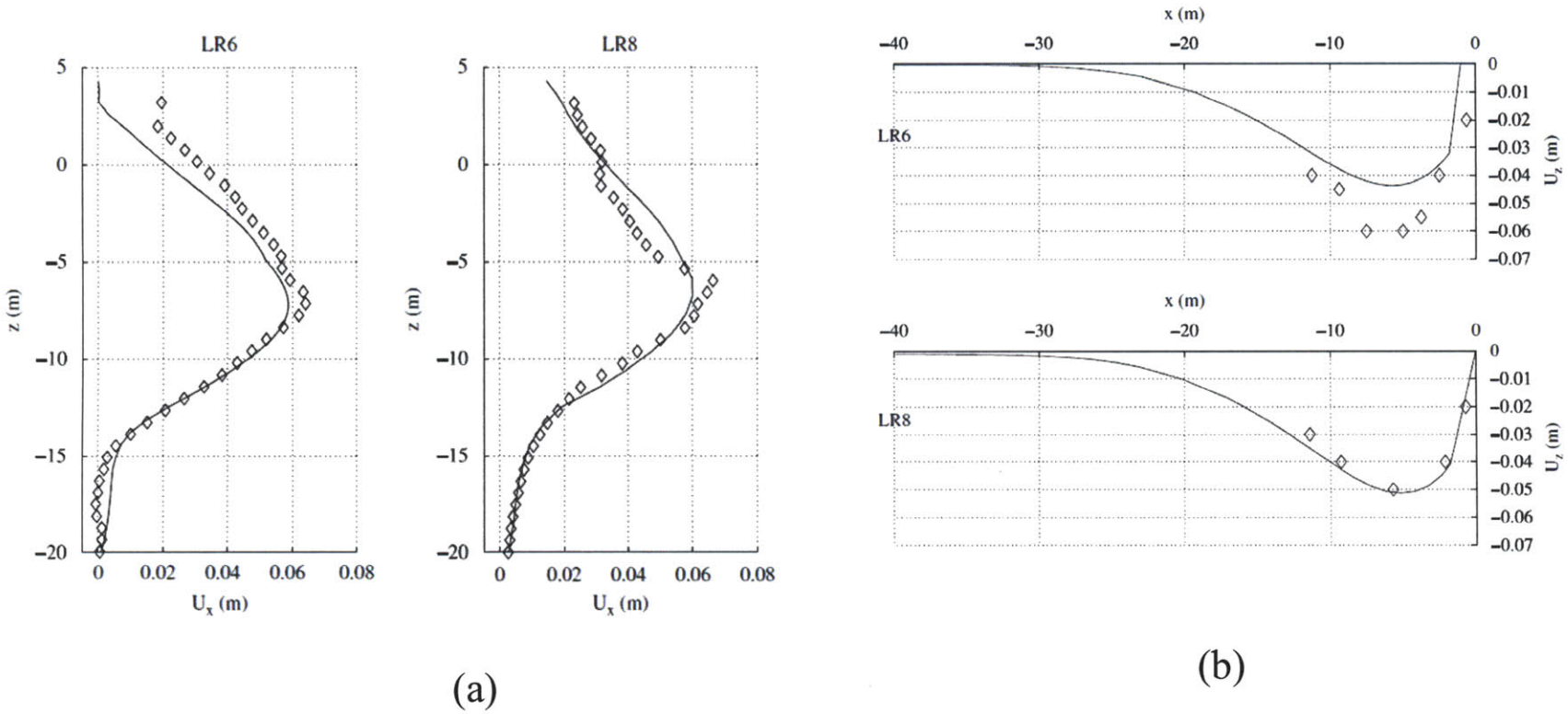

Figure 3-29: Measurements versus updated predictions for last excavation stage at Lurie Center (behind sheet wall): (a) horizontal soil movements, and (b) surface settlements (after Levasseur et al. 2009b)

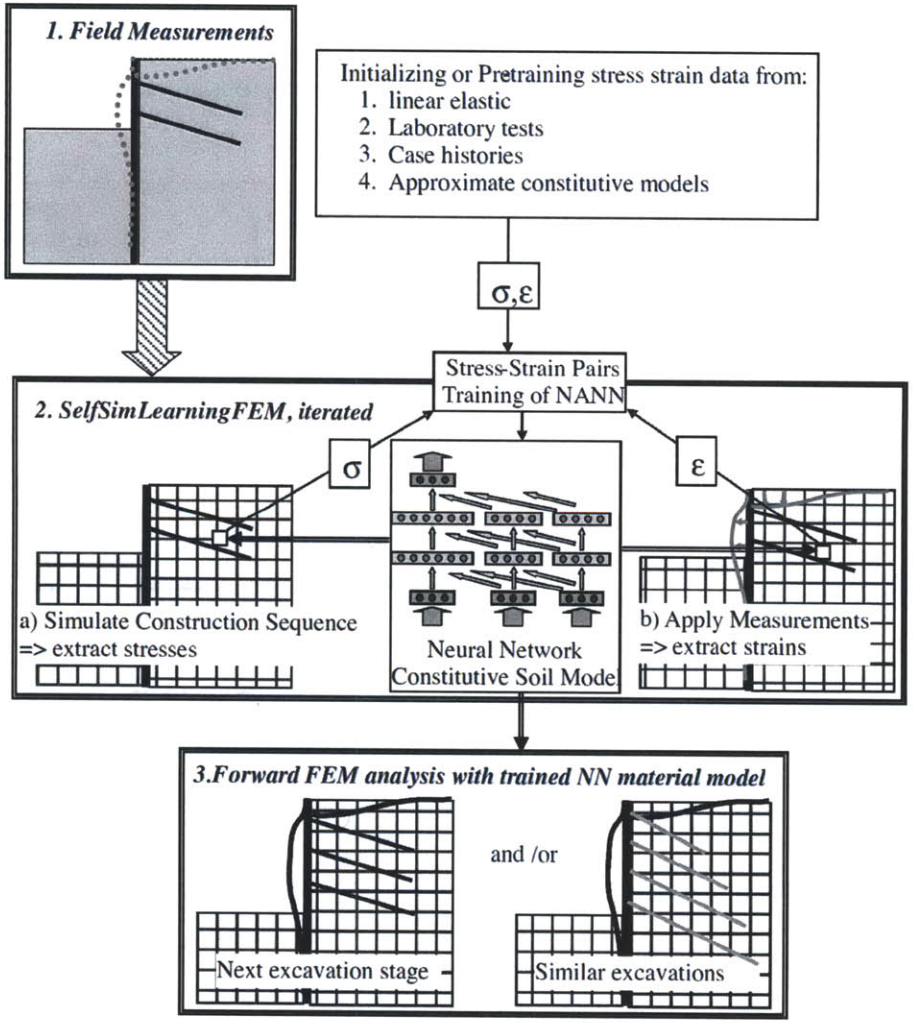

Figure 3-30: Application of self-learning simulations to deep excavation problems (Hashash et al., 2010)

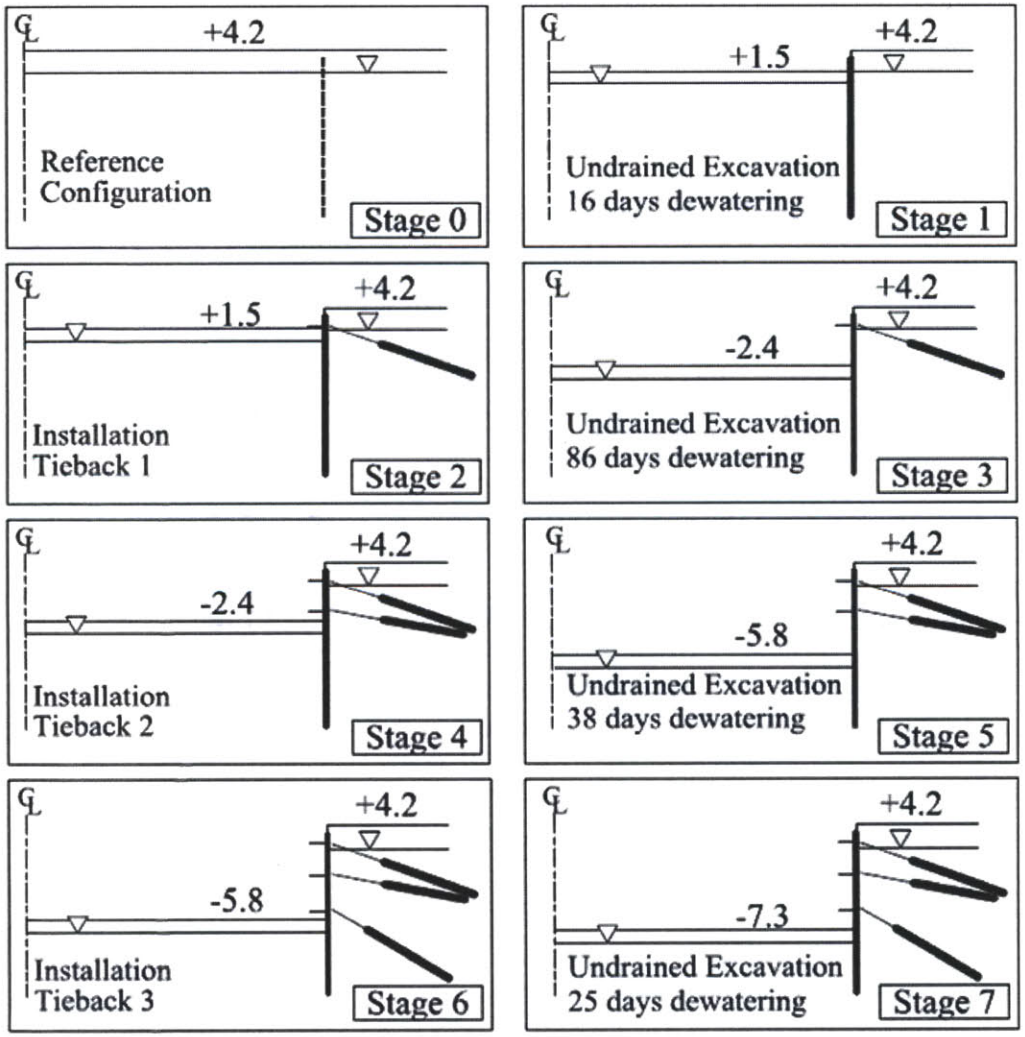

Figure 3-31: Construction sequence of Lurie Center excavation site (Hashash et al., 2010)

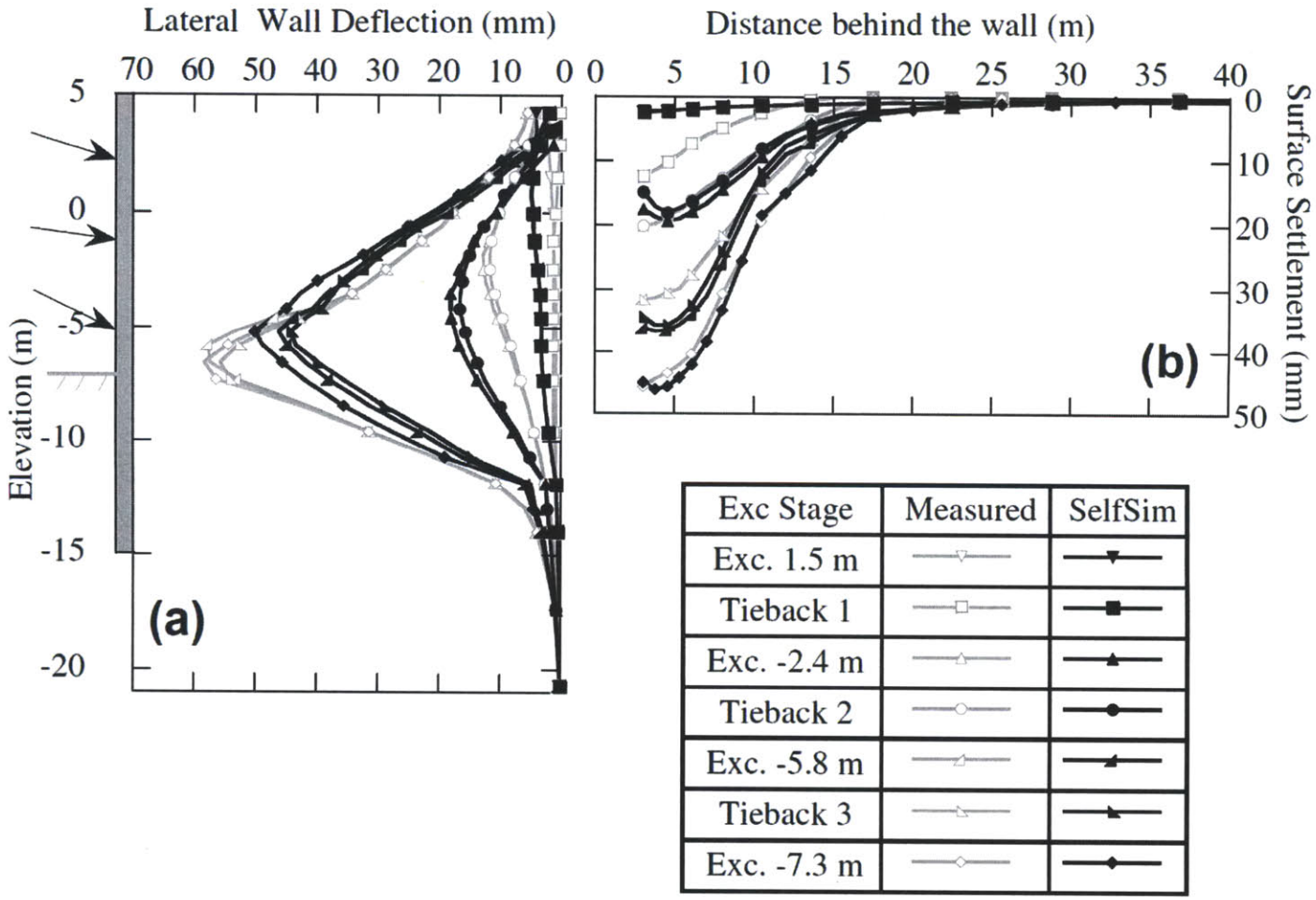

Figure 3-32: Comparison of measurements and computed (a) lateral wall deflections and (b) surface settlements after 12 passes of SelfSim learning (Hashash et al., 2010)

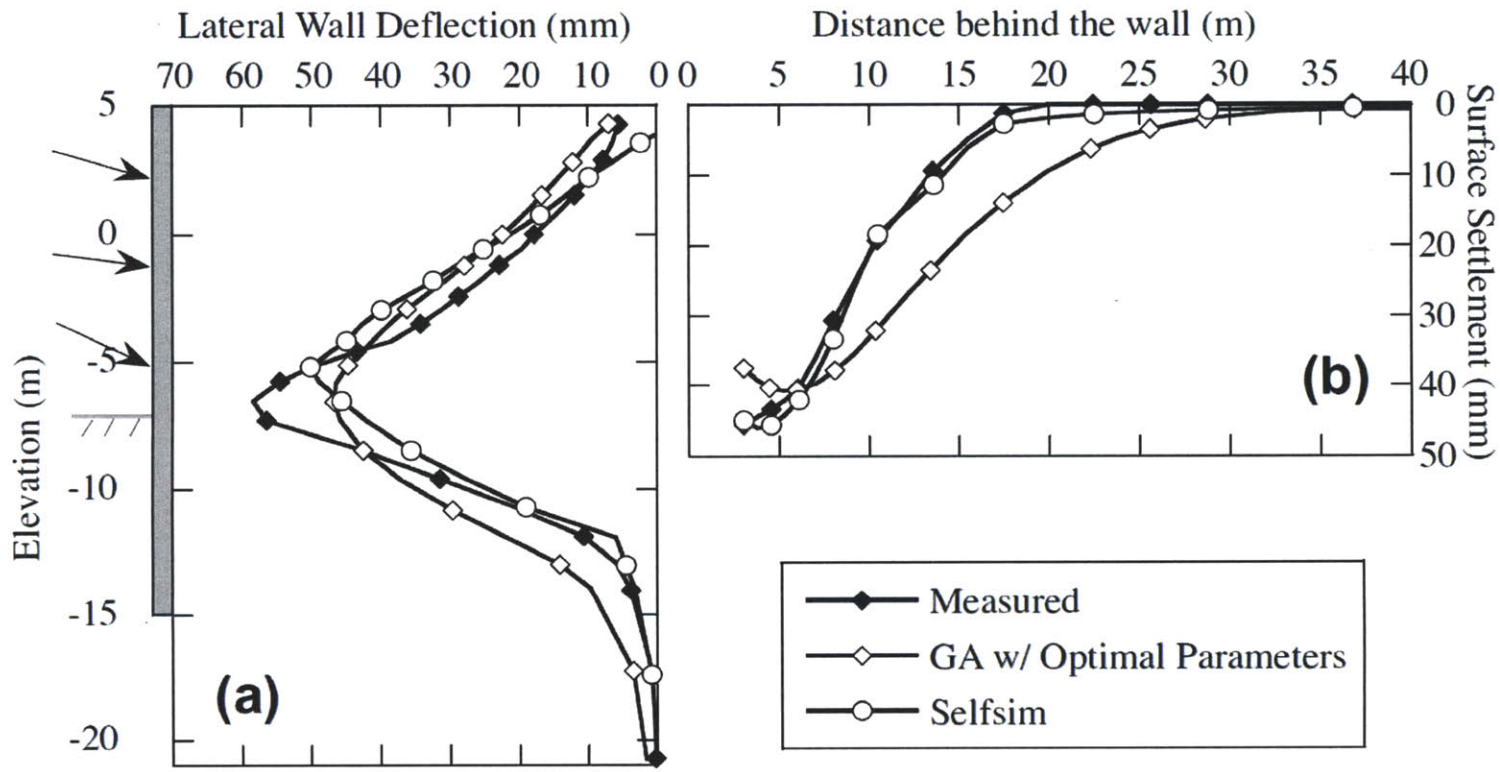

Figure 3-33: Comparison of measurements, GA (with Hardening Soil Model) and SelfSim computed (a) lateral wall deflections and (b) surface settlements for the stage 7 of excavation (Hashash et al., 2012)

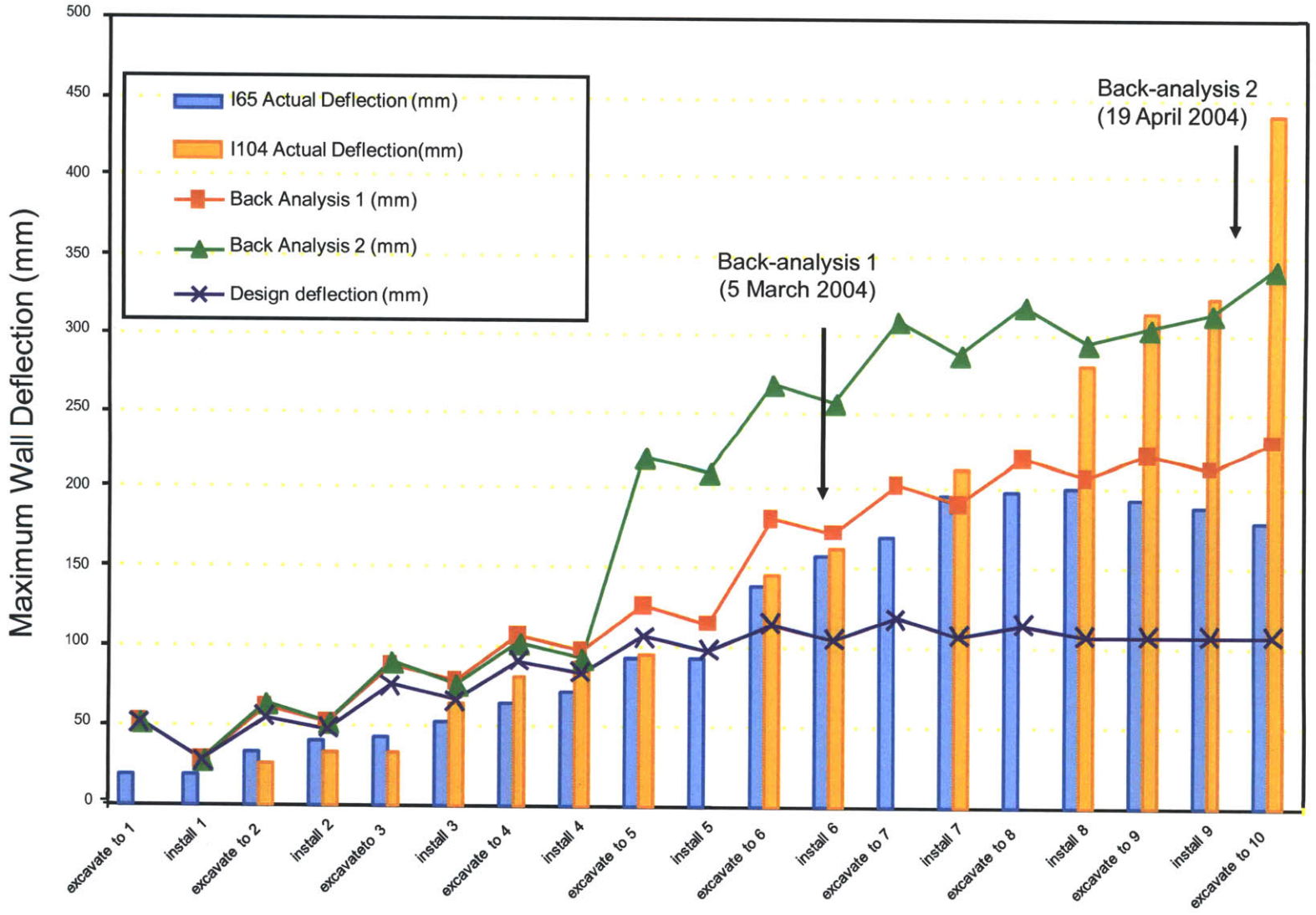

Figure 3-34: Maximum wall deflections and back-analyses performed at section M3, Nicoll Highway collapse (after COI, 2005)

4 METHODOLOGY FOR UPDATING FE PREDICTIONS OF EXCAVATION PERFORMANCE

4.1. Introduction

This chapter describes a methodology for updating FE predictions of excavation performance based principally on the maximum likelihood approach. Initially, a simplified version of this methodology is introduced and the main parts of the framework are described. This is followed by a description of the covariance matrices for field measurements and the error structures for some typical instruments used to monitor excavations. The proposed methodology uses sensitivity analyses to screen parameters to be used in inverse analyses. The chapter also presents a more detailed framework for using the updating approach in the project management through integration with alert or trigger criteria. Finally, some comments on 2-D and 3-D numerical modeling with the use of the proposed methodology are given.

4.2. Simplified Methodology for Updating FE Predictions of Excavations Performance

Figure 4-1 presents a simplified flowchart of the proposed methodology for updating FE predictions of excavation performance. This methodology contains the following sequential and iterative stages or processes:

1. Site Investigation: This includes all site information needed to define the stratigraphy, groundwater and bedrock conditions, as well as programs of field and laboratory tests needed to select input parameters for appropriate constitutive models.

2. FE model: In principle, the finite element model is derived from the site investigation data together with the data of the design of the structural support system and proposed construction sequence. In practice FE models are often limited to central cross-sections or other 2D approximations, while site investigations rarely include details of stratigraphy extending for beyond the locus of the project site.
3. Predictions: Initial predictions of performance are based on the finite element model.
4. Feedback from construction records: once excavation begins, new information will become available on soil stratigraphy while construction records will determine as –built conditions (with deviations from initial design conditions). The information is critical, as it provides basis for reducing modeling uncertainties. This feedback can be used continuously throughout the construction process.
5. Measurements: field monitoring measurements should become available during early phases of construction. Various statistical techniques can be used to identify outliers in data (malfunctioning or poorly calibrated devices) that should be removed from subsequent comparisons with performance predictions.
6. Computation of Squared Residuals and Variances: the consistency between computed and measured performance is assessed by computing two scalar quantities, the structured squared residuals (SSR) and structured global variances (SGV) for a defined set of field measurements. Section 4.4 describes the calculations of these quantities.
7. The magnitudes of SSR and SGV are used as a first filter on the methodology. If preset threshold values are exceeded then sensitivity analyses (SA) are performed in order to establish how individual input parameters affect predictions. The sensitivity analyses are

used to define a sub-set of Essential Improvement Parameters (EIP) that should be updated through inverse analyses (IA).

8. If there are no essential improvement parameters from SA, then there is no need to update the model and the model can be used to predict conditions at the next time step (construction state).

9. Inverse Analyses (IA) are performed using available measurement types and the essential improvement parameters (from SA). The inverse analysis is carried out using a maximum likelihood formulation that is solved using genetic algorithms.

10. The inverse analyses generate a set of updated input parameters that should be used to compute updated predictions of performance using the finite element model. The updated predictions should be validated against the prior history of the project (through computations of SSR) as well as predictions of performance for subsequent time steps (construction stages).

4.3. Covariance and Error Structure of Measurements

In the proposed methodology, the interpretation of field measurements and instrumentation requires the estimation of covariance and error structure matrices. Section 3.3.2.2 derived the objective function for estimating parameters in a geotechnical problem using the maximum likelihood approach. This approach involves covariance matrices of the measurements. In particular, it is necessary to derive the covariance matrix expressions for every instrument that is involved in a certain project. The maximum likelihood identification criterion was expressed as follows:

$$J = \sum_{j}^{t} \boldsymbol{r}_j^T \, \boldsymbol{C}_{\boldsymbol{m}_j}^{-1} \, \boldsymbol{r}_j \tag{4.1}$$

(3.19 bis)

where J is the maximum likelihood objective function; $\boldsymbol{C}_{\boldsymbol{m}_j}$ is the covariance matrix of the j-instrument; and $\boldsymbol{r}_j$ is the vector of residual of the j-instrument.

The covariance matrix of each instrument can be factorized as follows:

$$\boldsymbol{C}_{\boldsymbol{m}_j} = \sigma_j^2 \cdot \boldsymbol{E}_{\boldsymbol{m}_j} \tag{4.2}$$

where σ_j^2 is the scale factor that represents the global variance of the measurements by the j-instrument; and $\boldsymbol{E}_{\boldsymbol{m}_j}$ is the error structure matrix of the j-instrument which depends on the apparatus itself.

Typical geotechnical field instrumentation used in excavation support system and bored tunnels usually includes:1) inclinometers, 2) probe extensometers (e.g. sliding micrometers and heave gages), 3) piezometers, 4) load cells, 5) strain gages, 6) rod settlements, and 7) deflection monitoring points. In general, these can be subdivided into two groups: 1) pointwise instruments, and 2) linewise instruments (Kovári and Amstad, 1983; Naterop, 1998). The following section describes the covariance matrices for these measurements.

4.3.1. Pointwise Instruments

Typical pointwise instruments in excavation problems correspond to load cells, strain gages, single deflection monitoring points and rod extensometers, as well as a piezometric sensors.

Figure 4-2 shows examples of deflection monitoring and strain gage devices. Pointwise instruments measure physical parameters at a single point and are independent of other measurements. For example, load cells and strain gages are often used to measure axial forces of struts. The two measurements can be inter-related by assumptions of elasticity but are independent measures. Errors of measurements are attributed to random errors only.

Surface settlements are usually measured by deflection monitoring points, rod extensometers or surveying points where measurements at different locations are independent. Piezometers installed within a borehole are generally isolated from each other and hence also make discrete, pointwise measurements of pore pressures (i.e., no cross-coupling of pressures assumes good installation procedures).

When the measurements are independent, the covariance matrix follows the simplest form:

$$C_{m_j} = \sigma_j^2 \tag{4.3a}$$

$$\sigma_j^2 = \frac{1}{N_j}\sum_{i=1}^{N_j}(x_i - \bar{x})_j^{\,2} \tag{4.3b}$$

where σ_j^2 is the population* variance of pointwise instrument "j" at a given construction state; N_j is the total number of measurements of the j-instrument; x_i are the individual measurements; and $\bar{x}$ is the arithmetic average of N measurements.

* The population corresponds to the number of measurements for a single instrument (i.e., unique physical location)

Equation 4.3 presents the diagonal terms of the general covariance matrix, being the variance of each pointwise instrument considered in a certain excavation problem over a given time interval or construction stages. The time interval or construction stage plays a key role for the calculation of the variance because: 1) numerical predictions involve temporal discretization of a continuous process; thus a realistic time interval must be considered to integrate properly the measurements; and 2) the total number of measured data points in this time interval must be sufficient to have a valid and realistic estimation of variances. If there is insufficient data to estimate a variance, the measurements should not be included in this updating process.

It can be inferred that the pointwise case represents a particular case of the maximum likelihood approach being exactly the same to the so-called, weighted least squares method described, previously, in Chapter 3. In fact, for independent measurements only, Equation 4.2 can be simplified to pointwise measurements only and re-written to the following simple matrix form:

$$\boldsymbol{C_m} = \begin{bmatrix} \sigma_1^2 & 0 & 0 & \\ 0 & \sigma_2^2 & 0 & \cdots \\ 0 & 0 & \sigma_3^2 & \\ \vdots & & \ddots & \end{bmatrix} \tag{4.4a}$$

with error structure

$$\boldsymbol{E_m} = \begin{bmatrix} 1 & 0 & 0 & \\ 0 & 1 & 0 & \cdots \\ 0 & 0 & 1 & \\ \vdots & & \ddots & \end{bmatrix} = \mathbf{I} \tag{4.4b}$$

where $\boldsymbol{C_m}$ is the covariance matrix of pointwise measurements; σ_j^2 is the variance of the j-instrument; and $\boldsymbol{E_m}$ is the structure error matrix of pointwise measurements (I: identity matrix).

4.3.2. Linewise Instruments

Linewise instruments, based on measurements along a chain of geometrically continuous segments, provide enough data to estimate the distribution of deformations and/or strains along a line (Naterop, 1998). Typical linewise instruments used in excavations correspond to sliding micrometers, heave gages, inclinometers, fiber-optic strain sensors, etc. Figure 4-3 shows a schematic of a straight line deformed used in these three most common linewise instrument types in excavations.

4.3.2.1. Sliding Micrometers and Heave Gages

Sliding micrometers and mechanical heave gages are devices that monitor changing distance between two or more points along a common axis, by passing a probe through the access pipe. The measurements can be either electrical or mechanical (see Figure 4-4). While there are several types of probe extensometers (Dunnicliff, 1983), only mechanical heave gages and sliding micrometers are considered.

Following the work done by Ledesma et al. (1996), and considering that the initial point of a probe extensometer has an absolute movement, A, the parallel displacement to the instrument axis at a given sensor or point can be computed as follows (see Figure 4.2a):

$$v_n = \sum_{i=1}^{n} \epsilon_i + A \tag{4.4}$$

where v_n is the total displacement (parallel to the axis) assuming that instrument has n sensors; ϵ_i is the individual displacement of the sensor; and A is an integration constant or absolute reference movement.

The physical mechanism of this instrument can be simply thought as springs in series, where the total axial displacement is the sum of each spring displacement. Assuming that the integration constant or reference movement A is zero, the covariance matrix can be expressed by:

$$C_{m_{ij}} = \text{cov}(v_i, v_j) = \text{cov}\left(\sum_{r=1}^{i} \epsilon_r, \sum_{s=1}^{j} \epsilon_s\right) = \sum_{r=1}^{i}\sum_{s=1}^{j} \text{cov}(\epsilon_r, \epsilon_s) \tag{4.5}$$

$$= \sigma^2 \sum_{r=1}^{i}\sum_{s=1}^{j} \delta_{rs} = \sigma^2 \min(i,j)$$

where σ^2 is the global variance of measurements; and δ_{rs} is the Dirac delta function.

If the integration constant A is not fixed, the covariance matrix should be evaluated as follows:

$$C_{m_{ij}} = \sigma^2 \left\{\min(i,j) + \frac{var(A)}{\sigma^2}\right\} \tag{4.6}$$

where $var(A)$ is the variance of absolute reference movement or integration constant.

The covariance matrix can then be expressed and factorized as follows:

$$\boldsymbol{C_m} = \sigma^2 \begin{bmatrix} 1 & 1 & 1 & \\ 1 & 2 & 2 & \dots \\ 1 & 2 & 3 & \\ \vdots & & \ddots & \end{bmatrix} + var(A) \tag{4.7a}$$

$$= \sigma^2 \left\{ \begin{bmatrix} 1 & 1 & 1 & \\ 1 & 2 & 2 & \cdots \\ 1 & 2 & 3 & \\ \vdots & & & \ddots \end{bmatrix} + \frac{var(A)}{\sigma^2} \right\}$$

with error structure

$$\boldsymbol{E_m} = \begin{bmatrix} 1 & 1 & 1 & \\ 1 & 2 & 2 & \cdots \\ 1 & 2 & 3 & \\ \vdots & & & \ddots \end{bmatrix} + \frac{var(A)}{\sigma^2} \quad \textbf{(4.7b)}$$

It is important to note that the variance has dimension of squared length. This last factorization of the covariance matrix allows one to express the error structure matrix in a dimensionless form, having a particular advantage for sensitivity analyses that will be discussed later in Sections 4.4 and 4.5.

4.3.2.2. Inclinometers

Figure 4.5 shows the typical configuration of a conventional inclinometer and an in-place inclinometer (Hung et al., 2009). The conventional inclinometer system comprises a casing, an inclinometer probe and control cable, and readout unit, while the in-place inclinometer comprises a series of sensors attached at fixed points to the casing. Inclinometer probes measure tilt in fixed points along its axis and falls within the category of transverse deformation gages (Dunnicliff, 1993).

Again, following the work done by Ledesma et al. (1996), and considering that the bottom of the casing or the deepest point considered has a horizontal displacement B, the perpendicular displacement to the instrument axis at a given point can be computed as follows:

$$u_n = \sum_{i=1}^{n} l_i sin\alpha_i + B \tag{4.8}$$

where u_n is the total displacement (perpendicular to the axis) assuming that the line is divided by n segments; $sin\alpha_i$ is the sine function of slope segment; and B is an integration constant or absolute reference movement.

If it is assumed that the base of the casing is fixed (i.e., B =0), the covariance matrix of two continuous points can be expressed as follows:

$$\begin{aligned} C_{m_{ij}} &= \text{cov}(u_i, u_j) = \text{cov}\left(\sum_{r=1}^{i} l_r sin\alpha_r, \sum_{s=1}^{j} l_s sin\alpha_s\right) \\ &= \sum_{r=1}^{i}\sum_{s=1}^{j} l_r\, l_s\, \text{cov}(sin\alpha_r, sin\alpha_s) \\ &= \sigma^2 \sum_{r=1}^{i}\sum_{s=1}^{j} l_r\, l_s\, \delta_{rs} = \sigma^2 \sum_{r=1}^{\min(i,j)} {l_r}^2\, \delta_{rs} \end{aligned} \tag{4.9}$$

where σ^2 is the global variance of measurements (dimensionless); l_r is the segment length; and δ_{rs} is the Dirac delta function.

It is important to highlight that the global variance, σ^2, is dimensionless since it corresponds to global variance of the sine of the angles.

If the integration constant B is not fixed, the covariance matrix element should be evaluated as follows:

$$C_{m_{ij}} = \sigma^2 \left\{ \sum_{r=1}^{\min(i,j)} {l_r}^2 \, \delta_{rs} + \frac{var(B)}{\sigma^2} \right\} \tag{4.10}$$

where $var(B)$ is the variance of absolute reference movement or integration constant.

The covariance matrix of inclinometer measurements can then be expressed as:

$$\boldsymbol{C_m} = \sigma^2 \begin{bmatrix} {l_1}^2 & {l_1}^2 & {l_1}^2 & \\ {l_1}^2 & {l_1}^2 + {l_2}^2 & {l_1}^2 + {l_2}^2 & \cdots \\ {l_1}^2 & {l_1}^2 + {l_2}^2 & {l_1}^2 + {l_2}^2 + {l_3}^2 & \\ \vdots & & & \ddots \end{bmatrix} + var(B) \tag{4.11}$$

If the lengths between two consecutive points are chosen to be equal to l_i , along the inclinometer, the covariance matrix can be expressed as:

$$\begin{aligned} \boldsymbol{C_m} &= \sigma^2 {l_i}^2 \begin{bmatrix} 1 & 1 & 1 & \\ 1 & 2 & 2 & \cdots \\ 1 & 2 & 3 & \\ \vdots & & & \ddots \end{bmatrix} + var(B) \\ &= \sigma^2 {l_i}^2 \left\{ \begin{bmatrix} 1 & 1 & 1 & \\ 1 & 2 & 2 & \cdots \\ 1 & 2 & 3 & \\ \vdots & & & \ddots \end{bmatrix} + \frac{var(B)}{\sigma^2 {l_i}^2} \right\} \end{aligned} \tag{4.12a}$$

with error structure

$$\boldsymbol{E_m} = \begin{bmatrix} 1 & 1 & 1 & \\ 1 & 2 & 2 & \cdots \\ 1 & 2 & 3 & \\ \vdots & & & \ddots \end{bmatrix} + \frac{var(B)}{\sigma^2 {l_i}^2} \tag{4.12b}$$

This last factorization of the covariance matrix for inclinometers (Equation 4.12a) allows one to express the error structure matrix in a dimensionless form having a particular advantage for the two filters of this methodology that will be discussed later in Sections 4.4 and 4.5.

Figure 4-6 shows the derivation of covariance matrix and objective function for a hypothetical example of an inclinometer of three points. It is very important to observe how the final form of the objective function differs from the simple least squared method, discussed previously in Chapter 3. In fact, coupled terms of residuals (i.e., terms containing r_1r_2 and r_2r_3) as well as different scalar magnitudes multiplying each term, can be found in the objective function expression.

4.4. Structured Squared Residuals and Global Variances

This step involves the computation of two scalar magnitudes for each instrument: 1) residuals (difference between measurements and predictions) and 2) variances of field measurements. Since there is no error structure associated with pointwise measurements, the structured squared residual (SSR) corresponds to the squared residual of each instrument. Under the same logic, the structured global variance (SGV) corresponds simply to the measurement variance of each pointwise instrument. Therefore, the structured squared residual and global variance for each pointwise instrument type 'i' (e.g., all measurements of surface settlements) is as follows:

$$SSR_i = \boldsymbol{r}_i^T \boldsymbol{r}_i \tag{4.13}$$

where SSR_i is the cumulative structured squared residual (scalar) for pointwise instrument type 'i'; and $\boldsymbol{r}_i$ is the vector of residuals for a given instrument type 'i'.

Similarly, the structured global variance (SGV) for each pointwise instrument type 'i' can be expressed by:

$$SGV_i = \boldsymbol{\sigma}_i^T \ \boldsymbol{\sigma}_i \tag{4.14}$$

where SGV_i is the cumulative variances (scalar) for pointwise instrument type 'i' ; and $\boldsymbol{\sigma}_i$ is the vector of standard deviation of measurements for pointwise instrument type 'i'.

For the particular case of 2-D numerical analyses and for pointwise instruments, it is often possible to run sensitivity analyses based on groups of instrument types (rather than individual measurements). This means working with average values of both the residuals and variances of measurements, and therefore given a better physical sense of magnitudes of average values. The advantage of grouping pointwise measurements at different locations (e.g., settlements at different distances from wall) is that it permits the visualization and impact of specific observations on different model parameters, and thus provides a better understanding of the numerical problem. Under this logic, Equations 4.14 and 4.15 can be re-written as:

$$SSR_i^{ave} = \frac{\boldsymbol{r}_i^T \boldsymbol{r}_i}{n_i} \tag{4.15}$$

$$SGV_i^{ave} = \frac{\boldsymbol{\sigma}_i^T \boldsymbol{\sigma}_i}{n_i} \tag{4.16}$$

where n_i is the total number of measurements of pointwise instrument type 'i'.

In order to generalize the error structure matrix (for both pointwise and linewise measurements) the expressions can be modified as follows:

$$SSR_i = \boldsymbol{r}_i^T \boldsymbol{E}_{\boldsymbol{m}_i}^{-1} \boldsymbol{r}_i \tag{4.17}$$

$$SGV_i = \boldsymbol{\sigma}_i^T \, \boldsymbol{E}_{m_i}^{-1} \, \boldsymbol{\sigma}_i \tag{4.18}$$

$$\boldsymbol{E}_{m_i} = \begin{cases} \boldsymbol{E}_{m_i} & ; \text{ for linewise instruments} \\ \mathrm{I}_i & ; \text{ for pointwise instruments} \end{cases} \tag{4.19}$$

where, $\boldsymbol{E}_{m_i}$ is the error structure of the instrument type 'i' (from Equations 4.7b and 4.12b); and $\boldsymbol{I}_i$ is the identity matrix where the dimension depends on the number of independent measurements.

Summarizing, Equations 4.17, 4.18, and 4.19 allow one to compute the scalar values of SSR and SGV for each instrument type. It is very important to highlight that for linewise instruments, it is not necessary to work with average values, because of the error structure in the measurements, (Equations 4.7b and 4.7b).

4.5. Sensitivity Analysis

Having computed SSR_i and SGV_i for each instrument type 'i', the next step is to perform a sensitivity analysis. The sensitivity analysis proposed herein has three main objectives: 1) identify the most important model parameters needed for optimizing; 2) identify the instruments or measurement types that provide the most information for the inverse problem; and 3) quantify how much the SSR can be reduced by varying one parameter only.

The proposed sensitivity analysis involves the variation of a single model input parameter over a pre-defined search space, computing the squared structured residual (SSR) for each different parameter value. This makes it possible to study the relation between SSR and each model parameter.

Sensitivity analyses are carried out for input parameters where the structured squared residual is greater than the structured global variance:

$$SSR_i^{initial} > SGV_i \, ? \tag{4.20}$$

where $SSR_i^{initial}$ is the structured squared residual using the original/initial input parameters.

When using pointwise instruments only, Equation 4.20 can be simplified to compare squared residuals against measurement variances. Figure 4-7 shows an illustrative example that defines "essential" and "non-essential residuals", simplified for a single point measurement. The case when the absolute value of the residual ($|\boldsymbol{r}| = |\boldsymbol{m} - \boldsymbol{p}|$) is higher than the standard deviation of the measurement is defined as an "essential residual" (Fig. 4-7a). In contrast, when the absolute value of the residual is less than or equal to the measured standard deviation, the residual is "non-essential" (Fig. 4-7b).

A second filter considers how the structured squared residual varies over the parameter search space:

$$\Delta SSR_i = SSR_i^{initial} - SSR_i^{min} \tag{4.21}$$

where ΔSSR_i is the maximum reduction of SSR_i related to the initial value ($SSR_i^{initial}$) due to variation of a single model parameter.

Figures 4-8 and 4-9 show examples of two hypothetical sensitivity analyses that show variations in SSRi with a selected input parameter, pk. Figure 4-8 show the case when DSSRi is

higher than the value of SGVi; thus defines the parameter, p_k, as an "essential improvement parameter". On the other hand, when ΔSSRi is less than SGVi (Fig. 4-9), the parameter is a "non-essential improvement parameter". The goal of sensitivity analyses (SA) is to define the set of "essential improvement parameters".

Basically, Equation 4.21 measures how sensitive each parameter is in term of SSR of each instrument type. If ΔSSR_i is higher than SGV_i, the model parameter is immediately flagged as an "Essential Improvement Parameter" (EIP) for a specific measurement type, and therefore considered to be a parameter to be optimized in the inverse analysis or parameter estimation step (see Figure 4.8).

4.6. Inverse Analysis

The current methodology proposes the use of the maximum likelihood approach, as the identification criterion, and the use of genetic algorithms, as the optimization method.

Having defined the covariance matrices of the measurements and identified the set of the essential improvement parameters (including the search spaces for each parameter), the objective function based on the maximum likelihood approach, can be expressed as follows:

$$\min\{J\} = \min\{(\boldsymbol{m}-\boldsymbol{p})^T \boldsymbol{C_m}^{-1}(\boldsymbol{m}-\boldsymbol{p})\} \quad (4.22)$$

where $\boldsymbol{C_m}$ is the covariance matrix of all measurements and instrument types; $\boldsymbol{m}$ is the vector of all measurements considered; and $\boldsymbol{p}$ is the vector of all predictions considered

It is very important to highlight that the inverse maximum likelihood analysis, proposed herein, contains all of the measurements (and instrument types), regardless of the results of the sensitivity analysis. This means that although the sensitivity analysis give us the essential improvement parameters to optimize at a given excavation time, all instrument types must be considered in the minimization problem. In order to constrain the problem specified in Equation 4.22, it is also necessary to define the search space (lower and upper bounds) to each of the essential improvement parameters:

$$\min\{J\} = \min\{\boldsymbol{r}^T \boldsymbol{C_m}^{-1} \boldsymbol{r}\}$$

s.t. (4.23)

$$\boldsymbol{\theta_{LB}} \leq \boldsymbol{\theta} \leq \boldsymbol{\theta_{UB}}$$

where $\boldsymbol{r} = \boldsymbol{m} - \boldsymbol{p}$ is the vector of residuals of all measurements considered; $\boldsymbol{\theta}$ is the vector of essential improvement parameters to optimize; and $\boldsymbol{\theta_{LB}}$ and $\boldsymbol{\theta_{UB}}$ are the lower and upper bounds of $\boldsymbol{\theta}$, respectively.

Equation 4.23 generalizes and constrains the proposed inverse maximum likelihood analysis. In principle, this minimization problem can be solved by heuristic optimization methods. This thesis uses genetic algorithms (GA), described in Section 3.3.3. The selection of GA options such as: population size, fitness scaling, selection, reproduction, mutation, crossover, stopping criteria plays an important role in finding good approximations to the global minima or minimum, and highly depends on every specific problem.

4.7. Proposed Methodology for Updating FE Predictions

Figure 4-10 presents a more detailed flowchart on the proposed methodology for updating FE predictions (based on the outline shown in Figure 4.1). Additional details in this chart include: 1) use of the initial FE model predictions ("class A") as the basis for the initial support system design; and 2) the integration of the instrumentation plan to derive and specify the error structure matrix of each instrument type prior to construction. It is also recommended to remove outliers (e.g., T-tests) from field measurements to obtain more credible set of measured data. With the error structure matrix of the instrument i ($\mathbf{E}_{mi}$) and credible measurements (**m**), we can compute the covariance matrices for instrument i, and the global variance of the measurements ($\mathbf{C}_{mi}$; σ^2). This flowchart specifies also that the inverse analyses should be performed using the maximum likelihood approach (identification criterion), and genetic algorithms (optimization method).

4.8. Generalized Methodology for Management of Construction Process

A more generalized and detailed methodology for the management of construction process is shown in Figure 4-11. Although this figure uses the same previously proposed updating procedure, it includes some additional steps. These steps are basically related with the planning and initial design phases. In general terms, the planning should consist of a comprehensive site investigation, which would allow one to select the most appropriate excavation type and support system, and also to integrate an instrumentation plan and monitoring program before starting the excavation construction (see Figure 4-11a).

In addition, the site investigation should involve previous studies in the area, laboratory and field tests, and geological studies. This will clearly help to define properly the site geology and soil profiles which will play a critical role in the initial predictions (also referred to as class A predictions) and initial design. If available, this procedure suggests the use of any regional databases and local borings to help defining properly soil profiles and material properties. After defining more in detail the site geology, two sets of material properties should be defined: 1) most probable (MP); and 2) characteristic values (CV).

The MP set of parameters represent the probabilistic mean of all the data which usually requires a degree of engineering judgment to interpret the data, while the CV set of parameters represent a "cautious estimate of the value affecting the occurrence of the limit state" which, in principle, should result in predictions of the upper 5% fractile of the measured wall deflections, being not a precisely defined parameter (Patel et al., 2007). Figure 4-12a shows an example of these parameters for the case of Gaussian distribution of shear strength (after Nicholson et al., 1999). Figure 4-12b shows the Eurocode 7 (EC7) interpretation of predicted and measured performance for the most probable (MP), characteristic values (CV) and most unfavorable soil properties (after Patel et al., 2007). It is important to note that Figure 4.12b also shows colors or trigger zones based on the likelihood of exceeding movement predictions (referred to as green, amber, and red zones). Patel el al. (2007) describe the significance of these zones as follows: 1) "green zone" means to continue construction; 2) "amber zone" means to continue with caution and prepare to implement contingency, increase rate of monitoring (amber zone); and 3) "red zone" means to stop progress, do everything possible to slow movements, and implement contingency.

By using the two sets of material properties (MP and CV), one should capable of calibrating simple and/or advanced soil models, as well as defining and listing model parameters with high uncertainty (including each model parameter search spaces based on any correlation or information available). Once the initial FE model is ready, all possible modelling uncertainties should clearly be specified. Based on the sets of material properties, initial predictions (i.e. class A predictions) can be obtained (also referred to as vectors: $\mathbf{p}^{MP}$ and $\mathbf{p}^{CV}$) by using these two sets of materials and the initial numerical model (see Figure 4-11a). These will also allow one to establish initial trigger criteria, as exemplified in Figure 4-12.

These two initial steps of planning and predictions (as well as design) permit one to generalize the proposed methodology for updating predictions. Figure 4-11b shows a more generalized version of the proposed methodology, previously shown in Figure 4-10.

Finally, under the same logic of this proposed inverse approach, a proposed updating of the traffic light system for excavation is presented in Figure 4-12. This updating traffic light system plays a very important role in this framework in enabling communication among contractors, managers, design team, and the client. Figure 4-12 integrates, as an example from CIRIA report 185 (after Nicholson et al., 1999), the steps to follows under each color or trigger zones (green, amber, and red) already discussed.

4.9. Comments on Spatial Representation in Numerical Model

In order to be capable of applying this inverse procedure, enough measured data must be available to certainly compute covariance matrices of measurements. When construction site

approximates to 2-D conditions it is reasonable to focus on a 2-D numerical representation. Geotechnical engineers often adopt 2-D plane strain conditions to model excavation problems, and sometimes, the modeling is further simplified by adopting symmetric conditions.

In a simplified 2-D numerical model, the spatial representation allows one to group measurements at a single section for the proposed inverse analysis. In principle, this increases the number of measurements, and offers two main advantages: 1) more representative measurement errors (i.e., covariance matrices), and 2) grouping instruments by type (e.g., surface settlements behind a diaphragm wall; wall deflections from different in-wall inclinometers). Particularly, for pointwise instruments, it is possible to run sensitivity analyses based on group instrument types (instead of individual measurements). Hence, it is possible to work with average values of the residuals and measurement variances, and also to enable better visualization of the impacts of specific observations on different model parameters.

In contrast, 3-D numerical models present the advantage of more realistic spatial representation of construction processes. However, this involves more computational effort and time and restricts averaging measurements at one section or grouping instrument types. In this case, the main challenges are 1) to define properly the time intervals used in interpretation on performance construction records, and 2) to ensure there is sufficient data at each construction stage to enable updating of parameters. Application of updating methods for 3-D FE models is beyond the scope of this thesis. Chapter 5 provides a detailed case study based on 2-D modeling of an excavation support system.

4.10. References

Dunnicliff, J. (1993). "Geotechnical Instrumentation for Monitoring Field Performance." *A Wiley-Interscience Publication*, John Wiley & Sons.

Einstein, H. H. and Baecher, G. B. (1982). "Probabilistic and Statistical Methods in Engineering Geology. I. Problem Statement and Introduction to Solution." *Rock Mechanics*, Suppl. 12: 47-61.

Kovári, K., and Amstad, Ch (1982). "A new method of measuring deformations in diaphragm walls and piles." Géotechnique, 32(4): 402-406.

Kovári, K., and Amstad, Ch (1983). "Fundamentals of Deformation Measurements." International Symposium on Field Measurements in Geomechanics, Zurich, 219-239.

Hung, J.C., Monsees, J., Munfah, N., and Wisniwski, J. (2009): "Technical Manual for Design and Construction of Road Tunnels – Civil Elements." *US Department of Transportation Federal Highway Administration. Publication* No. FHWA-NHI-10-034, 704p.

Ledesma, A. (1987). "Identificación de Parámetros en Geotecnia. Aplicación a la Excavación de Túneles." *PhD Thesis - Escuela Técnica Superior de Ingenieros de Caminos, Canales y Puertos de Barcelona.*

Ledesma, A., Gens, A., and Alonso, E. (1996). "Estimation of Parameters in Geotechnical Backanalysis - I. Maximum Likelihood App." *Computers and Geotechnics* 18(1):1-27.

Naterop, D. (1998). "Linewise Deformation Measurements for solving geotechnical problems." *Development of Geotechnical Tests, Chinese Assoc. of Geotechnical Investigation*, Seminar Beijing, 10 p.

Nicholson, D., Tse, C. and Penny, C. (1999). "The Observational Method in ground engineering – principles and applications." Report 185, CIRIA, London.

Patel, D., Nicholson, D., Huybrechts, N., and Maertens, J. (2007). "The Observational Method in Geotechnics." Proceedings of XIV European Conference on Soil Mechanics and Geotechnical Engineering: Geotech. Eng. in urban environments, Madrid, 2:10p.

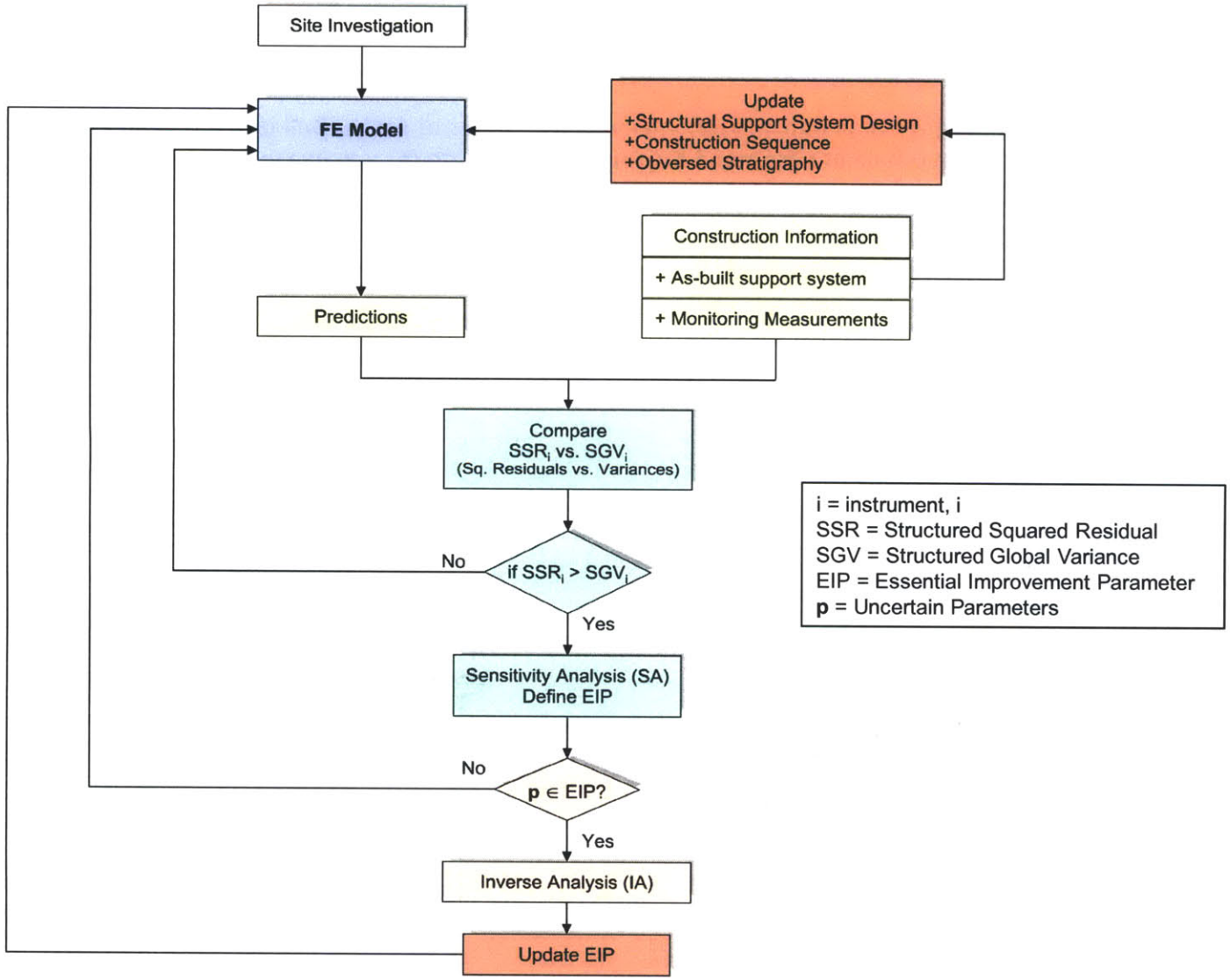

Figure 4-1: Proposed methodology for updating FE predictions of excavation performance (simplified version)

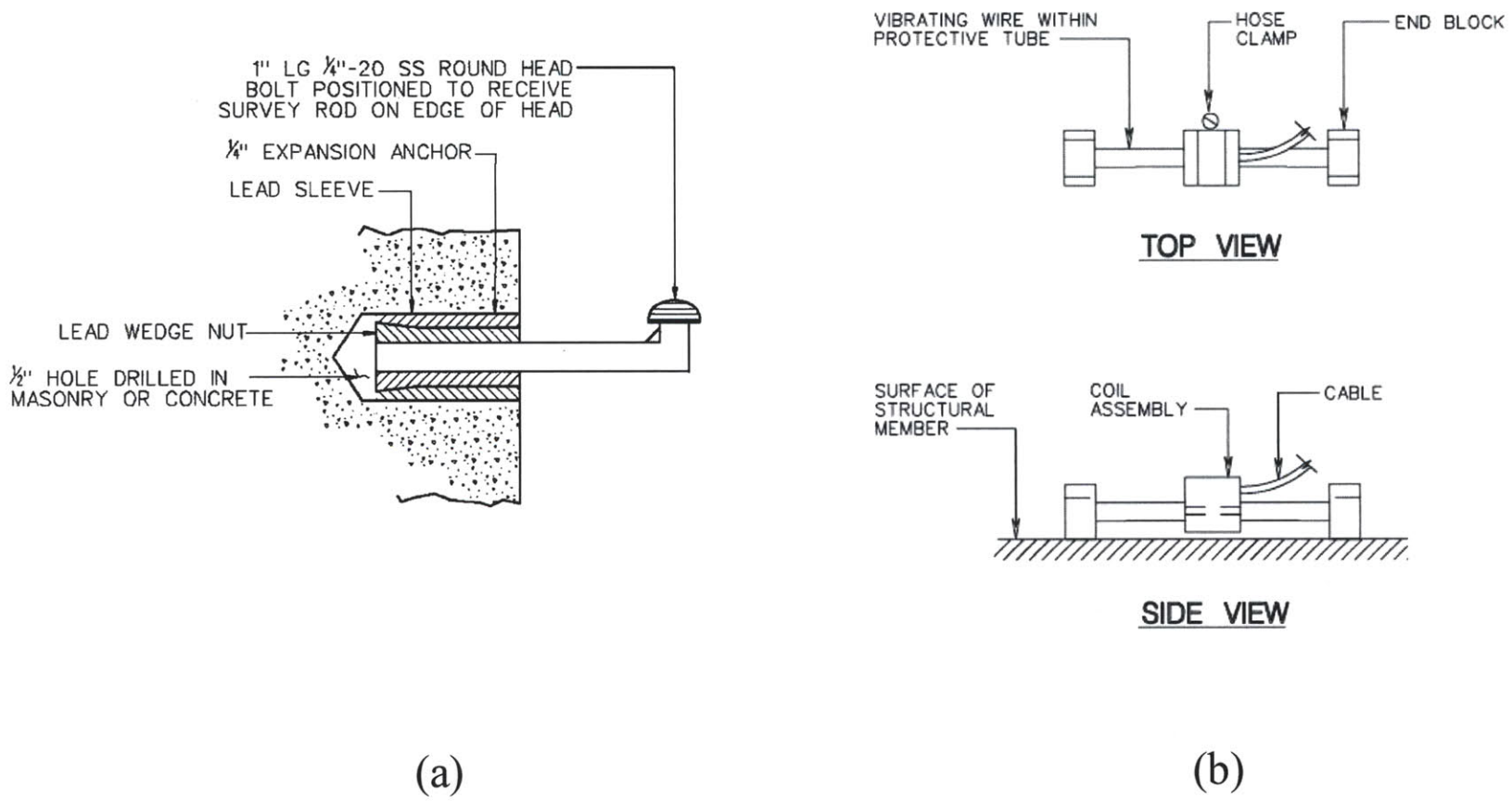

Figure 4-2: Example of pointwise measurements: (a) deflection monitoring point used in concrete surface or vertical masonry and (b) strain gages used in structural elements (after Hung et al., 2009)

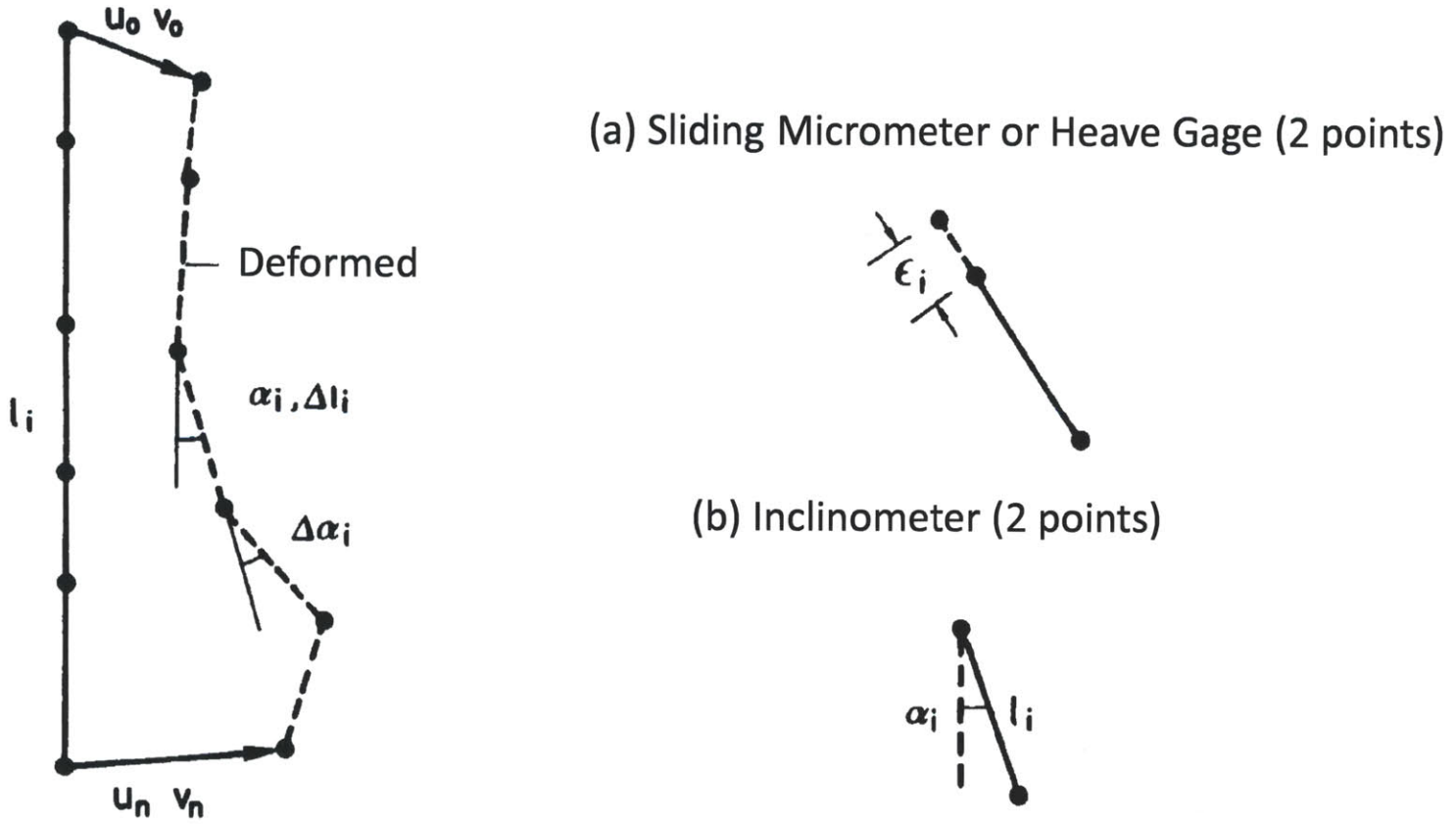

Figure 4-3: Linear deformed of straight line used in (a) sliding micrometer and heave gage and (b) inclinometer (after Ledesma, 1987)

(a)

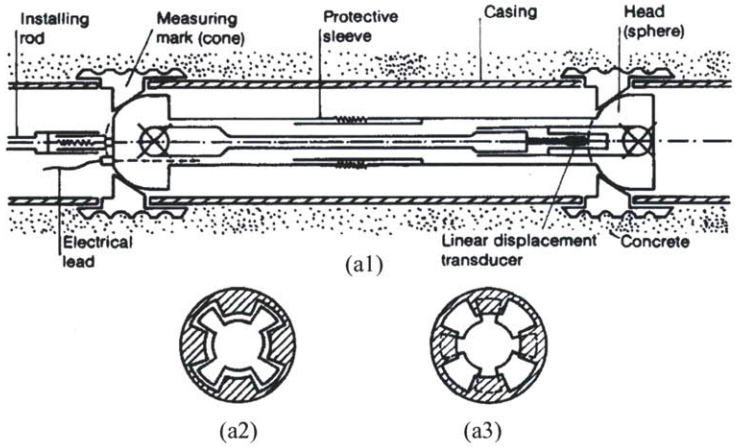

(b)

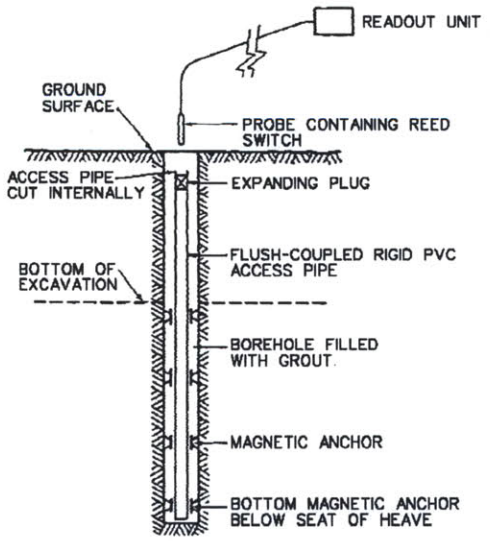

Figure 4-4: Example of linewise instruments: (a) Sliding Micrometer: (a1) schematic view, (a2) sliding position, and (a3) measuring position (after Kovári and Amstad, 1982); (b) Heave Gage (after Hung et al., 2009)

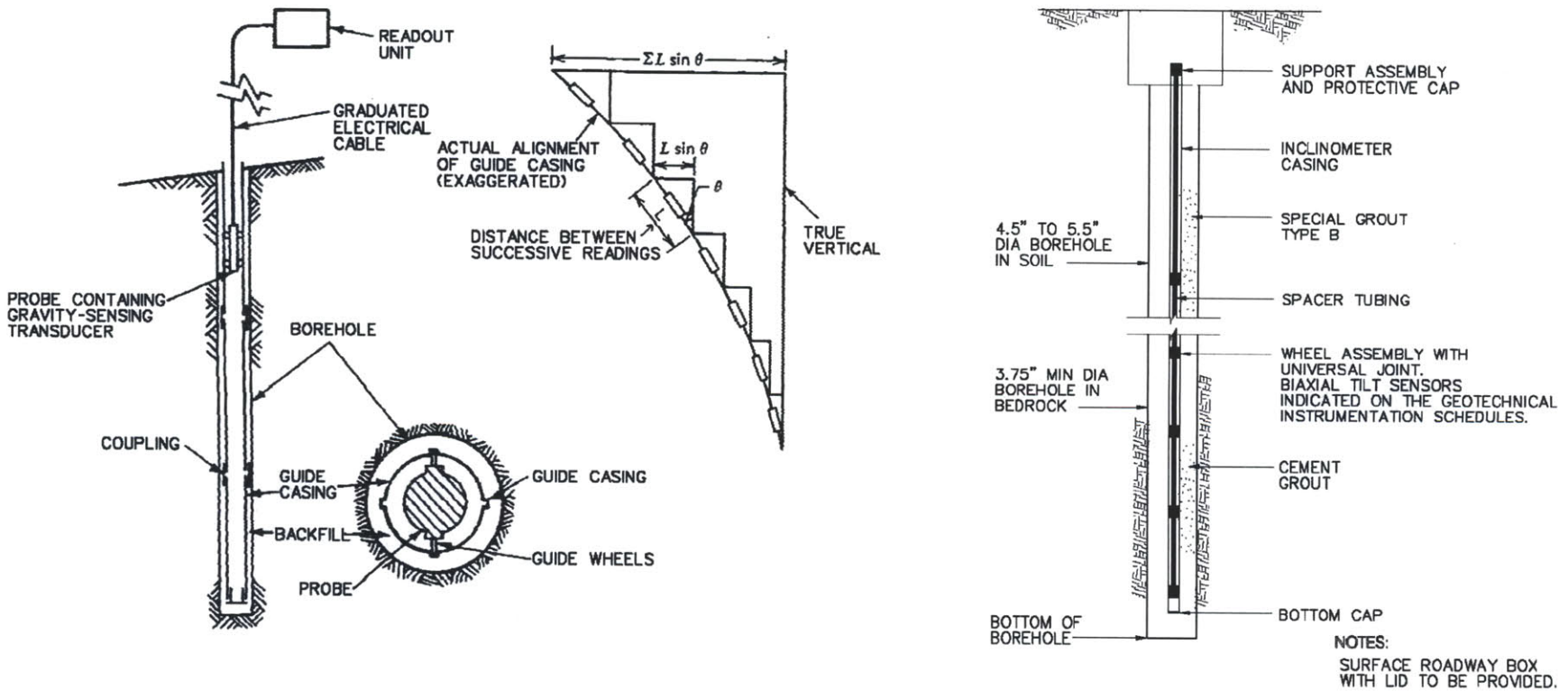

Figure 4-5: Examples of inclinometers: (a) conventional inclinometer (after Dunnicliff, 1993) and (b) in-place inclinometer (after Hung et al., 2009)

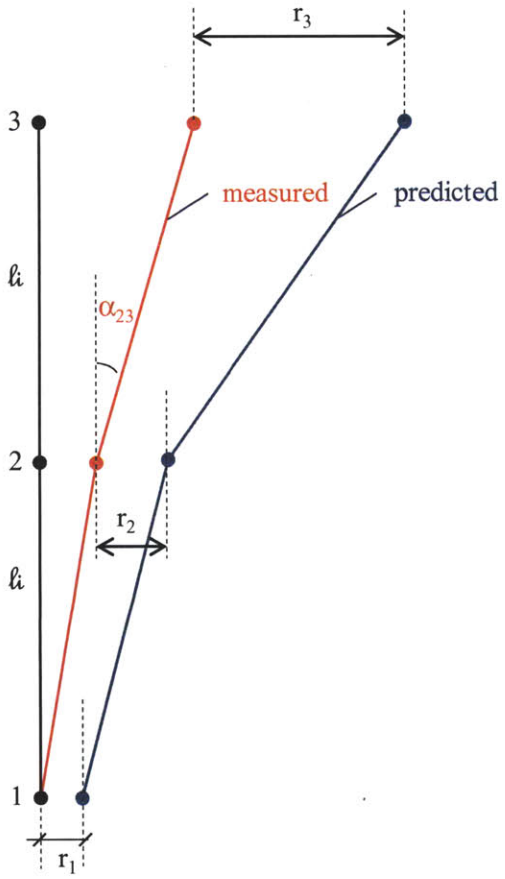

Assumptions:
1) ℓi constant
2) α_{ij} small
3) horizontal scale >> vertical scale
4) horizontal displacement only
5) variance of measurement at point 1 is zero

Covariance Matrix of Measurements
(3 points inclinometer)

$$\boldsymbol{C}_m = \sigma^2 {l_i}^2 \begin{bmatrix} 1 & 1 & 1 \\ 1 & 2 & 2 \\ 1 & 2 & 3 \end{bmatrix}$$

$$\rightarrow \quad \boldsymbol{C}_m{}^{-1} = \frac{1}{\sigma^2 {l_i}^2} \begin{bmatrix} 2 & -1 & 1 \\ -1 & 2 & -1 \\ 0 & -1 & 1 \end{bmatrix}$$

Objective Function
(Maximum Likelihood Approach)

$$J = [r_1 \quad r_2 \quad r_3]\, \boldsymbol{C}_m{}^{-1} \begin{bmatrix} r_1 \\ r_2 \\ r_3 \end{bmatrix}$$

$$\rightarrow \quad J = \frac{1}{\sigma^2 {l_i}^2} \{2{r_1}^2 - 2r_1 r_2 + 2{r_2}^2 - 2r_2 r_3 + {r_3}^2\}$$

Figure 4-6: Example of covariance matrix of measurements and objective function expressions for three point inclinometer.

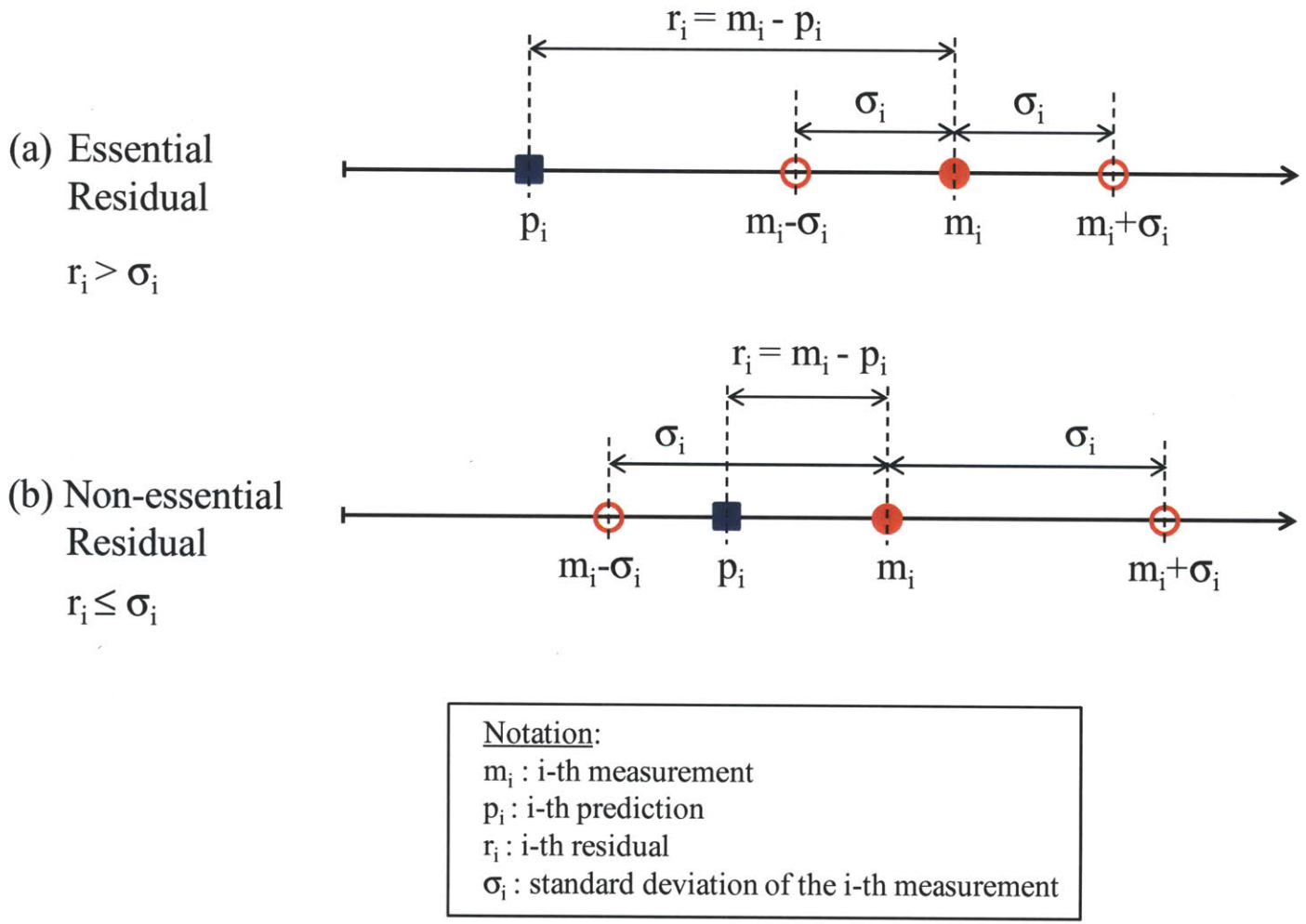

Figure 4-7: Illustrative example of essential and nonessential residuals for a single point measurement

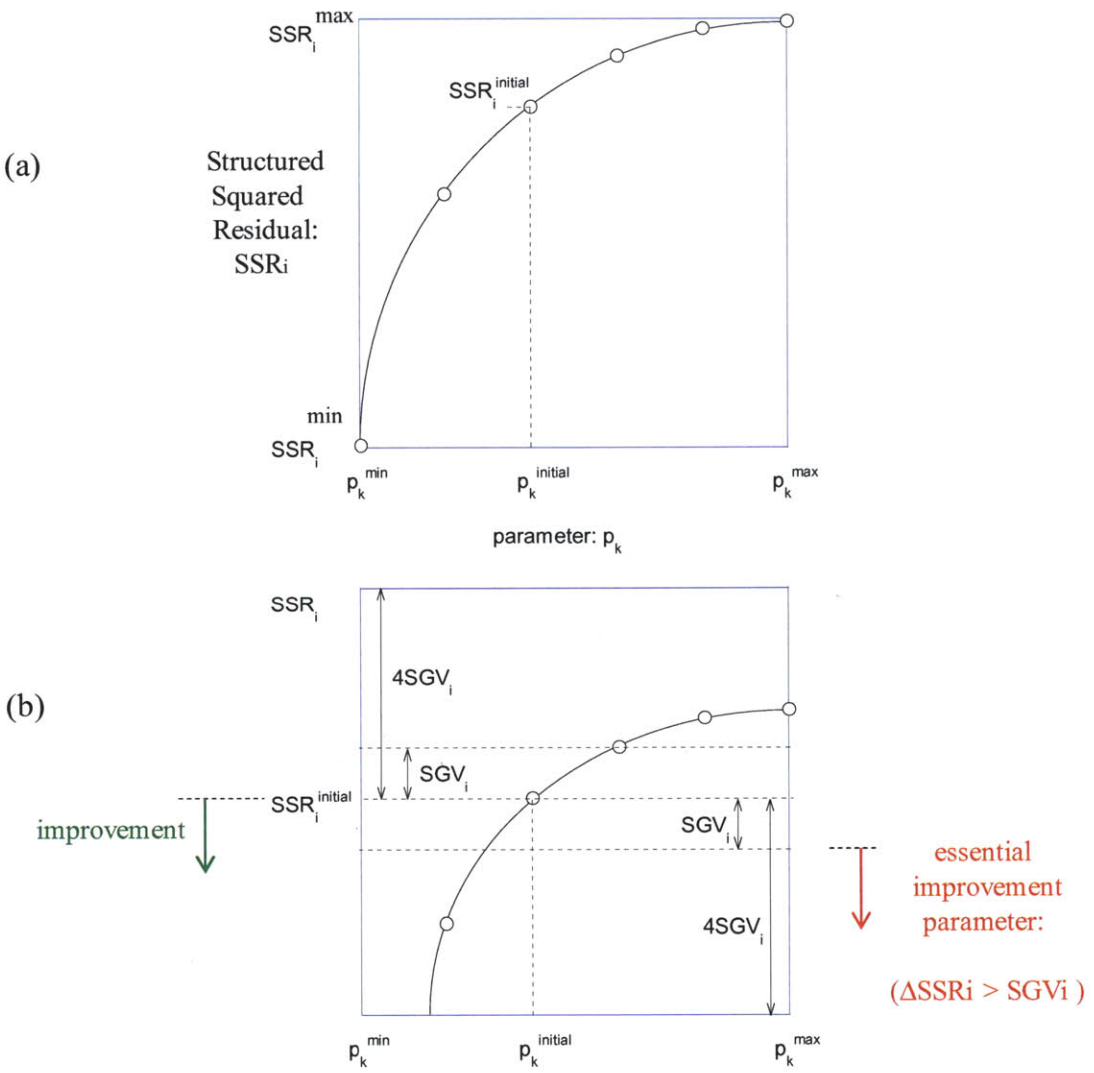

Figure 4-8: Illustrative example of sensitivity analysis for an essential improvement parameter: (a) showing maximum and minimum SSR_i, and (b) comparing SSR_i with SGV_i

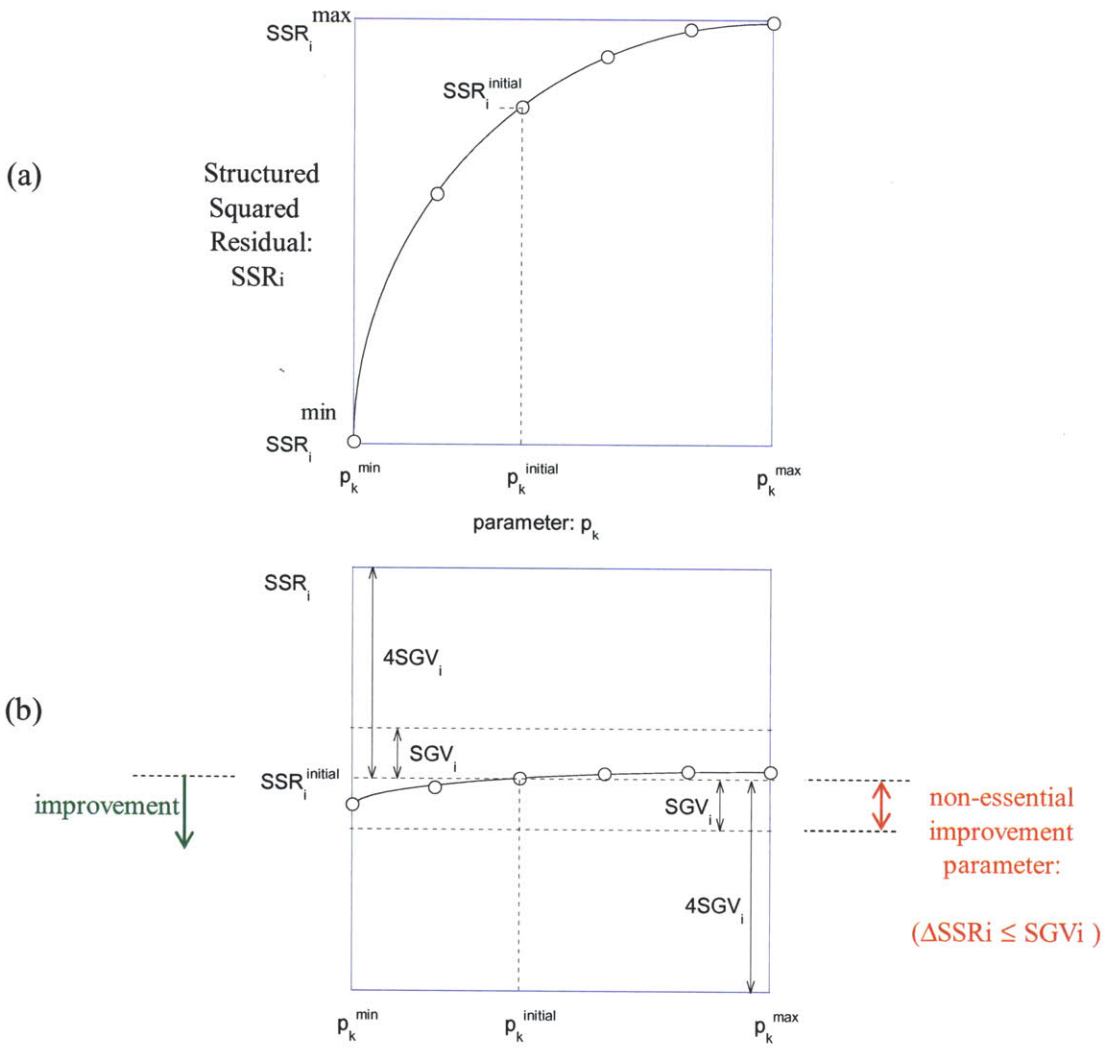

Figure 4-9: Illustrative example of sensitivity analysis for a nonessential improvement parameter: (a) showing maximum and minimum SSR_i, and (b) comparing SSR_i with SGV_i

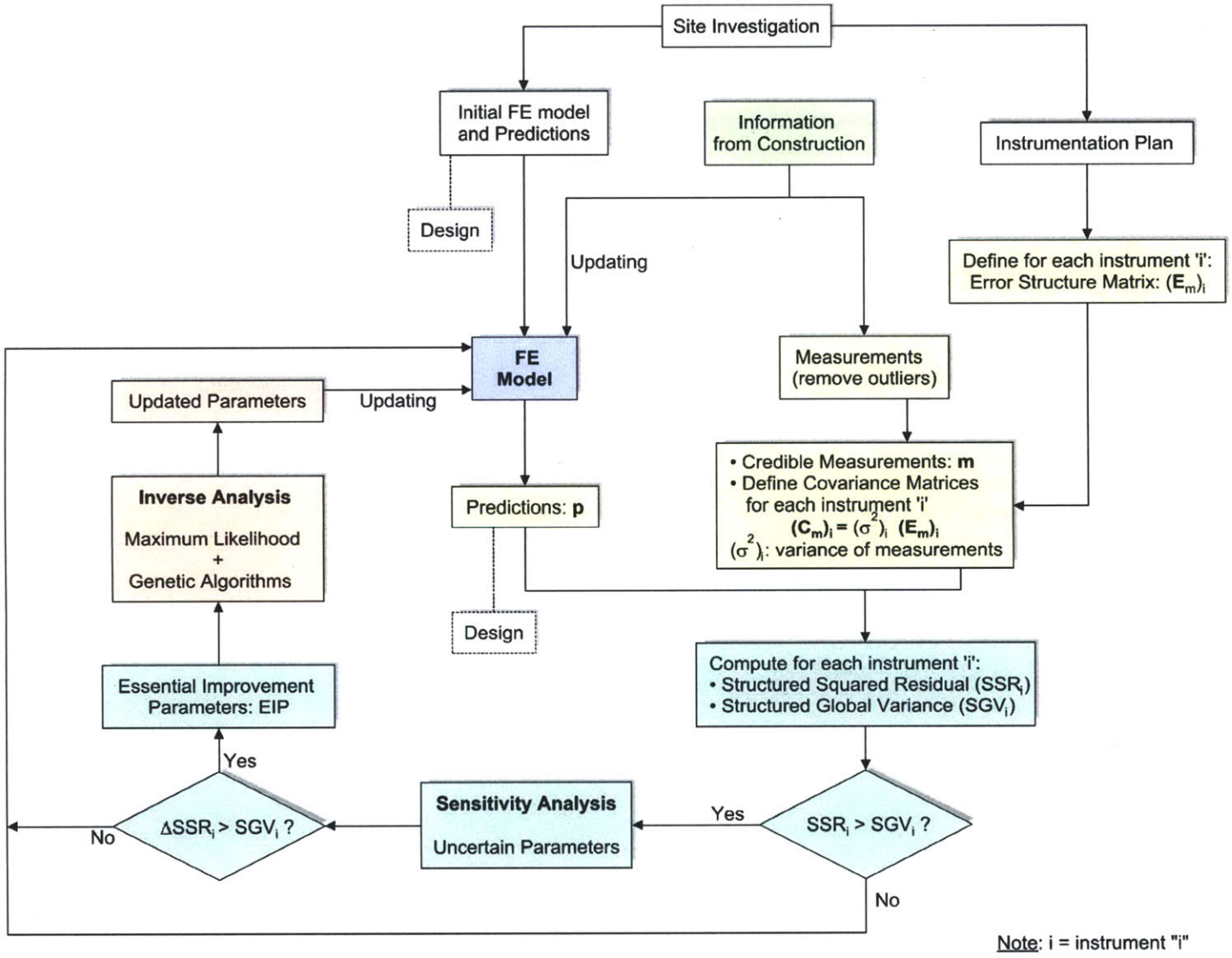

Figure 4-10: Proposed Methodology for updating FE predictions of excavation performance

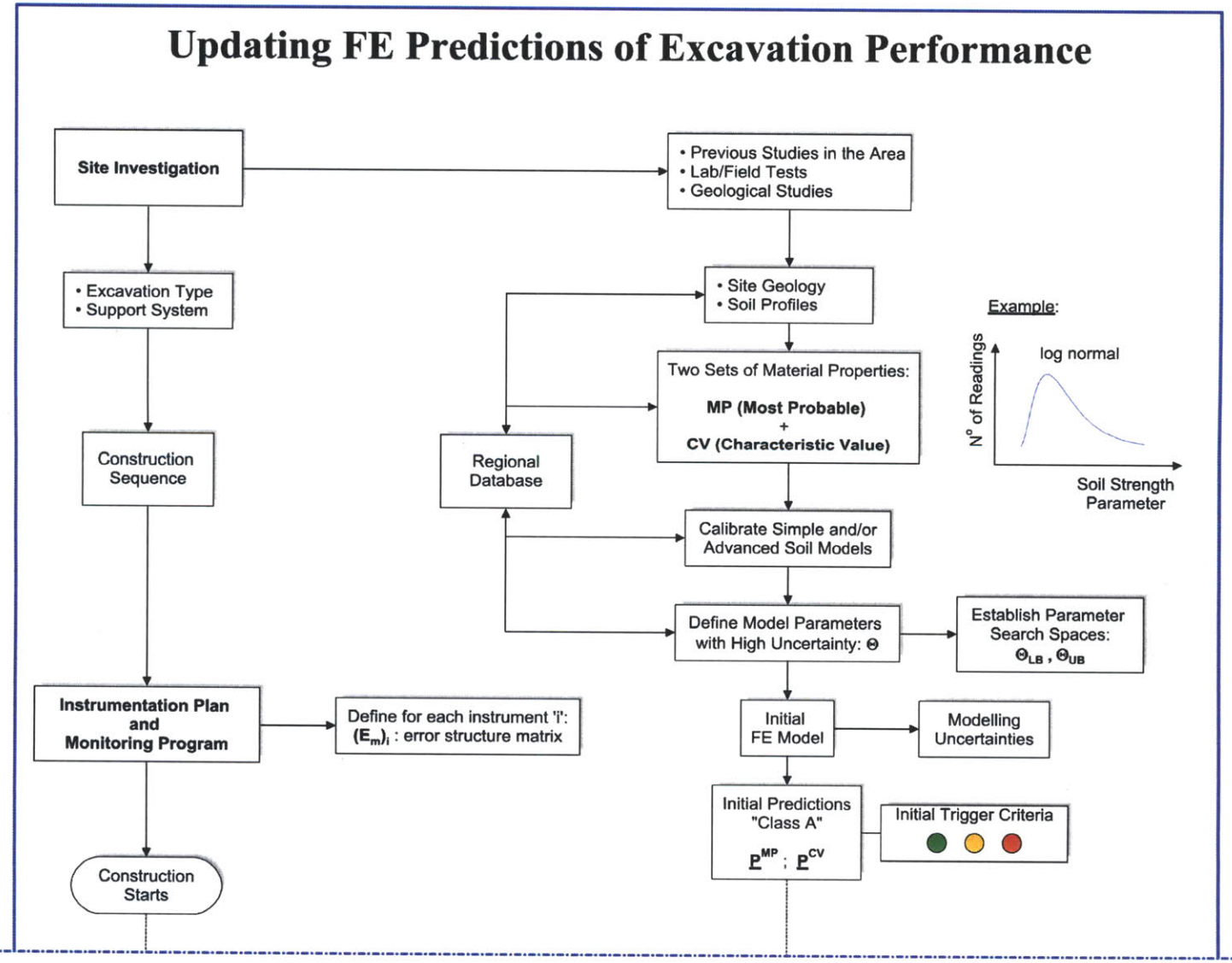

Figure 4-11a: Generalized methodology for management construction process of excavation performance (1/2)

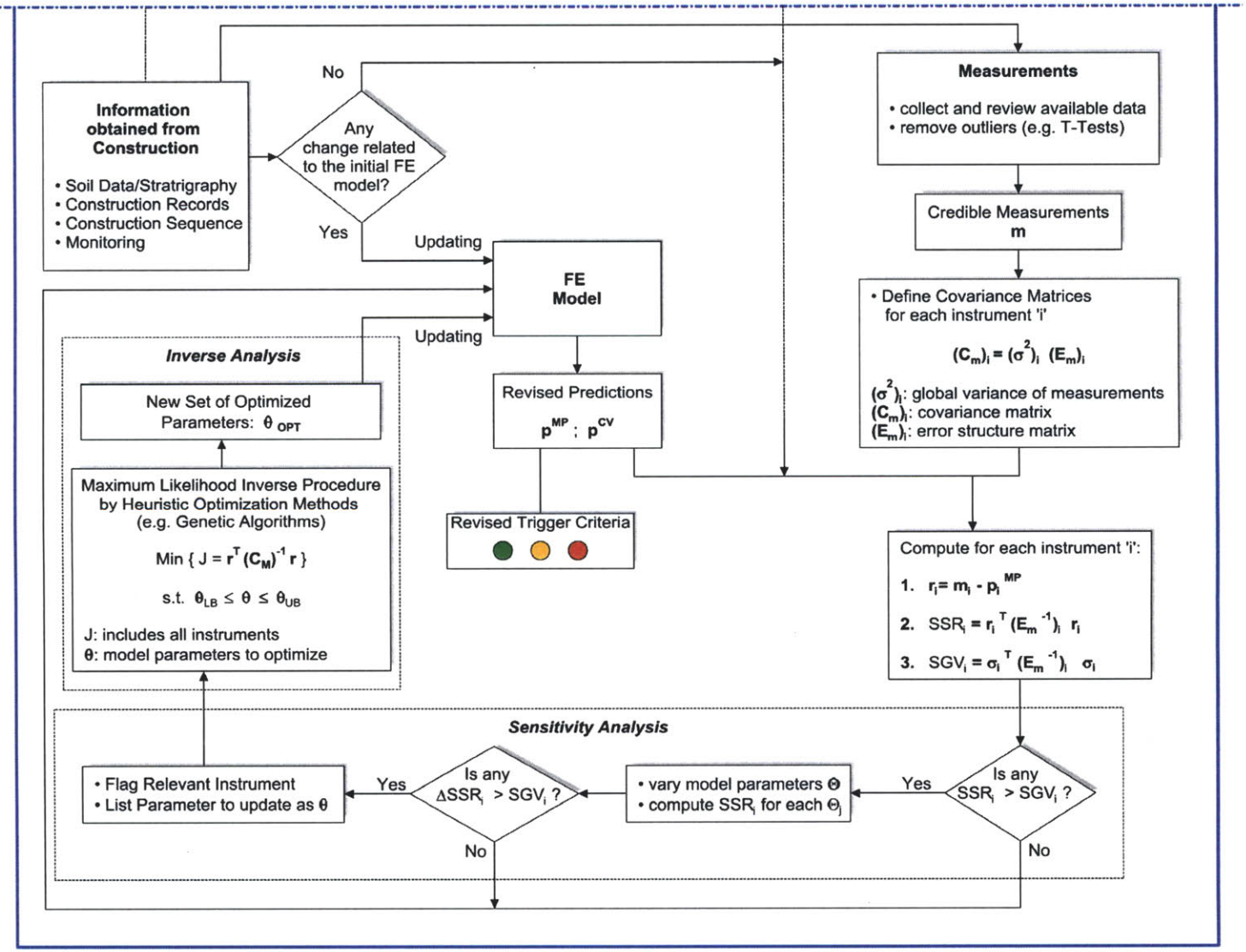

Figure 4-11b: Generalized methodology for management construction process of excavation performance (2/2)

(a)

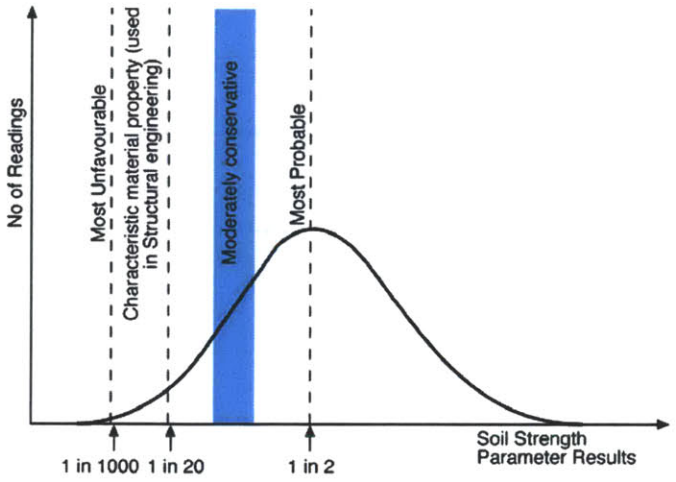

(b)

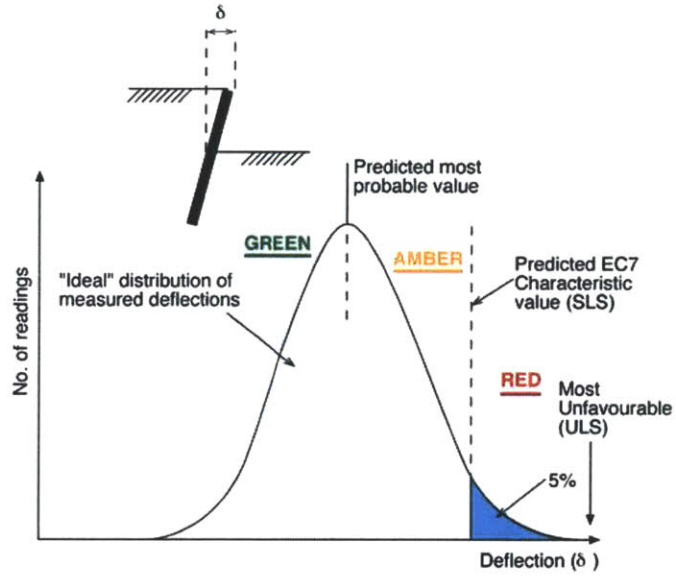

(c)

Most Probable	50% likelihood of movement predictions being exceeded
Characteristic Values (EC7) or moderately conservative (CIRIA185)	5% likelihood of movement predictions being exceeded
Most unfavourable (CIRIA 185)	0.1% likelihood of movement predictions being exceeded

Figure 4-12: Examples of: (a) Types of soil strength parameters (after Nicholson et al., 1999); (b) Ideal Eurocode 7 predicted versus measured performance; and (c) Definition of most probable, characteristic values, and most unfavorable values (after Patel et al., 2007)

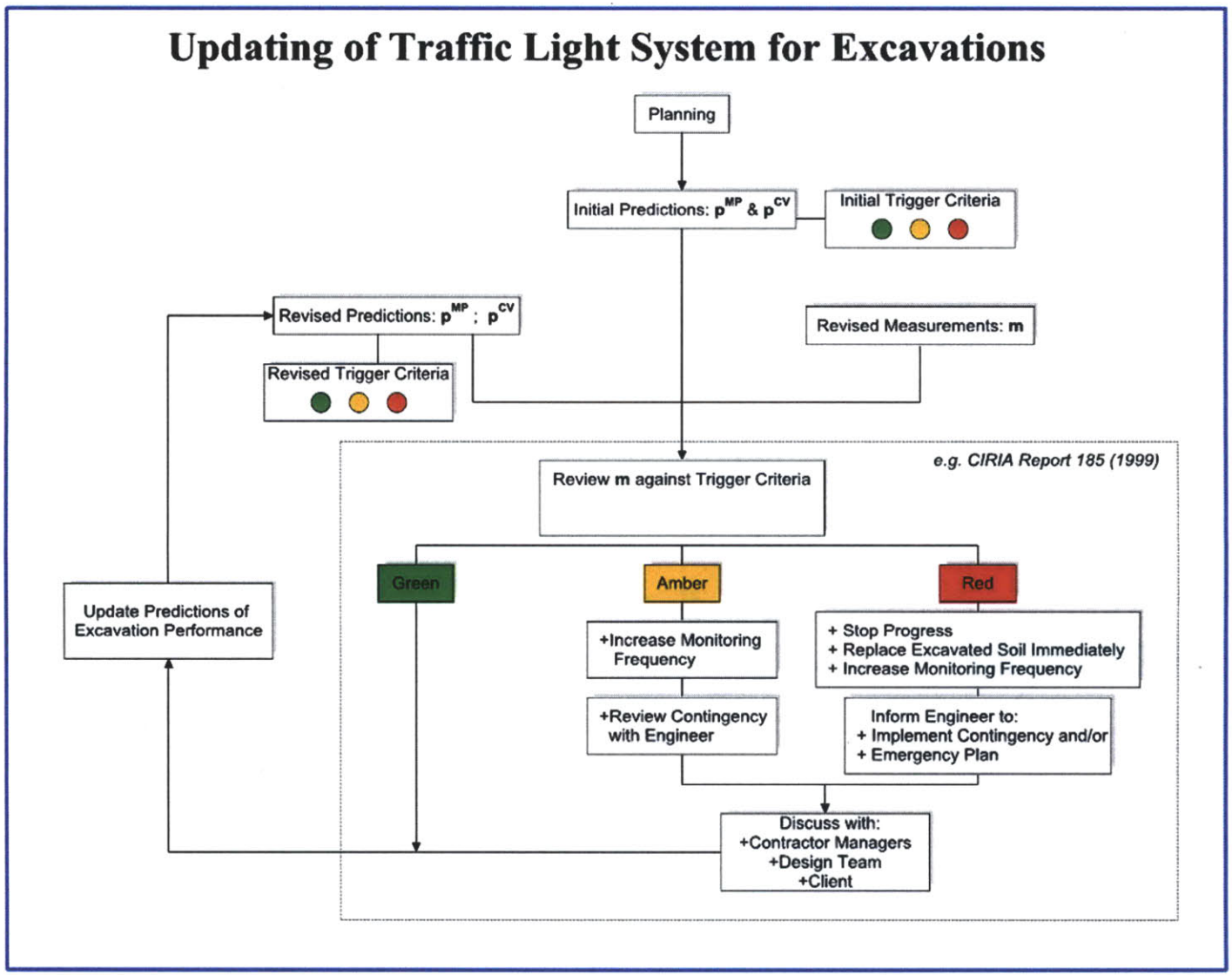

Figure 4-13: Updating of traffic light system for excavations using the proposed methodology

5 APPLICATION OF PROPOSED UPDATING PROCEDURE

5.1. Introduction

This chapter applies the proposed methodology for updating finite element predictions of excavation performance to the Transitway case study (Section 2.2). This project involves a 17.3m deep excavation for the MBTA Silver Line Courthouse Station. The excavation and support system diaphragm walls with 5 levels of cross-lot bracing are well represented by a 2D finite element model (Platform section) of the half-section (i.e., full model symmetry). This chapter describes the finite element model, identification of essential improvement parameters at each stage of construction through sensitivity analyses. The chapter gives full details of the inverse analyses and updating of parameters. The results show how model updating would be applied and how these analyses assist in reducing uncertainties through the course of the construction. The current analyses use simplified (MC) constitutive models. The final section compares these results with predictions using a more complex soil model (MIT-E3) that were presented in Chapter 2.

5.2. Transitway Project: Case Study

5.2.1. Finite Element Model

The Transitway project description and the platform section details were discussed in detail, previously in Section 2.2, and are not repeated here.

Figure 5-1 shows the assumed finite element model of the Platform section for the MBTA Courthouse Station excavation (class B; section 2.2). The phreatic level is set at 2.7m below ground level (El. + 31.1 m); there is a head loss of 2.9 m through the underlying Boston Blue Clay (BBC). At the base of the model (bottom of BBC) a constant head, H=28.2 m was adopted. Figure 5-1 also shows the initial vertical effective stresses and pore pressures. The model assumes symmetric conditions (horizontal soil layers and uniform excavated grade), such that only a half-model of the section is used. Coupled analyses of fluid flow and deformations in the soil are performed using 15-3 mixed interpolation, high order solid triangular finite elements to describe the soil and diaphragm wall. The cross lot bracing is simulated using node-to-node anchors (elastic spring elements with constant axial stiffness) with average horizontal strut spacing of 6.45 m (see Figure 2-3).

Figure 5-2 shows the construction sequence in 12 discrete construction stages. The excavation is supported by a reinforced concrete diaphragm wall (1.22 m thick and 26.2 m deep), with five level of cross-lot bracing. The excavation grades and duration of each excavation step are based on a detailed interpretation of the as-built construction records. Measurements of strut pre-loads were achieved by averaging data from the 4 strain gauges* installed at each strut level and at different strut lines (for strutting plan, see Figure 2-3). Average values of measured pre-loads ranges from 0† to 613 kN/m, as shown in Figure 5-2.

---

* Strain gauges that measure strut forces were installed in every other strut line at the same strut level

† The actual average strut level 1 pre-load was 41kN/m; however, since the standard deviation was larger than the value, a zero value was assumed in this case.

Table 5-1 summarizes the construction steps used in the finite element simulations. The diaphragm wall installation and the cross-lot bracing installations were represented as undrained events (i.e., "plastic analysis" in Plaxis), while excavation stages include partially drainage (i.e., "consolidation analysis" in Plaxis)[‡] with specified time periods. The final excavation grade El. +16.5 m is reached after 279 days of construction. The sequence of construction activities, elevations, and support system are identical to those used in the class B[§] presented in Chapter 2.

The constitutive modeling of soil behavior and selection of input parameters represents a major source of uncertainty in finite element analysis (Whittle et al., 1993). The lack of lab tests on high quality samples in the granular fill, cohesive fill, and silty sand limits current capabilities to describe these units. The only available data for the upper layers are standard penetration tests (SPT). Empirical correlations between N_{SPT} and friction angle as well as Young's modulus are available (e.g., Skempton, 1986; Stroud, 1989) although with high uncertainty. Although the Boston Blue Clay (BBC) has been extensively studied in the past 50 years, especially at MIT, and also calibrated with an advanced soil model (e.g., MIT-E3; Whittle et al., 1994), for the application of the proposed methodology and in order to assume a more typical case (i.e., where no advanced soil model calibrations are available), the simple linearly elasto-perfectly plastic constitutive model Mohr-Coulomb[**] (MC) was selected for the five soil layers. This very-well-

[‡] It is important to be aware that using MC model in Plaxis (referred to as Method B), it does not update strengths as it does not considered effective stress strengths.

[§] The only difference corresponds to the strut level 1 pre-load assumed.

[**] Although the correct name of this constitutive law is Coulomb model; in this thesis, it will be referred to as Mohr-Coulomb or MC model.

known MC model requires only five parameters[††]: 1) Young's modulus: E'; 2) Poisson's ratio: ν'; 3) apparent cohesion: c; 4) internal friction angle: ϕ'; and 5) initial effective stress ratio: K_0.

Table 5-2 summarizes the material properties for the five soil units, where each layer is represented by the MC model. The upper fill layers (granular fill, cohesive fill and silty sand) have relatively high hydraulic conductivities and are treated as drained materials[‡‡]; while the upper BBC (slightly overconsolidated) and the lower BBC (normally consolidated) are "undrained" materials. The material properties for the three upper layers used were estimated from SPT correlations (Stroud, 1989) and assumptions made by Jen (1998). The initial undrained shear strengths and shear stiffnesses selections for the BBC units were based on the stress history profile (Fig. 5-4) as well as some available correlations that will be discussed later in this chapter. The initial hydraulic conductivity profile (Fig. 5-5b) in the BBC unit, assumed to be 5×10^{-10} m/sec and isotropic (i.e., $k_x=k_y$), was estimated from constant rate of strain consolidation tests (CRSC) (after Whelan, 1995).

Table 5-3 shows the material properties of the diaphragm wall and strutting system used in the FE model.

Figure 5-3 shows the location of instrumentation used for updating predictions. Those are: 1) inclinometer; 2) surface settlement (DMP); 3) piezometric sensors; 4) heave sensor; and 5) strut elevations (i.e., elevations of strain gauges to measure strut forces).

[††] We assume zero dilation ($\psi=0°$) for all layers in order to assume zero volume strain conditions at failure.

[‡‡] i.e., no excess pore pressures develop in these layers.

The measurements used includes: 1) lateral soil/wall movements, measured by five inclinometers cast within the wall; 2) surface settlements by sixteen deflection monitoring points (denoted by DMP); 3) excavation heave by one multi-point heave gage located at the center of the excavation; 4) piezometric head measurements from one vibrating wire piezometer inside the excavation; and 6) strut forces measured by twenty strain gauges distributed at different strut lines and elevation in the Platform section (see Figure 2-3). The averages and variances of measurements were estimated with all measured data available between the following time frames (i.e., construction days): 1) excavation level 1 (CD 48-51); 2) excavation level 2 (CD 83-90); 3) excavation level 3 (CD 111-118); 4) excavation level 4 (CD 139-153); 5) excavation level 5 (CD 183-201); and 6) excavation level 6 (CD 274-284). Table 5-4 presents the magnitudes of the variances[§§] of the field measurements used in both the sensitivity analysis and inverse analysis.

5.2.2. Uncertain Parameters and Search Spaces

The initial predictions must correspond to class A predictions. The information that was obtained during construction (e.g. construction records, soil stratigraphy, strut pre-loads, etc.) was included in the initial FE model, which means that there is no need to update layer thickness, unit weights, and elevations (shown in Table 5-2) as well as excavation grades, and strut pre-loads (as the proposed methodology specifies to update as needed). This basically implies that the

[§§] In principle, two measured data are enough to approximately estimate a variance; however, the more number of data, the more representative and reliable the variance will be. It is recommended to include all available data and remove all possible outliers. In particular, for the Transitway project, four measured surface settlements behind the South wall (two at 24m and two at 37m) were considered outliers due to the presence of the building (see Figure 2-14). This was because of the symmetric conditions assumed in the FE model (see Section 5.2.1).

boundary conditions and stratigraphy are certain, which may not be case in other practical applications. Thus, the current application assumes that modelling uncertainty is due exclusively to uncertainties in the input parameters of constitutive behavior of the soil units.

Table 5-2 shows the material properties to study that will be included in the sensitivity analysis, discussed in the next section. In Table 5-2, it can be seen that for the three upper soil layers (granular fill, cohesive fill, and silty sand), three parameters of each upper layer are to be studied: 1) reference shear stiffness, G^{ref}; 2) internal friction angle, ϕ';and 3) initial effective stress ratio, K_0. Hence, 9 parameters are varied within these units.

In addition, for the upper BBC layer (see Table 5-2), the parameters considered with high level of uncertainty are: 1) hydraulic conductivity (assumed to be isotropic: k_x=k_y); 2) reference shear stiffness, G^{ref}; 3) change of stiffness with depth, $\Delta G/\Delta z$; 4) reference undrained shear strength, s_u^{ref}; 5) change of undrained shear strength with depth: $\Delta s_u/\Delta z$; and 6) initial effective stress ratio, K_0. Hence, 6 parameters are varied within this unit.

The lower BBC layer (see Table 5-2) has constant OCR and hence, the depth variation of undrained shear strength (s_u^{ref} and $\Delta s_u/\Delta z$) and K_0 are fixed. Hence, 3 parameters are varied within this unit.

Based on this assessment, there are 18 constitutive model input parameters that are considered highly uncertain. This list can be reduced by considering well-known correlations among engineering properties. For example, Equation 5-1 shows the very-well known expression

between K_0 and ϕ' (Jaky, 1944). The use of this relation allows one to reduce the nine uncertain parameters of the upper soil layers to 6 parameters (G^{ref} and ϕ' for each layer).

$$K_0 = 1 - \sin\phi' \tag{5.1}$$

where K_0 is the lateral earth pressure ration (at rest); and ϕ' is the effective internal friction angle.

In clays, there is also a well-known linkage between K_0 and OCR (Schmidt, 1966; Mayne and Kulhawy, 1982):

$$K_0 = K_{0\,NC}(OCR)^n \tag{5.2}$$

where [***]K_0 is the initial lateral effective stress ratio for overconsolidated BBC; $K_{0\,NC}$ is the value for normally consolidated clay; and OCR is the overconsolidation ratio. Prior laboratory studies for BBC at South Boston (Ladd et al., 1999) did $K_{0\,NC} = 0.53$ and $n = 0.4$.

The SHANSEP equation (Ladd and Foot, 1974) relates the undrained shear strength, shown in Equation 5.3. In this equation, the constants are obtained empirically from lab tests in different modes of shearing. Here we assumed the direct simple shear to be the most representative for the undrained shear strength of BBC. Based on the stress history data (Figure 5-4), it is possible to assumed that the lower BBC is normally consolidated. Assuming OCR =1.0

[***] For the MC model only, the K_0 value was assumed constant for the U-BBC unit; therefore, an average value of OCR was used: $OCR_{ave}=(OCR_{top}-OCR_{bot})/2$

in the lower BBC layer, Equations 5-2 and 5-3 allow one to correlate s_u^{ref}, $\Delta s_u/\Delta z$, and K_0 to the OCR at the top of the upper BBC layer (denoted by OCR_{TOP}; Figure 5-4).

$$\frac{s_u}{\sigma'_{v0}} = S(OCR)^m \tag{5.3}$$

More recently, Santagata et al. (2005) have proposed a correlation between G_{max} and OCR for Boston Blue Clay, where G_{max} is the shear modulus that controls elastic shear wave propagation (at very small strain levels). Given that σ'_{v0} is well defined (Figure 5-1) and K_0 depends on the OC, it is possible to relate G_{max} to the OCR at a given elevation:

$$\frac{G_{max}}{p_a} = 381(OCR)^{0.15}\left\{\frac{\sigma'_0}{p_a}\right\}^{0.8} \tag{5.4}$$

where p_a is the atmospheric pressure and σ'_0 is the mean effective stress, $\sigma'_0 = \frac{\sigma'_{v0}}{3}(1+2K_0)$.

The value of G_{max} corresponds to the shear stiffness at very small strain levels; thus, it is necessary to make further assumptions in estimating the average elastic shear stiffness used in the MC model. This is consistently achieved using a simple stiffness reduction parameter, α:

$$\alpha = \frac{G}{G_{max}} \tag{5.5}$$

$$\frac{G}{p_a} = \alpha \cdot 381(OCR)^{0.15}\left\{\frac{\frac{\sigma'_{v0}}{3}(1+2K_{0\,NC}(OCR)^n)}{p_a}\right\}^{0.8} \tag{5.6}$$

Thus, the four stiffness parameters of BBC (G^{ref} and $\Delta G/\Delta z$ in the upper and lower units) can be replaced by two parameters only; $\alpha_{U\text{-}BBC}$, and $\alpha_{L\text{-}BBC}$.

Table 5-5 summarizes these parameter relations and correlations used for updating MC model parameters. Table 5-6 proposes search spaces for each of these parameters. The lower and upper bounds for the three drained layers (GF, CF, and SM) were estimated from standard deviations of N_{SPT}[†††] (PB, 1998) and the use of some empirical correlations between N_{SPT} and both ϕ' and Young modulus, E (Stroud, 1989).

Figure 5-4 summarizes the stress history obtained from 1-D consolidation tests at the South Boston Special Test Site (SBSTS program; Ladd, et al. 1999). The upper and lower bound stress history profiles selected (OCR_{top} from 2 to 6) are also shown as well as the initial profile assumed (OCR_{top}=5). The measured data show important scatter, the reason why some data were deleted (Ladd et al., 1999). The reason for not going to higher OCR values is uniquely due to the inconsistency between the OCR profile and SHANSEP strengths, discussed previously in Section 2.2.2.2.

Figure 5-5a shows the initial undrained shear strength (estimated from SHANSEP DSS mode of shearing (Eqn. 5.3) assumed in the FE model. Additionally, this figure shows measured data of undrained shear strength performed at the SBSTS (Ladd et al., 1999) as well as the upper and lower bound s_u profiles. Figure 5-5b presents the measured hydraulic conductivity profiles

[†††] $\bar{N}_{GF}$=38 ± 28 bpf (n=13); $\bar{N}_{CF}$=4 ± 4 bpf (n=49). $\bar{N}_{SM}$=29 ± 13 bpf (n=40)

(data from Whelan, 1995) together with upper and lower bounds assumed in the analyses. It is important to highlight that for both the upper and lower BBC, the search space range is one order of magnitude (i.e., $k_{max}/k_{min}=10^1$).

Figure 5-6 shows the initial profiles, lower and upper search bounds for 1) undrained shear strength, 2) K_0, and 3) shear stiffness in the BBC in South Boston. The s_u profile is compared with field vane data reported from the project site investigation. In principle, the data should be in agreement with the SHANSEP DSS lab data. However, the field vane measured data show a large scatter with very low values in the lower BBC unit[‡‡‡]. This is one of reason why the lower and upper search bounds were selected. For the upper BBC layer, the K_0 profile was estimated for an average value of OCR and Equation 5.2. The shear stiffness profile for the BBC was selected for the average OCR of the upper BBC unit and OCR=1 in the lower unit. However, the values of α parameter ($\alpha=G/G_{max}$) were arbitrarily chosen to be initially equal to 0.35 and 0.65 for the upper and lower, respectively (see Equation 5-6). The reason why the upper BBC presents a wider search space range is because of the OCR was assumed constant at the lower BBC layer, reason also for having a constant K_0 profile at that layer.

Summarizing, the use of all of these relationships and correlations allows one to reduce from the eighteen uncertain parameters to only eleven: 1) G_{GF}^{ref}, 2) G_{CF}^{ref}, 3) G_{SM}^{ref}, 4) ϕ_{GF}', 5) ϕ_{CF}', 6) ϕ_{SM}', 7) OCR_{TOP}, 8) $\alpha_{U\text{-}BBC}$, 9) $\alpha_{L\text{-}BBC}$, 10) $k_{U\text{-}BBC}$ and 11) $k_{L\text{-}BBC}$. It is very important to emphasize that the use of empirical relations and correlations involves uncertainties and constrains the updating process.

[‡‡‡] These values are considered uncertain and most likely affected by disturbance caused by vane installation.

5.2.3. Sensitivity Analysis Results

Although most published comparisons between predictions and measured performance are qualitative (e.g., shape of deflections, good and bad agreements, etc.), these comparisons can be quantified. Table 5-7 summarizes the magnitudes of initial structured squared residuals (SSR) and structured global variances (SGV) at each excavation level. This table will be discussed later in the chapter, since it includes all excavation levels. It can be seen that set of predictions at excavation levels 1, 2, and 3 meet the criterion $SSR_i > SGV_i$ (see Eq. 4-21) and hence, sensitivity analyses are required. Sensitivity analyses for excavation levels 1, 2, 3 are shown in Figures A-1 – A-42 (Appendix A). Table 5-7 also shows that these cases generate sensitivity results where $\Delta SSR_i < SGV_i$ and therefore, there are no Essential Improvement Parameters (EIP) for these initial excavation phases (i.e., no updating is required).

The project has limited pore pressure data and these are the only parameters for which SSR < SGV throughout construction (Table 5-7). This result occurs at pore pressures measured below the center of the excavation and are controlled principally by equilibrium conditions (excavated grade levels) and are not affected by model input parameters.

The sensitivity analysis results of all excavation levels and of all 11 highly uncertain parameters are presented in Appendix A. Table 5-7 also shows that only excavation levels 4, 5, and 6 (stages 8, 10, and 12) generate conditions where $\Delta SSR_i > SGV_i$. These are the only stages where the existence of EIP's justifies inverse analyses and updating of predictions.

Table 5-8 presents a summary of the sensitivity analysis results showing both the essential and non-essential improvement parameters as defined in the previous chapter (see Figs. 4-8 and 4-9) at excavation levels 4, 5, and 6. This table reveals number of input parameters used in subsequent optimization. As all the sensitivity analyses are presented in Appendix A, only these parameters providing essential improvement are discussed in this chapter.

5.2.4. Measurements and Initial Predictions at Levels 1, 2, and 3

As previously mentioned, the structured squared residuals (SSR) and the structured squared variances (SGV) provide a rational quantification of the agreement of predictions and field measurements. It is important to highlight that the reported SSR and SGV values of surface settlement, strut forces, and pore pressures correspond to average values (i.e., cumulative SSR divided by the number of devices or sensors).

Figures 5-7, 5-8, and 5-9 compare the predicted and measured lateral wall/soil movements at excavation levels 1, 2, and 3, respectively (stages 2, 4, and 6; Table 5-1; Figure 5-2). In general, the predictions are in very close magnitudes and shapes with the measured inclinometer data. The SSR values are lower than the SGV for levels 1 and 3, implying very good predictions; however, the SSR at level 2 (Fig. 5-8) is slightly larger than the SGV, which is reflected in the difference in wall curvature.

Figures 5-10, 5-11, and 5-12 compare the predicted and measured surface settlements at excavation levels 1, 2, and 3, respectively. There is a clear under-prediction of settlement at excavation level 1, with the SSR value much higher than the SGV. For excavation level 2, there

is a reasonable agreement between measured and predicted settlements, with SSR < SGV. For excavation level 3, there is a very good prediction of surface settlement since the SSR is much lower than the SGV.

Figures 5-13 and 5-14 compare the predicted and measured strut at excavation levels 2, and 3, respectively. At excavation level 2, the strut force prediction agrees almost perfectly with the measured force, with a very low SSR value. However, at excavation level 3, both strut levels 1 and 2 under-predict the measured values, with SSR > SGV.

Figures 5-15, 5-16, and 5-17 compare the predicted and measured excavation heave at excavation levels 1, 2, and 3, respectively. Apart from the uppermost sensor discrepancy between measured and predicted values; predictions agree very well with the three other sensors at each level. The difference between the SSR and SGV values reflects this discrepancy.

Figures 5-18, 5-19, and 5-20 compare the predicted and measured pore water pressure at excavation levels 1, 2, and 3, respectively. Comparing the SSR and SGV values suggests that there is a good agreement between predictions and measurements at each level (see Table 5-4).

5.2.5. Updating Predictions: Excavation Level 4

The sensitivity analysis results (Table 5-7) at excavation level 4 indicate that there are 4 Essential Improvement Parameters, EIP (G_{GF}. G_{SM}, OCR_{TOP}, $\alpha_{U\text{-}BBC}$) to consider (Table 5-8).

In order to perform the optimization of maximum likelihood using genetic algorithms, a number of control parameters (see Section 3.3.3) must be selected (see Chapter 3). These include the population size, reproduction criterion, crossover function, and stopping criterion[§§§]. In this thesis, the population number adopted was equal to (10×EIP) , while the reproduction adopted was 80%, 10%, and 10%, for the crossover fraction, elitism, and mutation, respectively[****]. The crossover function used corresponds to the heuristic function which creates children that randomly lie on the line containing the two parents. The stopping criteria adopted is discussed later in this chapter.

The following paragraphs describe the results obtained from the sensitivity analysis and inverse analysis steps, as well as the comparisons between initial and updated parameter values, and comparisons between predictions and measurements.

5.2.9.1. Sensitivity Analysis

Figures 5-21 show the results of sensitivity analyses of the EIP only (for all parameters see Appendix A), as defined in Chapter 4, at excavation level 4 for three different types of measurements.

[§§§] Population size specifies how many individuals there are in each generation. Reproduction options determine how the genetic algorithm creates children at each new generation. Elitism specifies the number of individuals that are guaranteed to survive to the next generation. Crossover fraction specifies the fraction of the next generation that crossover produces. Mutation produces the remaining individuals in the next generation. Stopping criterion determines what causes the algorithm to terminate (after MATLAB 2004-2009).

[****] Selected percentages result from several parametric analyses performed on synthetic excavation problems.

Figure 5-21a shows variation of SSR for wall deflection with OCR_{TOP} (upper BBC). Clearly, it can be seen that the minimum SSR occurs at 3.0, while the ΔSSR is slightly larger than the structured global variance (SGV).

Figure 5-21b shows SSR for excavation heave versus α in both the upper and lower BBC units (only $\alpha_{U\text{-}BBC}$ is an EIP). The results show that SSR reduces significantly with $\alpha_{U\text{-}BBC}$ while $\alpha_{L\text{-}BBC}$ does not produce sufficient change in SSR to qualify as an EIP.

Figures 5-21c,d show SSR for strut forces versus the shear stiffness of the cohesive fill (CF) and silty sand (SM) layers. From this figure, it can be seen that both stiffnesses are classified as essential improvement parameters, being much more important the stiffness of the silty sand (because it decreases significantly more the SSR of strut forces).

5.2.9.2. Inverse Analysis

Figure 5-22 presents the convergence of the objective functions for the maximum likelihood from the GA analysis at excavation level 4 using all types of field measurements. Figure 5-23, 5-24, 5-25, 5-26, and 5-27 show similar convergence characteristics separately for wall deflections, surface settlements, excavation heave, pore pressures, and strut forces, respectively.

At this excavation level, a constant population of 40 individuals was used. The overall objective function J converges[††††] at generation 20, where the lowest value was selected. It is always useful to track the convergence of individual measurement types. From Figures 5-25 and 5-27, it can be seen that the objective function for excavation heave and strut forces converge to lower values than initial case (green horizontal line in the figures). However, this is not the case for the surface settlements and pore water pressures (Figures 5-24 and 5-26, respectively). Curiously, the converged value of the wall movements is almost equal to the initial one (see Figure 5-23). These results show that improvements on the maximum likelihood objective functions (J_{ALL}) are primarily due to better fitting of 1) excavation heave and 2) strut forces.

Figures 5-28, 5-29, 5-30, and 5-31 summarize the convergences of the 4 EIP parameters over 20 generations of GA analyses. The parameters converge to a set of optimal values (i.e., not to a unique value) due to the adopted stopping criteria. The values chosen were the ones that correspond to the minimum value of the overall objective function (min J_{ALL}) at the last generation. It can be seen that G_{CF}, G_{SM}, and $\alpha_{U\text{-}BBC}$ increase, while the OCRtop decreases. Table 5-9 summarizes these optimal parameter values.

Figure 5-32 compares the updated versus the initial undrained shear strength profiles as well as the SHANSEP strength profiles, showing clearly that there is a decrease in the s_u profile of the upper BBC layer (since the OCR_{TOP} decreases from 5.0 to 4.4, approximately).

[††††] The stopping criteria adopted, in this thesis, was a minimum of 10 generations and when at least 90% of the individuals converge to the same minimum objective function value.

Figure 5-33 compares the updated versus initial s_u profiles (including field vane data), K_0 profiles, and shear stiffness profiles. As s_u in the upper BBC decreases, the average K_0 also decreases. The shear stiffness variations show that the G_{CF} and G_{SM} increases substantially, while the $G_{U\text{-}BBC}$ decreases.

5.2.9.3. Predictions versus Measurements

Comparisons of predicted, updated (at level 4), and measured lateral wall/soil movements, surface settlements, strut forces, excavation heave, and pore pressures at each excavation level are shown from Figure 5-34 to 5-38. These figures show the archival, updated, and predicted results.

Figure 5-34 compares computed and measured lateral wall/soil movement measurements. The figure includes the average of the five inclinometers available plus and minus the standard deviation (i.e. square root of measurement variances at each point - assumed to be independent for visualization in this figure). The computed values at level 4 show a smaller wall displacement than the original predictions, but better wall flexure. This figure also shows that archival displacements (updated at level 4) for excavation levels 1, 2, and 3 are inconsistent with the measured data and the initial predictions. After updating at level 4, predictions for levels 5 and 6 show a very small change.

Figure 5-35 compares the surface settlement predictions and measurements. Results show little change in the computed surface settlements at all excavation levels.

Figure 5-36 compares the forces in the three strut levels. It can be seen that, at level 4, there is a clear improvement at strut level 2 due to updating, while no change at strut level 3. In general, there is a minor difference between the initial predictions and archival forces for excavation levels 2 and 3. After updating at level 4, predictions for levels 5 and 6 show a force increment at strut level 3. Minor changes can be seen for strut levels 4 and 5.

Figure 5-37 compares the excavation heave predictions with measurements of 4 sensors. At level 4, it can be observed that the difference between updated and initial predictions is only apparent at the upper sensor where the updated value presents a minor worsening in magnitude, but a minor improvement in heave shape with respect to the rest of the sensors. The archival heave values decrease significantly at excavation grades (level 1, 2 and 3), and this is attributed to the increase in stiffnesses of the upper layers. Minor variations can be seen for the predictions, after updating, for levels 5 and 6.

Figure 5-38 compares the pore water pressures at two different elevations (i.e. two sensors). In principle, at level 4, what is slightly improved in sensor 1, it is slightly worsened at sensor 2. Minor changes can be seen for both archival and predictions.

It is clear that no significant improvements were achieved through parameter updating at level 4 due to the unique combination of different measurement types. This is a very important fact when analyzing all facets of model predictions. In fact, Figures 5-24 and 5-26 already suggested this, since the minimum objective function value was not necessary the minimum for all the measurement types. The following paragraphs consider how predictions can be improved when only a single measurement type is used.

Figure 5-39 compares the wall/soil lateral movement predictions when different measurement types are used. It can be seen that the best prediction is obtained when only inclinometer data are used. However, when the rest of measurements are used separately, it can be observed that predictions worsen either under-predicting or over-predicting the measured values. Similarly, Figure 5-40 compares the surface settlement predictions using different measurements in the likelihood function. It is clear that the best predictions are achieved when settlement measurements are used, and worse predictions occur when heave only is used. Figure 5-41 compares the strut force predictions, and it is clear that the best predictions are achieved when only the measured strut forces are used. Figure 5-42 compares the excavation heave predictions, and, once again, there is no doubt that the best predictions are reached when only the heave measurements are used. Also, Figure 5-43 compares the pore water pressure predictions with measured data of the two sensors, and it is clear, once again, that the best predictions are achieved when only the measured pore pressures are used as measurements. These results reveal fundamental contradictions or limitations in the FE model, most likely related to the selected MC constitutive model.

5.2.6. Updating Predictions: Excavation Level 5

The sensitivity analysis results for excavation level 5 indicate that there are 5 EIP to be used in the inverse analyses.

5.2.6.1. Sensitivity Analysis

Figure 5-44 shows the results of sensitivity analyses of the 5 EIP only (others are in Appendix A) at excavation level 5 for different lateral wall/soil movements, and excavation heave, respectively.

Figure 5-44a shows that SSR for lateral wall/soil movement varies significantly with variations of OCR_{TOP} (upper BBC). For OCR_{TOP} (lower bound), SSR is minimum and ΔSSR is higher than the structured global variance (SGV). In Figures 5-44b,c,d, the SSR for excavation heave is reported as a function of OCR_{TOP}, α, and k_{BBC}. The results show that the SSR is strongly affected by all five model parameters: OCR_{TOP}, $\alpha_{U\text{-}BBC}$, $\alpha_{L\text{-}BBC}$, $k_{U\text{-}BBC}$, and $k_{L\text{-}BBC}$.

5.2.6.2. Inverse Analysis

Figure 5-45 presents the convergences of the objective functions from inverse analyses at excavation level 5, for all measurements, while Figures 5-46, 5-47, 5-48, 5-49, and 5-50 show the convergence using lateral wall/soil movement, surface settlements, excavation heave, pore water pressures, and strut forces, respectively.

In this excavation level, a constant population of 50 individuals was used. The objective function, J_{ALL}, converges[‡‡‡‡] at generation 11, where the lowest value was selected. From Figures 5-46 to 5-50, it can also be seen that all objective functions show lower values than the initial

[‡‡‡‡] The stopping criteria adopted, in this thesis, was a minimum of 10 generations and when at least 90% of the individuals converge to the same minimum objective function value.

ones (since the final values are below the horizontal lines), implying improvements in the fitting for all types of measurements.

Figures 5-51, 5-52, 5-53, 5-54, and 5-55 present the five parameter convergences after 11 generations. As mentioned previously, most parameters converge to a set of optimal values (i.e., not to a unique value). The values chosen were the ones that correspond to the minimum value of the objective function of all measurements at the last generation. From these figures, it can be observed that 1) OCR_{top} decreases substantially, 2) there is a little change in $\alpha_{U\text{-}BBC}$, 3) $\alpha_{L\text{-}BBC}$ decreases significantly from 0.65 to 0.42, 4) there is a little change in $k_{U\text{-}BBC}$, while 5) $k_{L\text{-}BBC}$ increases by a factor of 2 approximately. Table 5-9 summarizes these optimal parameter values reached in eleven generations.

Figure 5-56 compares the updated versus the initial (updated from previous excavation level) undrained shear strength and hydraulic conductivity profiles. The results show that updating at level 5 reduces the s_u profile in the upper BBC and increases hydraulic conductivity on the lower BBC. This can be explained as we are now mainly producing movements at the toe of the wall and passive (PSP) resistance controls this process, while prior strengths were focused on DSS mode.

Figure 5-57 compares the updated versus initial (updated from previous excavation level) s_u (including field vane data), K_0, and shear stiffness profiles. The average K_0 of the upper BBC layer decreases significantly because of the s_u change. The shear stiffness of both the upper and lower BBC layers decreases, being more important in the lower BBC stratum (see Figure 5-54).

5.2.6.3. Predictions versus Measurements

Comparisons of predicted, updated (at level 5), and measured lateral wall/soil movements, surface settlements, strut forces, excavation heave, and pore pressures at each excavation level are shown from Figure 5-58 to 5-62. These figures show the archival, updated, and predicted results.

Figure 5-58 compares the initial predictions (updated at level 4), computed (updated at level 5) and measured lateral wall/soil movements for all excavation levels. Also, in this figure, it has been included the average of the five inclinometers available plus and minus the standard deviation (i.e. squared root of measurement variances at each point - assumed to be independent for visualization in this figure). The level 5 update matches closely the measured wall/soil horizontal displacements, while the initial predictions (at level 5) underestimate significantly the maximum wall deflection. The results again show some inconsistency in wall flexure for the archival values at levels 1, 2, 3, and 4. After updating, the predictions of displacements at level 6 increases significantly, showing an important variation on the maximum predicted value at the toe of the wall (from 37 mm to almost 70 mm).

Figure 5-59 compares initial predictions (updated at level 4), computed (updated at level 5) and measured surface settlements. At level 5, the computed settlements are very well estimated. Also, the archival settlements at levels 1, 2 and 3 do not vary significantly. Archival settlements at levels 4 are consistently improved. After updating, the predictions of settlements at level 6 increase significantly (from 12 mm to 22 mm approximately).

Figure 5-60 compares the strut forces of the four strut levels. At level 5, it can be seen that: 1) no forces (or almost none) were predicted at the first two strut levels; 2) there is a clear improvement on force prediction after updating at the third strut level, and a minor worsening is revealed at the strut level 4, but acceptable, since it is in the range of the measured loads (± 1 S.D.). The increment on the strut forces at levels 3 and 4 are attributed to the decrease of s_u and stiffness in the BBC unit which is consistent with the important increment in wall displacements. Concerning the archival strut forces, it is possible to claim that: 1) the strut a level 1 does not experience any variation; 2) there is a clear improvement in the strut level 2; and 3) there is a little worsening in the strut level 3 (excavation level 4). After updating, predictions of strut forces are increased significantly for strut levels 3, 4, and 5.

Figure 5-61 compares the excavation heave with the four available sensors. It can be observed a great agreement between measured and current predictions at level 5. This excellent improvement is attributed to changes in OCR_{top} (s_{uTOP} and $G_{U\text{-}BBC}$), $\alpha_{L\text{-}BBC}$ ($G_{L\text{-}BBC}$), and $k_{L\text{-}BBC}$. Unfortunately, there is a clear inconsistency on the archival values, specifically, at the uppermost sensor elevation. The predictions of heave at excavation level 6 are also increased significantly at all levels below final grade.

Figure 5-62 compares the pore water pressures at two different elevations (i.e. two sensors). In principle, the pore pressure in sensor 2 slightly improved (at level 5), being closer to the measured value. No significant variations can be observed for the archival values (levels 1, 2, 3, and 4) and for the predicted ones (level 6). Results on pore pressures suggest that are controlled by boundary conditions rather than MC parameters.

Figures 5-58 to 5-62 prove that very good improvements were accomplished at excavation level 5 (also see section 5.2.7), particularly of computed/updated wall/soil displacements, settlements, strut forces, and heave. However, there is some inconsistency with archival predictions of some measurement types.

5.2.7. Updating Predictions: Excavation Level 6

The sensitivity analysis results on this excavation level (see Table 5-7) indicate that there are 6 EIP (G_{GF}, G_{CF}, G_{SM}, OCR_{TOP}, $\alpha_{U\text{-}BBC}$, and $\alpha_{L\text{-}BBC}$) that must be considered in inverse analyses.

5.2.7.1. Sensitivity Analysis

Figure 5-63 shows the results of sensitivity analyses of the EIP only (other are in Appendix A) at excavation level 6 on three different measurement types: 1) lateral wall/soil movements, 2) excavation heave, and 3) strut forces.

Figures 5-63a,b show that SSR for lateral wall/soil movement can be reduced by changes in G_{SM} and OCR_{top} (upper BBC).

Figures 5-63c-g show that the SSR for excavation heave is affected significantly by five EIP parameters, while only G_{SM}, OCR_{TOP}, $\alpha_{U\text{-}BBC}$ affect SSR for strut forces, in Figures 5-63h-j.

5.2.7.2. Inverse Analysis

Figure 5-64 presents the convergences of the objective functions from the inverse analyses at excavation level 6, for all measurements, while Figures 5-65, 5-66, 5-67, 5-68, and 5-69 show the convergence using lateral wall/soil movement, surface settlements, excavation heave, pore water pressures, and strut forces, respectively.

In this excavation level, a constant population of sixty individuals was used. The objective function, J_{ALL} converges[§§§§] at generation 17, where the lowest value was selected. From Figures 5-65 to 5-69, it can also be seen that most objective functions show some improvements (since the final values are below the initial reference results).

Figures 5-70, 5-71, 5-72, 5-73, and 5-74 present the six EIP convergences after 17 generations. As mentioned previously, most parameters converge in a set of optimal values (i.e. not to a unique value). The values chosen were the ones that correspond to the minimum value of the objective function of all measurements at the last generation. From these figures, it can be seen that G_{GF} and G_{SM} increase significantly, but the G_{CF} reaches a similar magnitude than the initial one. In fact, the G_{GF} increases to its upper bound. Also, the $\alpha_{U\text{-}BBC}$ increases to its upper bound, while the $\alpha_{L\text{-}BBC}$ decreases to it lower bound. The change in OCR_{TOP} is minor. Table 5-9 summarizes all the optimal parameter values reached in 17 generations (at excavation level 6).

[§§§§] The stopping criteria adopted, in this thesis, was a minimum of 10 generations and when at least 90% of the individuals converge to the same minimum objective function value.

Figure 5-76 compares the updated versus the initial (updated from previous excavation level) undrained shear strength profiles as well as the SHANSEP strength profiles, showing that there is an insignificant increase in the s_u profile of the upper BBC layer.

Figure 5-77 compares the updated versus initial (updated from previous excavation level) s_u (including field vane data), K_0, and shear stiffness profiles. The average K_0 of the Upper BBC layer increases insignificantly because of the s_u change. However, the shear stiffness of the upper BBC layer increases substantially, while for the lower BBC layer decreases to the lower boundary.

5.2.7.3. Predictions versus Measurements

Comparisons of predicted, updated (at level 6), and measured lateral wall/soil movements, surface settlements, strut forces, excavation heave, and pore pressures at each excavation level are shown from Figure 5-78 to 5-82. These figures show the archival, updated, and predicted results.

Figure 5-78 compares initial predictions (updated at level 5), computed (updated at level 6), and measured lateral wall/soil movements. As in previous summaries, the average of the five inclinometers available plus and minus the standard deviation is reported. The computed lateral wall/soil displacements match closely the measured results, while the initial predictions would overestimate maximum wall movement. Once again, the archival lateral wall/soil movements show inconsistency with the measured data at levels 1, 2, 3, 4, and 5.

Figure 5-79 compares initial predictions (updated at level 5), computed (updated at level 6), and measured surface settlements. The computed (updated at level 6) values are worse than the very good predictions previously obtained at excavation level 5. Figure 5-78, it is important to note that the predictions (at level 6) overestimates wall deflections (Figure 5-59), suggesting model inconsistency through the updating with different measurement types. Also, this figure shows inconsistency with archival settlements at levels 2, 3, 4, and 5.

Figure 5-80 compares the strut forces of the five strut levels (measured, predicted, and computed). At excavation level 6, it can be seen that: 1) once again, for the strut levels 1 and 2, no forces (or almost none) were computed, and only small value were measured), 2) for strut levels 3, 4, and 5, there is a notable improvement in the computing results. After updating at level 6, the archival strut forces seem to be more consistent for the rest of the levels.

Figure 5-81 compares the excavation heave with the four available sensors. Once again, it can be observed a very good agreement between measured and computed values (updated at level 6). This agreement is again primarily attributed to updating of the stiffness for the upper and lower BBC ($\alpha_{U\text{-}BBC}$ and $\alpha_{L\text{-}BBC}$). Also, the archival heave at level 5 agrees very well with the measured data. The rest of the archival predictions do not experience important variation; however, they are not consistent with the measured data.

Figure 5-82 compares the pore water pressures at two different elevations (i.e. two sensors). It can be seen that, at excavation level 6, the computed pore pressures do not improve; in fact, there is a minor worsening in sensor 2. Once again, no relevant variations on archival pore pressures can be observed.

Although there are no improvements on computed surface settlement and pore pressures, very good improvements of computed lateral wall/soil deflections, excavation heave, and strut forces are accomplished at excavation level 6 (also see Section 5.2.7). Also, it is important to highlight that the updated predictions from previous and current excavation levels show that predictions of each measurement type are not really needed at this excavation level (as it was at exc. level 4) to draw additional conclusions.

The results of computed wall/soil defections, excavation heave, and surface settlements, at this excavation level, show that they cannot agree well with the measured data. Although, an explanation for this issue cannot be drawn from these results, it is possible to claim that the use of simple constitutive law (MC model), and any possible omission and/or assumption in the FE model could be the reason for this discrepancy. However, the use of each individual measurement can be used to improve substantially each prediction (see Section 5.2.4).

5.2.8. Parameter Variations, Improvements, and Comments

Figure 5-83 shows the variation of reference shear stiffness of the three upper strata (see also Table 5-2) from the initial values adopted. The updating is associated with significant increases in shear stiffness for all three layers; while changes in these parameters are not surprisingly (there is a large uncertainty in these parameters and not enough measurements). It is surprising that they are only updated at later stages of excavation and no updating was found necessary at excavation levels 1-3.

Figure 5-84 shows the variation of the OCRtop, α parameter, s_u^{ref}, and G^{ref} of both the upper and lower BBC strata, from the initial values adopted. It can be seen that the undrained shear strength of the upper BBC decreases significantly after excavation level 4, suggesting that for this simple model, the initial OCR_{top} adopted was too high. Concerning the shear stiffnesses, there is an important increment for the upper BBC at the last stage, but a more significant decrease for the lower BBC layer.

Figure 5-85 shows the variation of hydraulic conductivities on the BBC units. It can be seen that there were a small change only in $k_{L\text{-}BBC}$ (increase by a factor of 2).

Table 5-9 presents a summary of the optimal parameter values obtained by the inverse analysis procedure based on genetic algorithms for excavation levels 4, 5, and 6. Also, the values of the minimum objective function that contains all measurement are shown as well as the initial objective function values (i.e. without updating). It can be seen important improvements are reached at each excavation level.

In order to quantify the improvement, an incremental improvement ratio is proposed:

$$I.R._{total} = \frac{J_{0\,ALL} - J_{\min\,ALL}}{J_{0\,ALL}} \tag{5.7}$$

where $I.R._{total}$ is the improvement ratio at a certain excavation level of all measurements; $J_{0\,ALL}$ is the initial value of objective function at a certain excavation level; and $J_{min\,ALL}$ is the minimum value of objective function after inverse analysis.

However, it is also very important to understand how each instrument type contributes to the final improvement, at a certain excavation level. Thus the following expression is also proposed:

$$I.R._i = \frac{J_{0\,i} - J_{\text{final}\,i}}{J_{0\,ALL}} \tag{5.8}$$

where $I.R._i$ is the improvement ratio contribution of the i-th instrument type; $J_{0\,i}$ is the initial value of objective function for the i-th instrument type; and $J_{min\,i}$ is the final value of objective function after inverse analysis for the i-th instrument type.

Figure 5-86 presents the incremental improvement ratios of updating predictions for the last three excavation stages. This figure shows a consistent improvement which increases as the excavation progresses. For example, for excavation level 4, 5, and 6, the incremental improvements were 29.3%, 58.9%, and 84.9%. This clearly confirms the effectiveness of the proposed rational methodology for updating predictions of excavation performance. Moreover, it is very important to highlight that the improvement presented herein is only due to some model parameters, as the FE model was kept constant (using from the beginning all information obtained from construction activities). In fact, in a real project, these improvements ratios should be performed between class A predictions and the updated ones.

Summarizing, the proposed updating procedure show consistent improvements of particular predictions types. Although there is a consistent improvement of all computed results at level 5, there is no consistency with improvements of all measurement types for levels 4 and 6.

Also, it is important to highlight that, after updating at levels 4, 5, and 6, archival results are not consistent with field measurements. This clearly reflects the limitations of the MC model.

5.2.9. Comparison of MIT-E3 and MC models

The following section compares previous MC results (initial, updated, and predicted) with MIT-E3 predictions. The BBC unit (upper and lower) has been modeled using the generalized effective stress soil model MIT-E3 (Whittle, 1987; Whittle and Kavvadas, 1994). The input parameters and state variables (e.g., stress history profile) have been previously discussed in Chapter 2. In fact, this MIT-E3 set of predictions corresponds to the class B predictions, previously described in Section 2.2. In order to quantify predictions and improvements, comparisons of SSR and SGV values are performed.

5.2.9.1. Excavation levels 1 (no updating required)

Figure 5-87 compares MIT-E3 and MC predictions with measurements of lateral wall/soil displacements at excavation level 1. Both models show very similar predictions and SSR values. The SGV and SSR values are almost the same in both cases, implying that the predictions agree very well with the measured data.

Figure 5-88 compares the both predictions with measured surface settlements. It is clear that both predictions (MIT-E3 and MC) do not agree with the measurements and have similar SSR values.

Figure 5-89 compares the predictions with the measured heave, where both predictions have similar SSR values and do not agree very well with the measured data (based on SSR and SGV values).

Also similar predictions between MC and MIT-E3 of pore pressures can be seen in Figure 5-90, with similar SSR values, suggesting that both predictions agree very well with the measurements (since SSR values are smaller than SGV).

5.2.9.2. Excavation levels 2 (no updating required)

Figure 5-91 compares MIT-E3 and MC predictions with measurements of lateral wall/soil displacements at excavation level 2. Although both SSR values are slightly larger than the SGV value, the $SSR_{MIT\text{-}E3}$ value is closer to the SGV value. This suggests that the MIT-E3 predictions are in better agreement than the MC ones.

Figure 5-92 compares both predictions with measured surface settlements. In this case, the SSR value of MC predictions is smaller to the SGV, suggesting a good agreement with the measured data. The $SSR_{MIT\text{-}E3}$ value is slightly larger than the SGV one.

Figure 5-93 compares the predictions with the measured strut forces. Both sets of predictions are in very good agreement with the measured data. While the SSR value of the MC predictions is extremely small, it is particularly interesting to note that the SSR value of the MIT-E3 predictions is zero, implying perfect match with the measured data.

Figures 5-94 compares the heave predictions of MIT-E3 and MC models. Although both predictions have SSR values larger than SGV, the SSR of MIT-E3 is smaller, suggesting a better agreement with the measured heave data.

Figures 5-95 compares MC and MIT-E3 predictions with pore pressure measurements. It can be seen that both SSR values are very small (MIT-E3 is in slightly better agreement with the measured data).

5.2.9.3. Excavation levels 3 (no updating required)

Figure 5-96 compares MIT-E3 and MC predictions with measurements of lateral wall/soil displacements at excavation level 3. Although both SSR values are smaller than the SGV value (i.e., very good agreement with measurements), the SSR_{MC} value is closer to the SGV, suggesting that the MC predictions are in better agreement than the MIT-E3 ones.

Figure 5-97 compares both predictions with measured surface settlements at excavation level 3. Both SSR values are very similar and both are smaller than the SGV value (i.e., very good agreement with measurements).

Figure 5-98 compares the predictions with the measured strut forces. MIT-E3 predictions are in better agreement with the measured strut forces, while being larger than the SGV value.

Figures 5-99 compares the heave predictions of both models that have similar SSR values and are larger than the SGV value.

Figures 5-100 compares MC and MIT-E3 predictions with pore pressure measurements. It can be seen that SSR_{MC} value is very small, suggesting a very good agreement with the measured data. Although the SSR_{MIT-E3} is around 5 times the SSR_{MC} value, it is still smaller than the SGV value.

5.2.9.4. Excavation level 4 (updating MC model)

Figure 5-101 compares MIT-E3 and MC predictions with measurements of lateral wall/soil displacements at excavation level 4. At this excavation level, updating was required (Section 5.2.4), therefore both the initial and updated MC predictions are shown. It is important to clarify that predictive model capabilities should be carried out by comparing the MC initial with MIT-E3. Thus, the SSR_{MIT-E3} value is smaller than the SSR_{MC} value and also close to the SGV value, implying that MIT-E3 predictions agree well with the data (at least better than MC predictions). After the updating, the SSR_{MC-UP} value slightly increases indicating a small worsening in the predictions; however a better flexure can be observed (similar to the measured flexure).

Figure 5-102 compares MIT-E3 and MC predictions with measurements of surface settlements at excavation level 4. MIT-E3 predictions agree very well with the measured data, having a very small SSR value (close to zero). The MC predictions have a larger SSR value than the SSR_{MIT-E3}. After updating, once again, the SSR_{MC-UP} increases, making slightly worse the MC computed value.

Figure 5-103 compares MIT-E3 and MC predictions with measurements of strut forces. While MC initial and MIT-E3 predictions show similar SSR values, the SSR_{MC-UP} decreases,

indicating that the computed values improved after updating but larger than the SGV value. This is primarily due to difference between measured and computed strut level 2 forces.

Figure 5-104 compares the predictions of both models together with the measured heave at the centerline. Although larger than the SGV value, the MC initial predictions are in better agreement with the measured data. After updating, there is a minor improvement on the computed values (smaller SSR value).

Figure 5-105 compares both model predictions of pore pressures with the measured data. Initial MC predictions agree very well with the measured data, while MIT-E3 predictions do not. After updating there is a slightly worsening of computed values.

From section 5.2.4, it is clear that the MC model shows limitations when using different measurement types, reason for not consistently achieving improvements.

5.2.9.5. Excavation level 5 (updating MC model)

Since updating occurred in the previous excavation level, now it is possible to evaluate the predictive capabilities of the updating procedure together the MC model.

Figure 5-106 compares MIT-E3 and MC predictions with measurements of lateral wall/soil displacements at excavation level 5. At this excavation level, updating was required (Section 5.2.5), therefore both the initial (updated level 4) and updated level 5 MC predictions are shown. Comparing SSR_{MC} with $SSR_{MIT\text{-}E3}$, it is clear that MIT-E3 predictions achieve much better agreement with the measured data, especially with the maximum wall displacement value

(occurring at the toe of the wall). After updating the $SSR_{MC\text{-}UP}$ value is reduced significantly, being closer to the SGV value (also $SSR_{MC\text{-}UP}$ is smaller than $SSR_{MIT\text{-}E3}$).

Figure 5-107 compares MIT-E3 and MC predictions with measurements of surface settlements at excavation level 5. MIT-E3 predictions agree very well with the measured data, having a very small SSR value. The MC predictions have a much larger SSR value than the $SSR_{MIT\text{-}E3}$. However, after updating the $SSR_{MC\text{-}UP}$ value is reduced significantly. Also the $SSR_{MC\text{-}UP}$ value is slightly smaller than $SSR_{MIT\text{-}E3}$.

Figure 5-108 compares MIT-E3 and MC predictions with measured strut forces. MIT-E3 and MC predictions have similar SSR values. After updating the SSR value slightly increases. Since the SGV value is larger than all SSR values, it is possible to claim that very good agreements are achieved between predictions and measurements, as well as between computed values and measurements.

Figure 5-109 compares the predictions of both models together with the measured heave. MIT-E3 predictions agree well with the measured data, resulting in a smaller SSR value than the SSR_{MC} (updated level 4), but larger than the SGV. After updating at this level, the computed values improve, reducing significantly the SSR value.

Figure 5-110 compares both model predictions of pore pressures with the measured data. Initial MC predictions (updated level 4) agree very well with the measured data, while MIT-E3 predictions do not. After updating the $SSR_{MC\text{-}UP}$ value is reduced significantly from the SSR_{MC} value.

At this excavation level, the results show consistently improvements of computed values. This fact demonstrates the powerful capabilities of the proposed updating procedure; however, this does not reflect the predictive capabilities. In fact, the MC predictions (updated level 4) are not in good agreement with the data which is attributed to the model limitations.

5.2.9.6. Excavation level 6 (updating MC model)

Once again, since updating occurred in the previous excavation level, now it is possible to evaluate the predictive capabilities of the updating procedure together the MC model.

Figure 5-111 compares MIT-E3 and MC predictions with measurements of lateral wall/soil displacements at excavation level 6. At this excavation level, updating was required (Section 5.2.6), therefore both the initial MC (updated level 5) predictions and computed (updated level 6) values are shown. Comparing SSR_{MC} with $SSR_{MIT\text{-}E3}$, once again, it is clear that MIT-E3 predictions achieve much better agreement with the measured data, especially with the maximum wall displacement value (occurring at the toe of the wall). The initial MC predictions overestimate the maximum wall displacement. However, after updating, the SSR value is reduced significantly, being smaller than the $SSR_{MIT\text{-}E3}$ value.

Figure 5-112 compares MIT-E3 and MC predictions with measurements of surface settlements at excavation level 6. Surprisingly, the MC predictions almost match the measured data (having a SSR value very close to zero). The $SSR_{MIT\text{-}E3}$ value is larger than the SSR_{MC}, but is smaller than the SGV. Although both settlement predictions agree very well with the measured data, the MC predictions of surface settlements are superior. This result is extremely important

because it shows that to reproduce such good MC predictions of settlements, the MC predictions of wall deflections must be overpredicted, confirming once again the limitations of the MC model. After updating, the SSR value of MC predictions increases significantly but does not go beyond the SGV value.

Figure 5-113 compares MIT-E3 and MC predictions with measured strut forces at excavation level 6. MIT-E3 predictions are in very good agreement with the measured data, resulting in a SSR value smaller than the SGV one. After updating the SSR value significantly decreases, but does not go below the SGV. It is important to highlight the MIT-E3 prediction of the strut level 5 force is close to the range of measured value (± 1 SD).

Figure 5-114 compares the predictions of both models together with the measured heave. MIT-E3 predictions agree well with the measured data, resulting in a smaller SSR value than the SSR_{MC} (updated level 5), but larger than the SGV. After updating at this level, the computed values (updated level 6) improve significantly. It is important to note how small the SGV value is at this excavation level.

Figure 5-115 compares both model predictions of pore pressures with the measured data. Both the initial MC predictions (updated level 5) and the MIT-E3 agree very well with the measured data. After updating, the SSR value of the MC predictions increases, but does not go beyond the SGV value.

These results confirm, once again the limitation of the MC model, since it cannot predict and improve the computed values at the same time when different measurement types are used.

5.3. References

Jaky, J. (1944), "The coefficient of earth pressure at rest. In Hungarian (A nyugalmi nyomas tenyezoje)." *J. Soc. Hung. Eng. Arch. (Magyar Mernok es Epitesz-Egylet Kozlonye)*, 355-358.

Jen, L. C. (1998), "The design and performance of deep excavations in clay." *PhD Thesis. Department of Civil and Environmental Engineering, Cambridge, MIT*, 698p.

Kempfert, H.G., Gebreselassie, B. (2006), "Excavations and Foundations in Soft Soils." Springer Berlin Heidelberg New York.

Ladd, C.C., Young, G.A., Kraemer, S.R. and Burke, D.M. (1999). "Engineering properties of Boston Blue Clay from Special Testing Program." *Proceedings, Special Geotechnical Testing: Central Artery/Tunnel Project in Boston, Massachusetts*, ASCE GSP 91, GeoCongress '98, National Convention, Boston, 1-24.

MATLAB (2004-2009). "Genetic Algorithm and Direct Search Toolbox TM 2 - User's Guide." The MathWorks, INC.

Mayne, P.W. and Kulhawy, F.H. (1982). "K_0-OCR Relationships in Soil." *Journal of the Geotechnical Engineering Division. Proceedings of ASCE*. 108 (GT6): 851-872.

Parsons Brinckerhoff (1998), "Final Design Geotechnical Report, South Boston Piers Transitway Project", MBTA Contract E02CN14, Courthouse Station and Tunnel Construction, contracts CC07, CC08 & CC10.

Santagata, M., Germaine, J.T., Ladd, C.C. (2005), "Factors Affecting the Initial Stiffness of Cohesive Soils." *Journal of Geotechnical and Geoenvironmental Engineering, ASCE*. 131 (4): 430-441.

Santagata, M., Germaine, J.T., Ladd, C.C. (2007), "Small-Strain Nonlinearity of Normally Consolidated Clay." *Journal of Geotechnical and Geoenvironmental Engineering, ASCE*. 133 (1): 72-82.

Schmidt, B. (1966). Discussion of "Earth pressures at rest related to stress history" by E.W. booker and H.O. Ireland. *Canadian Geotechnical Journal*, 3(4): 239-242.

Stroud, M. A. (1989), "The Standard Penetration Test – its Applications and Interpretations.", Penetration Testing in the UK, Thomas Telford, London, 29-49.

Whelan, M.P. (1995), "Performance of deep excavations in Boston." *SM Thesis. Department of Civil and Environmental Engineering, Cambridge, MIT*, 356p.

Whittle, A.J. (1987) "A Constitutive Model for Overconsolidated Clays with Application to the Cyclic Loading". *Sc.D Thesis. Department of Civil and Environmental Engineering, Cambridge, MIT.* 641p.

Whittle, A.J. and M. J. Kavvadas (1994). "Formulation of MIT-E3 Constitutive Model for Overconsolidated Clays." - *ASCE Journal of Geotechnical Engineering* 120(1): 173-198.

Whittle, A.J., DeGroot, D.J., Ladd, C.C. & Seah, T-H. (1994). "Model prediction of the anisotropic behavior of Boston Blue Clay." *ASCE Journal of Geotechnical Engineering* 120(1): 199-225.

Table 5-1: Construction sequences assumed in FE simulation

Activity					
Stage	Description	† FE Analysis Type	CD (days)	Project Elev. (m)	Depth (m)
0	Initial Phase (geostatic condition)	P	-	-	
1	D. Wall Installation (1.22m thick)	P	-	7.6 (toe)	26.2 (toe)
2	Exc. Level 1 (reset displacements)	C	51	32.0	1.8
3	Strut Level 1 (no pre-load)	P	-	33.2	0.6
4	Exc. Level 2	C	84	27.4	6.4
5	Strut Level 2 (pre-load=110 kN/m)	P	-	28.7	5.1
6	Exc. Level 3	C	111	25.0	8.8
7	Strut Level 3 (pre-load=429 kN/m)	P	-	26.5	7.3
8	Exc. Level 4	C	153	21.6	12.2
9	Strut Level 4 (pre-load=501 kN/m)	P	-	23.2	10.6
10	Exc. Level 5	C	185	18.9	14.9
11	Strut Level 5 (pre-load=613 kN/m)	P	-	19.5	14.3
12	Exc. Level 6	C	279	16.5	17.3

† P≡Plastic; C≡Consolidation (EPP)

Table 5-2: Soil units and initial material properties

Initial Material Properties of Soil Layers					
	Granular Fill (GF)	**Cohesive Fill (CF)**	**Silty Sand (SM)**	**Upper BBC**	**Lower BBC**
Thickness (m)	1.8	5.2	3.7	18.3	14.0
Material Type	Drained - MC			Undrained -MC	
Ref. Elevation, z_0 (m)	33.8	32.0	25.6	23.2	4.9
γ (kN/m^3)	18.9	18.1	18.9	18.1	
k (m/day)	0.31			4.32E-05	
G^{ref} (MPa)	1.0	0.7	3.0	17.6	42.2
$\Delta G/\Delta z$ (MPa/m)	0.66	0.20	0.30	0.97	1.04
ν'	0.3			0.28	
s_u^{ref} (kPa)	-			82.0	56.3
$\Delta s_u/\Delta z$ (kPa/m)				-1.4	1.8
ϕ' (°)	37.5	25.0	35.0	0.0	
K_0	0.39	0.58	0.43	0.83	0.53

assumed constant/fixed values

18 uncertain parameters

Note: $s_u = s_u^{ref} + \frac{\Delta s_u}{\Delta z}(z - z_0)$

$G = G^{ref} + \frac{\Delta G}{\Delta z}(z - z_0)$

Table 5-3: (Table 2-3 bis) Material properties of excavation support system

[1] Diaph. Wall	Thickness (m)	E (MPa)	ν	Unit Weight, γ (kN/m^3)
Concrete	1.22	2.26E+04	0.15	22.8

[1] D. Wall modeled as an elastic non-porous material.

[2] Strut Level	Typical Section	E (MPa)	A (cm^2)	EA (kN)	EA/$\bar{s}$ [3] (kN/m)	Ultimate Capacity (kN/m)
1	24"ϕ x 5/8"	2.0E+05	296.1	5.9E+06	9.2E+05	609
2	36"ϕ x 5/8"		448.1	9.0E+06	1.4E+06	810
3	36"ϕ x 1"		709.4	1.4E+07	2.2E+06	1223
4	2-W36 x 135		512.3	1.0E+07	1.6E+06	1328
5	2-W36 x 230		872.3	1.7E+07	2.7E+06	1977

[2] Struts modeled as elasto-plastic anchors with null tensile strength.

[3] Average horizontal spacing, $\bar{s}$=6.45m.

Table 5-4: Variances of Field Measurements

Instrument Type	Measurement Type	Data Points or Sensors	Variance (units)		Excavation Level					
					1	2	3	4	5	6
Linewise	Wall/Soil Measurements	5 inclinometers (71 points) [c]	$\sigma^2 {l_i}^2$ (mm^2)		0.014	0.049	0.052	0.086	0.798	1.932
		1 (base)	$varB$ (mm^2)		0.155	0.152	0.245	0.543	1.665	1.587
	Excavation Heave	4 sensors	σ^2 (mm^2)		8.129	1.394	1.548	4.583	2.690	0.373
		1 (base)	$varA$ (mm^2)		0.0					
Pointwise	Surface Settlement [a]	15 DMPs (5 groups) [d]	σ^2_{ave} (mm^2)		1.753	6.350	8.041	15.224	21.628	24.200
	Pore Pressures [a]	2 sensors	σ^2_{ave} (kPa^2)		1303	1109	376	462	543	635
	Strut Forces [b]	32 strain gauges (5 levels)	σ^2_{ave} (kN/m)^2	L1	-	1436				
				L2	-	-	615			
				L3	-	-	-	1225		
				L4	-	-	-	-	19210	
				L5	-	-	-	-	-	8446

[a] Only average value of variances are shown (different magnitudes were considered)

[b] Constant values of variances were assumed for each strut level during the excavation (due to the lack of measurements)

[c] Each inclinometer contains sensors every 0.6m; therefore the total data points considered (on the FE model) were 71 (every 0.6m).

[d] A total of 12 DMP devices from South and North locations were used. They were grouped into 5 independent sets with similar distance behind the diaphragm wall. OBS: 4 DMP devices installed behind the South side at 24 and 37m (see Fig. 2-14) were not considered due to the presence of the Building (i.e., they were assumed to be outliers).

Table 5-5: Relations and correlations used for updating model parameters

Soil Layers	Relations and Correlations used	Notes	References
Upper Fill Layers: **GF** **CF** **SM**	$K_0=1-\sin\phi'$ $G/\sigma'=30$ (GF and SM) $G/\sigma'=20$ (CF)	- $\sigma'=\sigma'_{vo}(1+2K_0)/3$	Jaky (1944) Whelan(1995) Jen (1998)
Boston Blue Clay (BBC): **U-BBC & L-BBC**	* $K_0 = K_{0\,NC}(OCR)^n$	$K_{0\,NC}=0.533$ n=0.4	Schmidt (1966) Mayne and Kulhawy (1982) Ladd et al. (1999)
	$s_u/\sigma'_{vo} = S\,(OCR)^m$	DSS mode of Shearing (BBC): S=0.20 m=0.775	Ladd et al. (1999)
	$G_{max}/p_a = 381\,OCR^{0.15}(\sigma'/p_a)^{0.8}$	p_a=101.3 kPa $\sigma'=\sigma'_{vo}(1+2K_0)/3$	Santagata et al. (2005)
	$G=\alpha\,G_{max}$	α represents stiffness reduction (G for the MC model)	proposed

* For the MC model only, the K_0 value was assumed constant for the U-BBC unit; therefore, an average value of OCR was used: $OCR_{ave}=(OCR_{top}-OCR_{bot})/2$

Table 5-6: Selected search spaces of model parameters

Soil Layers	Parameter	Lower Bound	Upper Bound	Notes	Reference
Upper Fill Layers: **GF CF SM**	G_0	$G_0/10$	$10G_0$	Estimated from high values of N_{SPT} standard deviations and with the use of empirical correlations	PB(1998) Stroud (1989)
	ϕ'	ϕ'-7.5°	ϕ'+7.5 °		
U- BBC & L- BBC	OCR_{TOP}	2.0	6.0	Estimated from OCR profile based on lab and field tests	PB (1998) Ladd et al. (1999) Jen (1998)
	$\alpha_{U\text{-}BBC}$ $\alpha_{L\text{-}BBC}$	0.35	0.65	Estimated from coefficient of variation of G_{max}, shear strain level, and uncertainty of being 0.5 for MC model.	Santagata et al. (2005) Kempfert and Gebreselassie (2006)
	$k_{U\text{-}BBC}$ (m/s)	$0.5 \cdot 10^{-9}$	$5 \cdot 10^{-9}$	range of 1 order of magnitude for each sub-layer	Whelan (1995)
	$k_{L\text{-}BBC}$ (m/s)	$0.2 \cdot 10^{-9}$	$2 \cdot 10^{-9}$		

Table 5-7: Comparison of Initial Structured Squared Residuals and Structured Global Variances

Measurement Type	Excavation Level											
	1		2		3		4		5		6	
	SSR_i	SGV_i	SSR_i	SGV_i	SSR_i	SGV_i	SSR_i	SGV_i	SSR_i	SGV_i	SSR_i	SGV_i
Wall/Soil Deflection (mm^2)	0.481	0.388	1.667	1.056	0.823	1.593	3.841	2.407	60.056	14.852	90.784	10.268
Surface Settlement † (mm^2)	7.429	1.753	5.490	6.350	3.247	8.041	4.237	15.224	13.530	21.628	0.1897	24.200
Heave at CL (mm^2)	27.300	9.290	46.725	1.860	36.610	3.100	59.408	3.887	94.178	1.988	141.470	0.351
Pore Pressures † (kPa^2)	587	1303	94	1109	50	376	435	462	509	549	178	635
Strut Forces † $(kN/m)^2$	-		11	1436	2098	615	7811	1225	7364	19210	45964	8446
Is any $SSR_i > SGV_i$? (see Eq. 4-20)	**YES**		**YES**		**YES**		**YES**		**YES**		**YES**	
Is any $\Delta SSR_i > SGV_i$? (see Eq. 4-21 and appendix A)	**NO**		**NO**		**NO**		**YES**		**YES**		**YES**	

† Average values of residuals and variances (pointwise instrument types)

Table 5-8: Summary of essential and nonessential improvement parameters obtained from sensibility analysis for excavation levels 4, 5 and 6

Meas. / Instrument Type	Improvement Parameters from Sensitivity Analyses					
	Level 4		Level 5		Level 6	
	Essential $\Delta SSR_i > SGV_i$	Nonessential $0 < \Delta SSR_i < SGV_i$	Essential $\Delta SSR_i > SGV_i$	Nonessential $0 < \Delta SSR_i < SGV_i$	Essential $\Delta SSR_i > SGV_i$	Nonessential $0 < \Delta SSR_i < SGV_i$
Wall/Soil Deflection / Inclinometer (linewise)	OCR_{TOP}	G_{CF} G_{SM}	OCR_{TOP}	$\alpha_{U\text{-}BBC}$ $k_{L\text{-}BBC}$	G_{SM} OCR_{TOP} $\alpha_{U\text{-}BBC}$ $\alpha_{L\text{-}BBC}$	G_{GF} G_{CF} $k_{L\text{-}BBC}$
Surface Settlement / DMP (pointwise)	-	OCR_{TOP}	-	OCR_{TOP} $\alpha_{U\text{-}BBC}$ $\alpha_{L\text{-}BBC}$	-	-
Heave at CL / Multi-Heave Gage – 4 sensors (linewise)	$\alpha_{U\text{-}BBC}$	OCR_{TOP}	OCR_{TOP} $\alpha_{U\text{-}BBC}$ $\alpha_{L\text{-}BBC}$ $k_{U\text{-}BBC}$ $k_{L\text{-}BBC}$	G_{CF} G_{SM}	G_{GF} G_{CF} G_{SM} OCR_{TOP} $\alpha_{U\text{-}BBC}$ $\alpha_{L\text{-}BBC}$	ϕ'_{CF} ϕ'_{SM} $k_{U\text{-}BBC}$ $k_{L\text{-}BBC}$
Pore Pressures / Piezometer - 2 sensors (pointwise)	-	OCR_{TOP}	-	OCR_{TOP} $\alpha_{U\text{-}BBC}$ $\alpha_{L\text{-}BBC}$ $k_{L\text{-}BBC}$	-	$\alpha_{U\text{-}BBC}$ $\alpha_{L\text{-}BBC}$
Strut Forces / Strain Gauges (pointwise)	G_{CF} G_{SM}	G_{GF} $k_{U\text{-}BBC}$	-	G_{GF} OCR_{TOP} $\alpha_{U\text{-}BBC}$ $k_{L\text{-}BBC}$	G_{SM} OCR_{TOP} $\alpha_{U\text{-}BBC}$	G_{GF} G_{CF} ϕ'_{SM} $k_{L\text{-}BBC}$
Relevant parameters to optimize	4	-	5	-	6	-

Table 5-9: Optimal and initial parameters values, and initial and minimum objective function values

Optimal Parameters & †Initial and Minimum Objective Function Values	Initial Parameters	Excavation L4	Excavation L5	Excavation L6
Number of Generation	-	20	11	17
OCR_{TOP}	5.0	4.36	2.35	2.45
$\alpha_{U\text{-}BBC}$	0.35	0.41	0.41	0.65
$\alpha_{L\text{-}BBC}$	0.65	-	0.42	0.36
$k_{U\text{-}BBC}$ [m/sec]	5.0×10^{-10}	-	5.1×10^{-10}	-
$k_{L\text{-}BBC}$ [m/sec]	5.0×10^{-10}	-	9.7×10^{-10}	-
†G_{GF} [MPa]	1.0	-	-	10.0
†G_{CF} [MPa]	0.7	4.9	-	5.2
†G_{SM} [MPa]	3.0	15.8	-	29.54
Min J_{ALL} [-]	-	82.19	59.79	113.15
Initial J_{ALL}[-]	-	116.19	145.62	751.79

† GF: granular fill, CF: cohesive fill, SM: silty sand

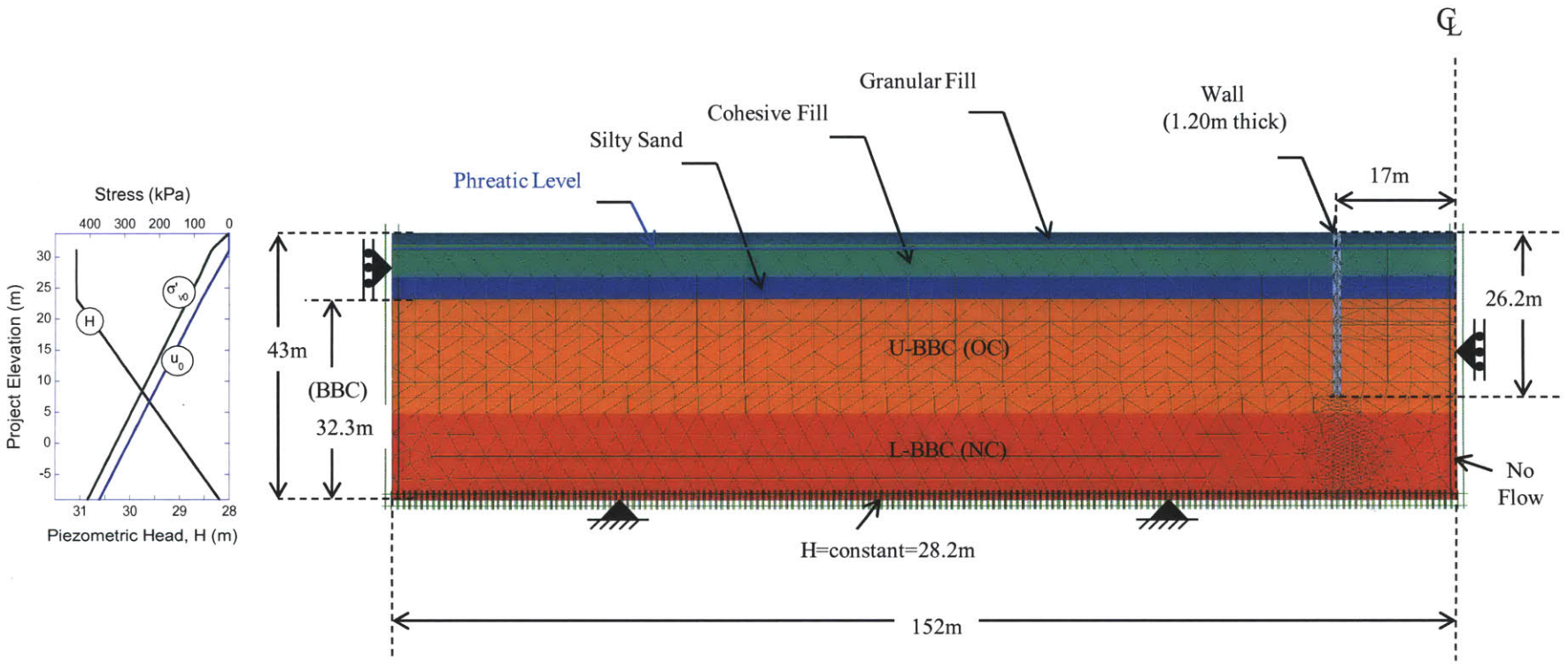

Note:
BBC: Boston Blue Clay
U-BBC: Upper BBC
L-BBC: Lower BBC

Additional Information:
Elements (15-nodes plane strain): 1857
Number of Nodes: 15119
Average Element Size: 1.8m
Phreatic Level: 2.7m from surface

Figure 5-1 (Figure 2-7 bis): Finite Element Model at the Platform section for the Transitway Project

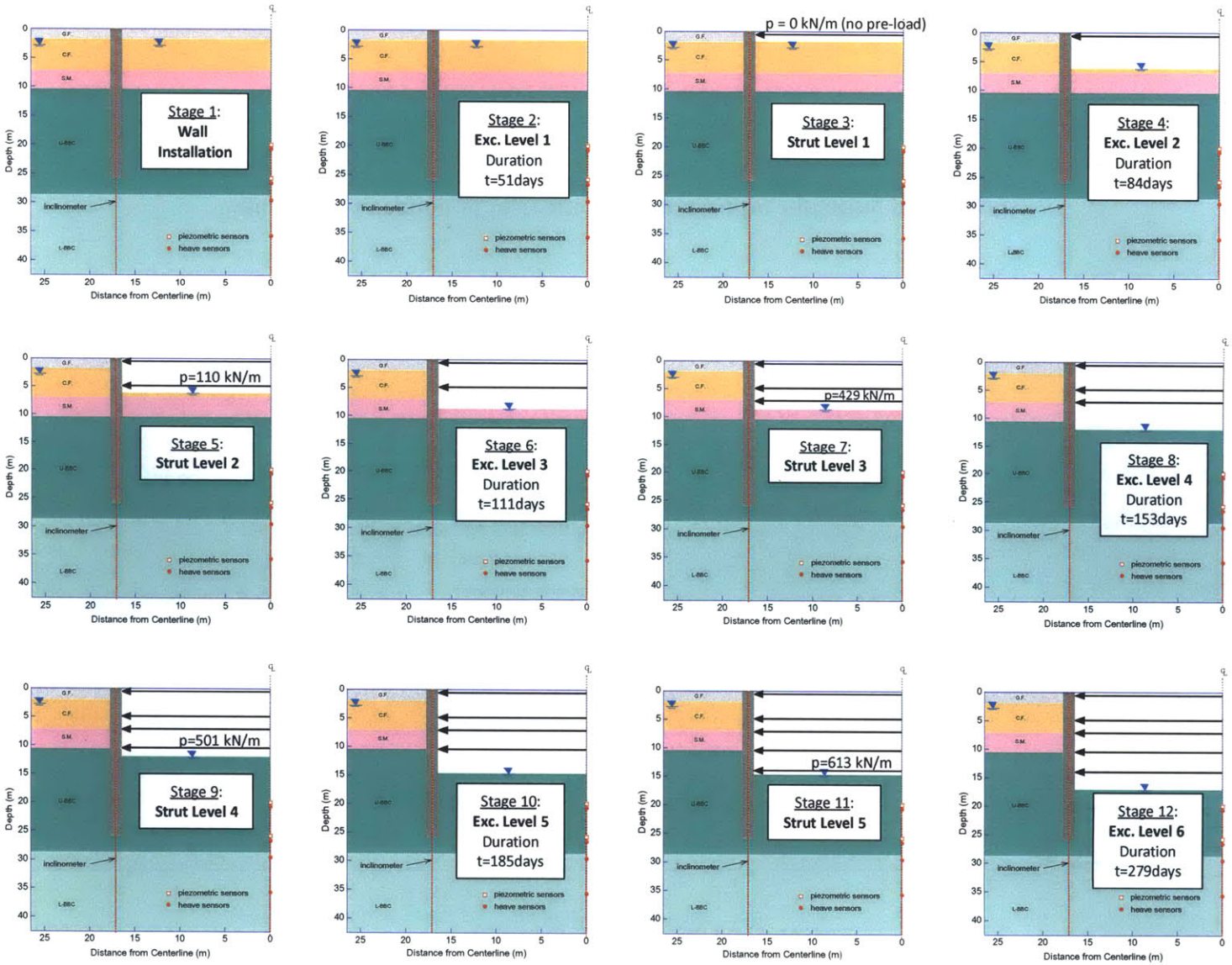

Figure 5-2: Schematic Construction Sequence assumed in FE model

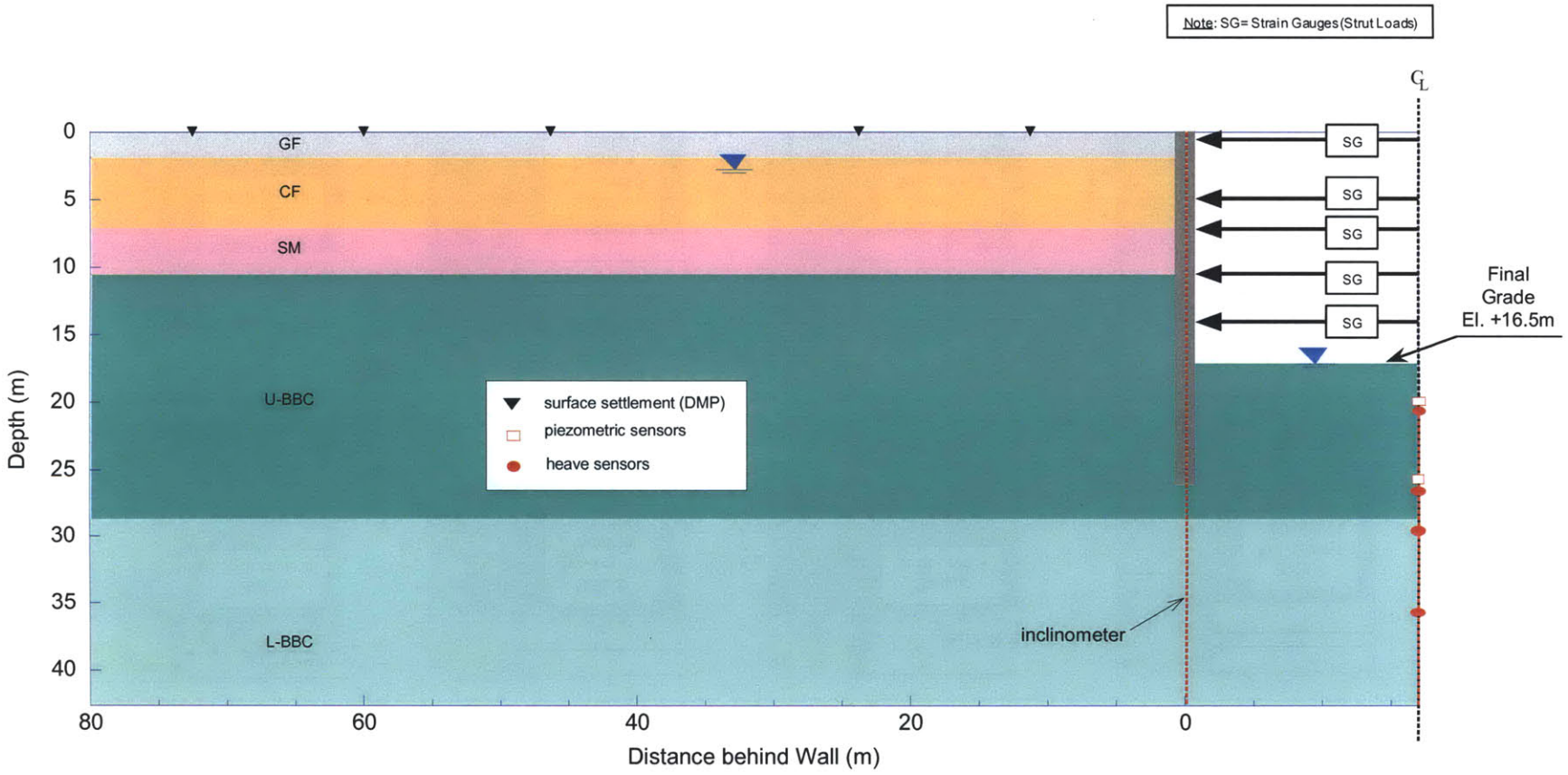

Figure 5-3: Location of instrumentation used for updating predictions

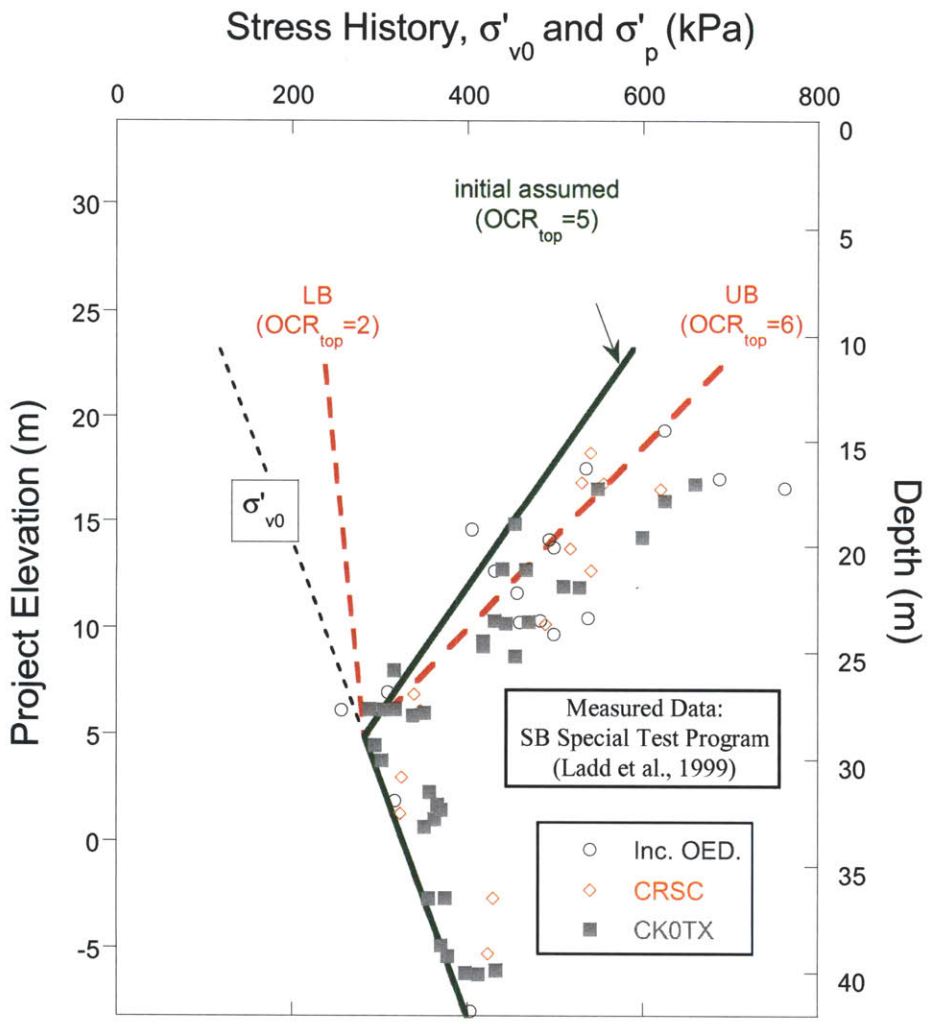

Figure 5-4: Stress history from 1-D consolidation tests in South Boston (after Ladd et al., 1999), and search space for OCR used in inverse analyses

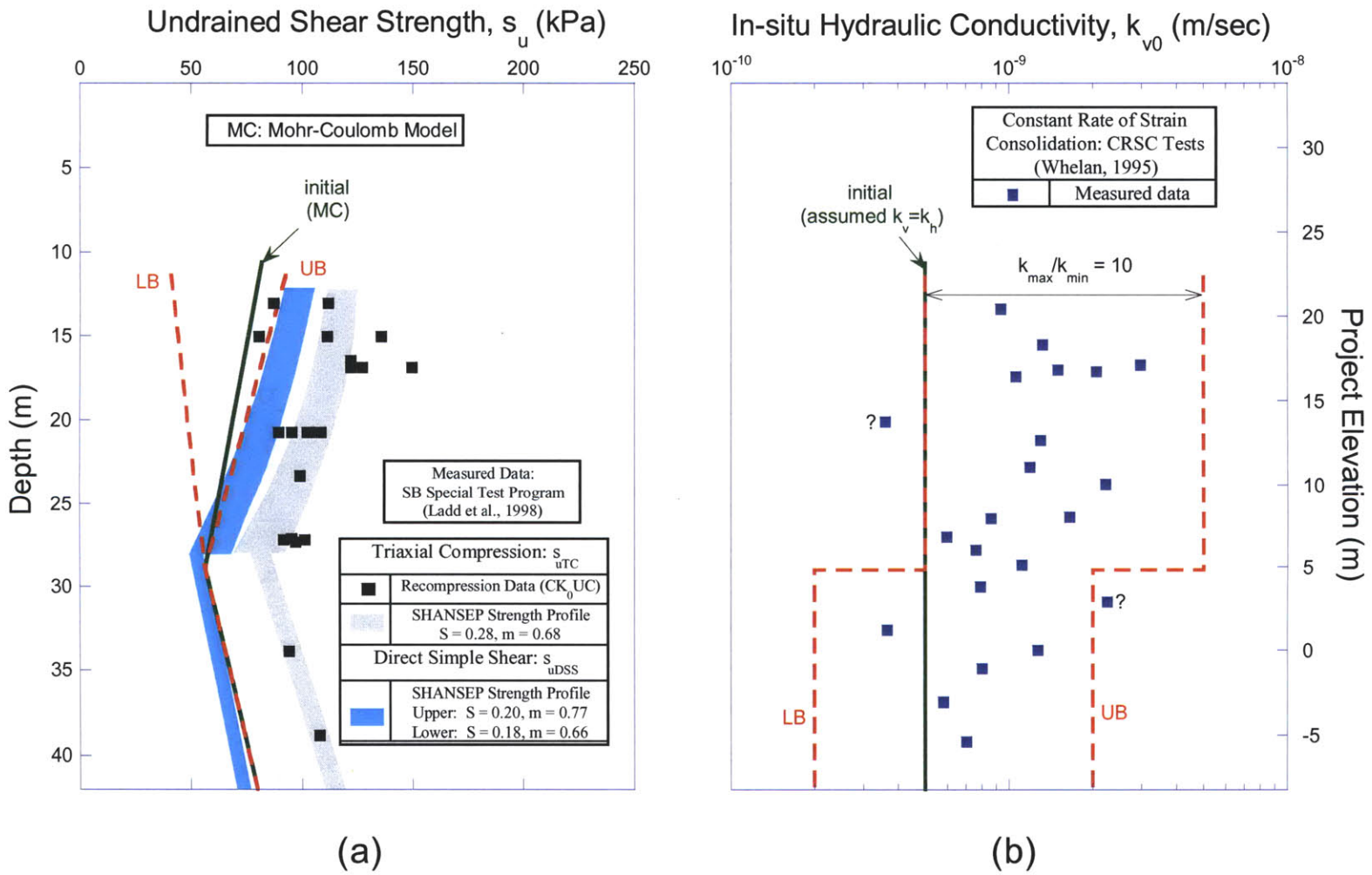

Figure 5-5: Measured undrained shear strength and hydraulic conductivity properties for BBC in South Boston together with search space ranges used in inverse analyses

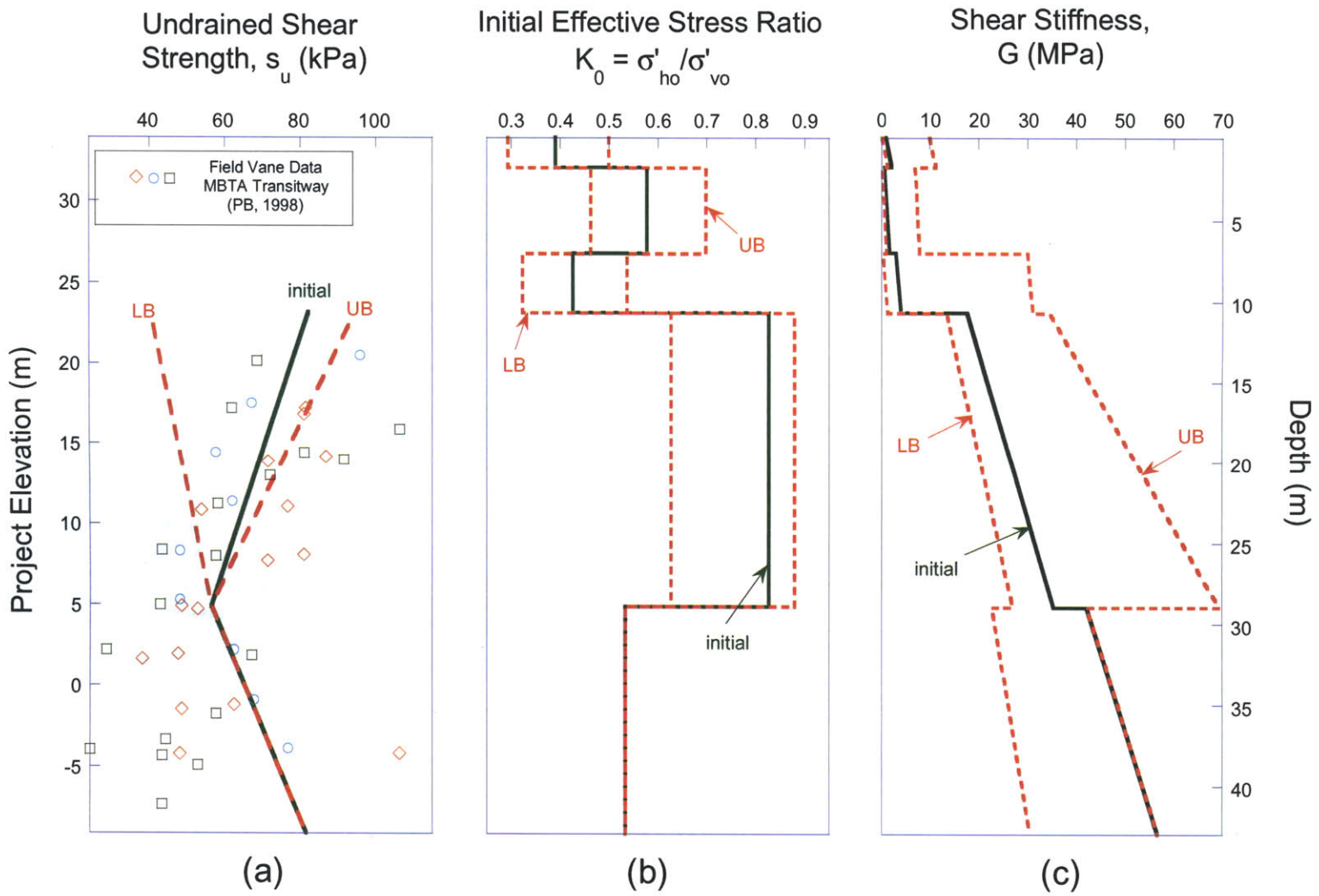

Figure 5-6: Initial, lower, and upper bounds profiles for BBC in South Boston of (a) undrained shear strengths (compared with field vane data), (b) lateral earth pressure ratios, K_0, and (c) elastic shear moduli for MC soil model

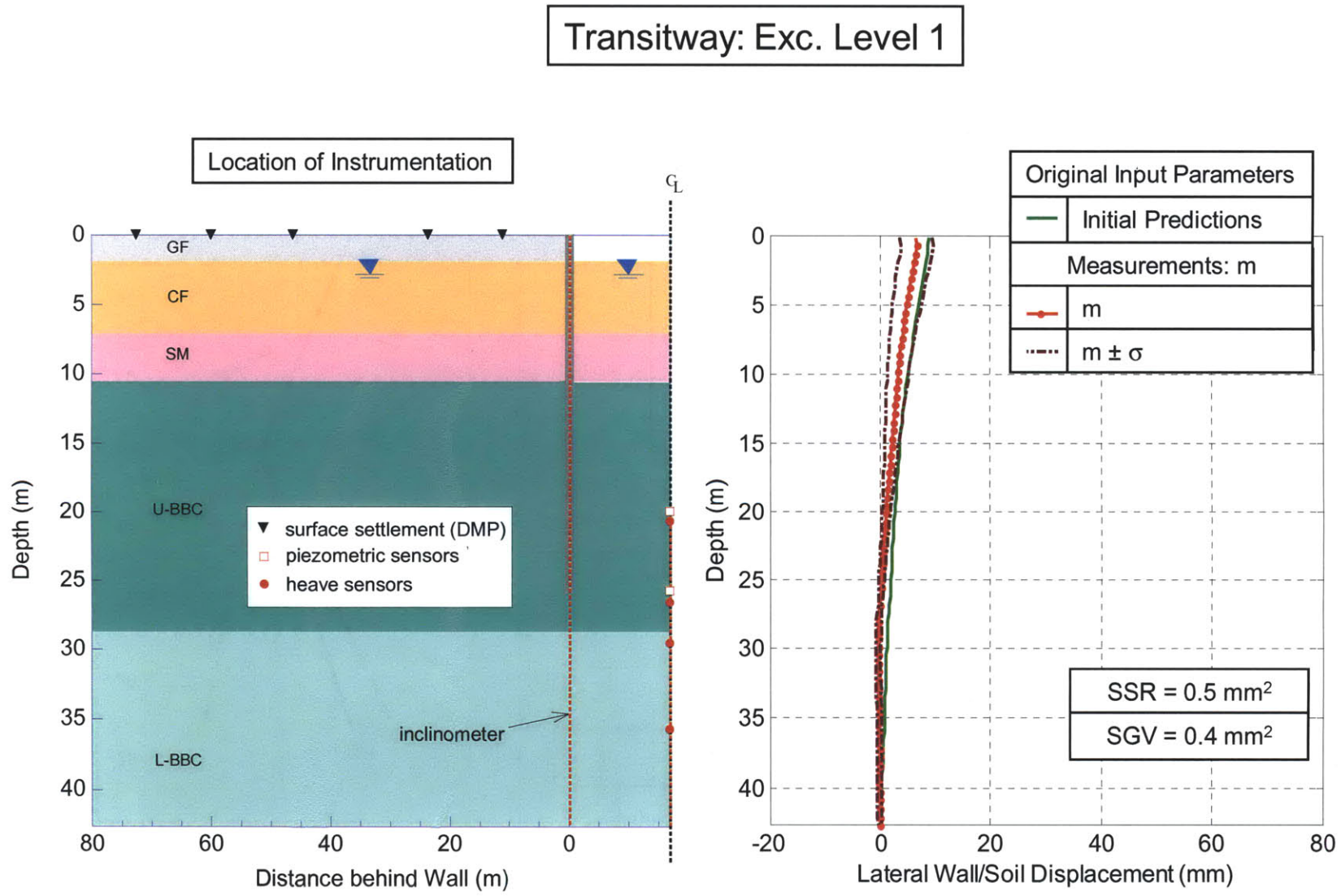

Figure 5-7: Measurements vs. Initial Predictions of Lateral Wall/Soil Movement at Excavation Level 1

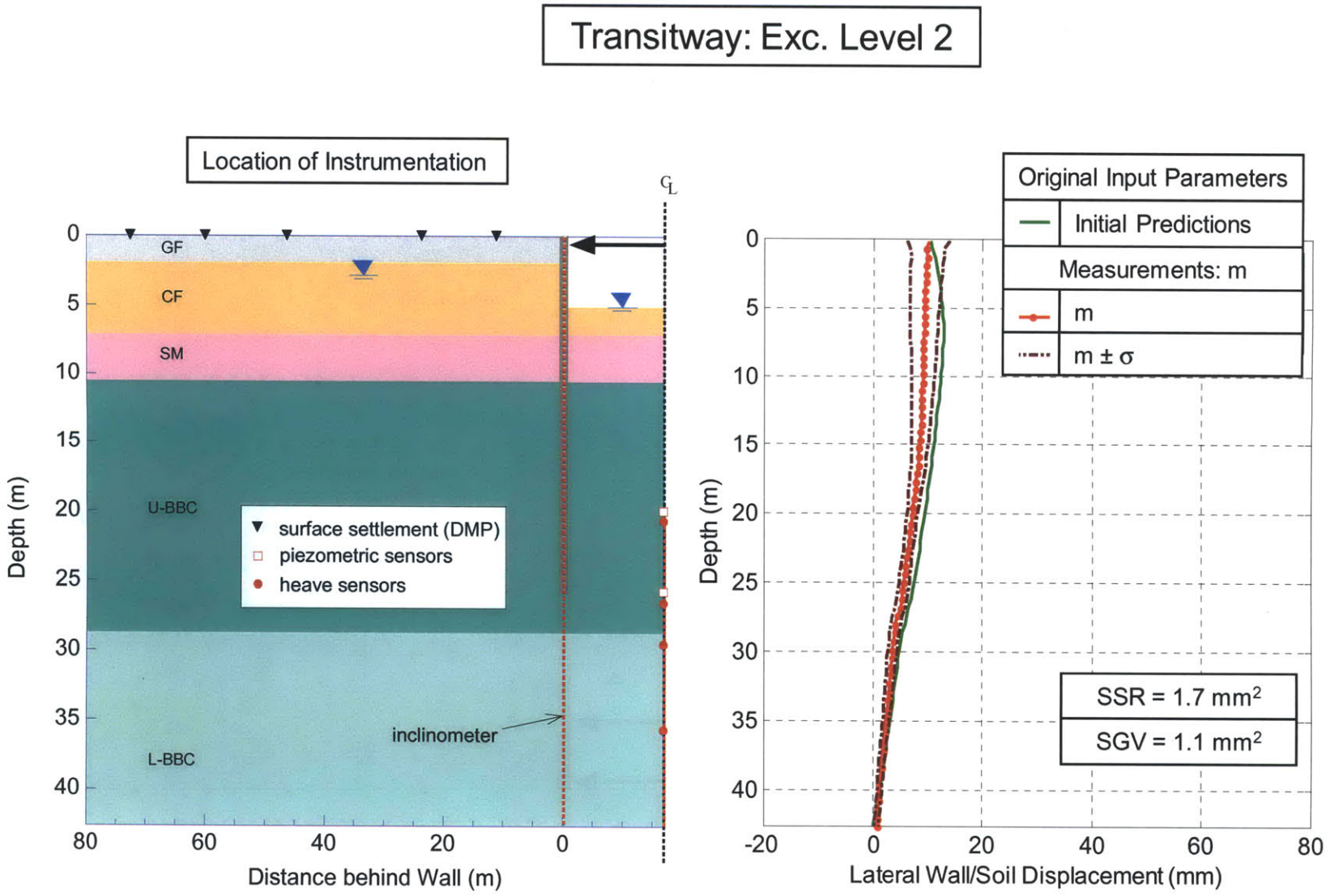

Figure 5-8: Measurements vs. Initial Predictions of Lateral Wall/Soil Movement at Excavation Level 2

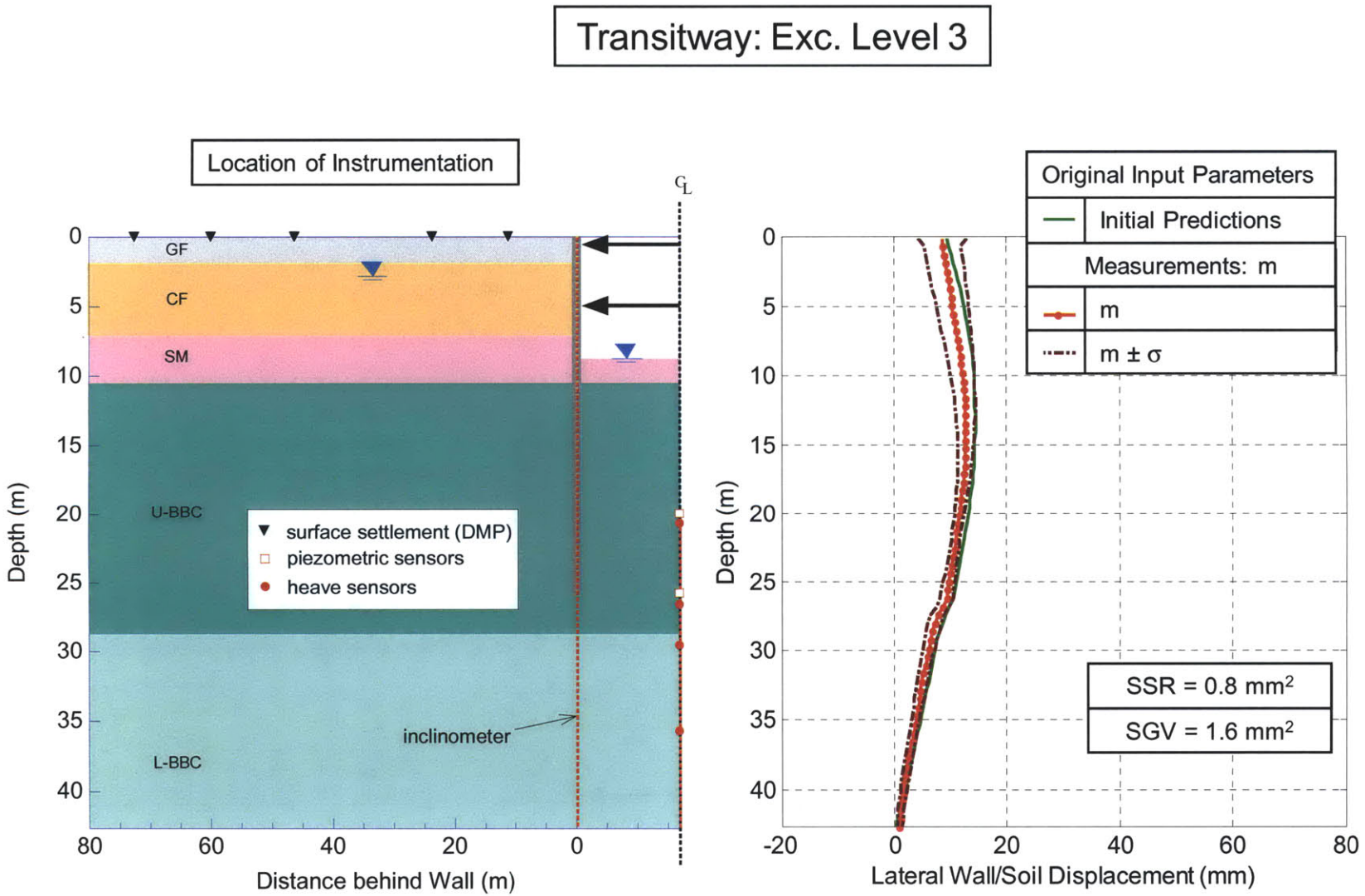

Figure 5-9: Measurements vs. Initial Predictions of Lateral Wall/Soil Movement at Excavation Level 3

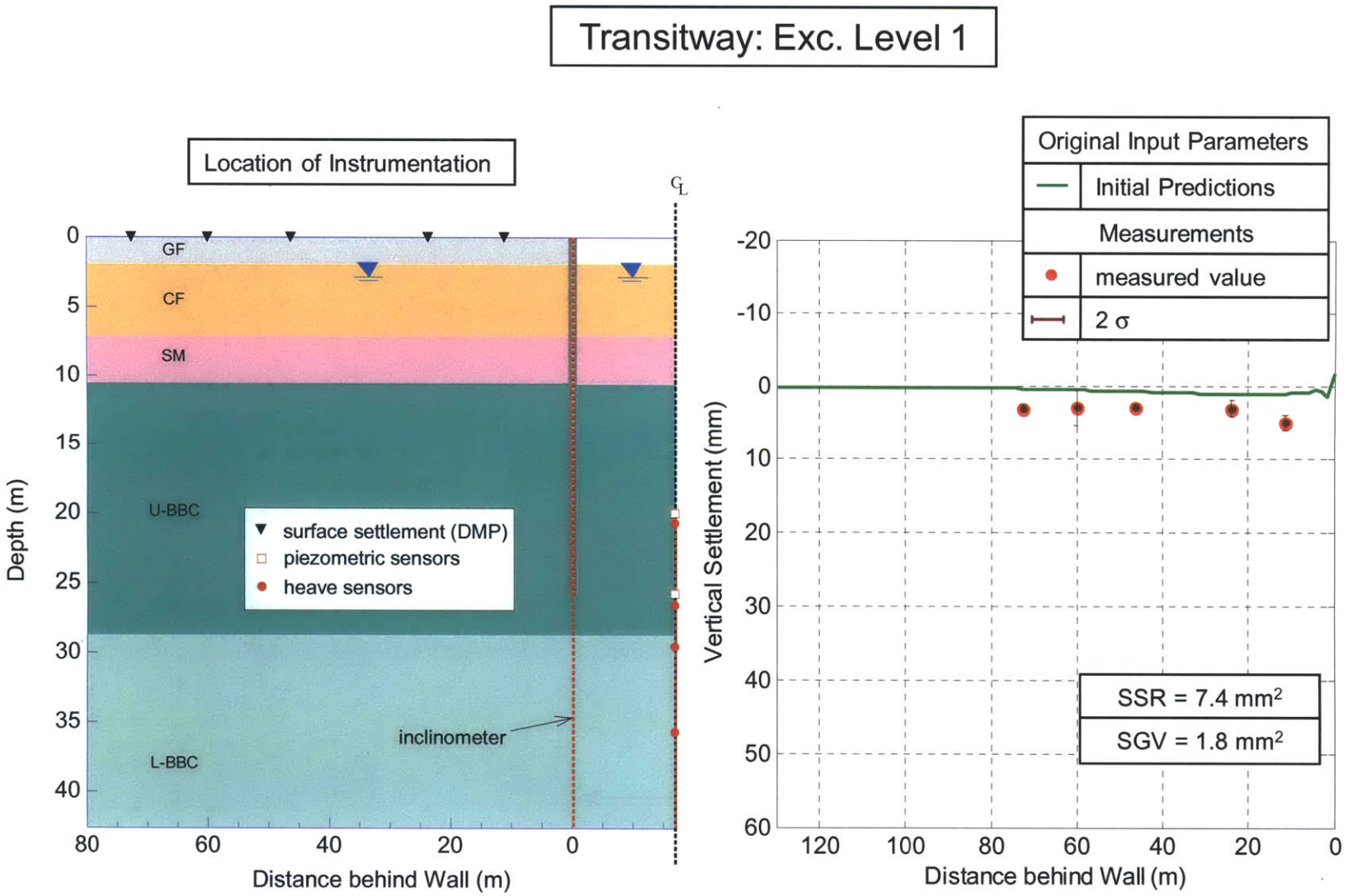

Figure 5-10: Measurements vs. Initial Predictions of Surface Vertical Settlement at Excavation Level 1

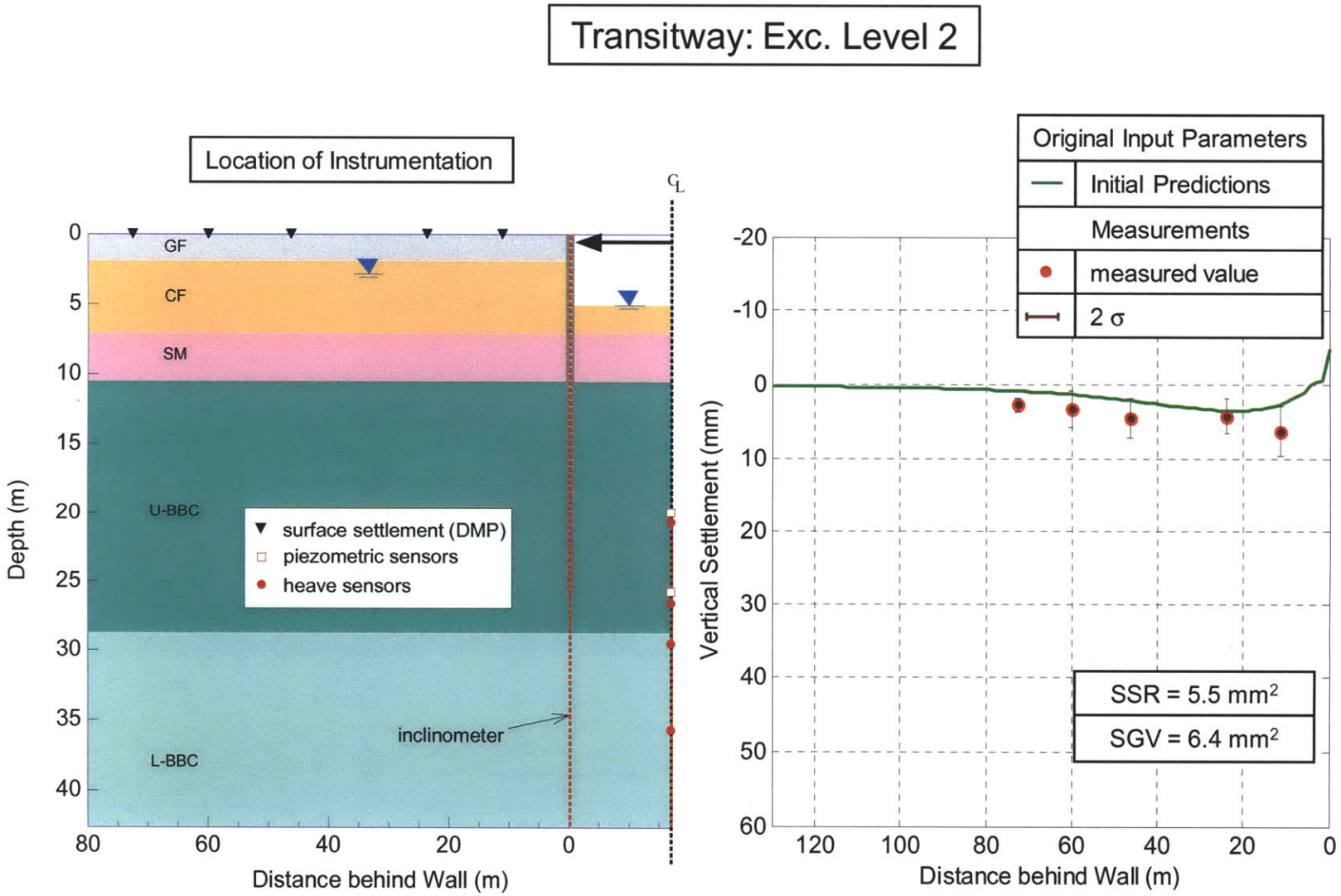

Figure 5-11: Measurements vs. Initial Predictions of Surface Vertical Settlement at Excavation Level 2

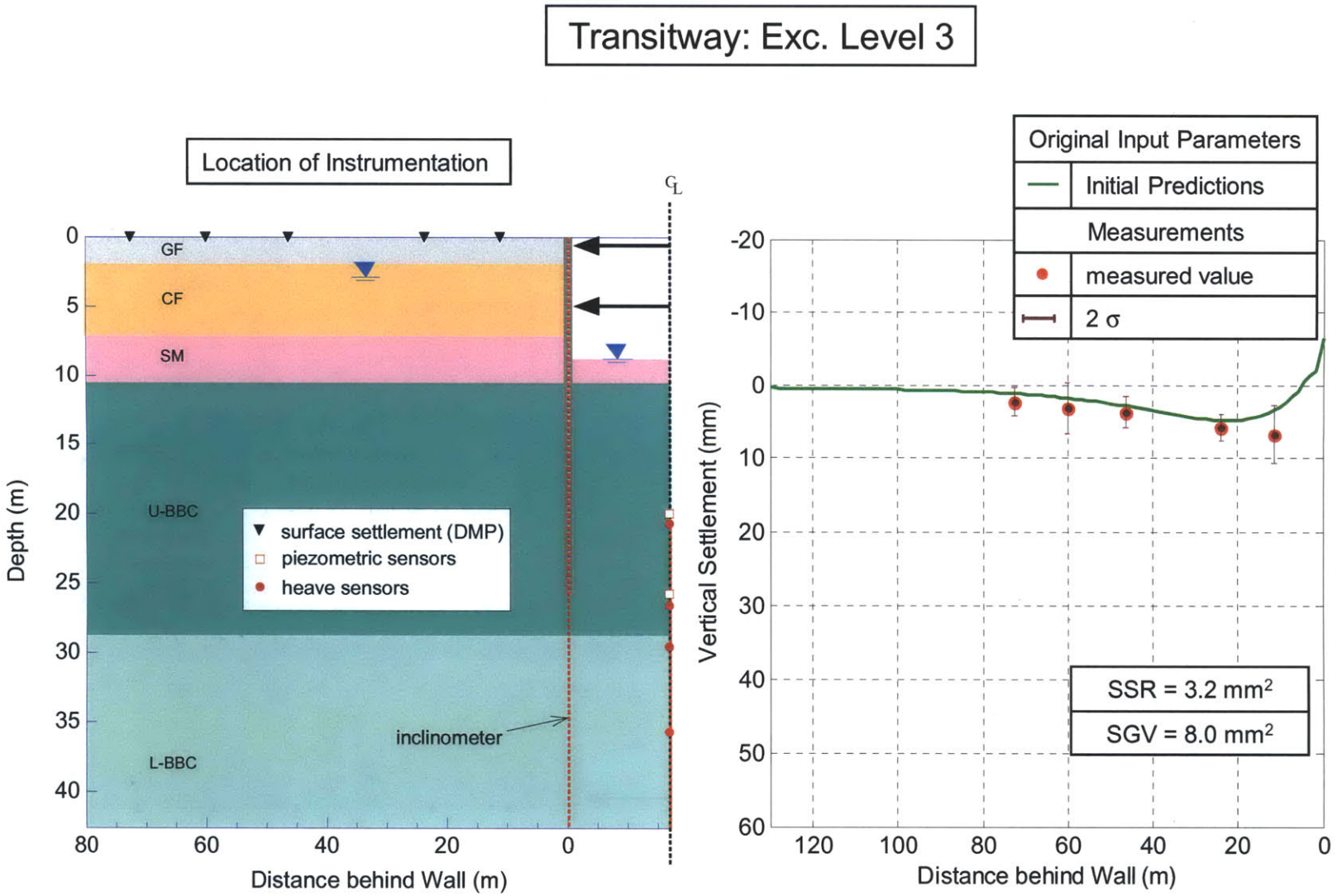

Figure 5-12: Measurements vs. Initial Predictions of Surface Vertical Settlement at Excavation Level 3

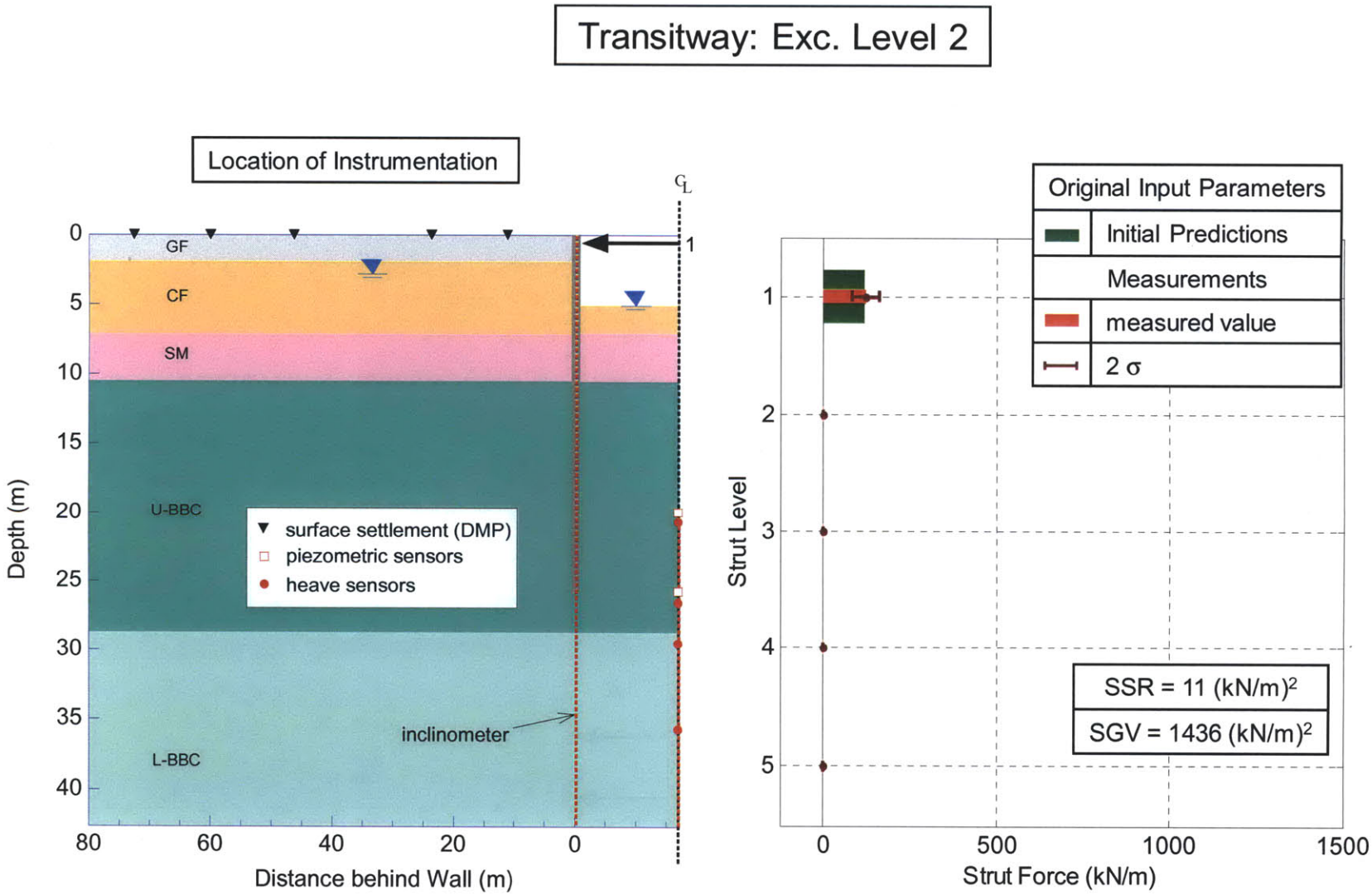

Figure 5-13: Measurements vs. Initial Predictions of Strut Forces at Excavation Level 2

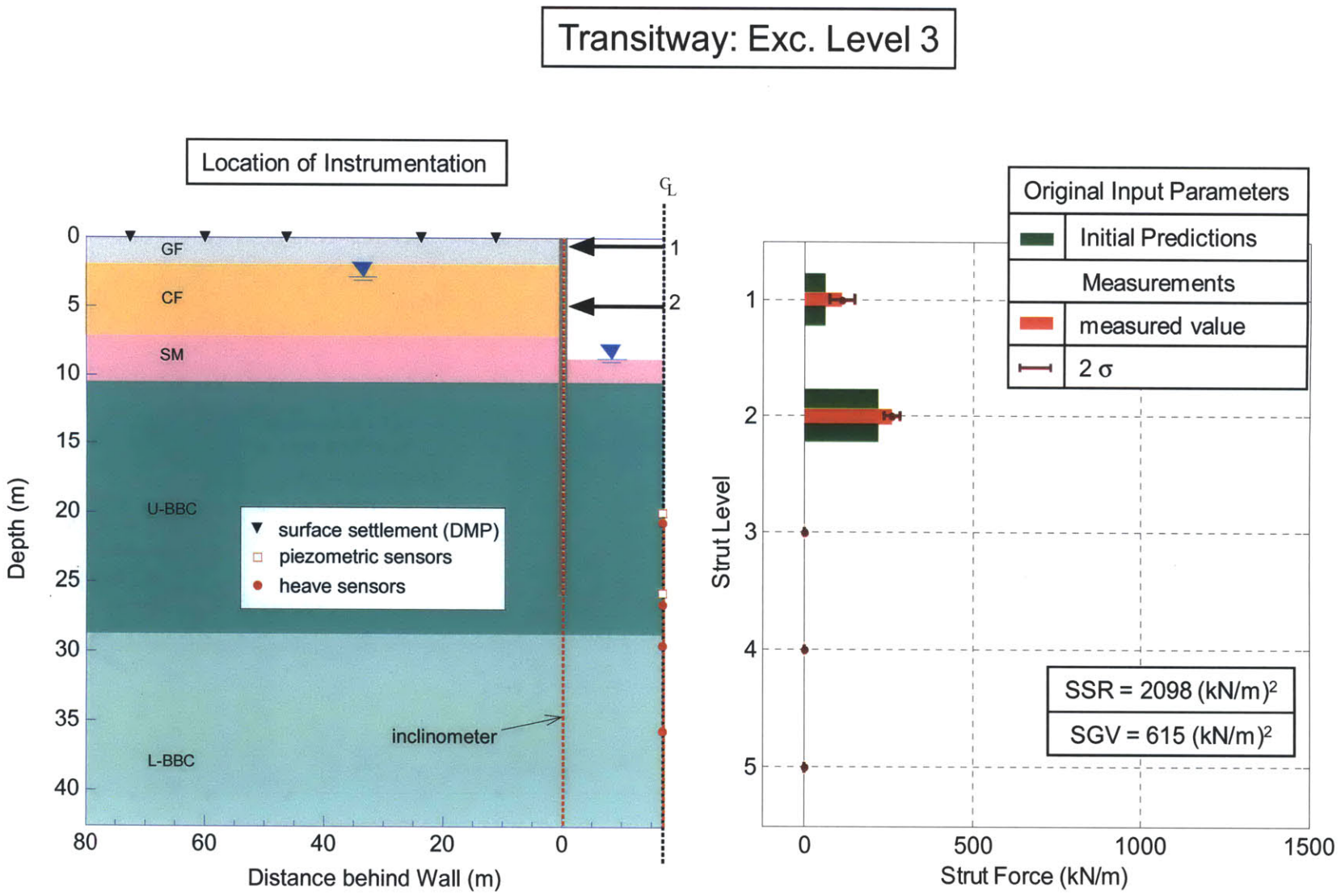

Figure 5-14: Measurements vs. Initial Predictions of Strut Forces at Excavation Level 3

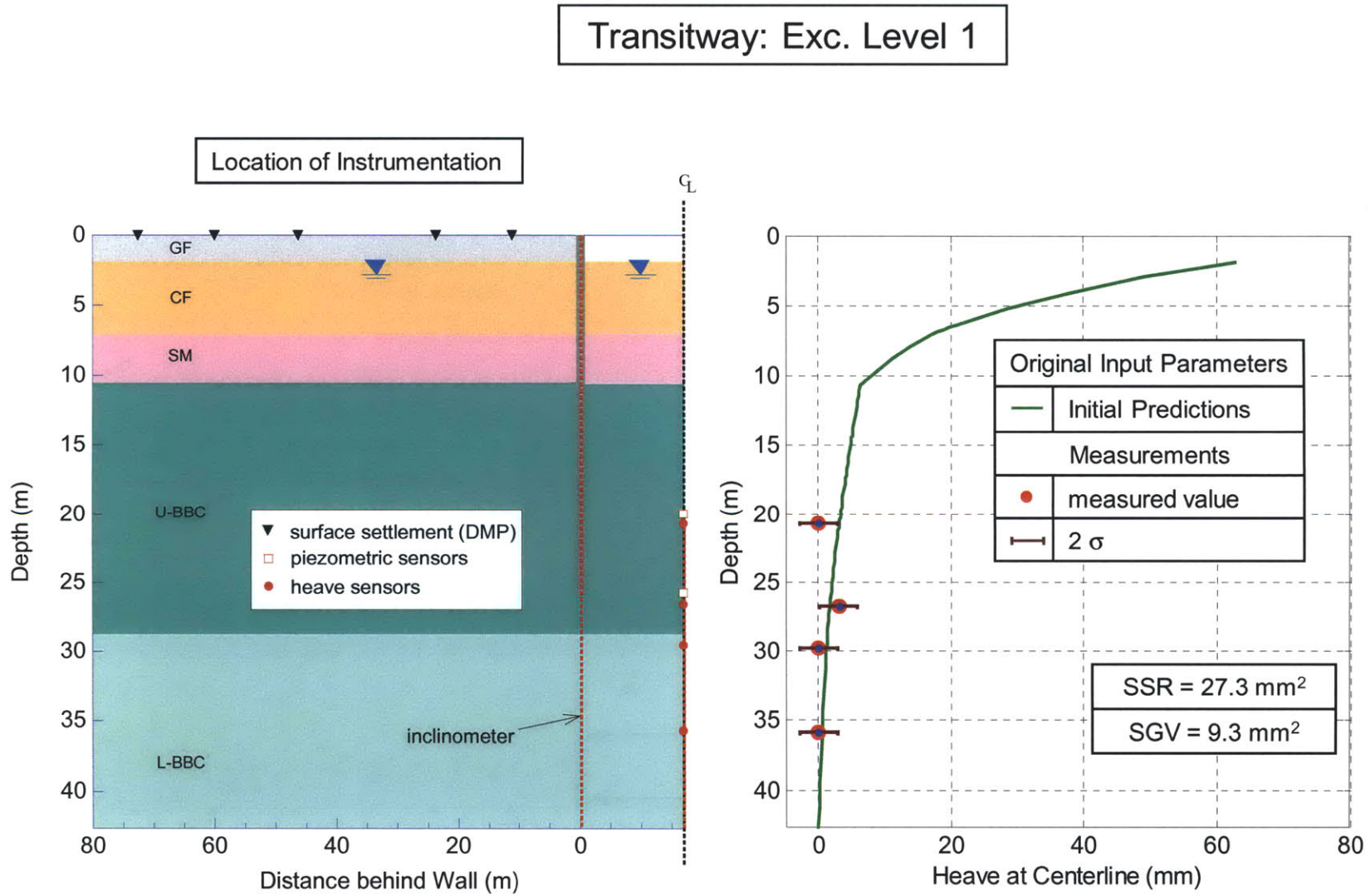

Figure 5-15: Measurements vs. Initial Predictions of Centerline Heave at Excavation Level 1

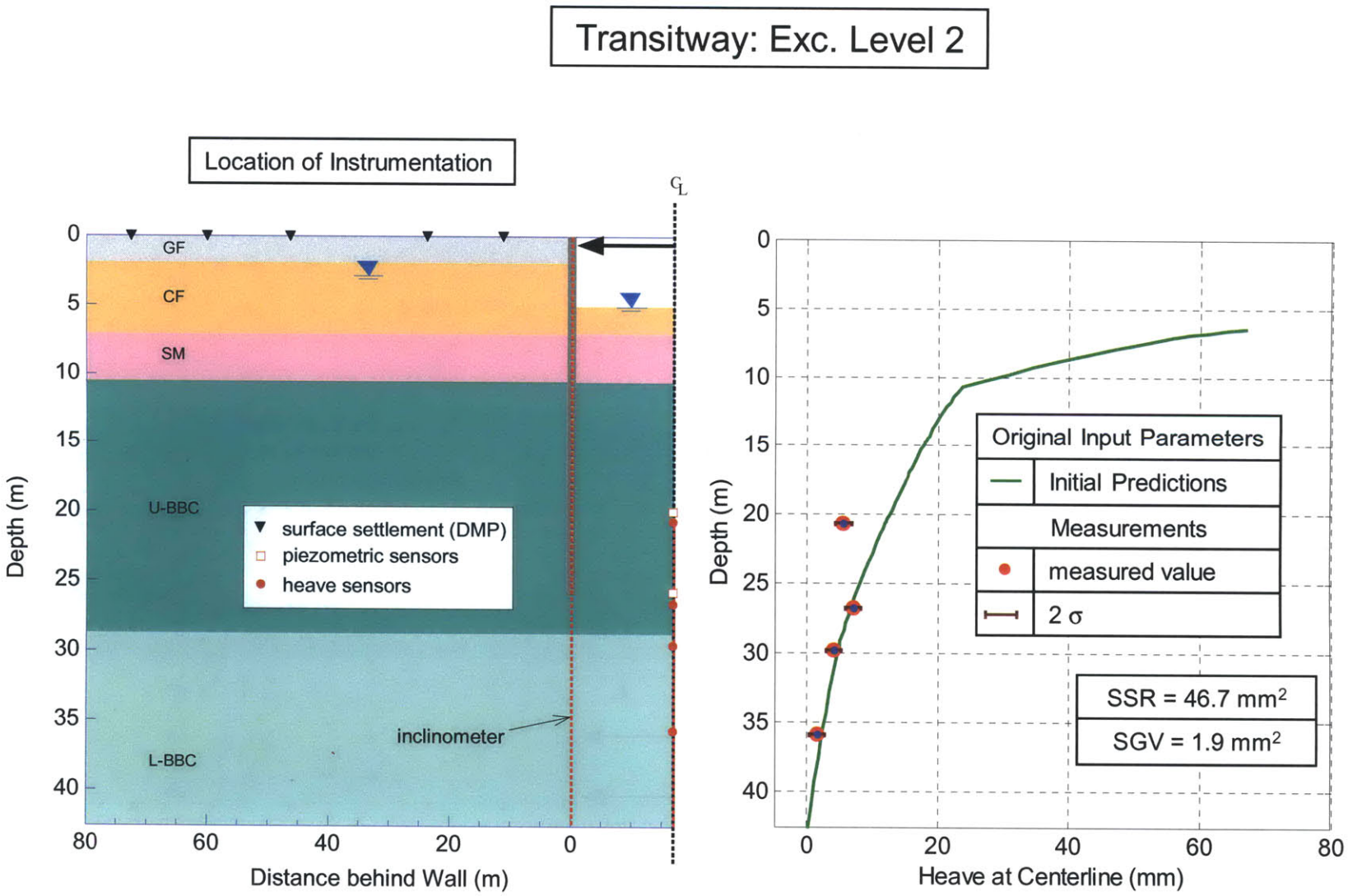

Figure 5-16: Measurements vs. Initial Predictions of Centerline Heave at Excavation Level 2

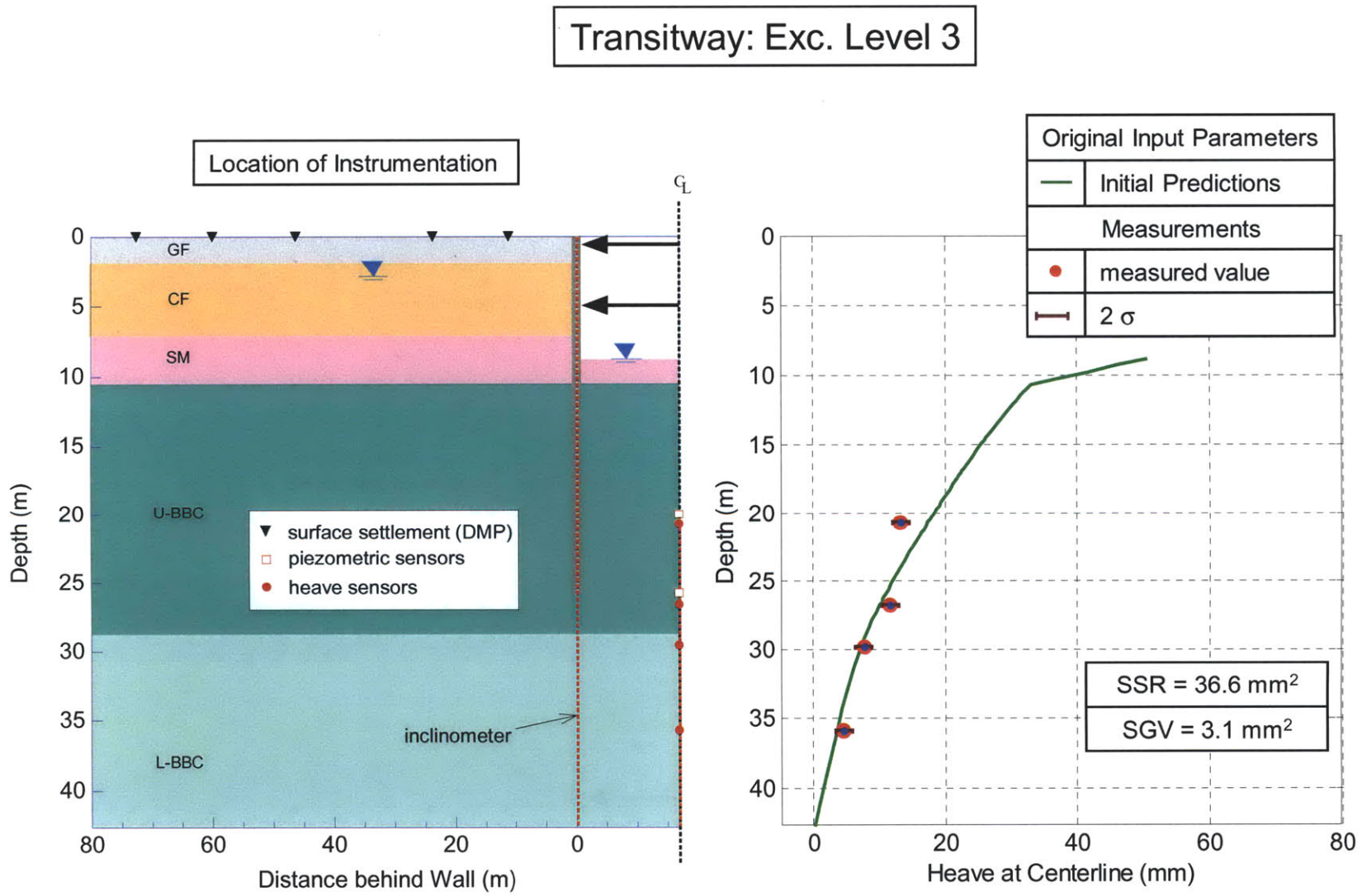

Figure 5-17: Measurements vs. Initial Predictions of Centerline Heave at Excavation Level 3

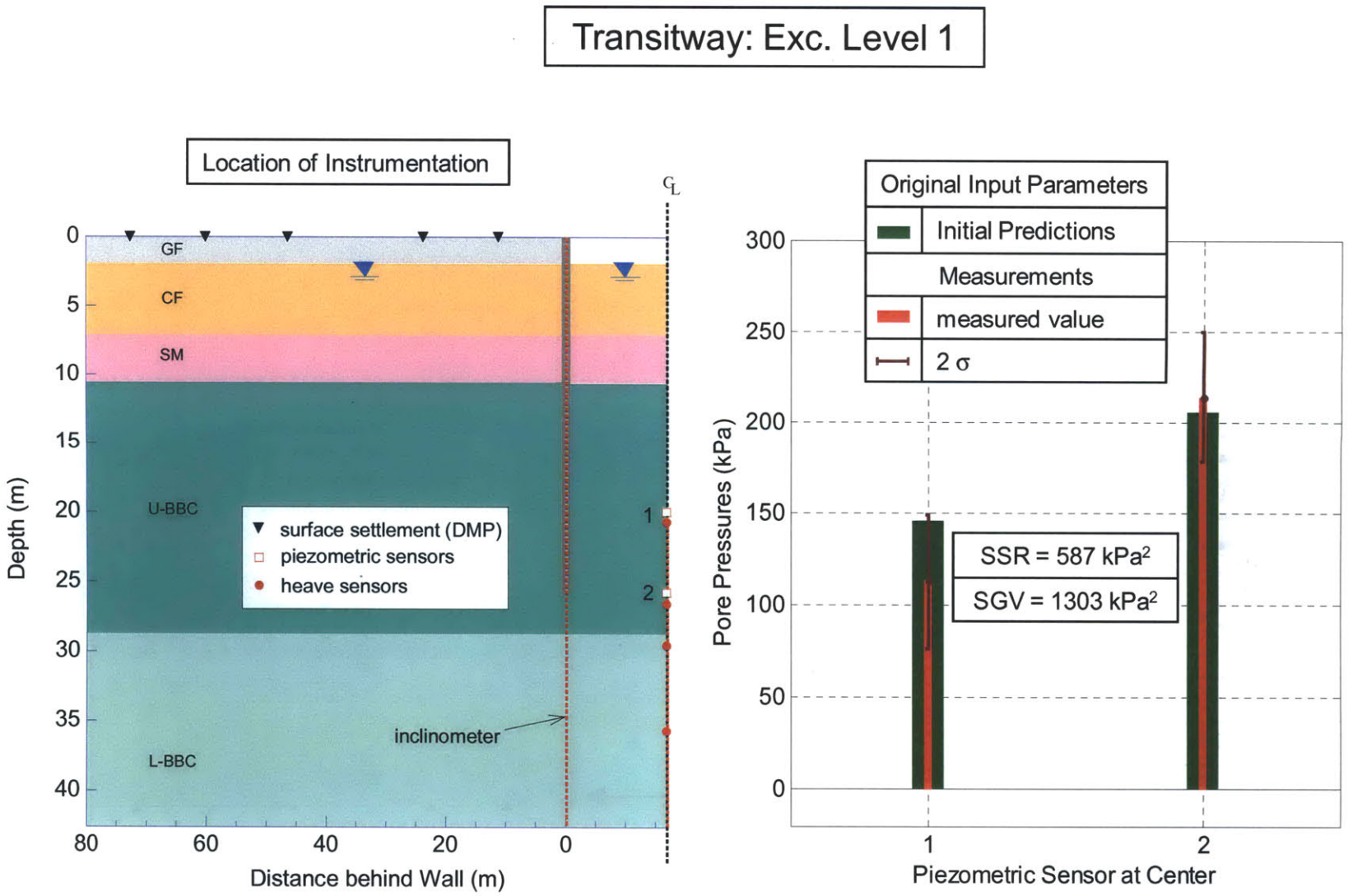

Figure 5-18: Measurements vs. Initial Predictions of Pore Water Pressures (2 sensors at CL) at Excavation Level 1

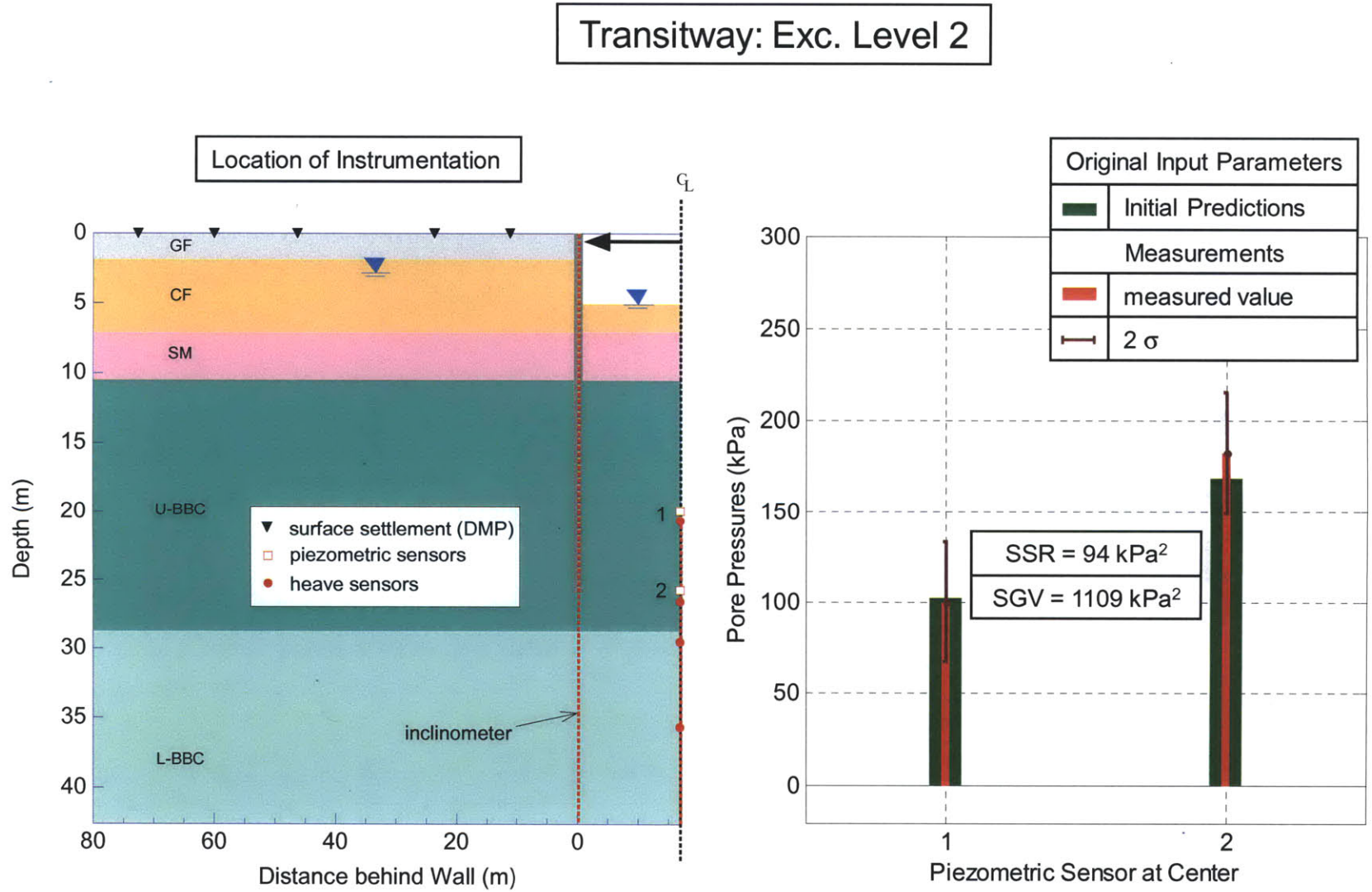

Figure 5-19: Measurements vs. Initial Predictions of Pore Water Pressures (2 sensors at CL) at Excavation Level 2

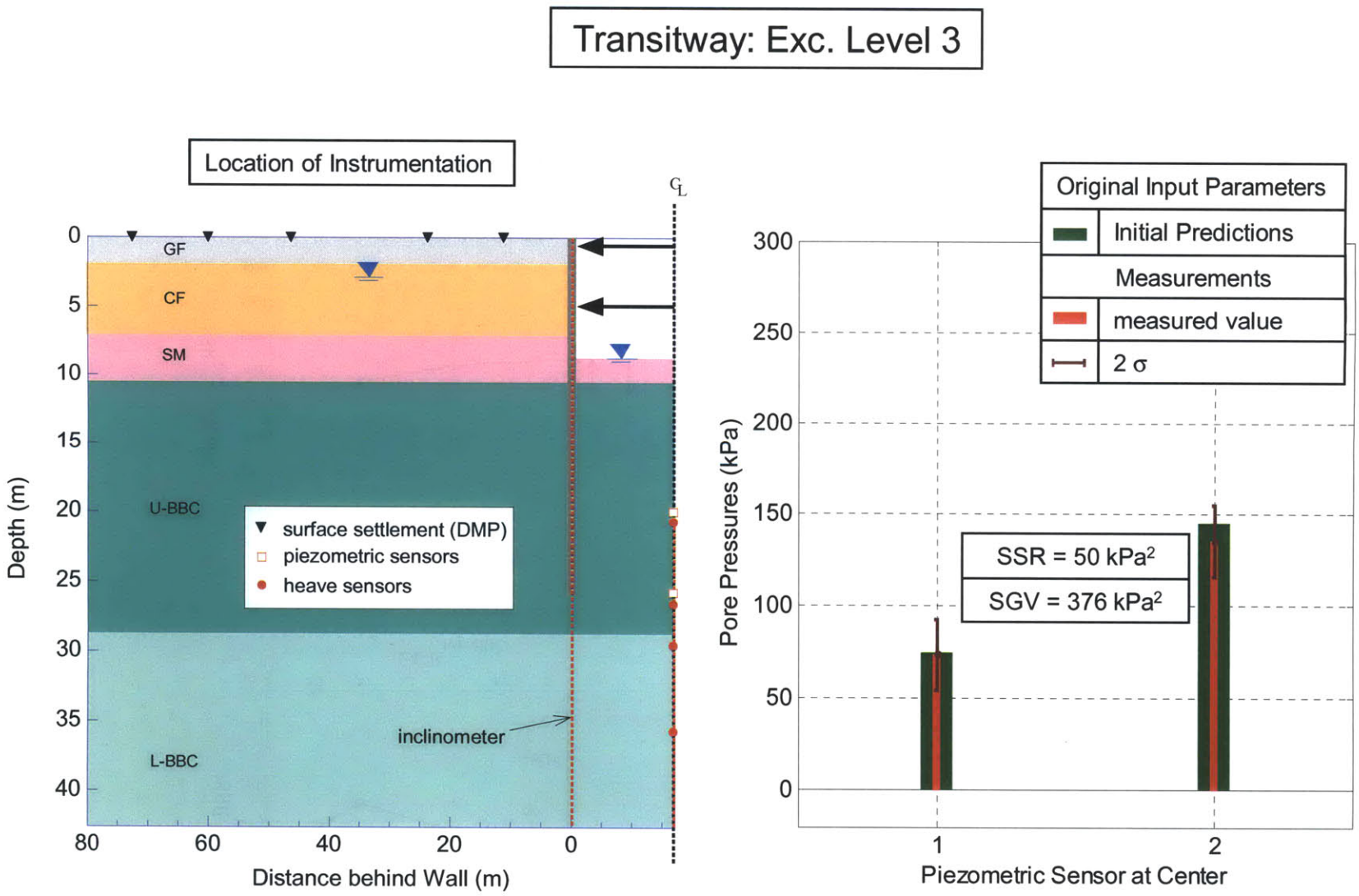

Figure 5-20: Measurements vs. Initial Predictions of Pore Water Pressures (2 sensors at CL) at Excavation Level 3

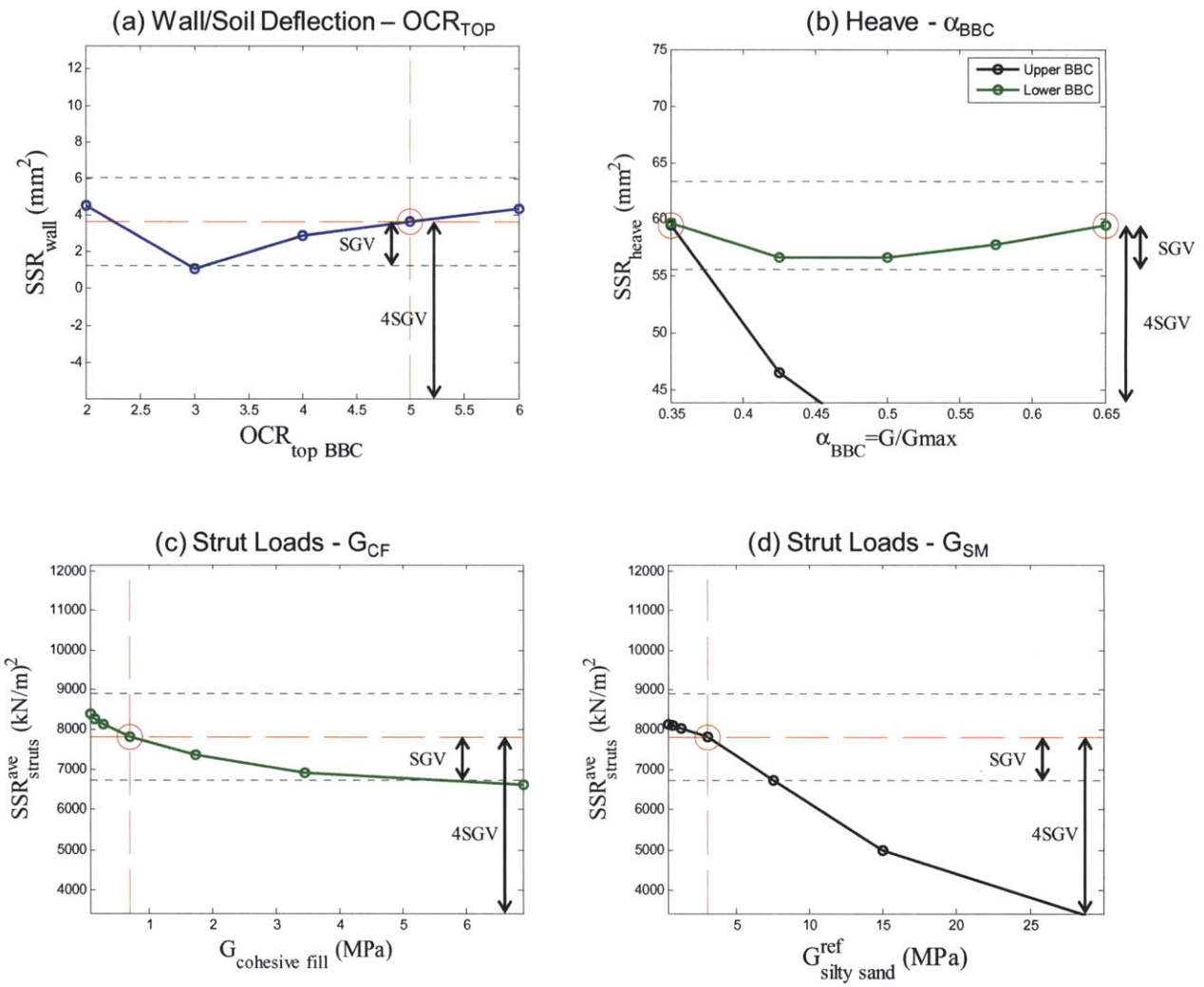

Figure 5-21: Sensitivity analyses of essential improvement parameters (EIP) at excavation level 4

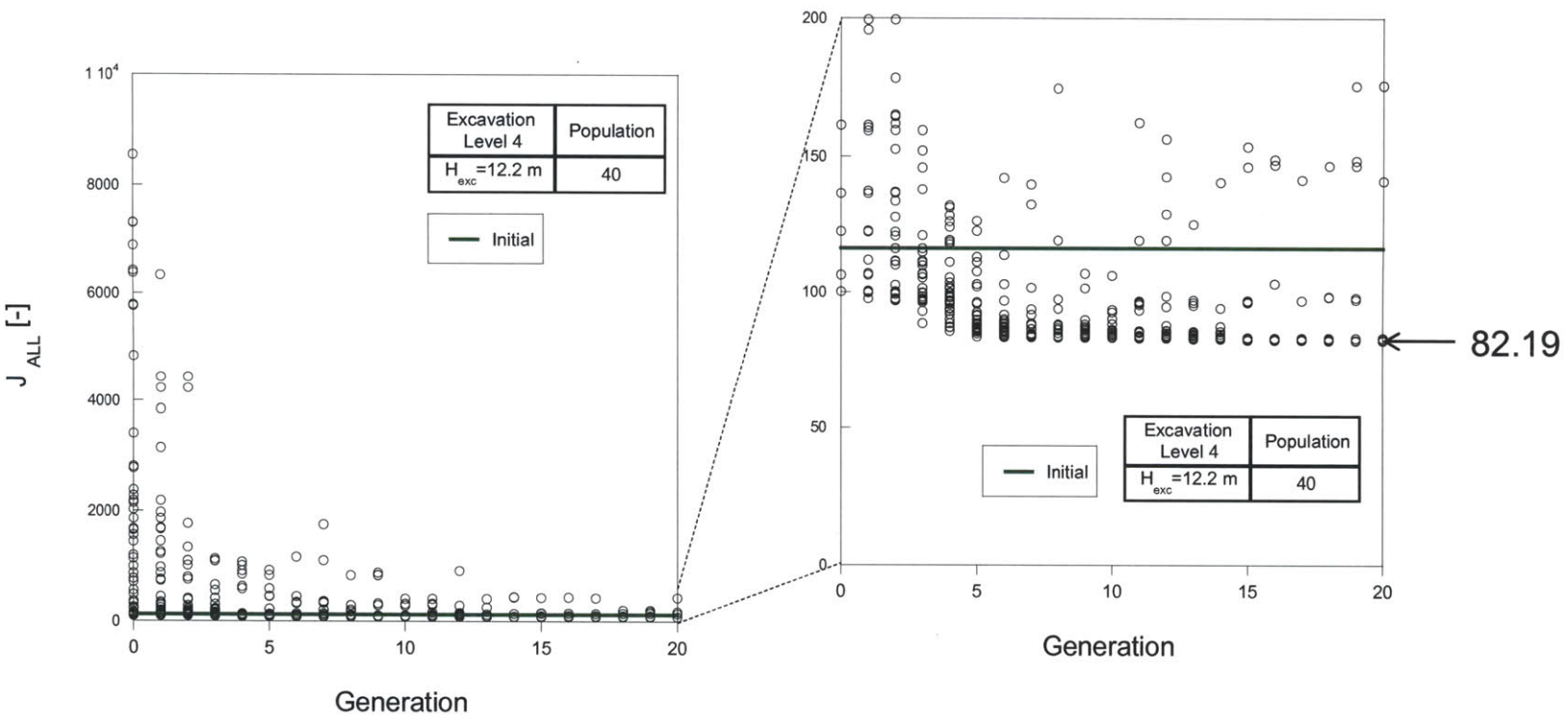

Figure 5-22: Convergence of objective function for all measurements obtained by genetic algorithms at excavation level 4

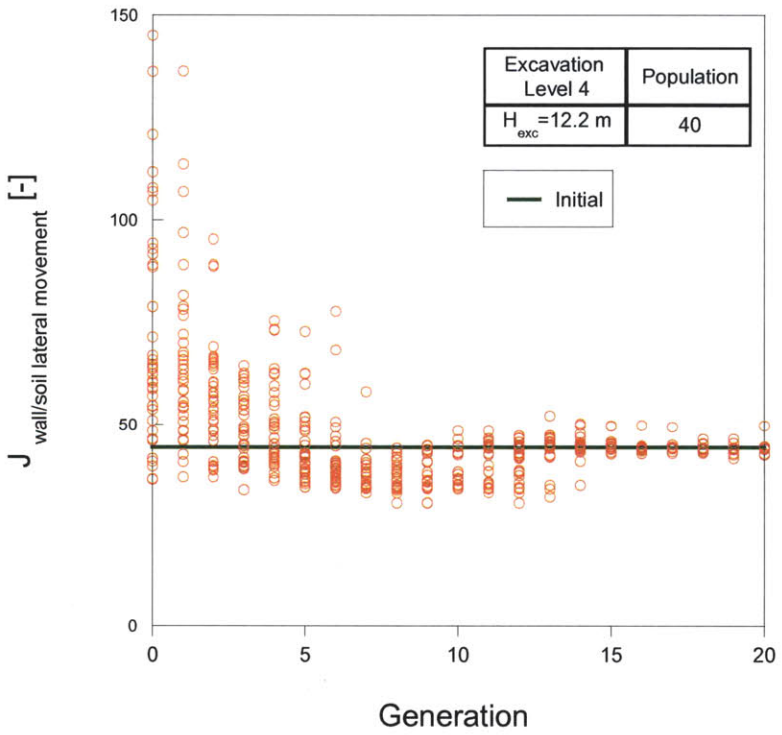

Figure 5-23: Convergence of objective function for lateral wall/soil movements obtained by genetic algorithms at excavation level 4

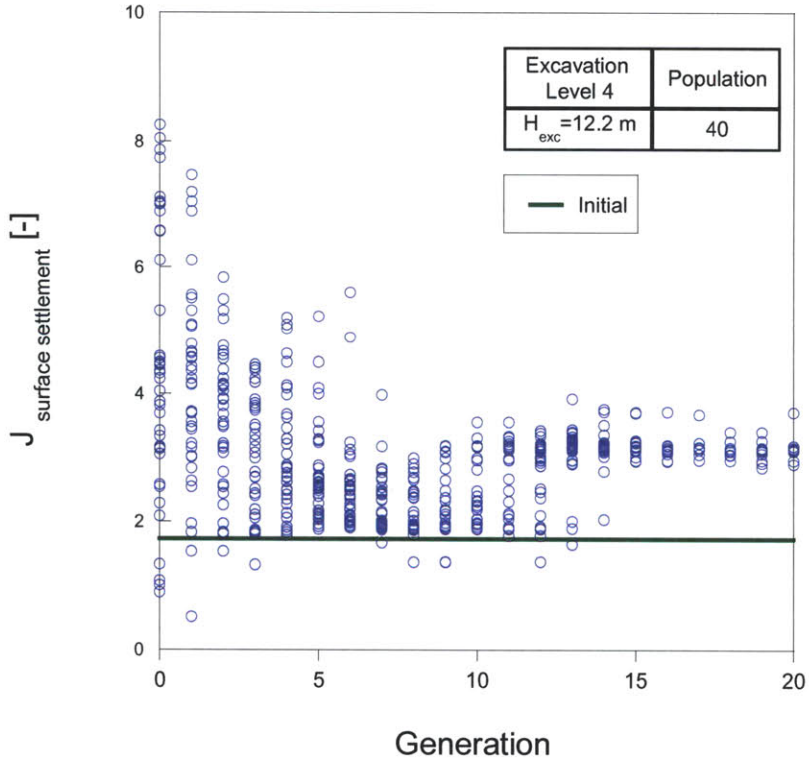

Figure 5-24: Convergence of objective function for surface settlements obtained by genetic algorithms at excavation level 4

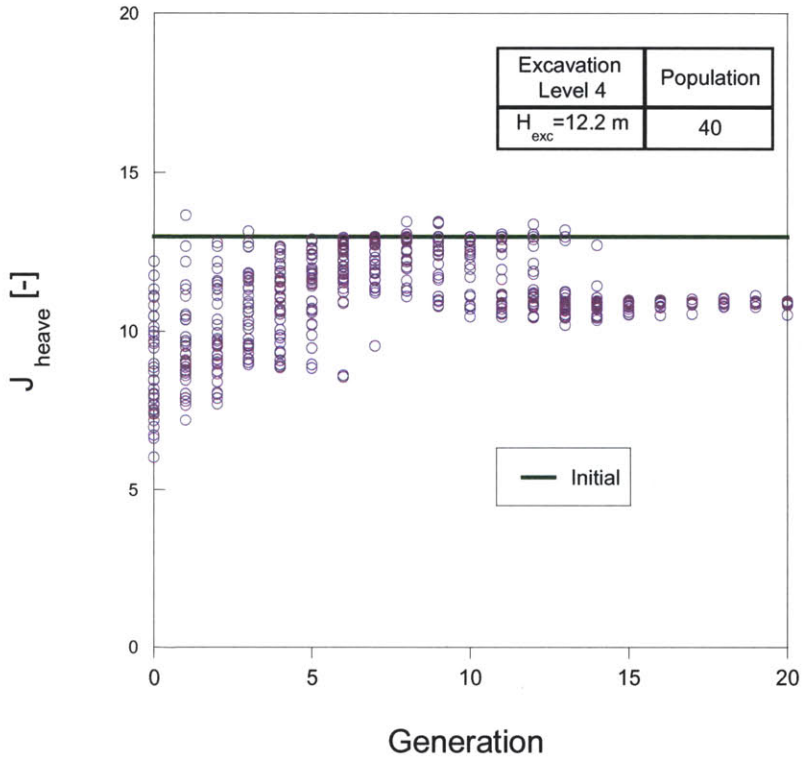

Figure 5-25: Convergence of objective function for excavation heave obtained by genetic algorithms at excavation level 4

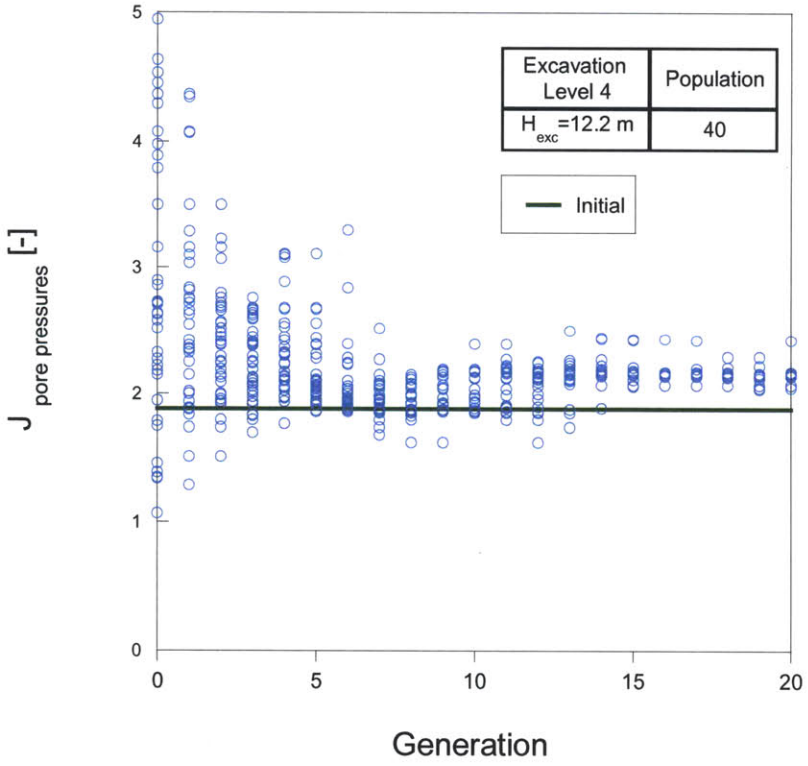

Figure 5-26: Convergence of objective function for pore water pressures obtained by genetic algorithms at excavation level 4

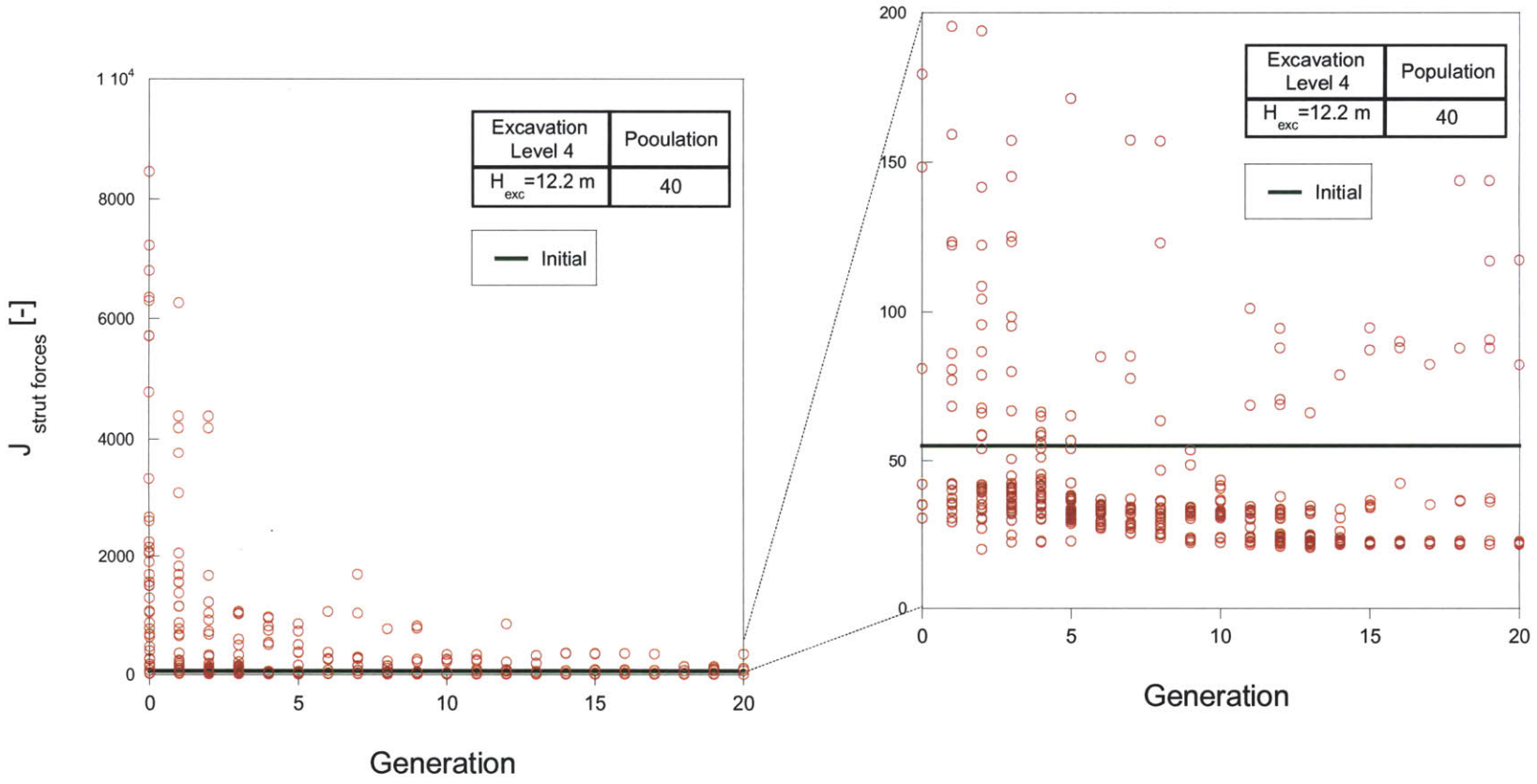

Figure 5-27: Convergence of objective function for strut forces obtained by genetic algorithms at excavation level 4

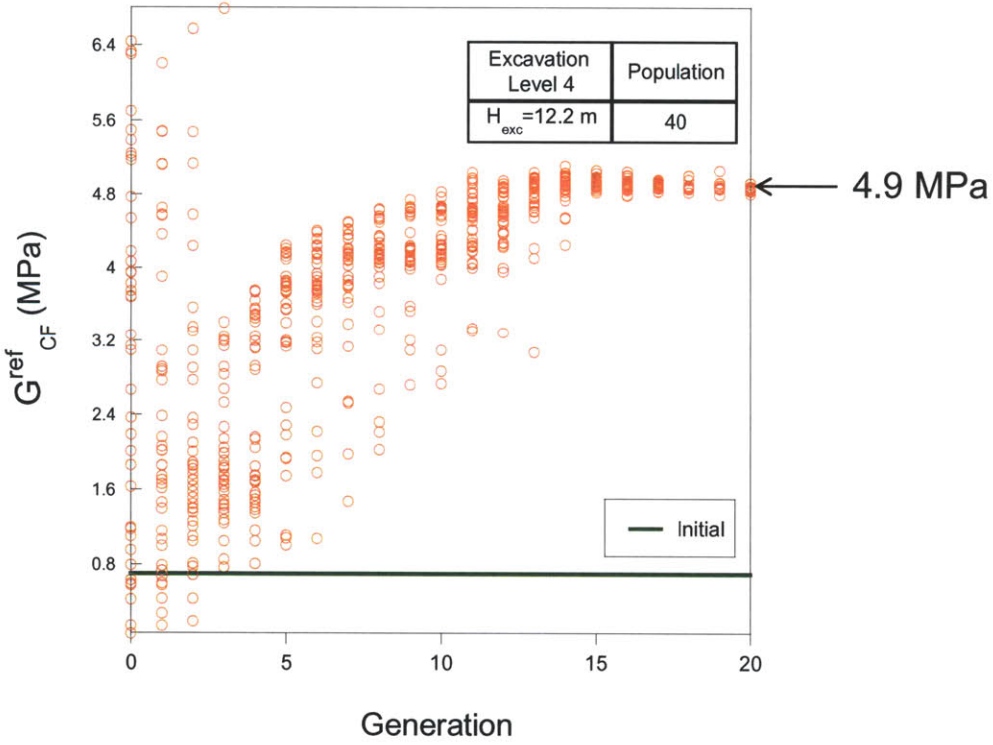

Figure 5-28: Convergence of G^{ref} of the cohesive fill layer obtained by genetic algorithms at excavation level 4

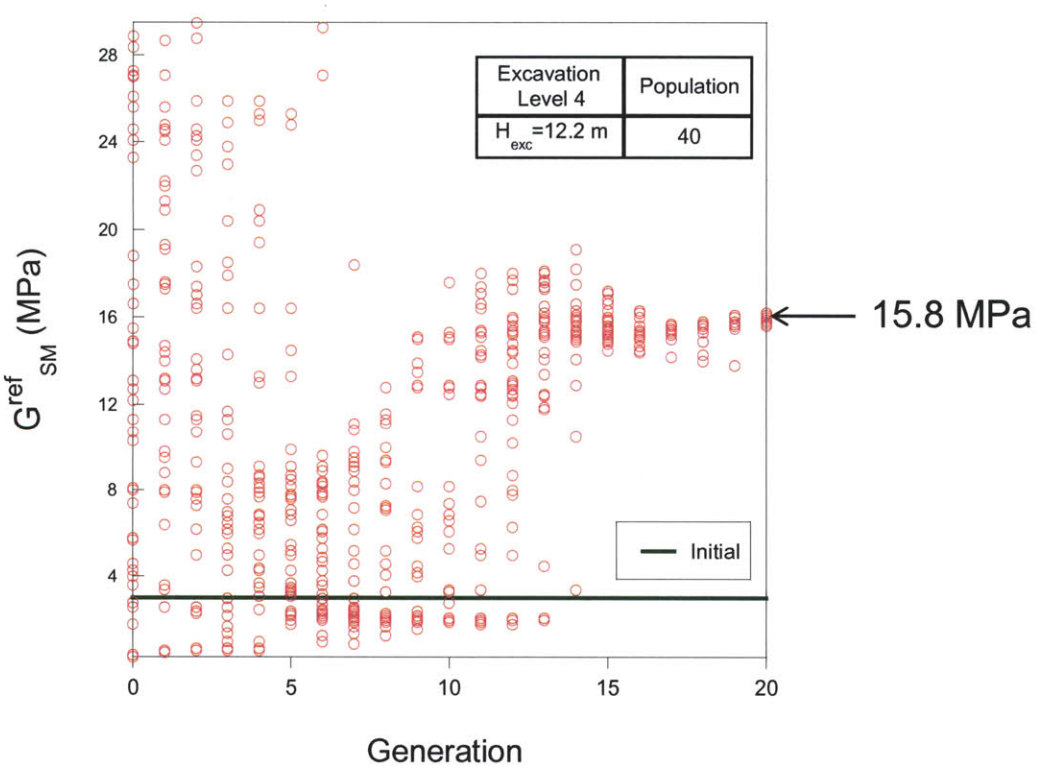

Figure 5-29: Convergence of G^{ref} of the silty sand layer obtained by genetic algorithms at excavation level 4

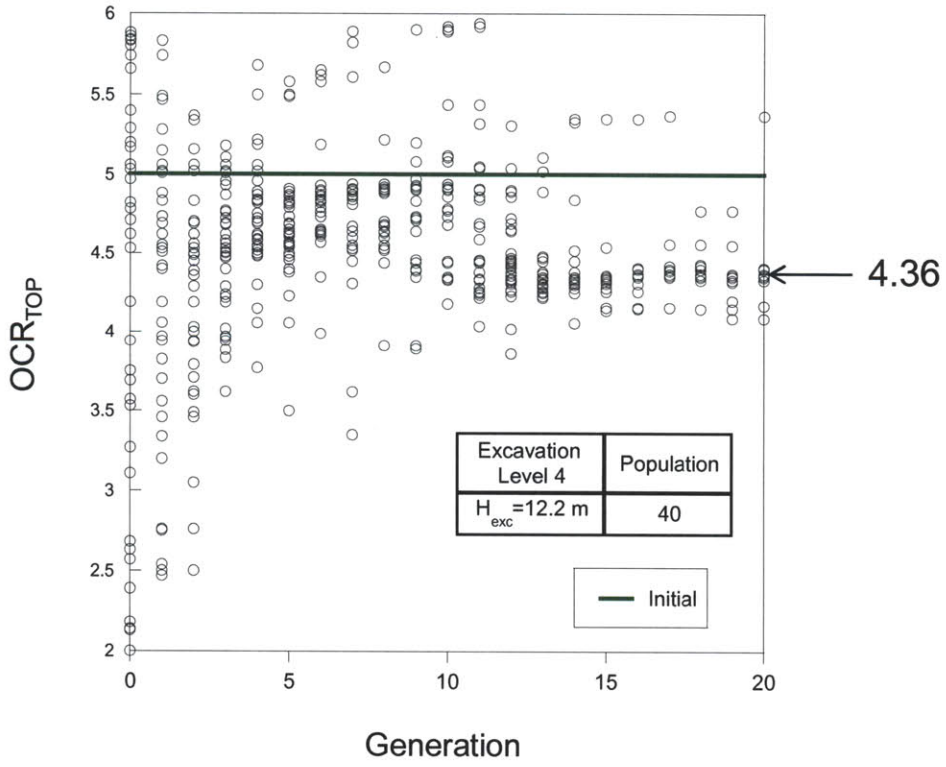

Figure 5-30: Convergence of OCR_{TOP} of the U-BBC layer obtained by genetic algorithms at excavation level 4

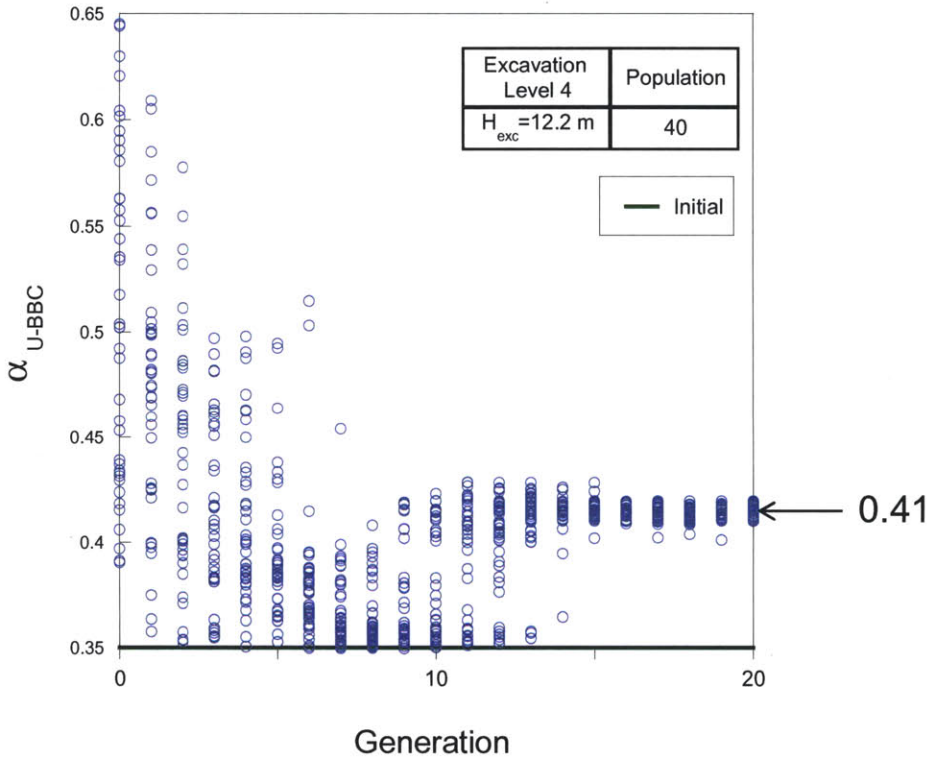

Figure 5-31: Convergence of α parameter of the U-BBC layer obtained by genetic algorithms at excavation level 4

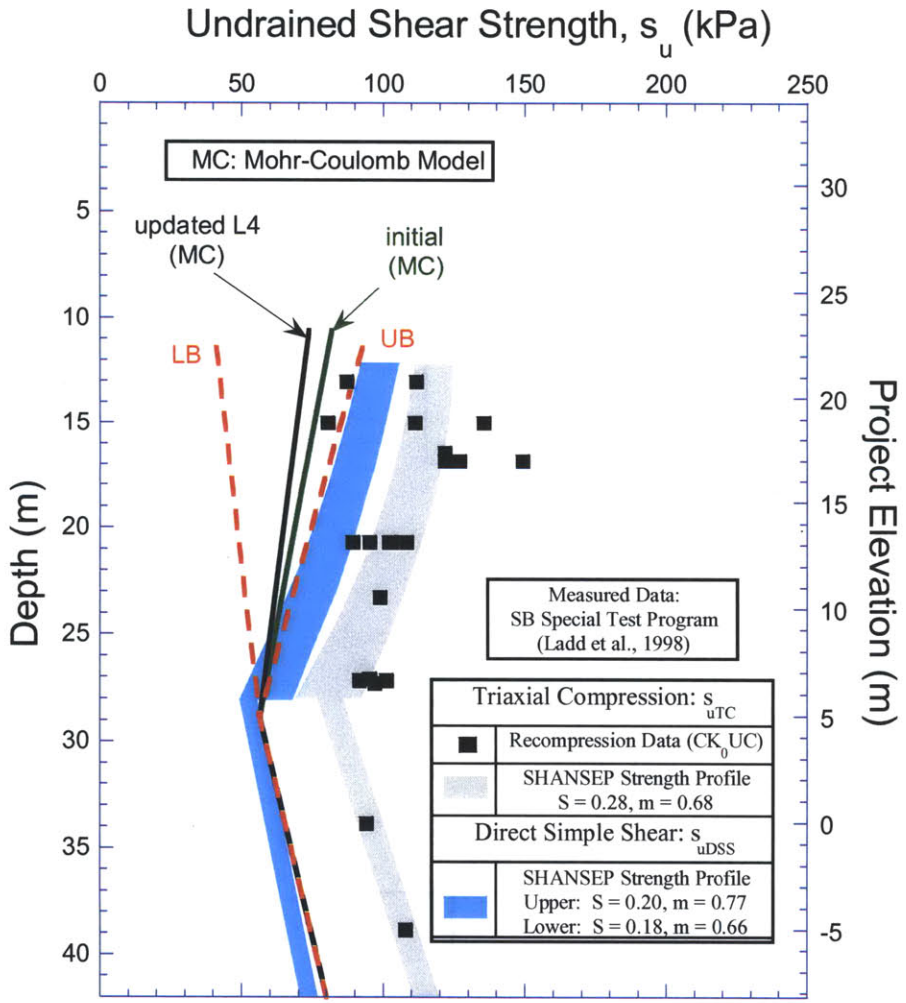

Figure 5-32: Updated Exc. L4 vs. Initial MC s_u profiles (showing lower and upper bounds) and SHANSEP strength profiles

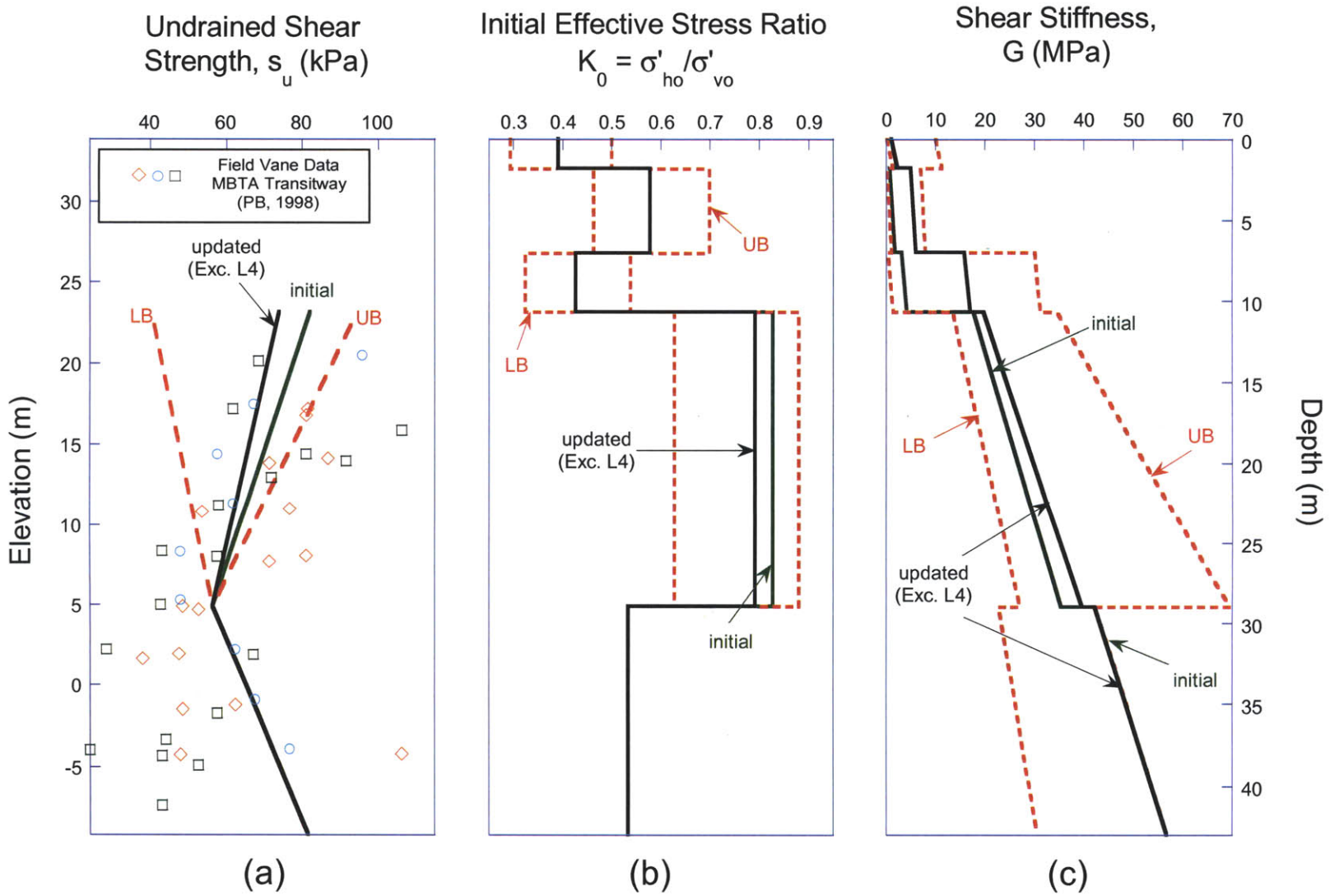

Figure 5-33: Updated Exc. L4 versus Initial profiles of undrained shear strengths (compared with field vane data), effective stress ratios, and shear stiffnesses

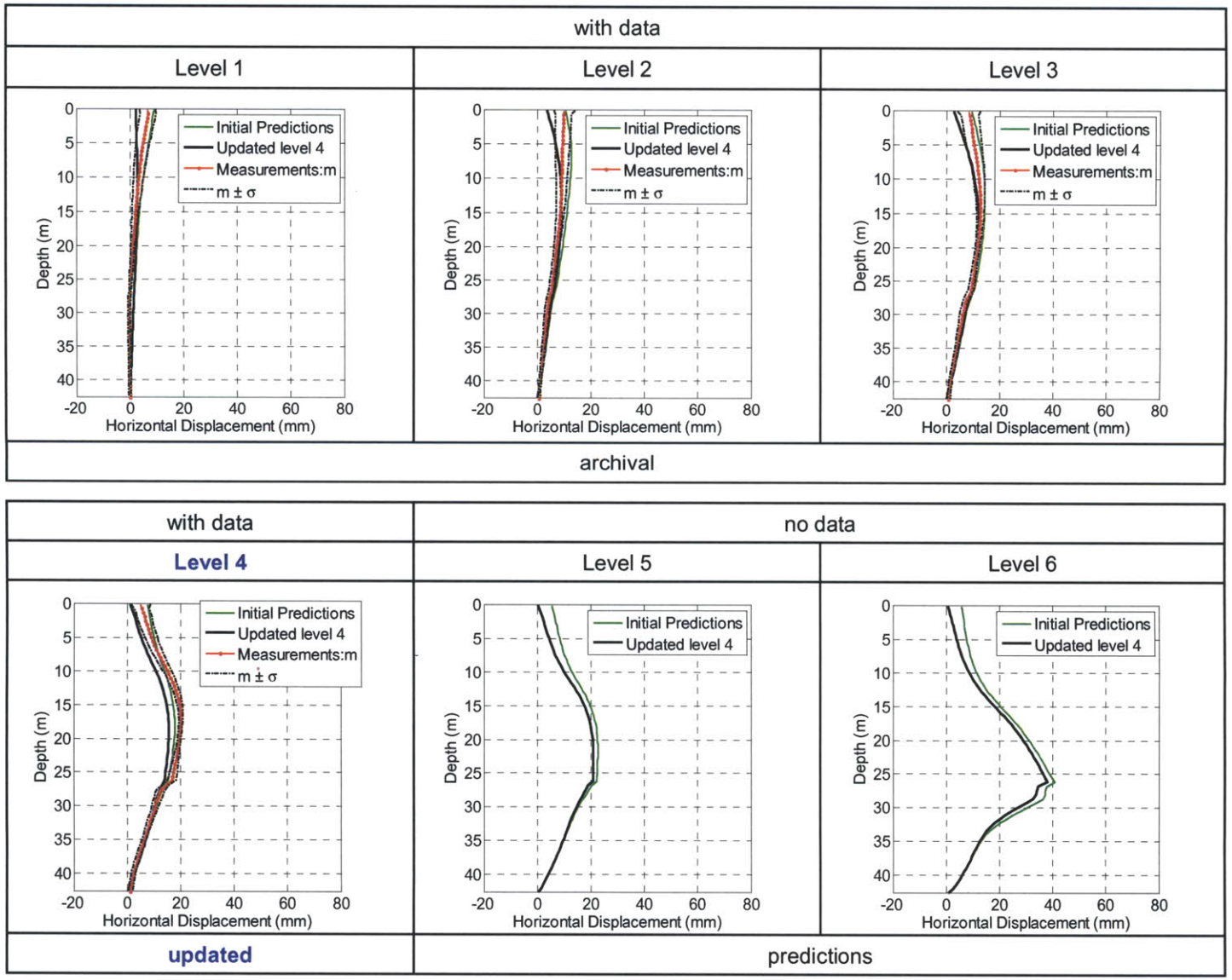

Figure 5-34: Comparison of measurements, initial predictions, and updated level 4 of lateral wall/soil movements

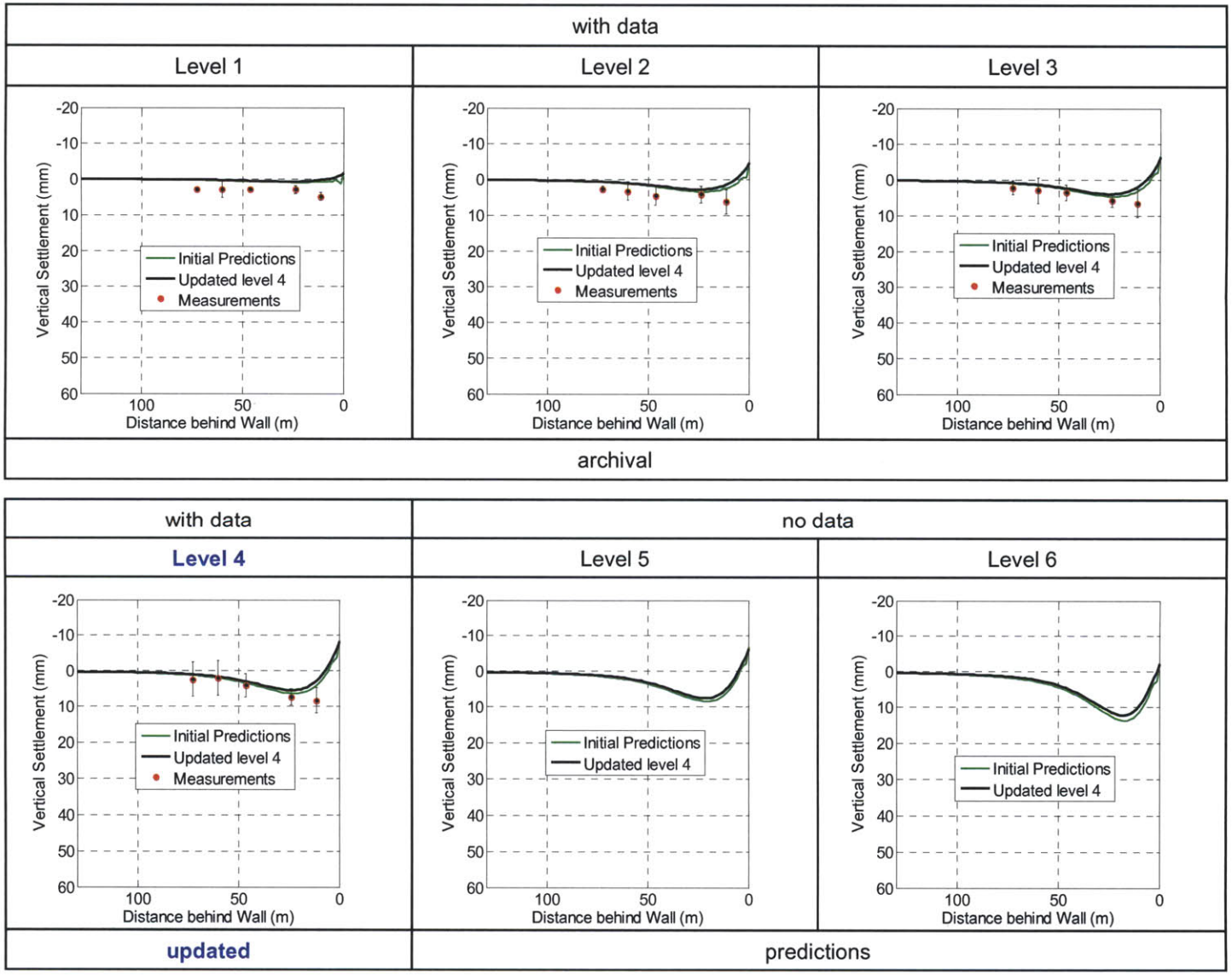

Figure 5-35: Comparison of measurements, initial predictions, and updated level 4 of surface settlements

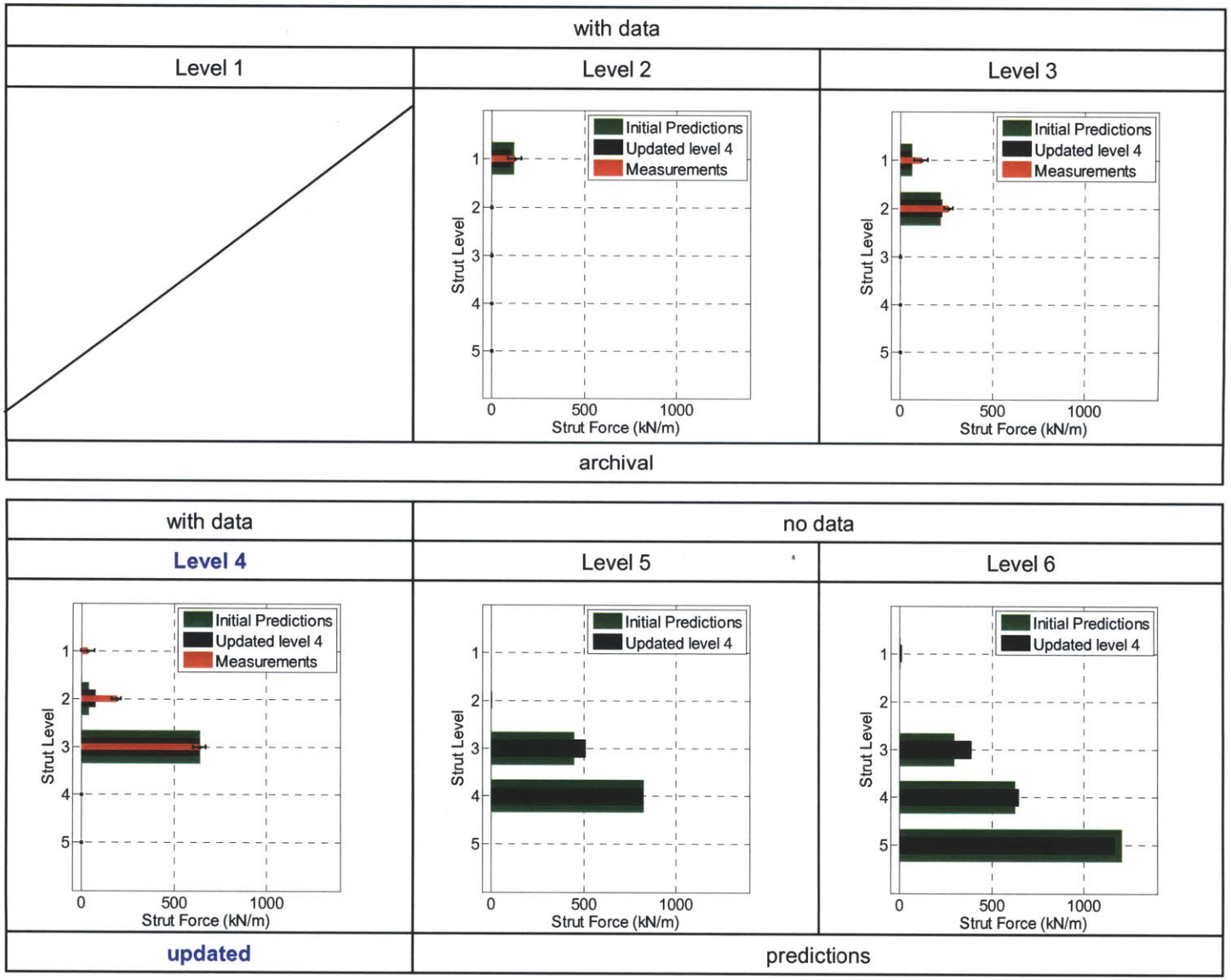

Figure 5-36: Comparison of measurements, initial predictions, and updated level 4 of strut forces

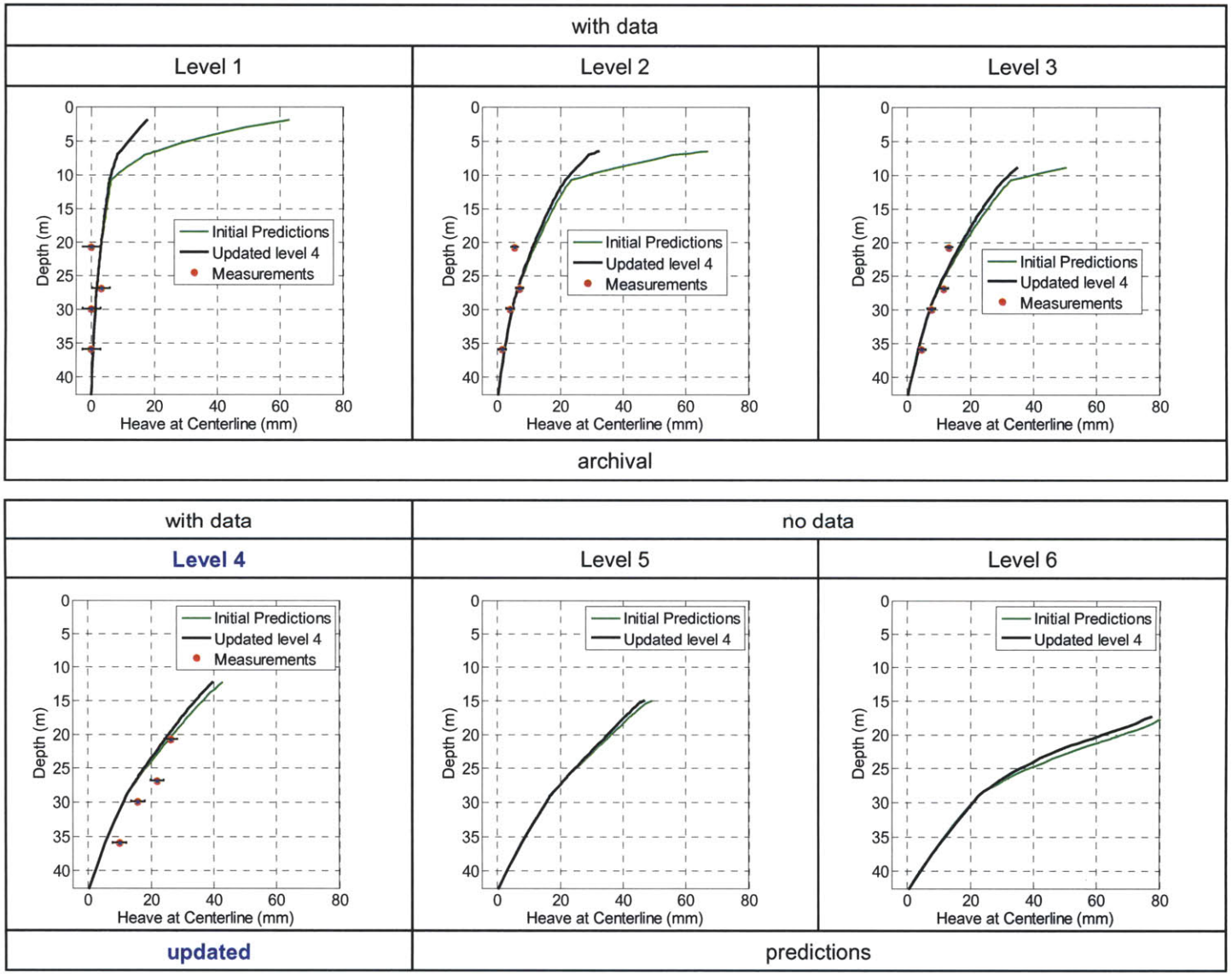

Figure 5-37: Comparison of measurements, initial predictions, and updated level 4 of excavation heave

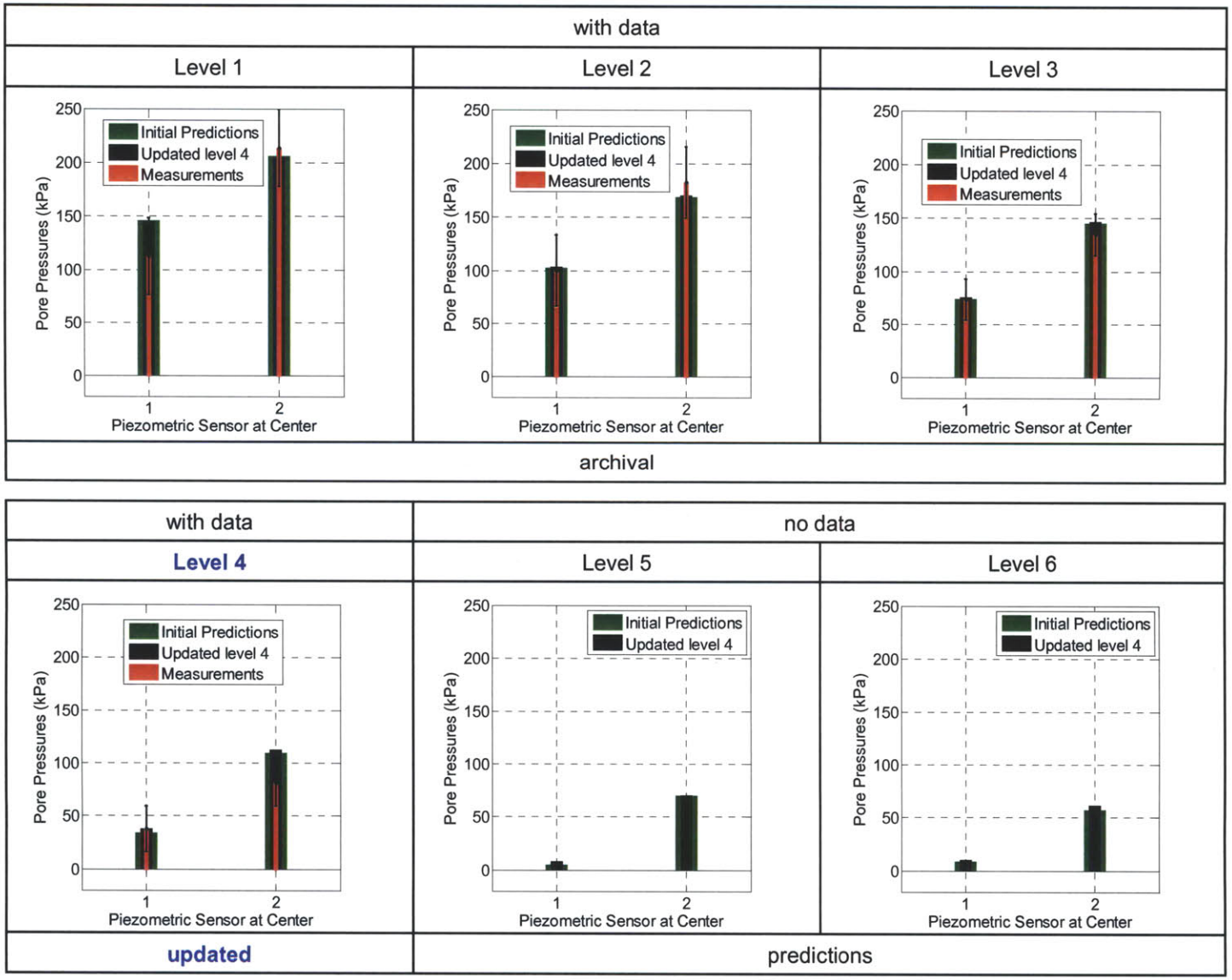

Figure 5-38: Comparison of measurements, initial predictions, and updated level 4 of pore water pressures

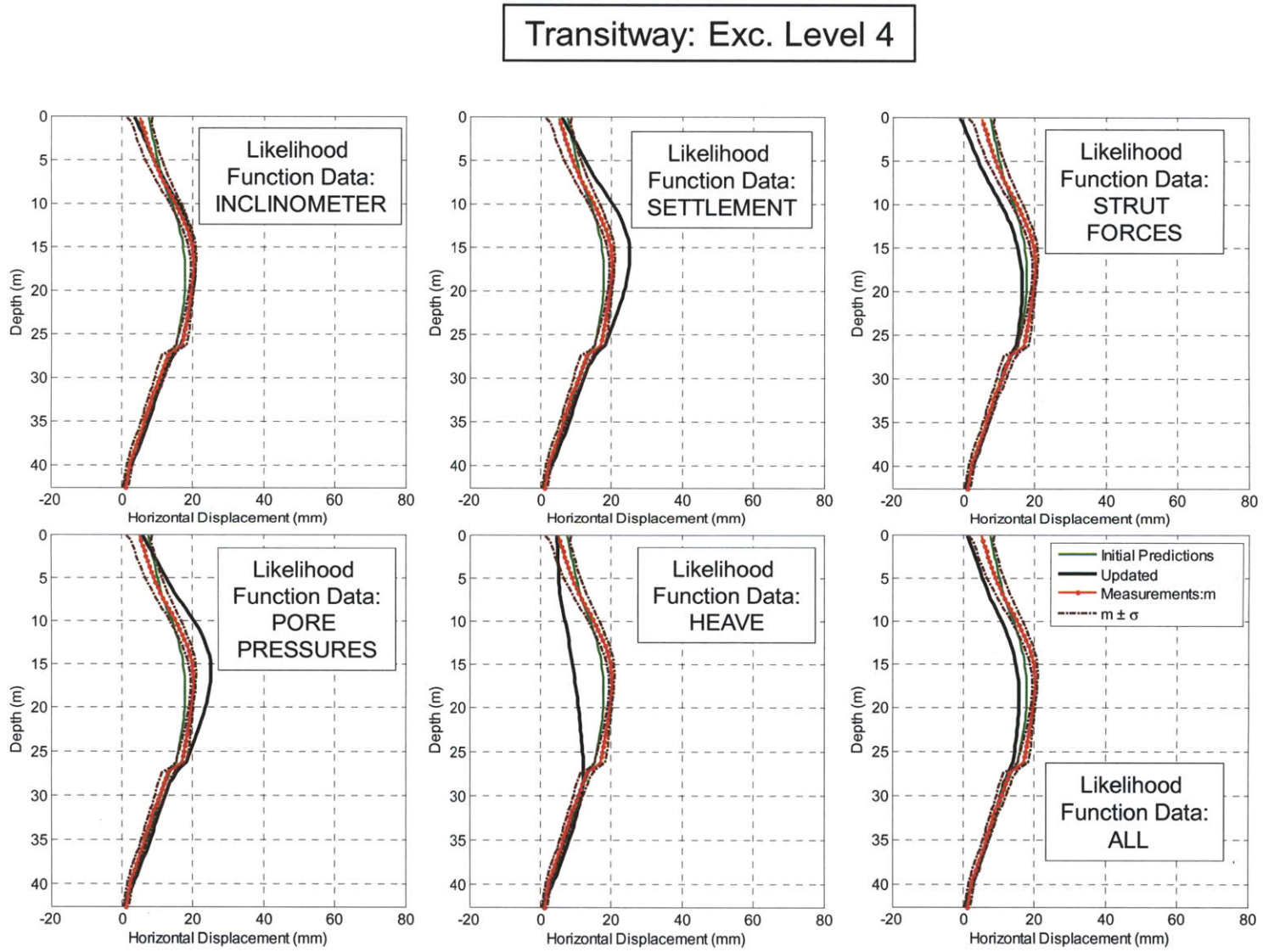

Figure 5-39: Comparison of lateral wall/soil movement predictions when using different types of measurements at exc. level 4

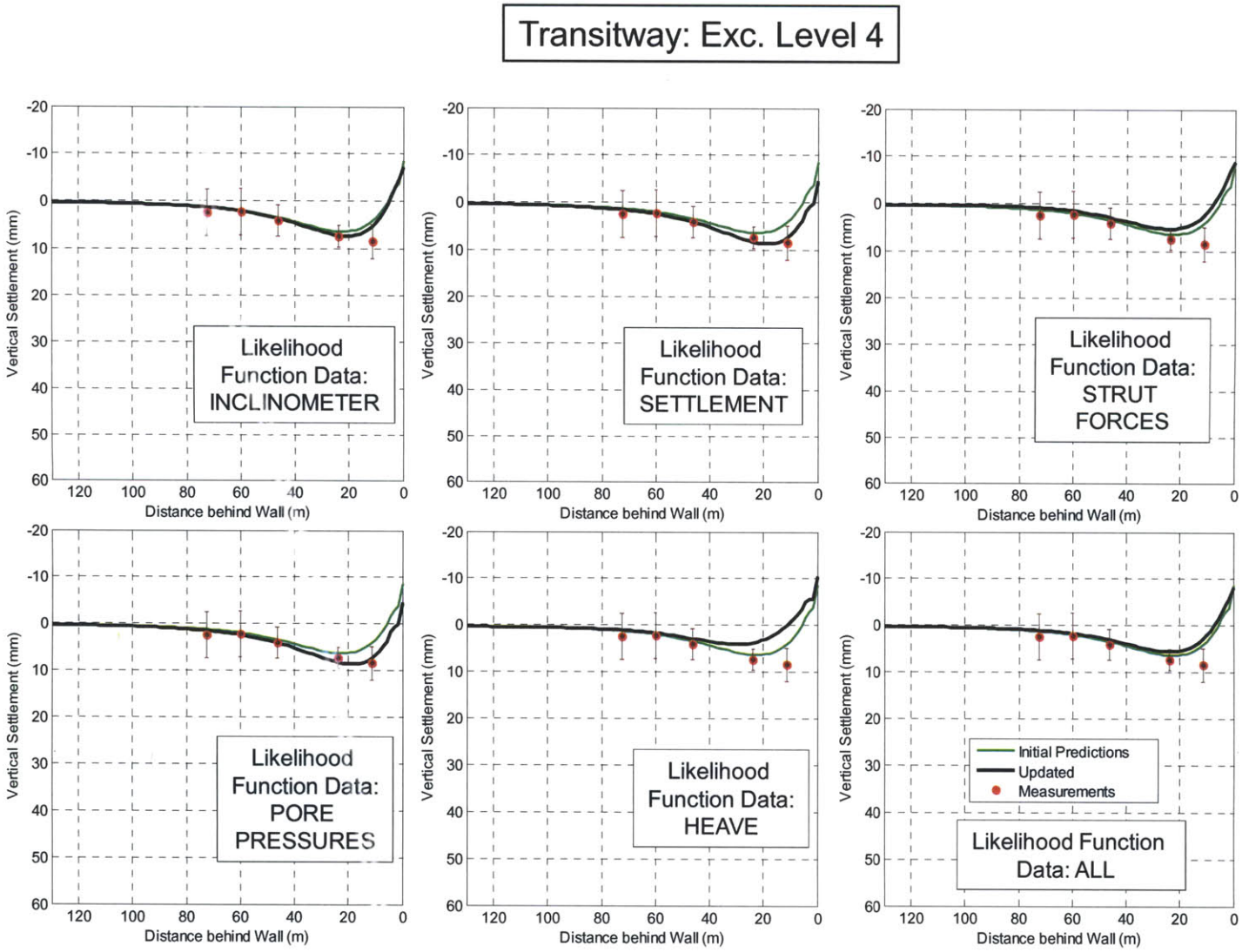

Figure 5-40: Comparison of surface settlement predictions when using different types of measurements at exc. level 4

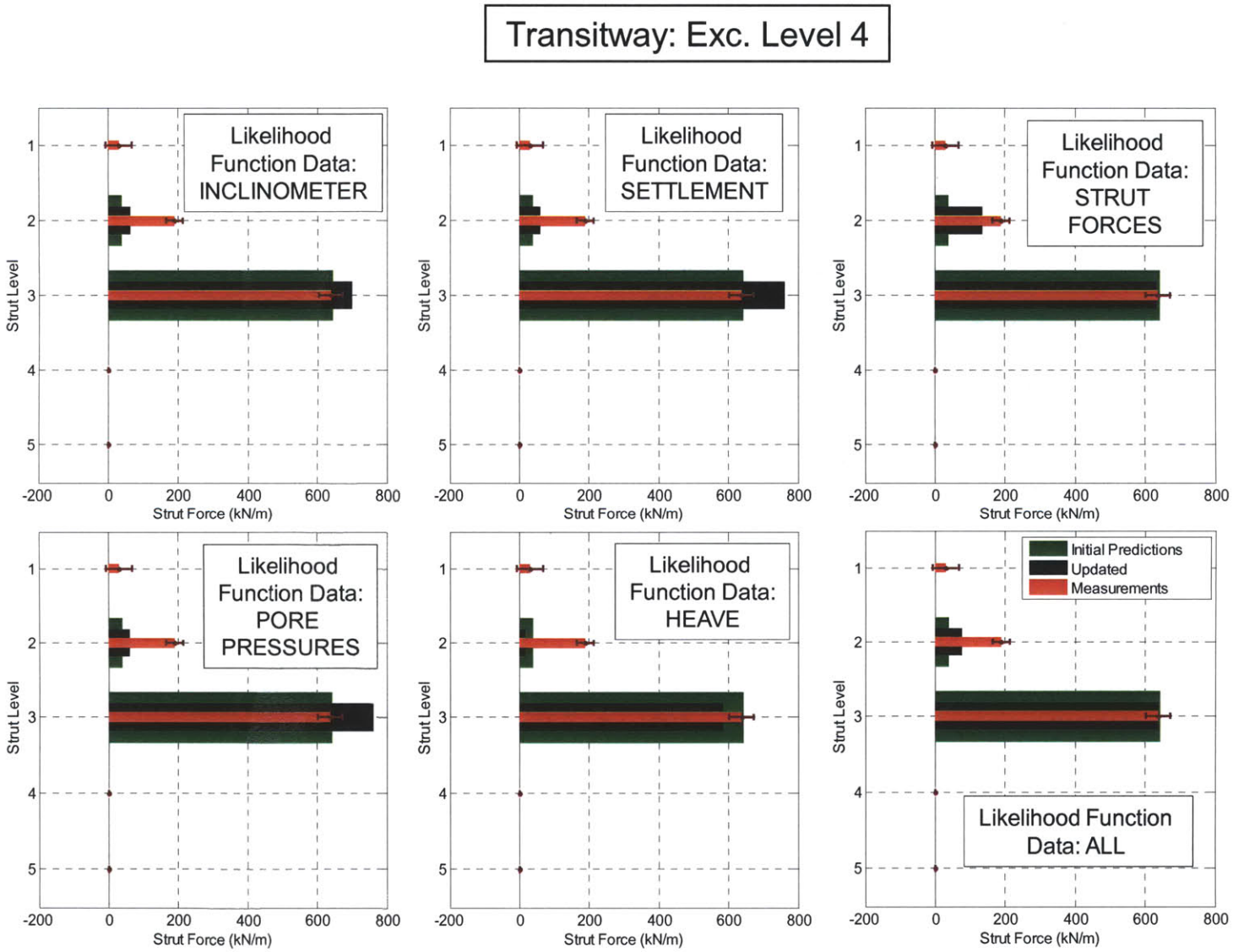

Figure 5-41: Comparison of strut forces predictions when using different types of measurements at exc. level 4

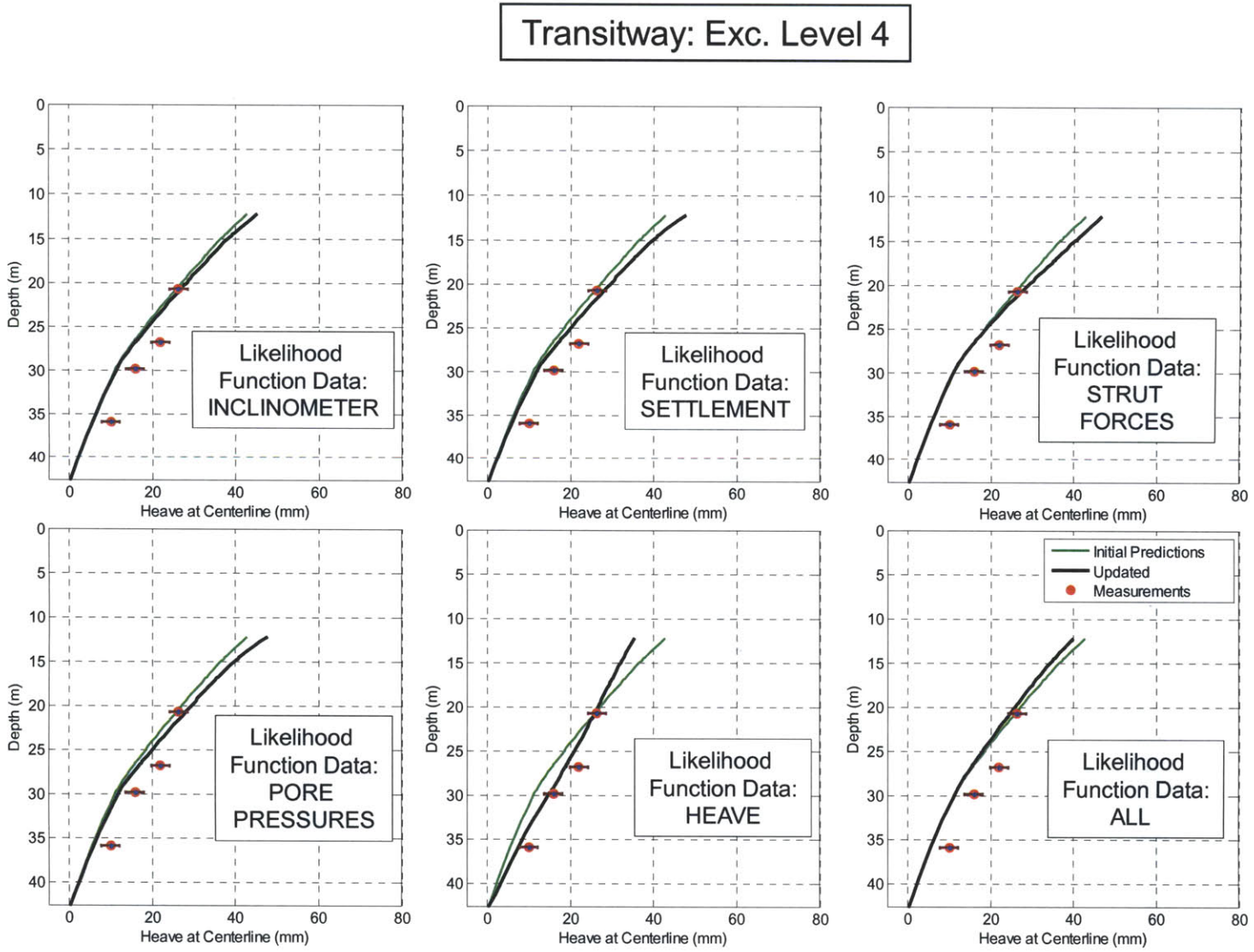

Figure 5-42: Comparison of excavation heave predictions when using different types of measurements at exc. level 4

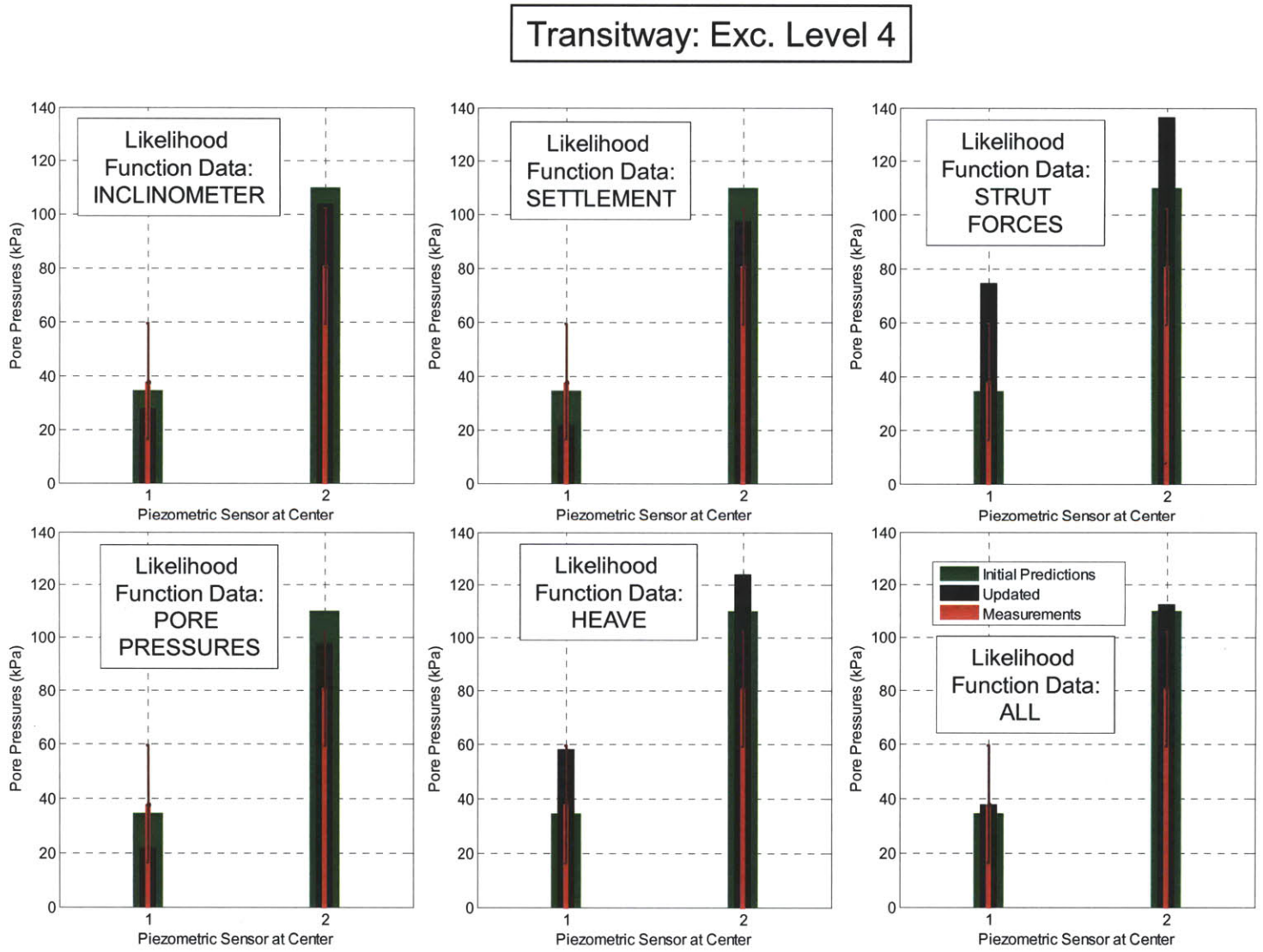

Figure 5-43: Comparison of centerline pore water pressures when using different types of measurements at exc. level 4

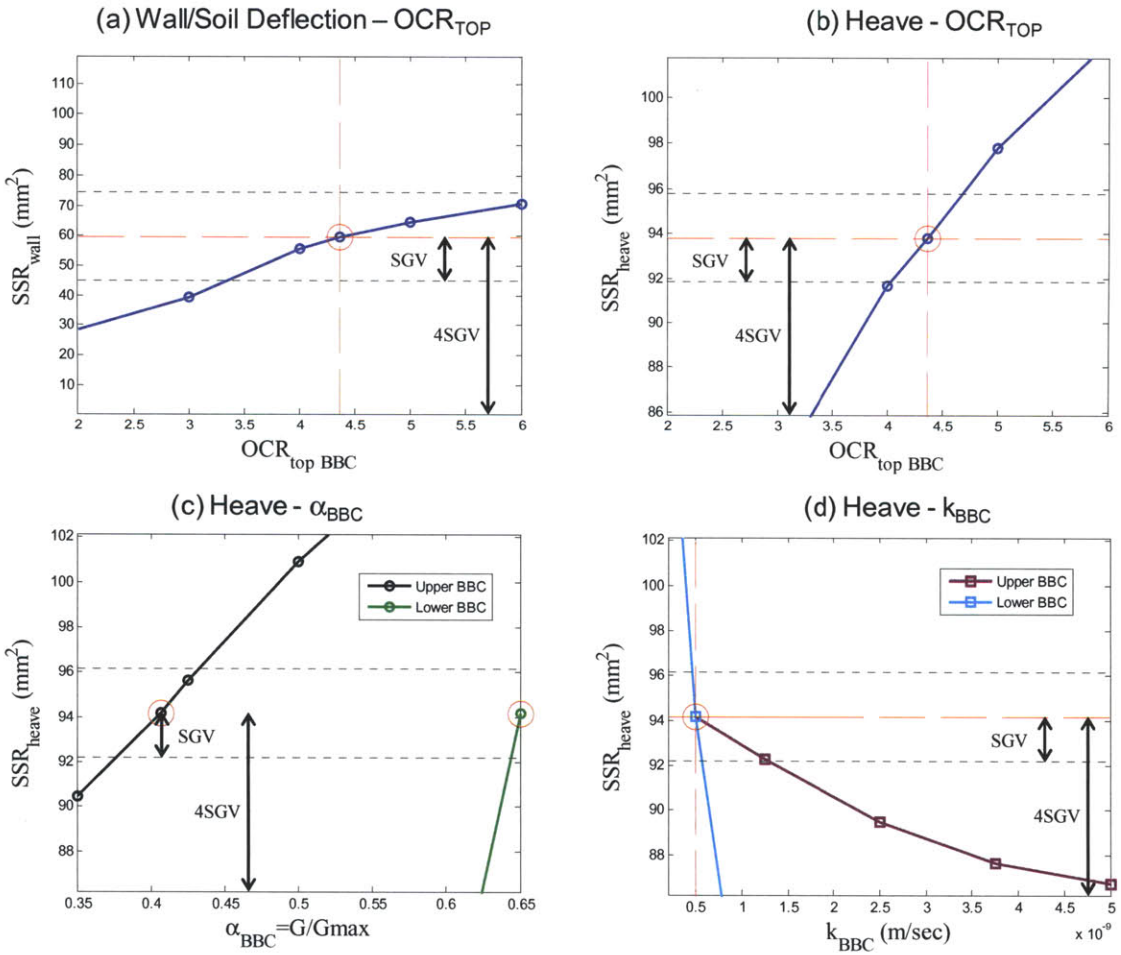

Figure 5-44: Sensitivity analyses of essential improvement parameters (EIP) at excavation level 5

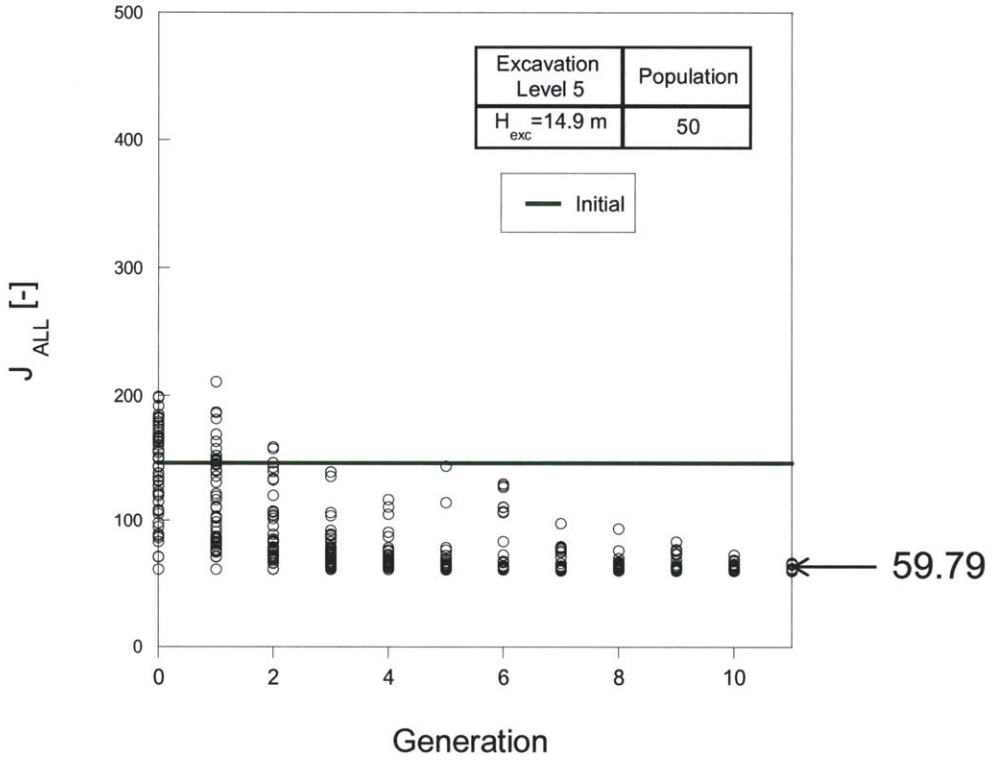

Figure 5-45: Convergence of objective function for all measurements obtained by genetic algorithms at excavation level 5

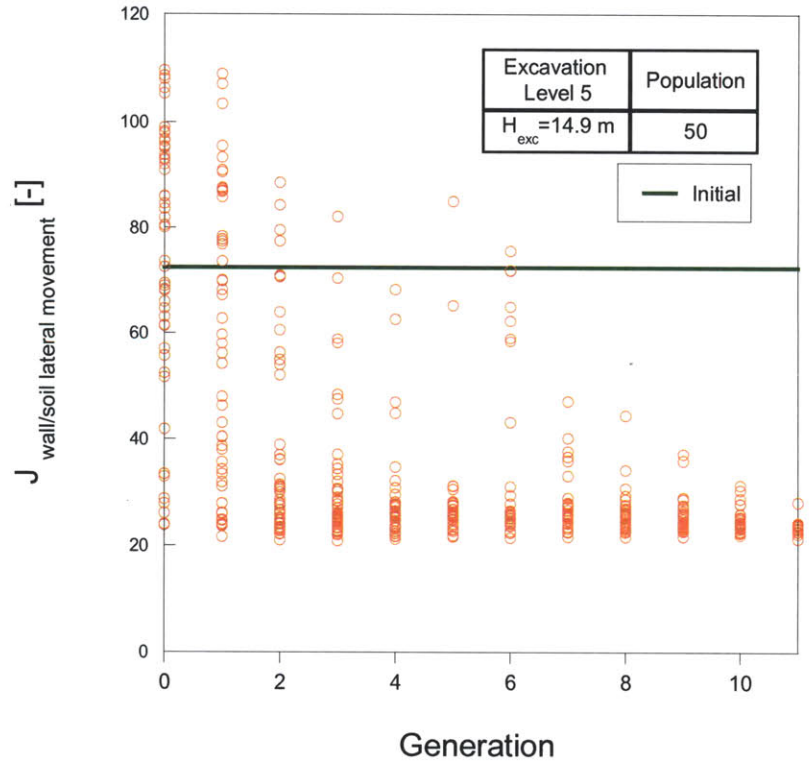

Figure 5-46: Convergence of objective function for lateral wall/soil movements obtained by genetic algorithms at excavation level 5

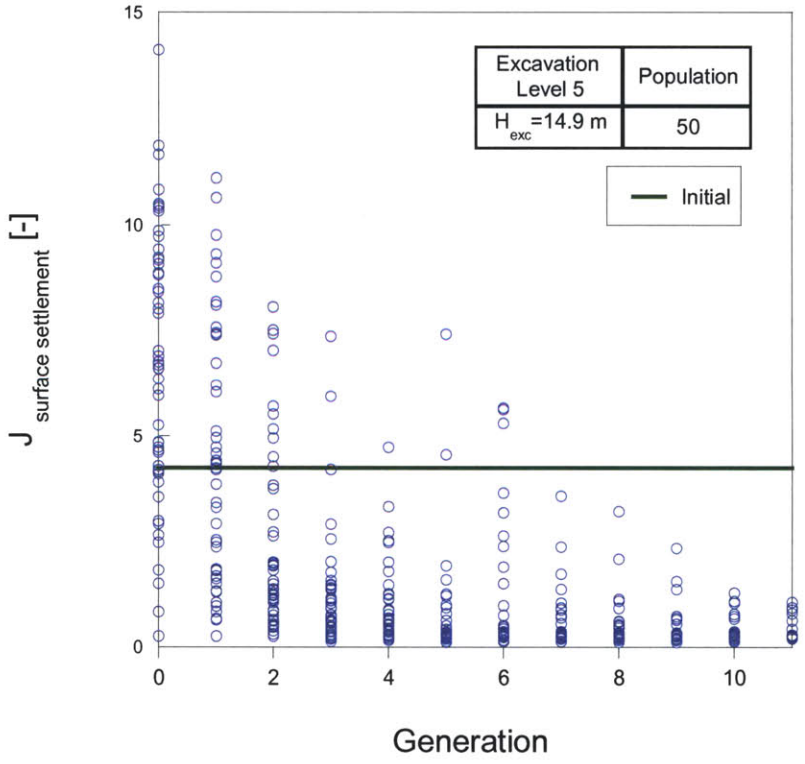

Figure 5-47: Convergence of objective function for surface settlements obtained by genetic algorithms at excavation level 5

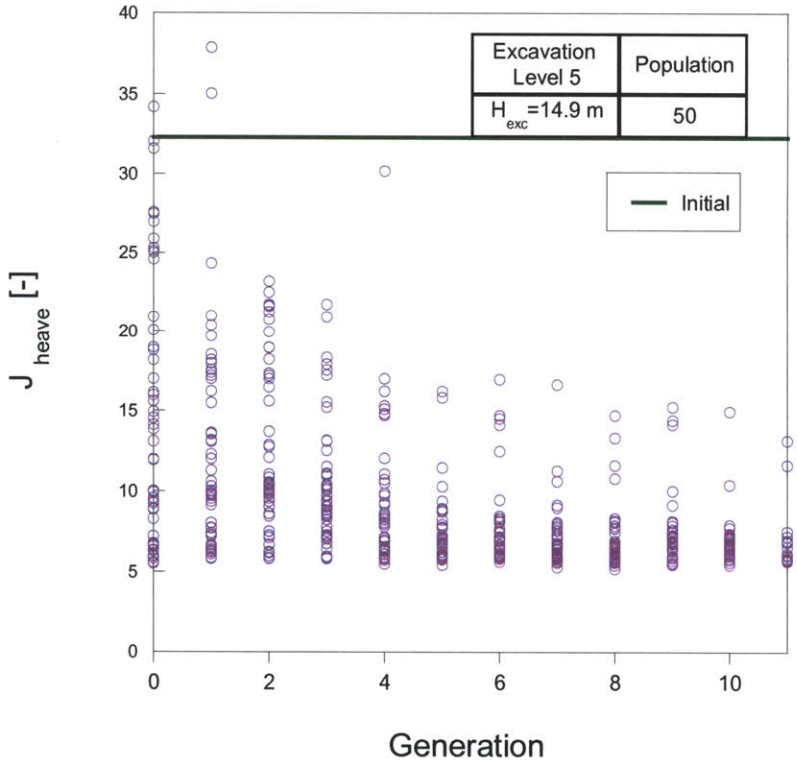

Figure 5-48: Convergence of objective function for excavation heave obtained by genetic algorithms at excavation level 5

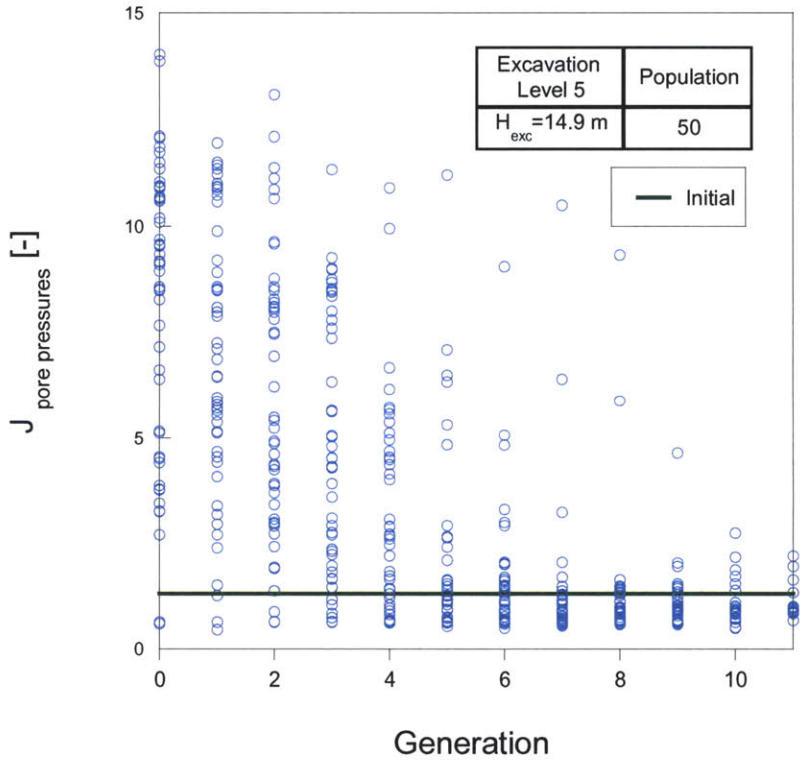

Figure 5-49: Convergence of objective function for pore water pressures obtained by genetic algorithms at excavation level 5

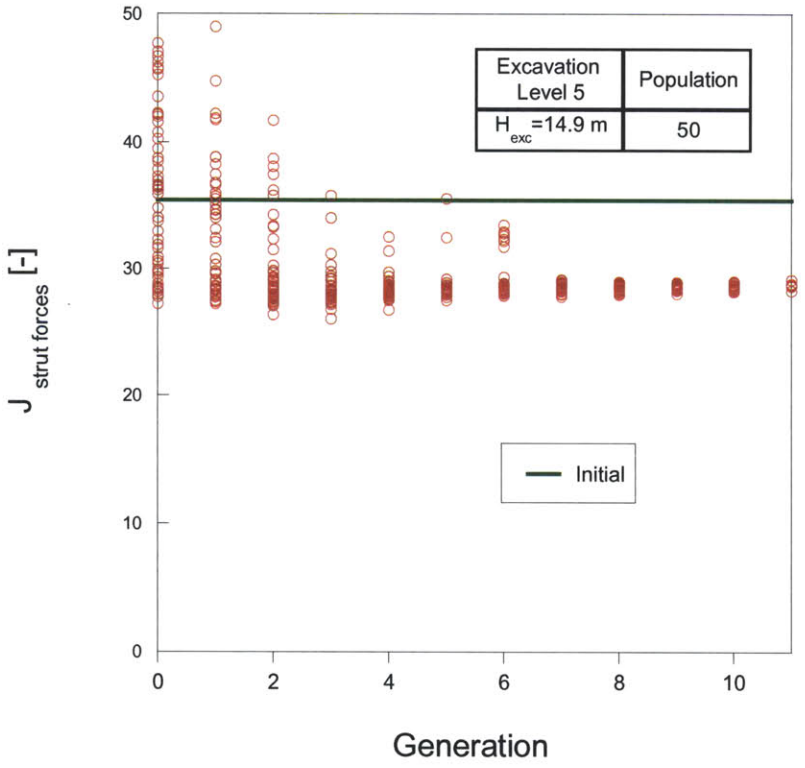

Figure 5-50: Convergence of objective function for strut forces obtained by genetic algorithms at excavation level 5

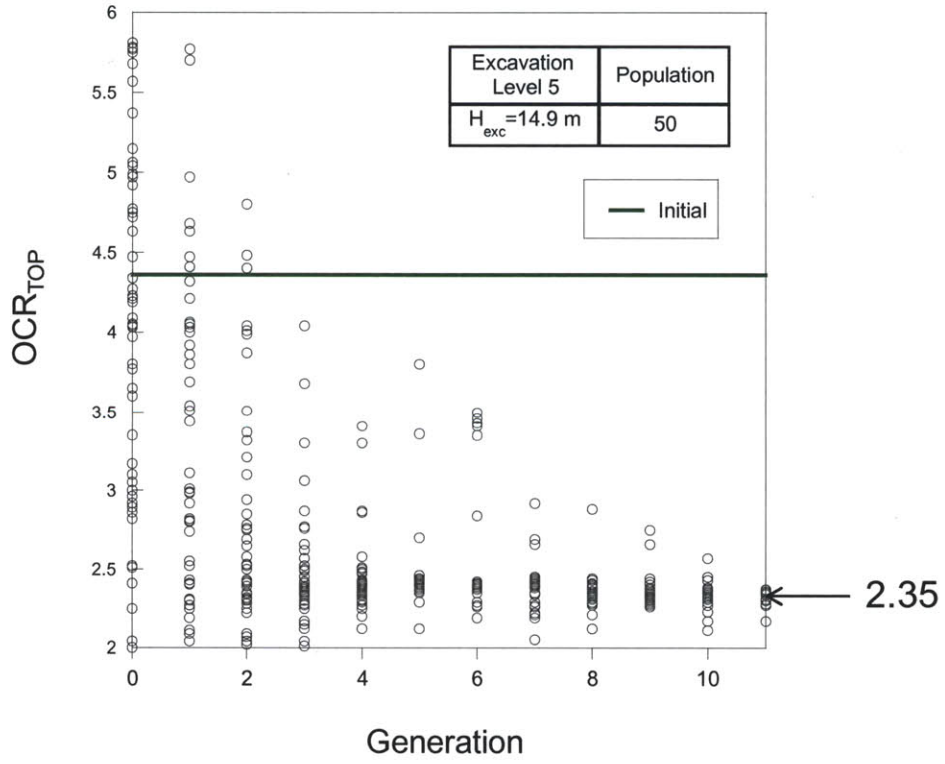

Figure 5-51: Convergence of OCR_{TOP} of the U-BBC layer obtained by genetic algorithms at excavation level 5

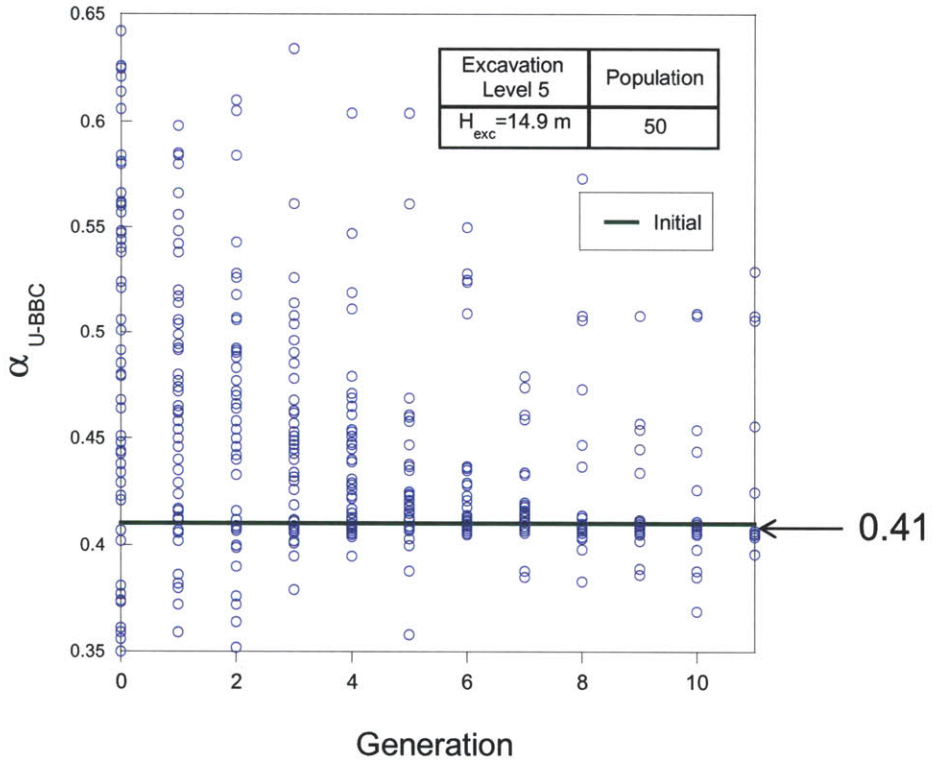

Figure 5-52: Convergence of α parameter of the U-BBC layer obtained by genetic algorithms at excavation level 5

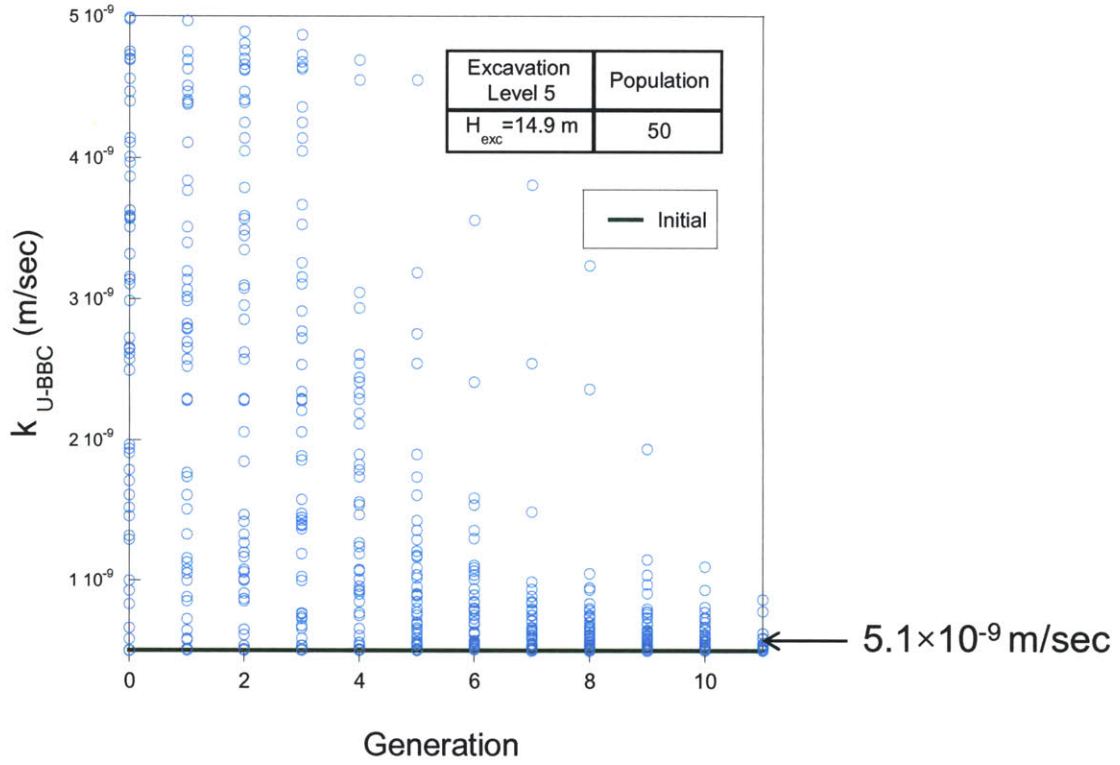

Figure 5-53: Convergence of hydraulic conductivity of the U-BBC layer obtained by genetic algorithms at excavation level 5

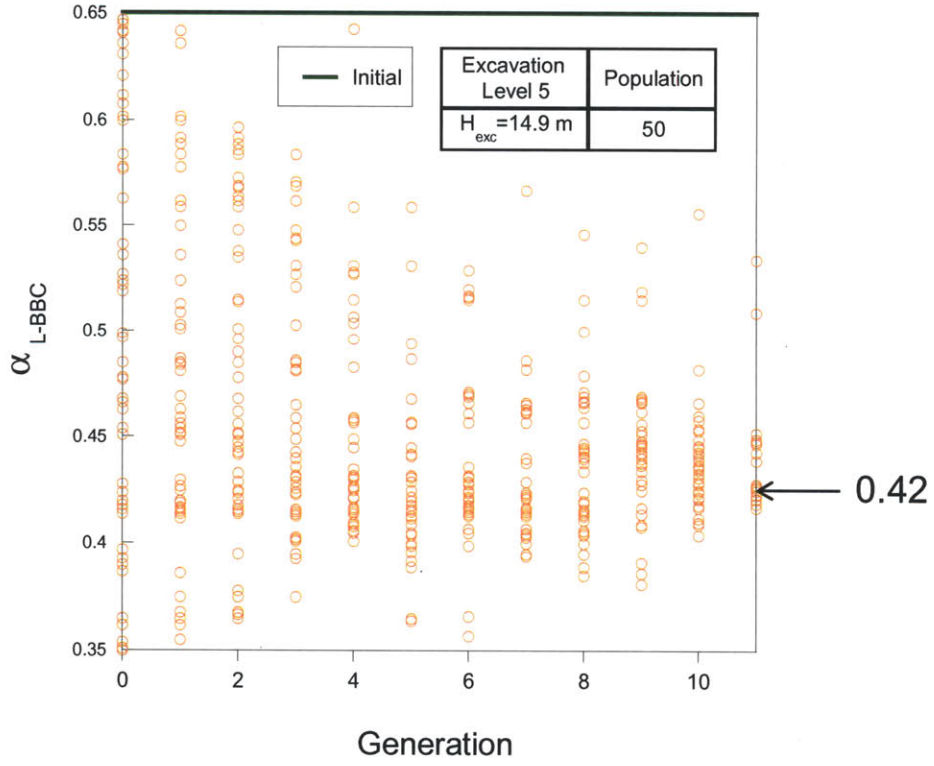

Figure 5-54: Convergence of α parameter of the L-BBC layer obtained by genetic algorithms at excavation level 5

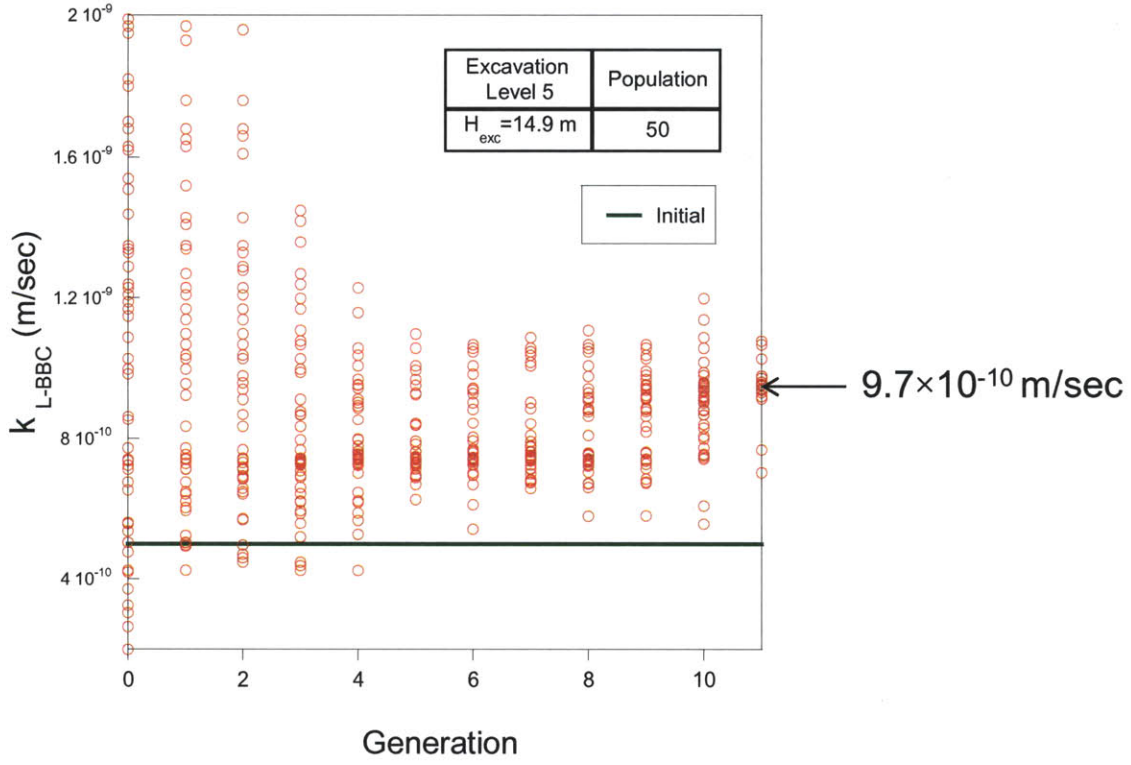

Figure 5-55: Convergence of hydraulic conductivity of the L-BBC layer obtained by genetic algorithms at excavation level 5

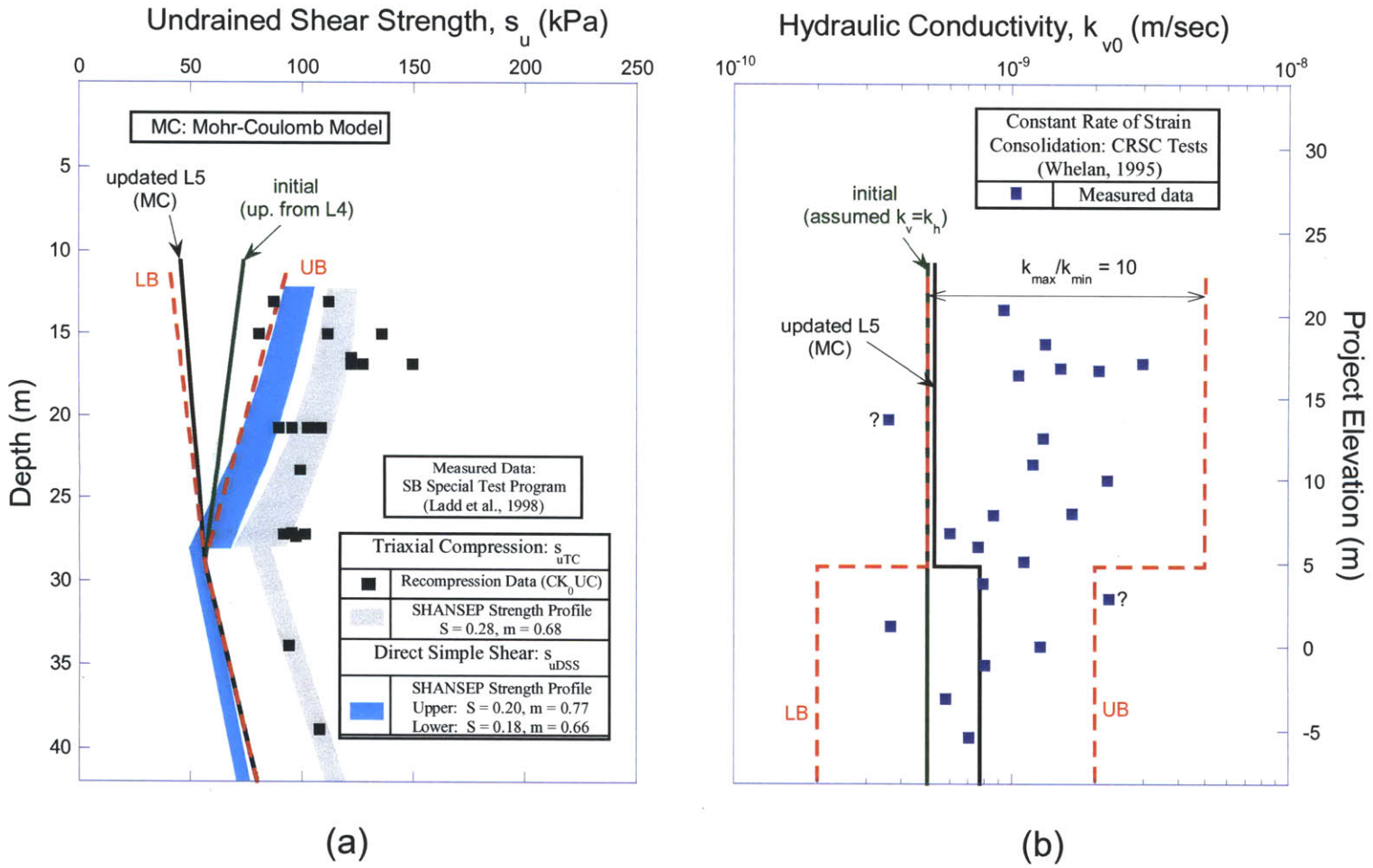

Figure 5-56: Updated Exc. L5 vs. Initial (updated from L4) MC undrained shear strength and hydraulic conductivity profiles (showing lower and upper bounds) and SHANSEP strength profiles

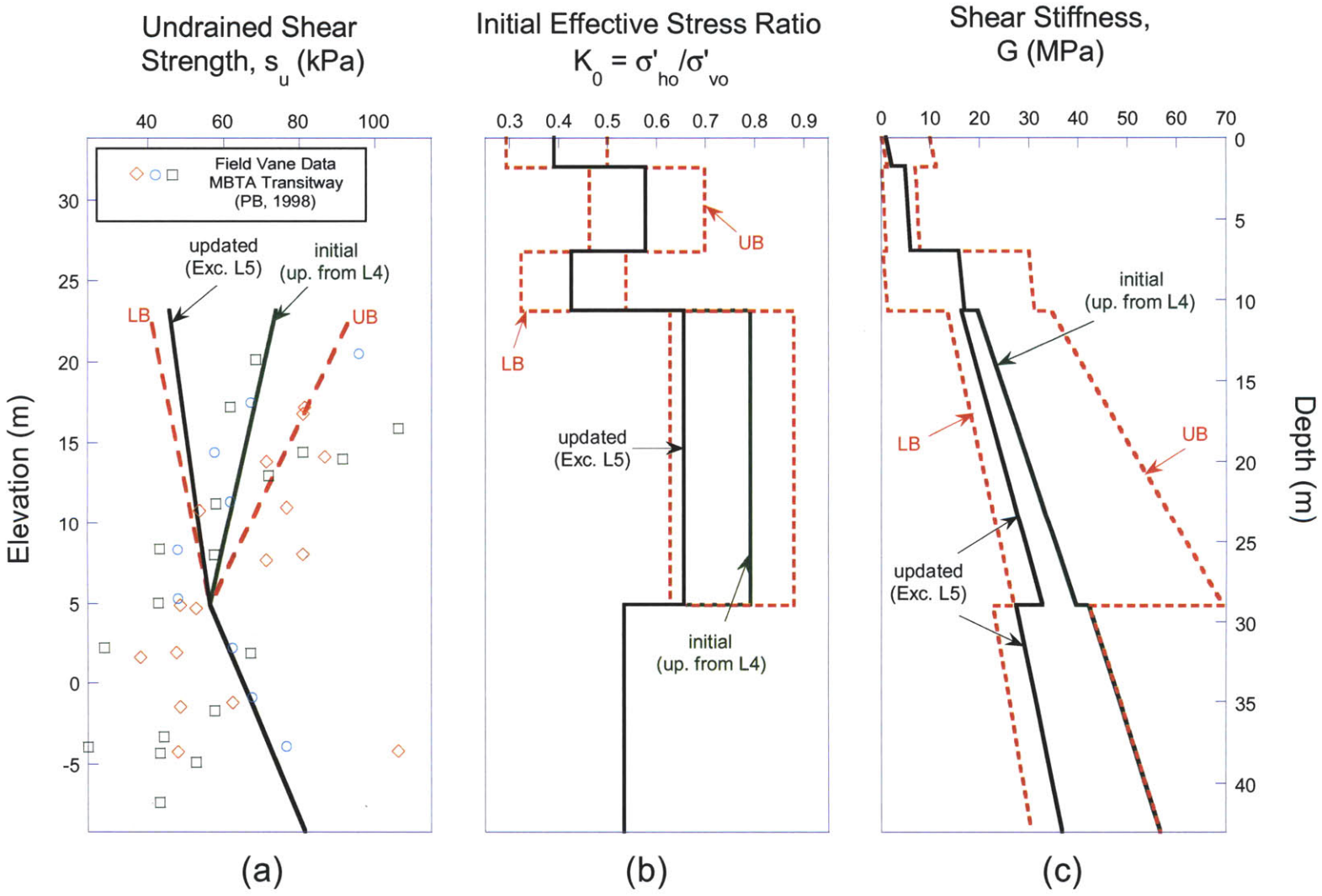

Figure 5-57: Updated Exc. L5 versus Initial (updated from L4) profiles of undrained shear strengths (compared with field vane data), effective stress ratios, and shear stiffnesses

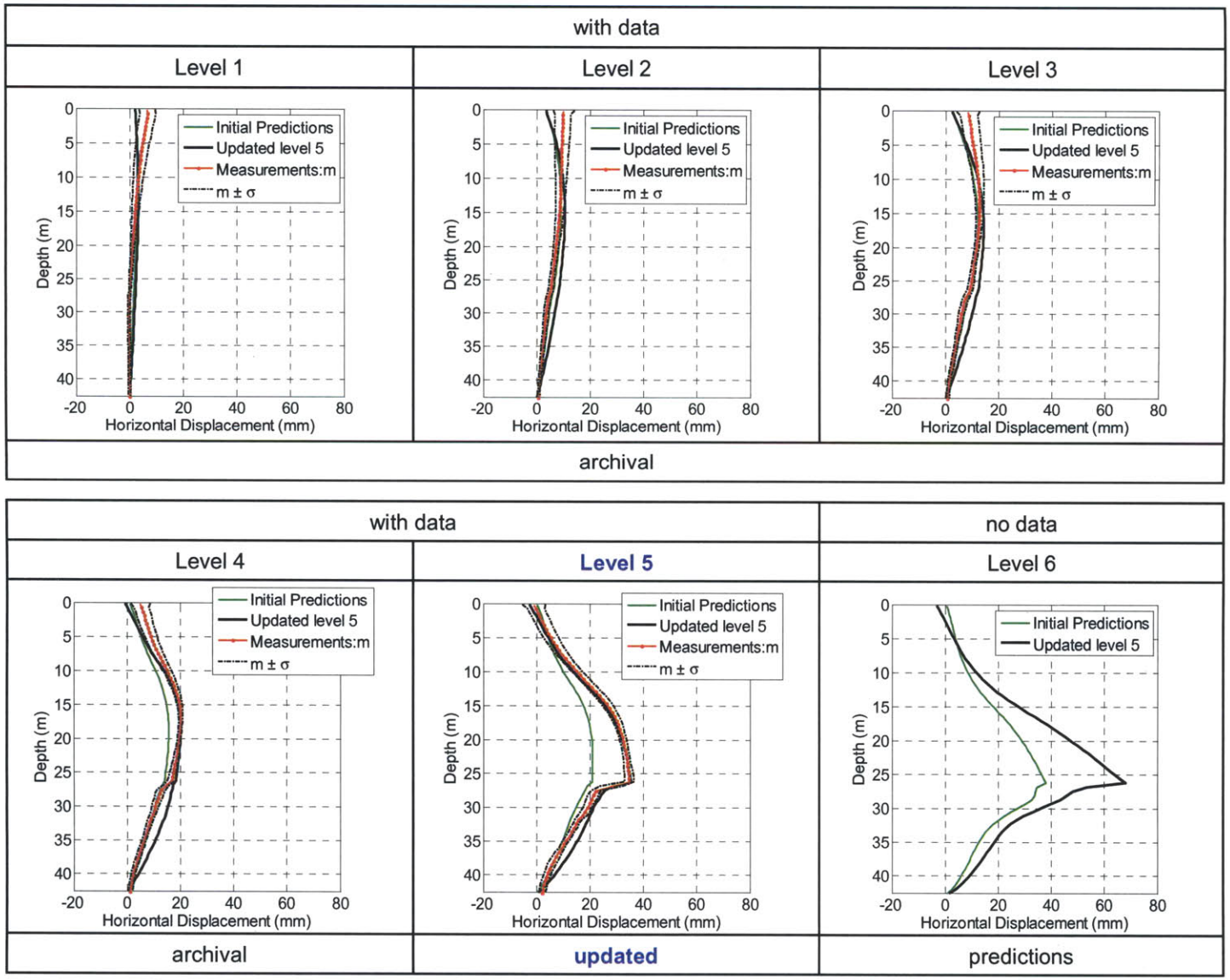

Figure 5-58: Comparison of measurements, initial predictions, and updated level 5 of lateral wall/soil movements

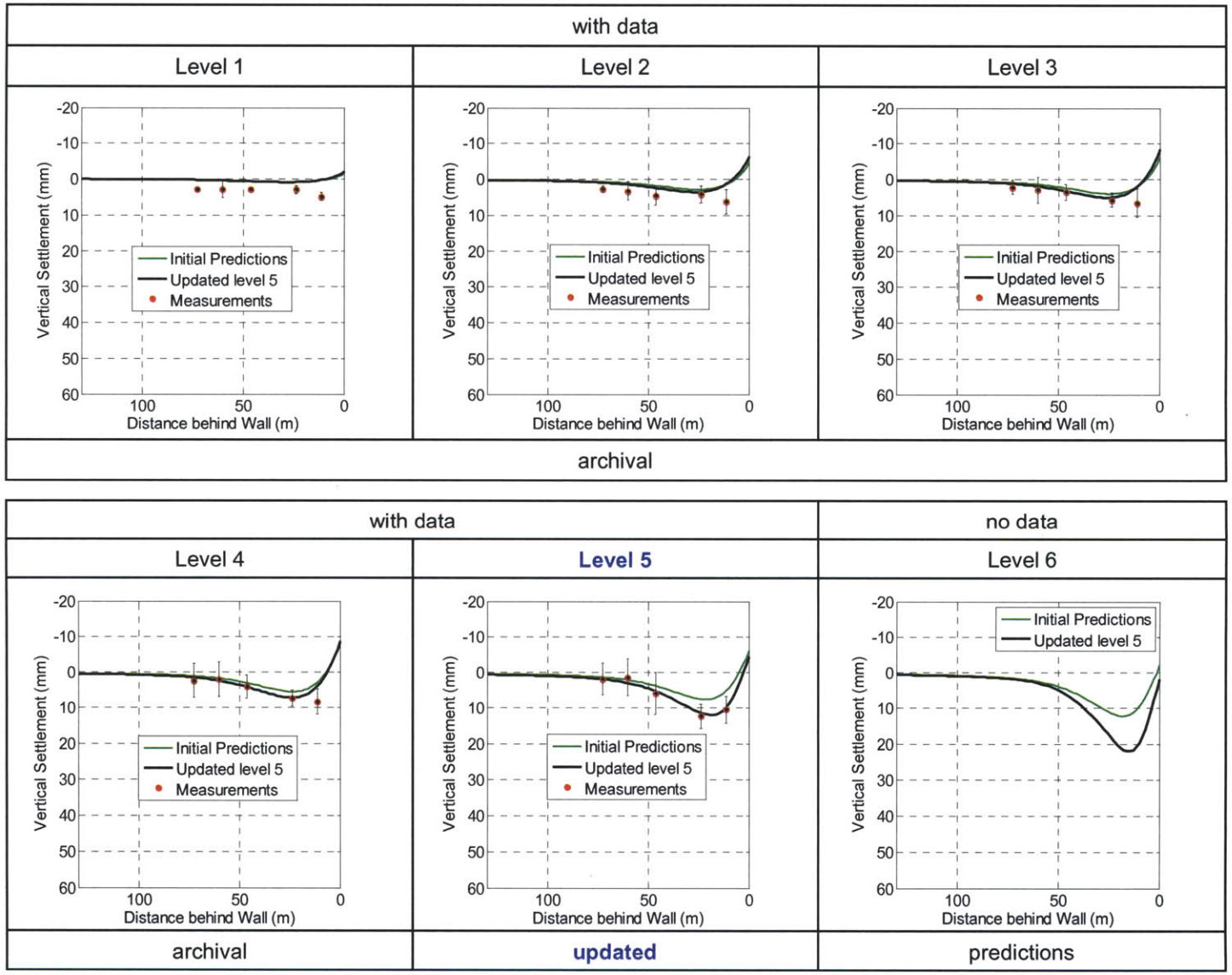

Figure 5-59: Comparison of measurements, initial predictions, and updated level 5 of surface settlements

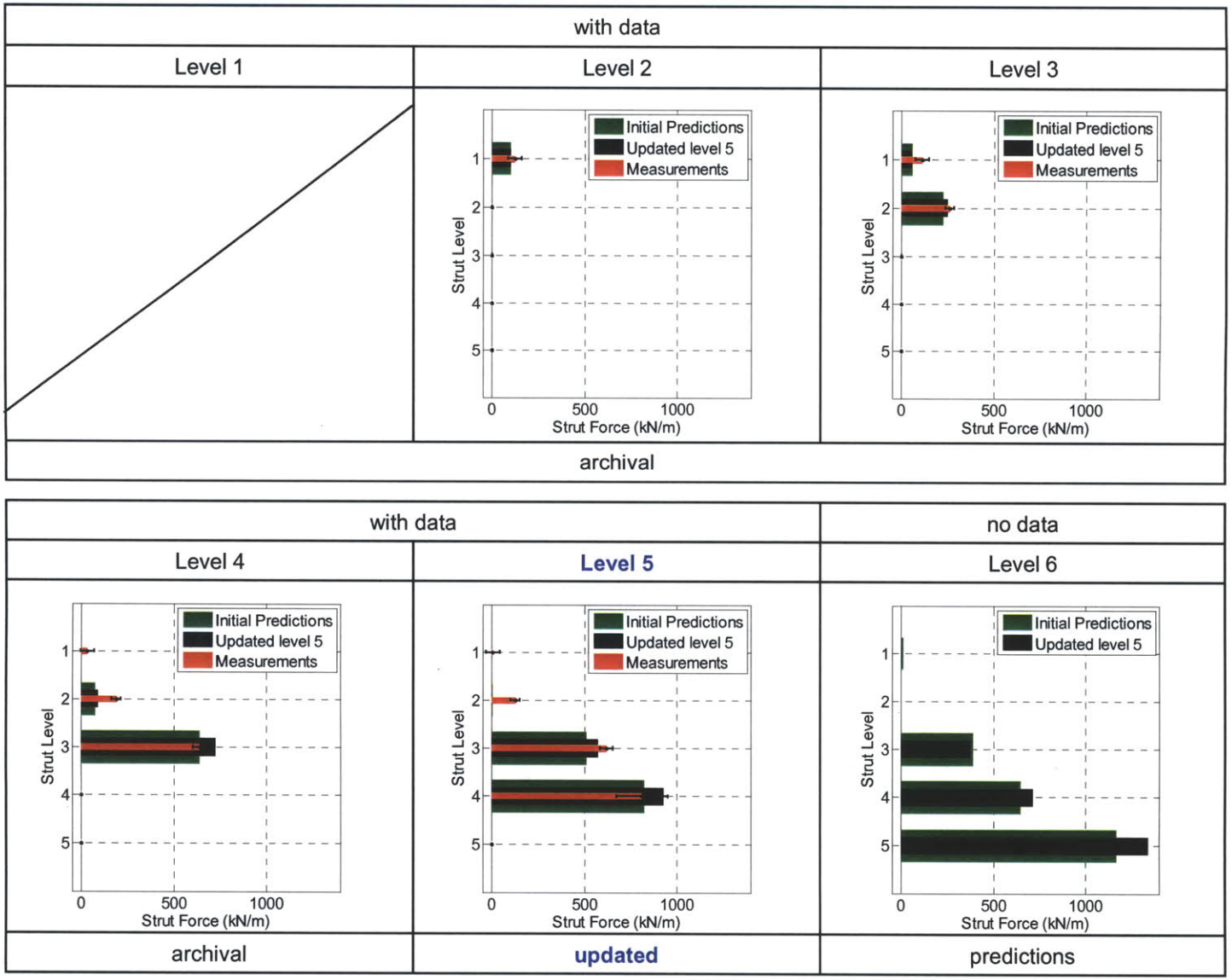

Figure 5-60: Comparison of measurements, initial predictions, and updated level 5 of strut forces

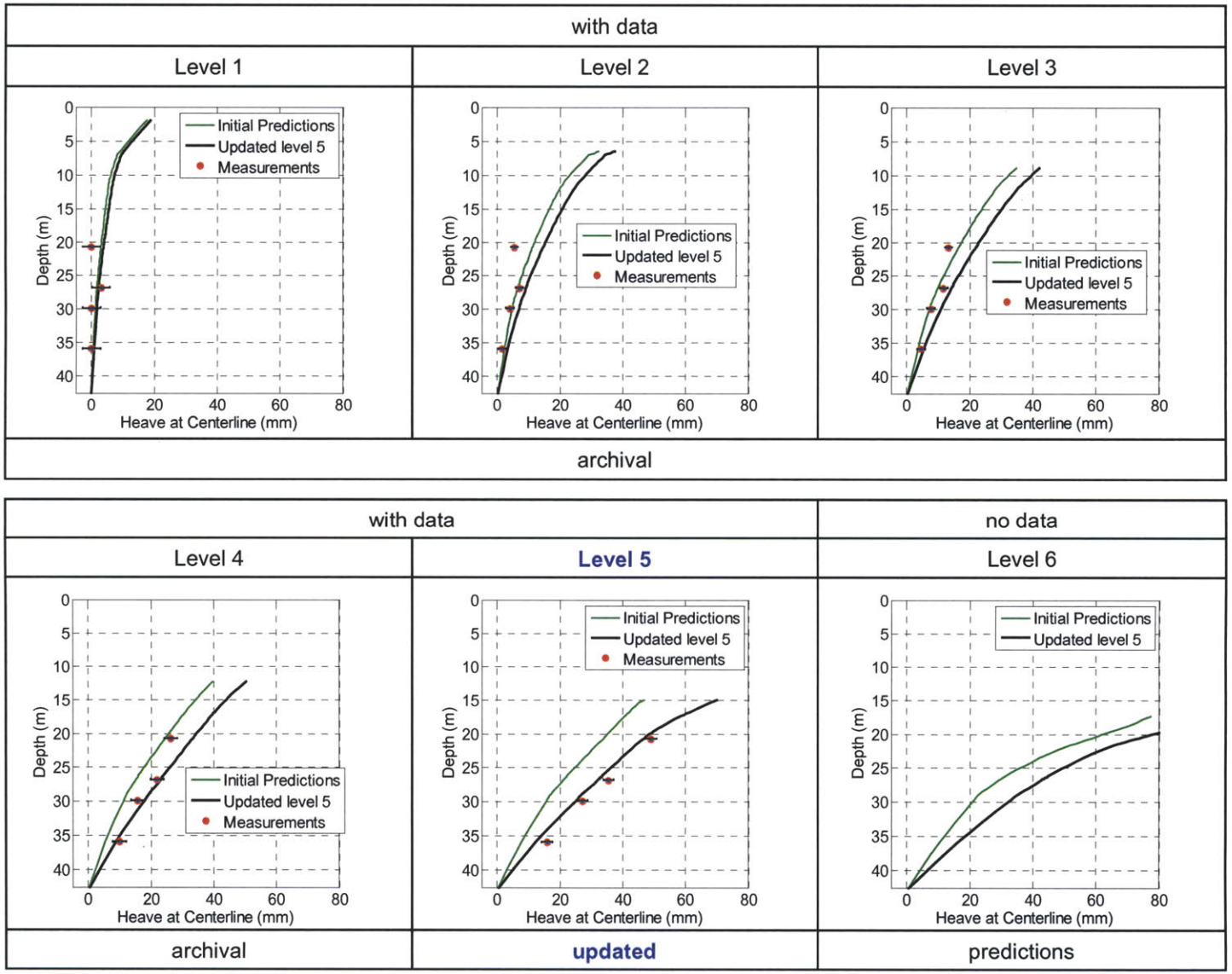

Figure 5-61: Comparison of measurements, initial predictions, and updated level 5 of excavation heave

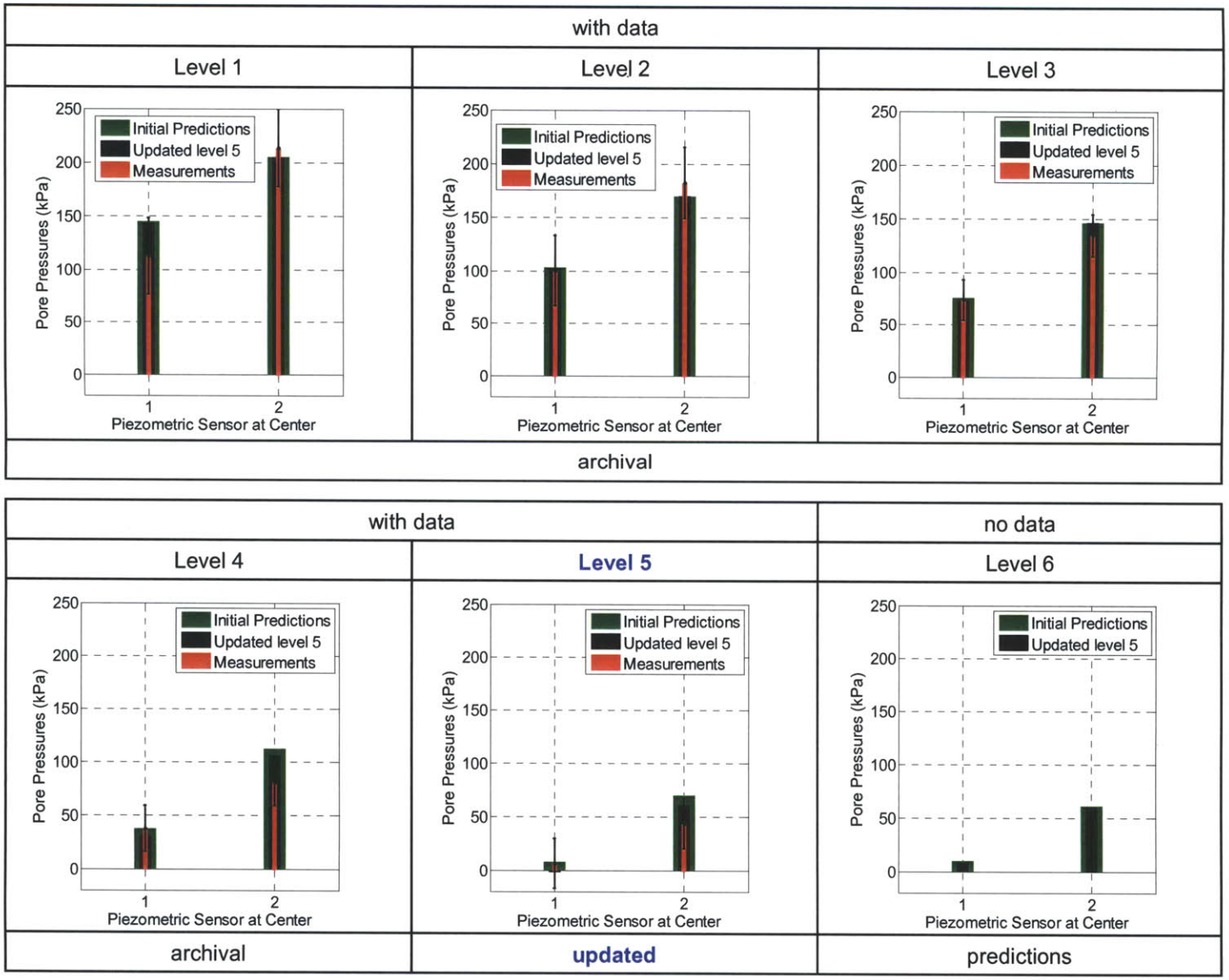

Figure 5-62: Comparison of measurements, initial predictions, and updated level 5 of pore water pressures

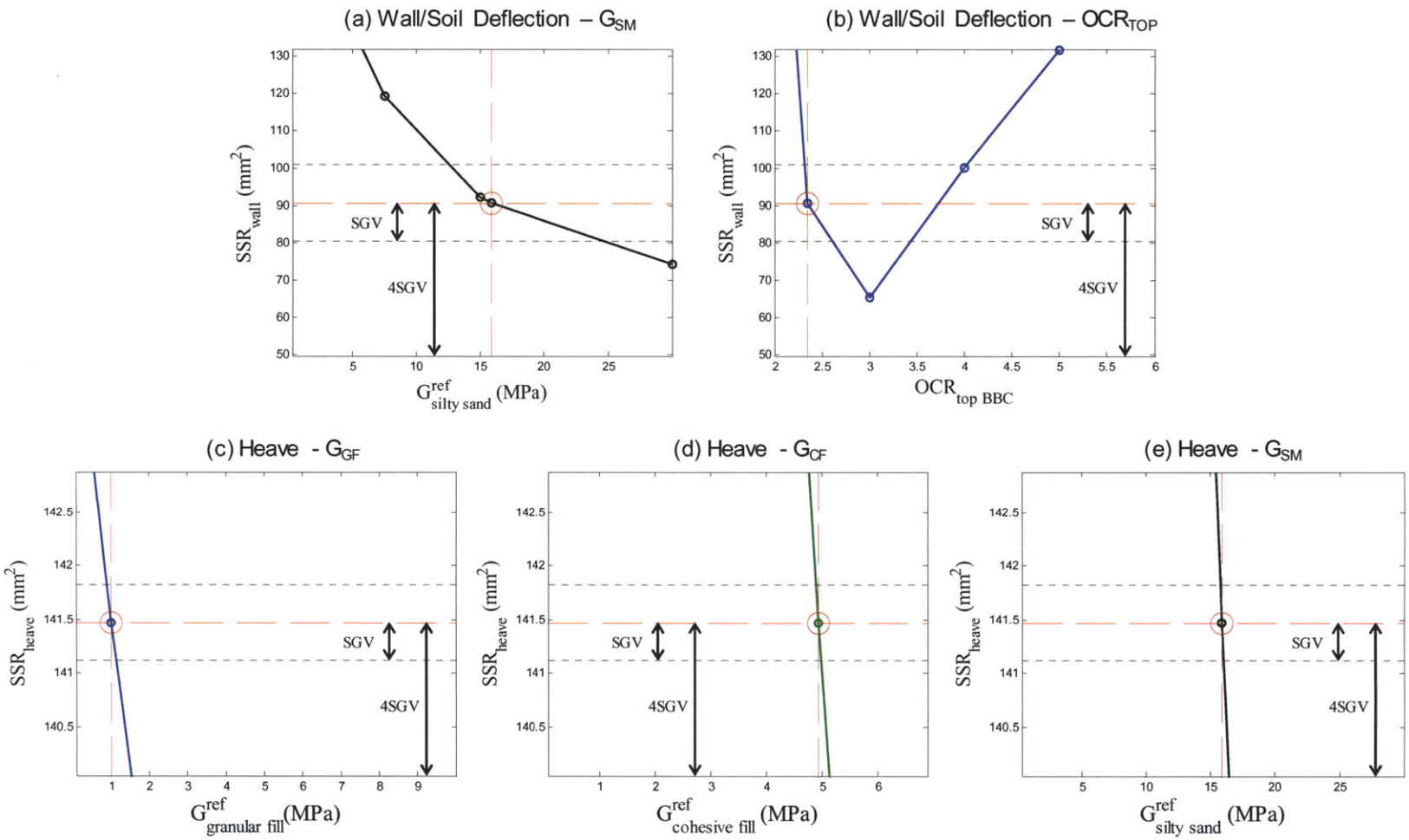

Figure 5-63: Sensitivity analyses of essential improvement parameters (EIP) at excavation level 6

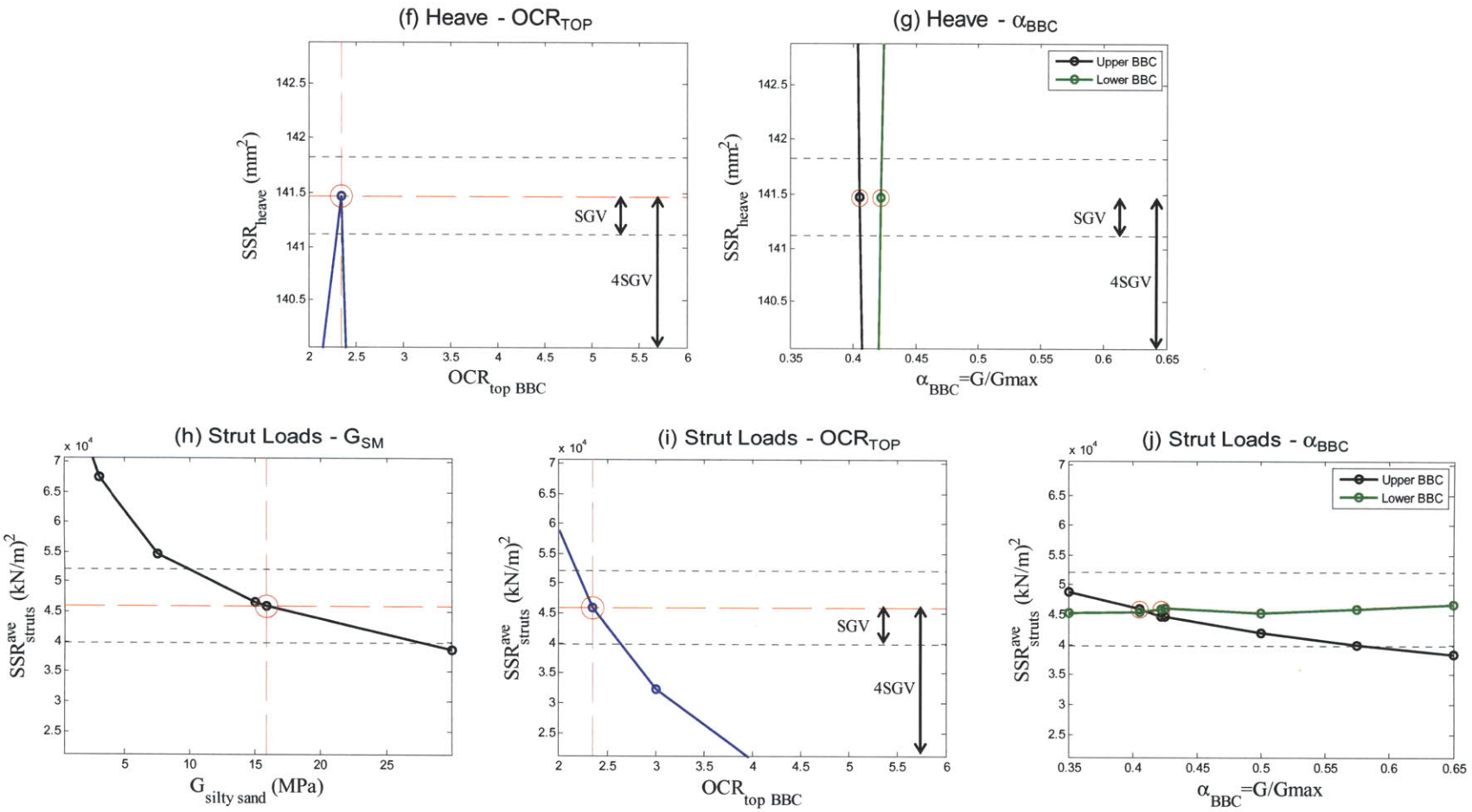

Figure 5-63: Sensitivity analyses of essential improvement parameters (EIP) at excavation level 6 (con't)

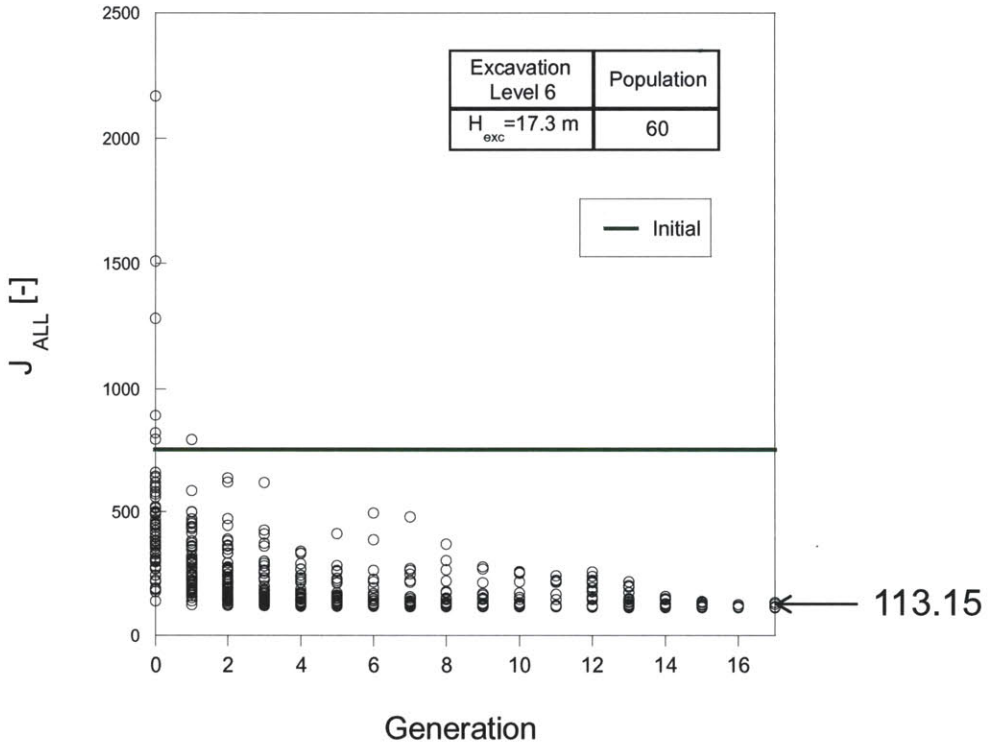

Figure 5-64: Convergence of objective function for all measurements obtained by genetic algorithms at excavation level 6 (also the initial value is shown by the green horizontal line)

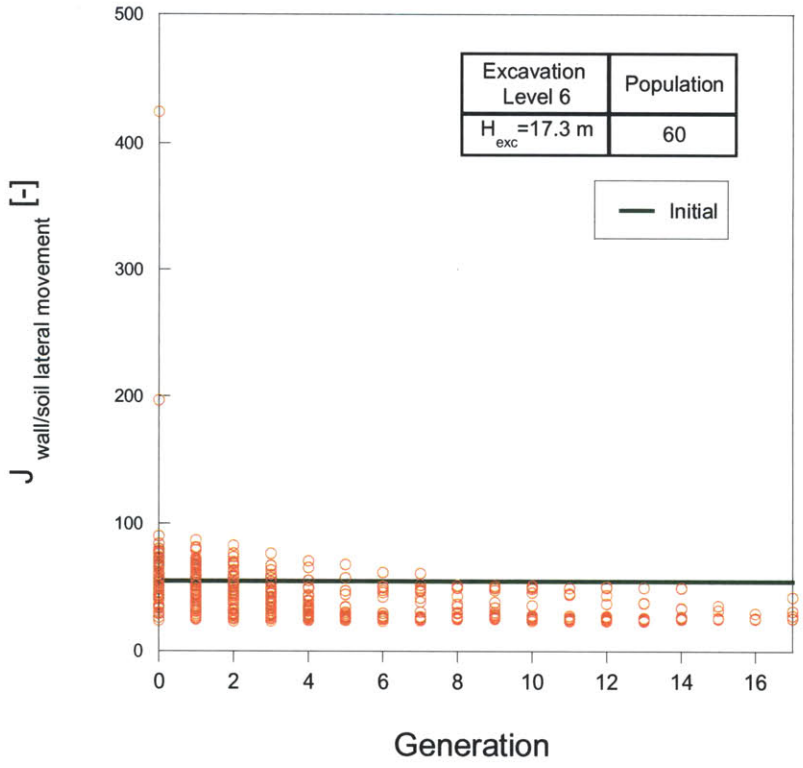

Figure 5-65: Convergence of objective function for wall/soil lateral movement obtained by genetic algorithms at excavation level 6 (also the initial value is shown by the green horizontal line)

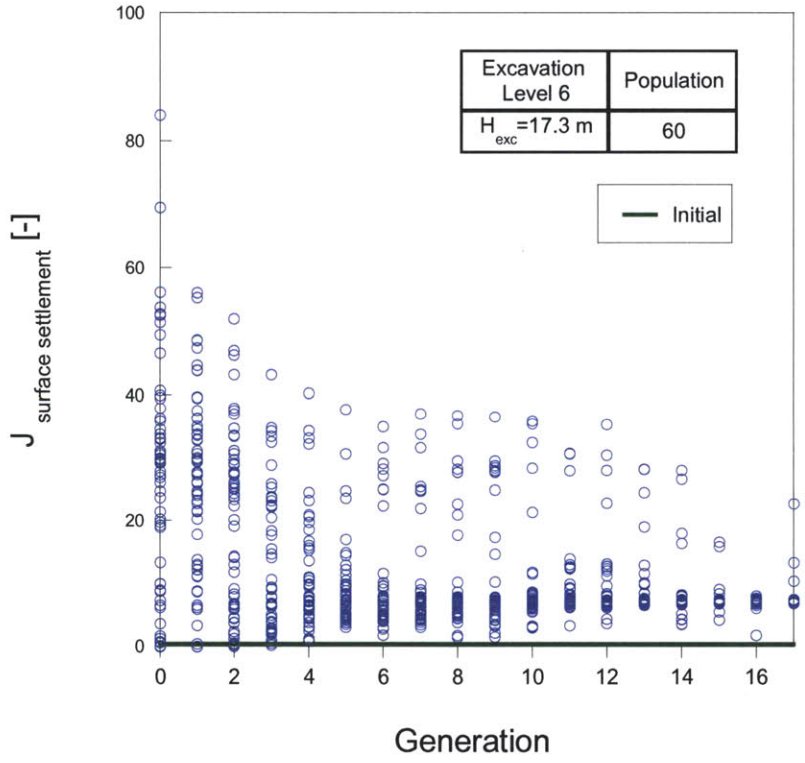

Figure 5-66: Convergence of objective function for surface settlements obtained by genetic algorithms at excavation level 6

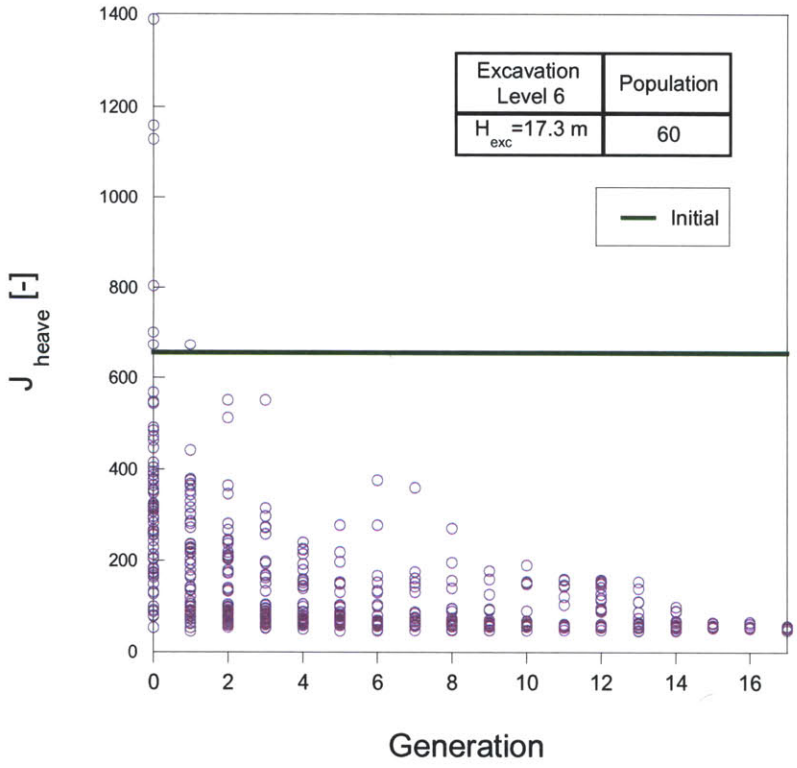

Figure 5-67: Convergence of objective function for excavation heave obtained by genetic algorithms at excavation level 6

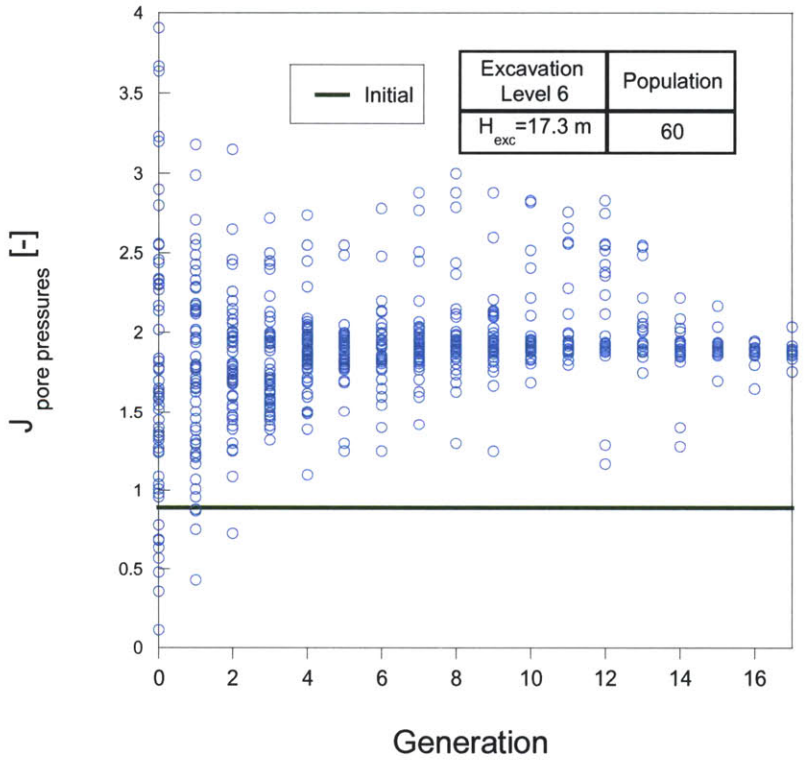

Figure 5-68: Convergence of objective function for pore water pressures obtained by genetic algorithms at excavation level 6

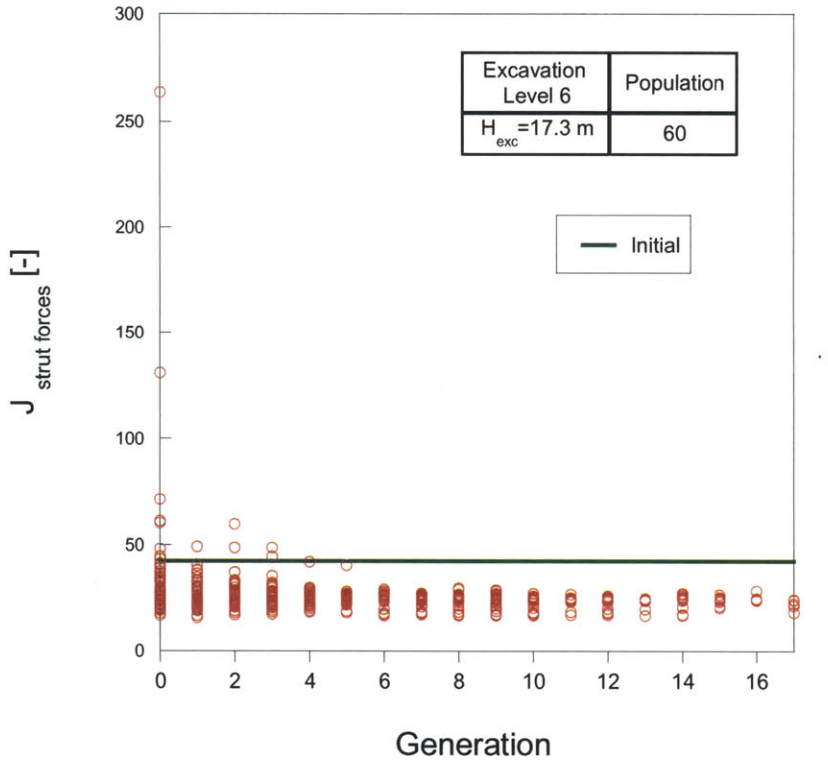

Figure 5-69: Convergence of objective function for strut forces obtained by genetic algorithms at excavation level 6

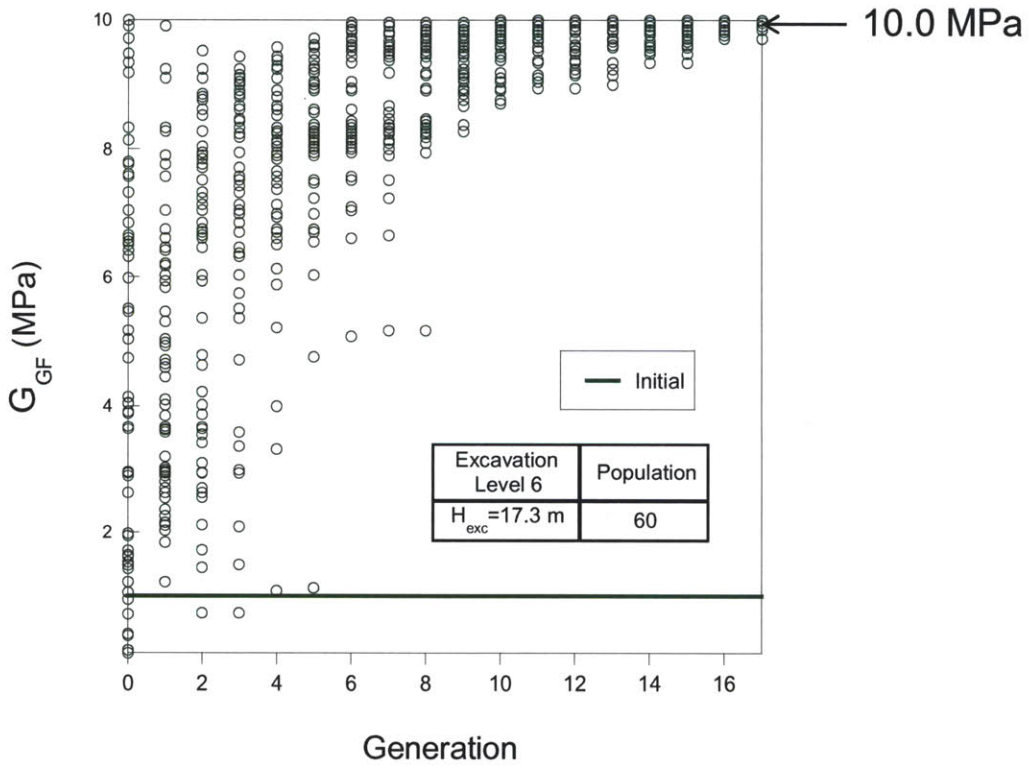

Figure 5-70: Convergence of G^{ref} of the GF layer obtained by genetic algorithms at excavation level 6

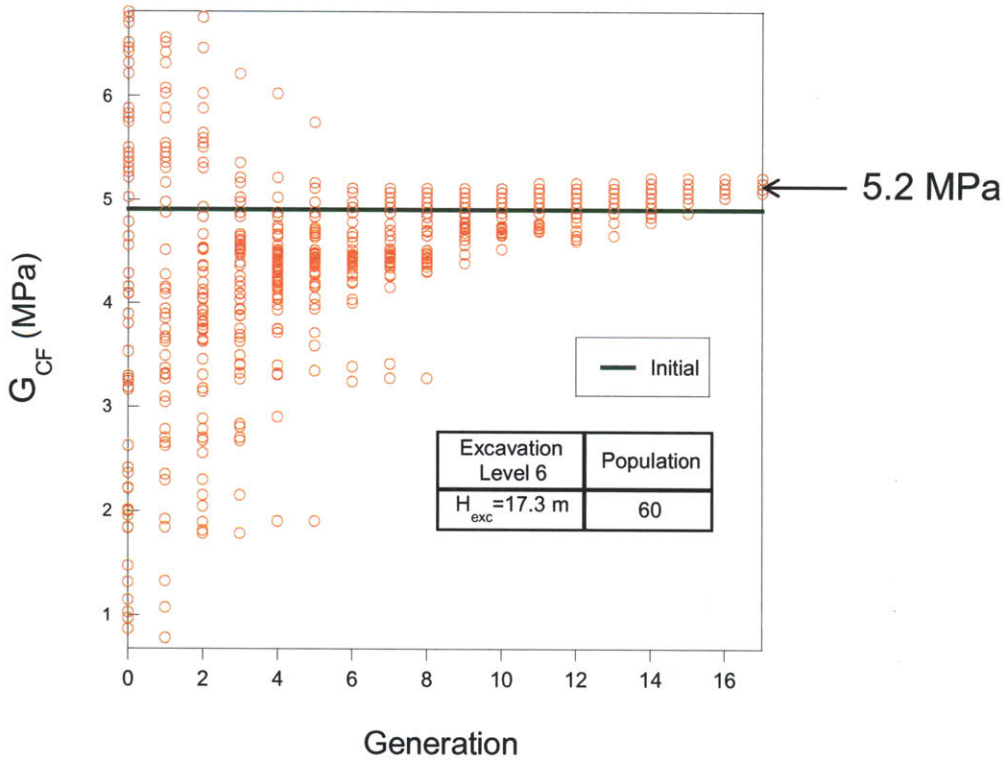

Figure 5-71: Convergence of G^{ref} of the CF layer obtained by genetic algorithms at excavation level 6

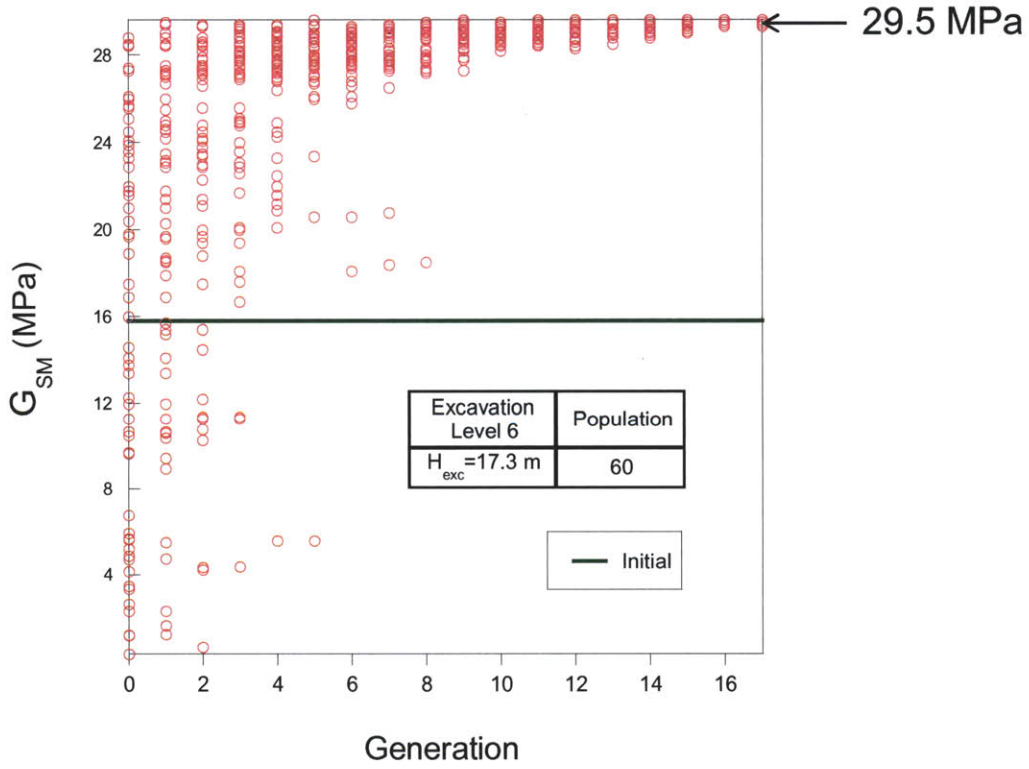

Figure 5-72: Convergence of G^{ref} of the SM layer obtained by genetic algorithms at excavation level 6

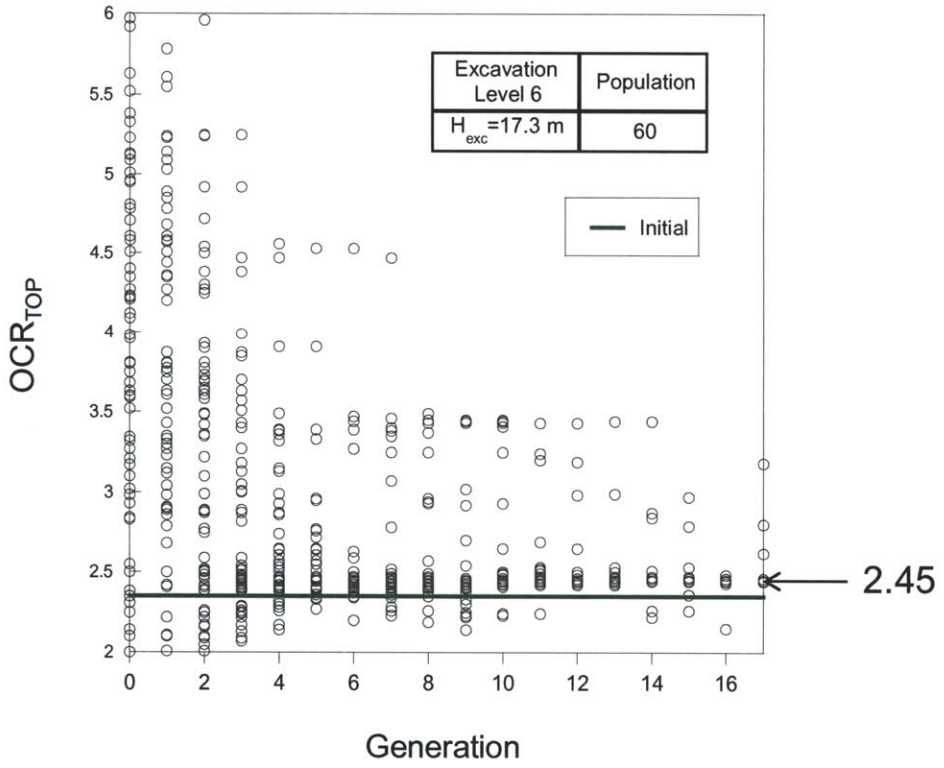

Figure 5-73: Convergence of OCR_{TOP} of the U-BBC layer obtained by genetic algorithms at excavation level 6

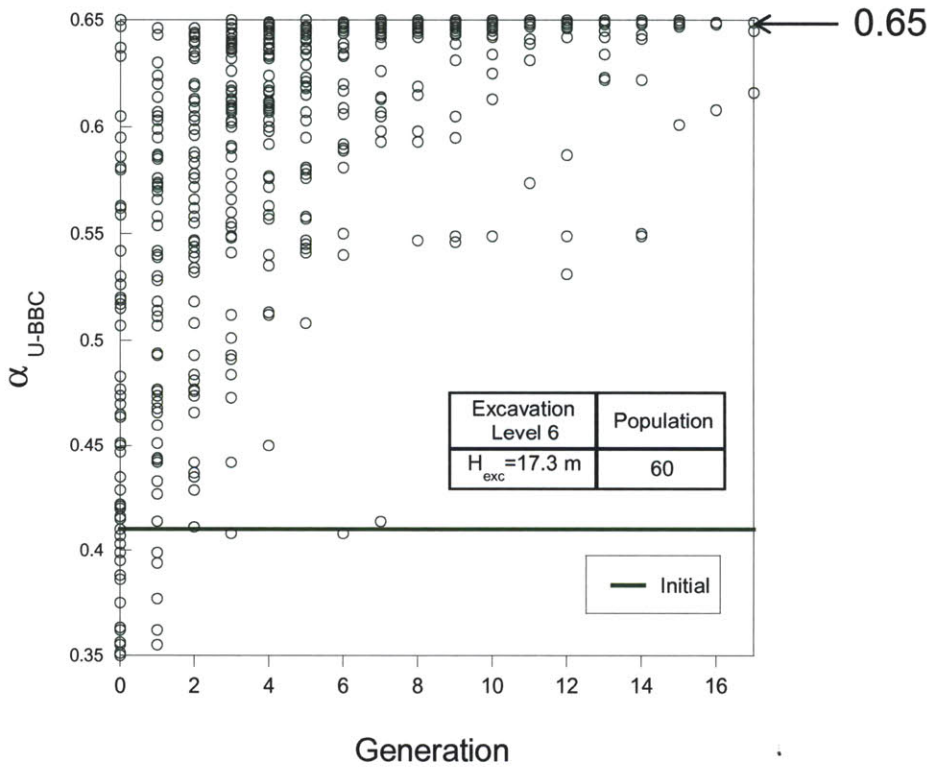

Figure 5-74: Convergence of α parameter of the U-BBC layer obtained by genetic algorithms at excavation level 6

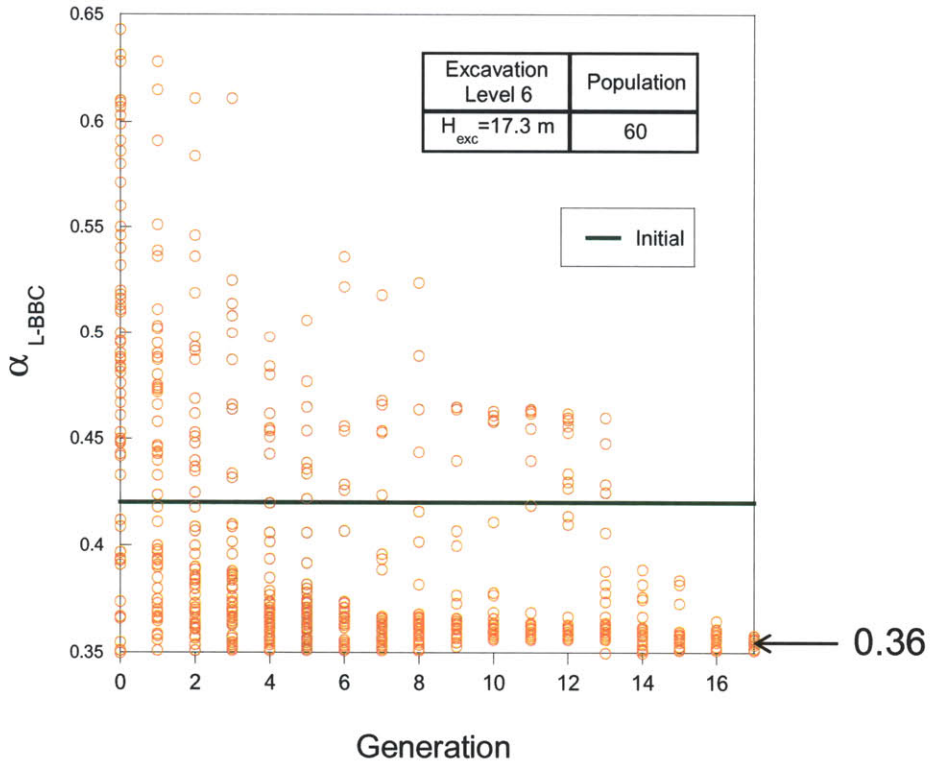

Figure 5-75: Convergence of α parameter of the L-BBC layer obtained by genetic algorithms at excavation level 6

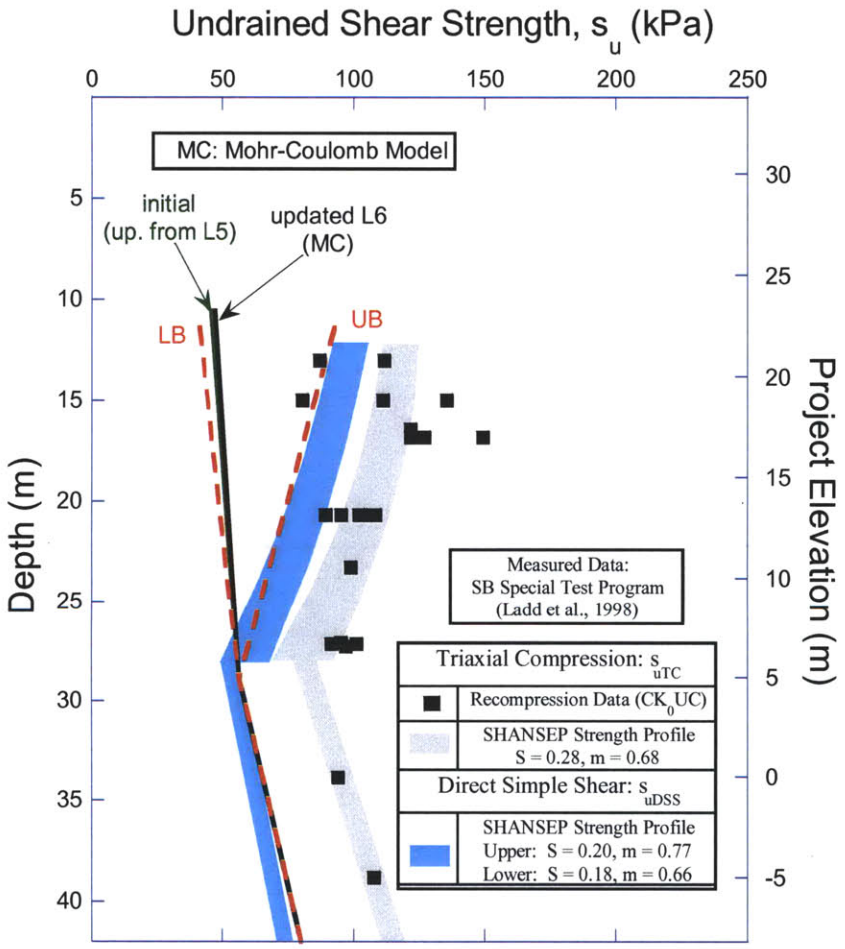

Figure 5-76: Updated Exc. L6 vs. Initial (updated from L5) MC s_u profiles (showing lower and upper bounds) and SHANSEP strength profiles

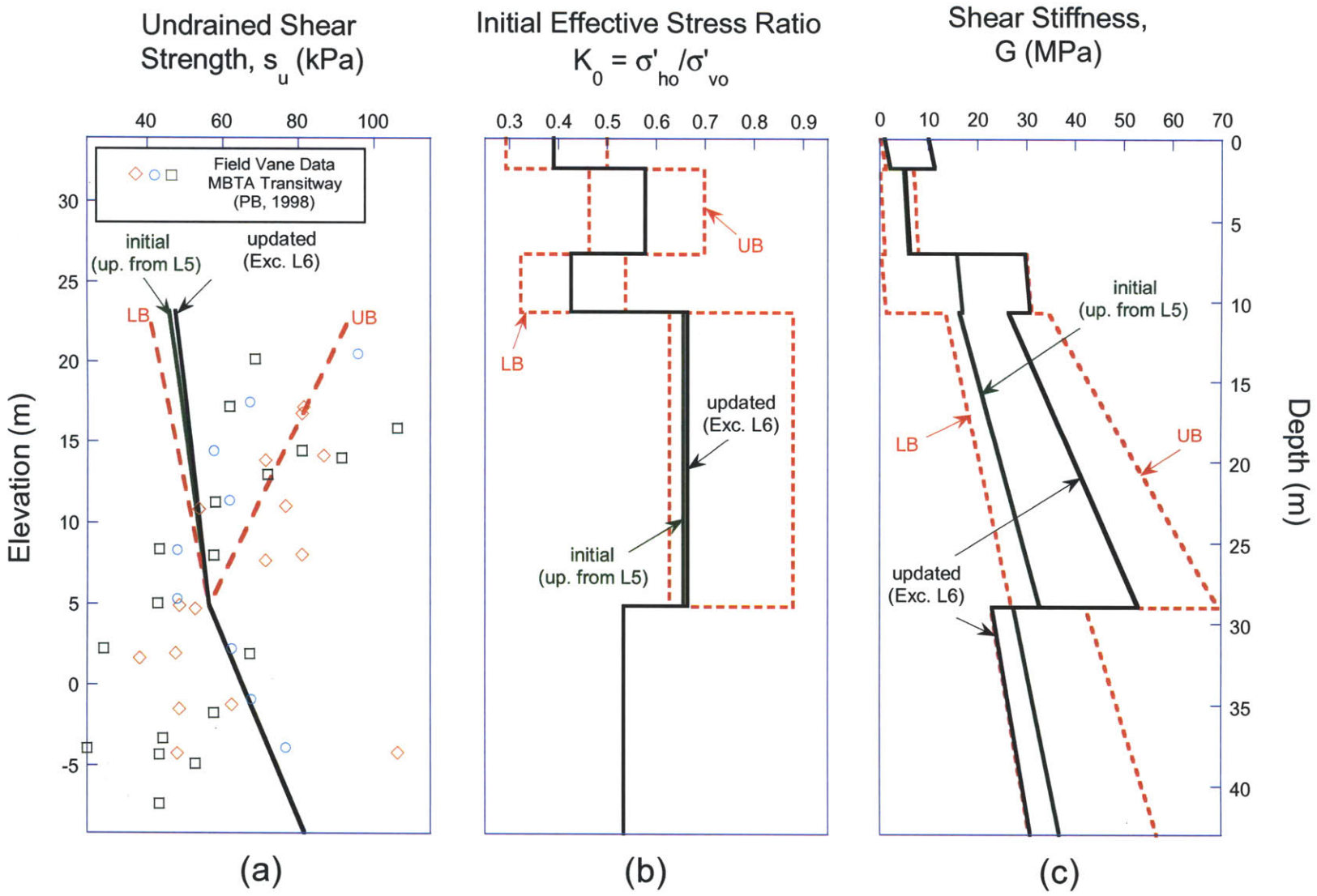

Figure 5-77: Updated Exc. L6 versus Initial (updated from L5) profiles of undrained shear strengths (compared with field vane data), effective stress ratios, and shear stiffnesses

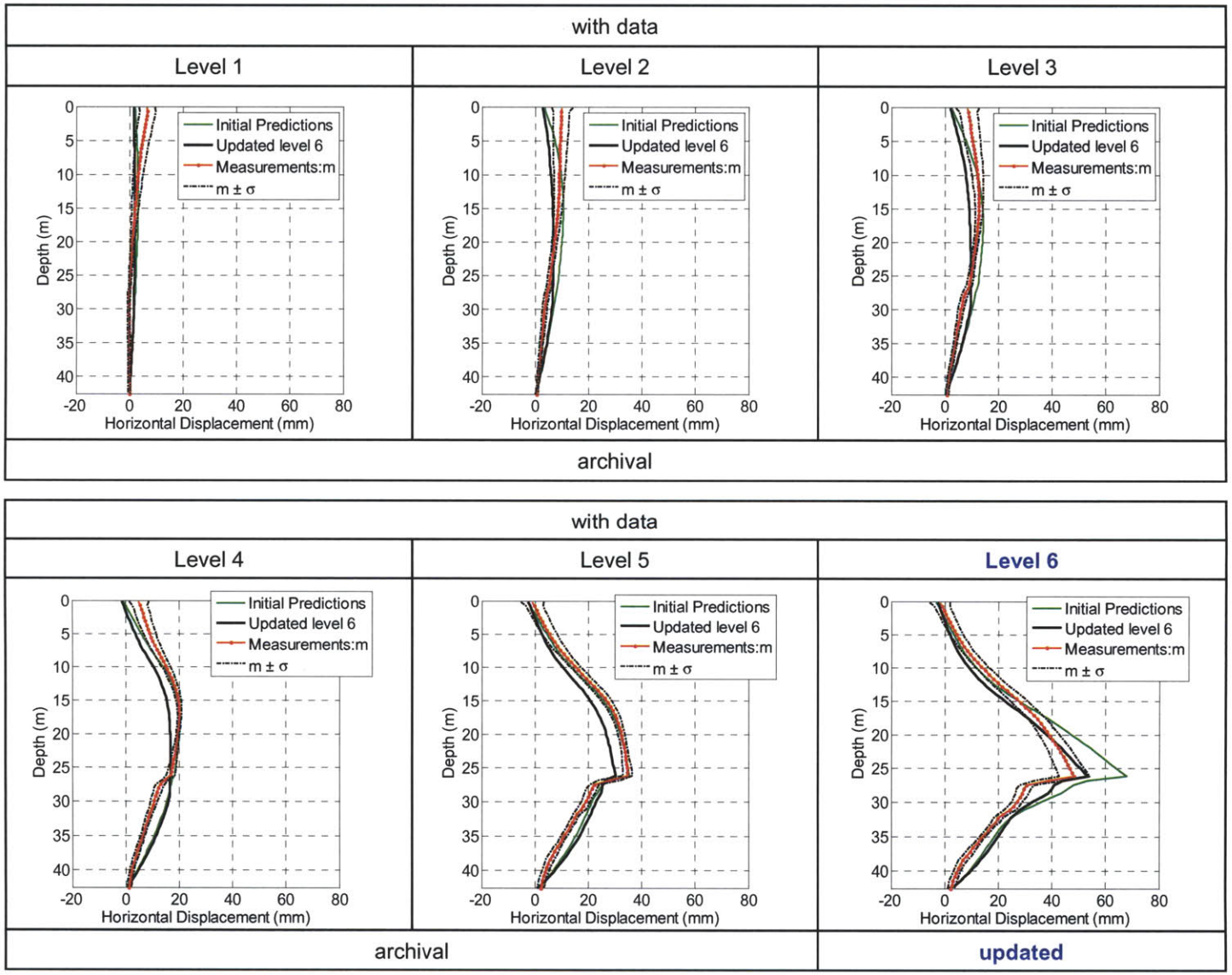

Figure 5-78: Comparison of measurements, initial predictions, and updated level 6 of lateral wall/soil movements

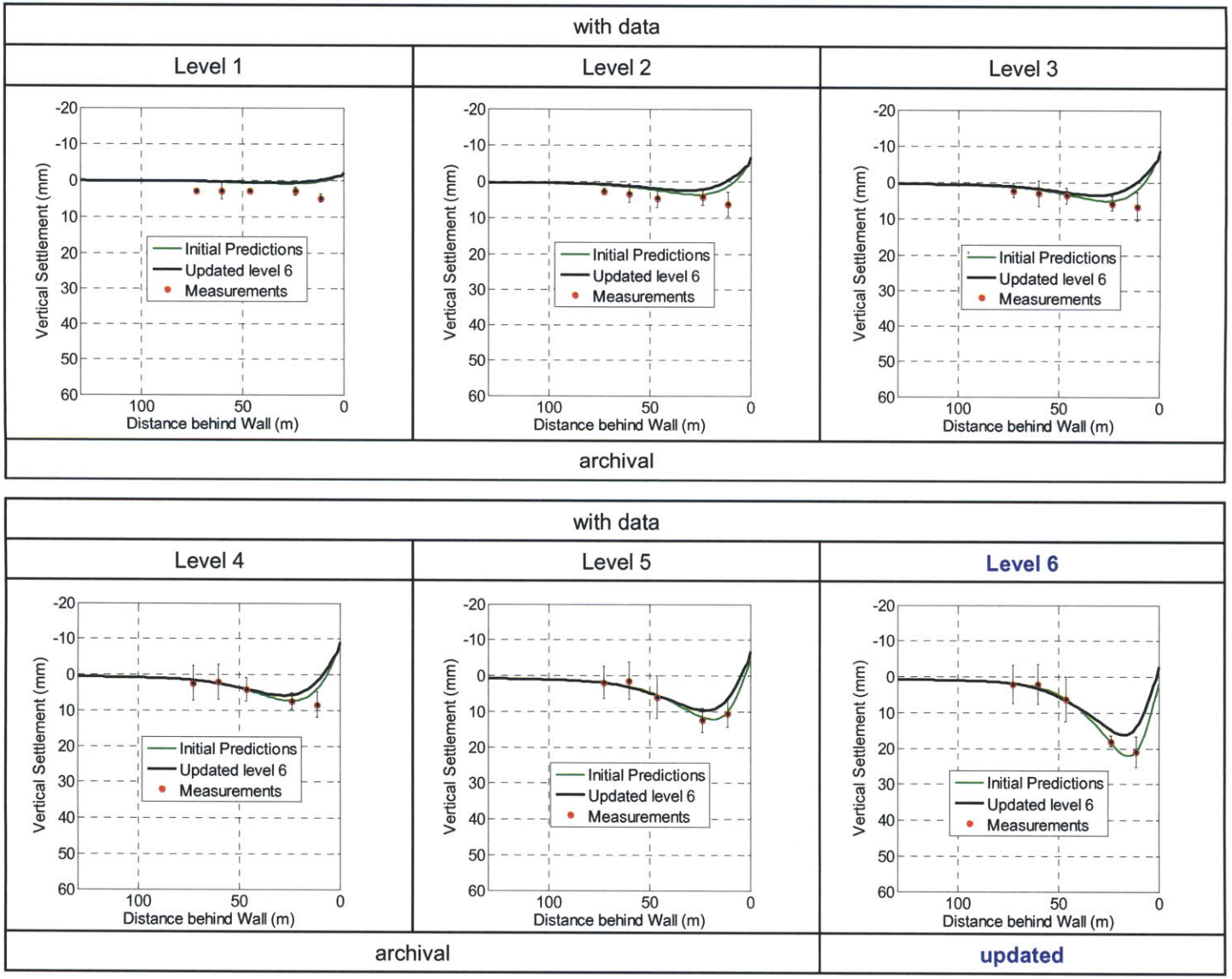

Figure 5-79: Comparison of measurements, initial predictions, and updated level 6 of surface settlements

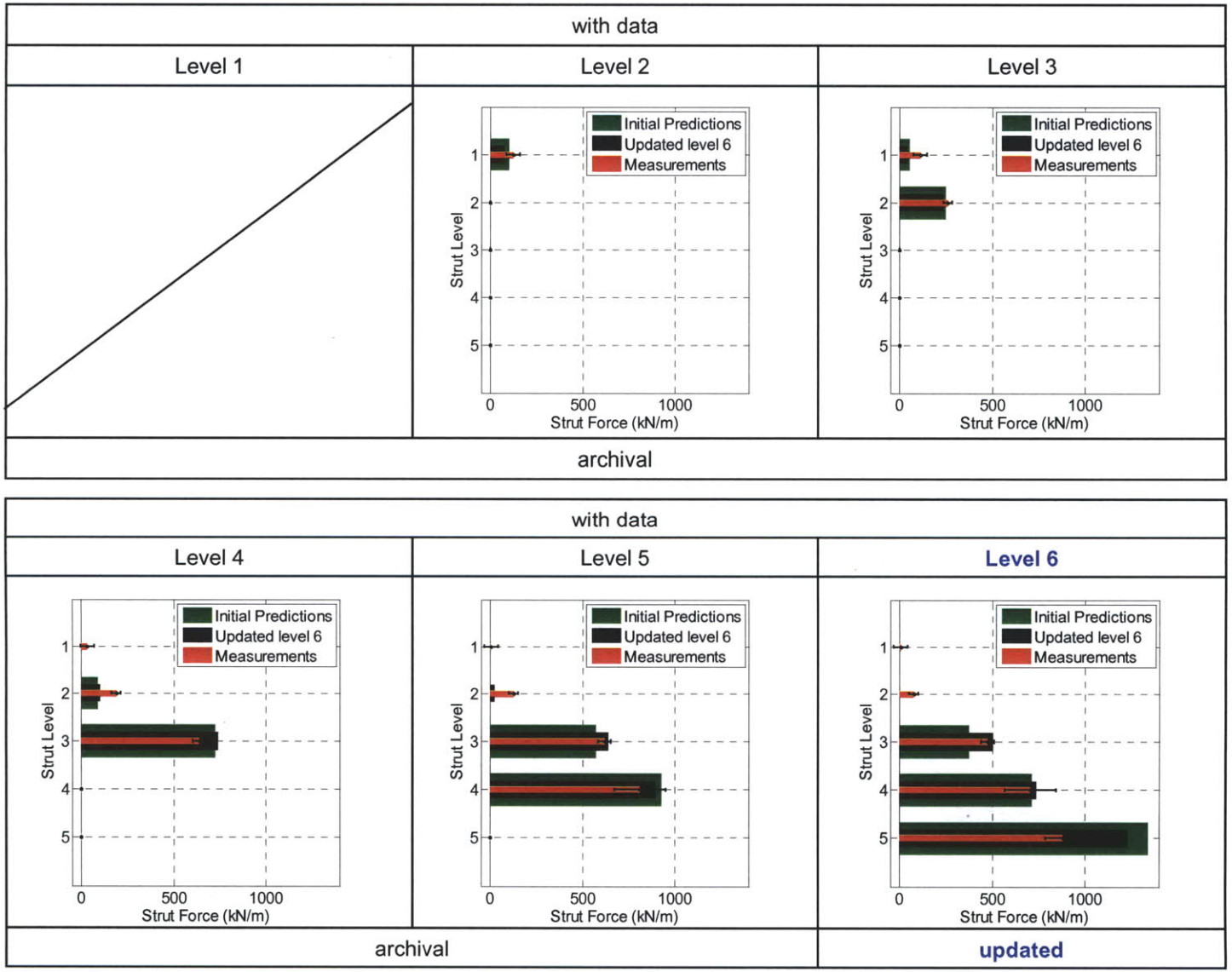

Figure 5-80: Comparison of measurements, initial predictions, and updated level 6 of strut forces

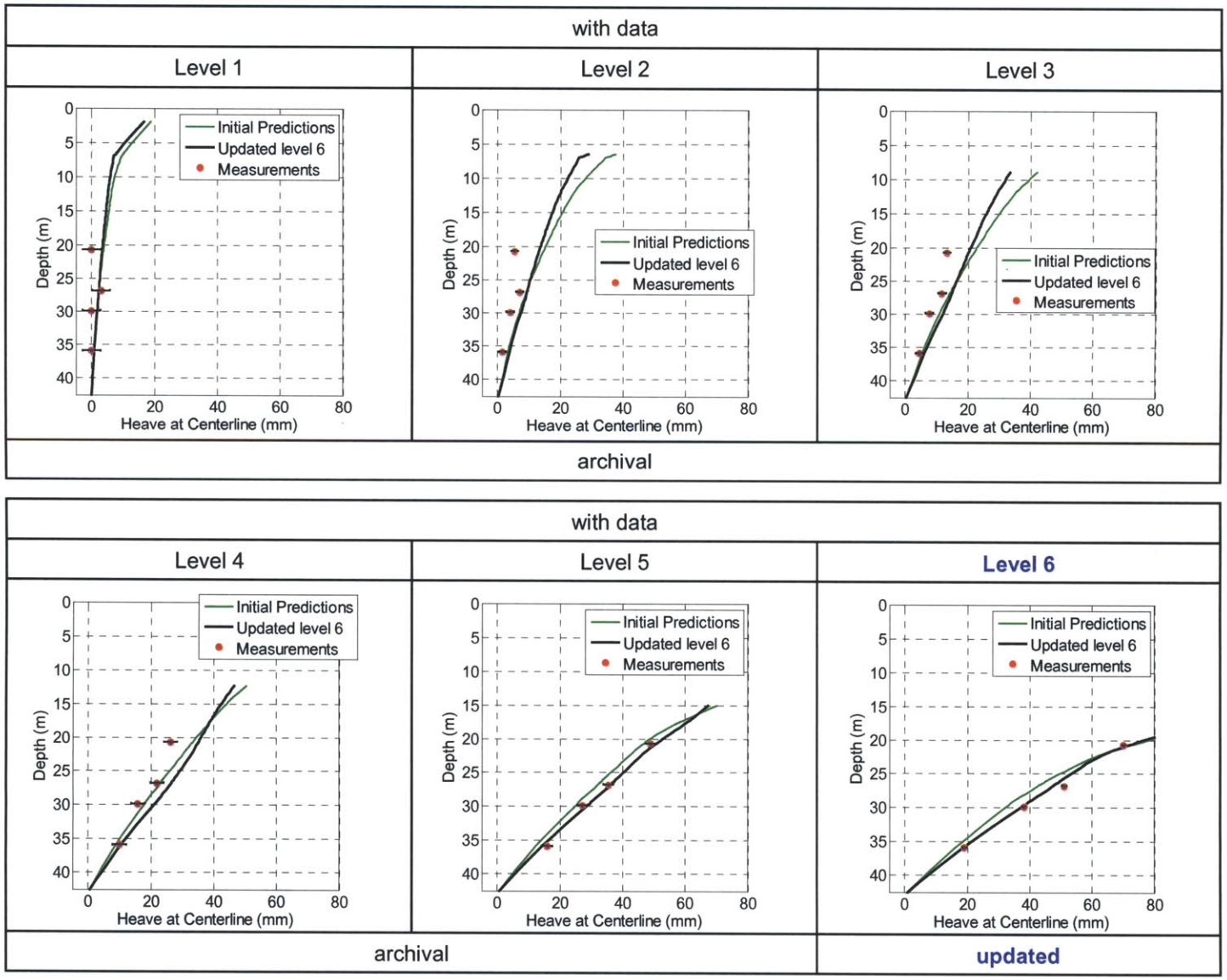

Figure 5-81: Comparison of measurements, initial predictions, and updated level 6 of excavation heave

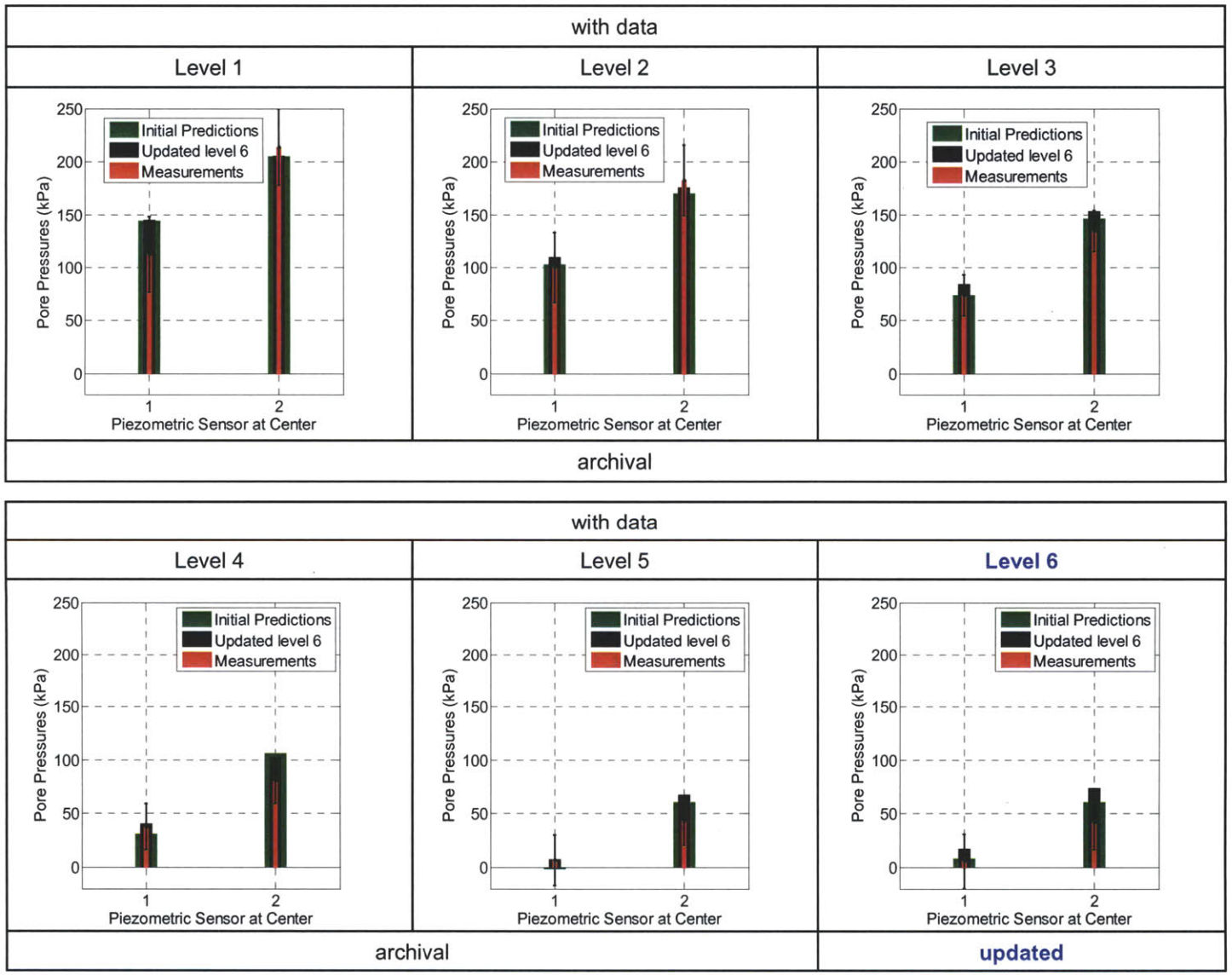

Figure 5-82: Comparison of measurements, initial predictions, and updated level 6 of pore water pressures

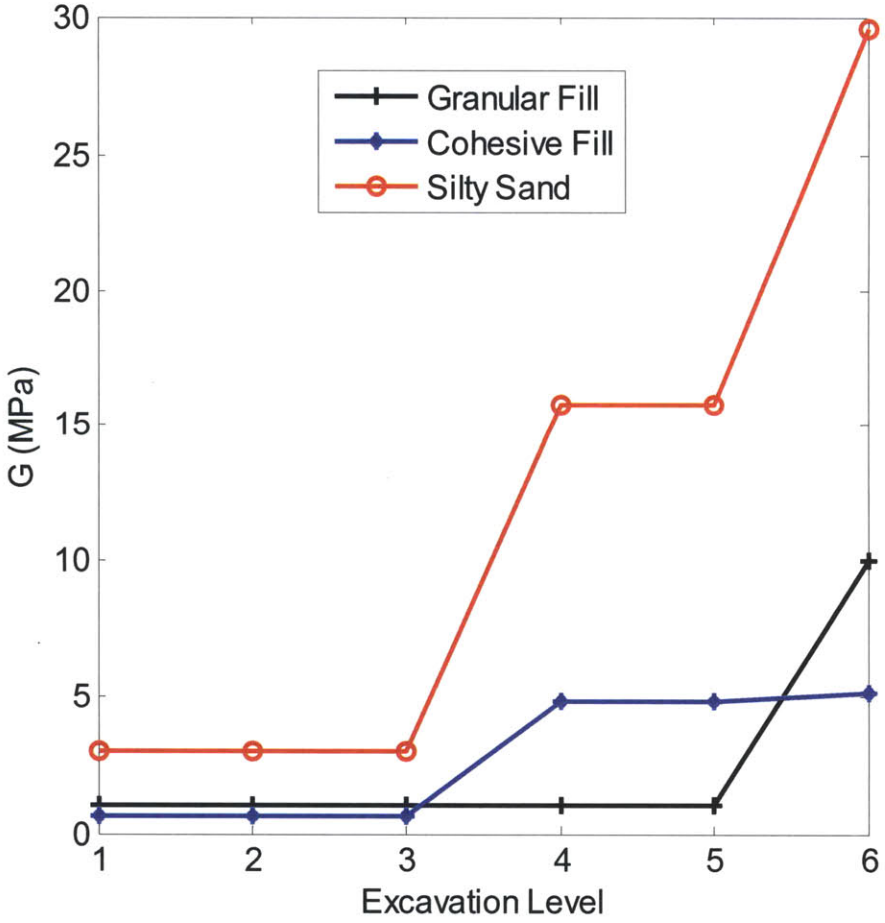

Figure 5-83: Shear Stiffness variations for granular fill, cohesive fill, and silty sand layers versus excavation level

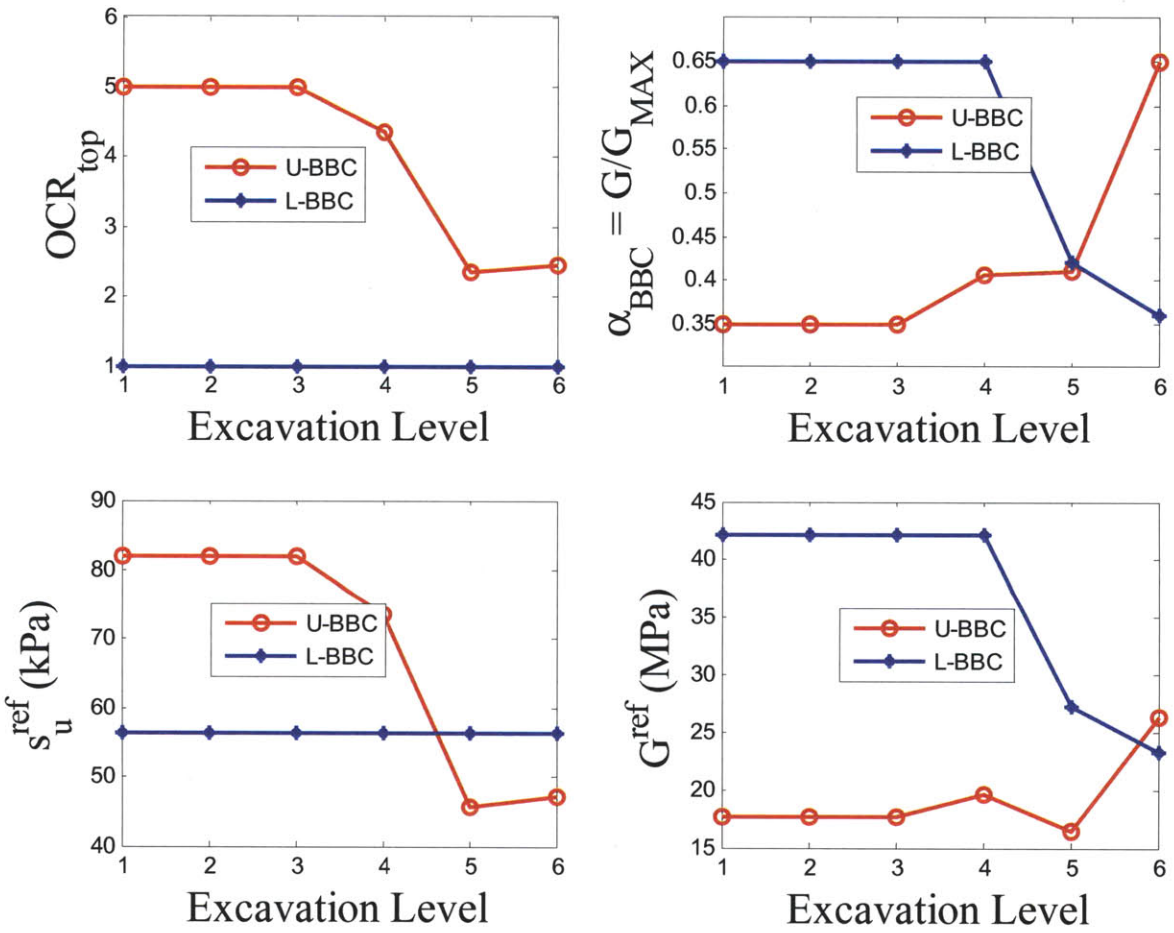

Figure 5-84: Undrained shear strength and shear stiffness variations of BBC layer (as well as OCR top and a) versus excavation level

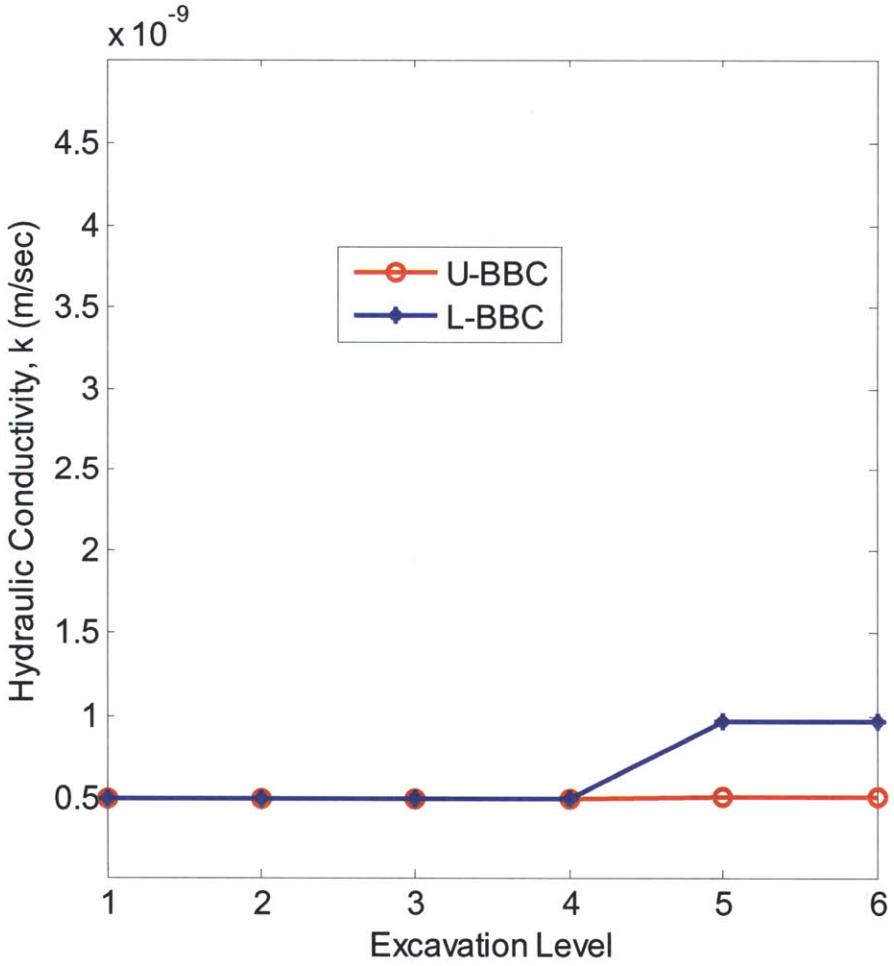

Figure 5-85: Hydraulic conductivity variations of BBC layer versus excavation level

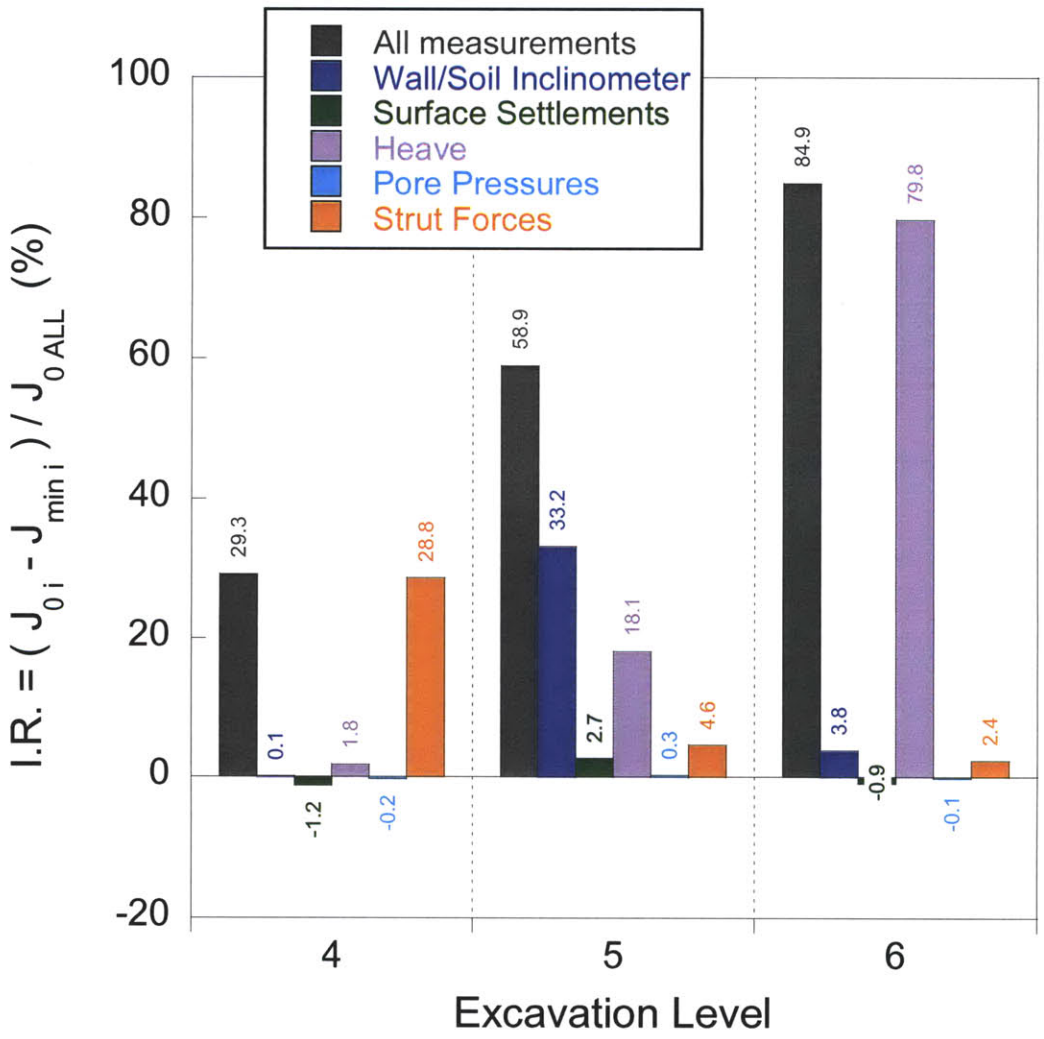

Figure 5-86: Incremental improvement ratios of updating predictions for excavation levels 4, 5, and 6

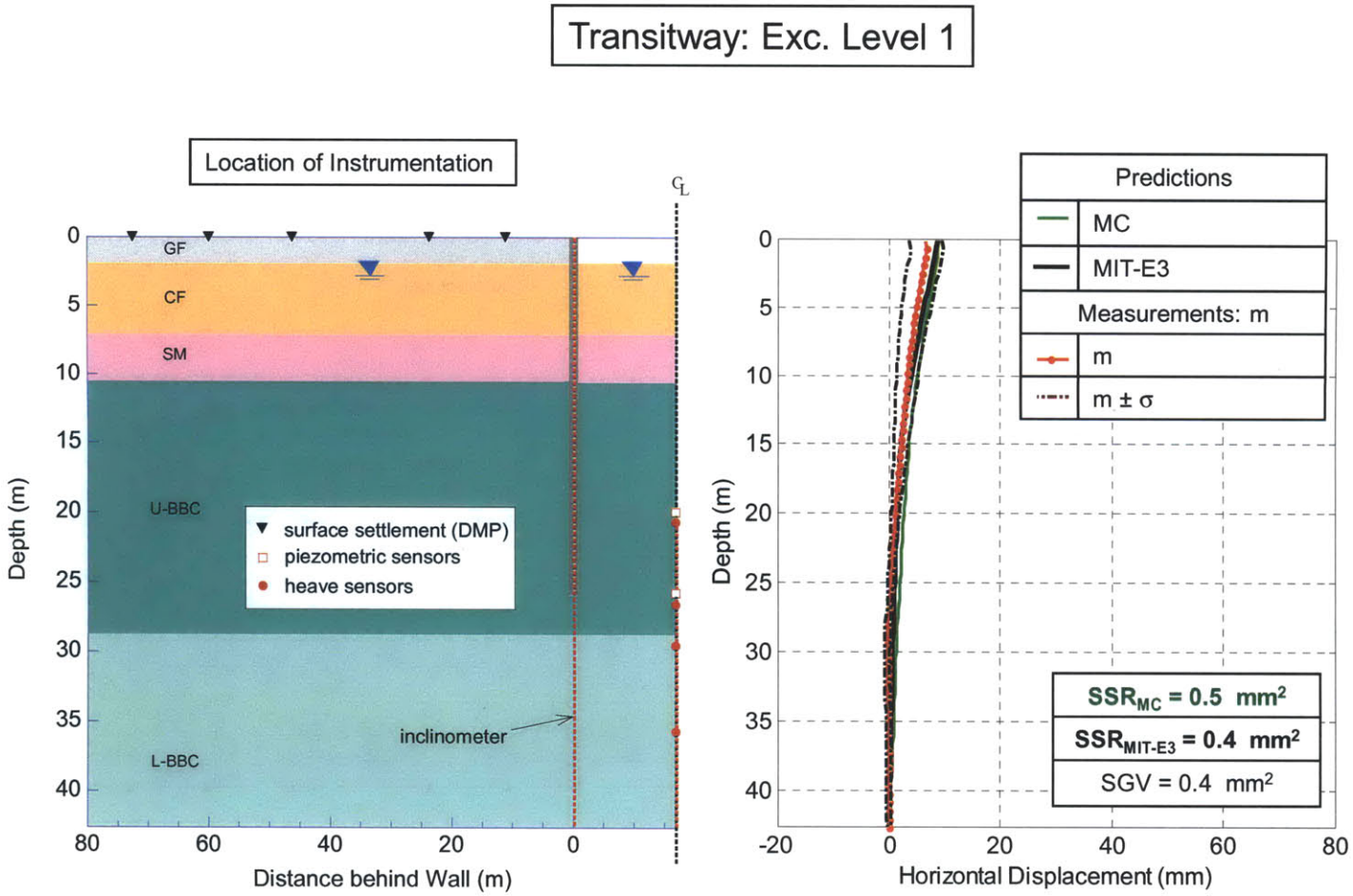

Figure 5-87: MIT-E3 and MC comparisons with measured lateral wall/soil movements at excavation level 1

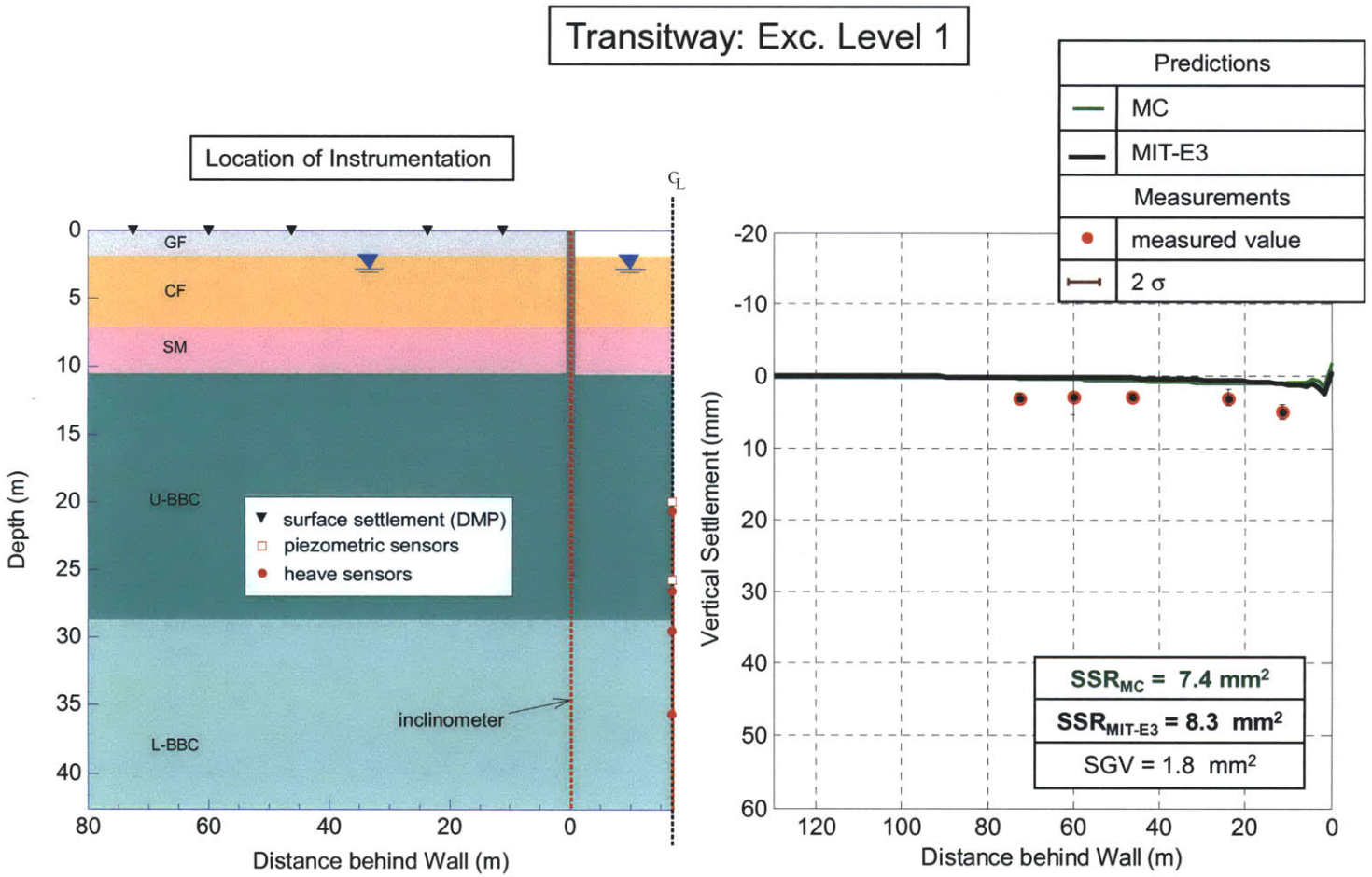

Figure 5-88: MIT-E3 and MC comparisons with measured surface settlements at excavation level 1

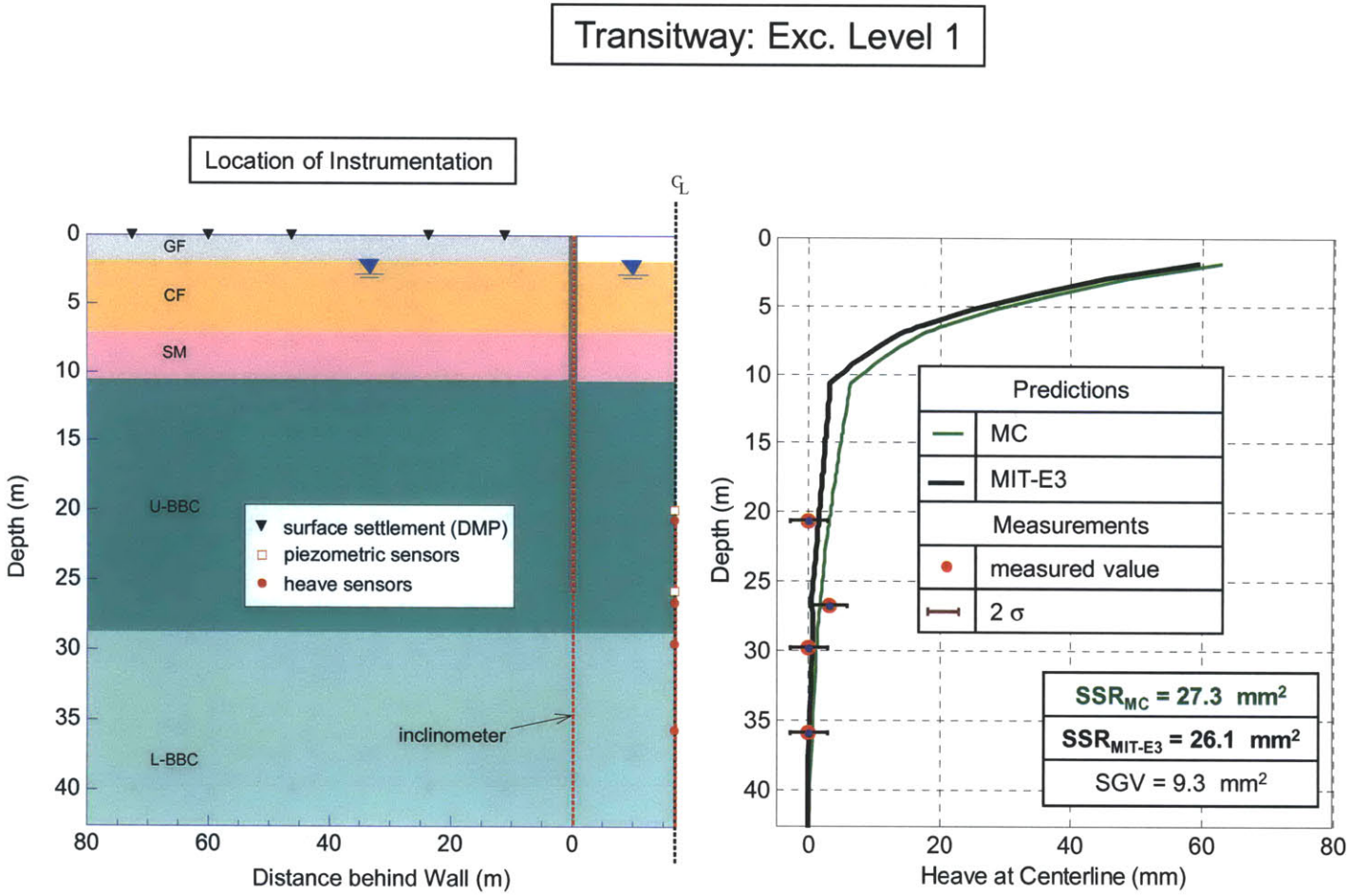

Figure 5-89: MIT-E3 and MC comparisons with measured heave at excavation level 1

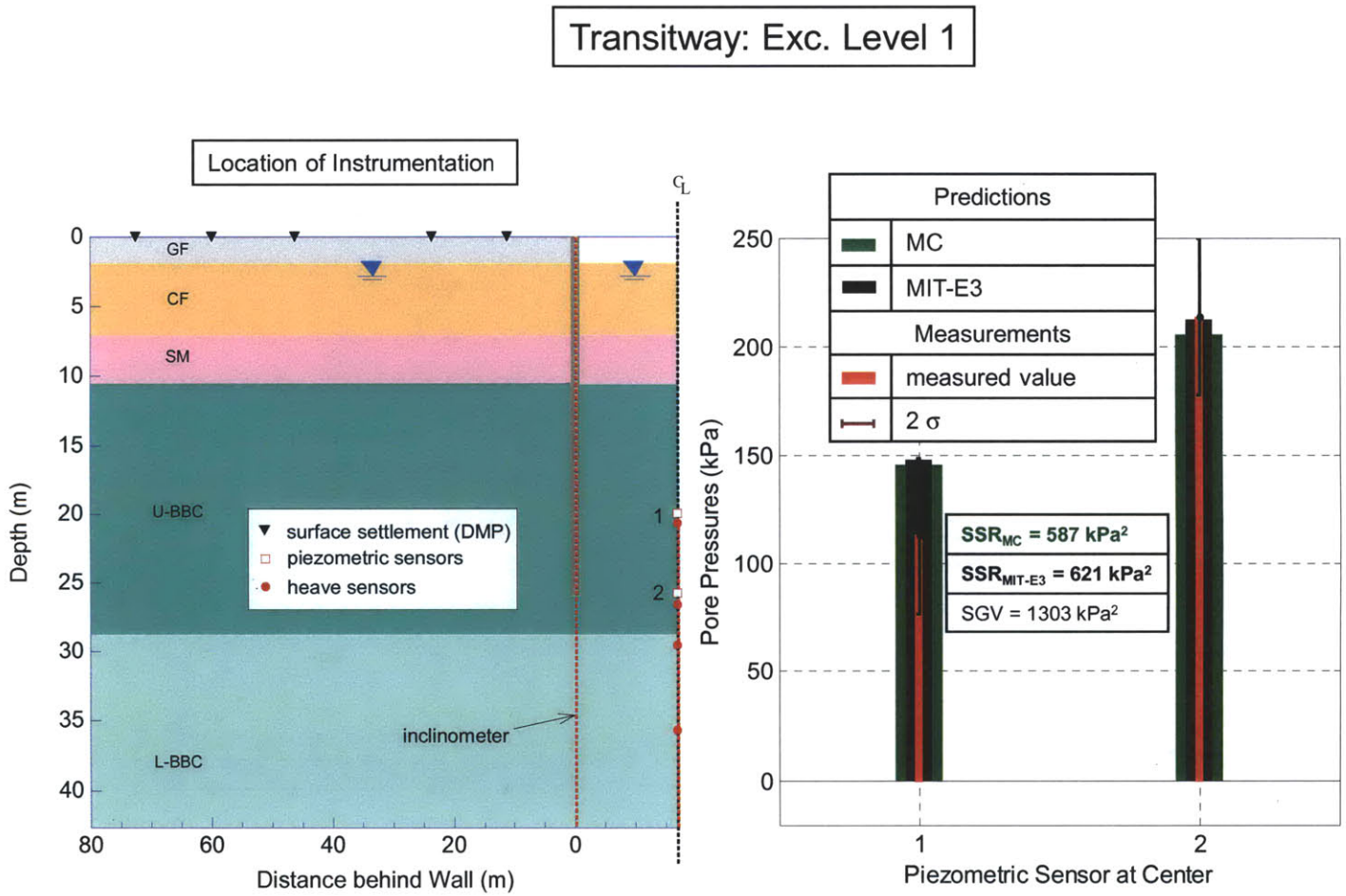

Figure 5-90: MIT-E3 and MC comparisons with measured pore pressures at excavation level 1

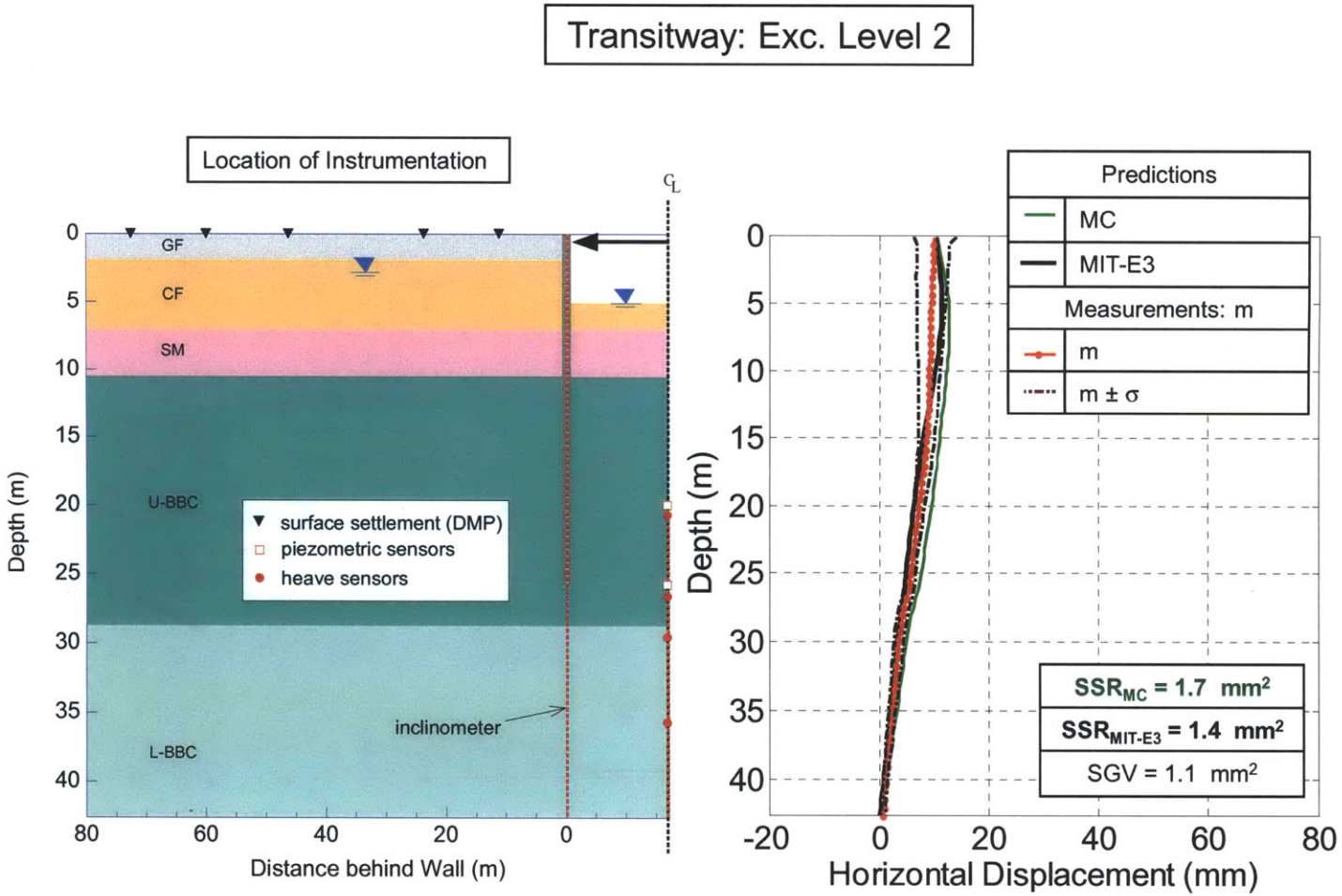

Figure 5-91: MIT-E3 and MC comparisons with measured lateral wall/soil movements at excavation level 2

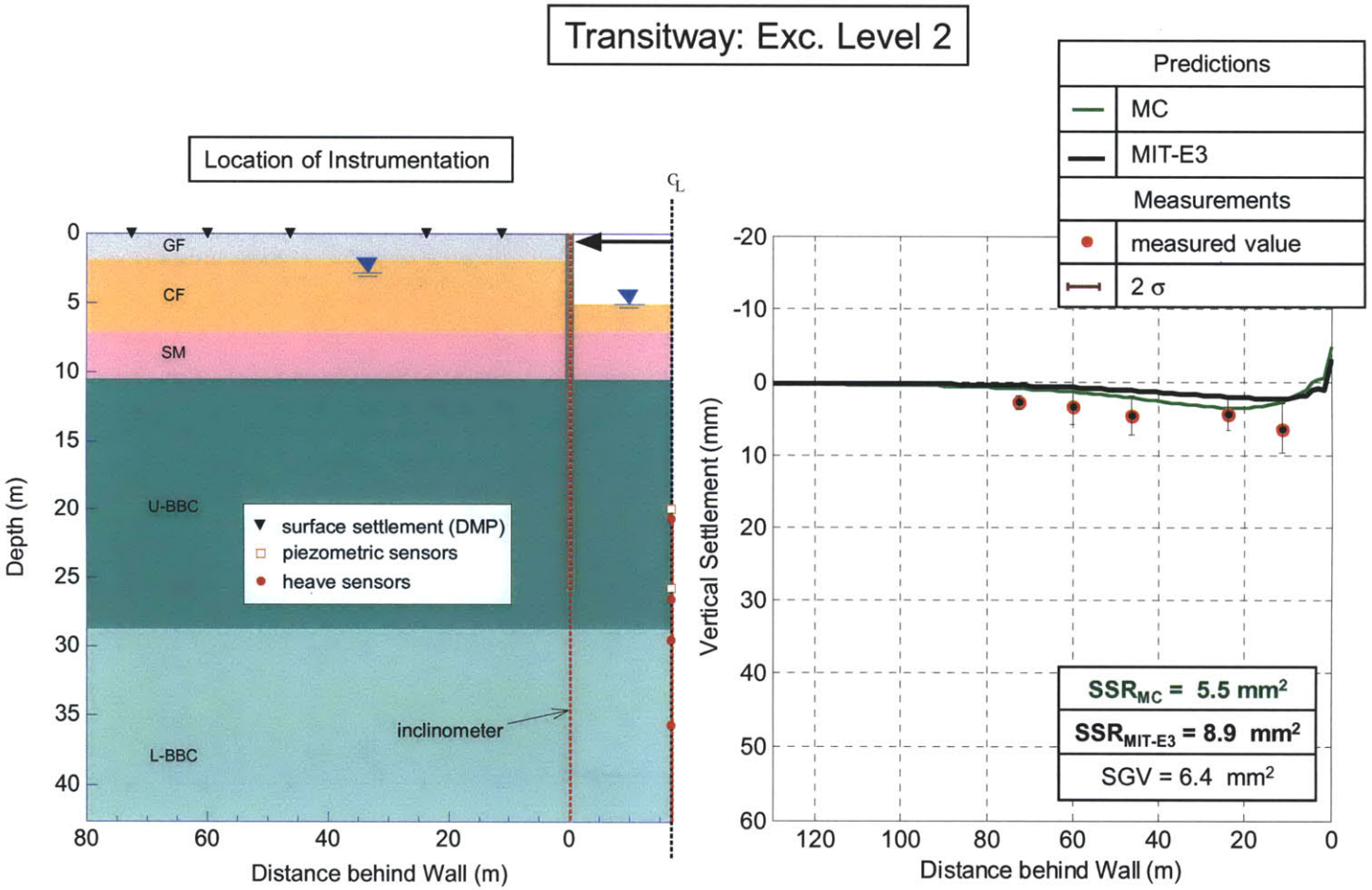

Figure 5-92: MIT-E3 and MC comparisons with measured surface settlements at excavation level 2

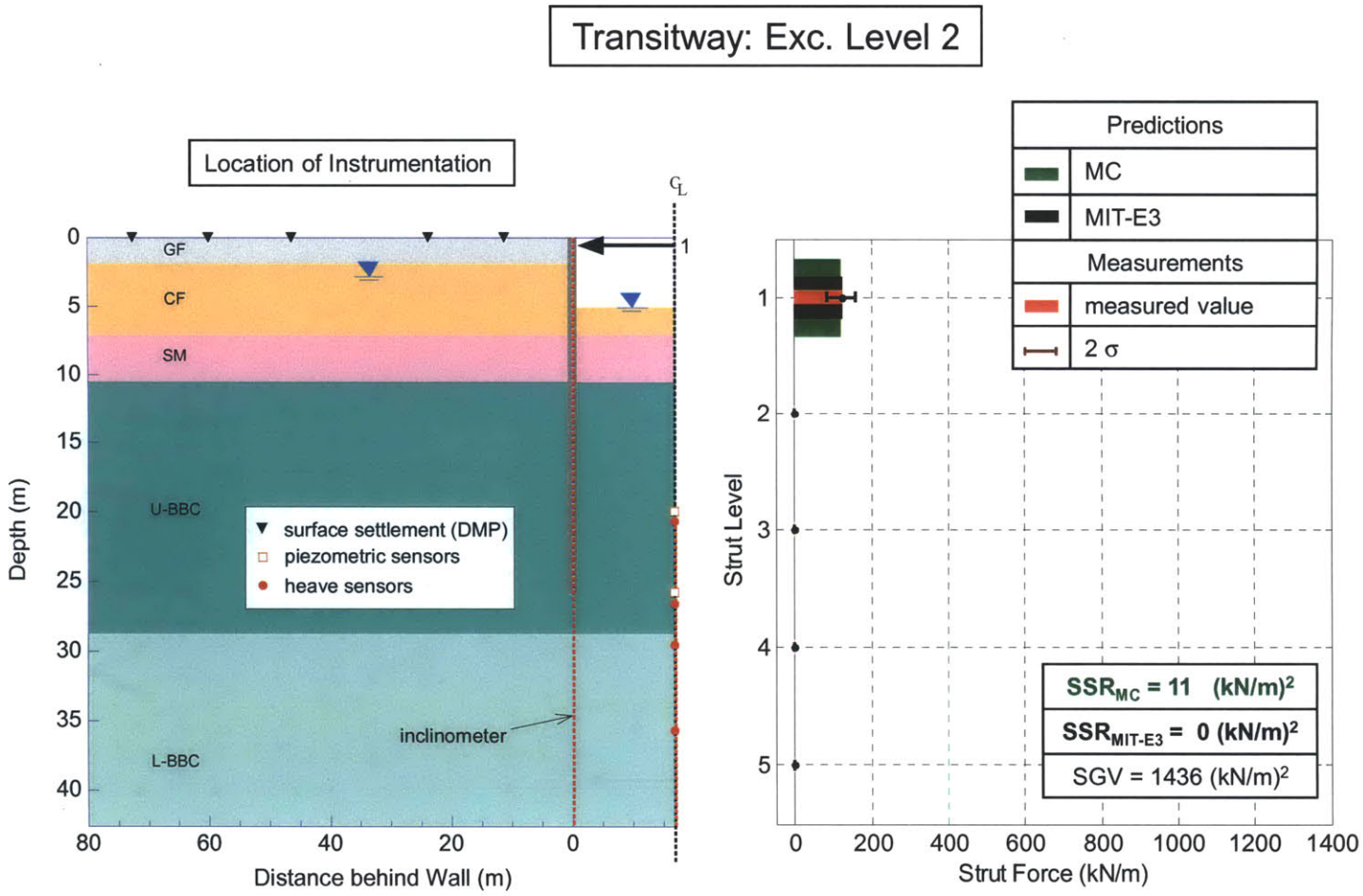

Figure 5-93: MIT-E3 and MC comparisons with measured strut forces at excavation level 2

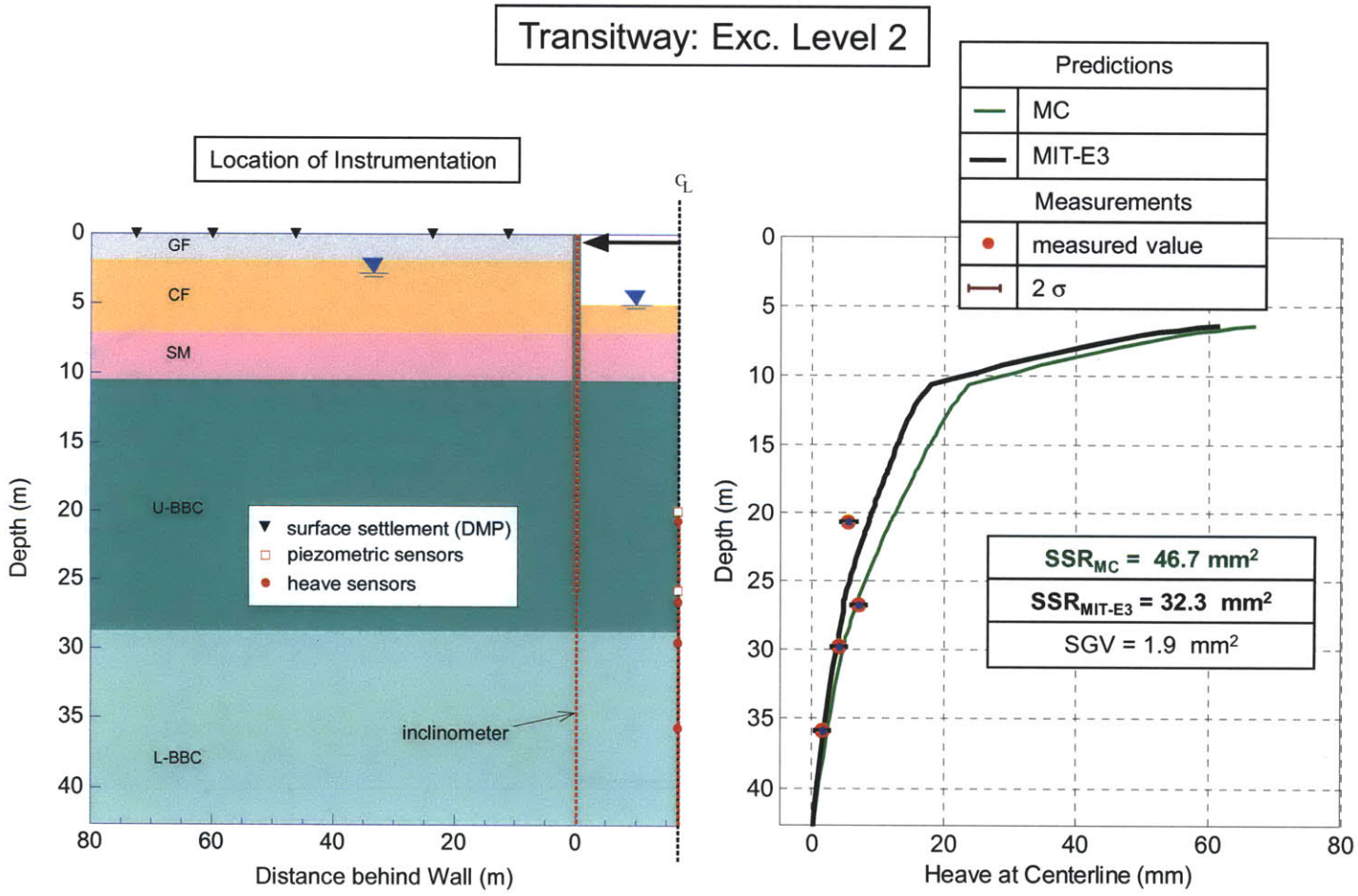

Figure 5-94: MIT-E3 and MC comparisons with measured heave at excavation level 2

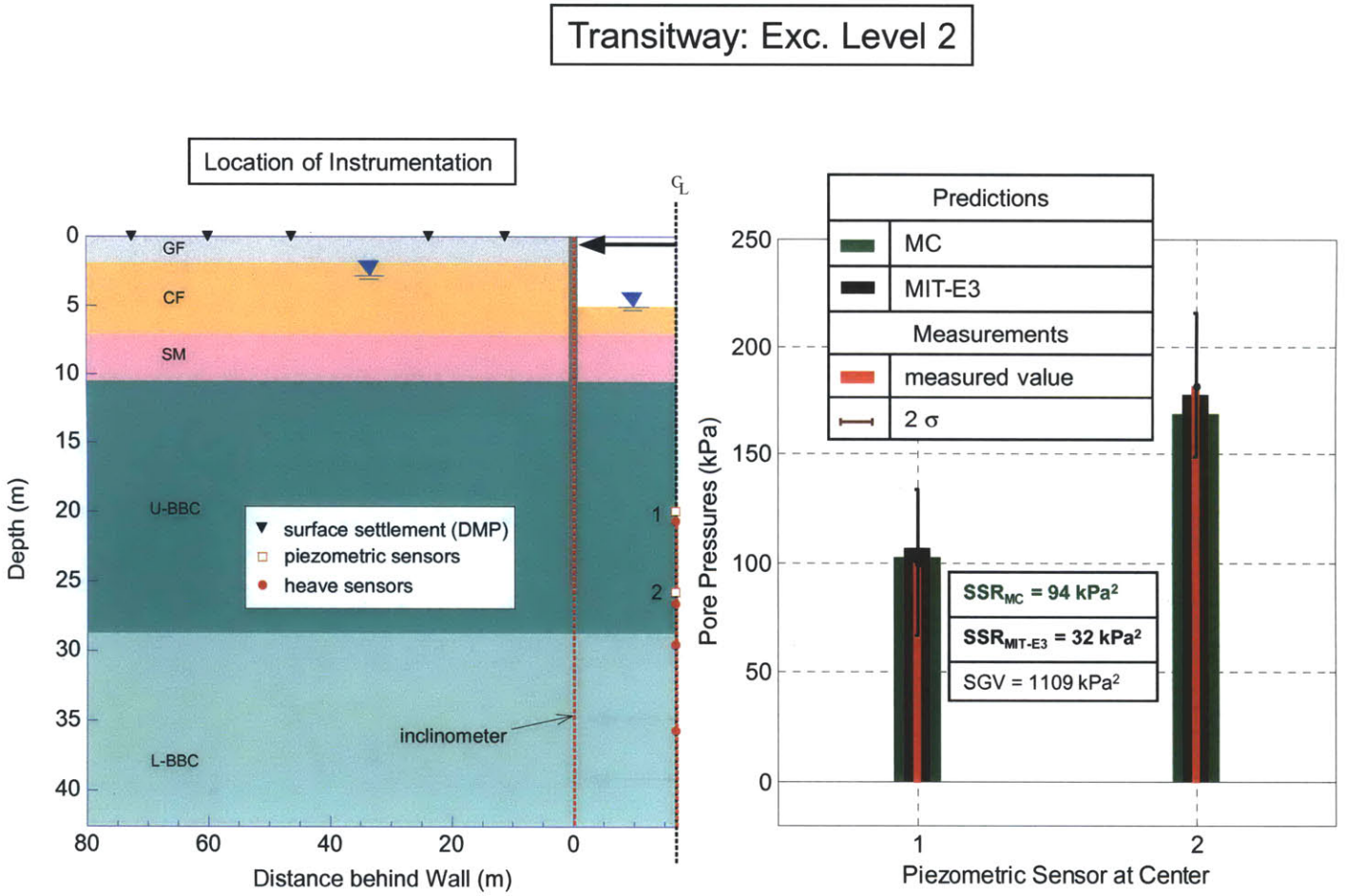

Figure 5-95: MIT-E3 and MC comparisons with measured pore pressures at excavation level 2

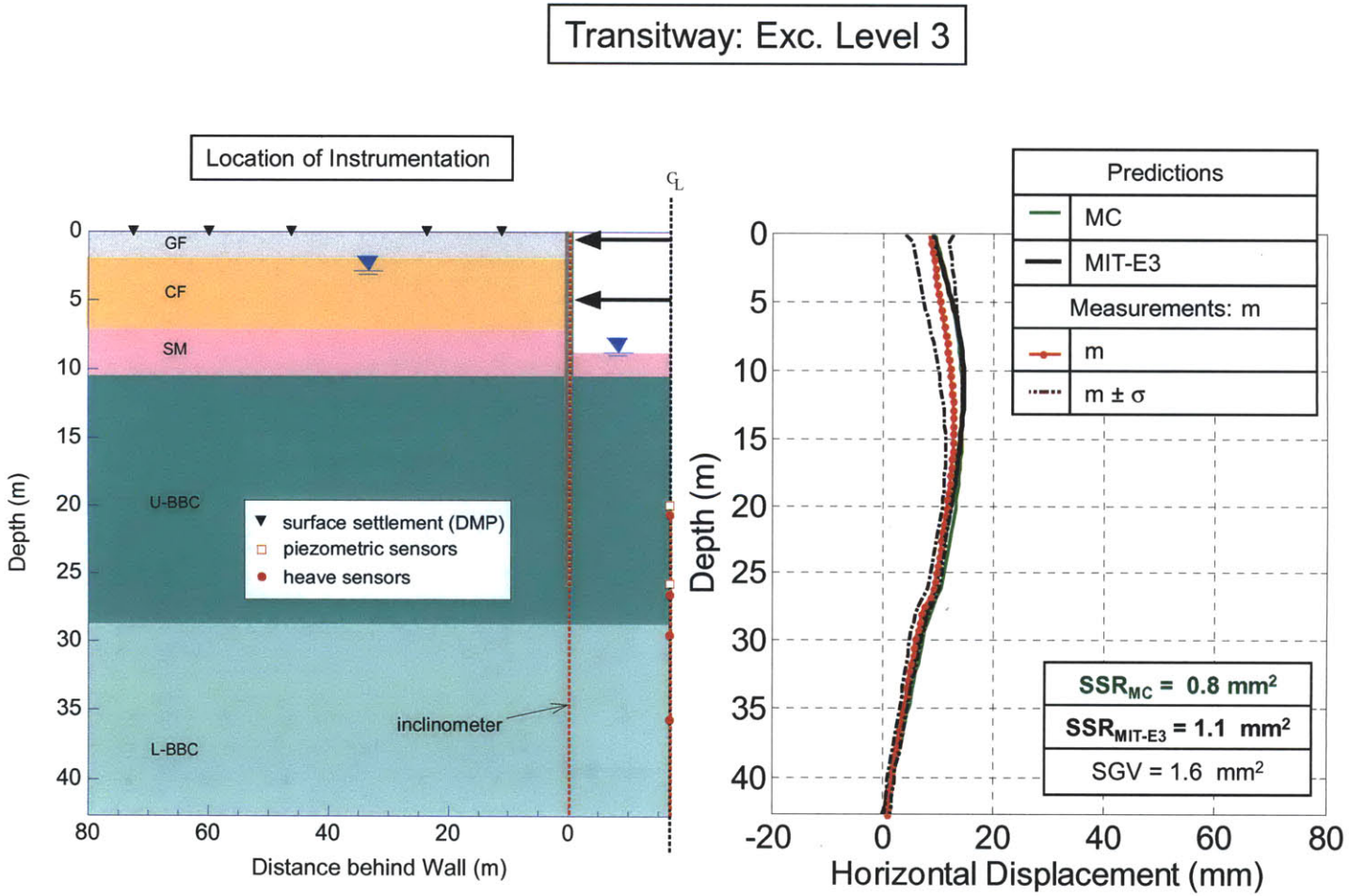

Figure 5-96: MIT-E3 and MC comparisons with measured lateral wall/soil movements at excavation level 3

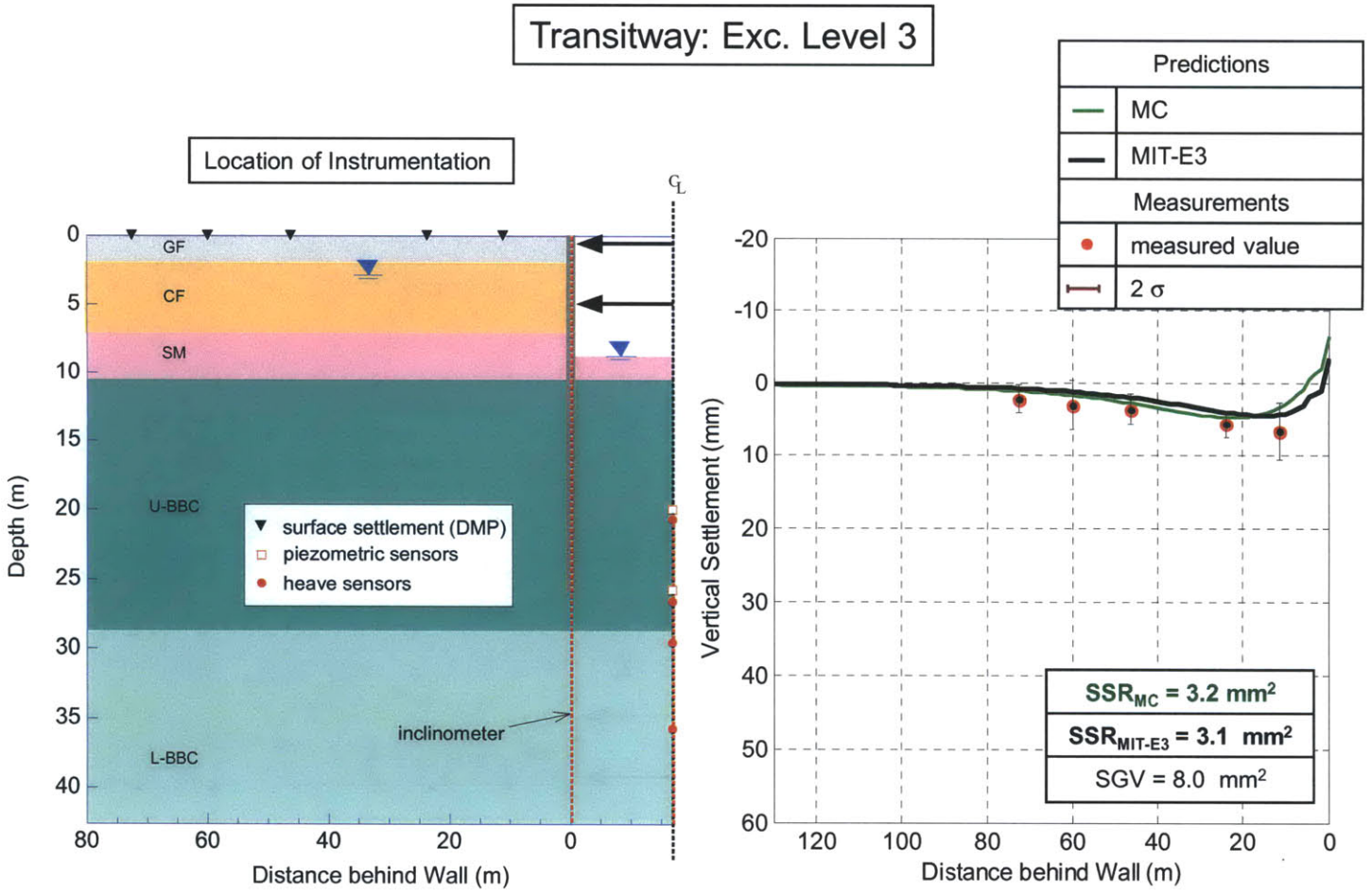

Figure 5-97: MIT-E3 and MC comparisons with measured surface settlements at excavation level 3

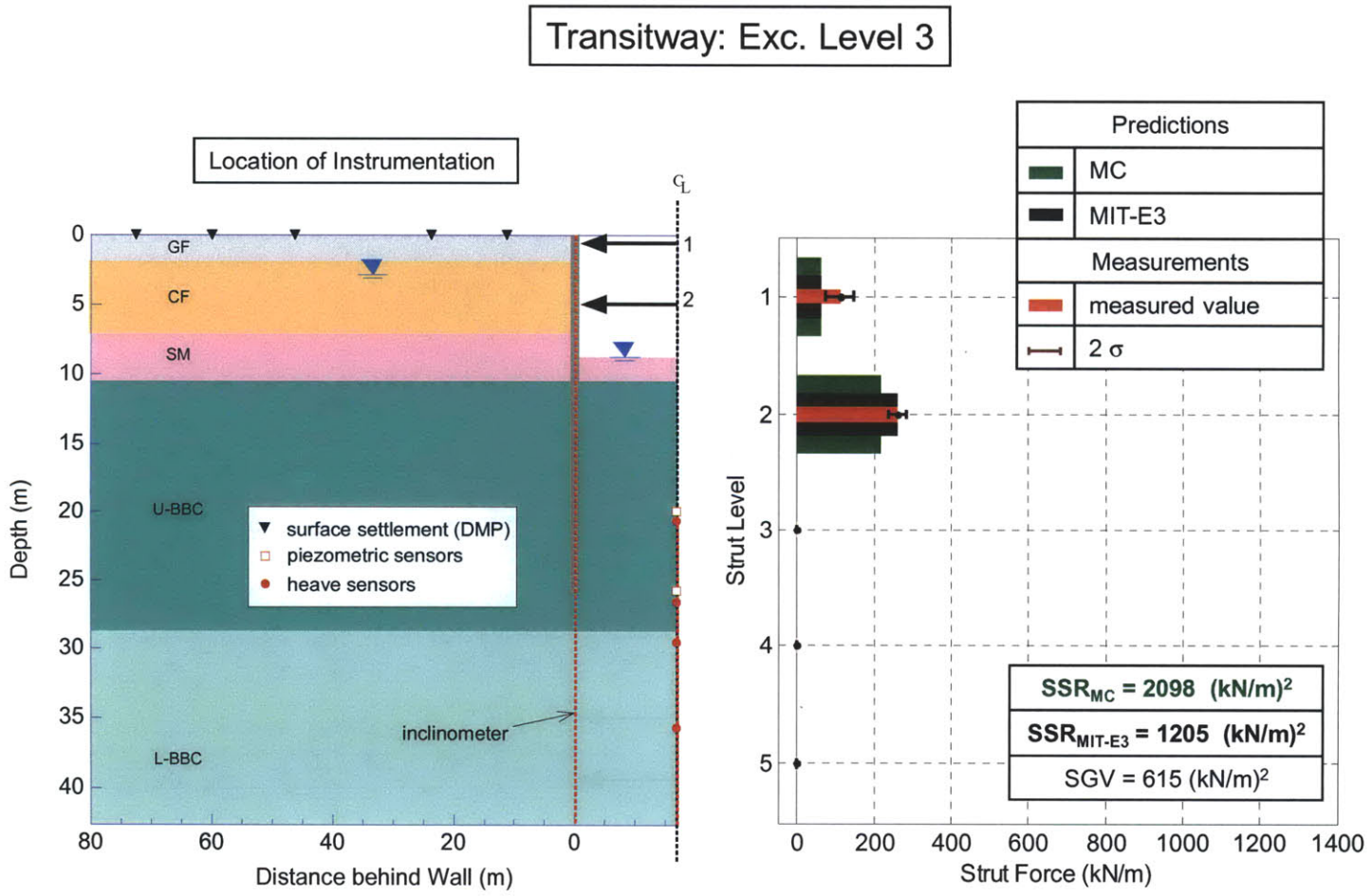

Figure 5-98: MIT-E3 and MC comparisons with measured strut forces at excavation level 3

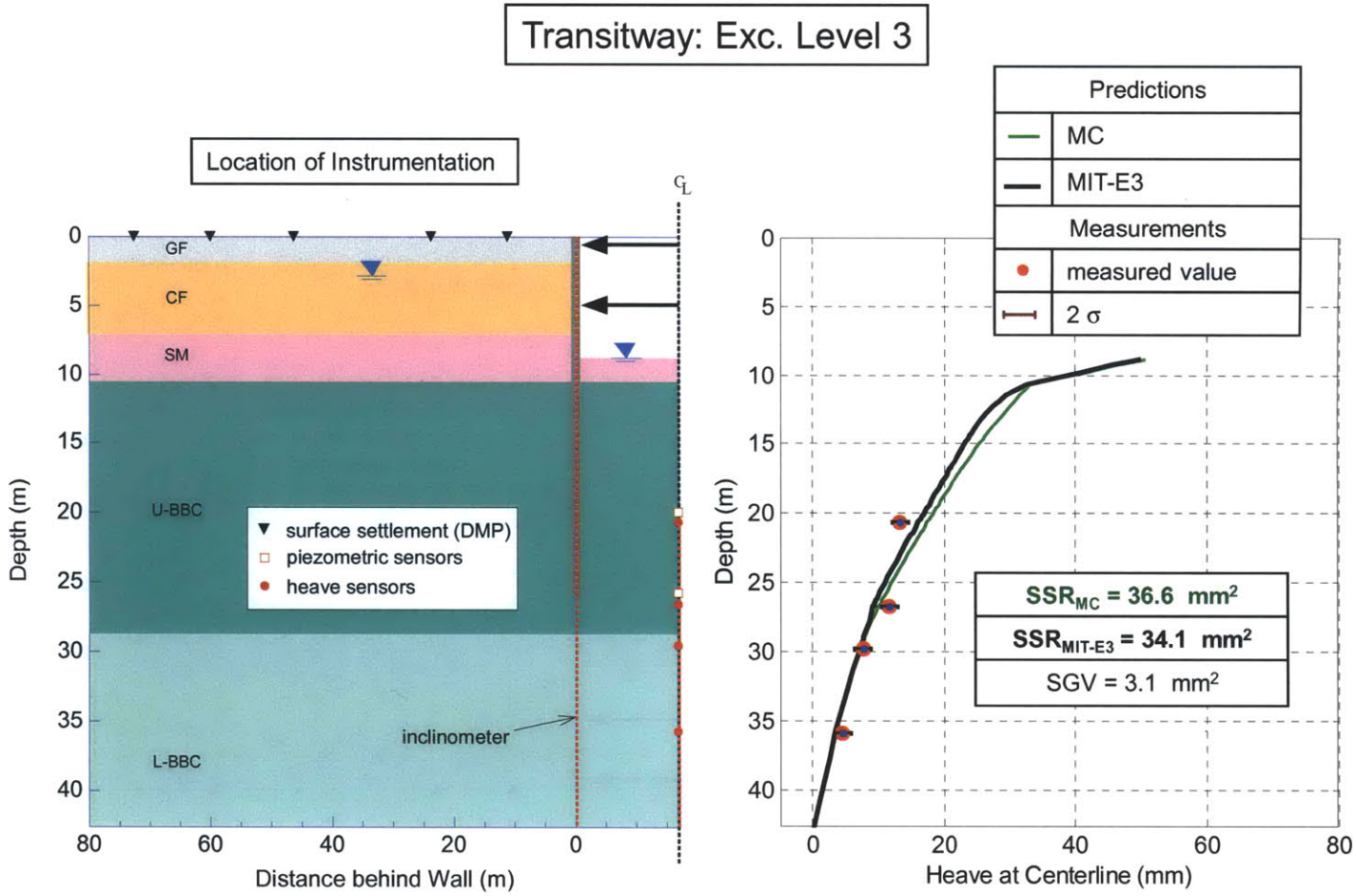

Figure 5-99: MIT-E3 and MC comparisons with measured heave at excavation level 3

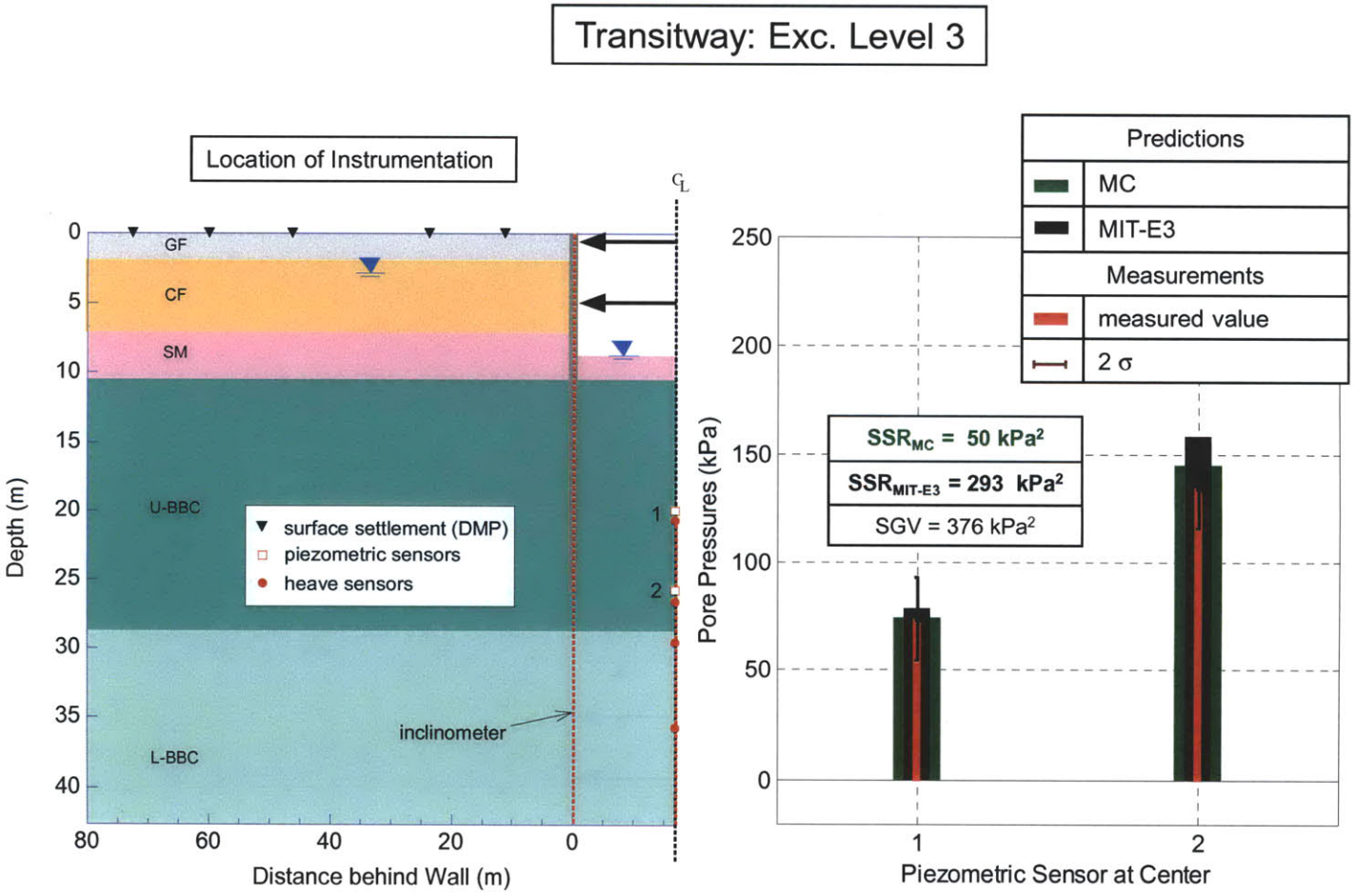

Figure 5-100: MIT-E3 and MC comparisons with measured pore pressures at excavation level 3

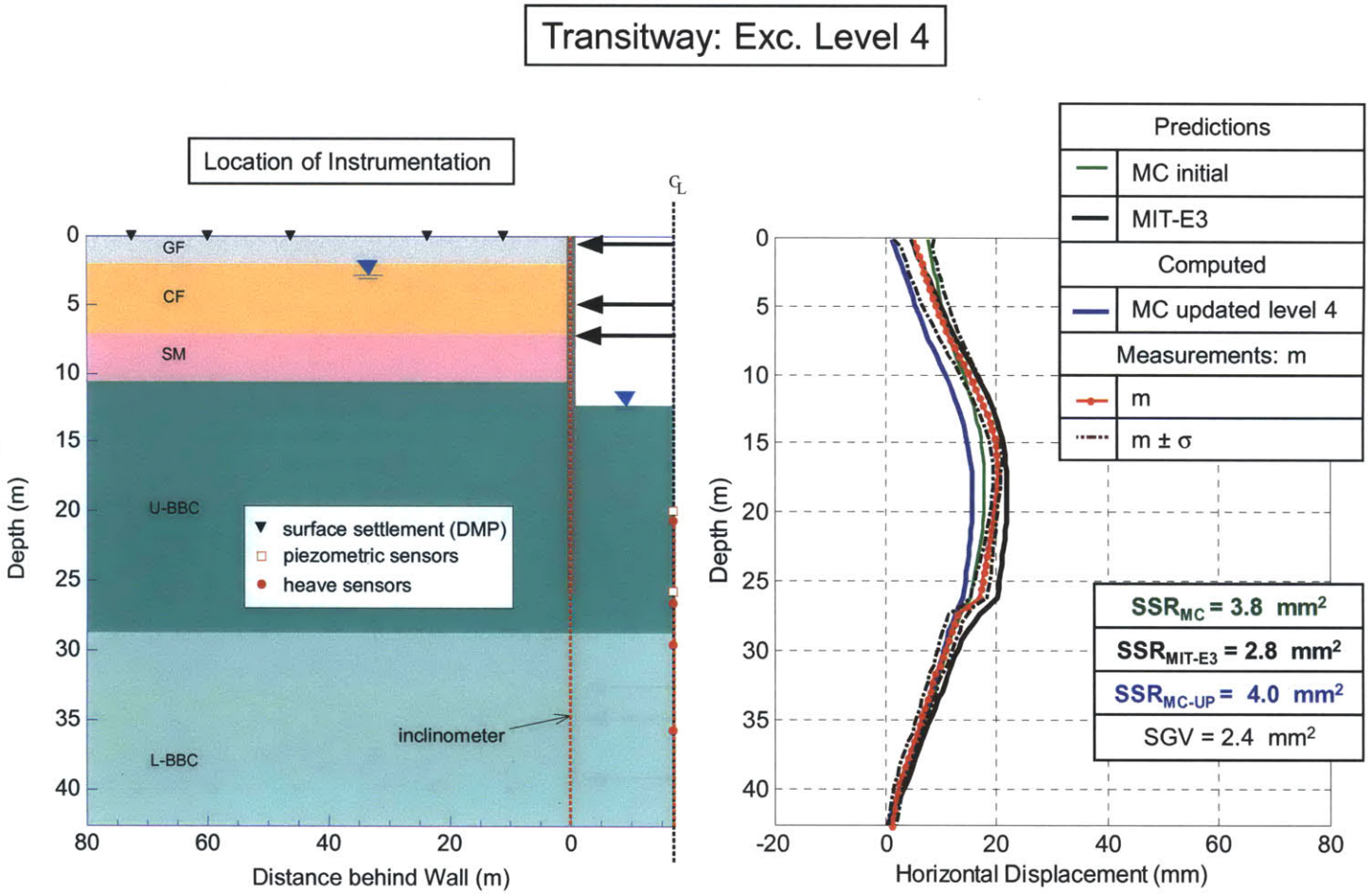

Figure 5-101: MIT-E3 and MC comparisons with measured lateral wall/soil movements at excavation level 4

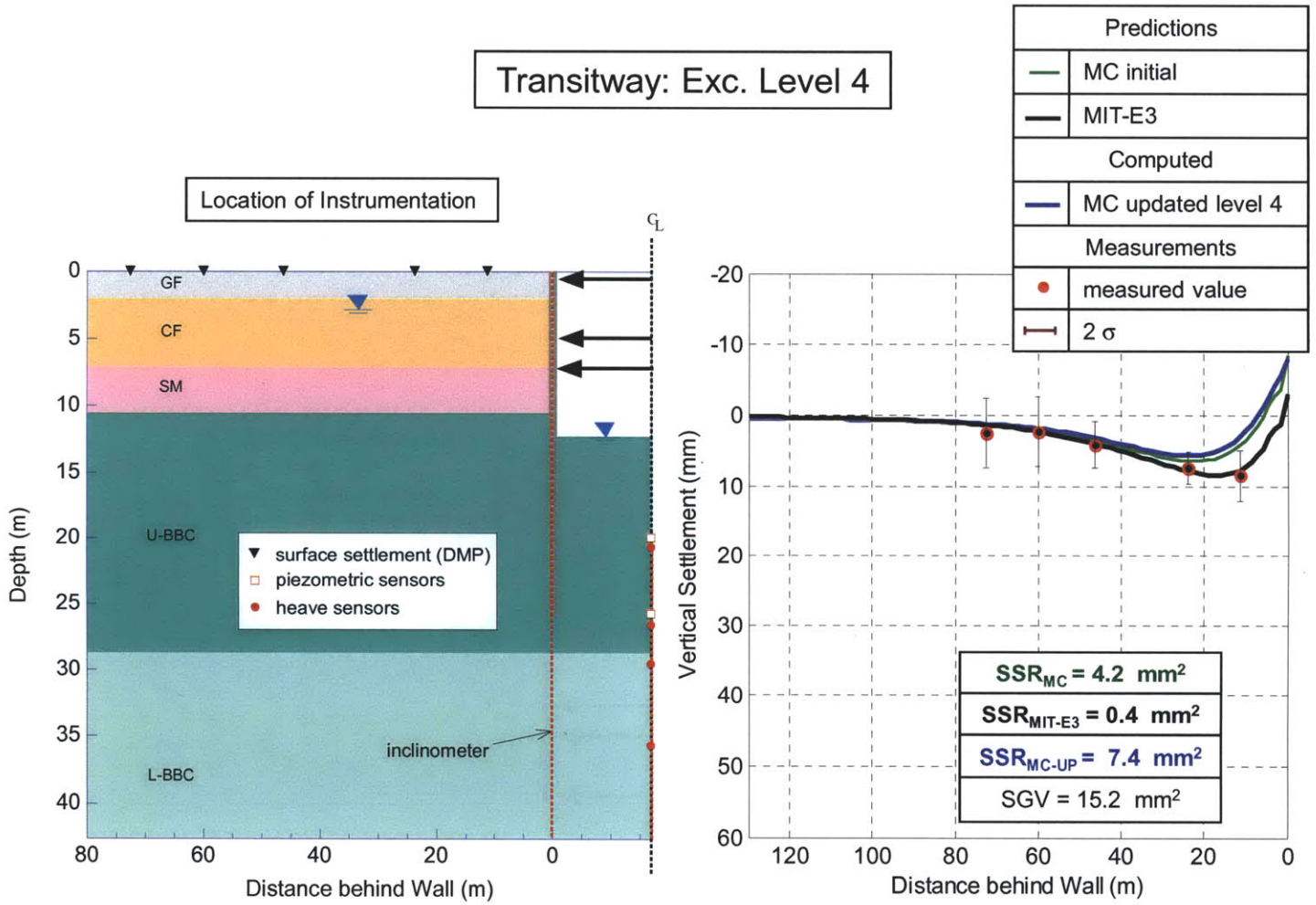

Figure 5-102: MIT-E3 and MC comparisons with measured surface settlements at excavation level 4

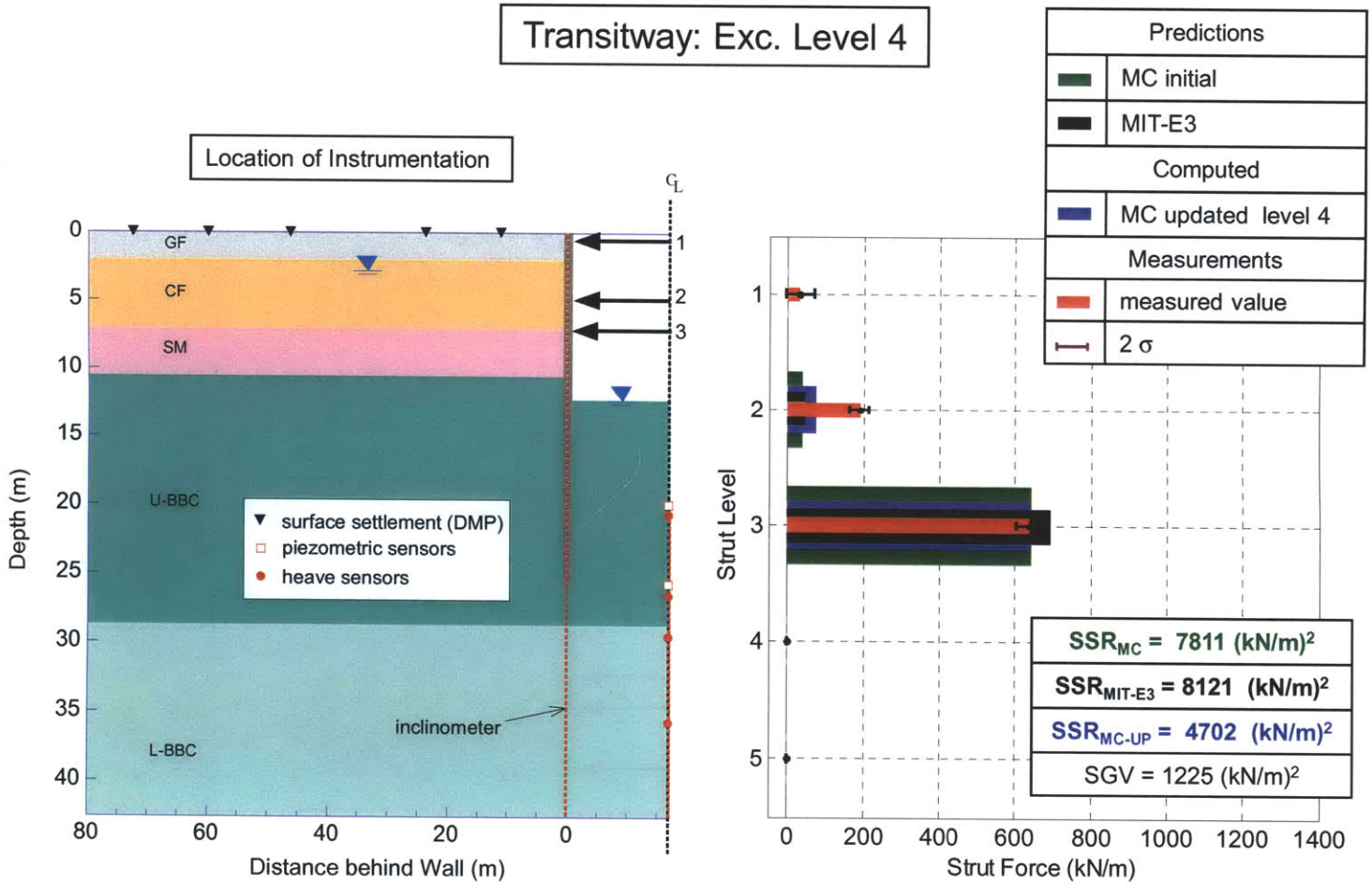

Figure 5-103: MIT-E3 and MC comparisons with measured strut forces at excavation level 4

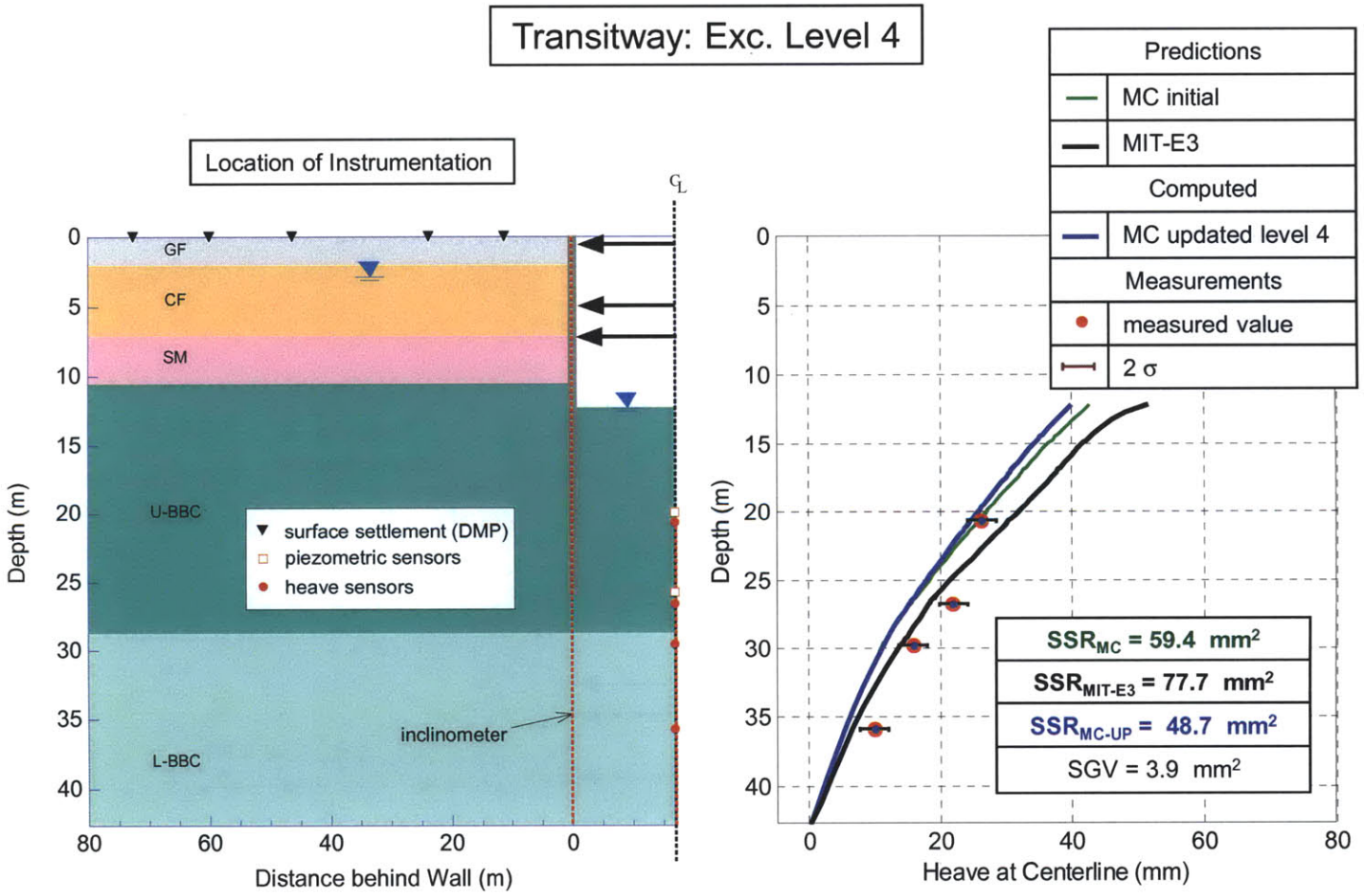

Figure 5-104: MIT-E3 and MC comparisons with measured heave at excavation level 4

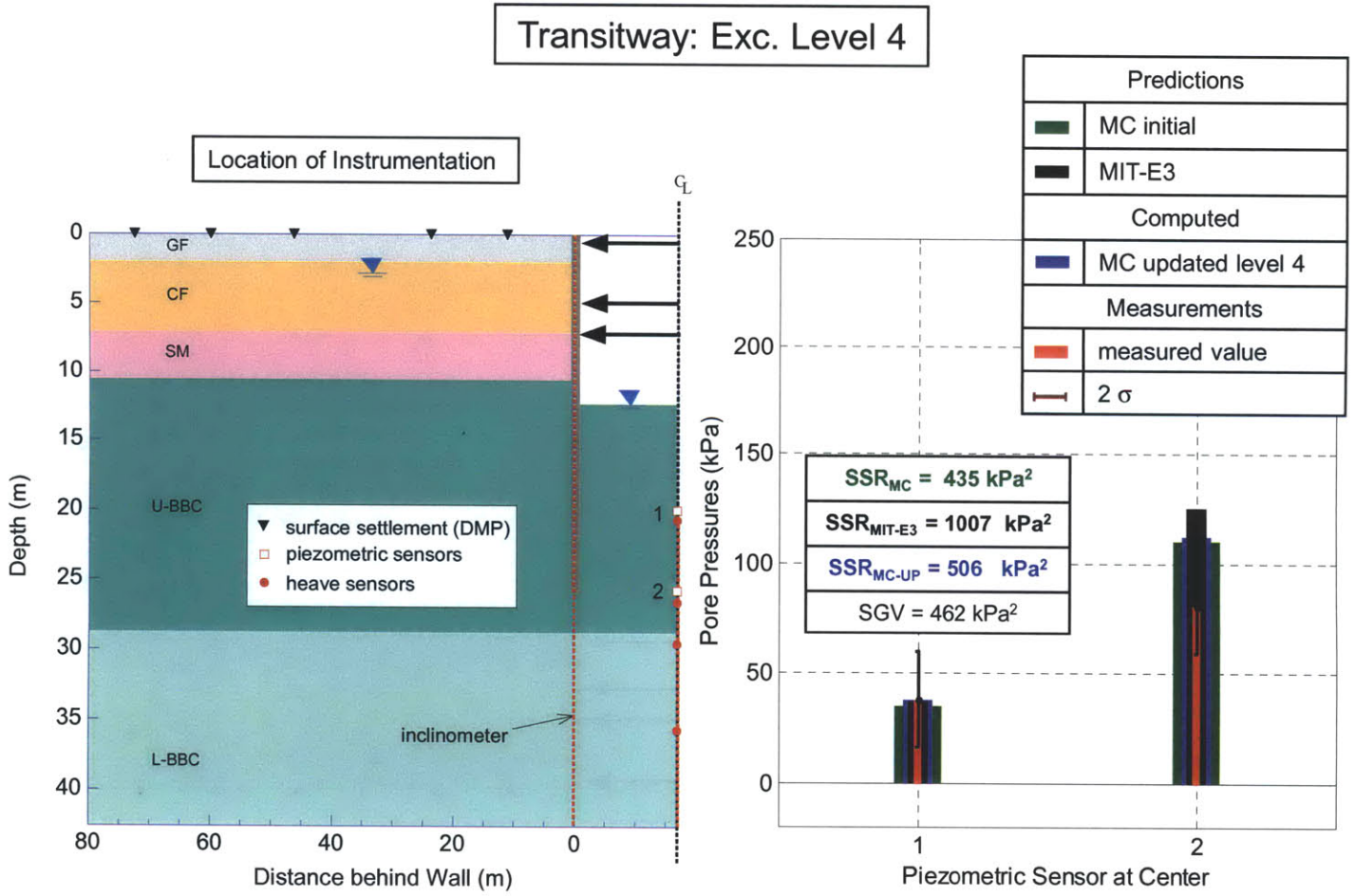

Figure 5-105: MIT-E3 and MC comparisons with measured pore pressures at excavation level 4

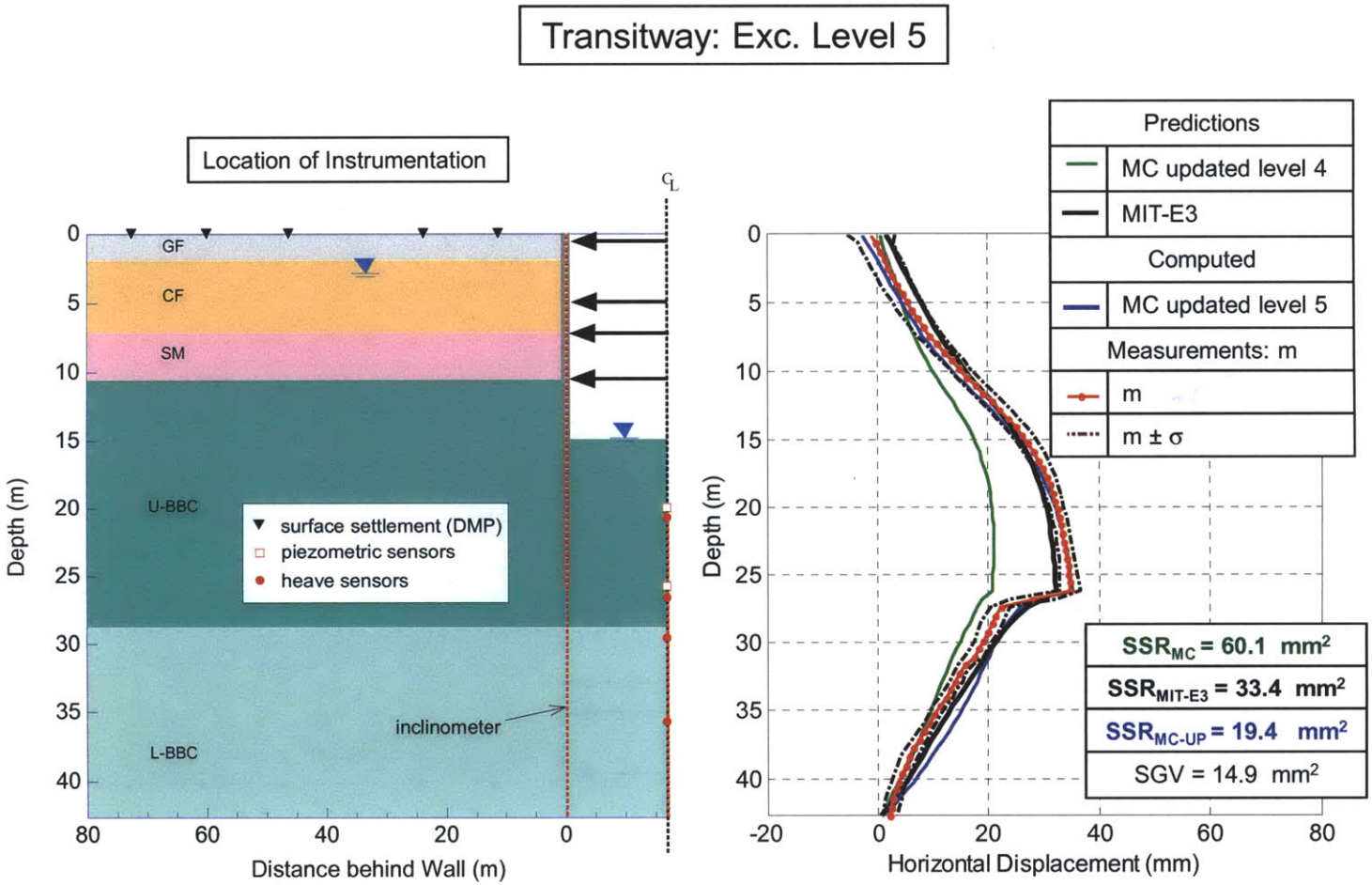

Figure 5-106: MIT-E3 and MC comparisons with measured lateral wall/soil movements at excavation level 5

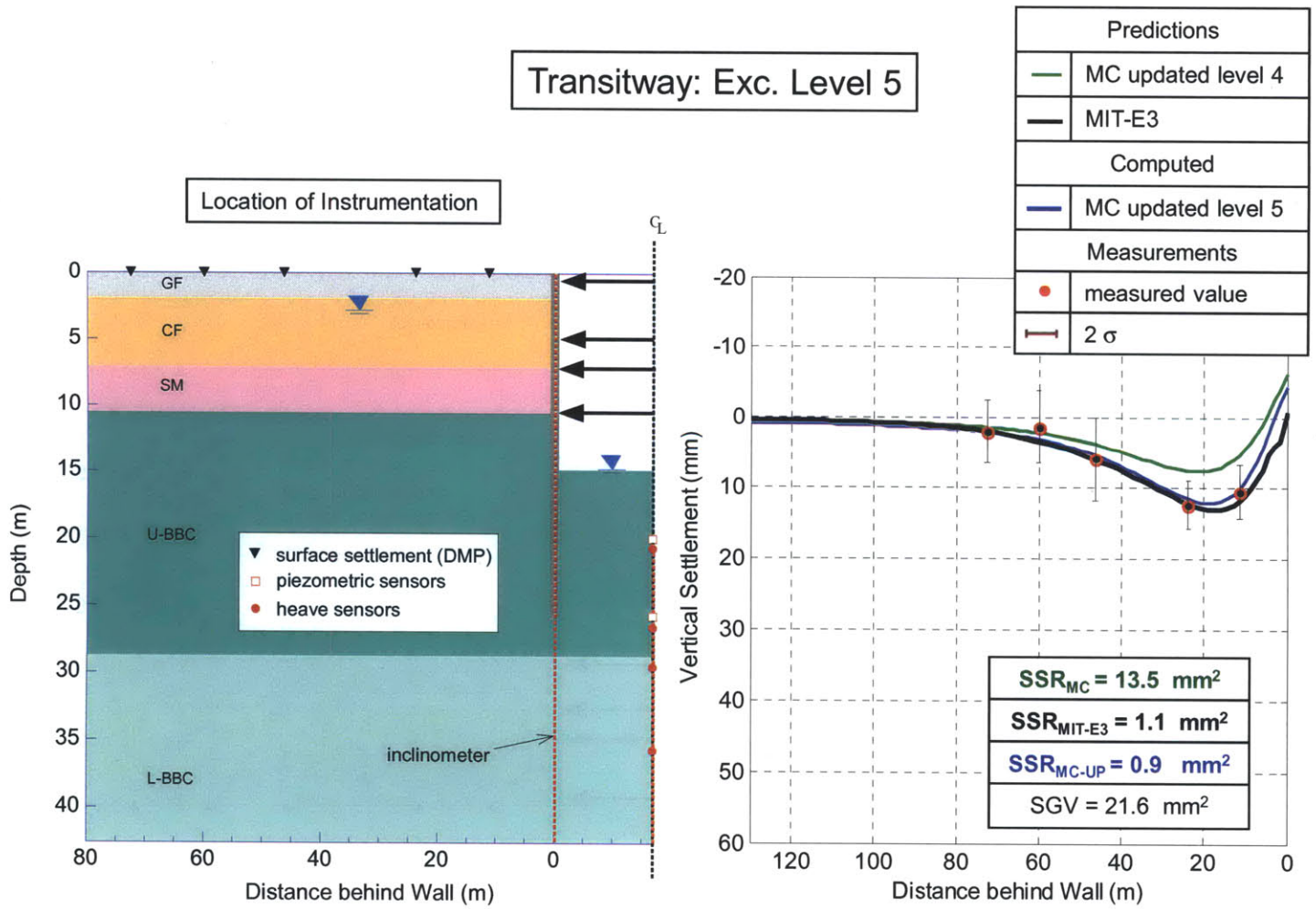

Figure 5-107: MIT-E3 and MC comparisons with measured surface settlements at excavation level 5

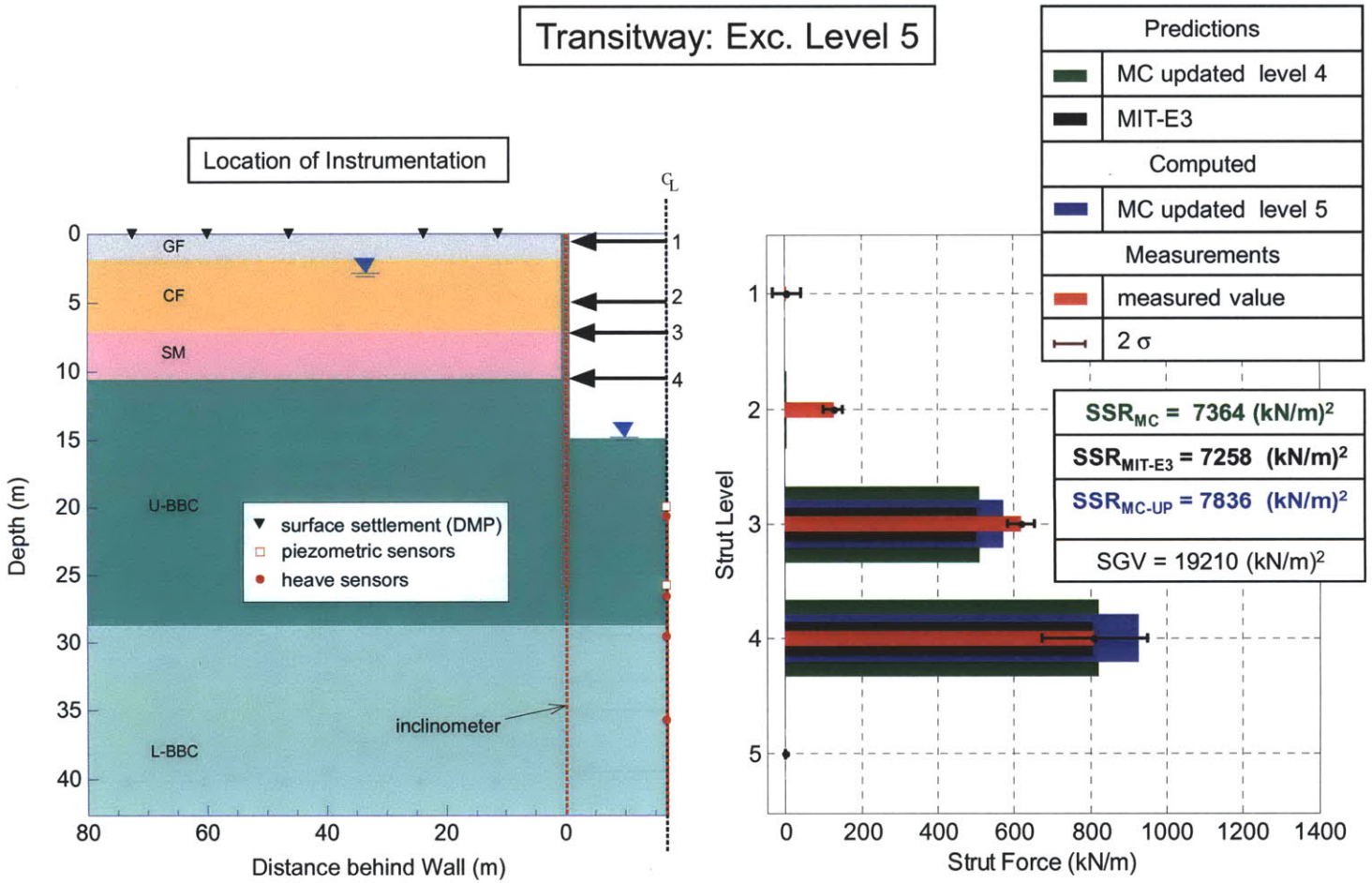

Figure 5-108: MIT-E3 and MC comparisons with measured strut forces at excavation level 5

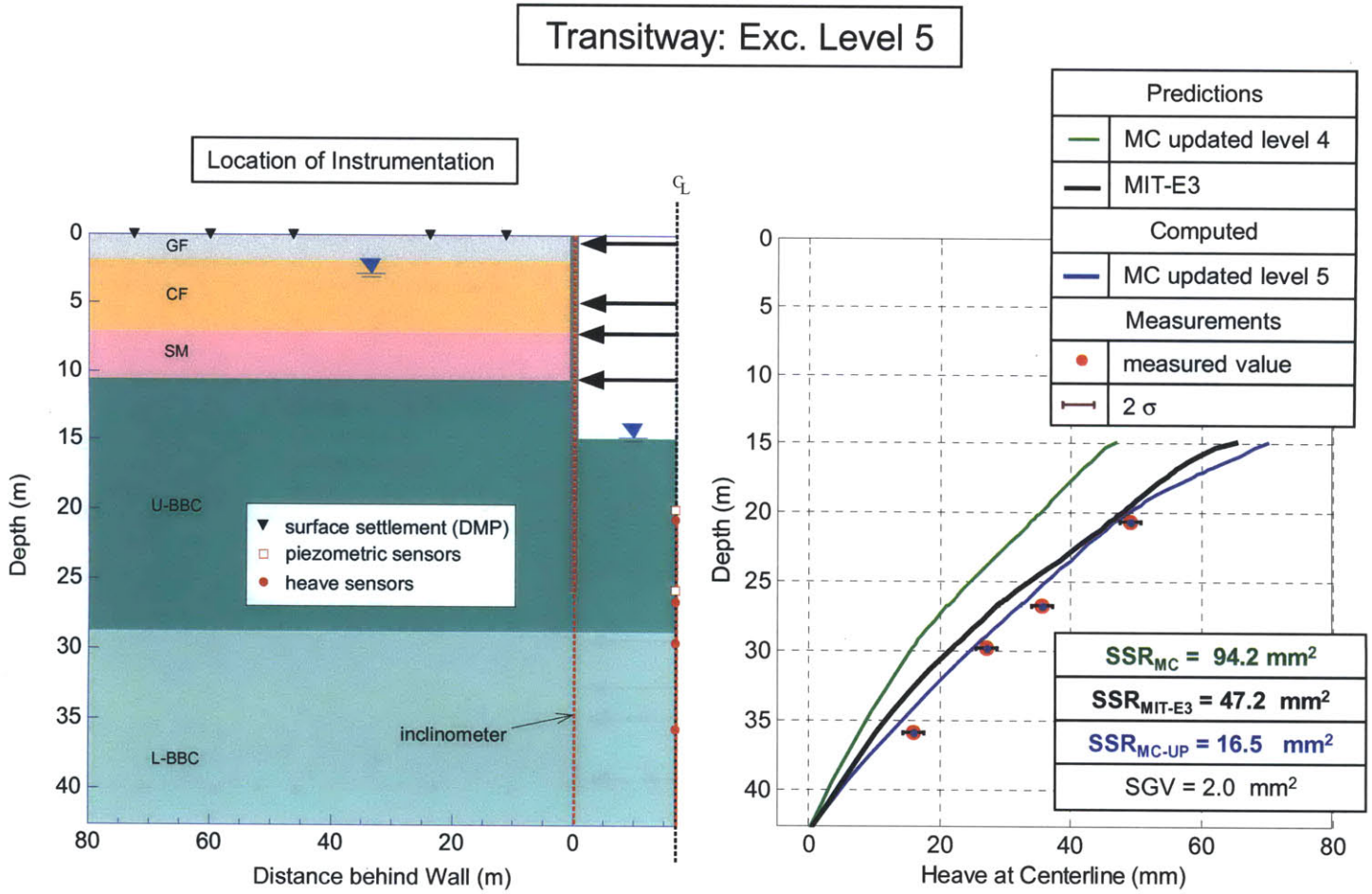

Figure 5-109: MIT-E3 and MC comparisons with measured heave at excavation level 5

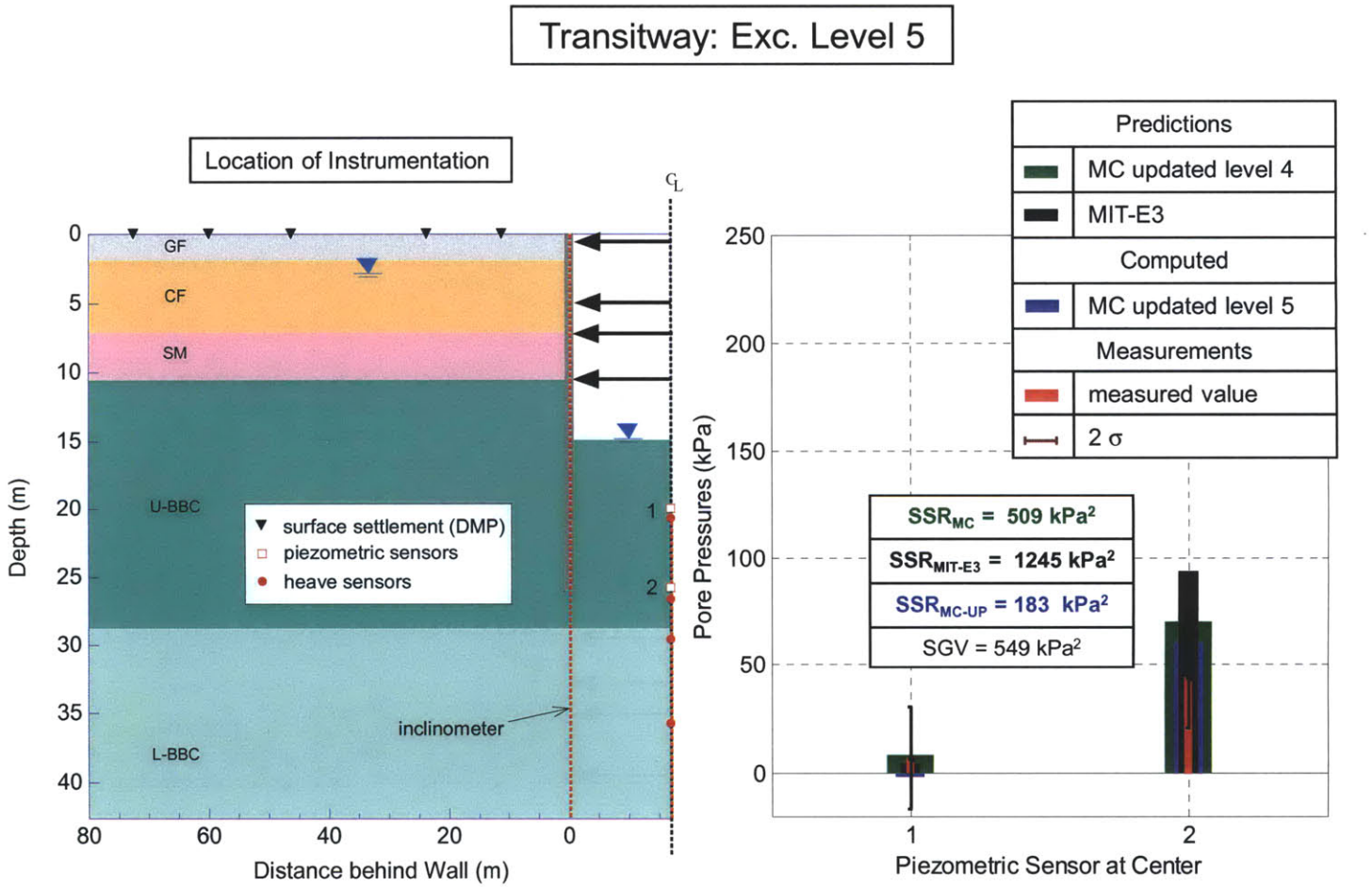

Figure 5-110: MIT-E3 and MC comparisons with measured pore pressures at excavation level 5

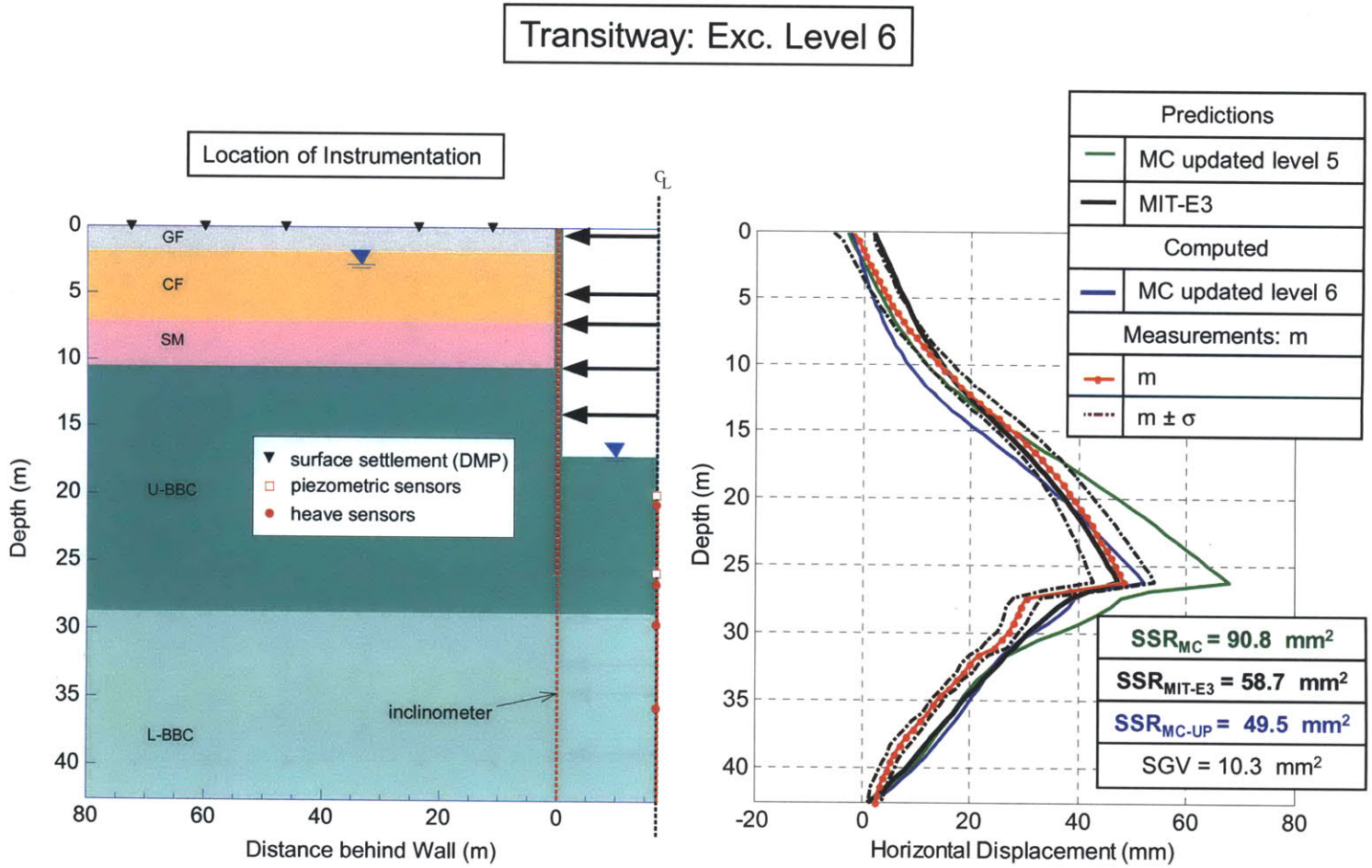

Figure 5-111: MIT-E3 and MC comparisons with measured lateral wall/soil movements at excavation level 6

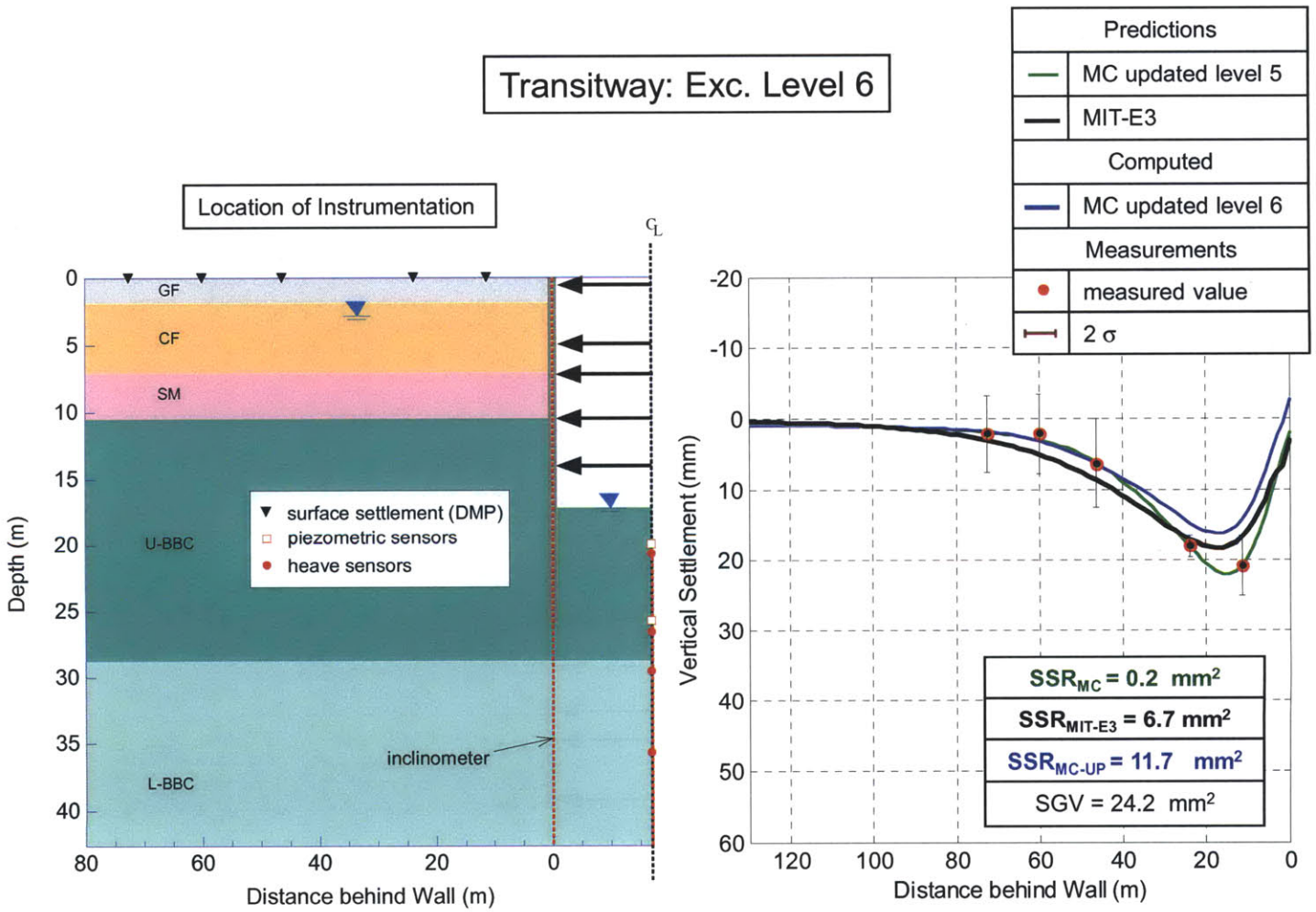

Figure 5-112: MIT-E3 and MC comparisons with measured surface settlements at excavation level 6

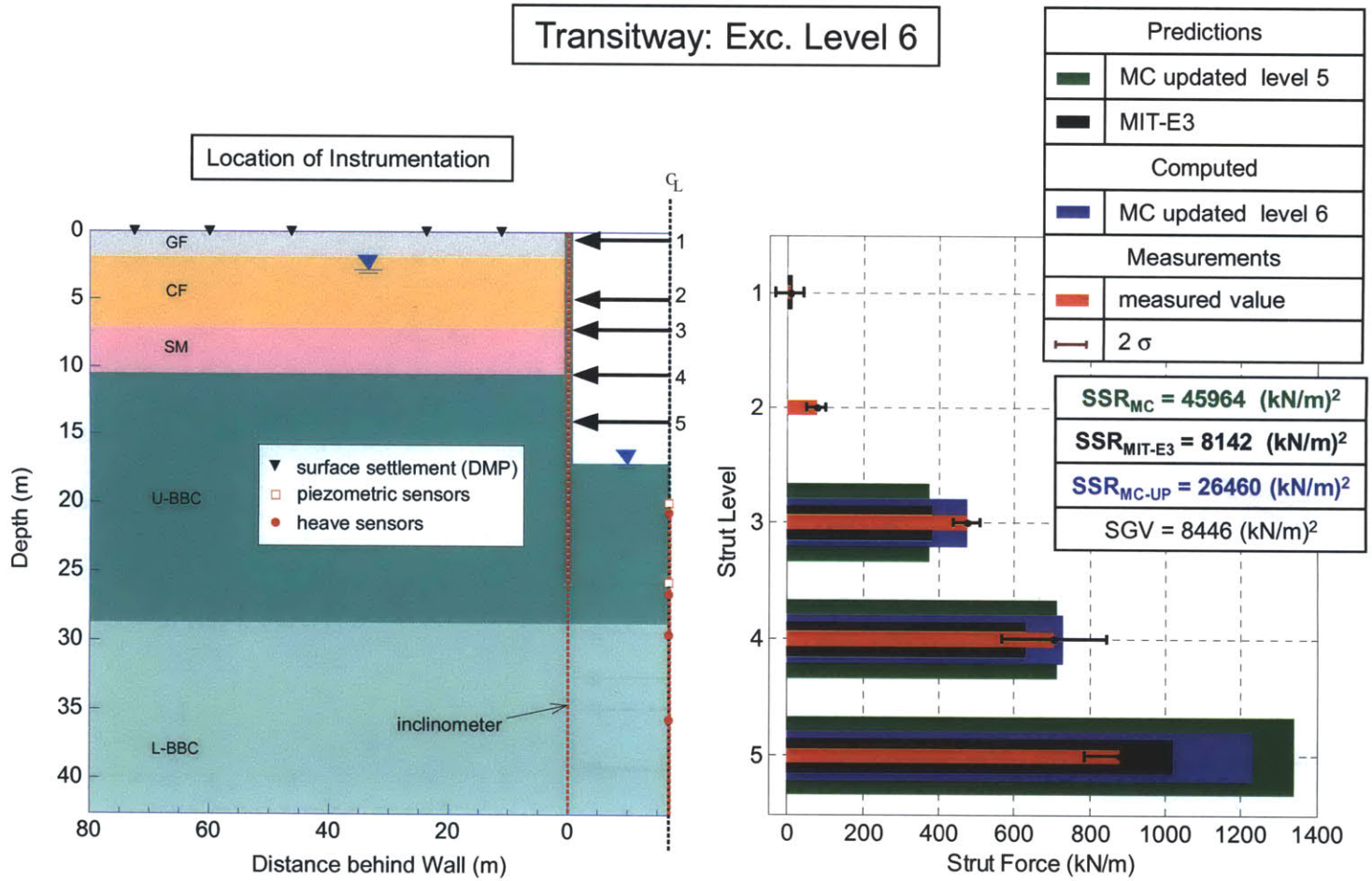

Figure 5-113: MIT-E3 and MC comparisons with measured strut forces at excavation level 6

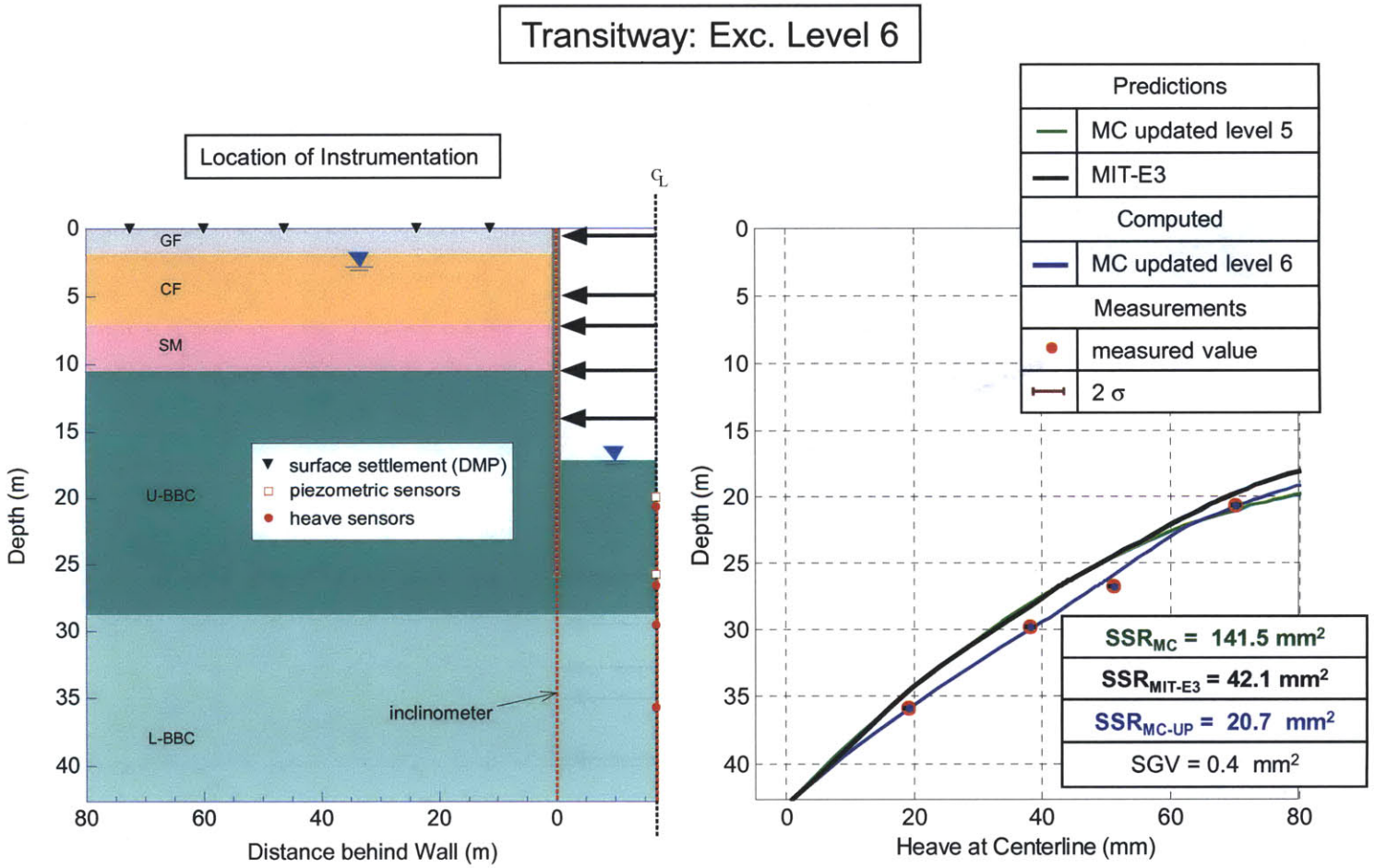

Figure 5-114: MIT-E3 and MC comparisons with measured heave at excavation level 6

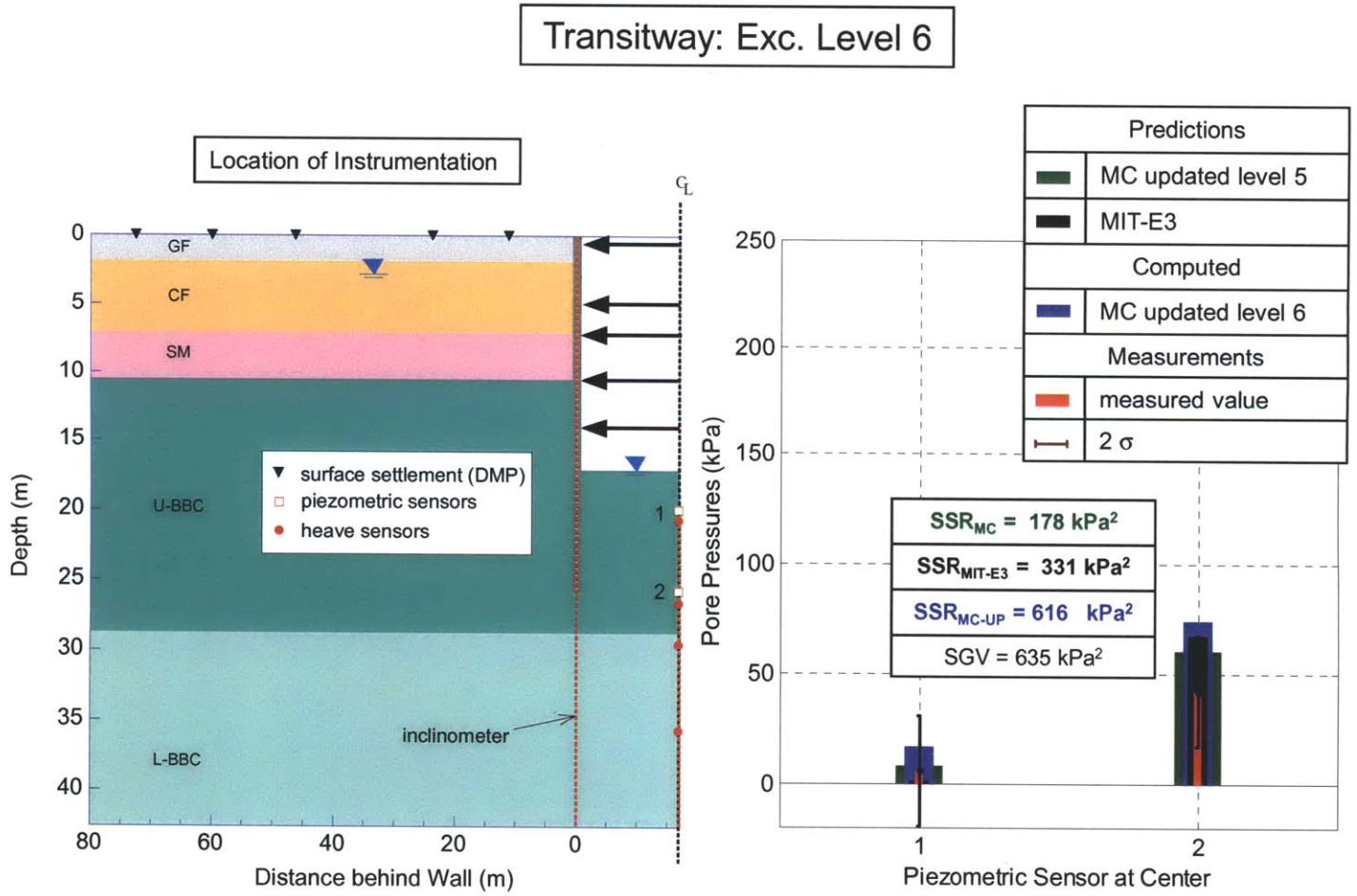

Figure 5-115: MIT-E3 and MC comparisons with measured pore pressures at excavation level 6

6 CONCLUSIONS AND FURTHER RESEARCH

6.1. Summary

The main goal of this thesis was to develop a methodology for updating FE predictions of excavation performance that can handle diverse designs, ground conditions, and sources of information during construction. This will improve the use of FE analyses by using monitoring data in an objective updating procedure. Well documented case studies play a crucial role to evaluate predictive capabilities of numerical analyses using all available site investigation data, construction records, and monitoring data.

Initially, two case studies of numerical predictions of excavation performance in Boston and Singapore have been described, in detail, in Chapter 2. These case studies are: 1) Transitway Project: Courthouse Station for South Boston Piers*, a case study that compares class A, class B, and class C predictions for a deep, wide excavation, supported by a floating diaphragm wall and five levels of pre-loaded struts. The site is underlain by a 30 m deep layer of soft-medium Boston Blue Clay; 2) Nicoll Highway collapse (Corral, 2010; Corral and Whittle, 2010), the well-documented failure of a 30m deep braced excavation in Singapore (Circle Line Phase 1) in underconsolidated marine clay is re-analyzed using data available from extensive post-failure site investigation program (including laboratory tests on high quality undisturbed samples of marine clay). Both cases studies are analyzed using an advanced effective stress soil model (MIT-E3) with parameters calibrated from laboratory tests. These cases provide a clear

* Now known as the Massachusetts Bay Transportation Authority (MBTA) Silver Line

validation of the important role of constitutive modeling for predicting the performance of braced excavations in soft clays.

Chapter 3 provides a detailed literature review on updating predictions using field measurements, varying from the Observational Method to inverse analysis of FE predictions in geotechnical problems. The description of the inverse problem was subdivided into two parts: 1) identification criteria (i.e., selection of objective function), and 2) optimization algorithms. The main focus was on inverse analyses for finite element predictions of geotechnical problems, and included a comprehensive grouping of literature published in the last 30 years. The literature review concludes that a rational methodology for updating FE predictions of excavation performance that can handle diverse designs, ground conditions, and sources of information during construction is indeed needed. This methodology should integrate at least: 1) rational sensitivity analyses; 2) error structures of field measurements; and 3) heuristic optimization methods.

A rational methodology for updating finite element predictions of excavation performance based on the maximum likelihood approach was presented in Chapter 4. This was followed by a description of the covariance matrices for field measurements and the error structures for some typical instruments used to monitor excavations. The proposed methodology uses sensitivity analyses to screen parameters that are later used in inverse analyses. In addition, a more detailed framework for using the updating approach in the project management through integration with alert or trigger criteria is presented.

To validate and evaluate the proposed methodology for updating FE predictions of excavation performance, 2-D analyses of the platform section of the Courthouse Station (Transitway project; Section 2.2) were used. The finite element model and the identification of Essential Improvement Parameters, EIP's, at each stage of construction through sensitivity analyses were described. Also full details were given of the inverse analyses and updating of parameters. The numerical analyses used simplified (MC) constitutive models. Comparisons of these results with predictions using a more complex soil model (MIT-E3) were carried out. The results show consistent improvements in the updating of computed performance, but also highlight inconsistencies obtained among difficult types of measured parameters. These are attributed, in part, to limitations in the MC soil model.

6.2. Conclusions

A rational methodology for updating FE predictions of excavation performance that can handle diverse designs, ground conditions, and sources of information during construction has been developed and validated through a unique case study. This methodology integrates three main components: (1) sensitivity analyses; (2) error structures of field measurements (maximum likelihood approach); and (3) heuristic optimization methods (genetic algorithms). Since there is no such methodology available up-to-date, the proposed methodology plays a very important contribution in improving the used of FE analyses in geotechnical engineering, specifically, in soil-structure interaction problems. Additionally, a detailed framework for using the updating approach in the project management through integration with alert or trigger criteria has been proposed.

From the application of the case study (Transitway project), the following conclusions can be drawn:

1. A powerful tool to quantify agreements between predictions and field measurements has been proposed. This is based on comparisons of SSR and SGV scalar values.
2. The rational methodology for updating FE predictions has been proved to be robust and efficient. In fact, with a very simple constitutive law (MC model), very good predictions can be obtained with individual measurement types. The calculated improvement ratios demonstrate important individual improvements.
3. The results show the effectiveness of the proposed updating procedure, but also highlight the challenge of updating predictions using simplified models of soil behavior. The application of this case study shows that the pore pressures at the centerline of the excavation are in general controlled by boundary conditions rather than model parameters.
4. The MIT-E3 analyses demonstrate more consistency in predictions of the measured performance (for all excavation levels of wall/soil deflections, surface settlements, excavation heave, and strut forces), and confirm the value of using more advanced constitutive models calibrated using high quality laboratory tests, achieving comparable results with MC (after updating).
5. The proposed methodology provides: (1) increase in safety (safer predictions); (2) possibility of the application of the observational method (vary design as needed); (3) control of construction schedules (avoid additional fines); and (4) decrease construction costs in cases when the original design can be modified to a less expensive option.

6.3. Further Research

Based on the summary and conclusions, the following research paths are proposed:

1. An application of the detailed framework for using the updating approach in the project management through integration with trigger criteria (see Chapter 4) in an actual, real-time project.
2. An application of the same case study with other constitutive soil models to investigate consistency of archival and predicted results.
3. An application of other case studies to re-validate the proposed methodology.
4. An application of the proposed methodology for a 3-D modeling of excavation support system.

6.4 References

Corral, G. (2010). "Re-analysis of Deep Excavation Collapse Using Generalized Effective Stress Soil Model." *CE Thesis, Department of Civil and Environmental Engineering, Cambridge, MIT*. 138p.

Orazalin, Z. (2010). "Three-Dimensional Finite Element Analysis of a Complex Excavation on the MIT Campus." *S.M. Thesis, Department of Civil and Environmental Engineering, Cambridge, MIT*. 143p.

Whittle, A.J. (1987) "A Constitutive Model for Overconsolidated Clays with Application to the Cyclic Loading". *Sc.D Thesis. Department of Civil and Environmental Engineering, Cambridge, MIT*. 641p.

Whittle, A.J., Hashash, Y.M.A., and Whitman, R. (1993). "Analysis of Deep Excavation in Boston." *ASCE Journal of Geotechnical Engineering* 119(1): 69-90.

Whittle, A.J. and Kavvadas, M.J. (1994). "Formulation of MIT-E3 Constitutive Model for Overconsolidated Clays." *ASCE Journal of Geotechnical Engineering* 120(1): 173-198.

A. SENSITIVITY ANALYSES ON UNCERTAIN PARAMETERS FOR TRANSITWAY PROJECT

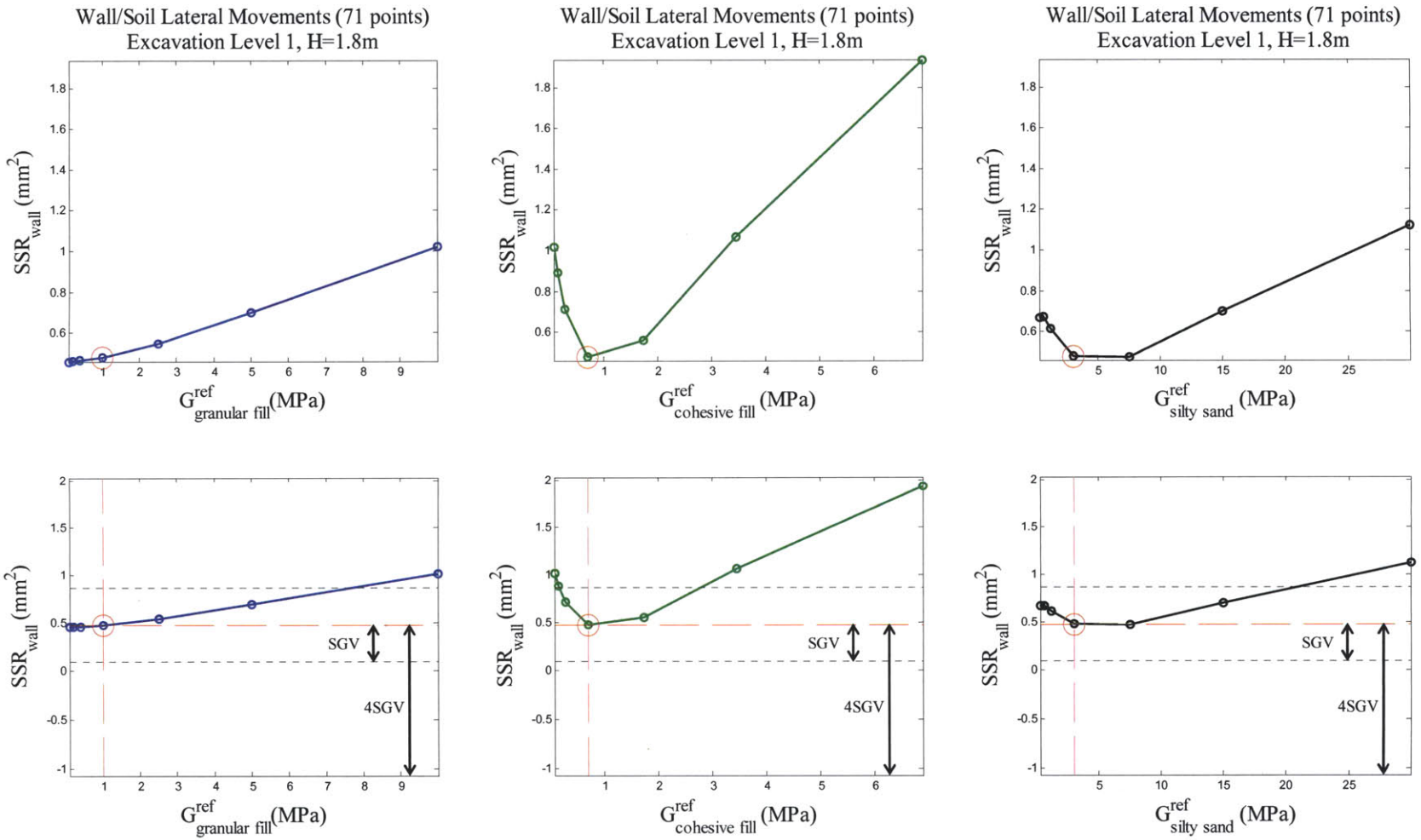

Figure A- 1: Sensitivity analysis of shear stiffness of granular fill, cohesive fill, and silty sand layers on lateral wall/soil movements at excavation level 1

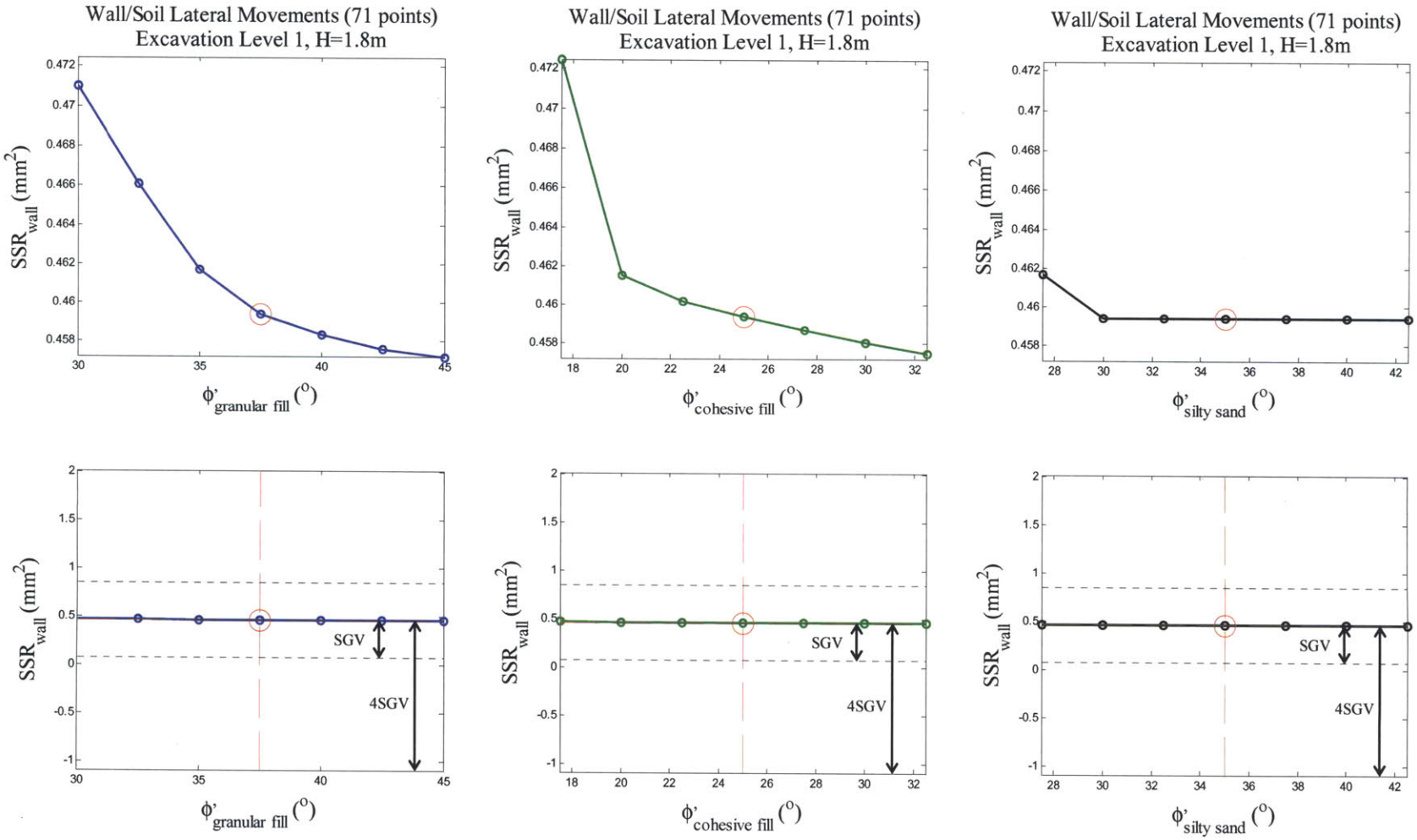

Figure A- 2: Sensitivity analysis of friction angles of granular fill, cohesive fill, and silty sand layers on lateral wall/soil movements at excavation level 1

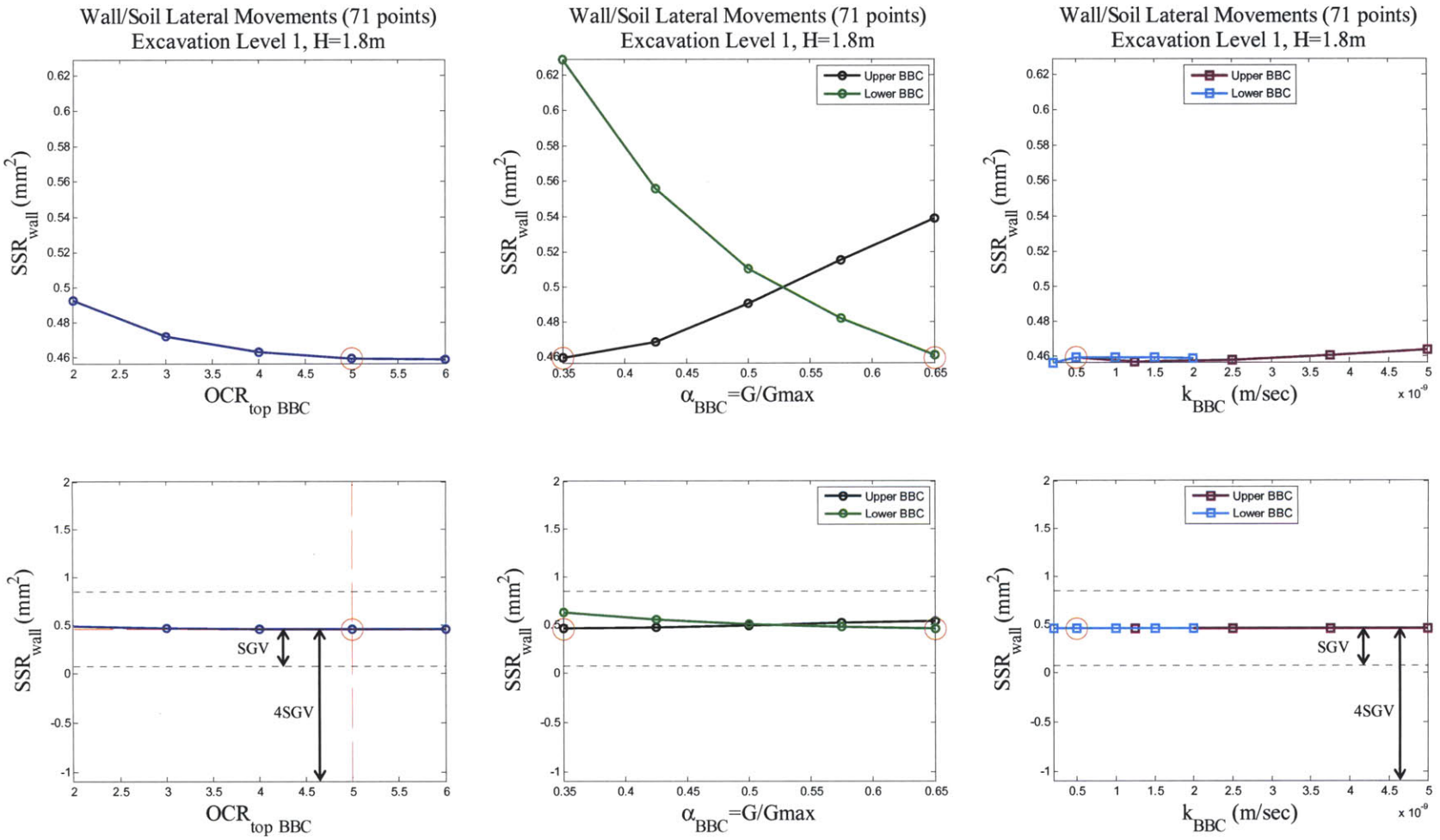

Figure A- 3: Sensitivity analysis of OCR (top), α parameter, and hydraulic conductivities of BBC layers on lateral wall/soil movements at excavation level 1

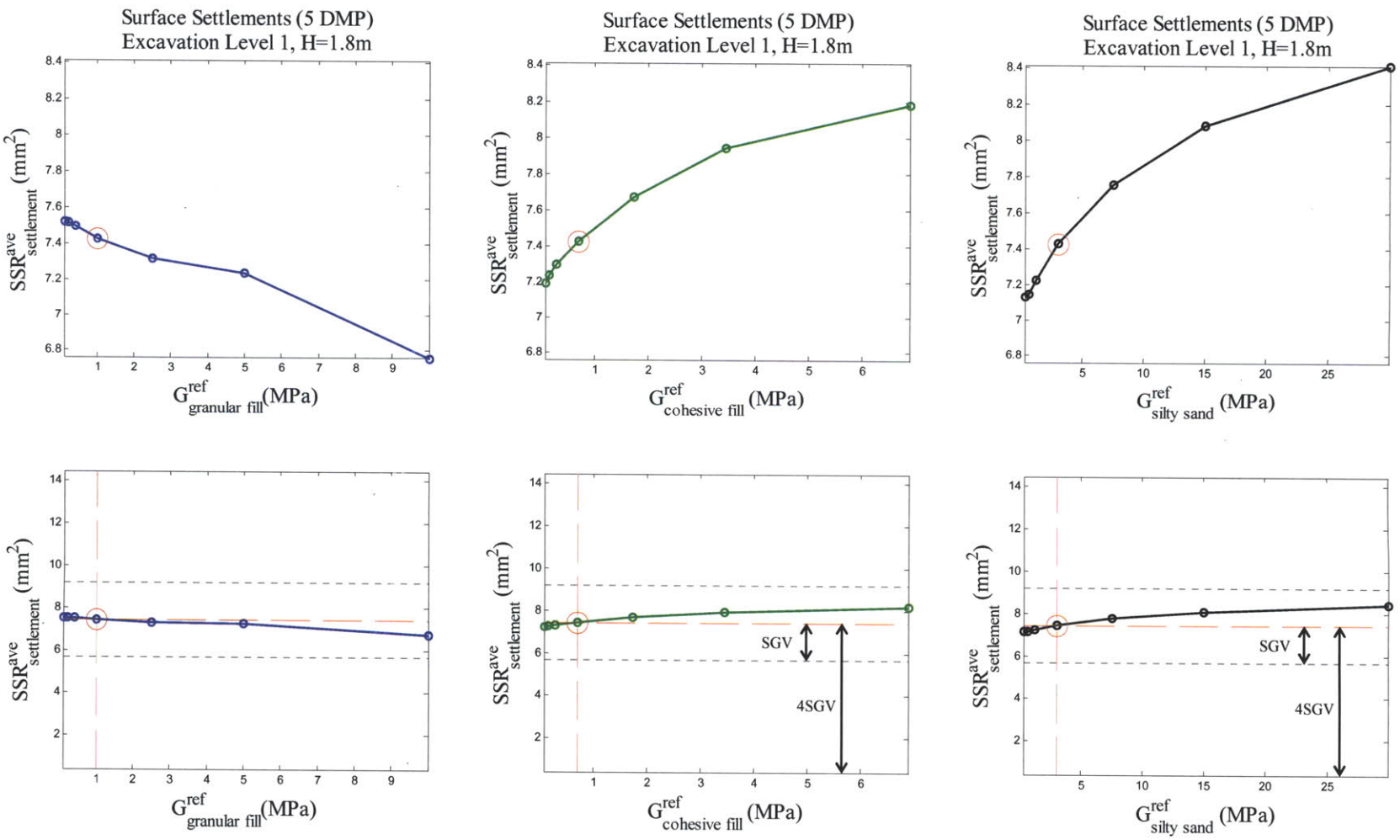

Figure A- 4: Sensitivity analysis of shear stiffness of granular fill, cohesive fill, and silty sand layers on surface settlement at excavation level 1

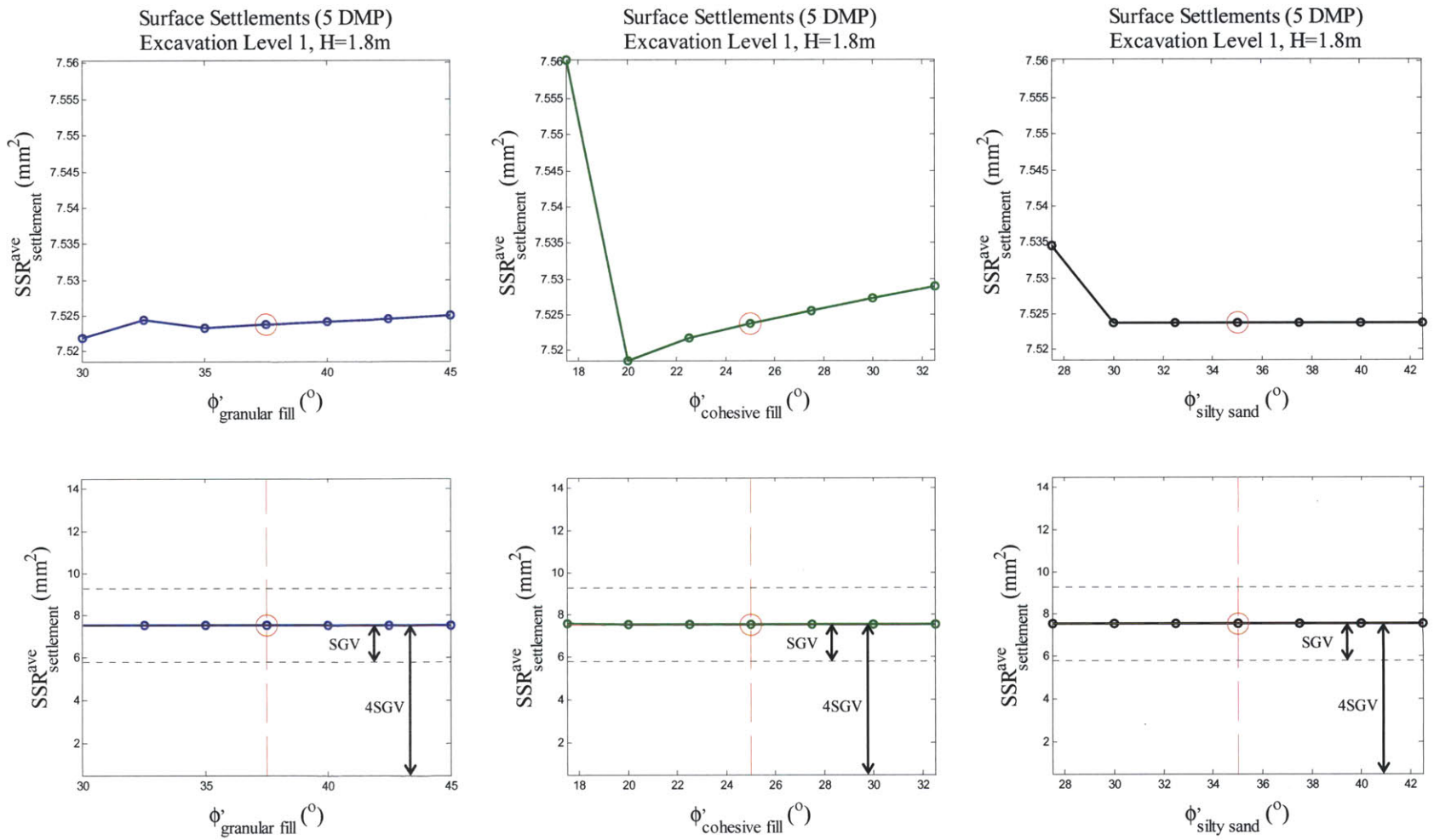

Figure A- 5: Sensitivity analysis of friction angles of granular fill, cohesive fill, and silty sand layers on surface settlement at excavation level 1

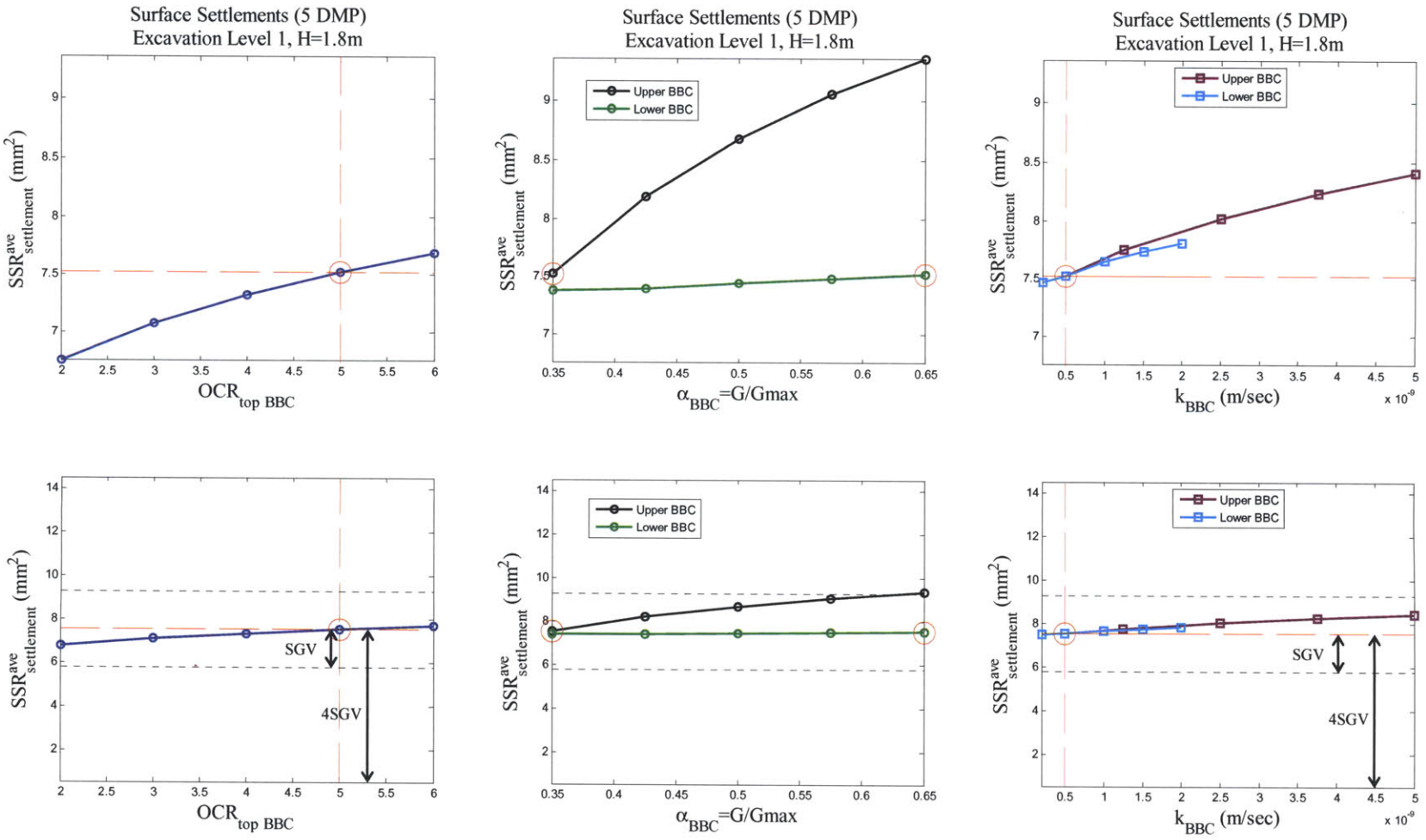

Figure A- 6: Sensitivity analysis of OCR (top), α parameter, and hydraulic conductivities of BBC layers on surface settlement at excavation level 1

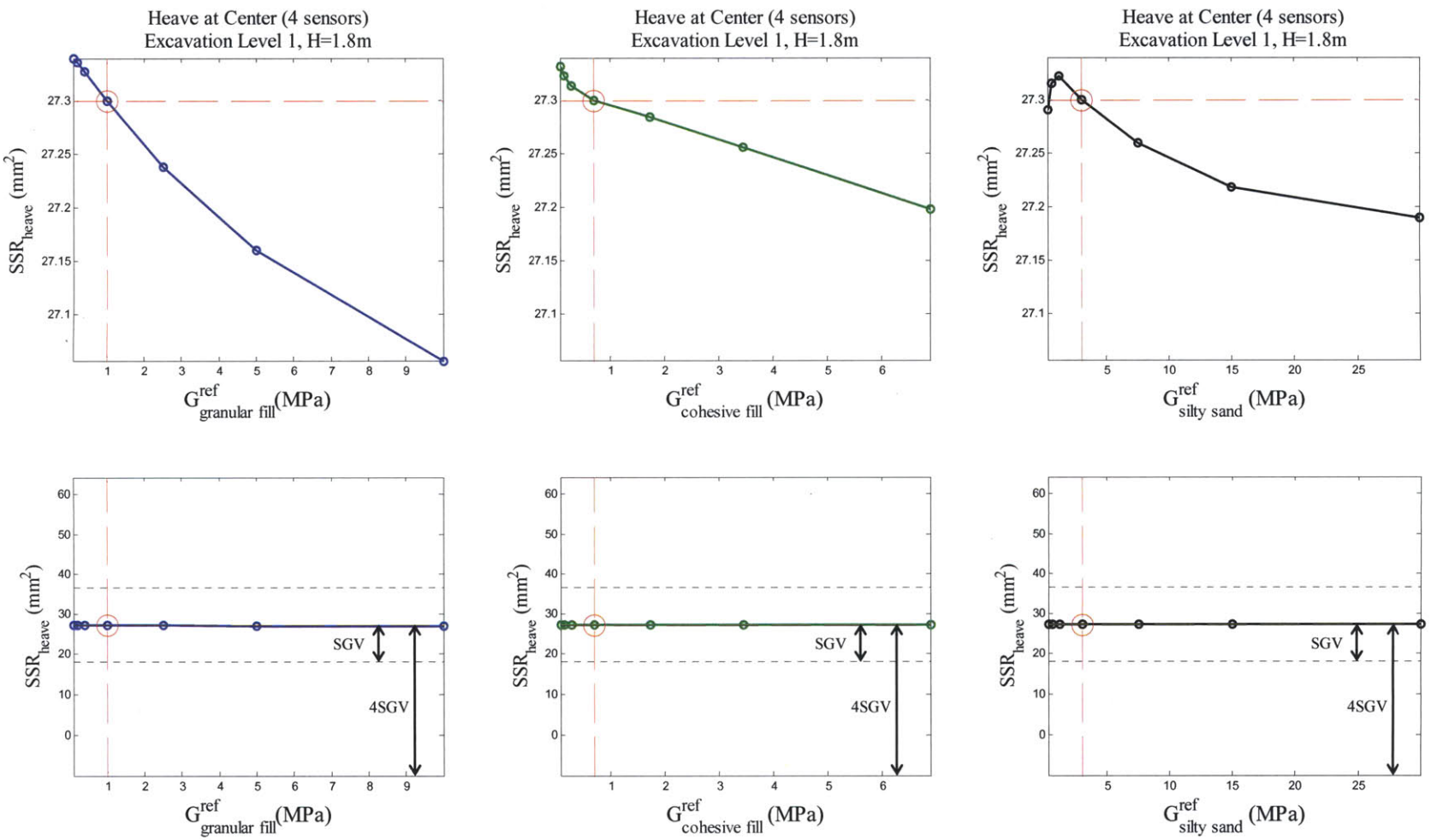

Figure A- 7: Sensitivity analysis of shear stiffness of granular fill, cohesive fill, and silty sand layers on excavation heave at excavation level 1

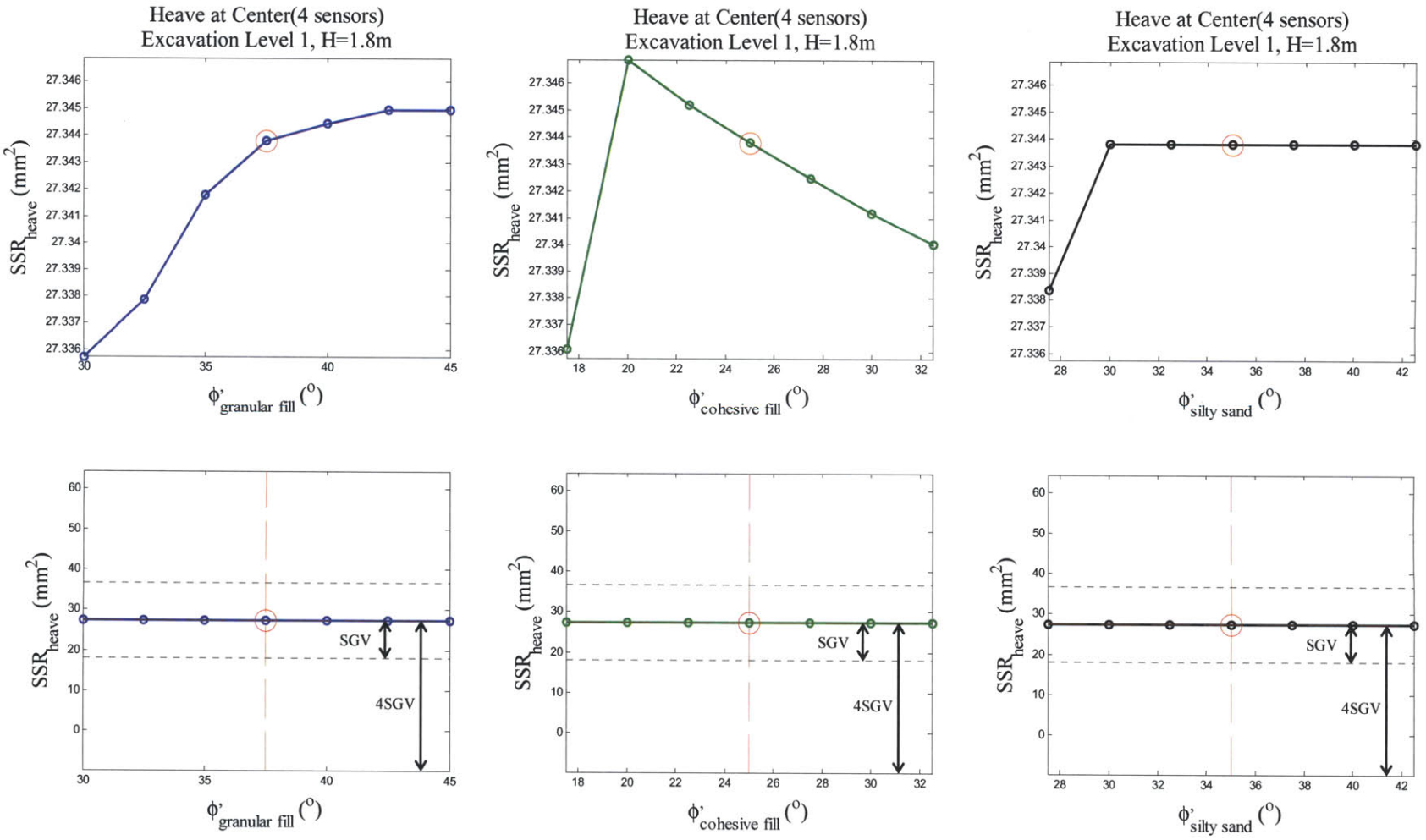

Figure A- 8: Sensitivity analysis of friction angles of granular fill, cohesive fill, and silty sand layers on excavation heave at excavation level 1

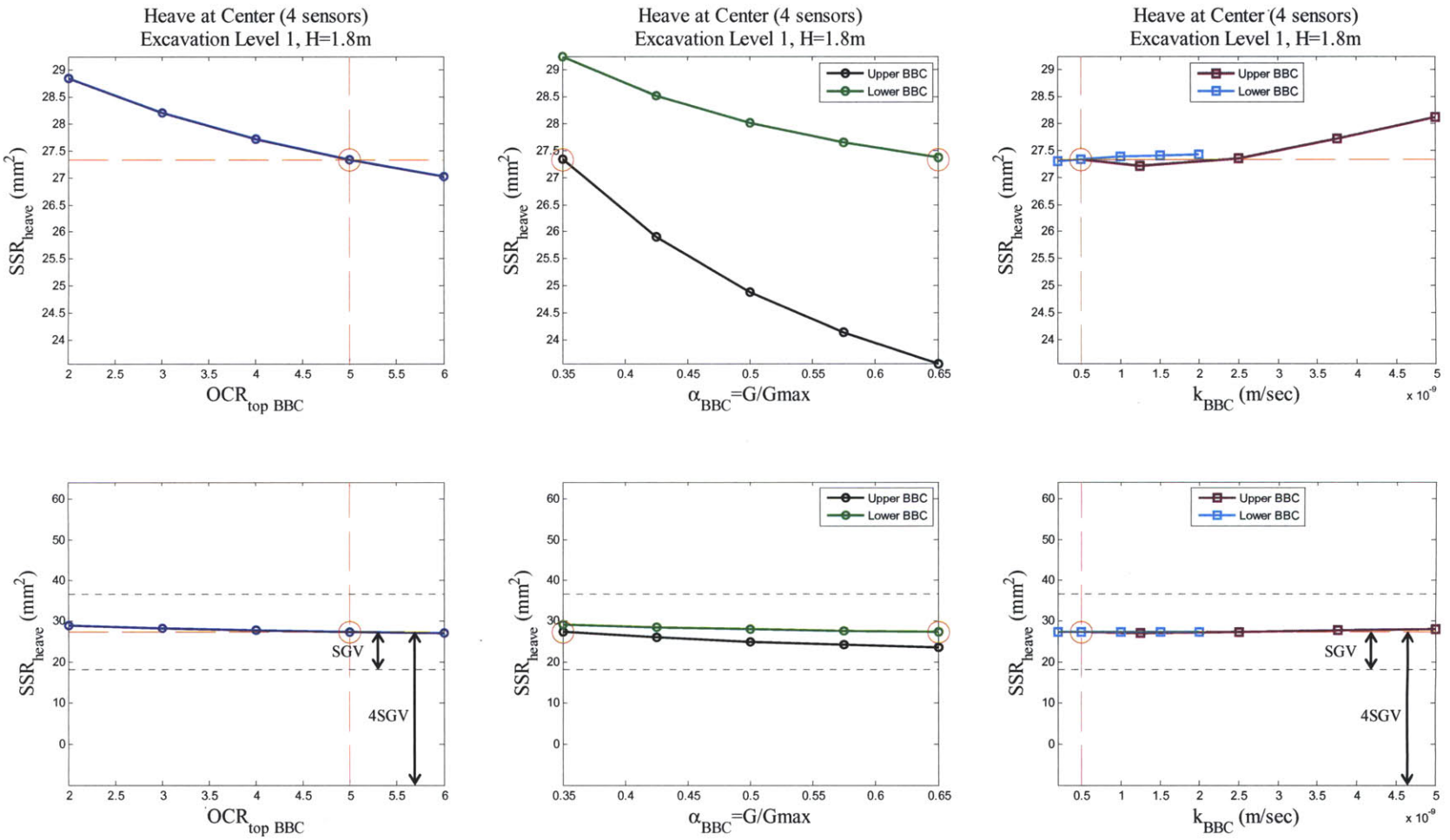

Figure A- 9: Sensitivity analysis of OCR (top), α parameter, and hydraulic conductivities of BBC layers on excavation heave at excavation level 1

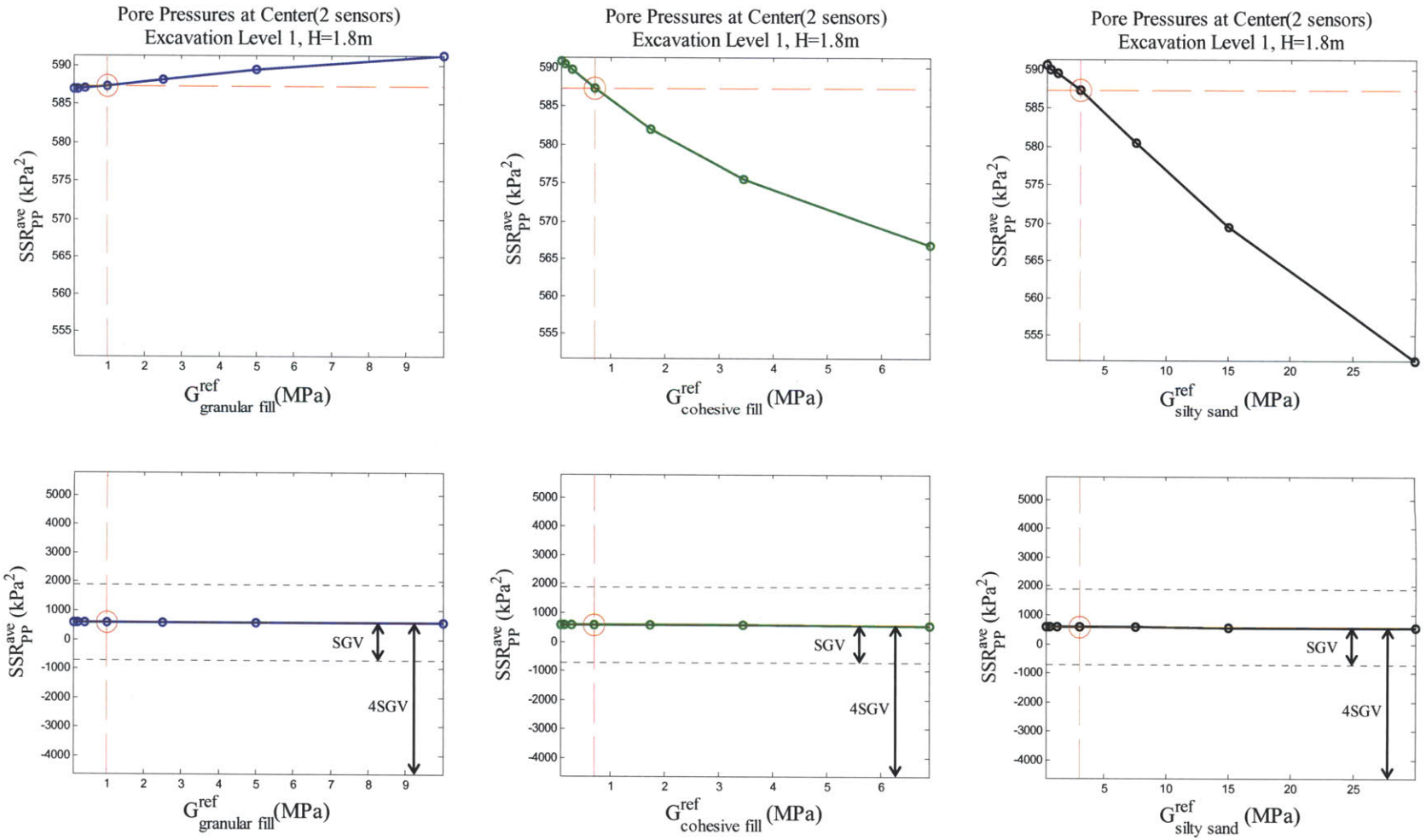

Figure A- 10: Sensitivity analysis of shear stiffness of granular fill, cohesive fill, and silty sand layers on pore pressures at excavation level 1

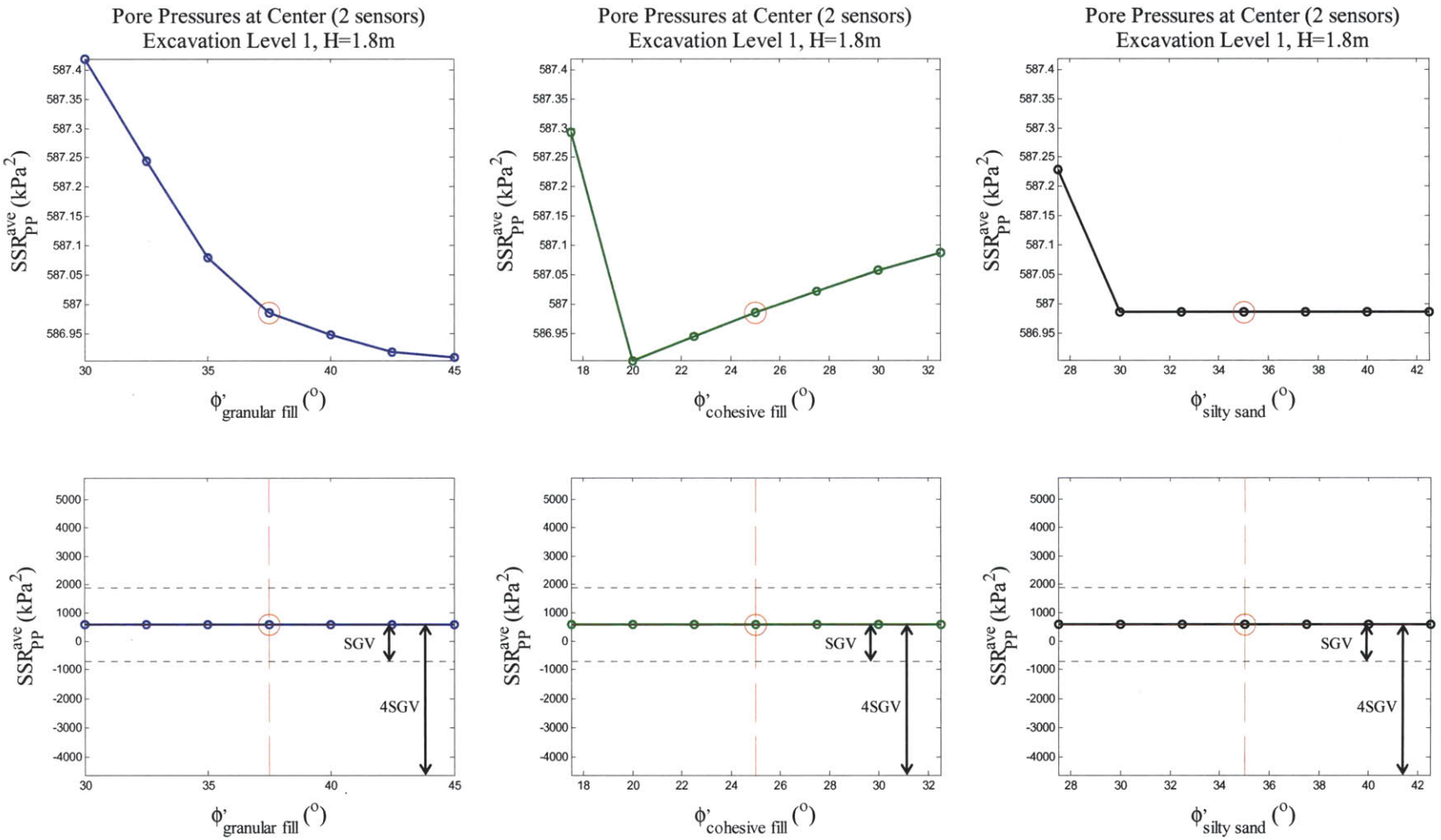

Figure A- 11: Sensitivity analysis of friction angles of granular fill, cohesive fill, and silty sand layers on pore pressures at excavation level 1

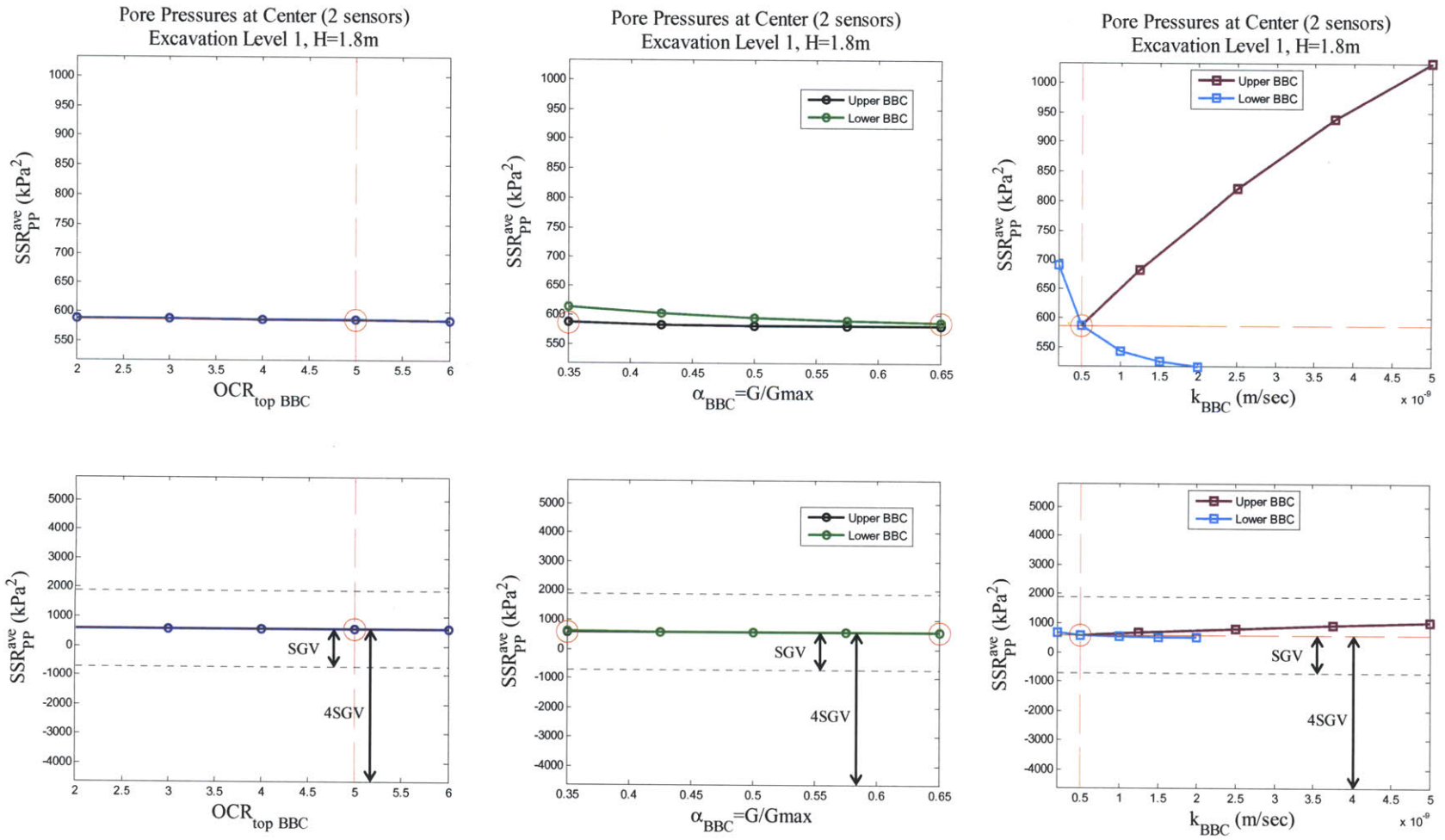

Figure A- 12: Sensitivity analysis of OCR (top), α parameter, and hydraulic conductivities of BBC layers on pore pressures at excavation level 1

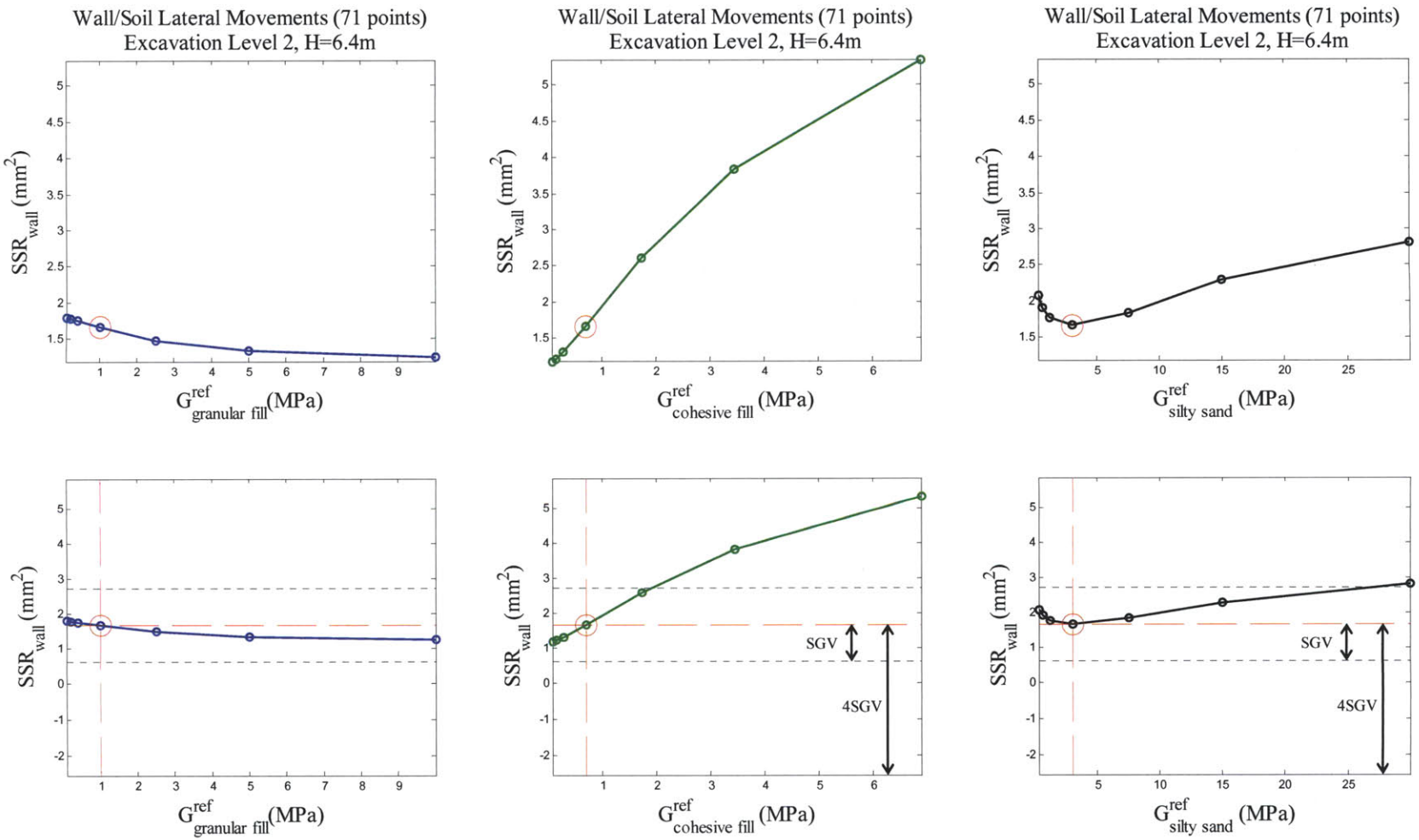

Figure A- 13: Sensitivity analysis of shear stiffness of granular fill, cohesive fill, and silty sand layers on lateral wall/soil movements at excavation level 2

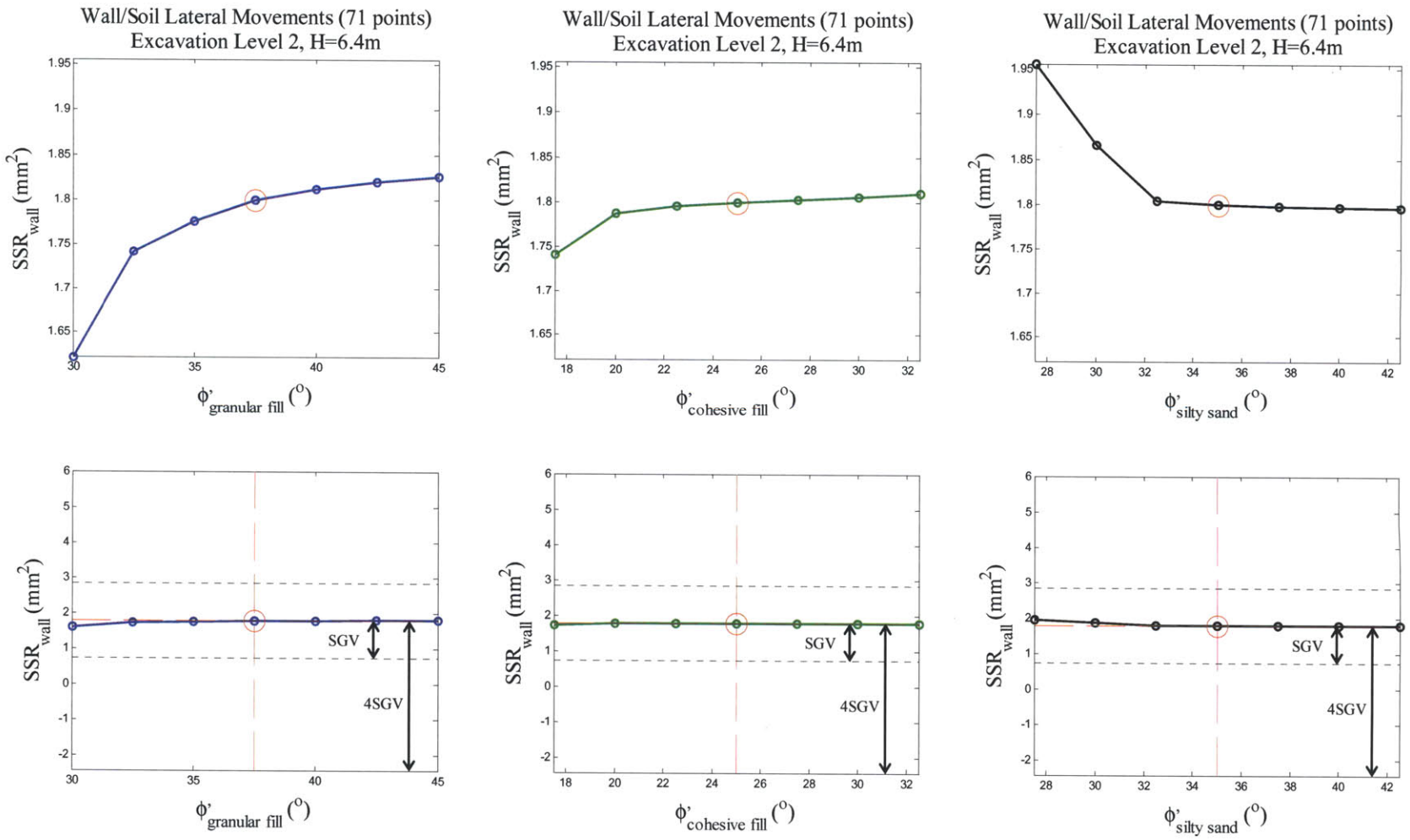

Figure A- 14: Sensitivity analysis of friction angles of granular fill, cohesive fill, and silty sand layers on lateral wall/soil movements at excavation level 2

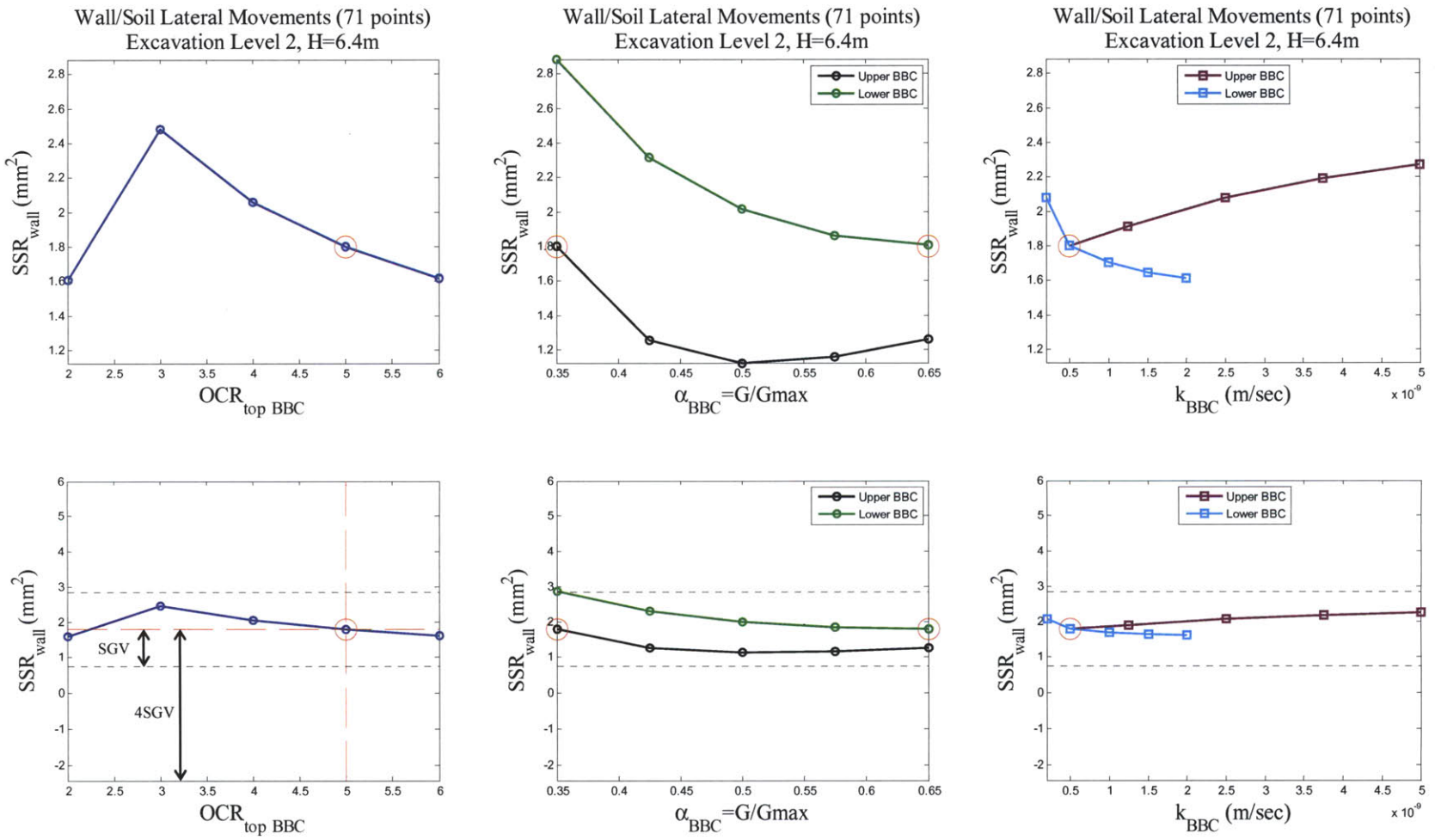

Figure A- 15: Sensitivity analysis of OCR (top), α parameter, and hydraulic conductivities of BBC layers on lateral wall/soil movements at excavation level 2

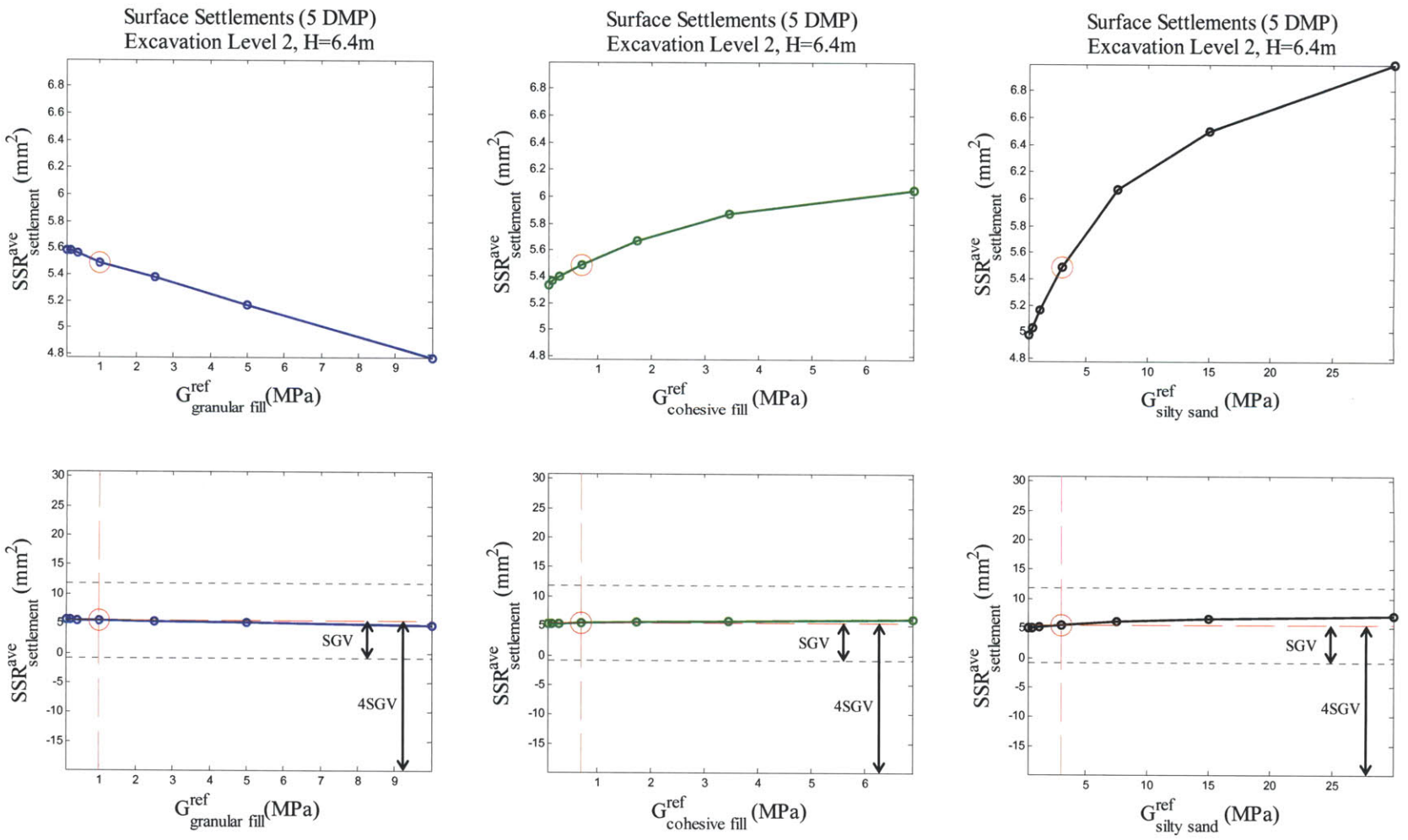

Figure A- 16: Sensitivity analysis of shear stiffness of granular fill, cohesive fill, and silty sand layers on surface settlement at excavation level 2

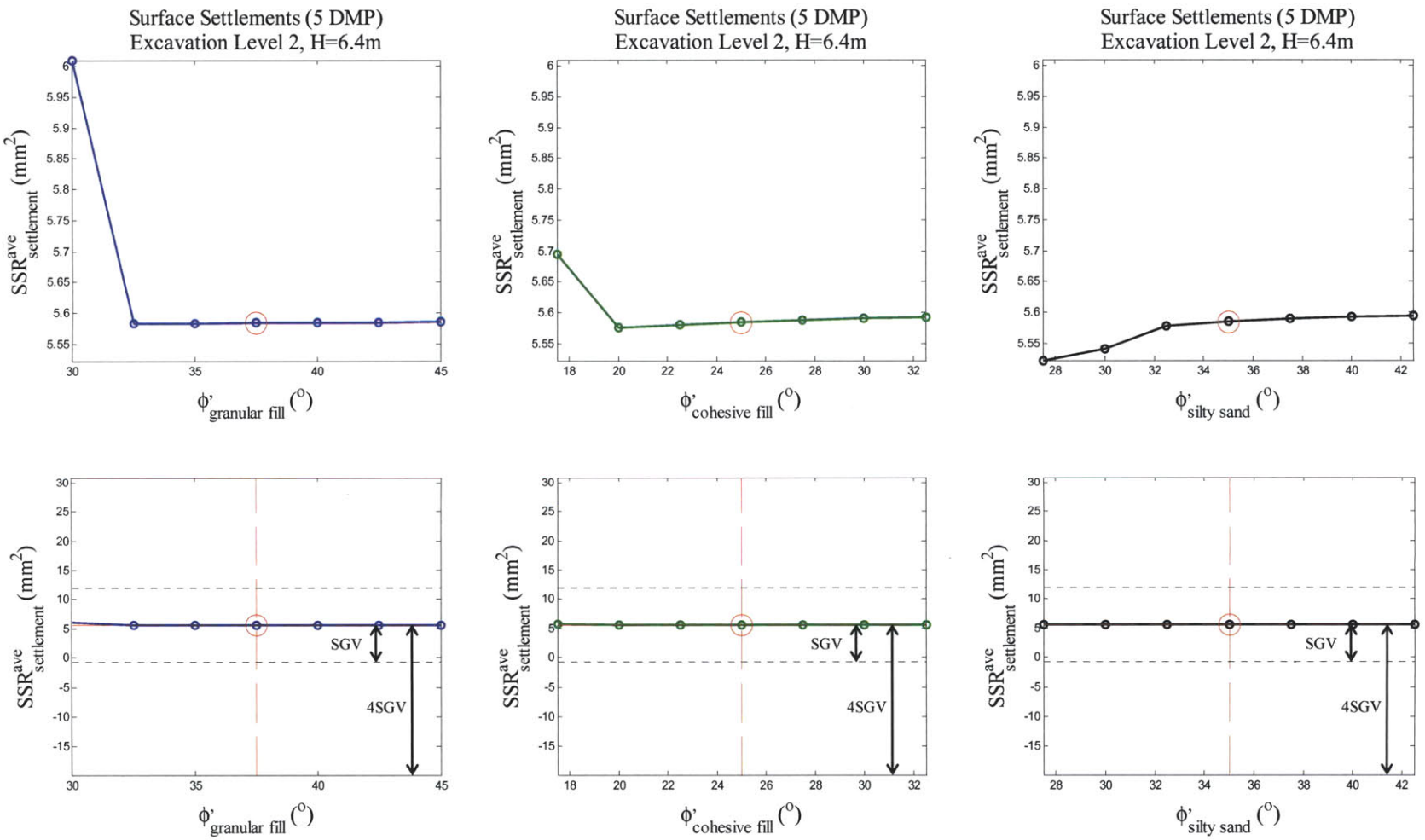

Figure A- 17: Sensitivity analysis of friction angles of granular fill, cohesive fill, and silty sand layers on surface settlement at excavation level 2

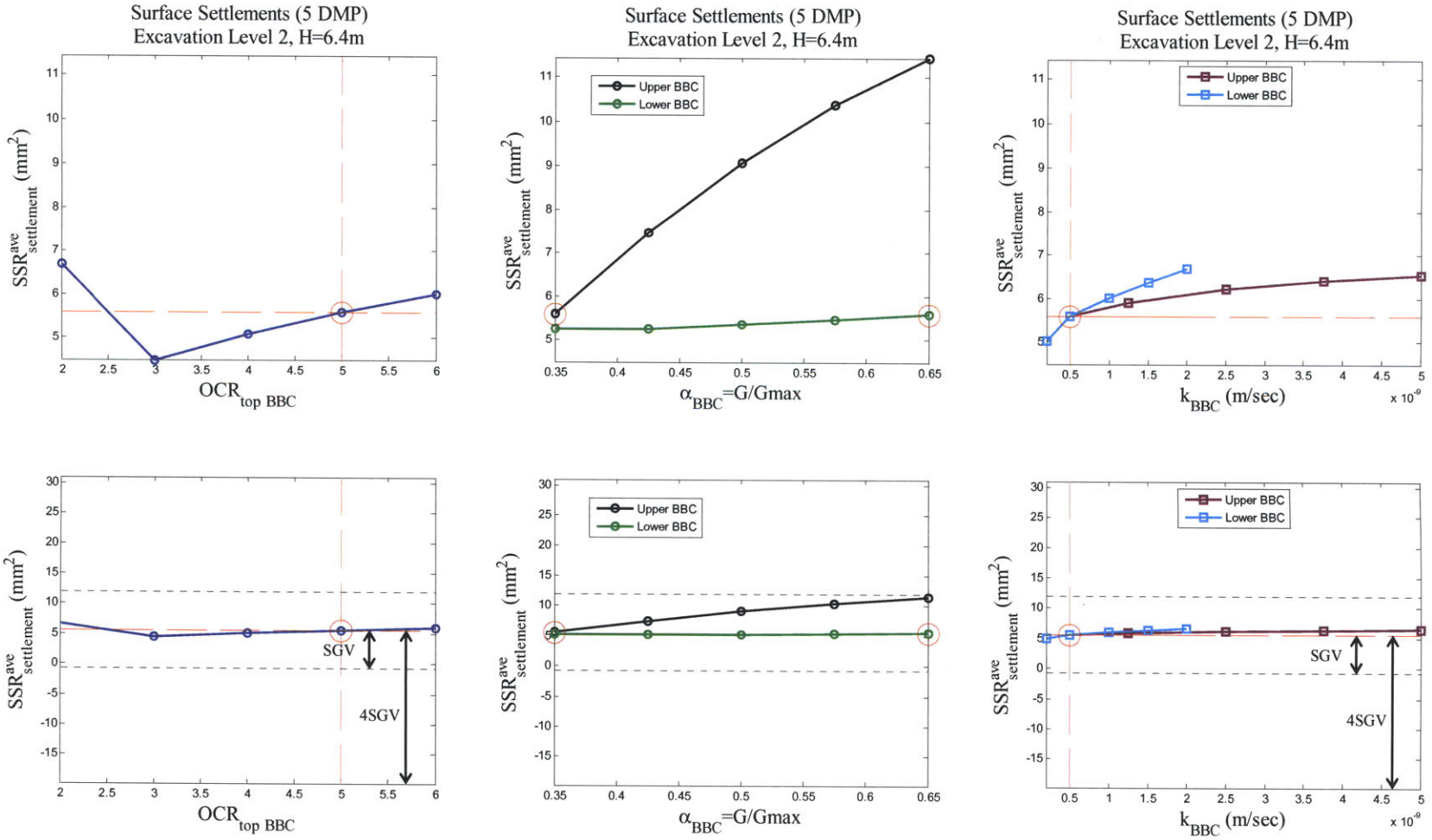

Figure A- 18: Sensitivity analysis of OCR (top), α parameter, and hydraulic conductivities of BBC layers on surface settlement at excavation level 2

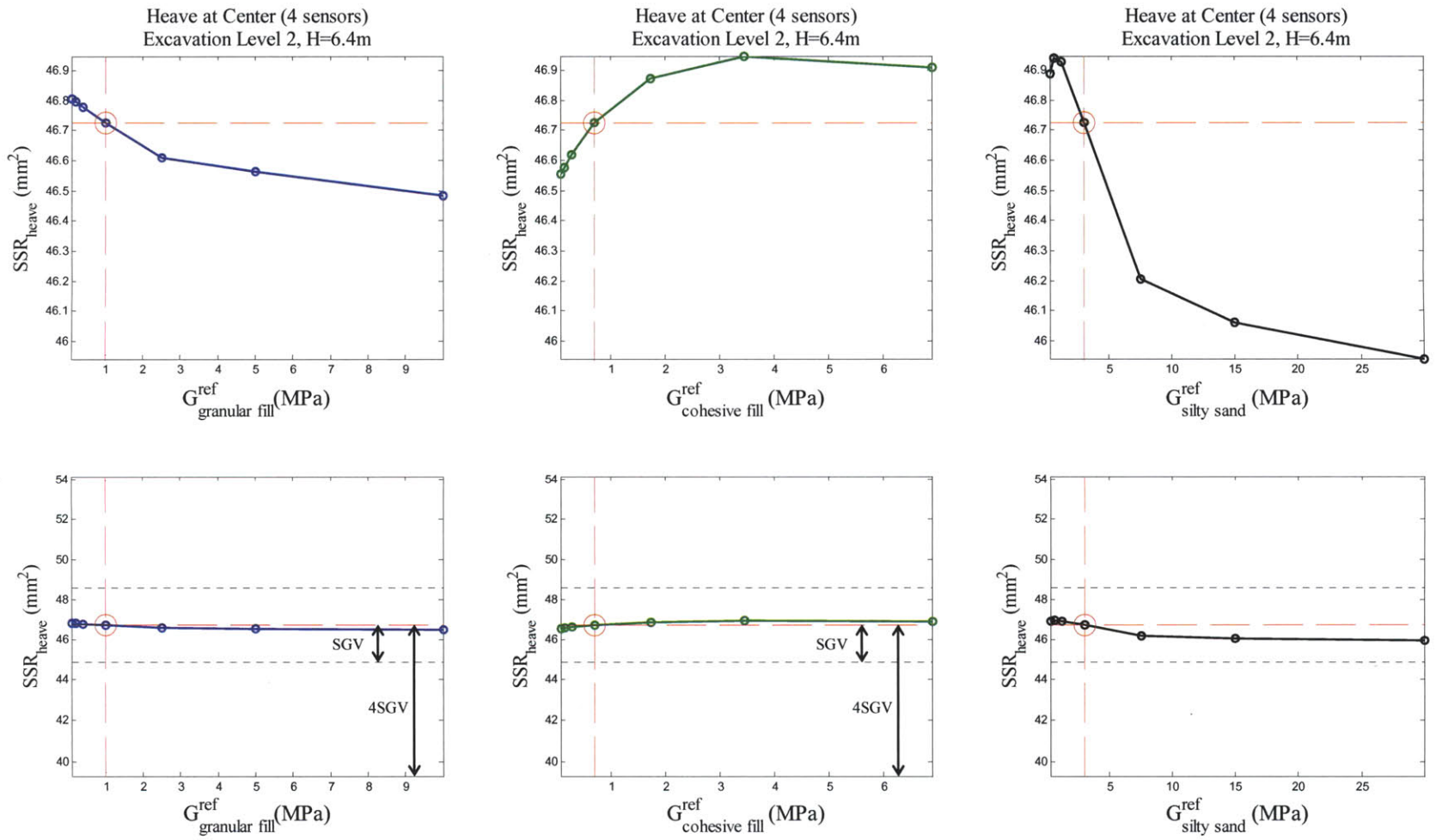

Figure A- 19: Sensitivity analysis of shear stiffness of granular fill, cohesive fill, and silty sand layers on excavation heave at excavation level 2

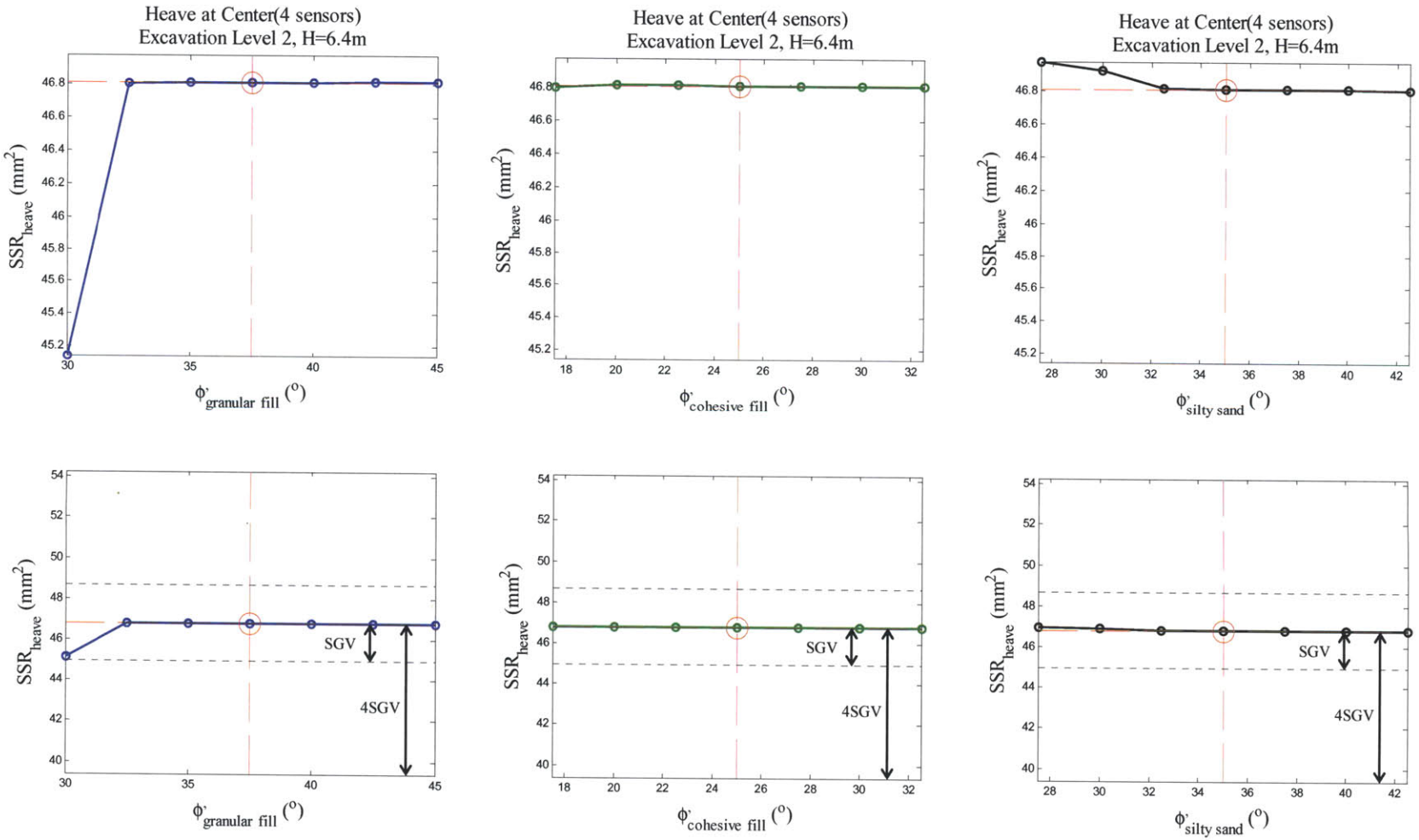

Figure A- 20: Sensitivity analysis of friction angles of granular fill, cohesive fill, and silty sand layers on excavation heave at excavation level 2

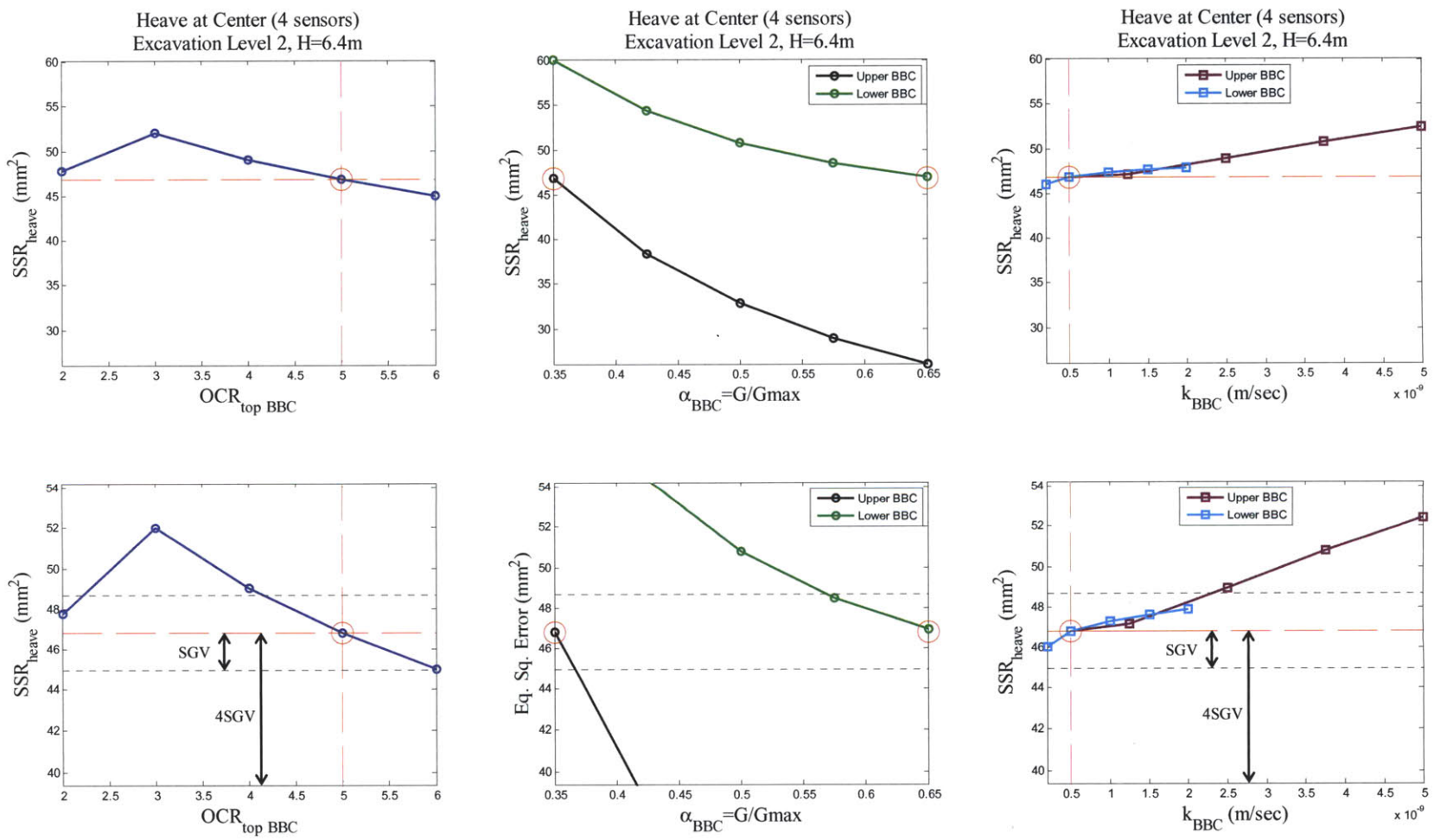

Figure A- 21: Sensitivity analysis of OCR (top), α parameter, and hydraulic conductivities of BBC layers on excavation heave at excavation level 2

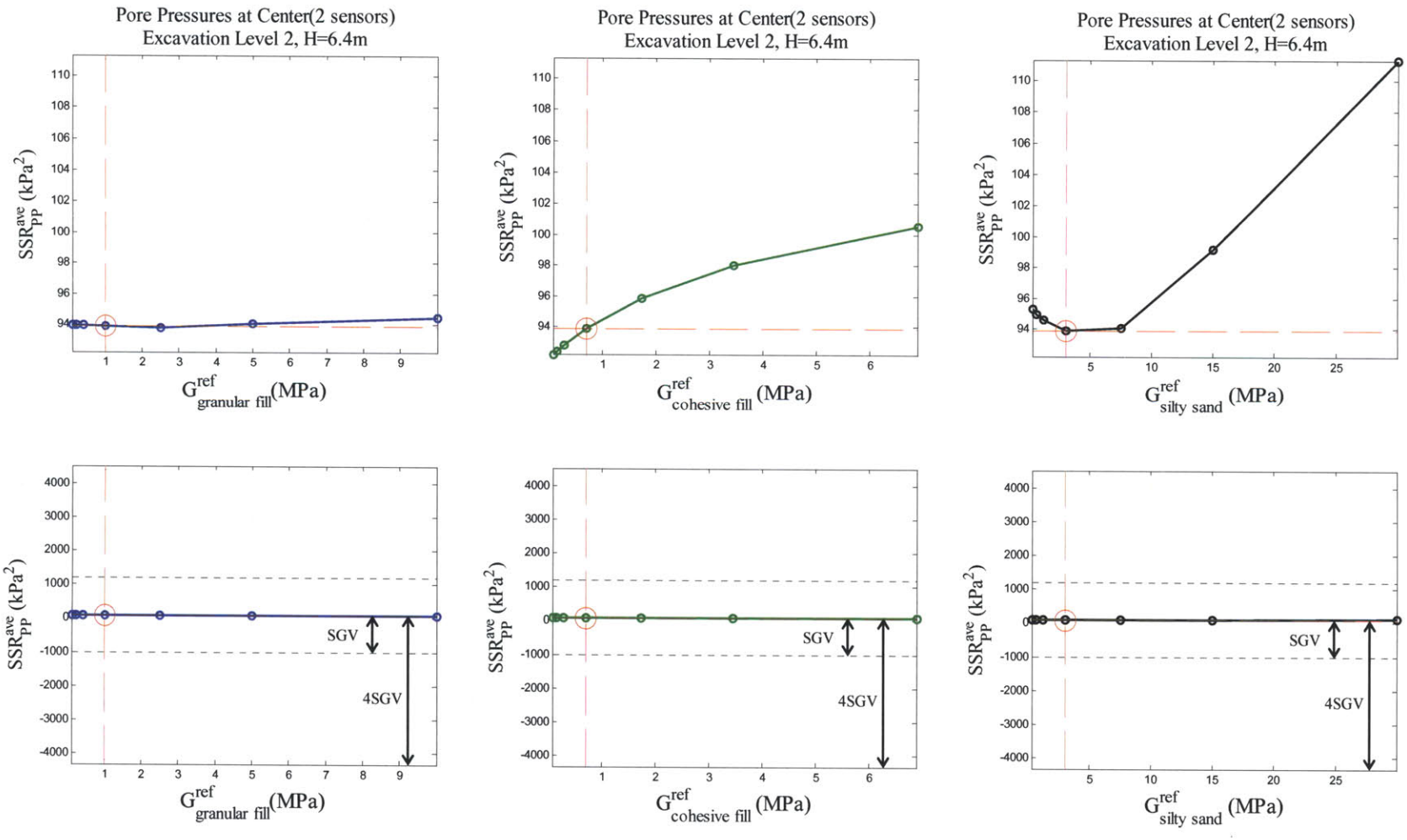

Figure A- 22: Sensitivity analysis of shear stiffness of granular fill, cohesive fill, and silty sand layers on pore pressures at excavation level 2

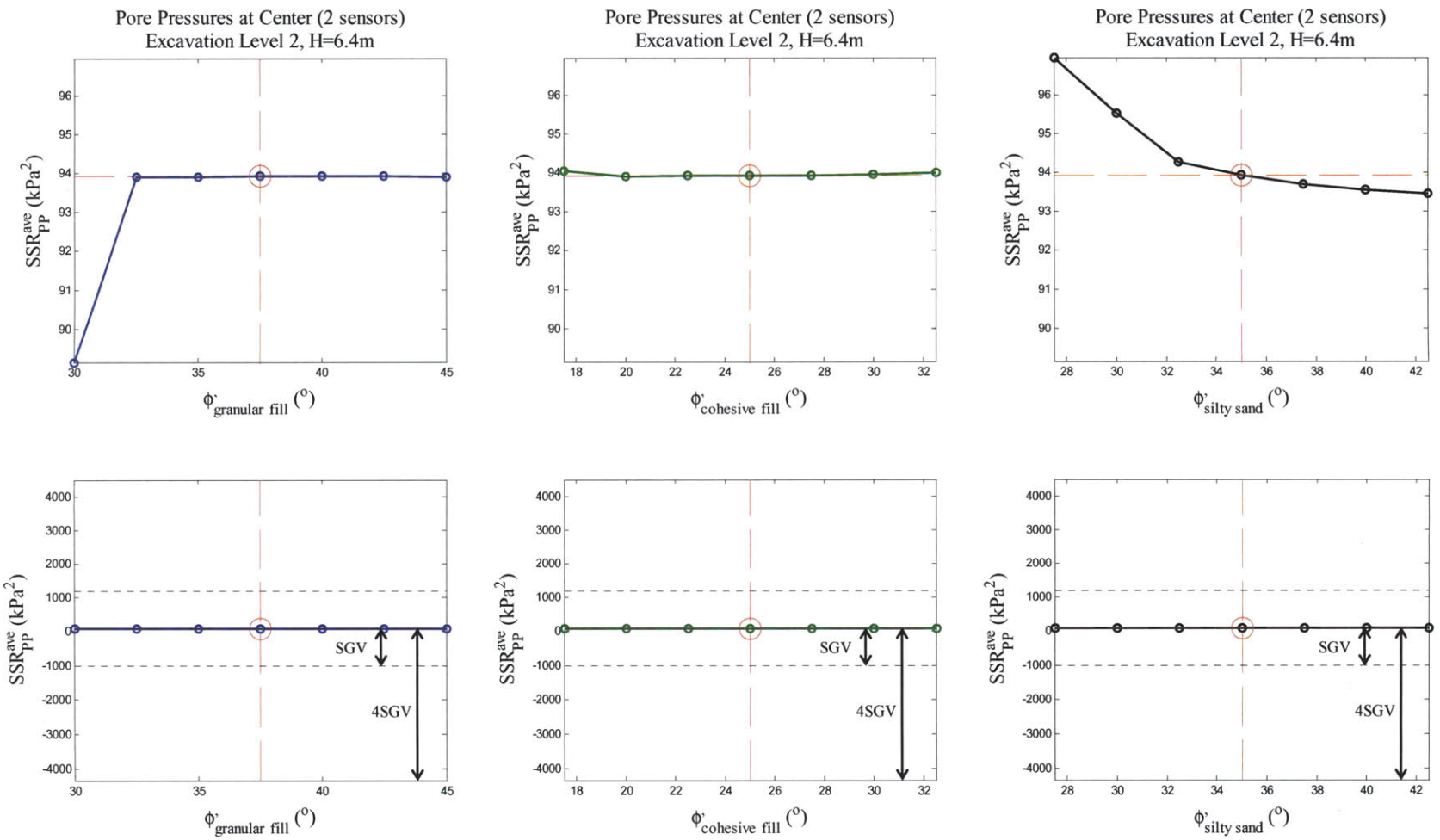

Figure A- 23: Sensitivity analysis of friction angles of granular fill, cohesive fill, and silty sand layers on pore pressures at excavation level 2

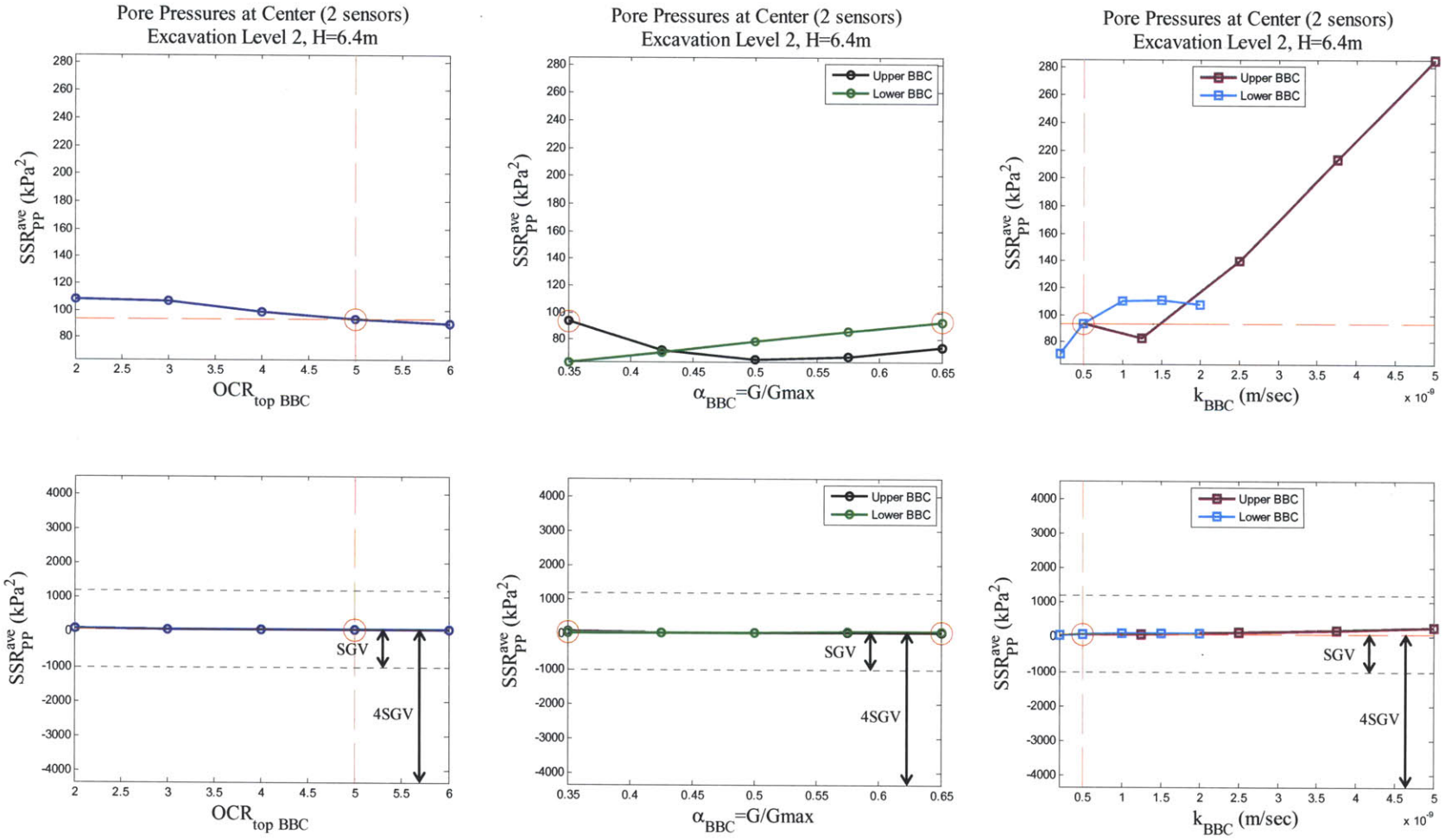

Figure A- 24: Sensitivity analysis of OCR (top), α parameter, and hydraulic conductivities of BBC layers on pore pressures at excavation level 2

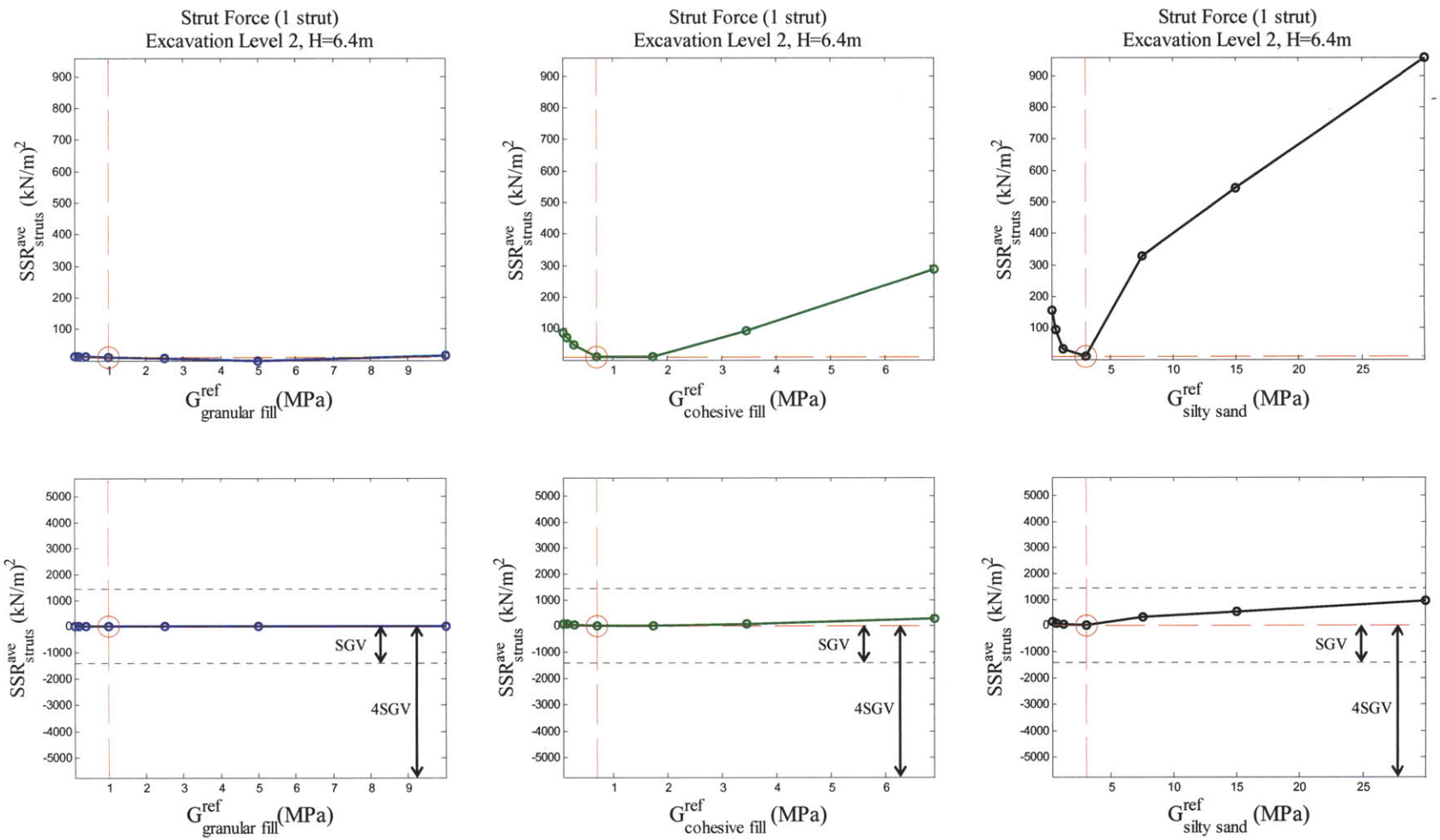

Figure A- 25: Sensitivity analysis of shear stiffness of granular fill, cohesive fill, and silty sand layers on strut forces at excavation level 2

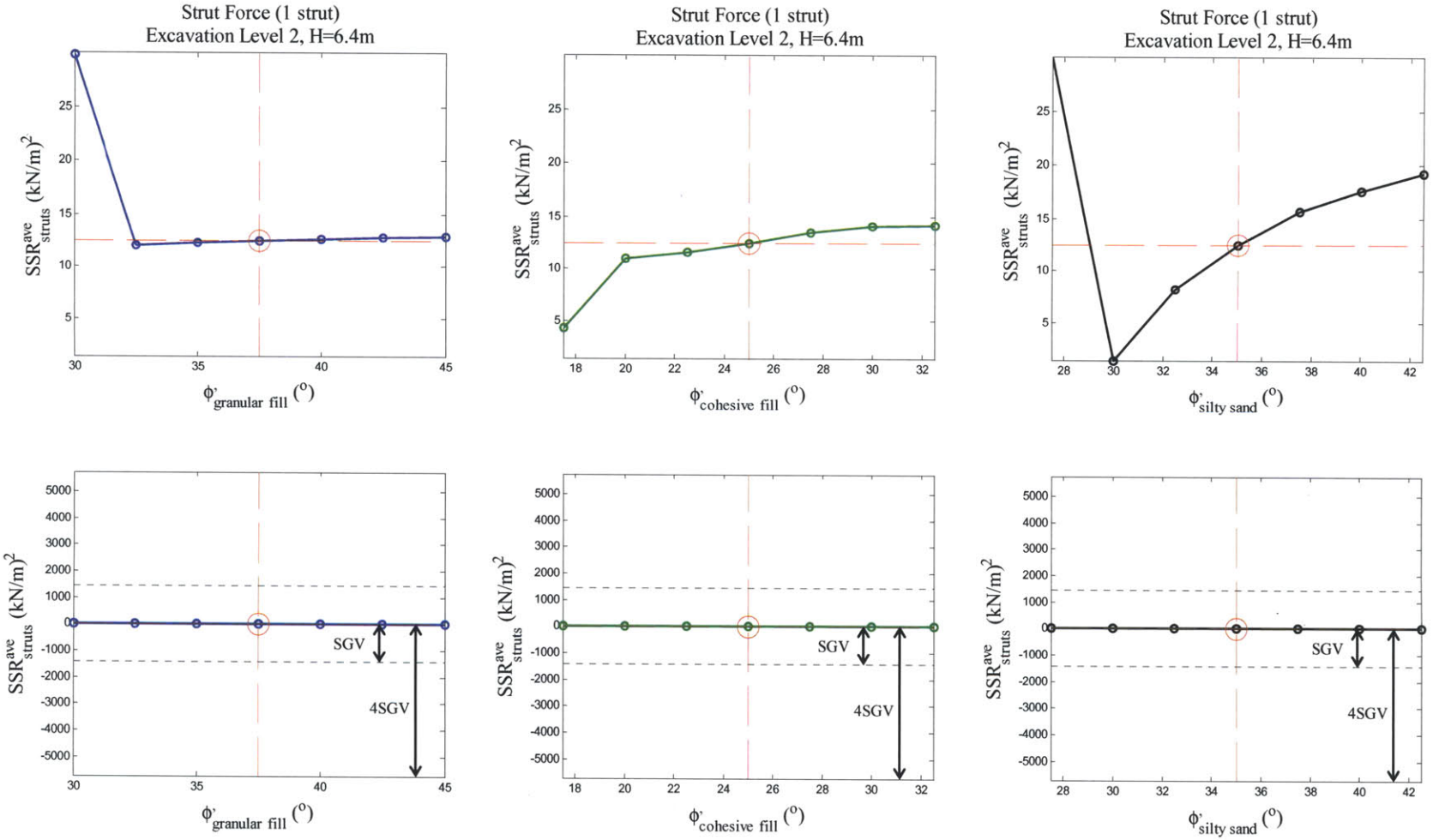

Figure A- 26: Sensitivity analysis of friction angles of granular fill, cohesive fill, and silty sand layers on strut forces at excavation level 2

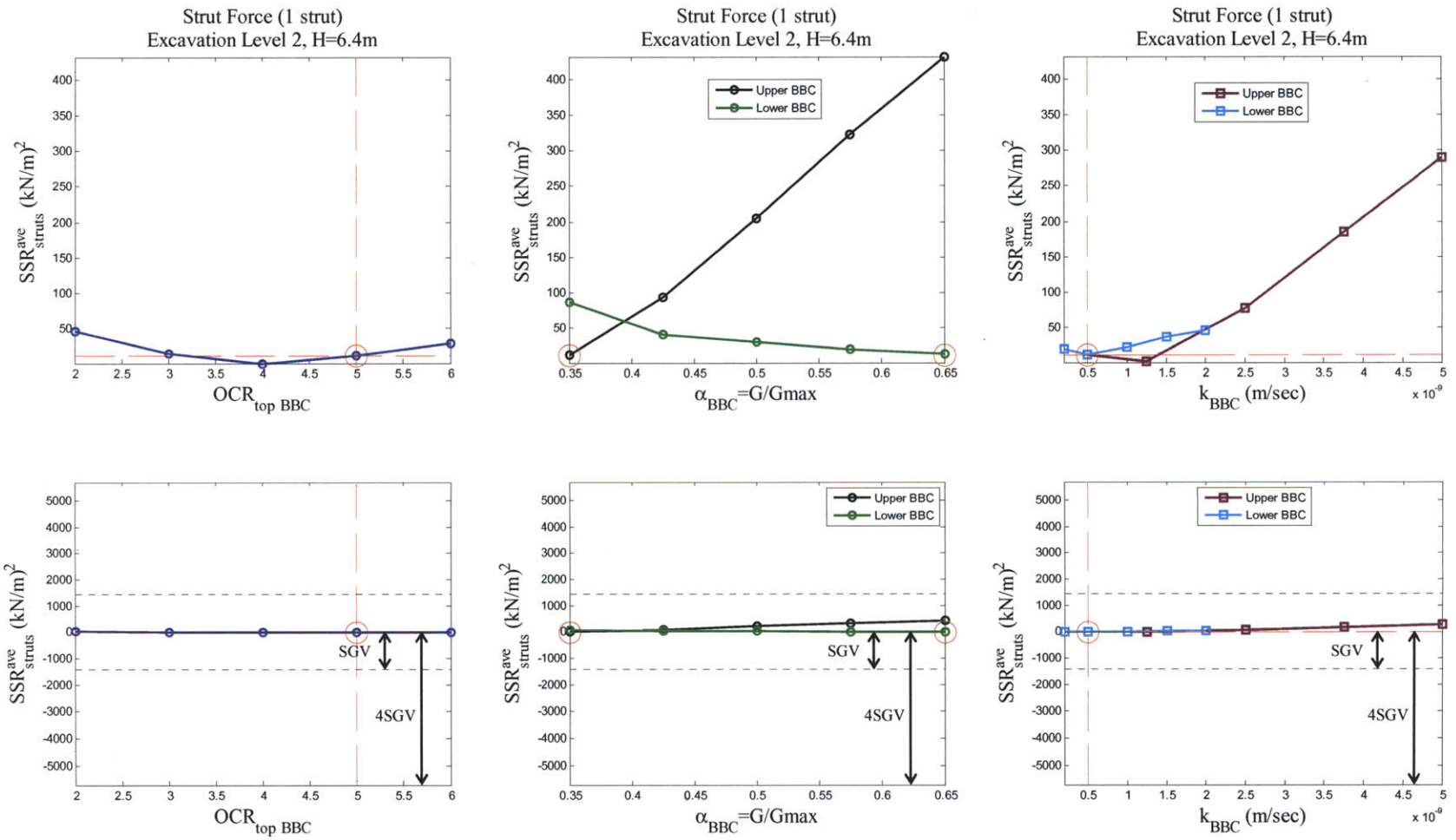

Figure A- 27: Sensitivity analysis of OCR (top), α parameter, and hydraulic conductivities of BBC layers on strut forces at excavation level 2

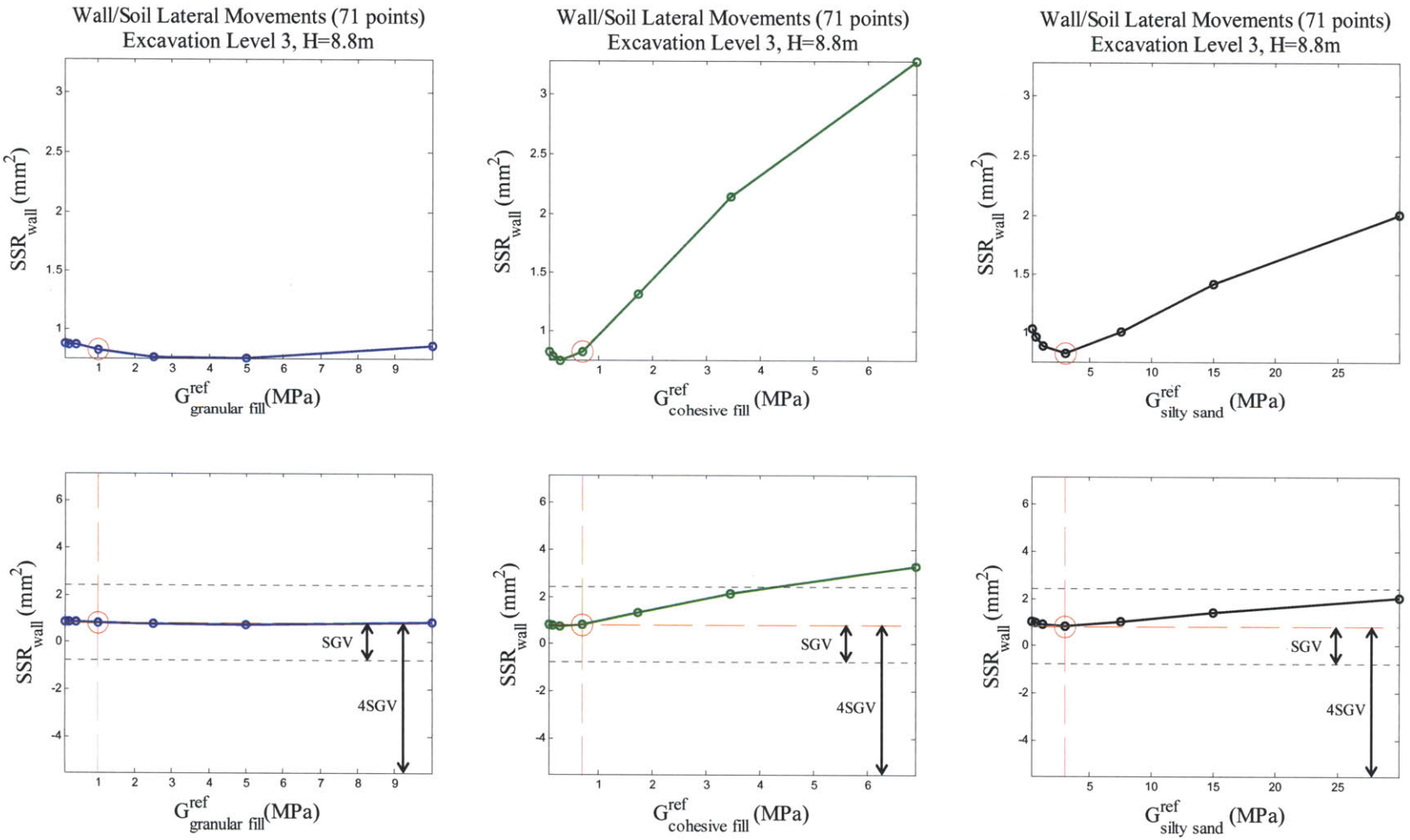

Figure A- 28: Sensitivity analysis of shear stiffness of granular fill, cohesive fill, and silty sand layers on lateral wall/soil movements at excavation level 3

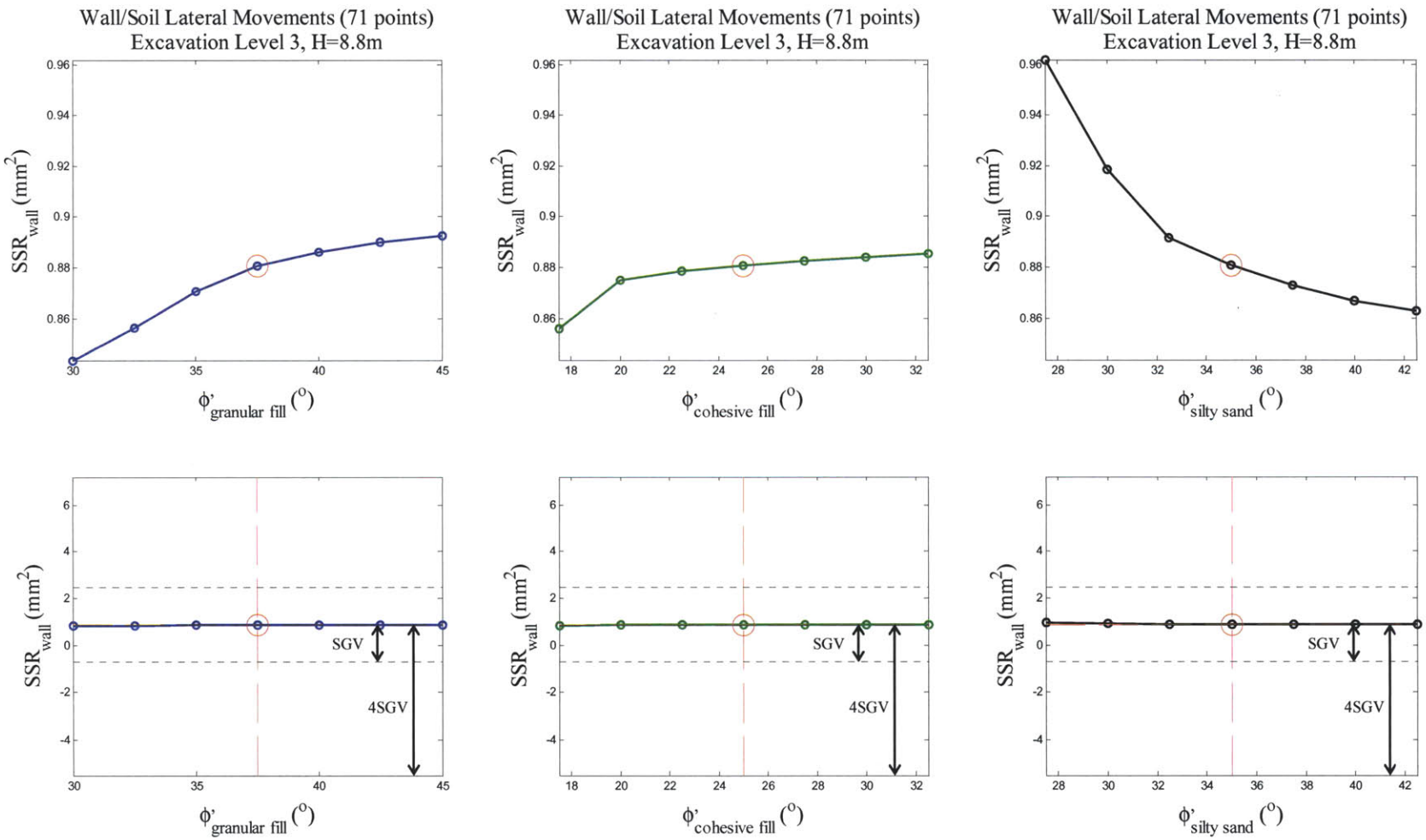

Figure A- 29: Sensitivity analysis of friction angles of granular fill, cohesive fill, and silty sand layers on lateral wall/soil movements at excavation level 3

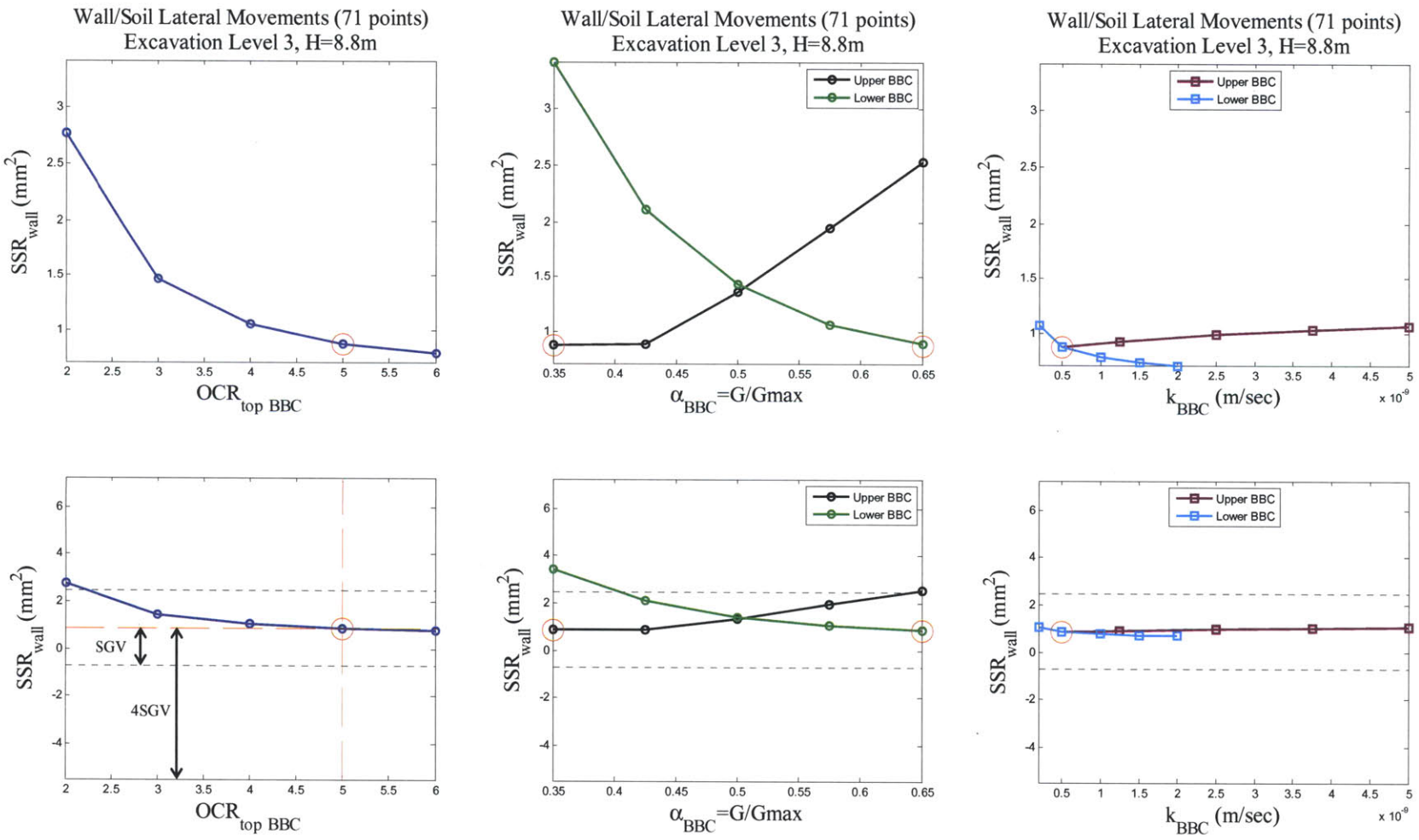

Figure A- 30: Sensitivity analysis of OCR (top), α parameter, and hydraulic conductivities of BBC layers on lateral wall/soil movements at excavation level 3

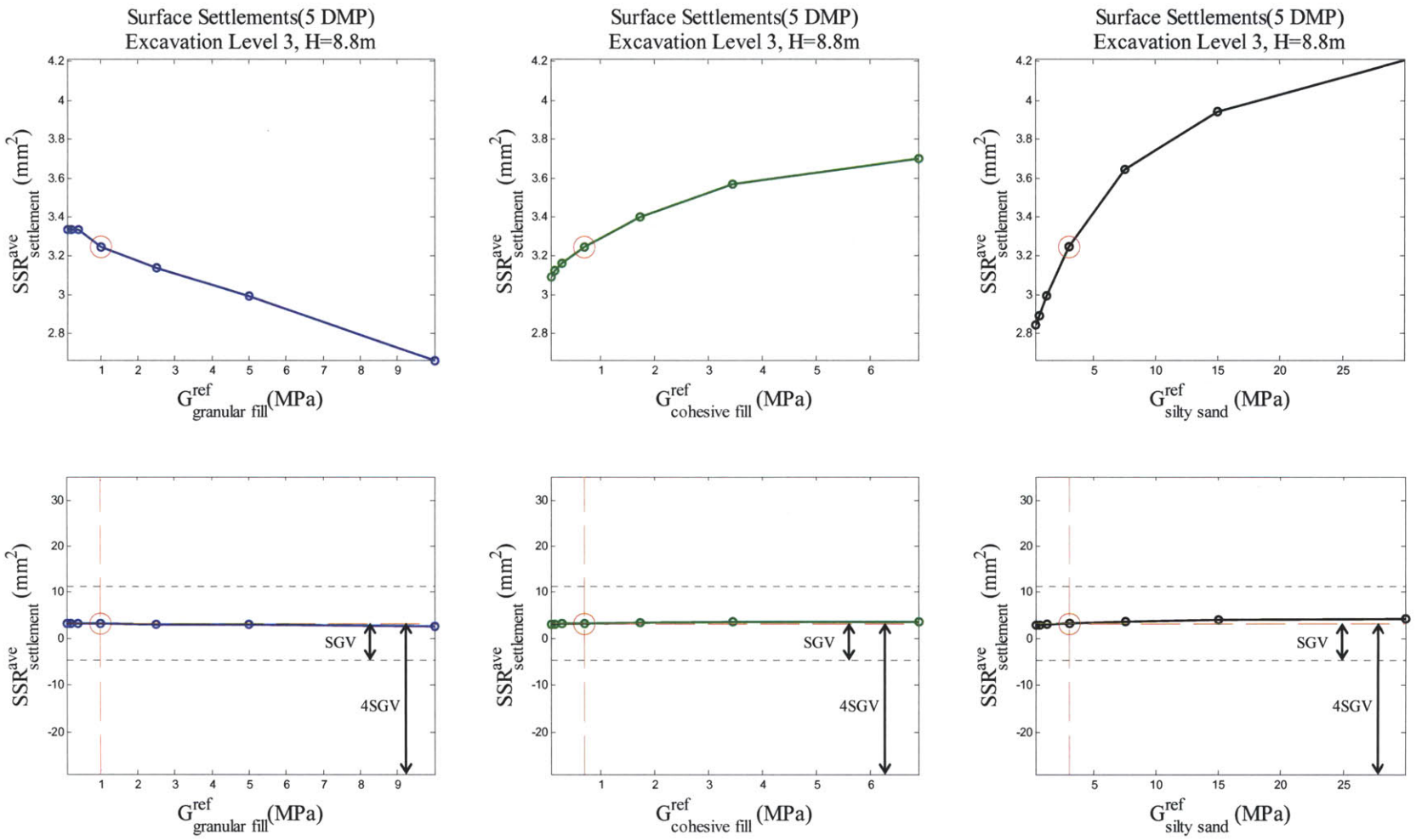

Figure A- 31: Sensitivity analysis of shear stiffness of granular fill, cohesive fill, and silty sand layers on surface settlement at excavation level 3

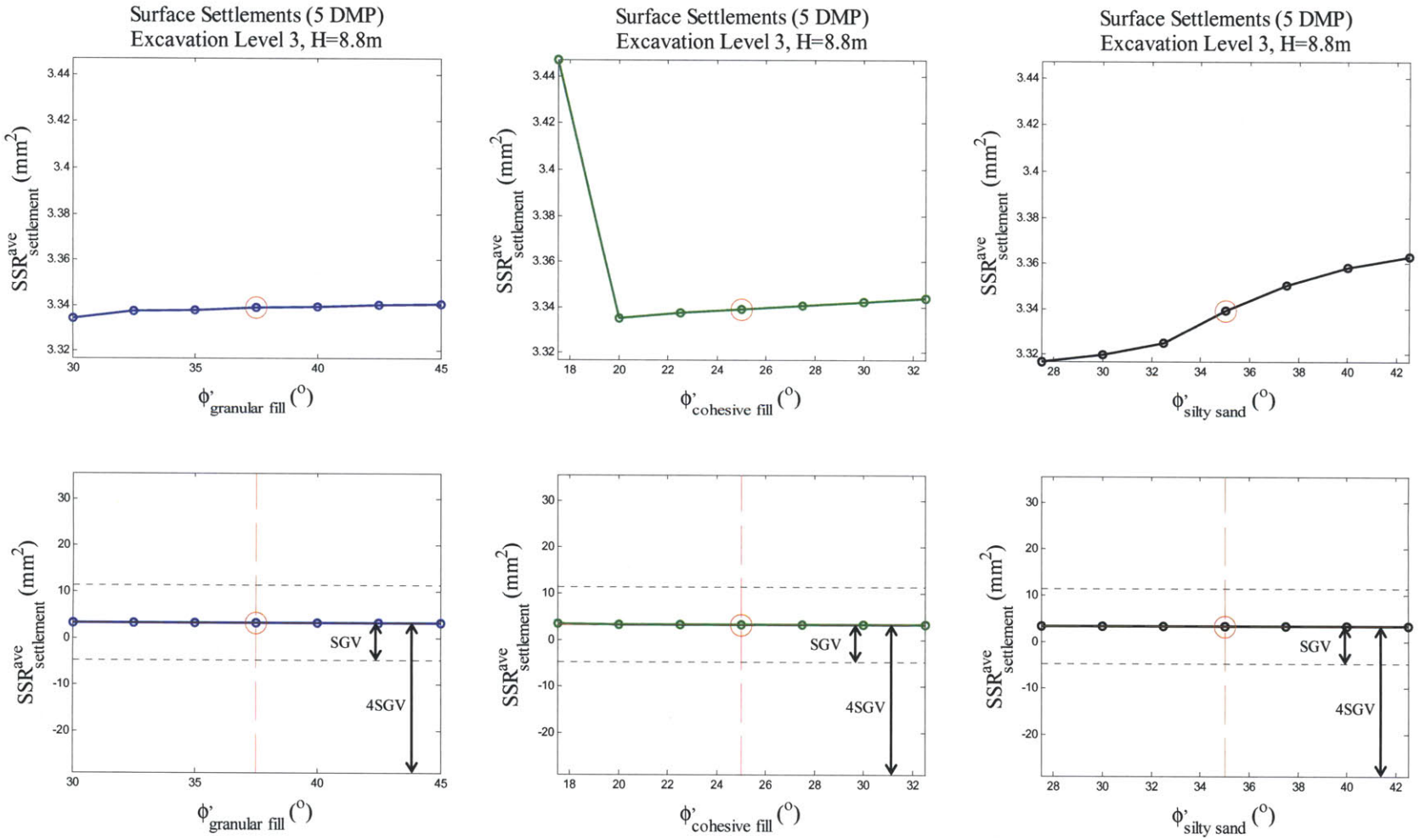

Figure A- 32: Sensitivity analysis of friction angles of granular fill, cohesive fill, and silty sand layers on surface settlement at excavation level 3

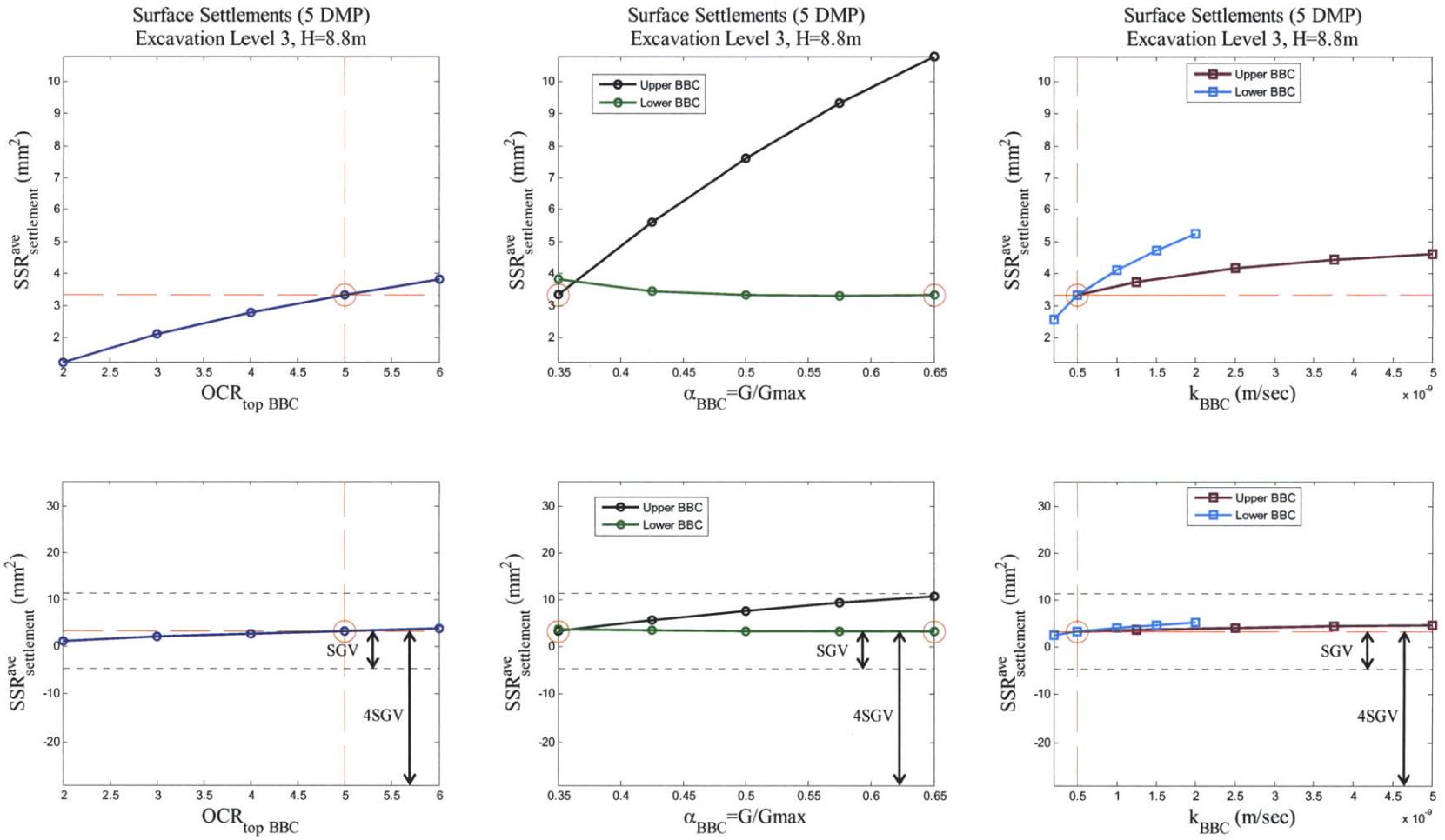

Figure A- 33: Sensitivity analysis of OCR (top), α parameter, and hydraulic conductivities of BBC layers on surface settlement at excavation level 3

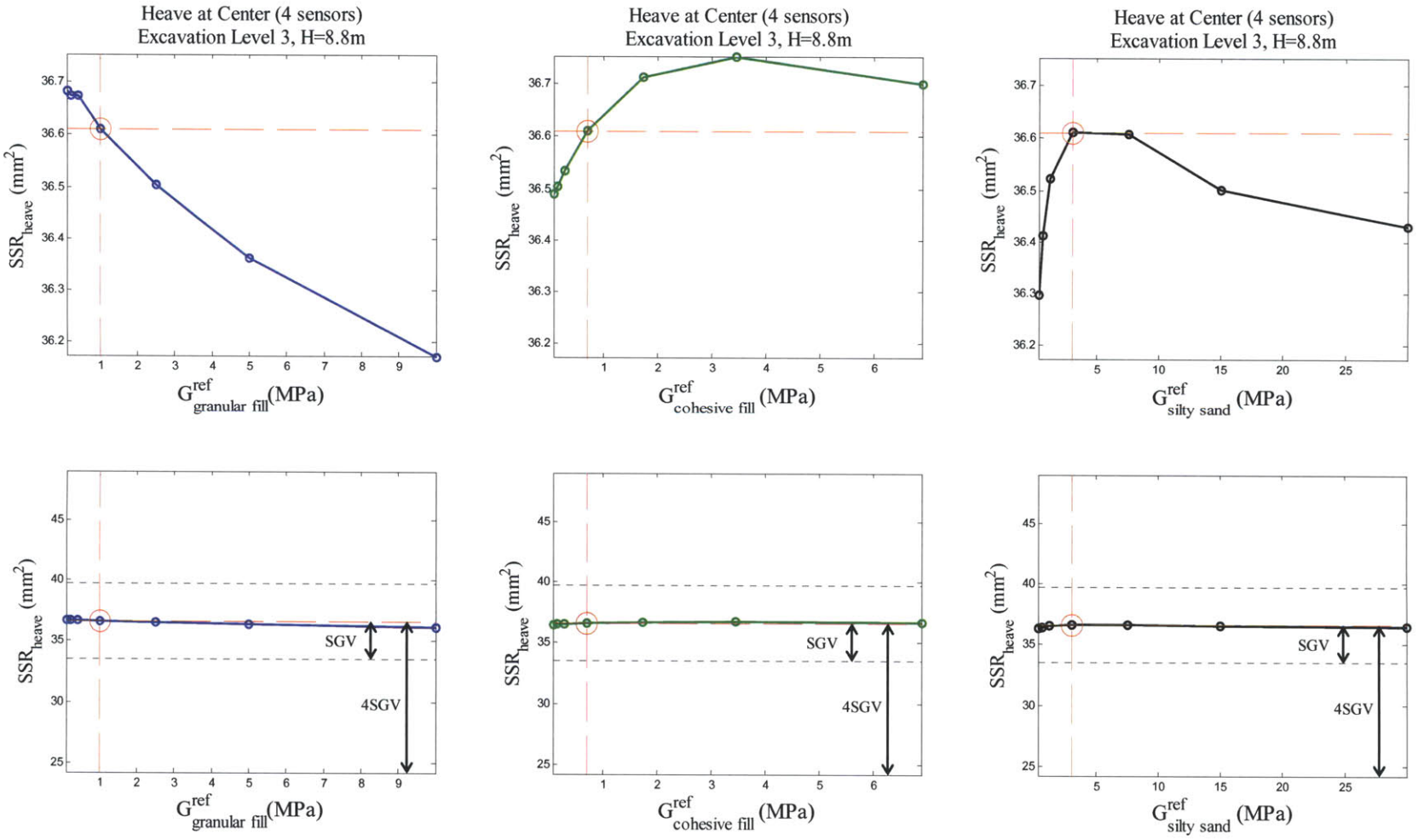

Figure A- 34: Sensitivity analysis of shear stiffness of granular fill, cohesive fill, and silty sand layers on excavation heave at excavation level 3

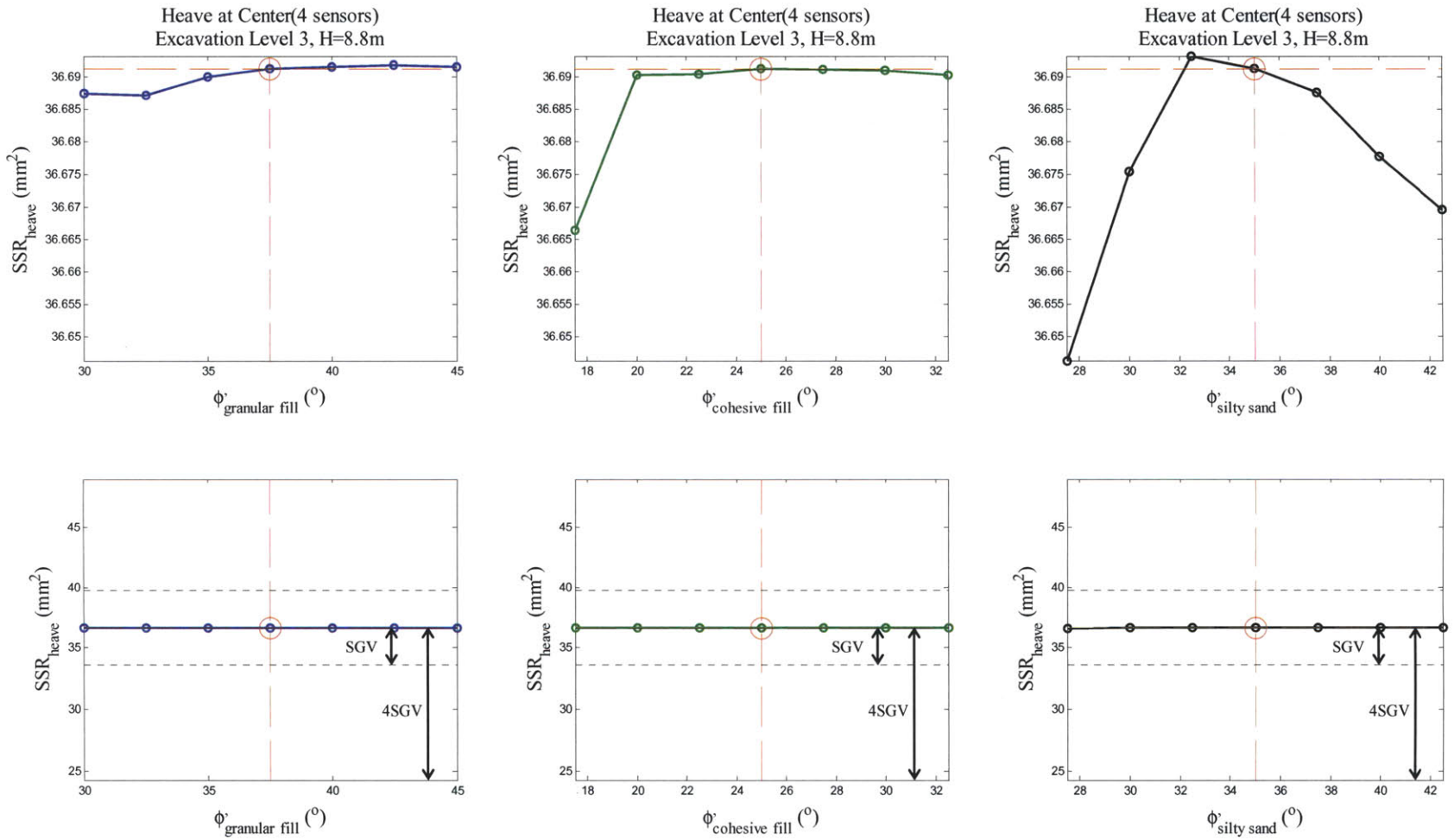

Figure A- 35: Sensitivity analysis of friction angles of granular fill, cohesive fill, and silty sand layers on excavation heave at excavation level 3

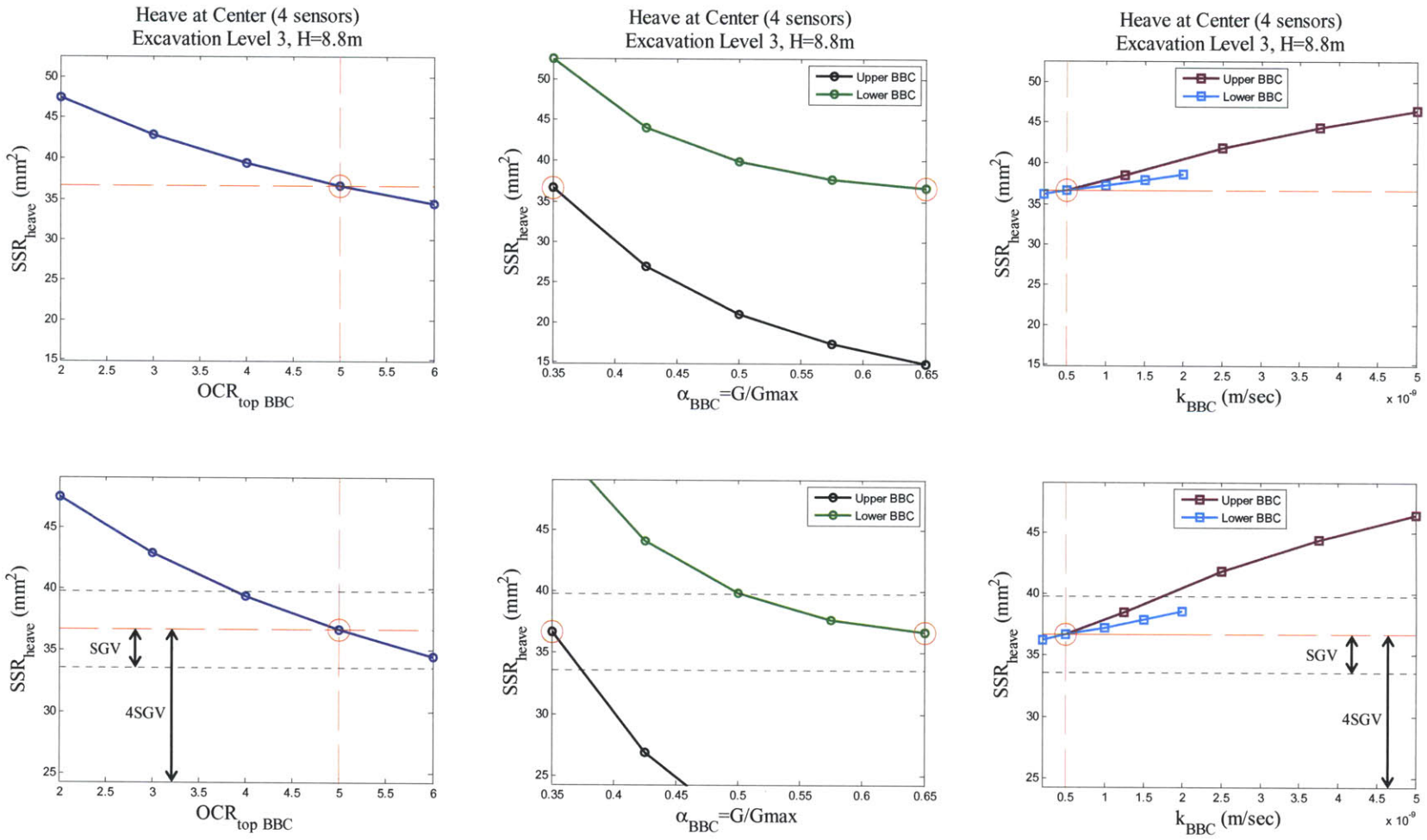

Figure A- 36: Sensitivity analysis of OCR (top), α parameter, and hydraulic conductivities of BBC layers on excavation heave at excavation level 3

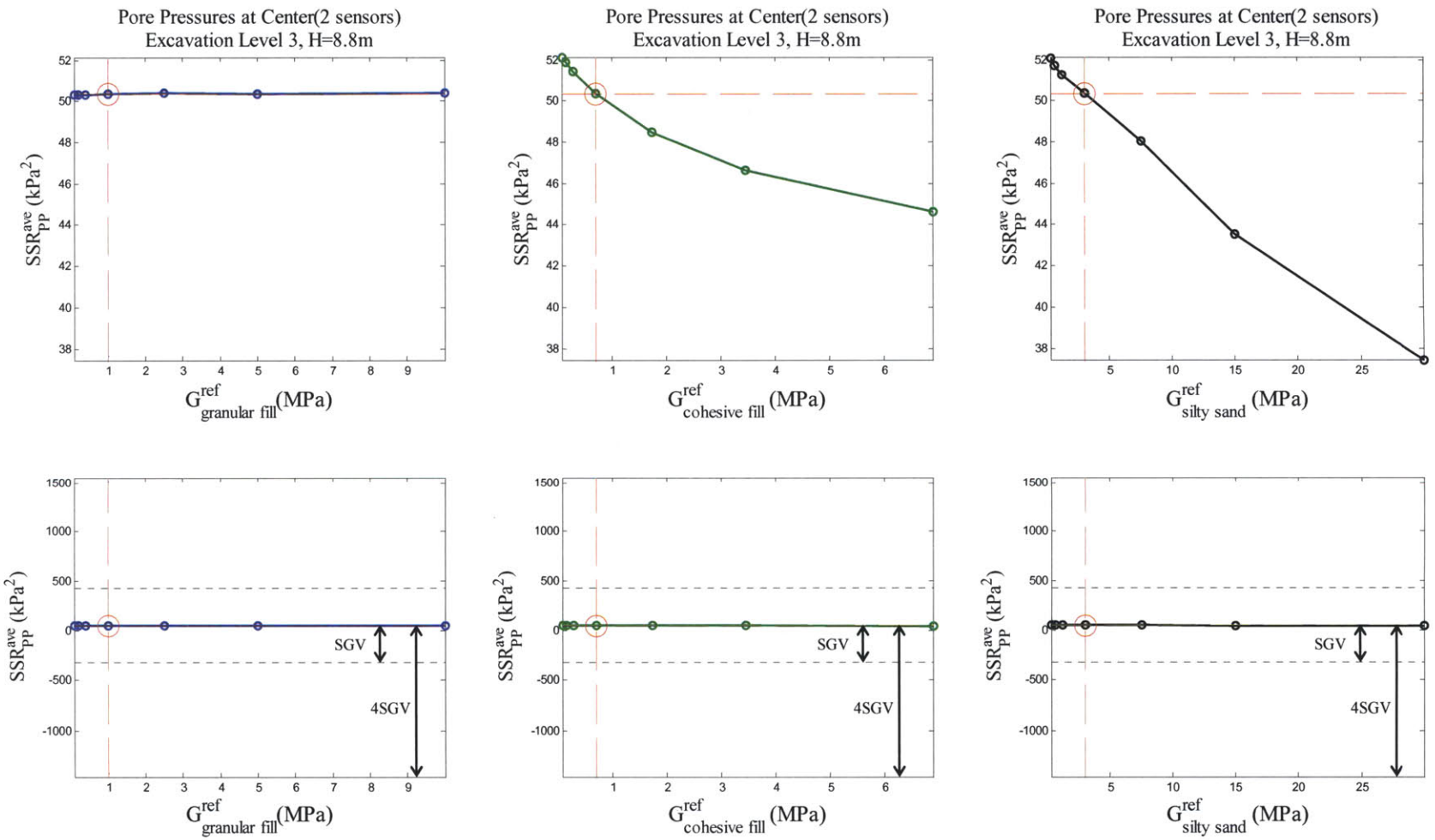

Figure A- 37: Sensitivity analysis of shear stiffness of granular fill, cohesive fill, and silty sand layers on pore pressures at excavation level 3

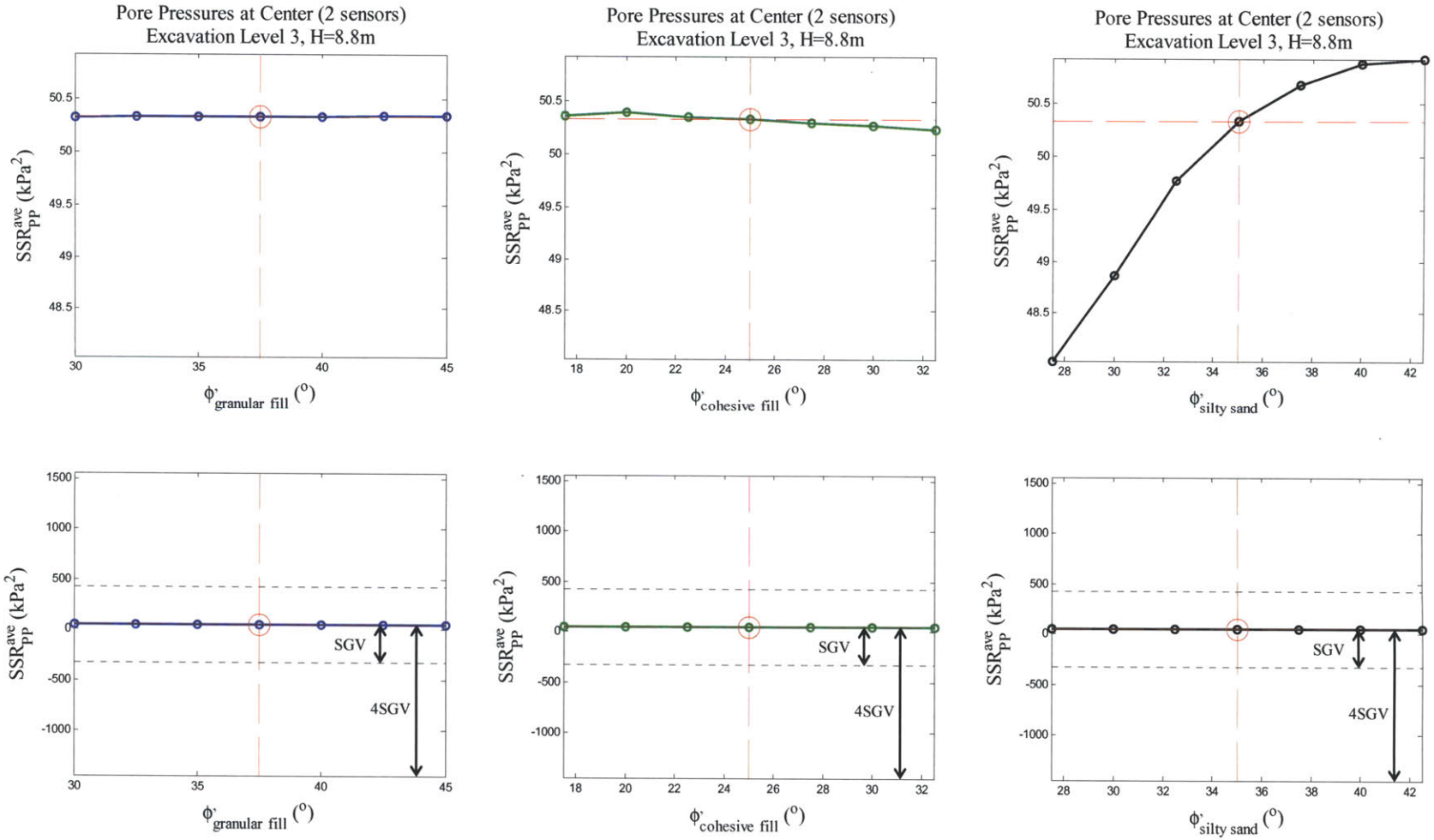

Figure A- 38: Sensitivity analysis of friction angles of granular fill, cohesive fill, and silty sand layers on pore pressures at excavation level 3

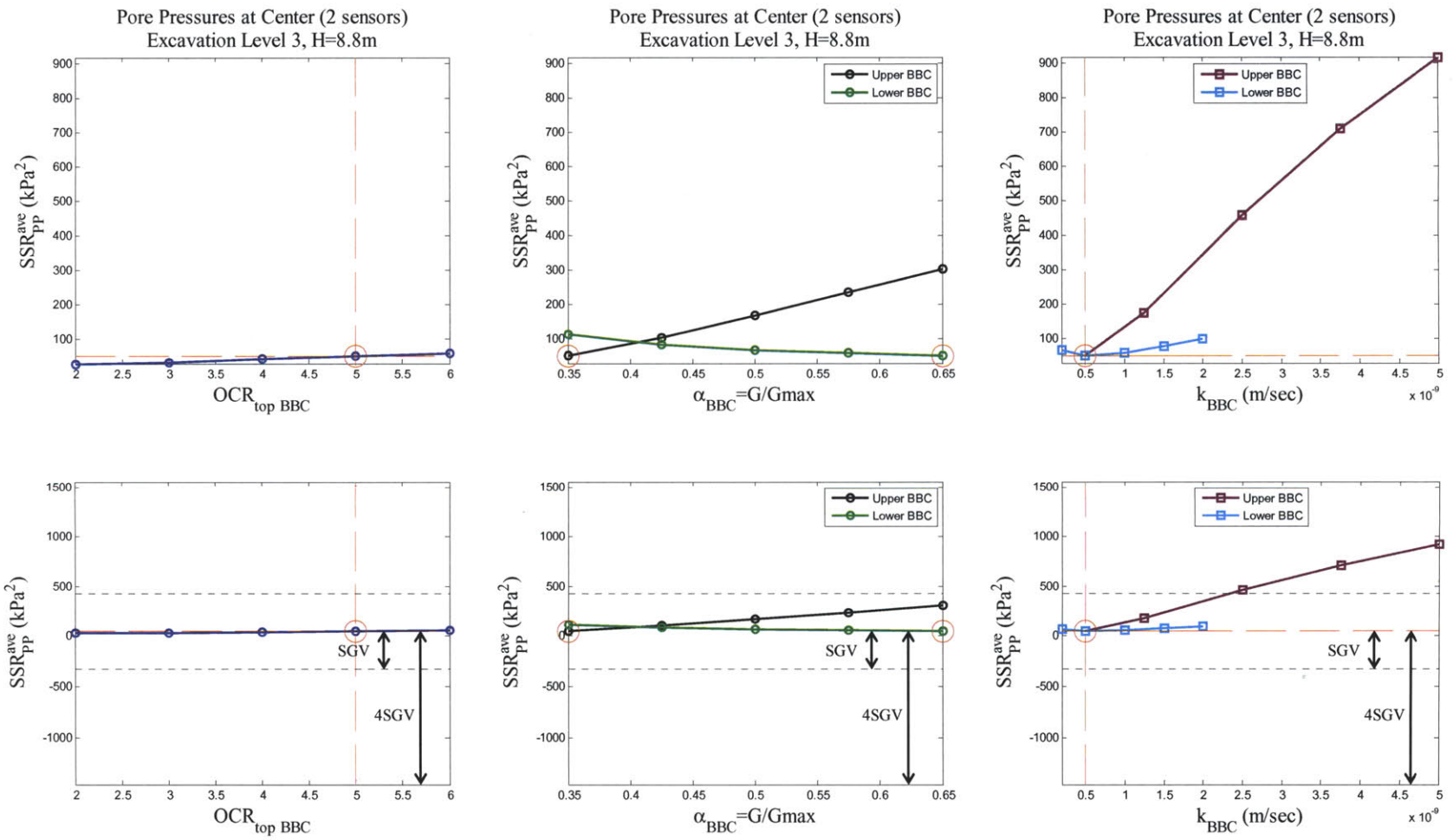

Figure A- 39: Sensitivity analysis of OCR (top), α parameter, and hydraulic conductivities of BBC layers on pore pressures at excavation level 3

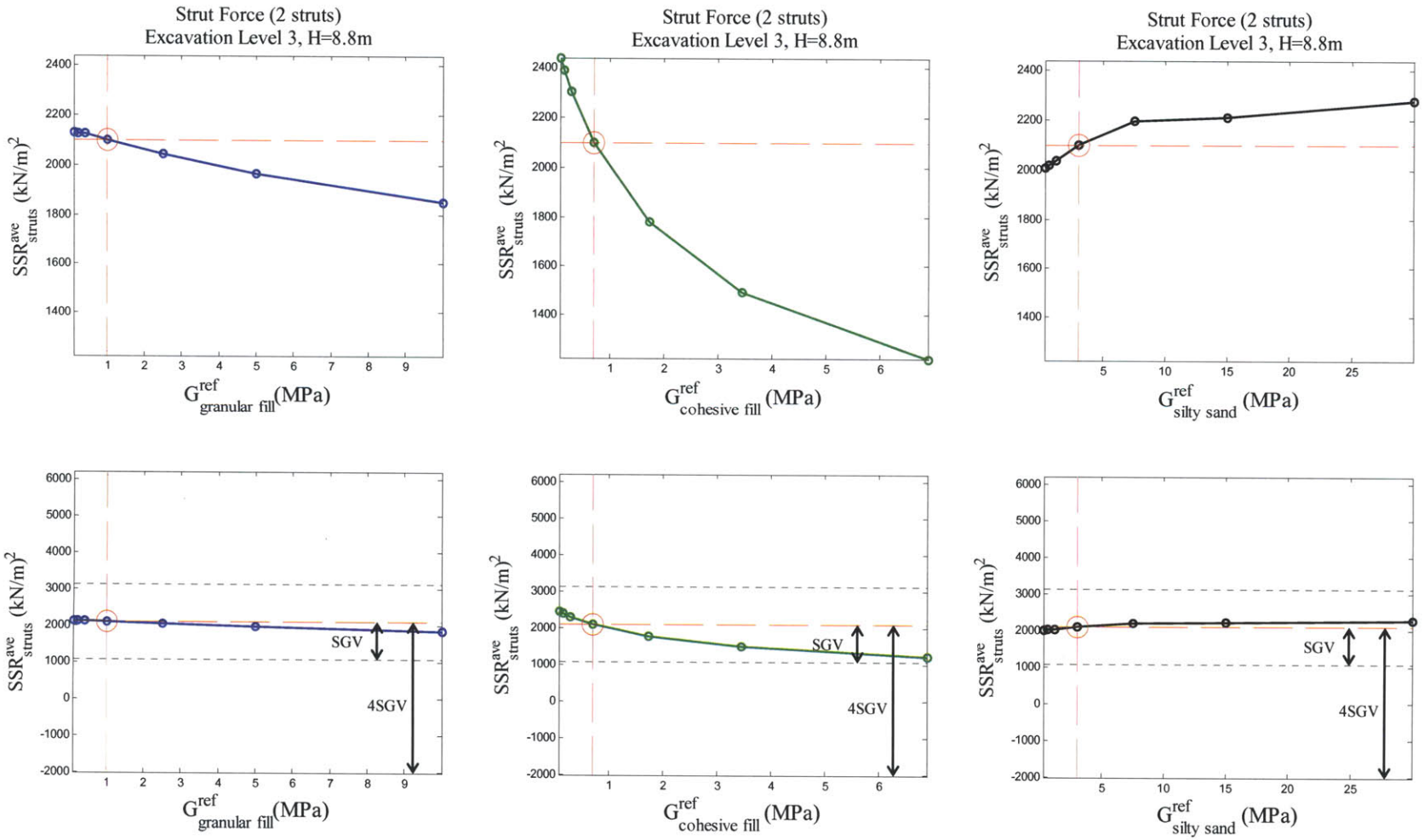

Figure A- 40: Sensitivity analysis of shear stiffness of granular fill, cohesive fill, and silty sand layers on strut forces at excavation level 3

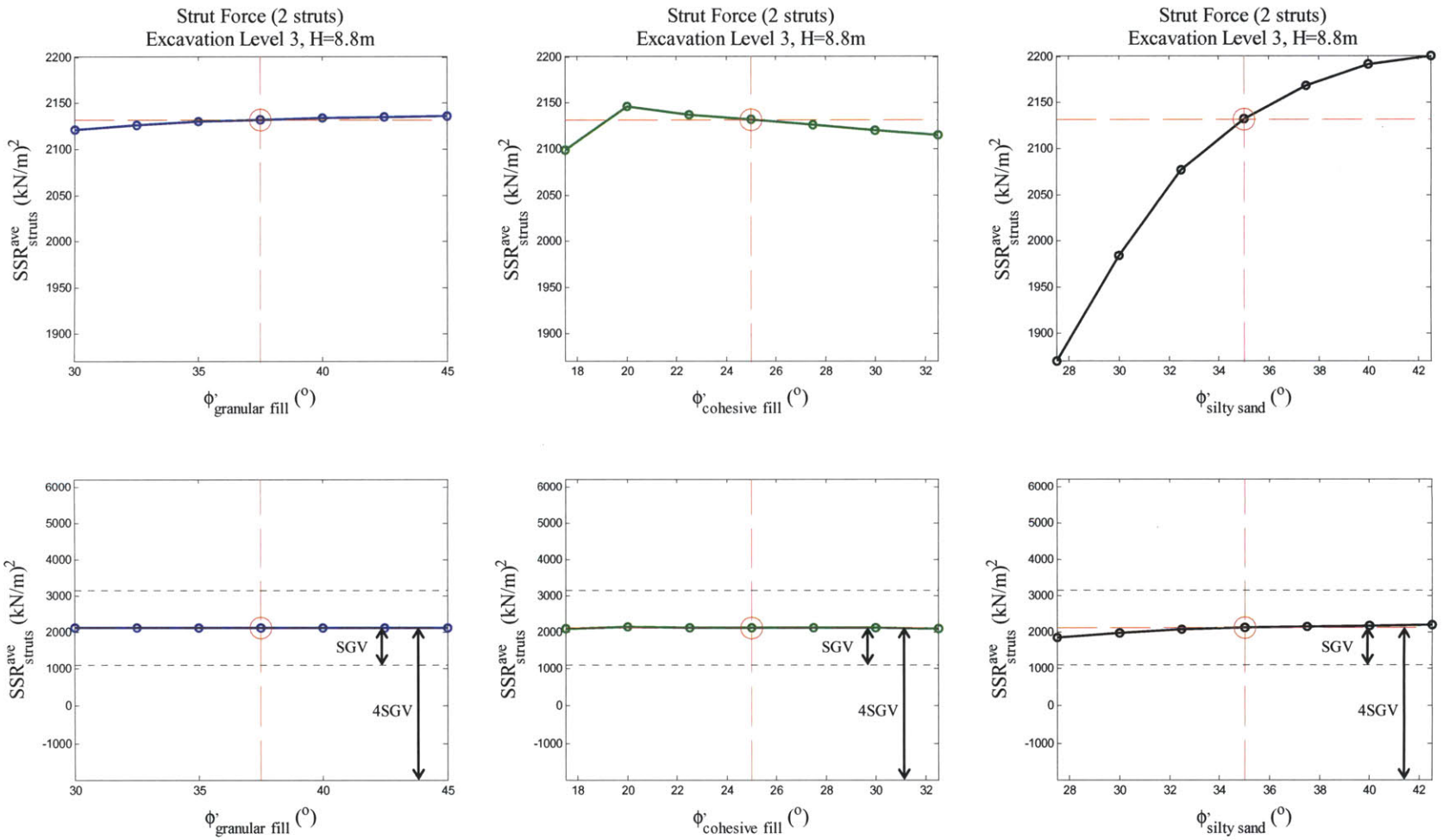

Figure A- 41: Sensitivity analysis of friction angles of granular fill, cohesive fill, and silty sand layers on strut forces at excavation level 3

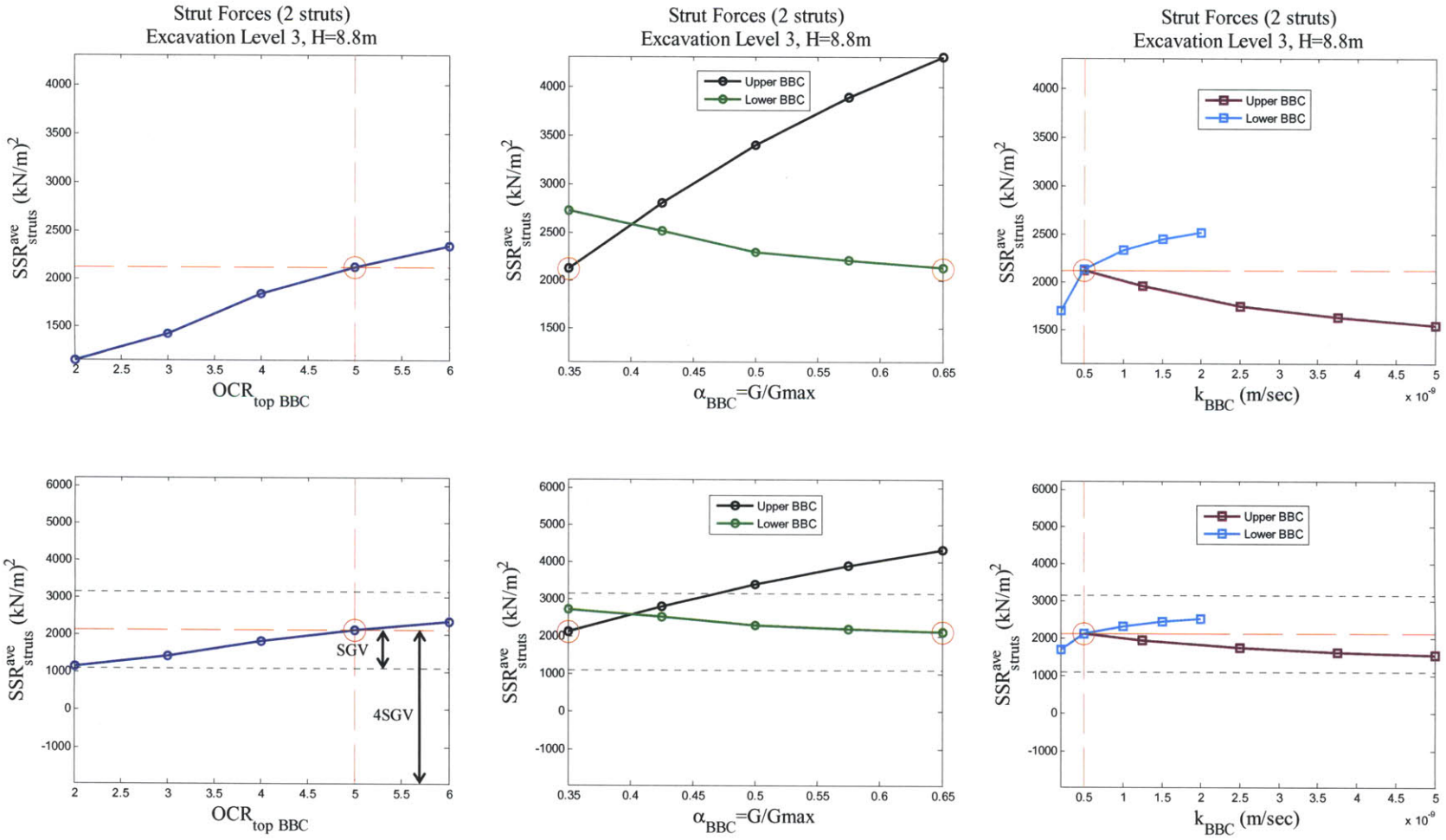

Figure A- 42: Sensitivity analysis of OCR (top), α parameter, and hydraulic conductivities of BBC layers on strut forces at excavation level 3

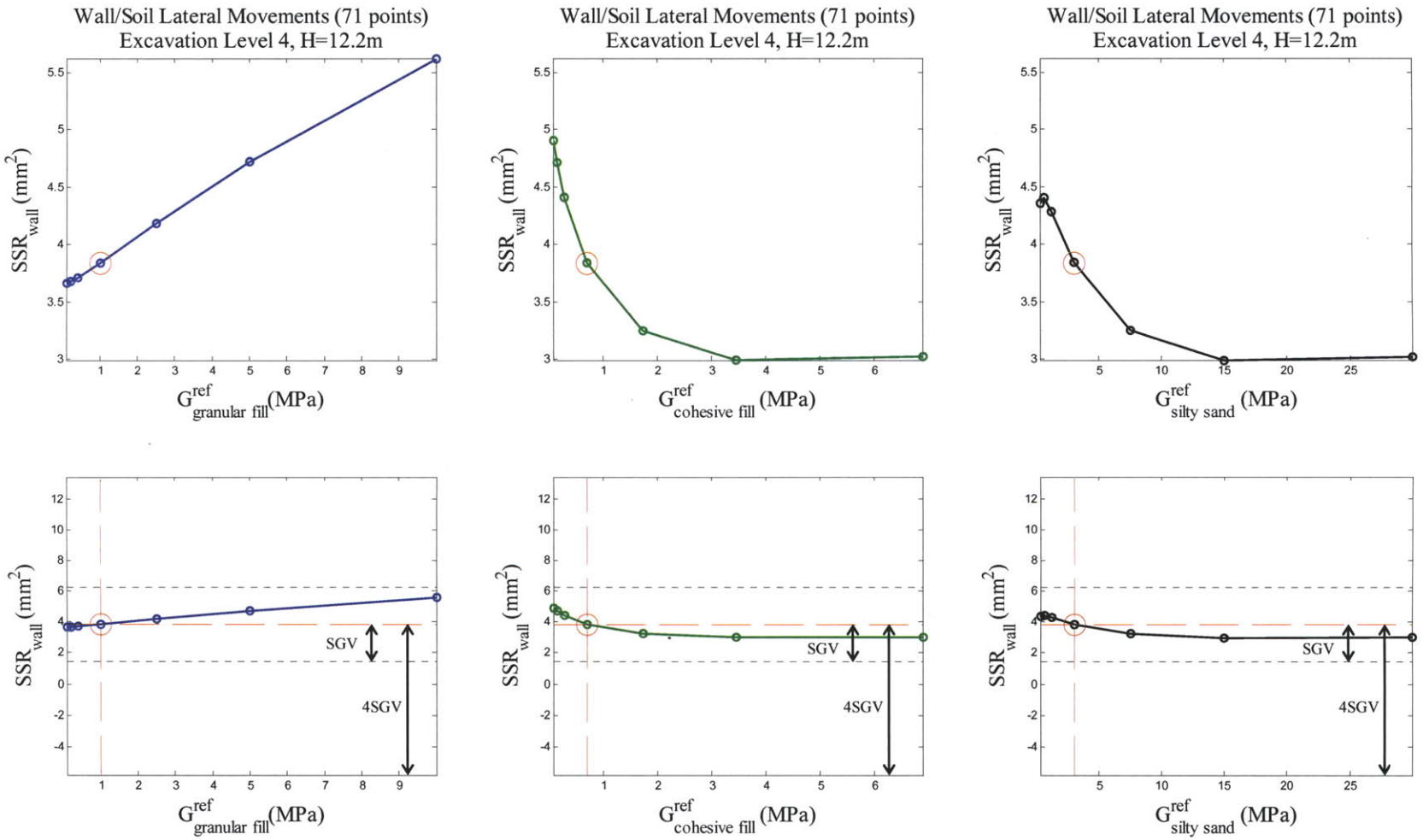

Figure A- 43: Sensitivity analysis of shear stiffness of granular fill, cohesive fill, and silty sand layers on lateral wall/soil movements at excavation level 4

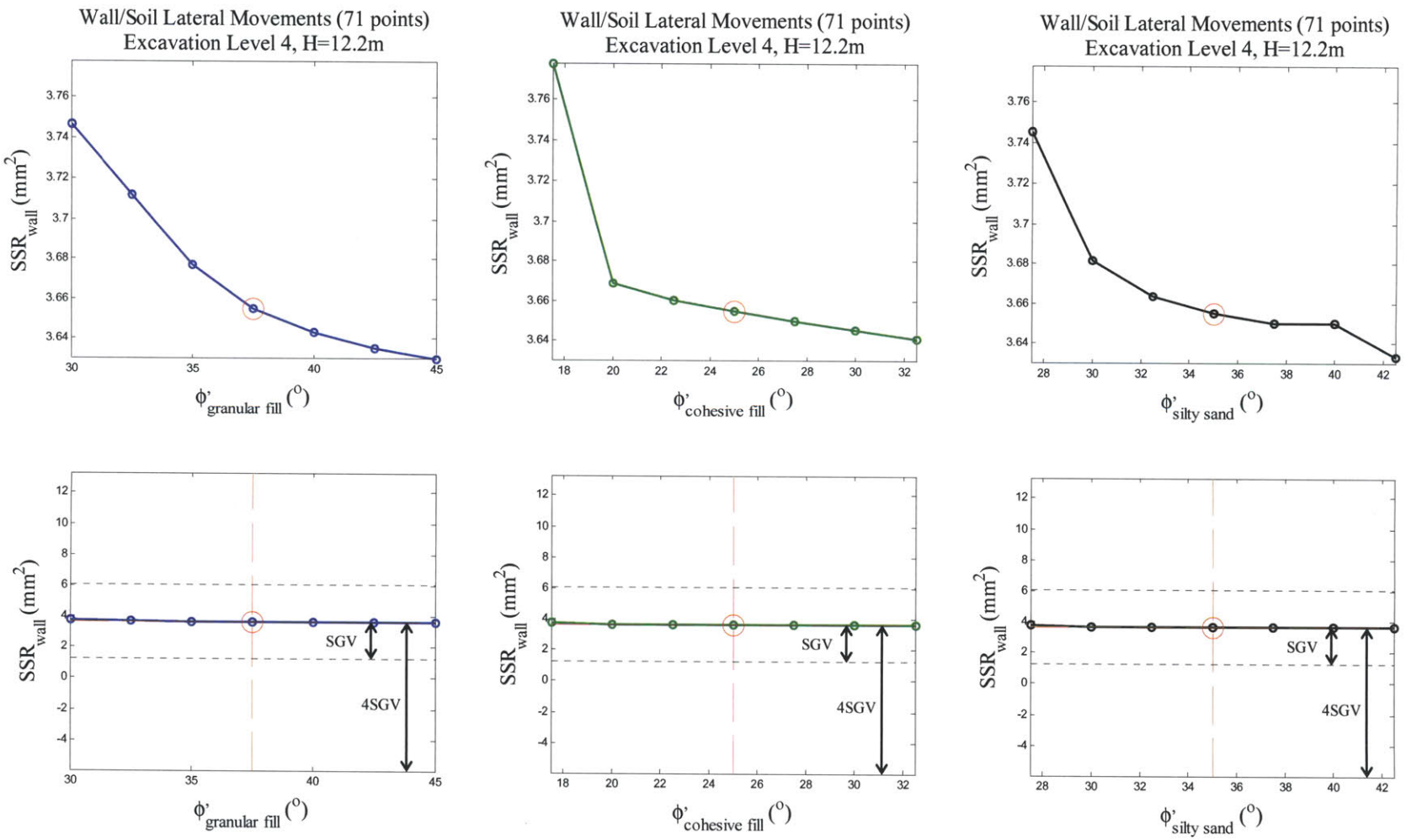

Figure A- 44: Sensitivity analysis of friction angles of granular fill, cohesive fill, and silty sand layers on lateral wall/soil movements at excavation level 4

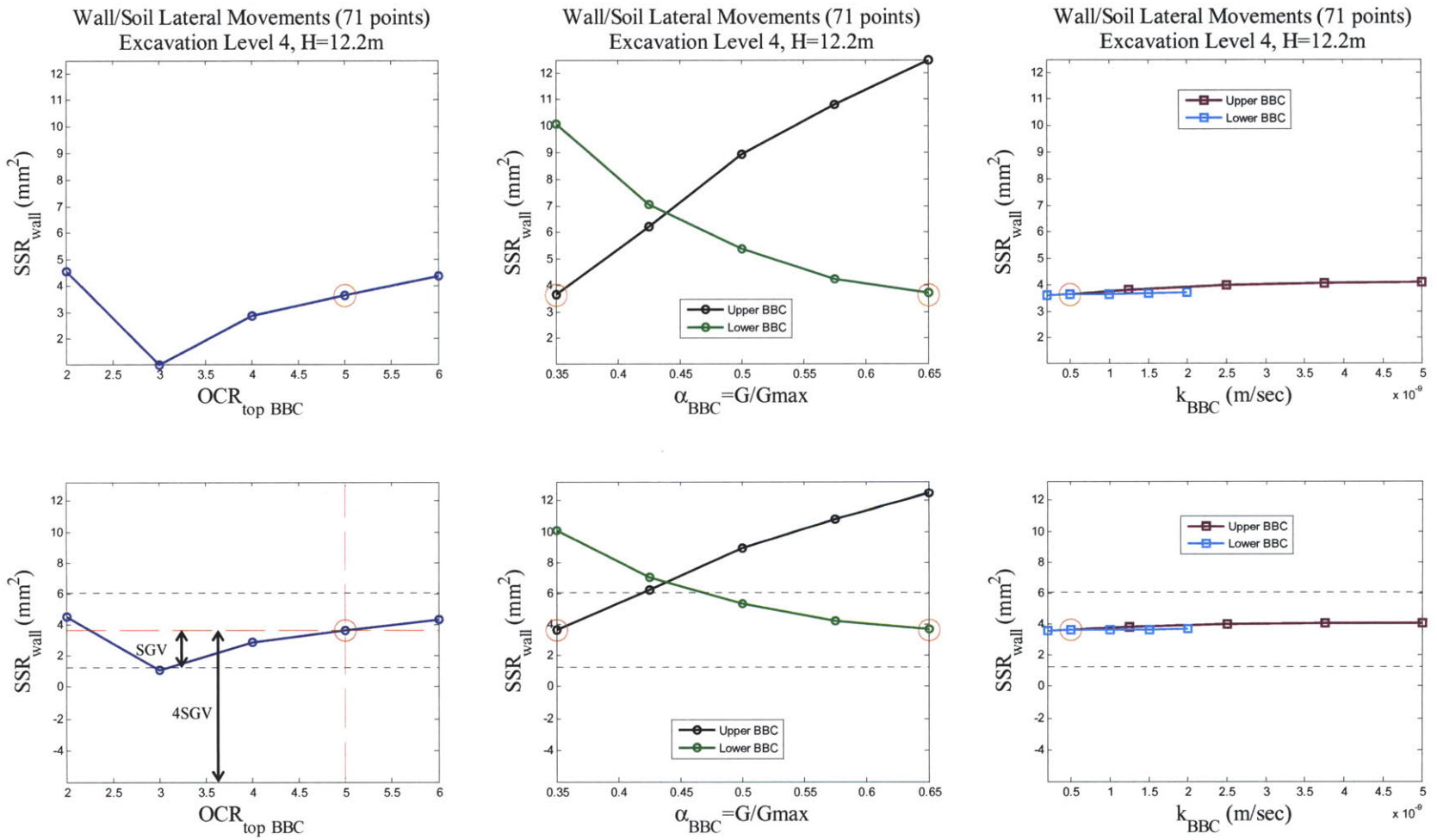

Figure A- 45: Sensitivity analysis of OCR (top), α parameter, and hydraulic conductivities of BBC layers on lateral wall/soil movements at excavation level 4

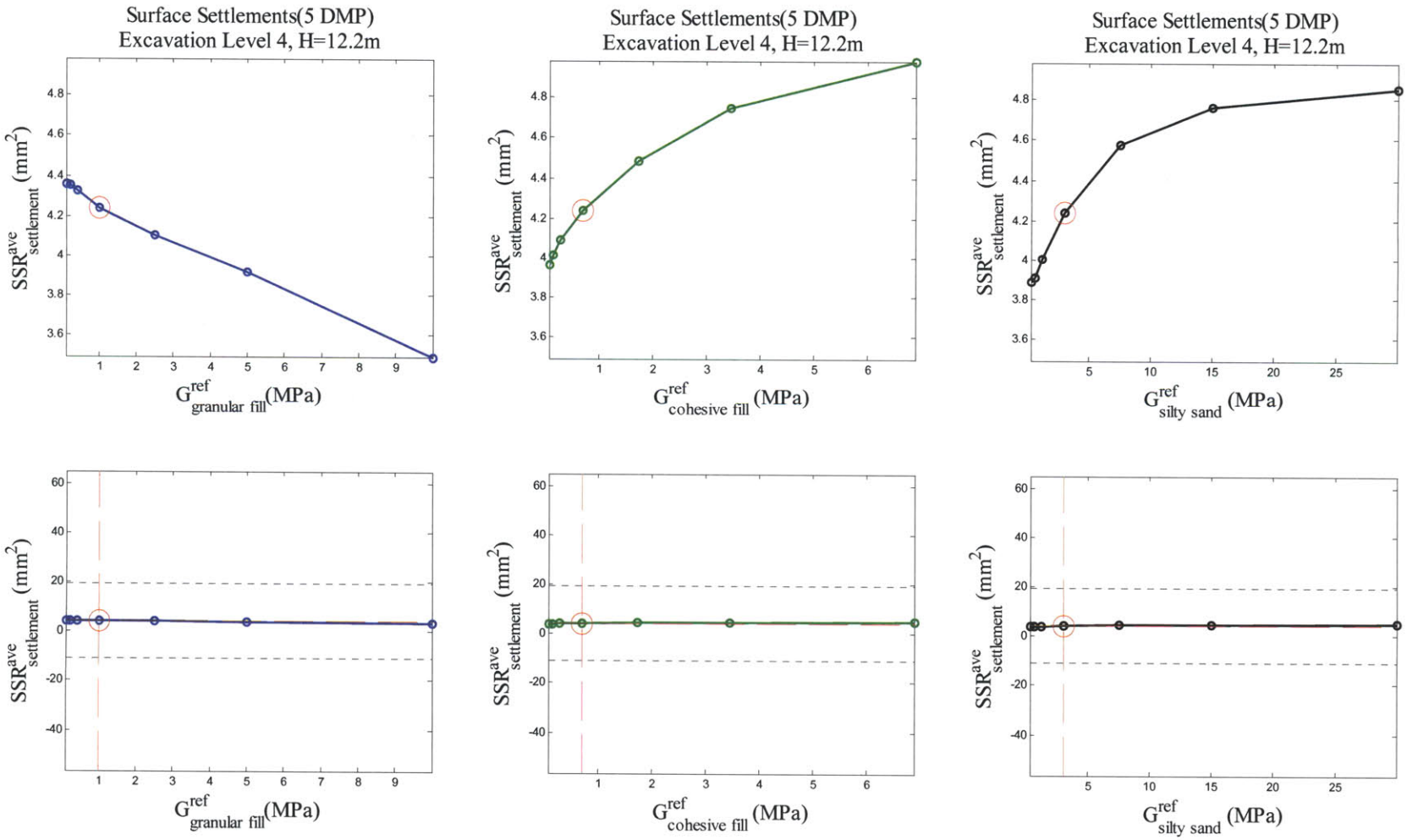

Figure A- 46: Sensitivity analysis of shear stiffness of granular fill, cohesive fill, and silty sand layers on surface settlement at excavation level 4

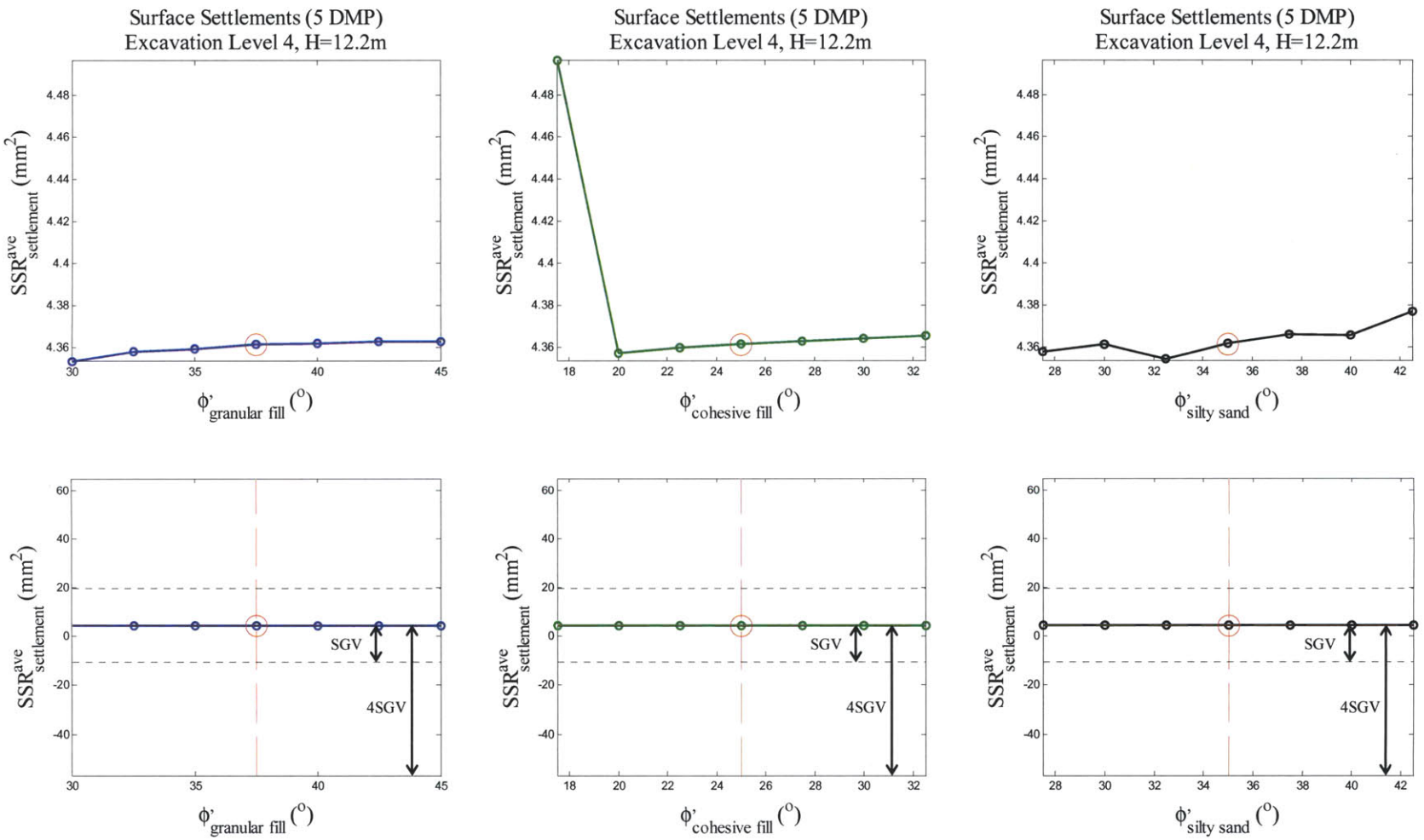

Figure A- 47: Sensitivity analysis of friction angles of granular fill, cohesive fill, and silty sand layers on surface settlement at excavation level 4

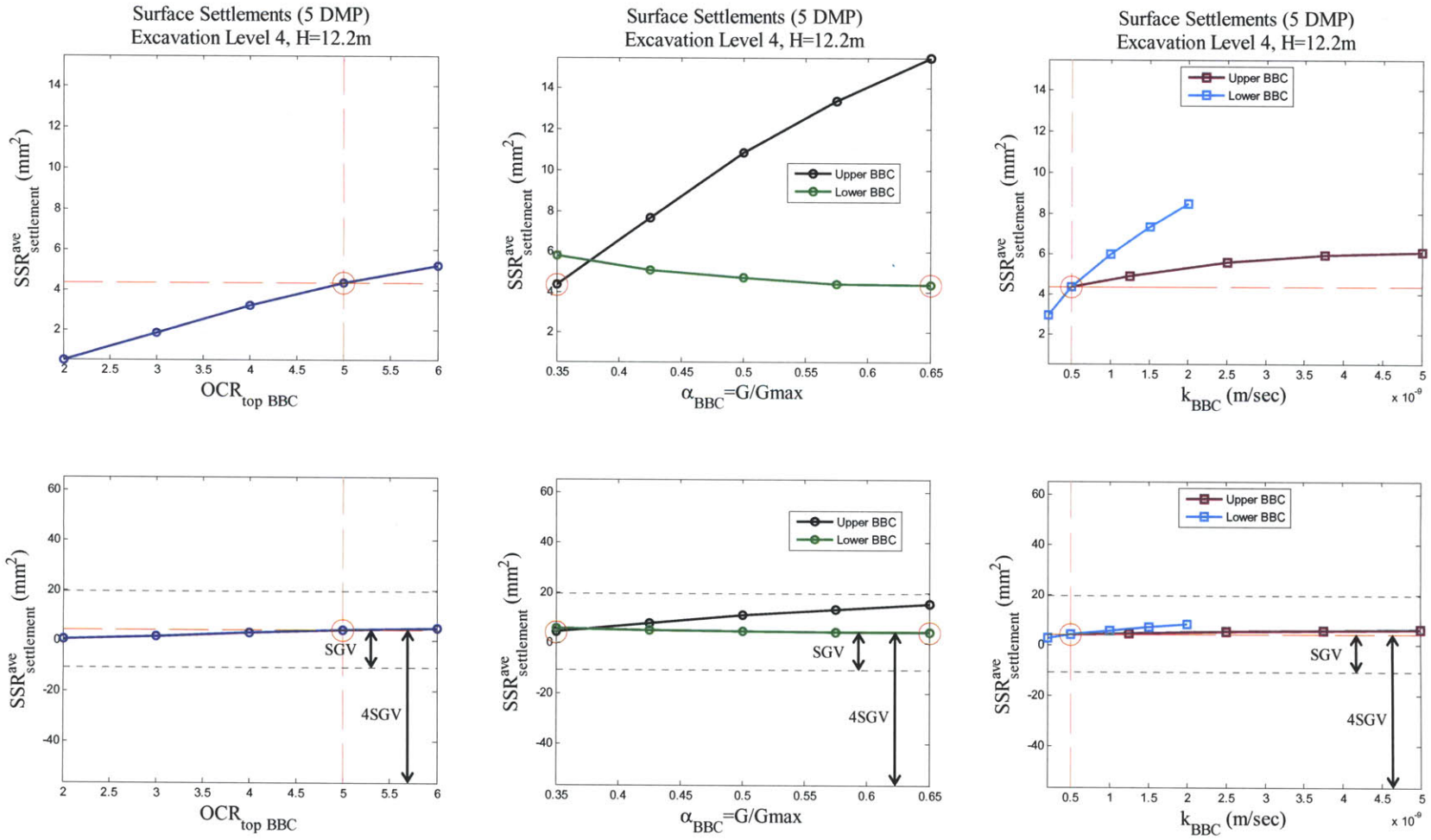

Figure A- 48: Sensitivity analysis of OCR (top), α parameter, and hydraulic conductivities of BBC layers on surface settlement at excavation level 4

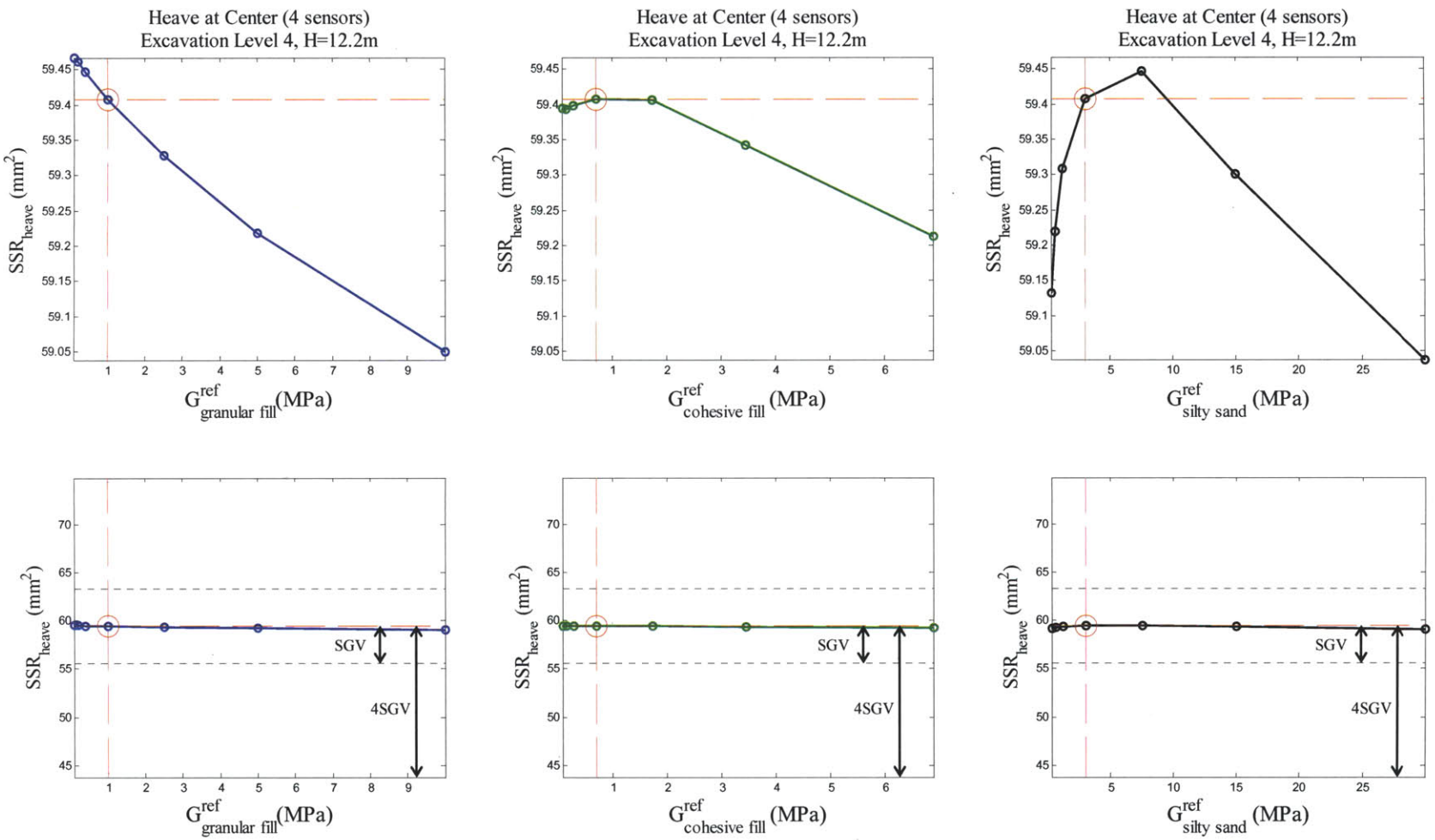

Figure A- 49: Sensitivity analysis of shear stiffness of granular fill, cohesive fill, and silty sand layers on excavation heave at excavation level 4

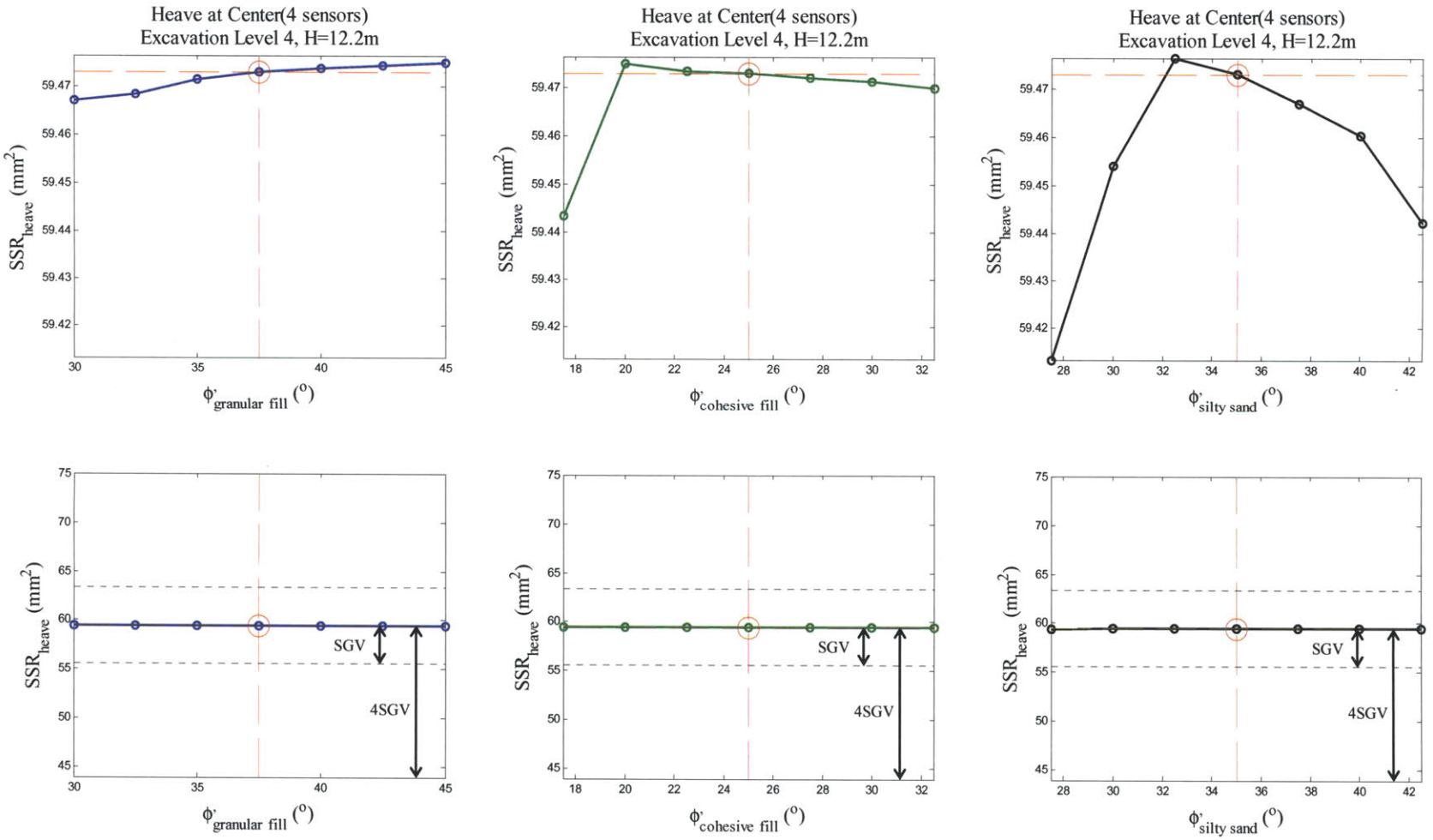

Figure A- 50: Sensitivity analysis of friction angles of granular fill, cohesive fill, and silty sand layers on excavation heave at excavation level 4

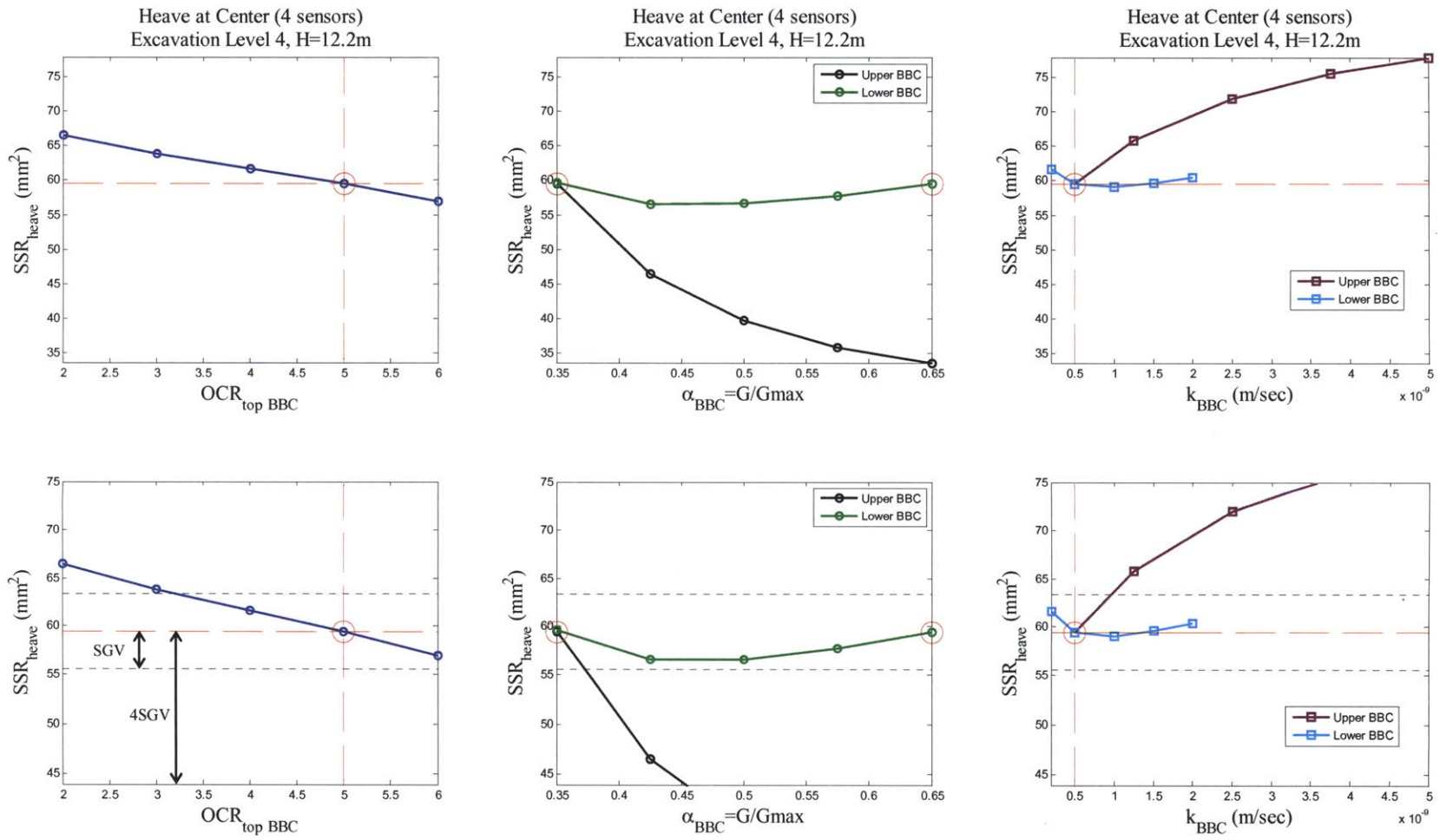

Figure A- 51: Sensitivity analysis of OCR (top), α parameter, and hydraulic conductivities of BBC layers on excavation heave at excavation level 4

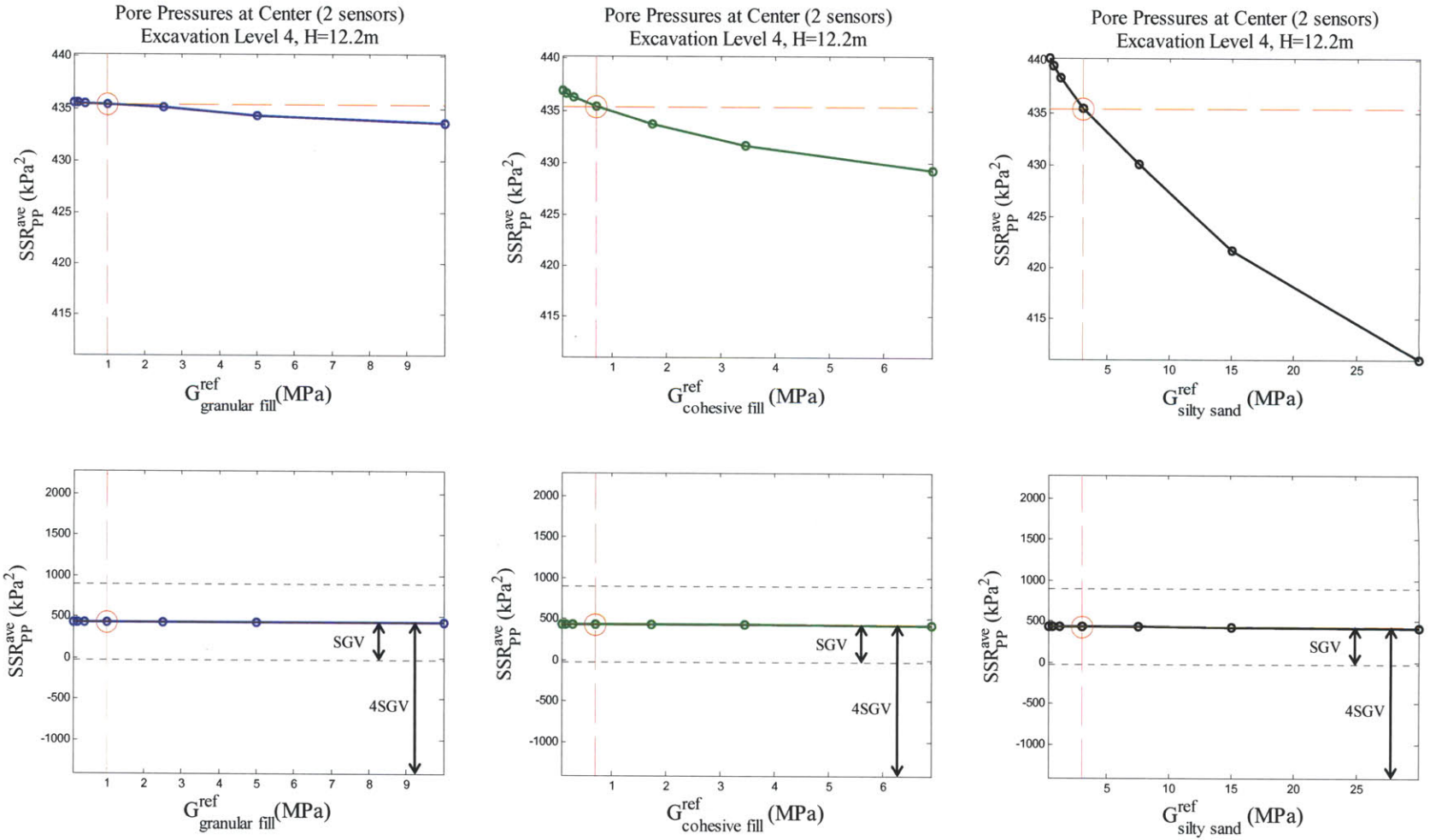

Figure A- 52: Sensitivity analysis of shear stiffness of granular fill, cohesive fill, and silty sand layers on pore pressures at excavation level 4

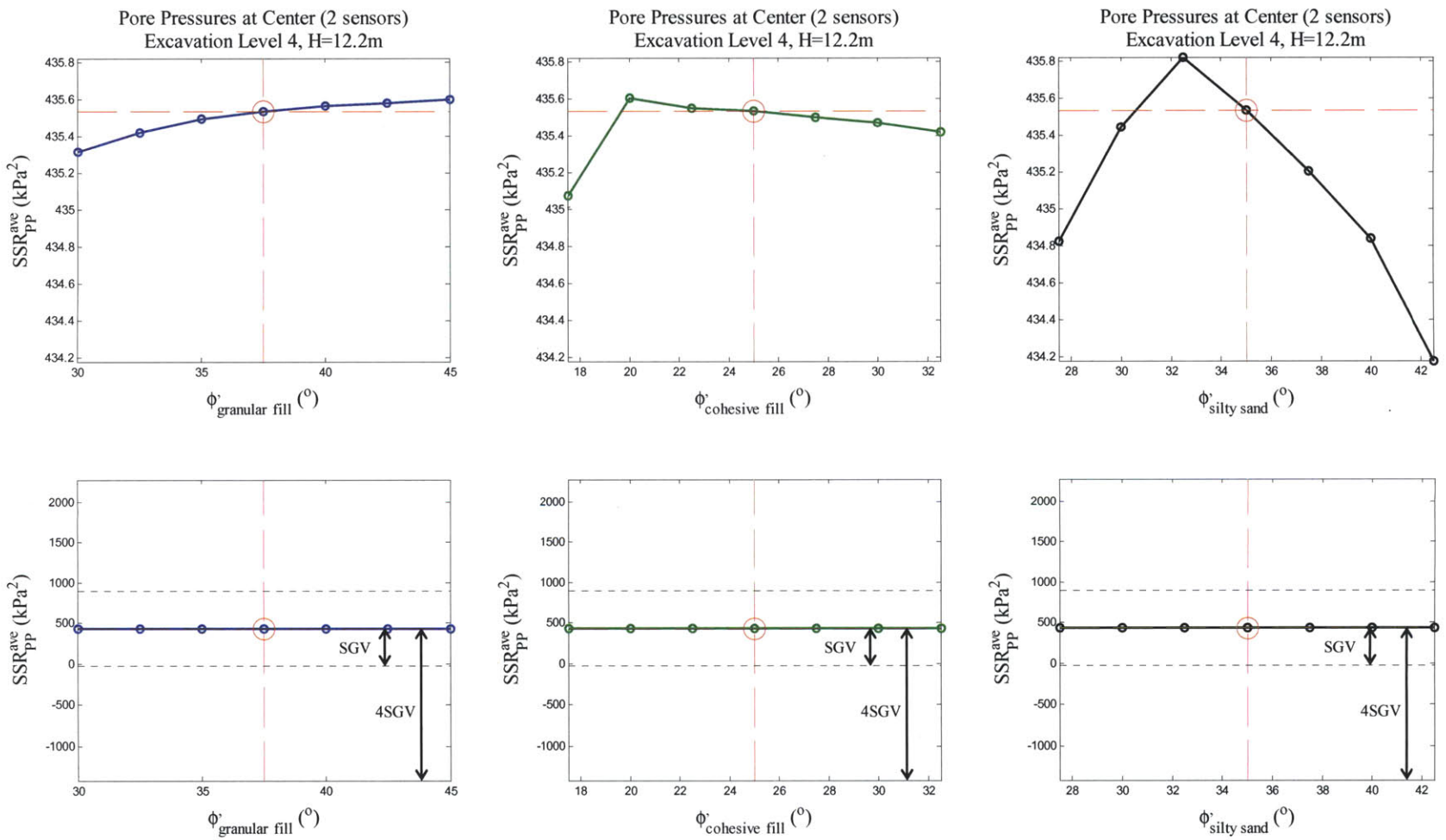

Figure A- 53: Sensitivity analysis of friction angles of granular fill, cohesive fill, and silty sand layers on pore pressures at excavation level 4

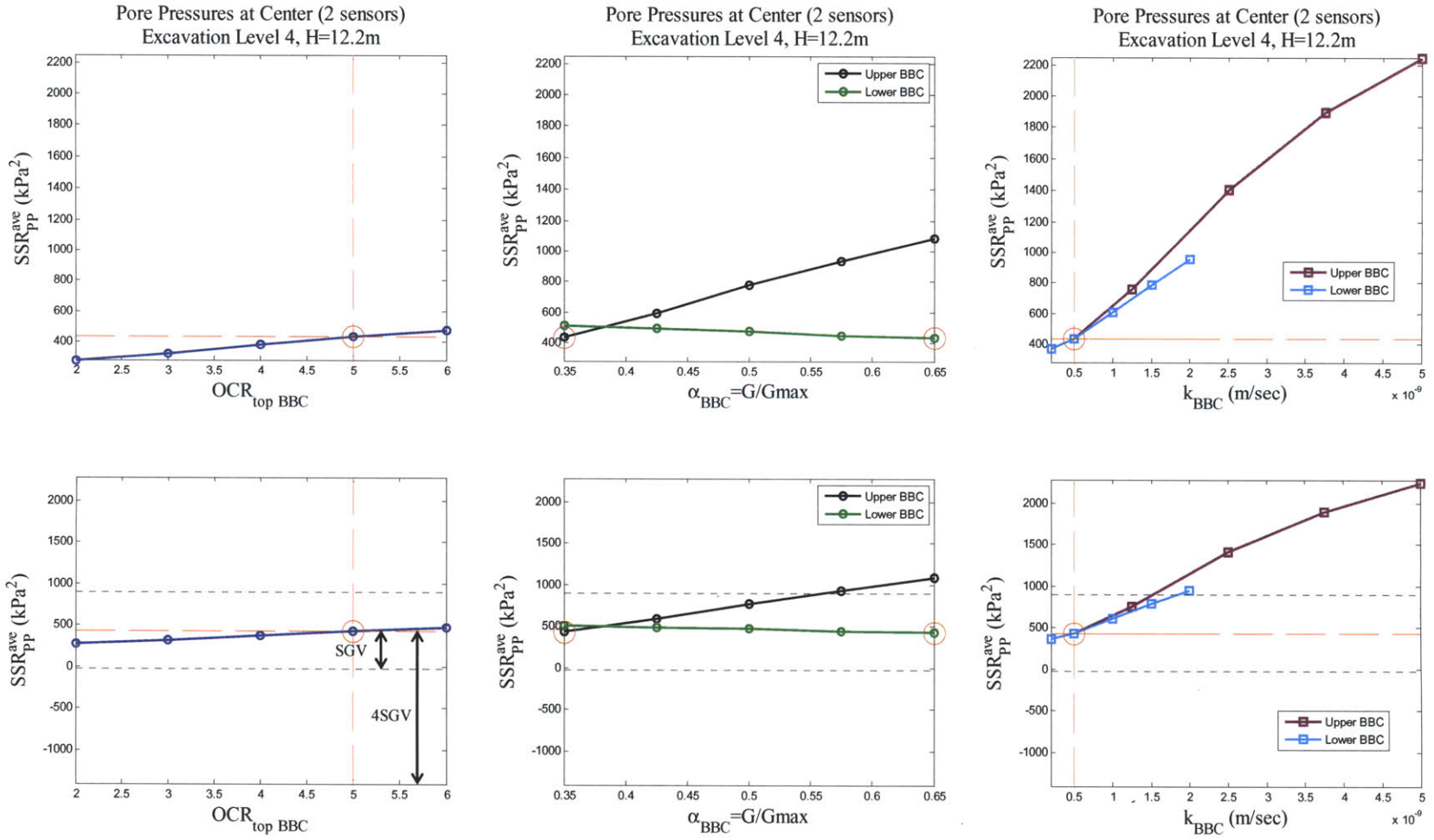

Figure A- 54: Sensitivity analysis of OCR (top), α parameter, and hydraulic conductivities of BBC layers on pore pressures at excavation level 4

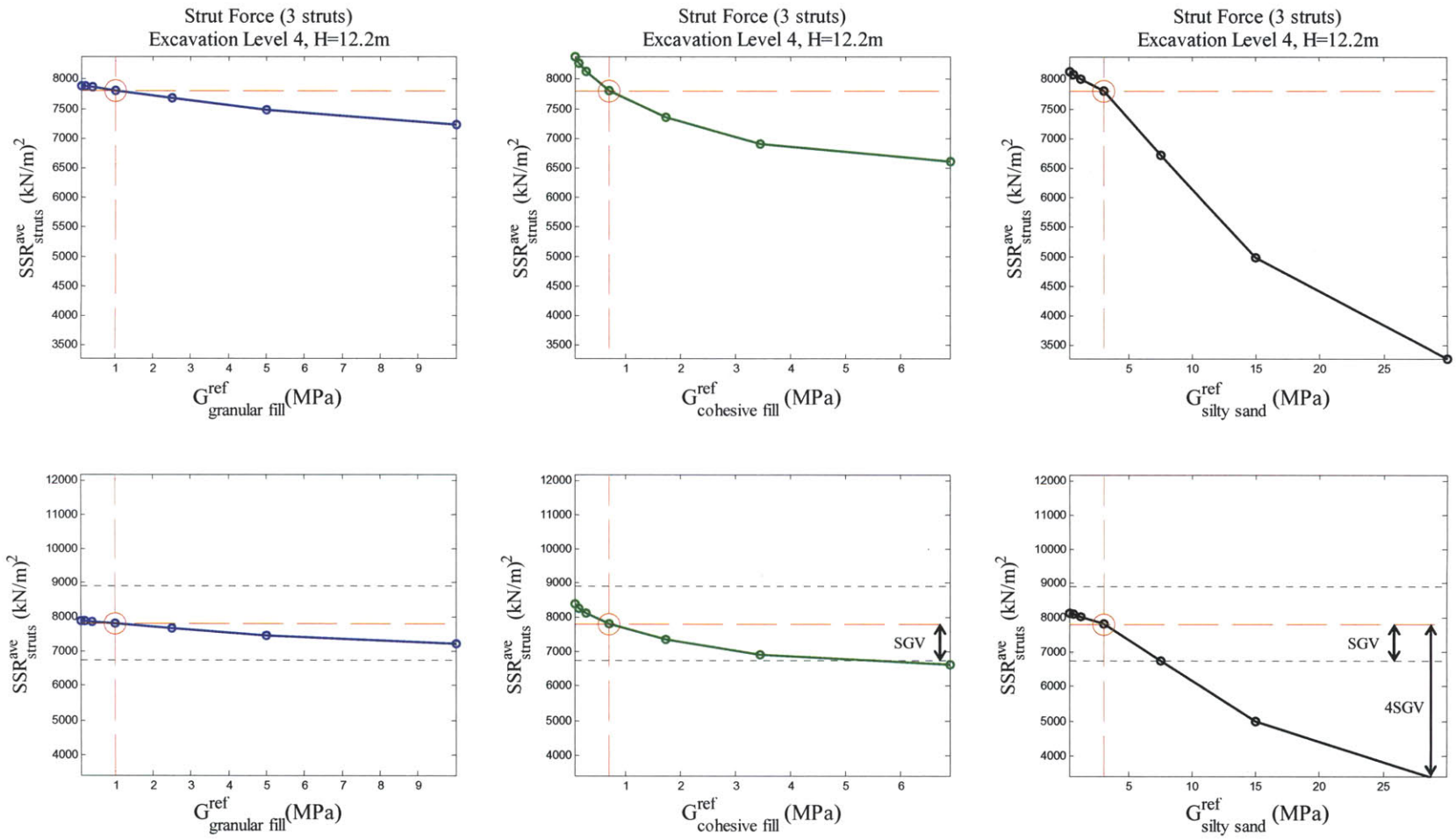

Figure A- 55: Sensitivity analysis of shear stiffness of granular fill, cohesive fill, and silty sand layers on strut forces at excavation level 4

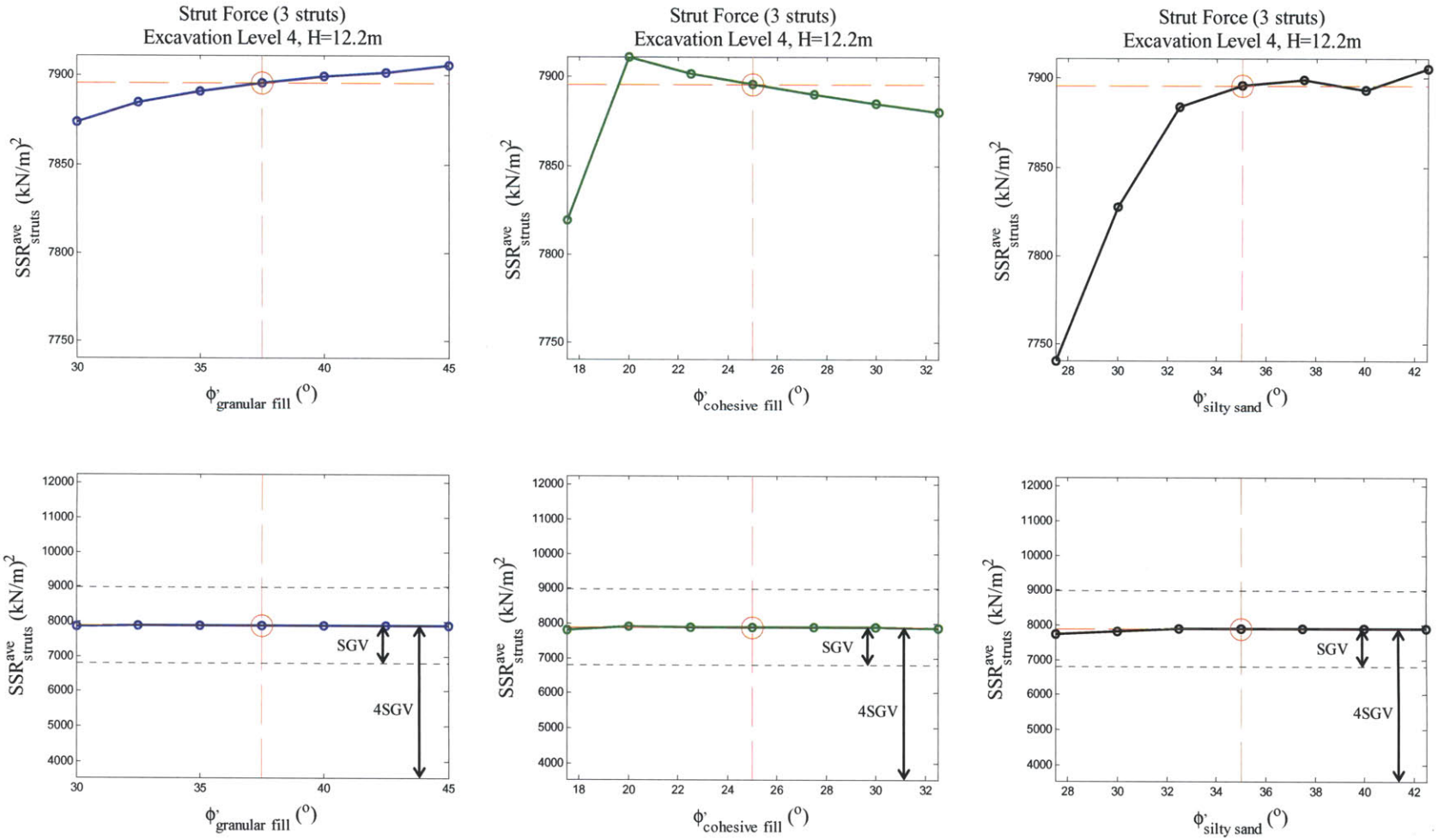

Figure A- 56: Sensitivity analysis of friction angles of granular fill, cohesive fill, and silty sand layers on strut forces at excavation level 4

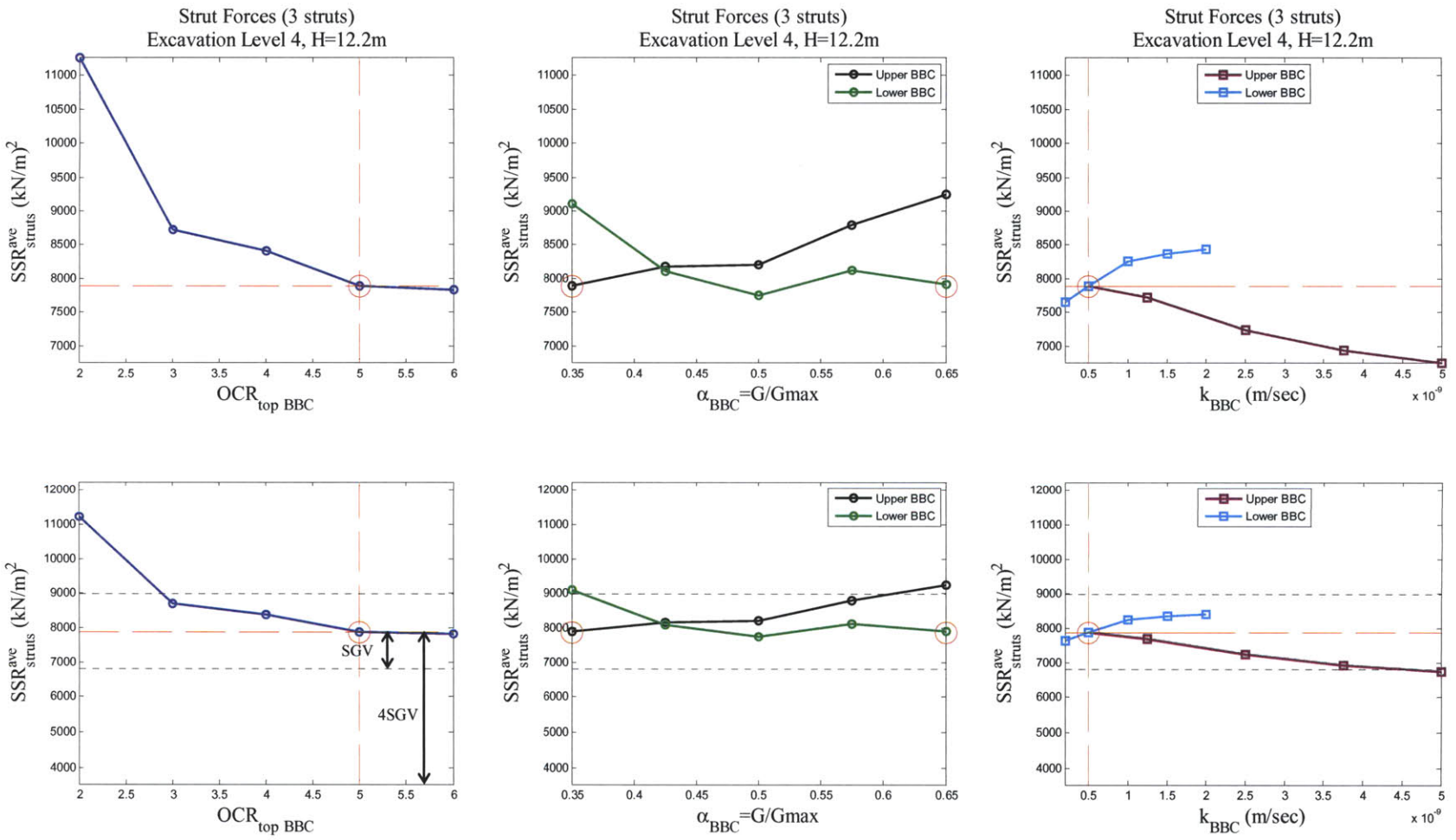

Figure A- 57: Sensitivity analysis of OCR (top), α parameter, and hydraulic conductivities of BBC layers on strut forces at excavation level 4

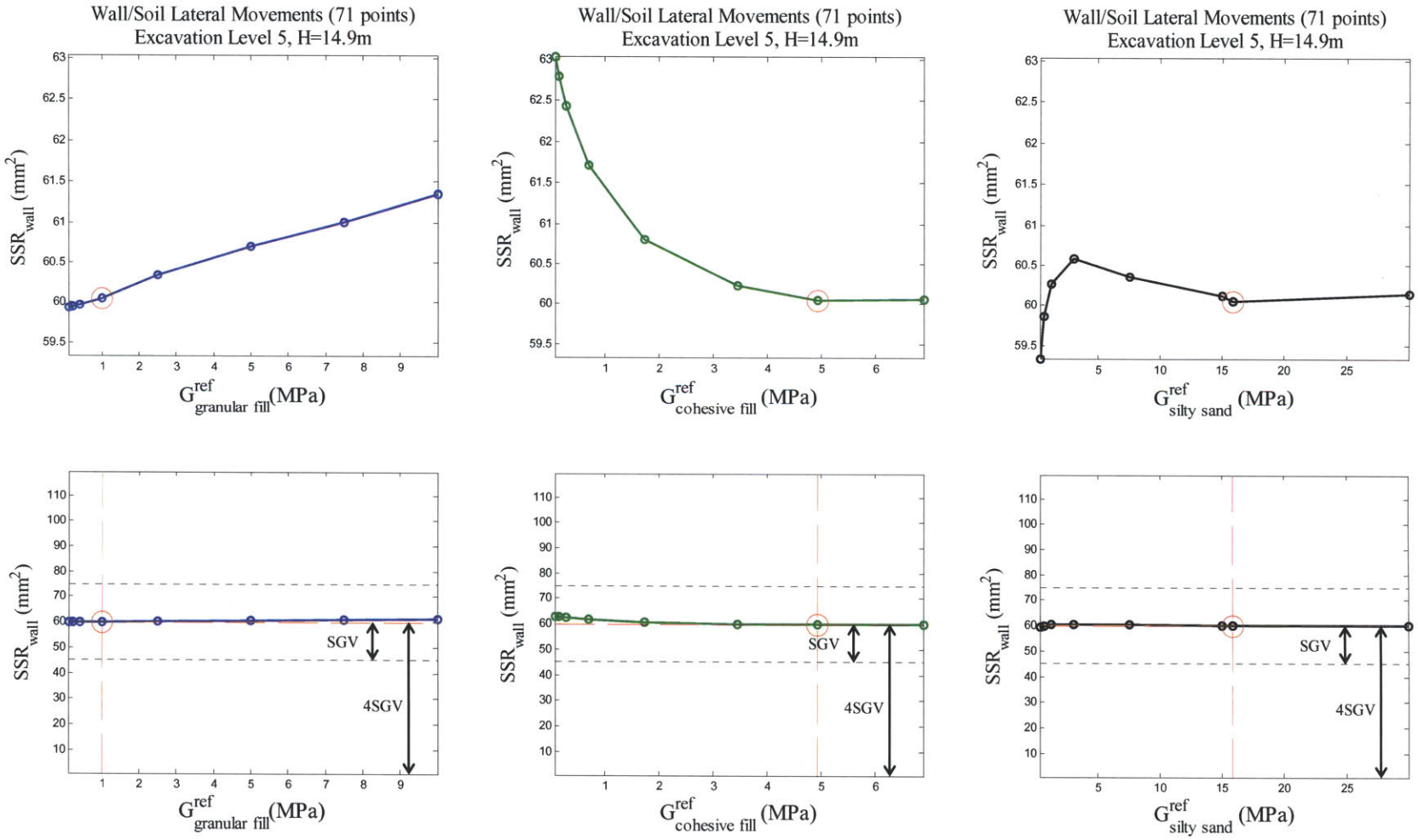

Figure A- 58: Sensitivity analysis of shear stiffness of granular fill, cohesive fill, and silty sand layers on lateral wall/soil movements at excavation level 5

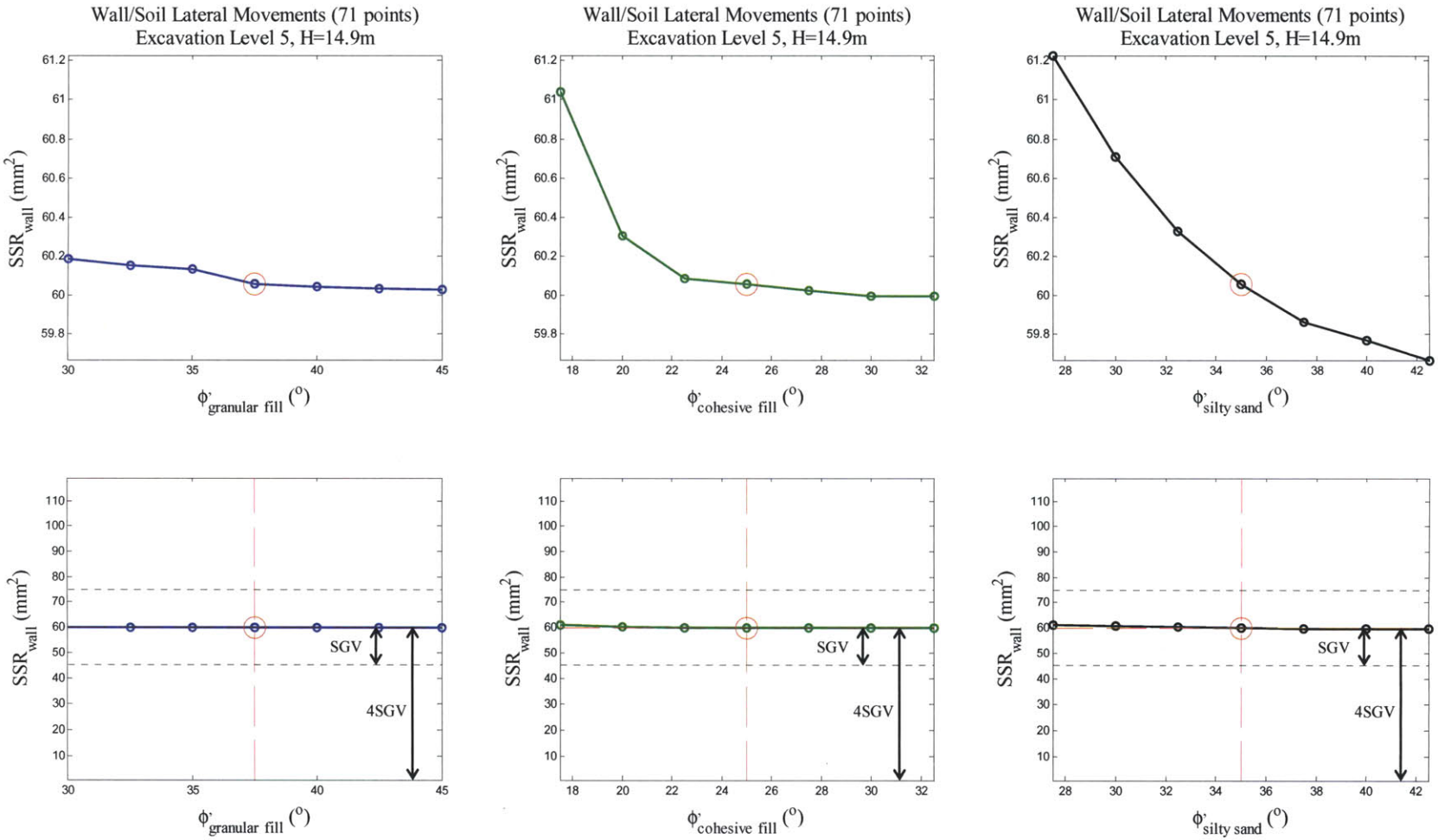

Figure A- 59: Sensitivity analysis of friction angles of granular fill, cohesive fill, and silty sand layers on lateral wall/soil movements at excavation level 5

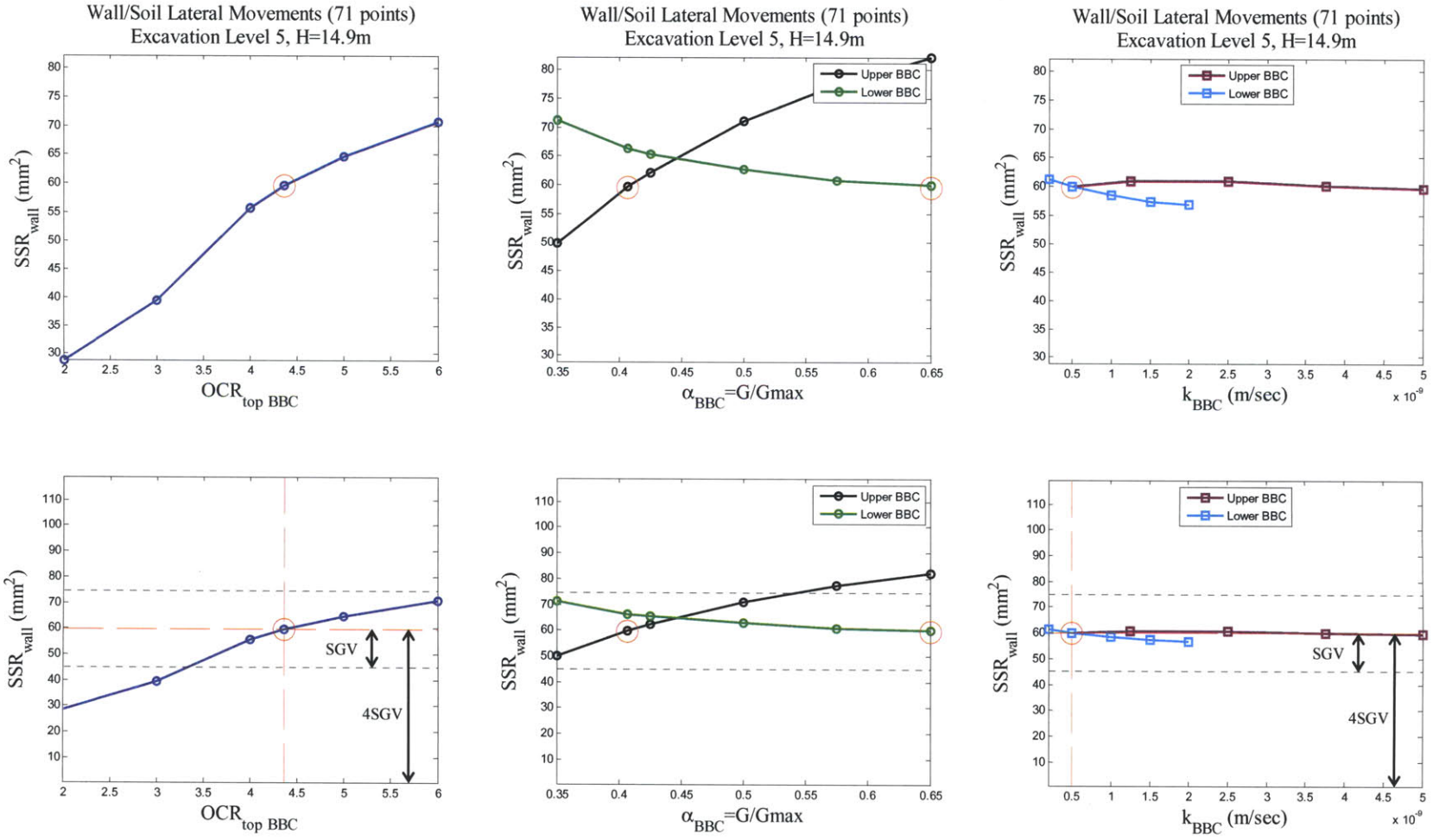

Figure A- 60: Sensitivity analysis of OCR (top), α parameter, and hydraulic conductivities of BBC layers on lateral wall/soil movements at excavation level 5

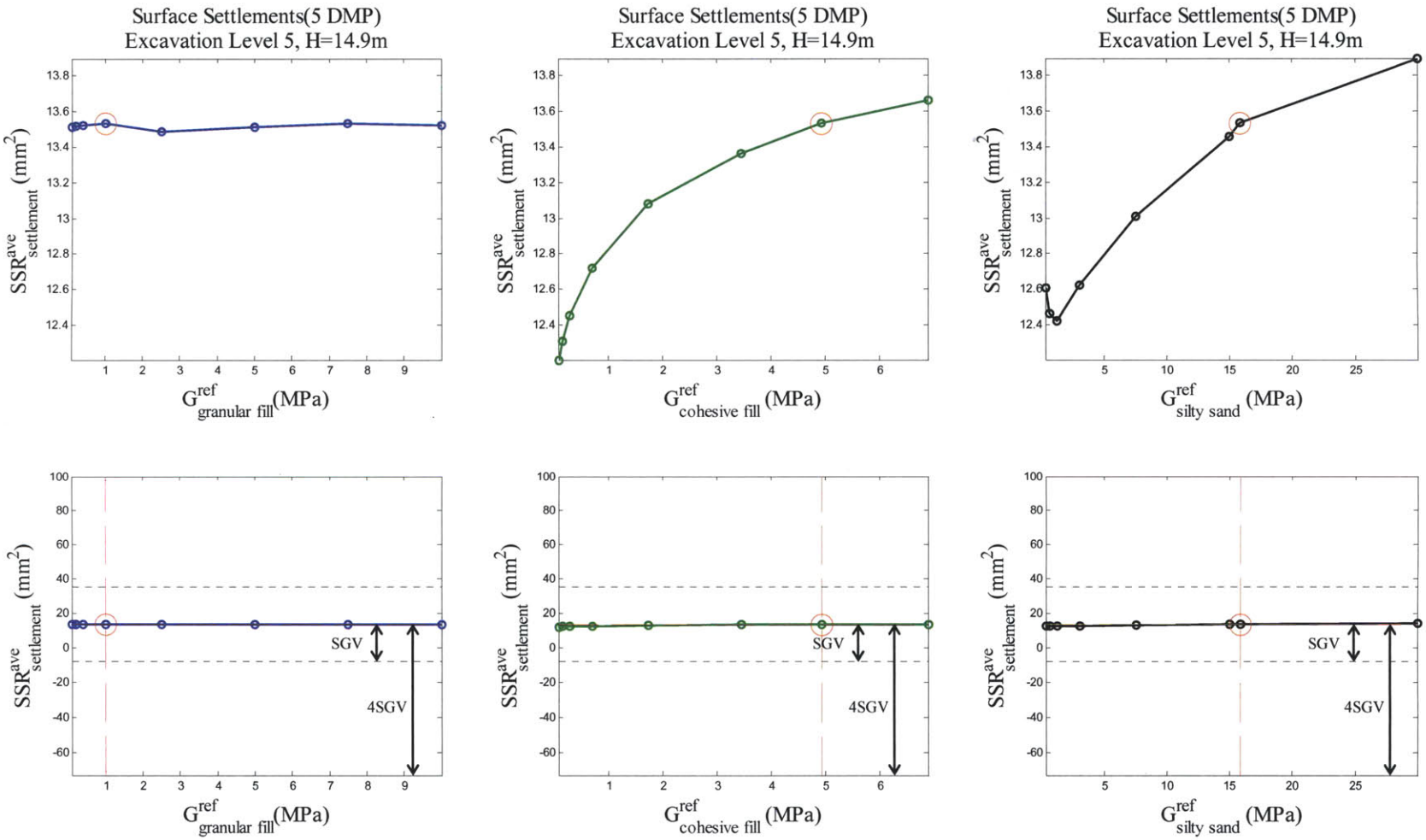

Figure A- 61: Sensitivity analysis of shear stiffness of granular fill, cohesive fill, and silty sand layers on surface settlement at excavation level 5

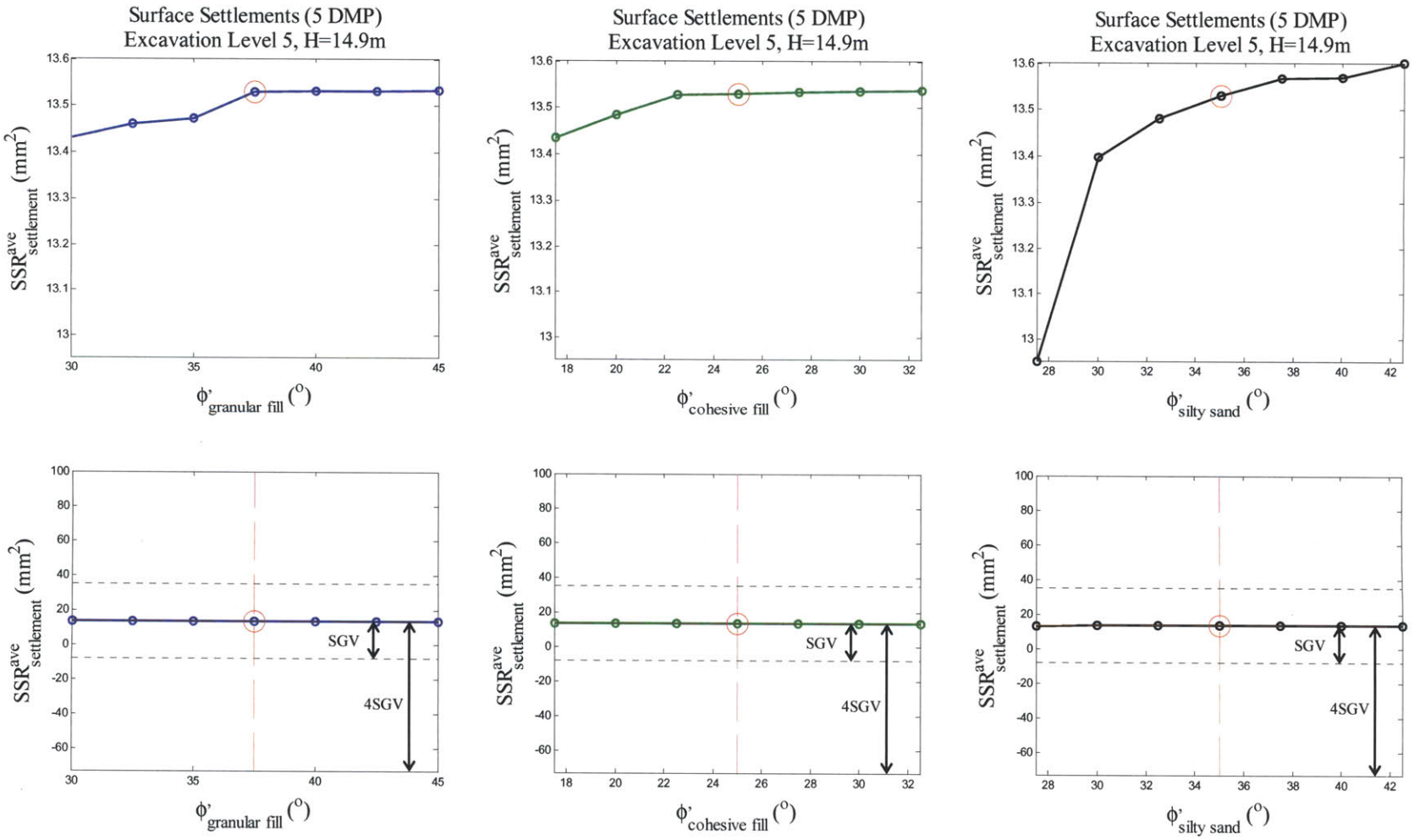

Figure A- 62: Sensitivity analysis of friction angles of granular fill, cohesive fill, and silty sand layers on surface settlement at excavation level 5

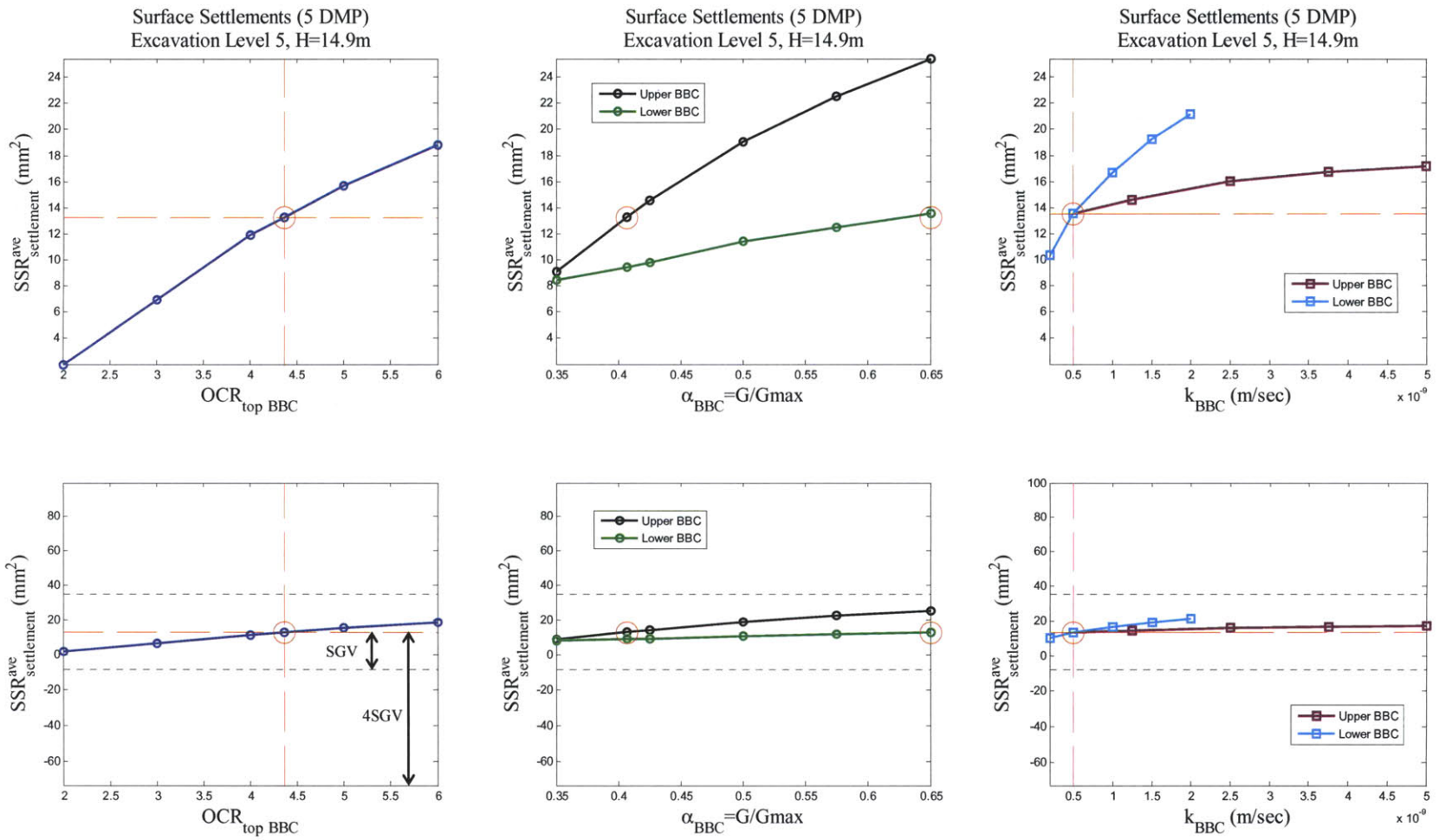

Figure A- 63: Sensitivity analysis of OCR (top), α parameter, and hydraulic conductivities of BBC layers on surface settlement at excavation level 5

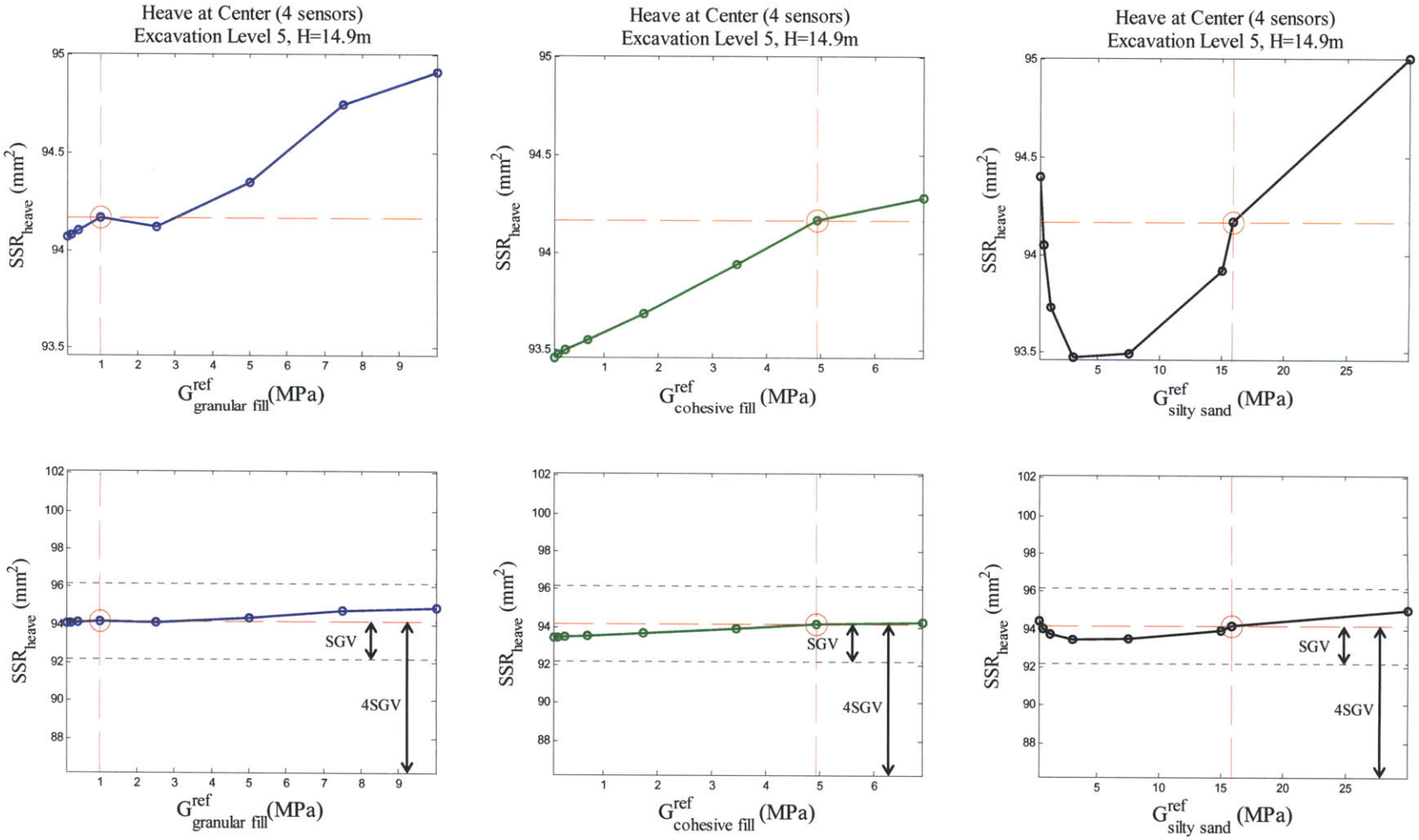

Figure A- 64: Sensitivity analysis of shear stiffness of granular fill, cohesive fill, and silty sand layers on excavation heave at excavation level 5

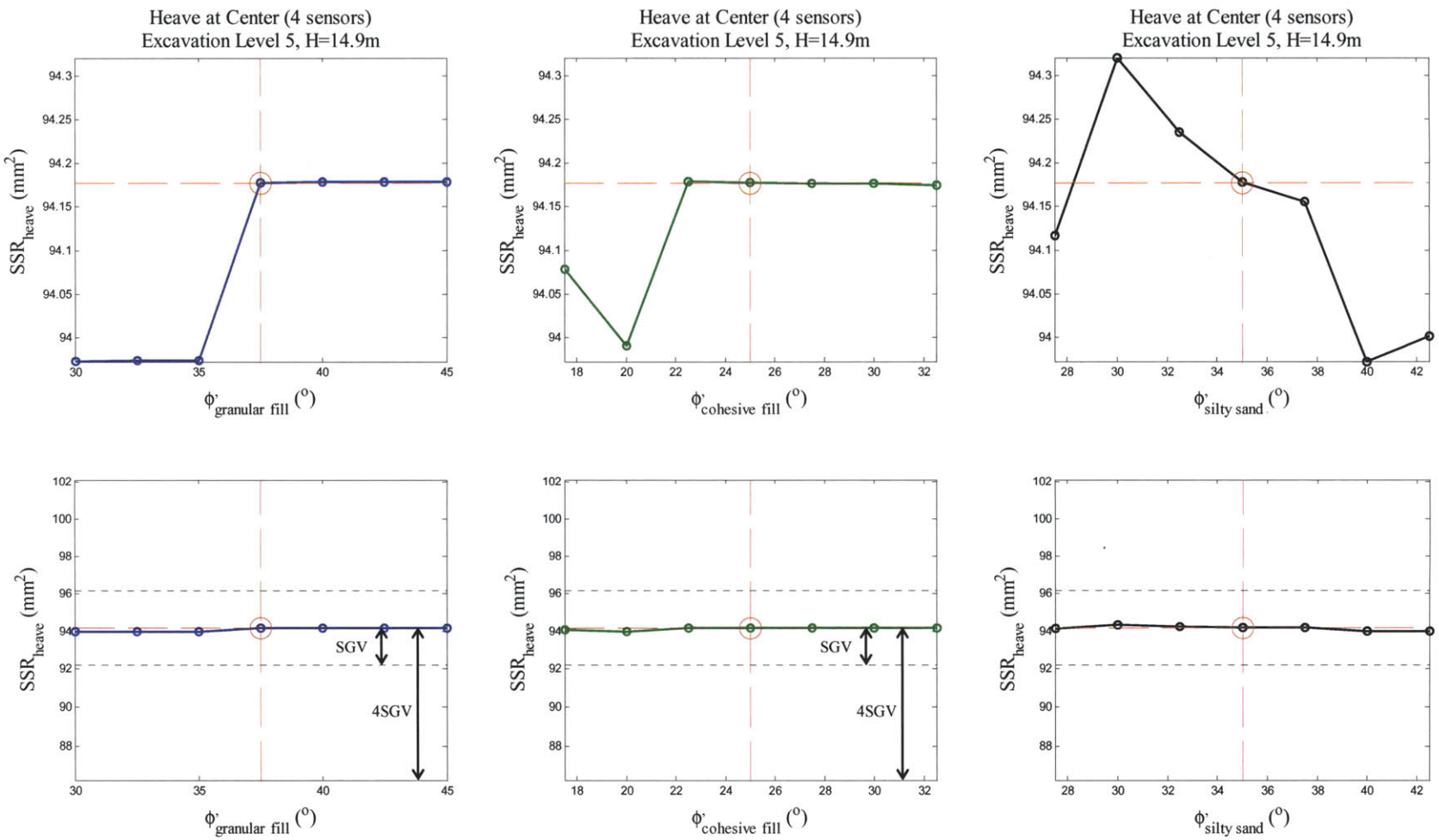

Figure A- 65: Sensitivity analysis of friction angles of granular fill, cohesive fill, and silty sand layers on excavation heave at excavation level 5

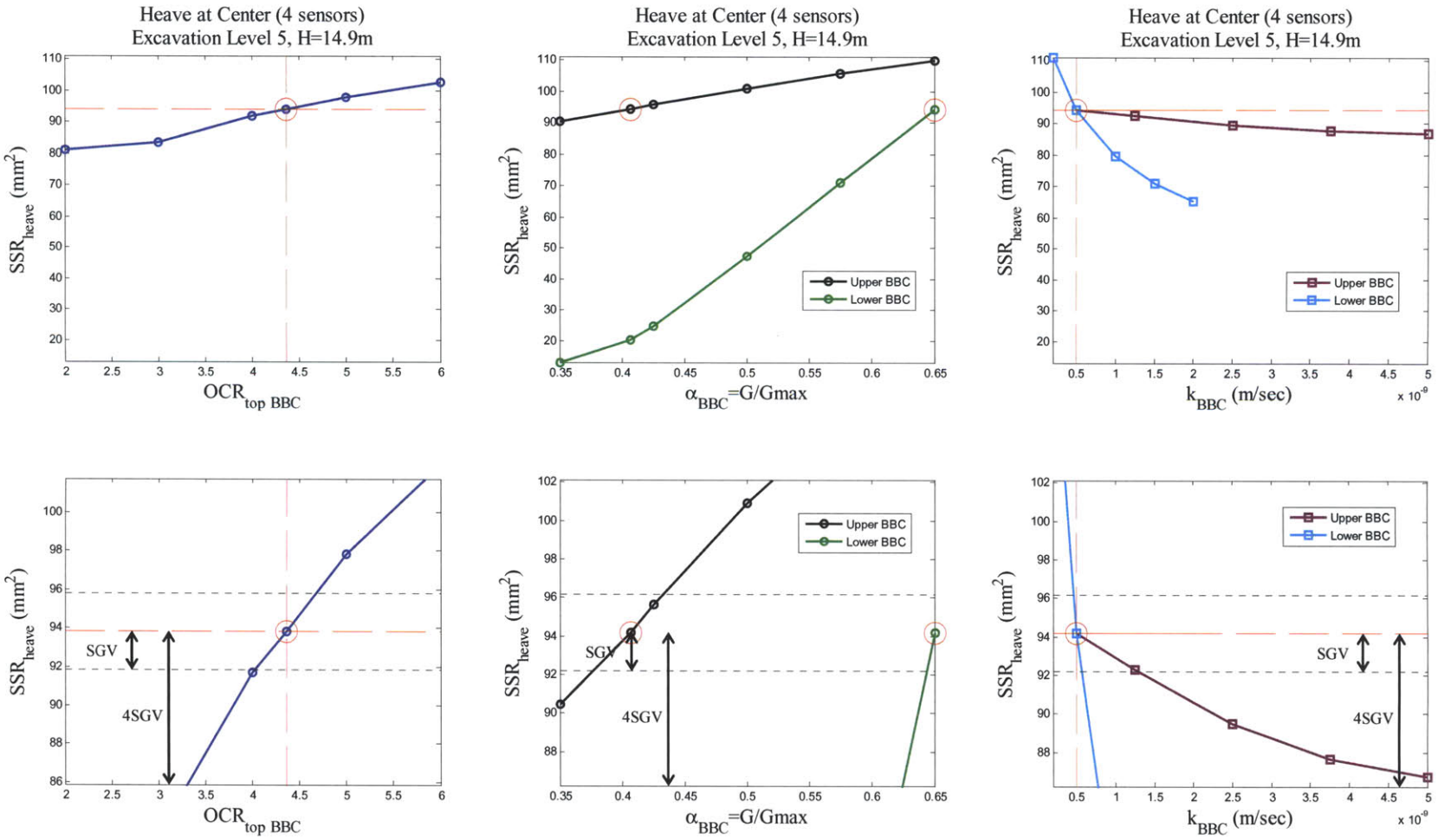

Figure A- 66: Sensitivity analysis of OCR (top), α parameter, and hydraulic conductivities of BBC layers on excavation heave at excavation level 5

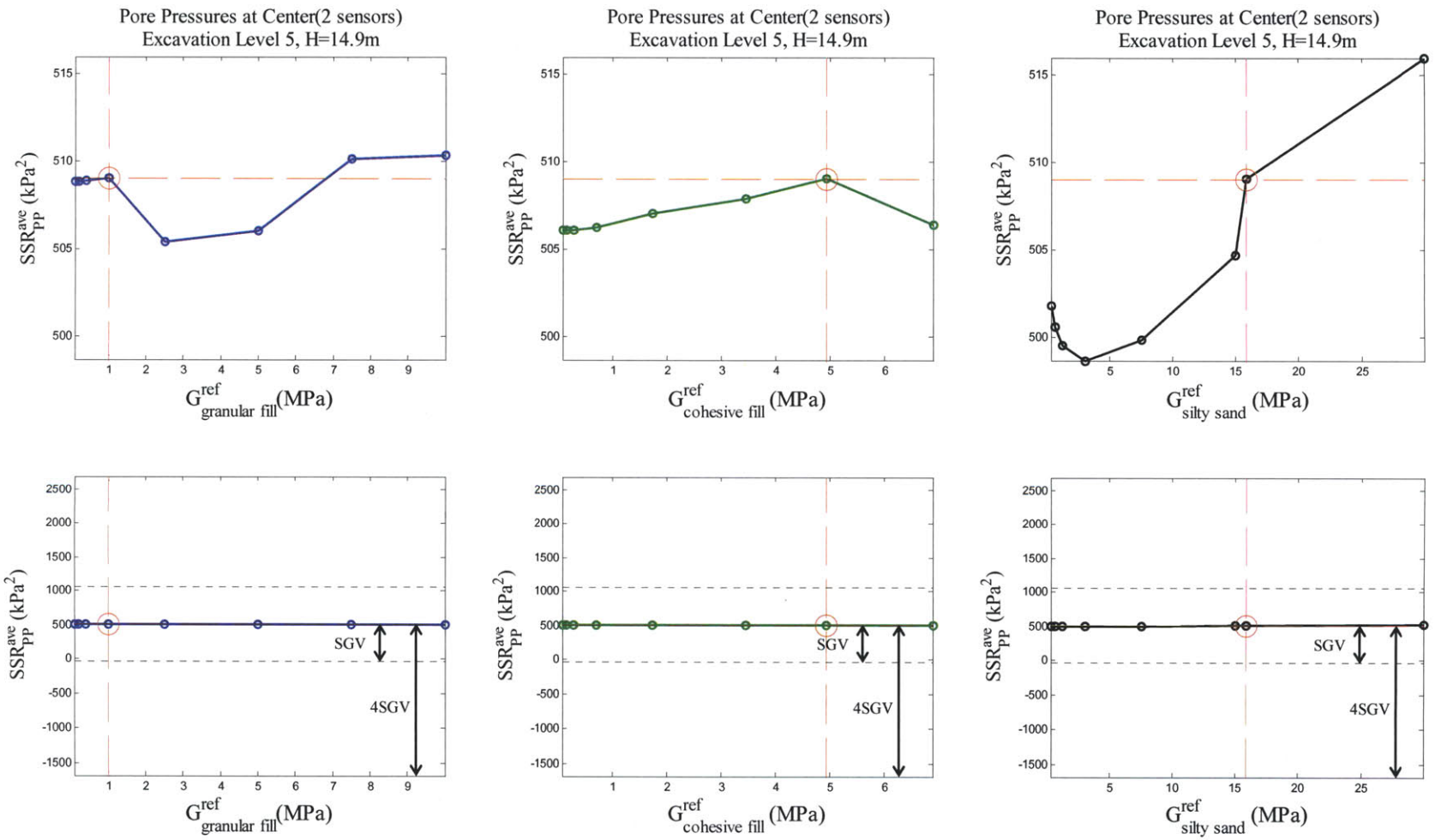

Figure A- 67: Sensitivity analysis of shear stiffness of granular fill, cohesive fill, and silty sand layers on pore pressures at excavation level 5

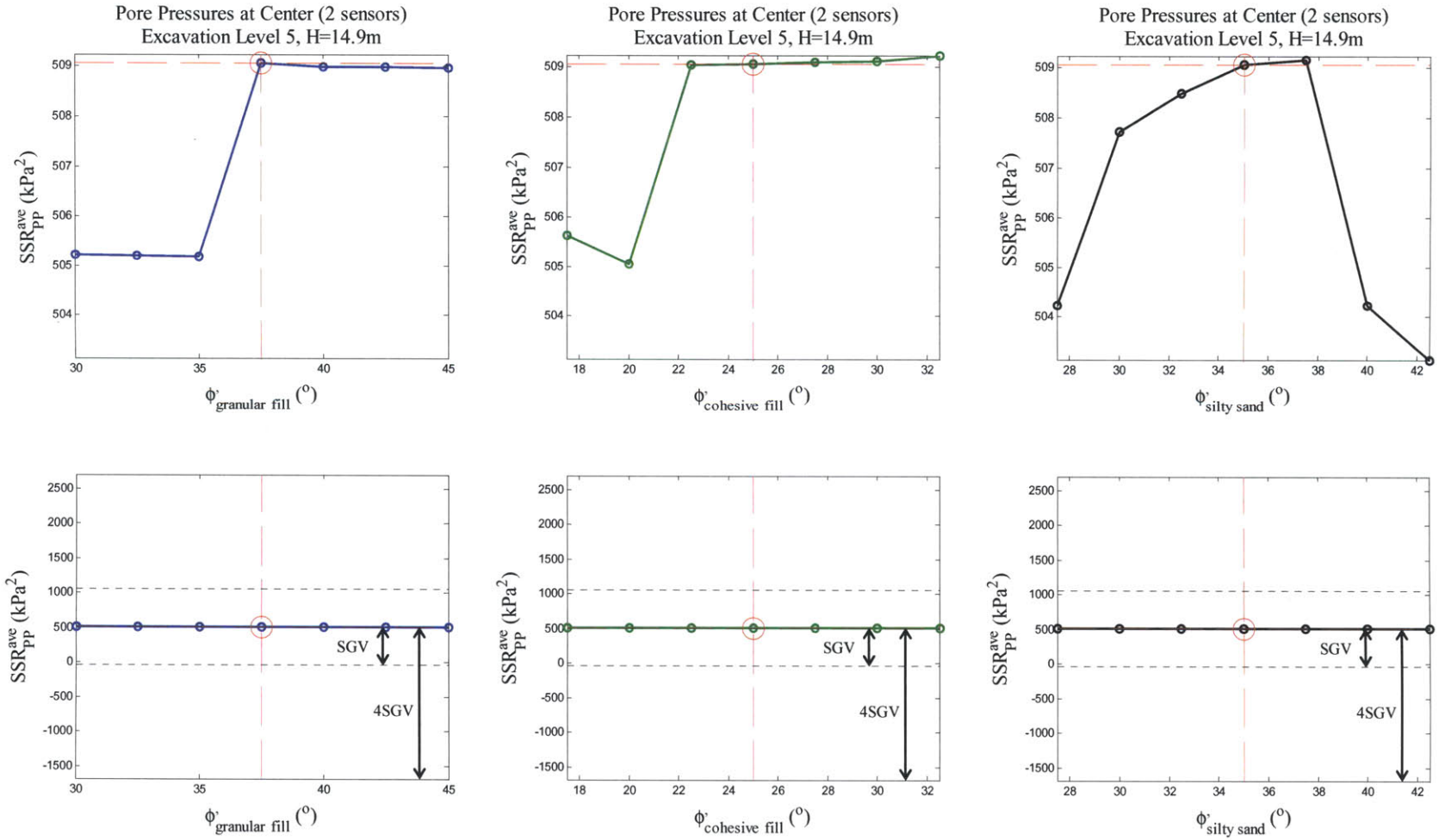

Figure A- 68: Sensitivity analysis of friction angles of granular fill, cohesive fill, and silty sand layers on pore pressures at excavation level 5

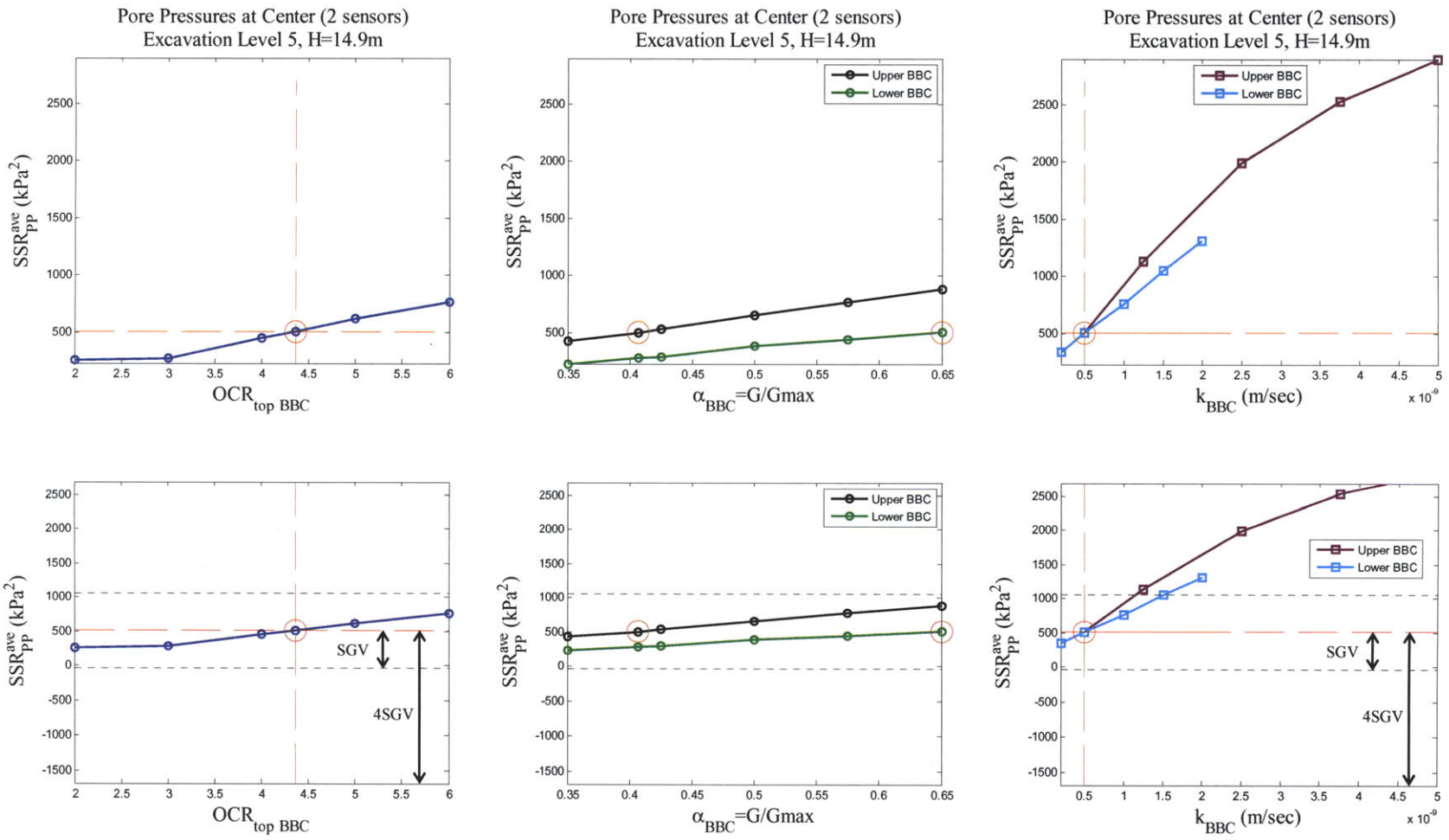

Figure A- 69: Sensitivity analysis of OCR (top), α parameter, and hydraulic conductivities of BBC layers on pore pressures at excavation level 5

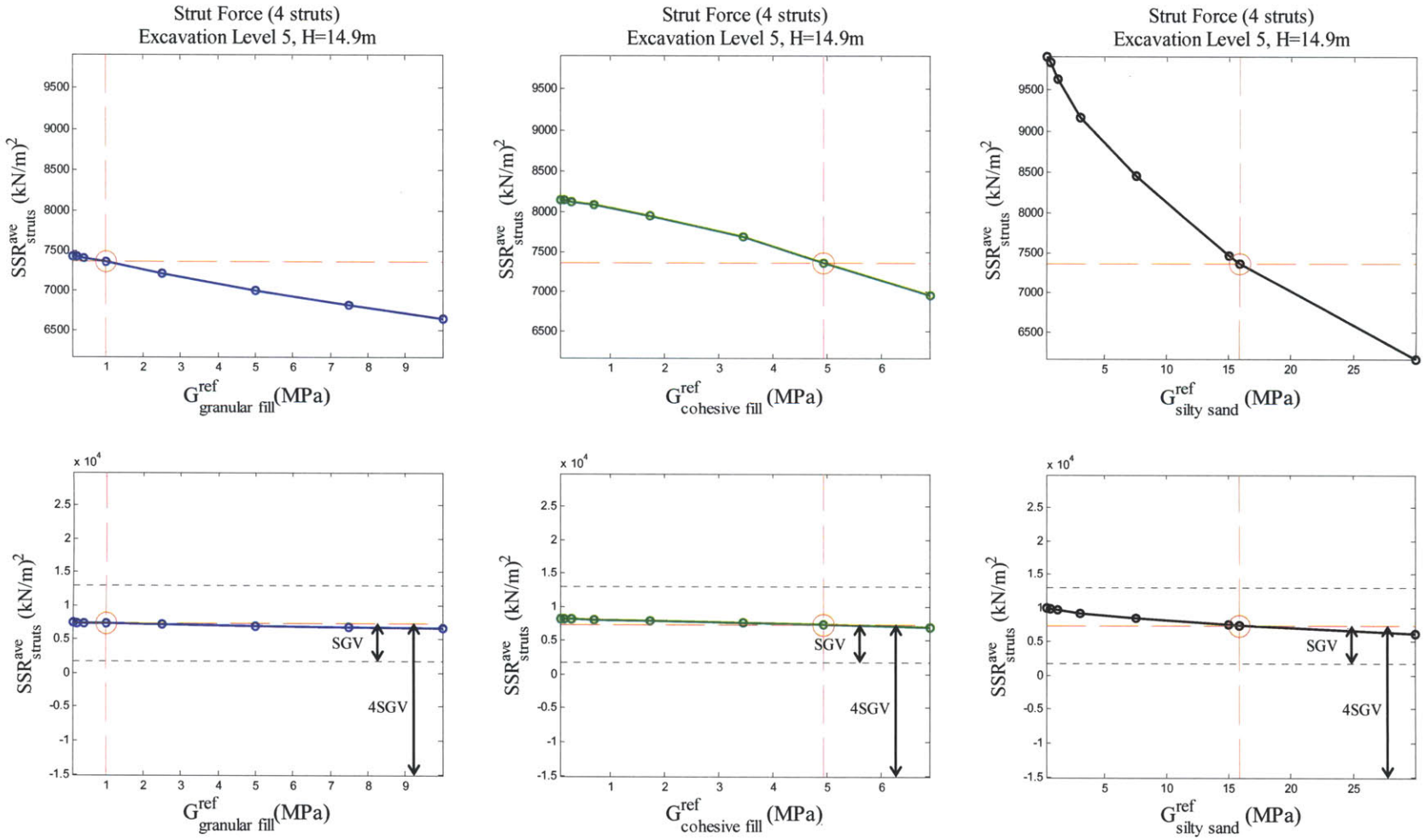

Figure A- 70: Sensitivity analysis of shear stiffness of granular fill, cohesive fill, and silty sand layers on strut forces at excavation level 5

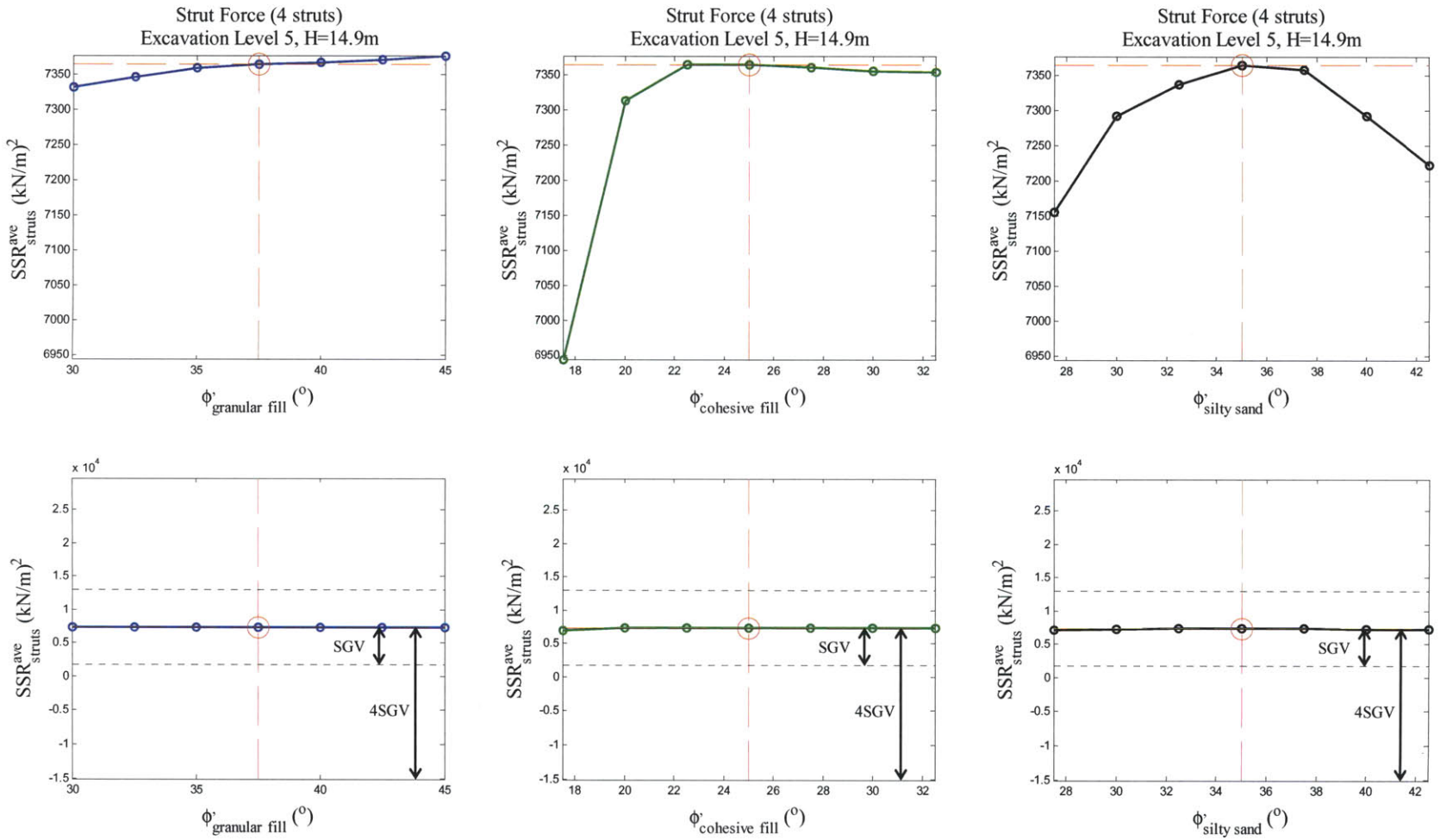

Figure A- 71: Sensitivity analysis of friction angles of granular fill, cohesive fill, and silty sand layers on strut forces at excavation level 5

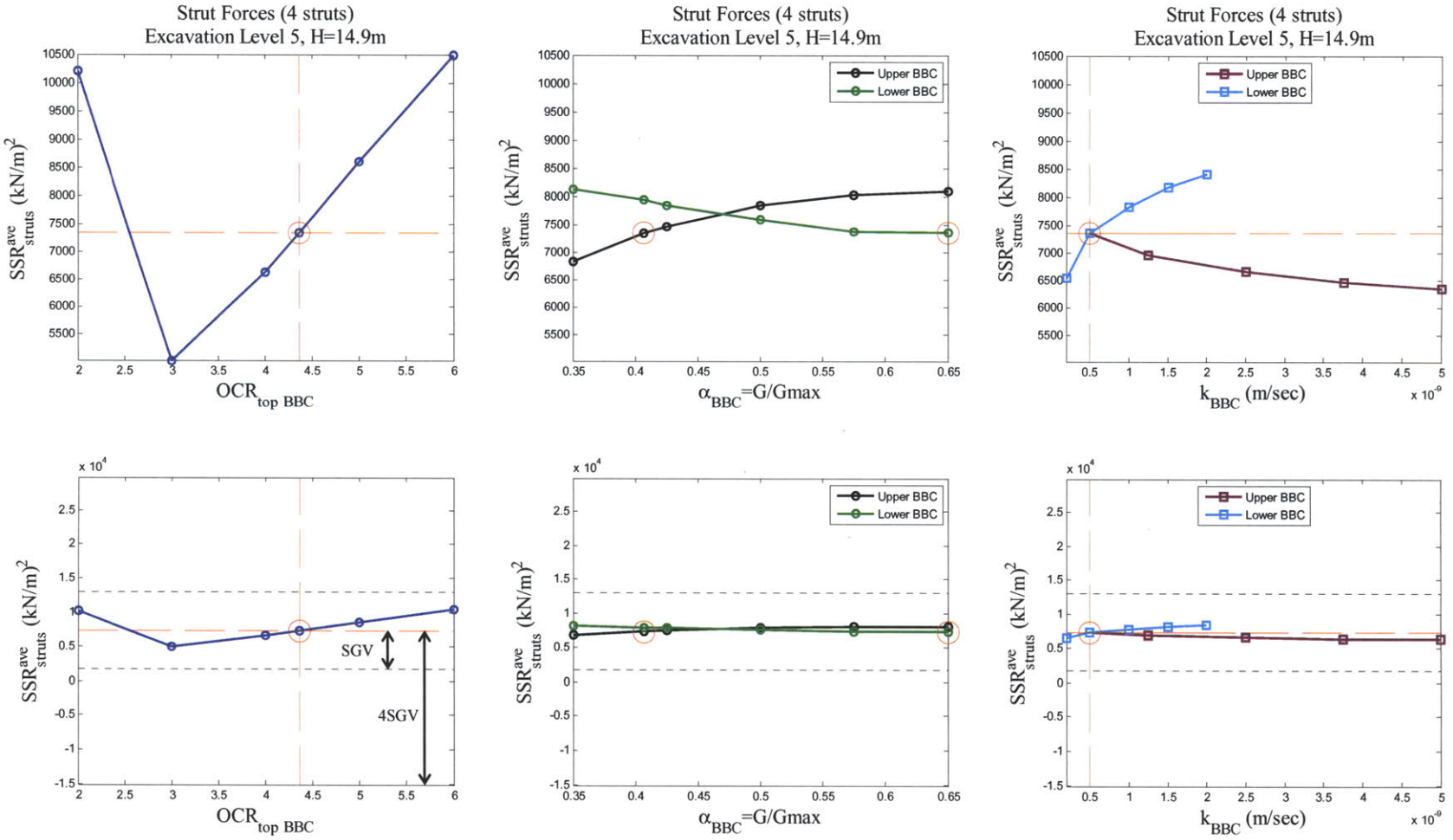

Figure A- 72: Sensitivity analysis of OCR (top), α parameter, and hydraulic conductivities of BBC layers on strut forces at excavation level 5

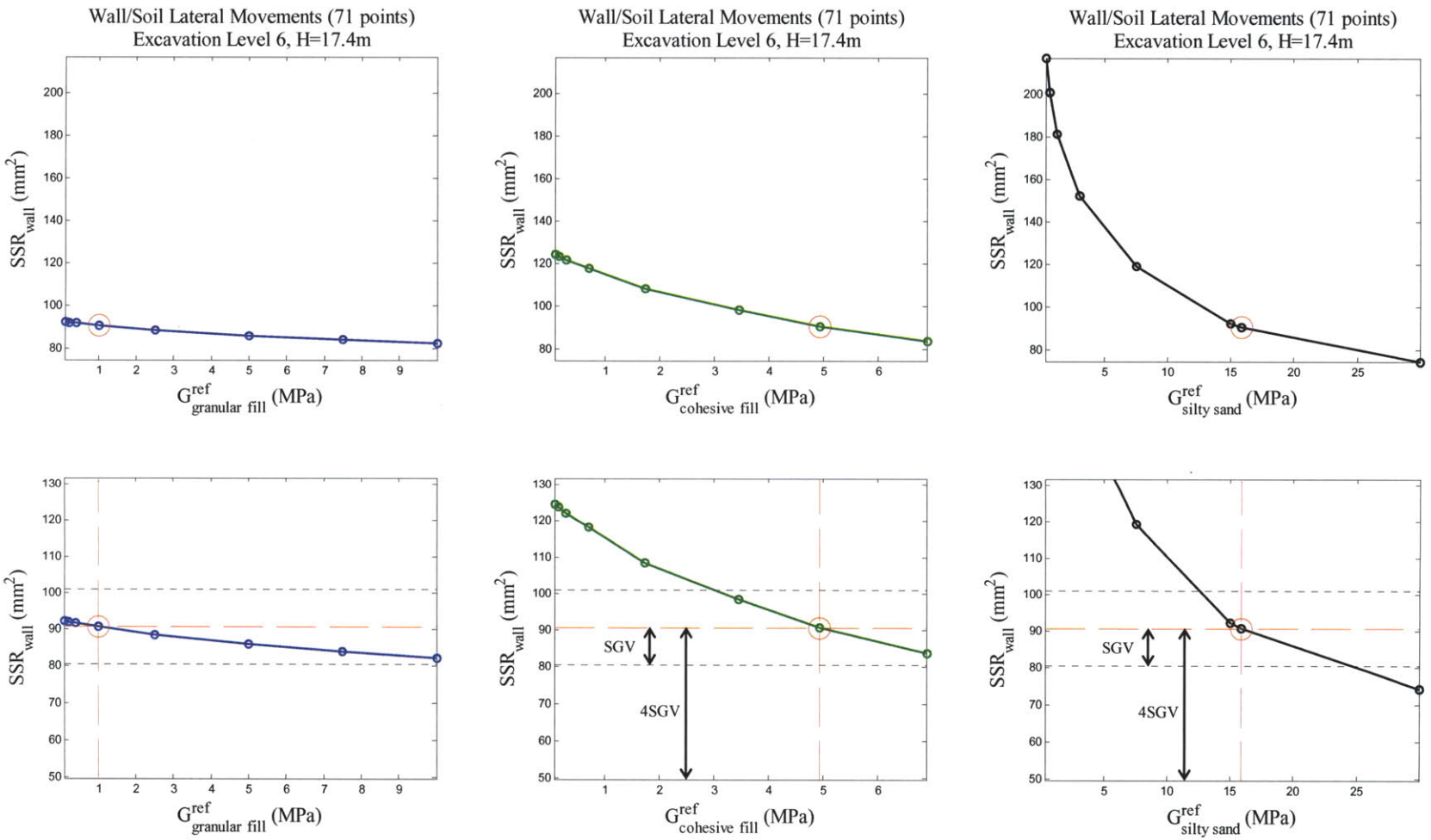

Figure A- 73: Sensitivity analysis of shear stiffness of granular fill, cohesive fill, and silty sand layers on lateral wall/soil movements at excavation level 6

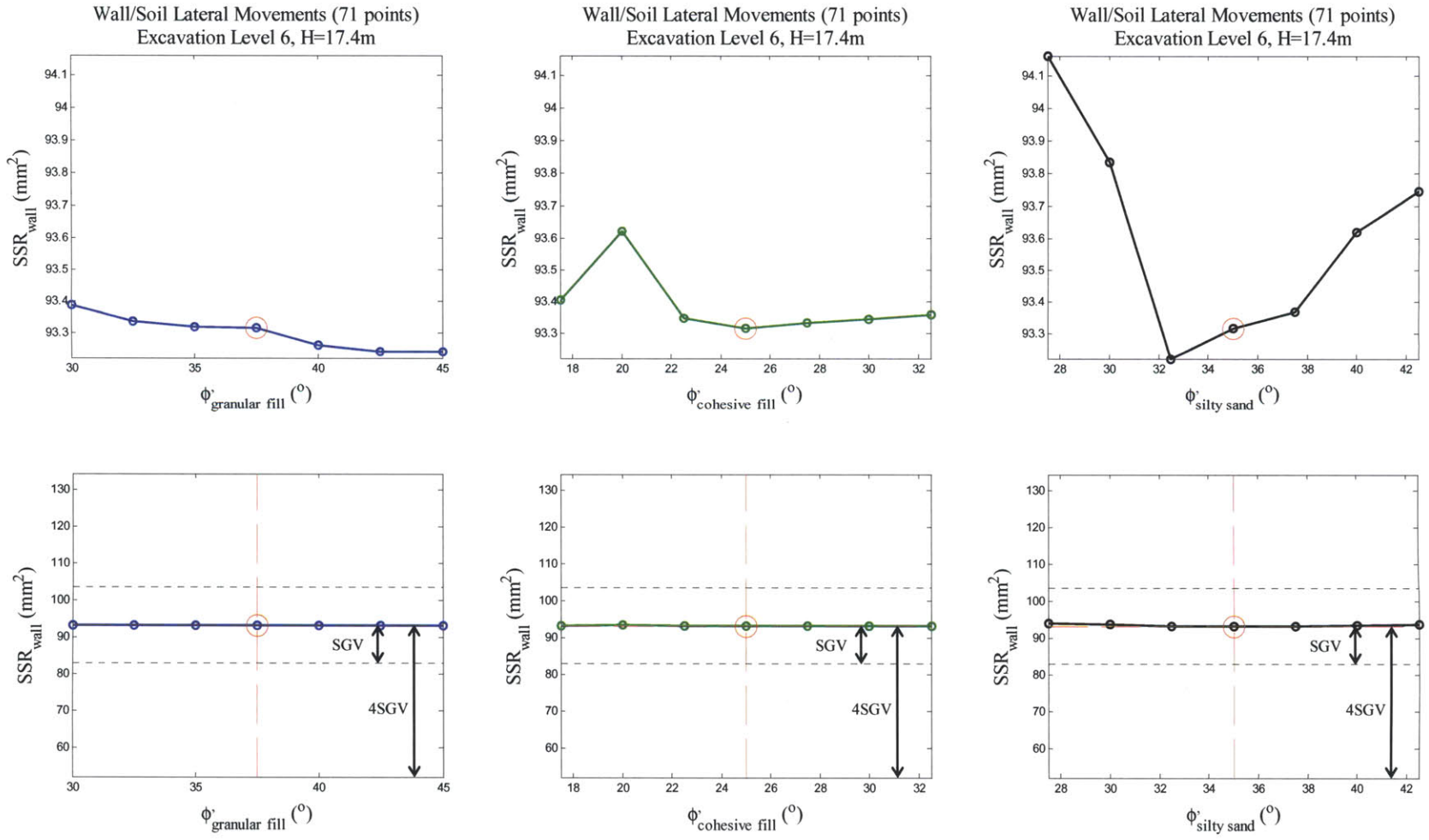

Figure A- 74: Sensitivity analysis of friction angles of granular fill, cohesive fill, and silty sand layers on lateral wall/soil movements at excavation level 6

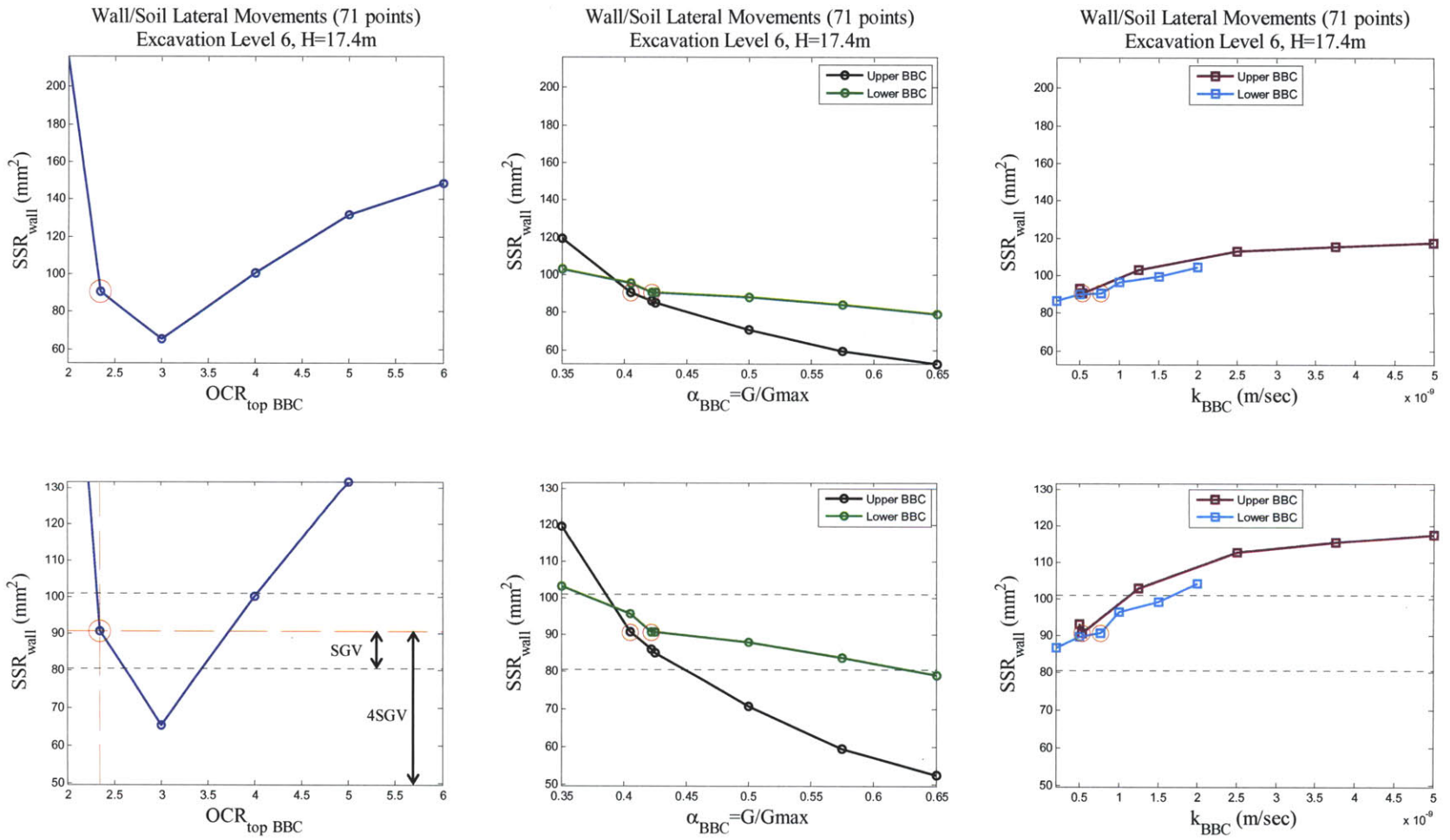

Figure A- 75: Sensitivity analysis of OCR (top), α parameter, and hydraulic conductivities of BBC layers on lateral wall/soil movements at excavation level 6

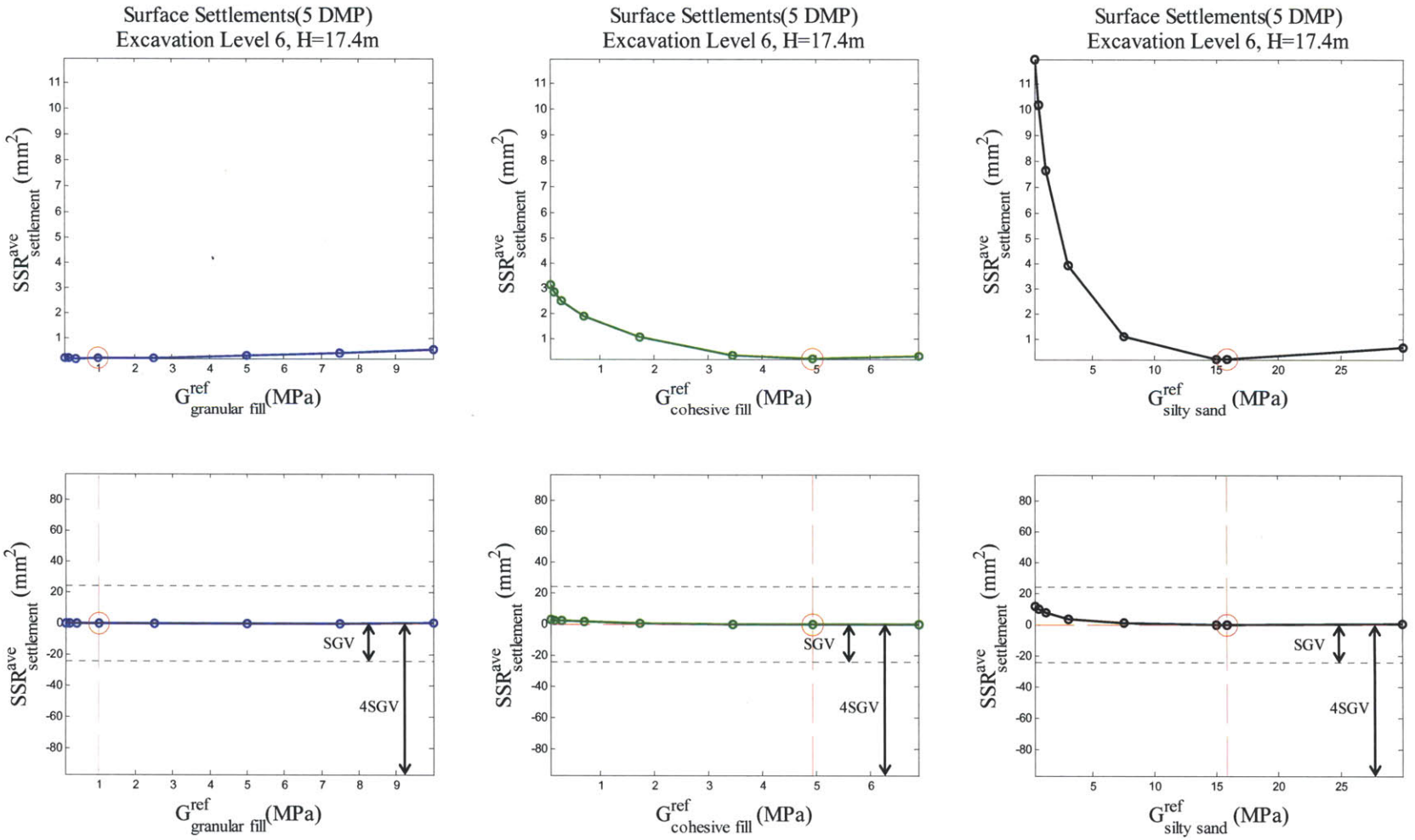

Figure A- 76: Sensitivity analysis of shear stiffness of granular fill, cohesive fill, and silty sand layers on surface settlement at excavation level 6

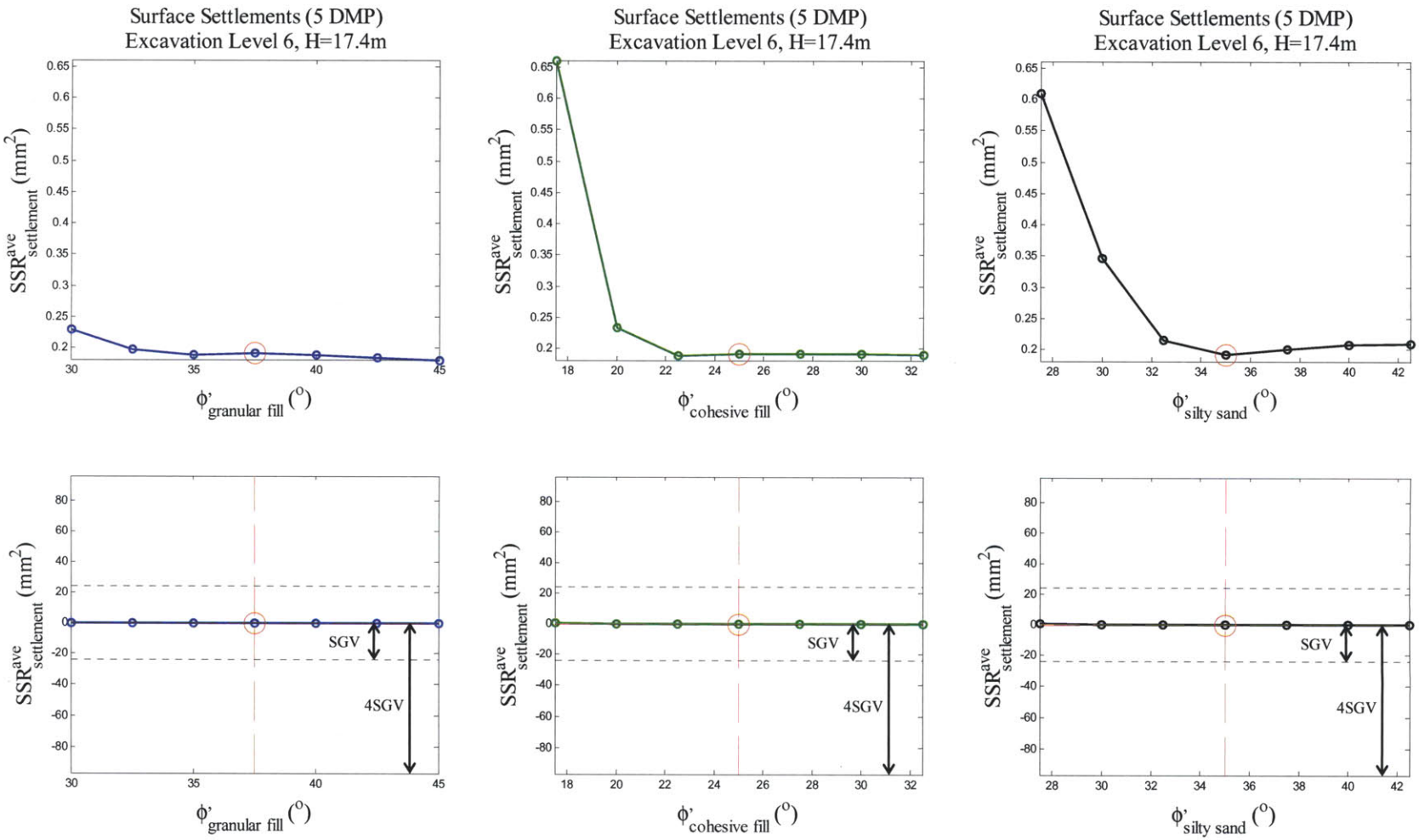

Figure A- 77: Sensitivity analysis of friction angles of granular fill, cohesive fill, and silty sand layers on surface settlement at excavation level 6

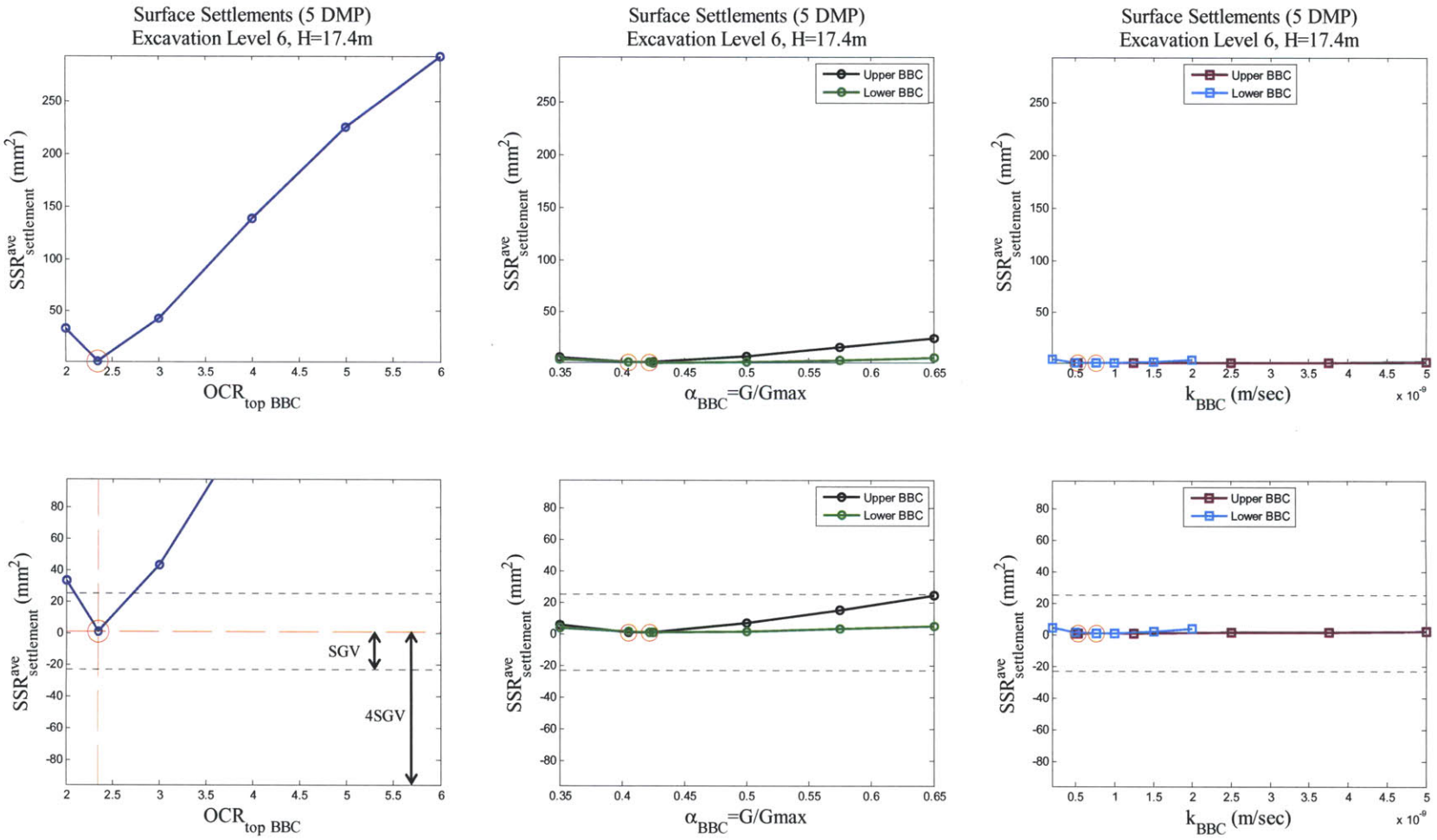

Figure A- 78: Sensitivity analysis of OCR (top), α parameter, and hydraulic conductivities of BBC layers on surface settlement at excavation level 6

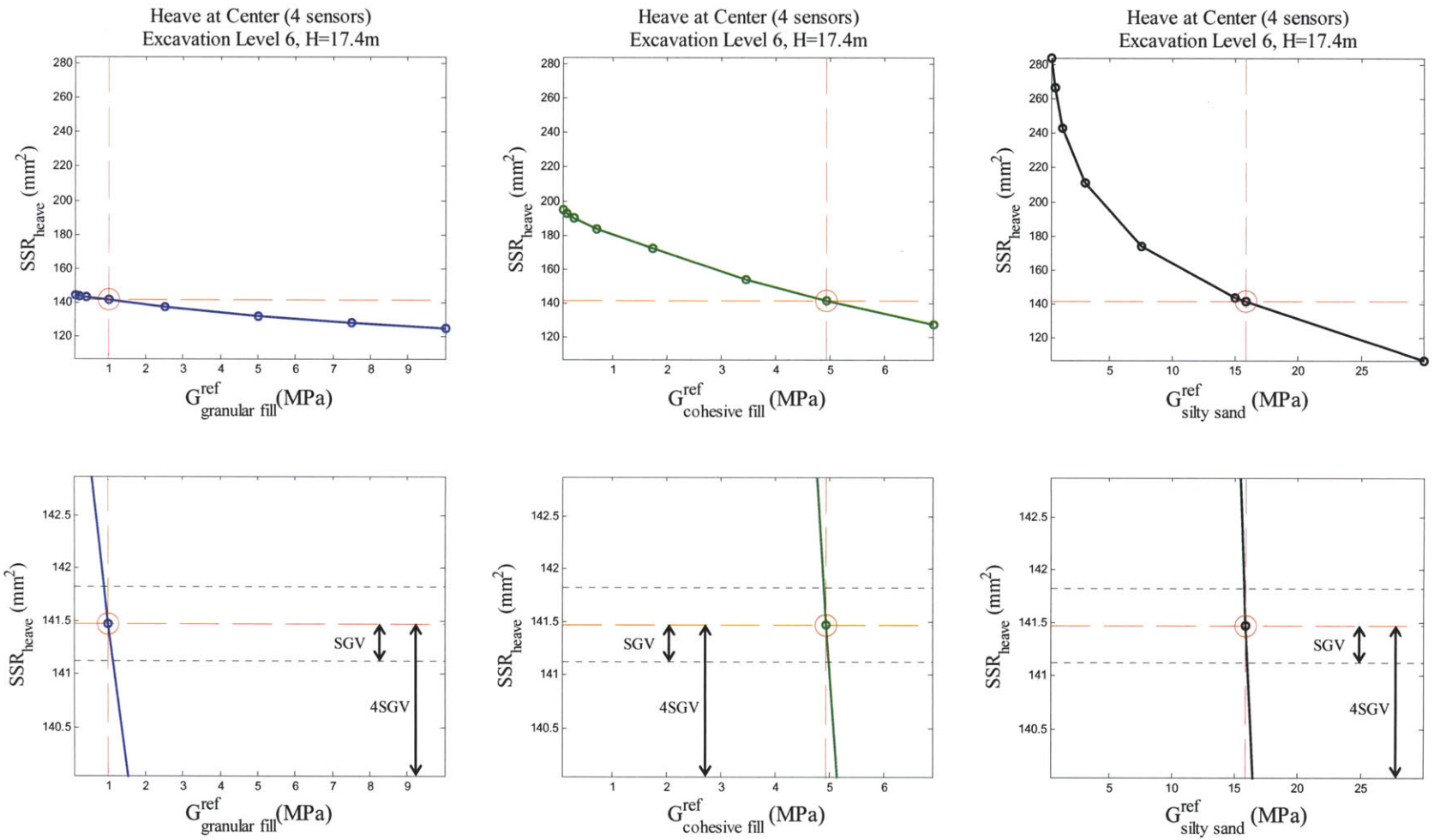

Figure A- 79: Sensitivity analysis of shear stiffness of granular fill, cohesive fill, and silty sand layers on excavation heave at excavation level 6

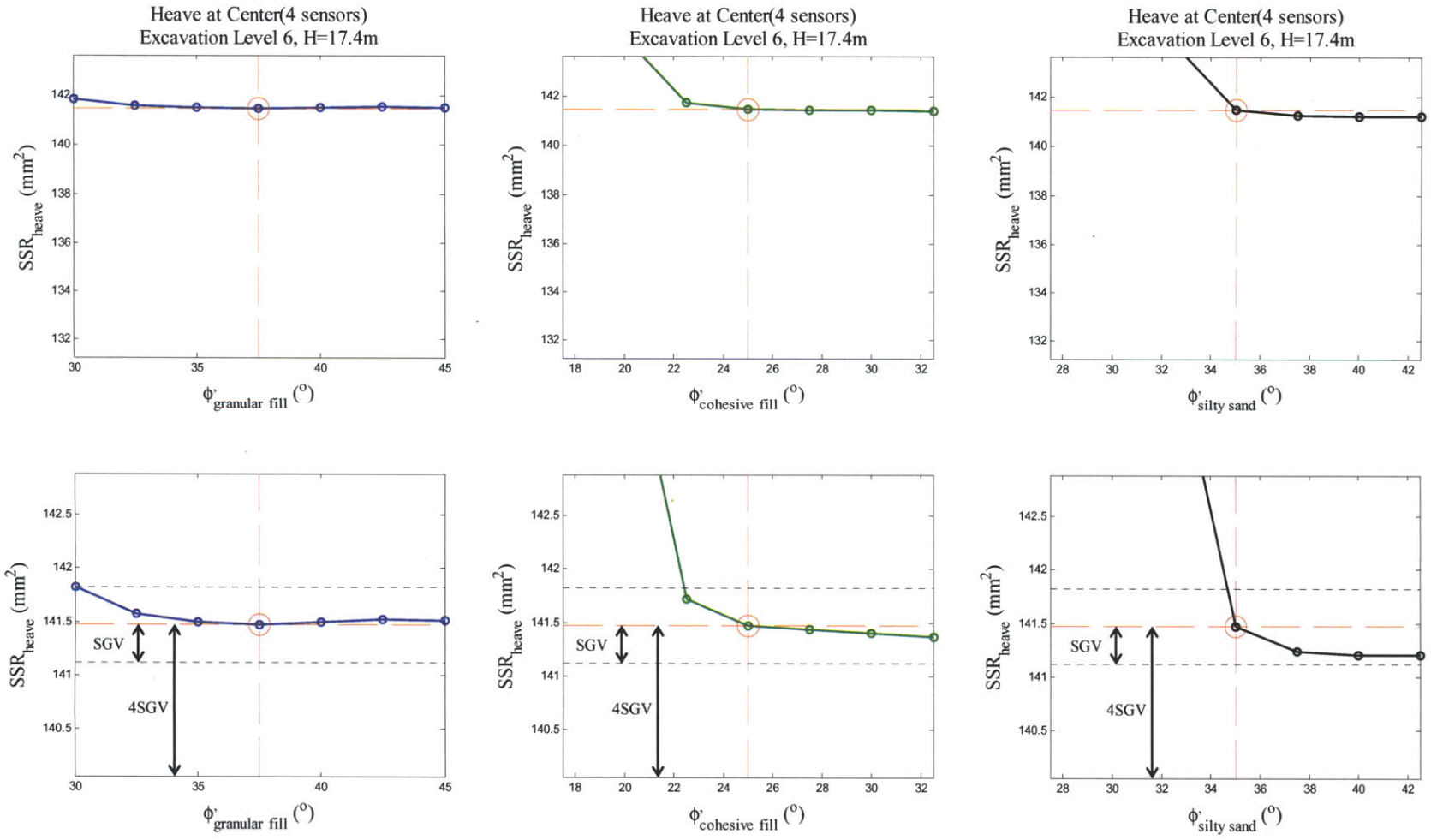

Figure A- 80: Sensitivity analysis of friction angles of granular fill, cohesive fill, and silty sand layers on excavation heave at excavation level 6

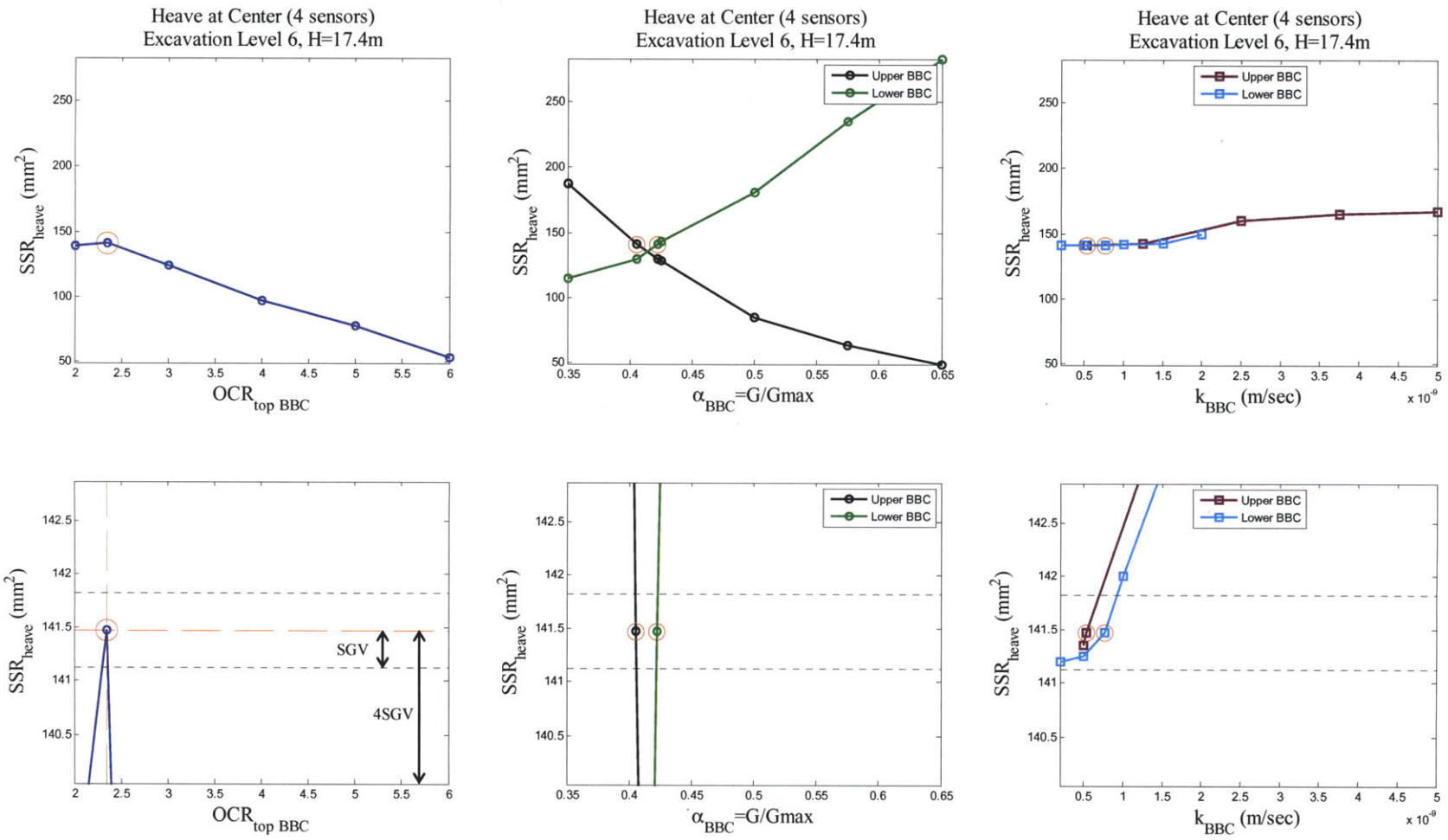

Figure A- 81: Sensitivity analysis of OCR (top), α parameter, and hydraulic conductivities of BBC layers on excavation heave at excavation level 6

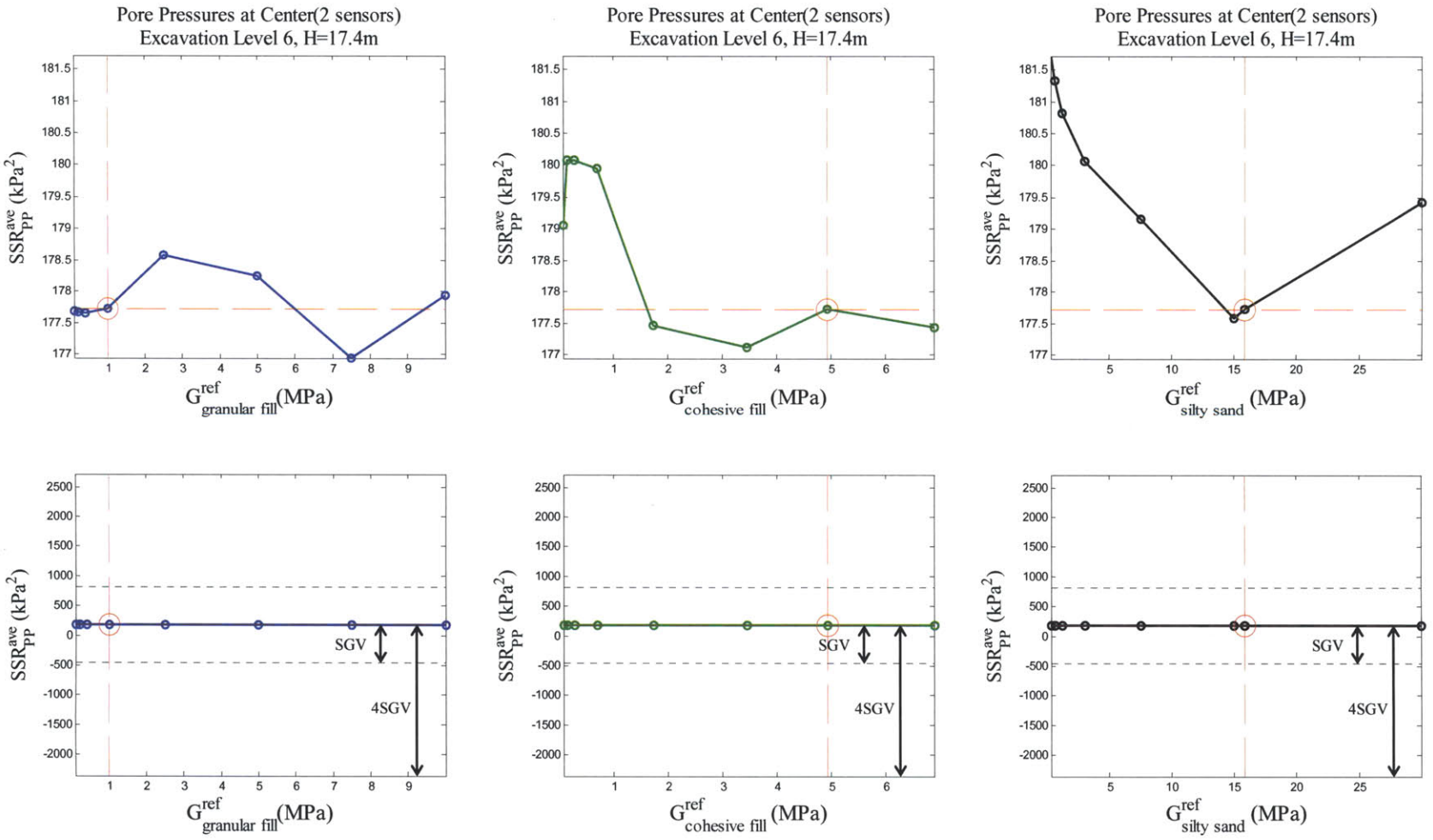

Figure A- 82: Sensitivity analysis of shear stiffness of granular fill, cohesive fill, and silty sand layers on pore pressures at excavation level 6

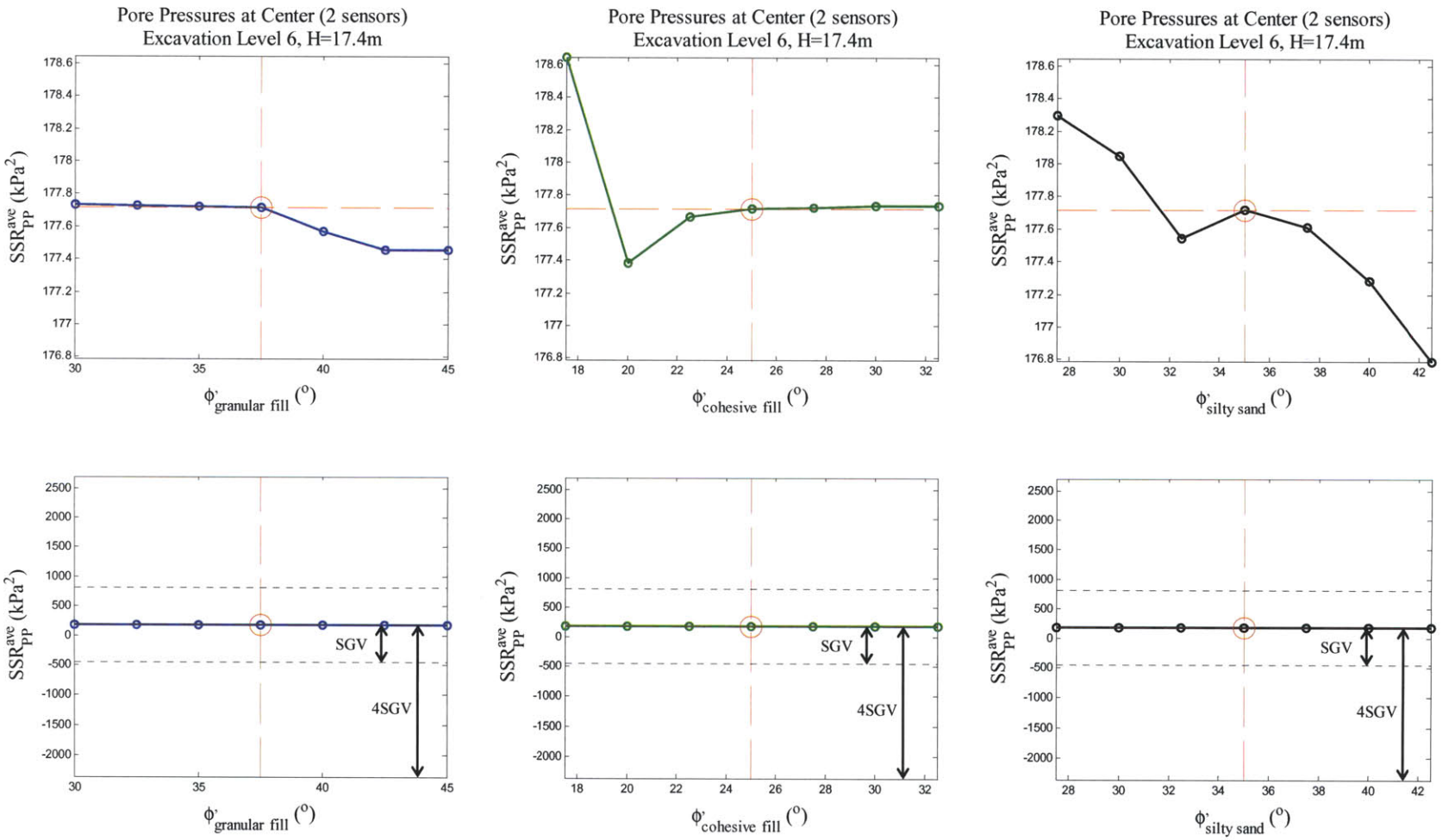

Figure A- 83: Sensitivity analysis of friction angles of granular fill, cohesive fill, and silty sand layers on pore pressures at excavation level 6

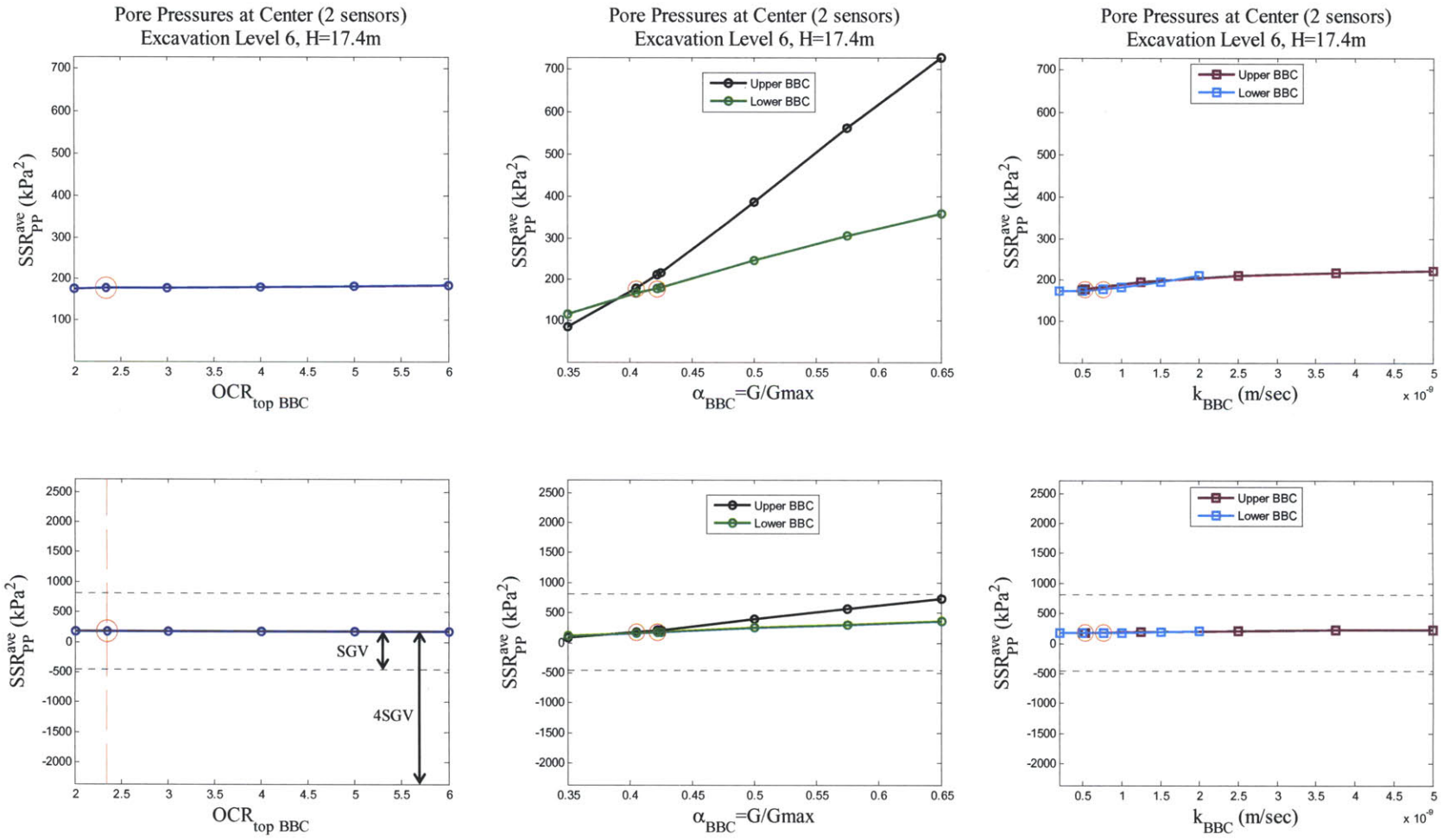

Figure A- 84: Sensitivity analysis of OCR (top), α parameter, and hydraulic conductivities of BBC layers on pore pressures at excavation level 6

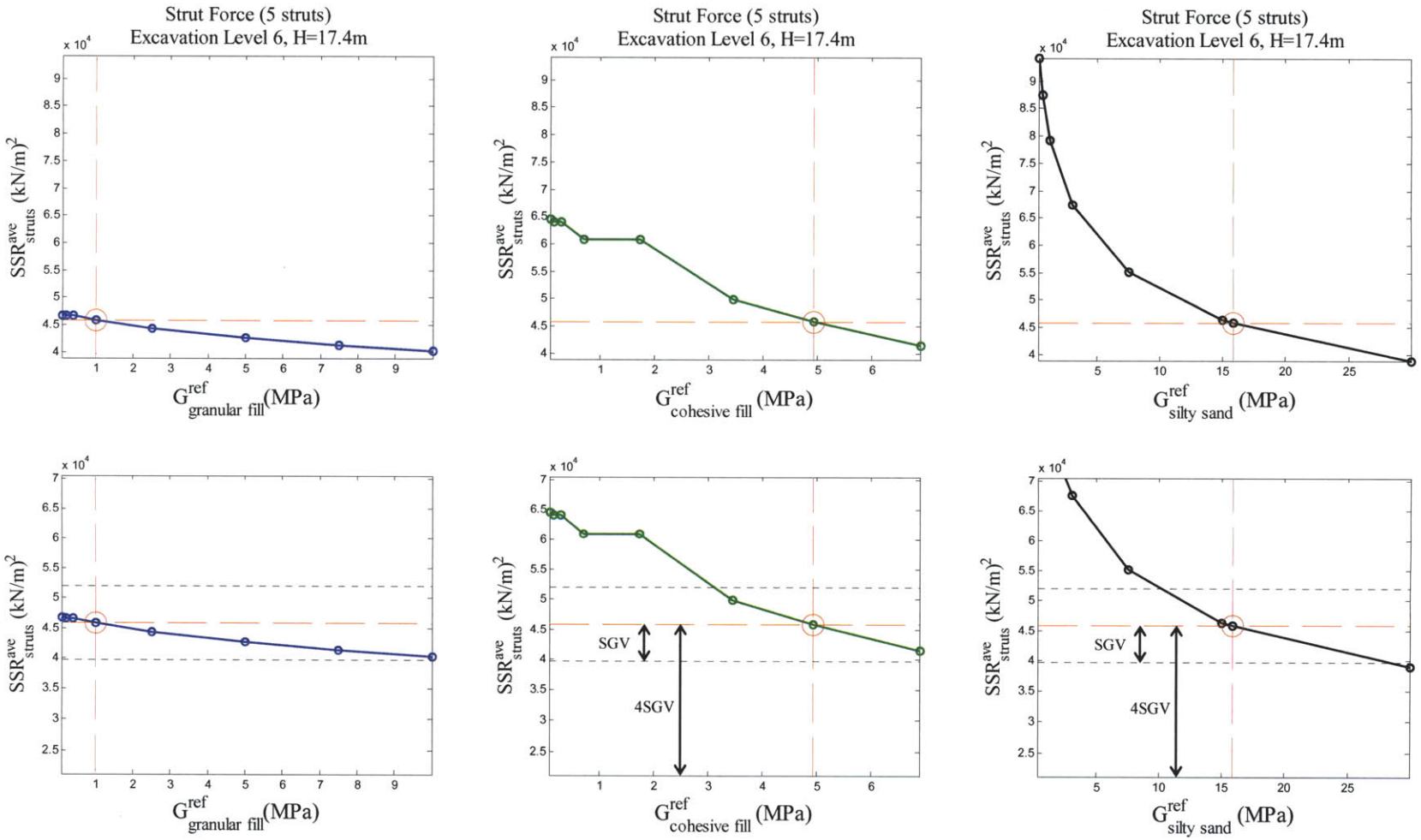

Figure A- 85: Sensitivity analysis of shear stiffness of granular fill, cohesive fill, and silty sand layers on strut forces at excavation level 6

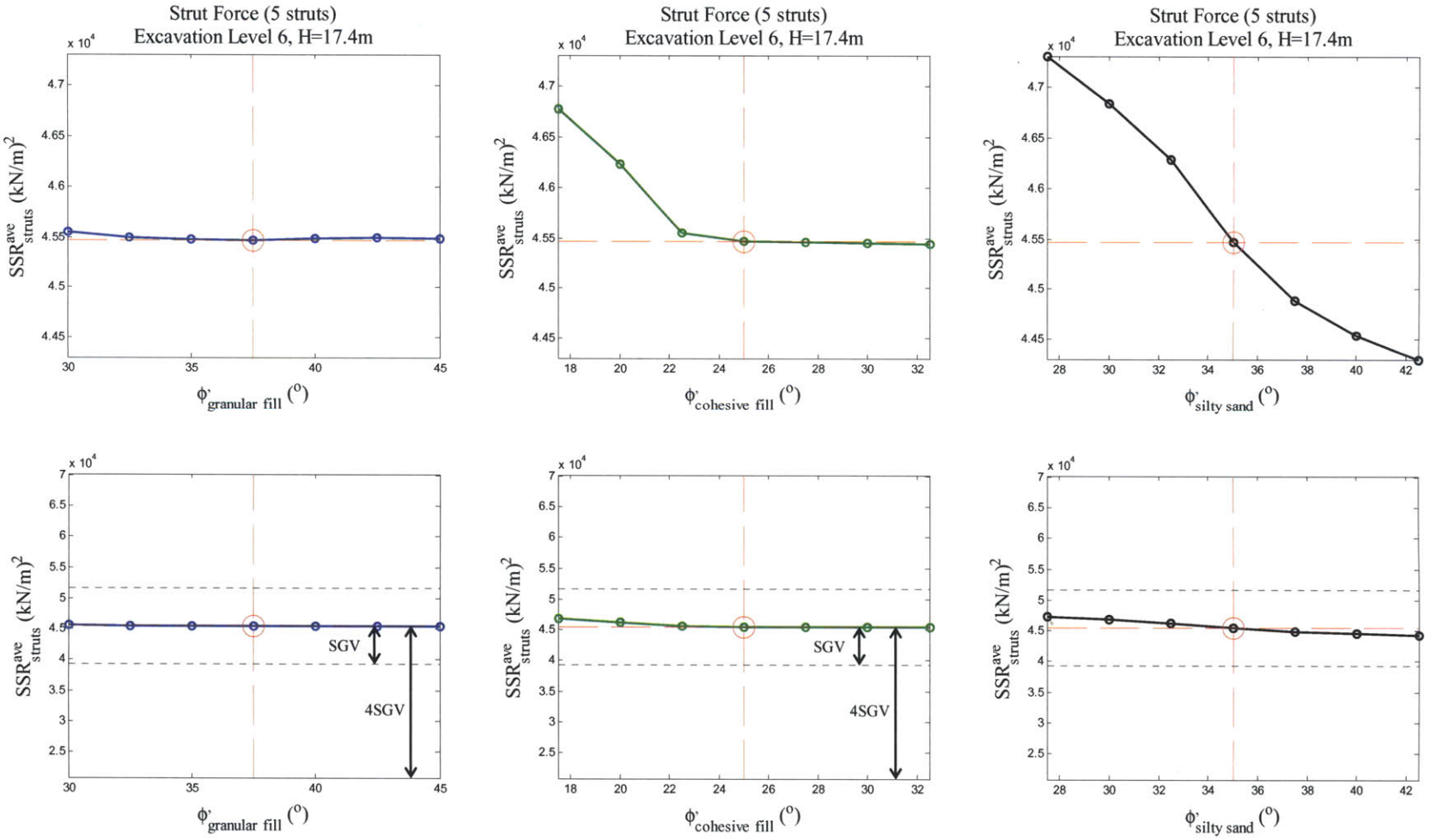

Figure A- 86: Sensitivity analysis of friction angles of granular fill, cohesive fill, and silty sand layers on strut forces at excavation level 6

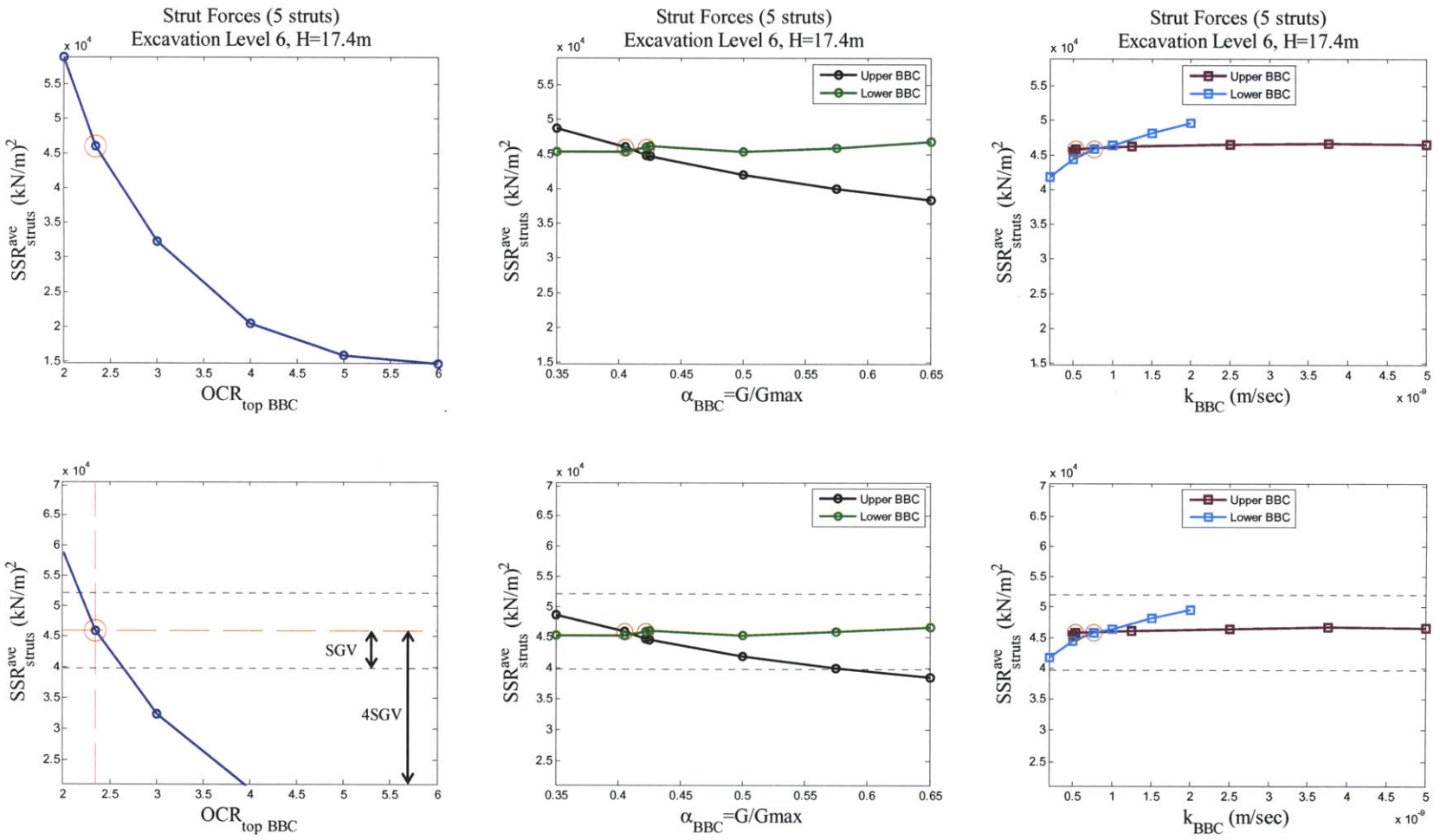

Figure A- 87: Sensitivity analysis of OCR (top), α parameter, and hydraulic conductivities of BBC layers on strut forces at excavation level 6

B. INITIAL PREDICTIONS (ORIGINAL – NO UPDATING) VERSUS FINAL PREDICTIONS (UPDATED LEVEL 6) WITH MC MODEL

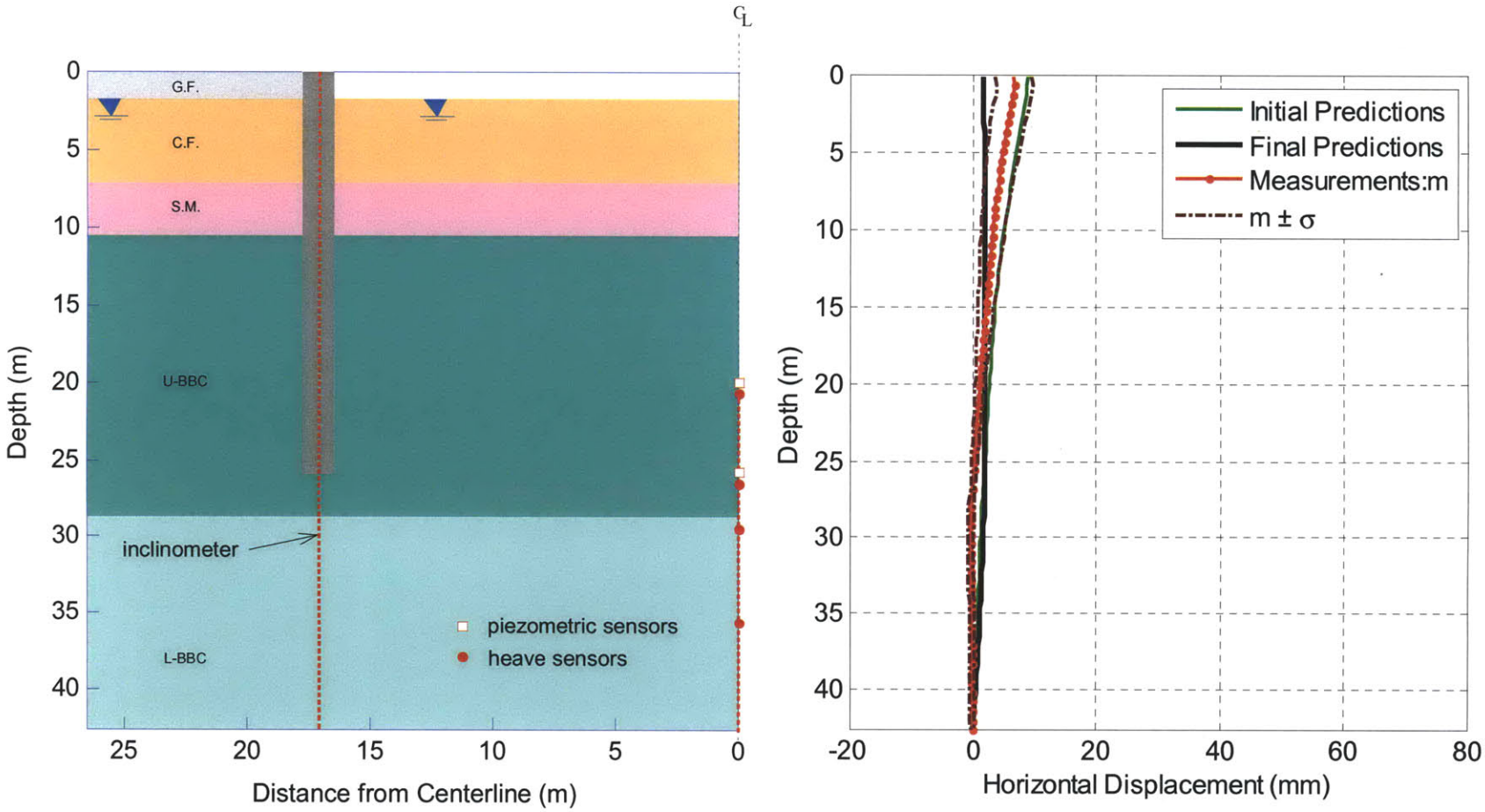

Figure B- 1: Measurements vs. Initial and Final Predictions of Lateral Wall/Soil Movement at Excavation Level 1

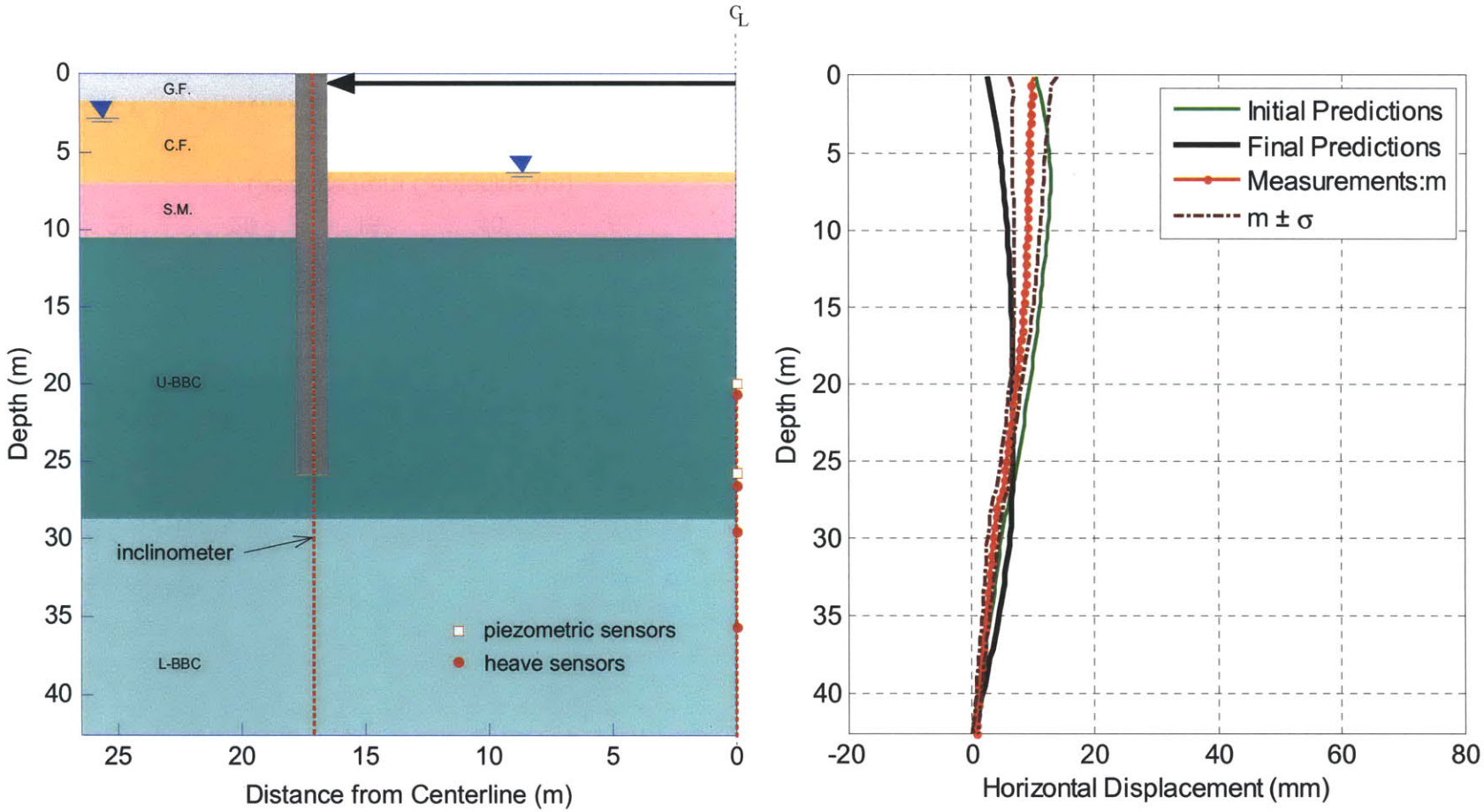

Figure B- 2: Measurements vs. Initial and Final Predictions of Lateral Wall/Soil Movement at Excavation Level 2

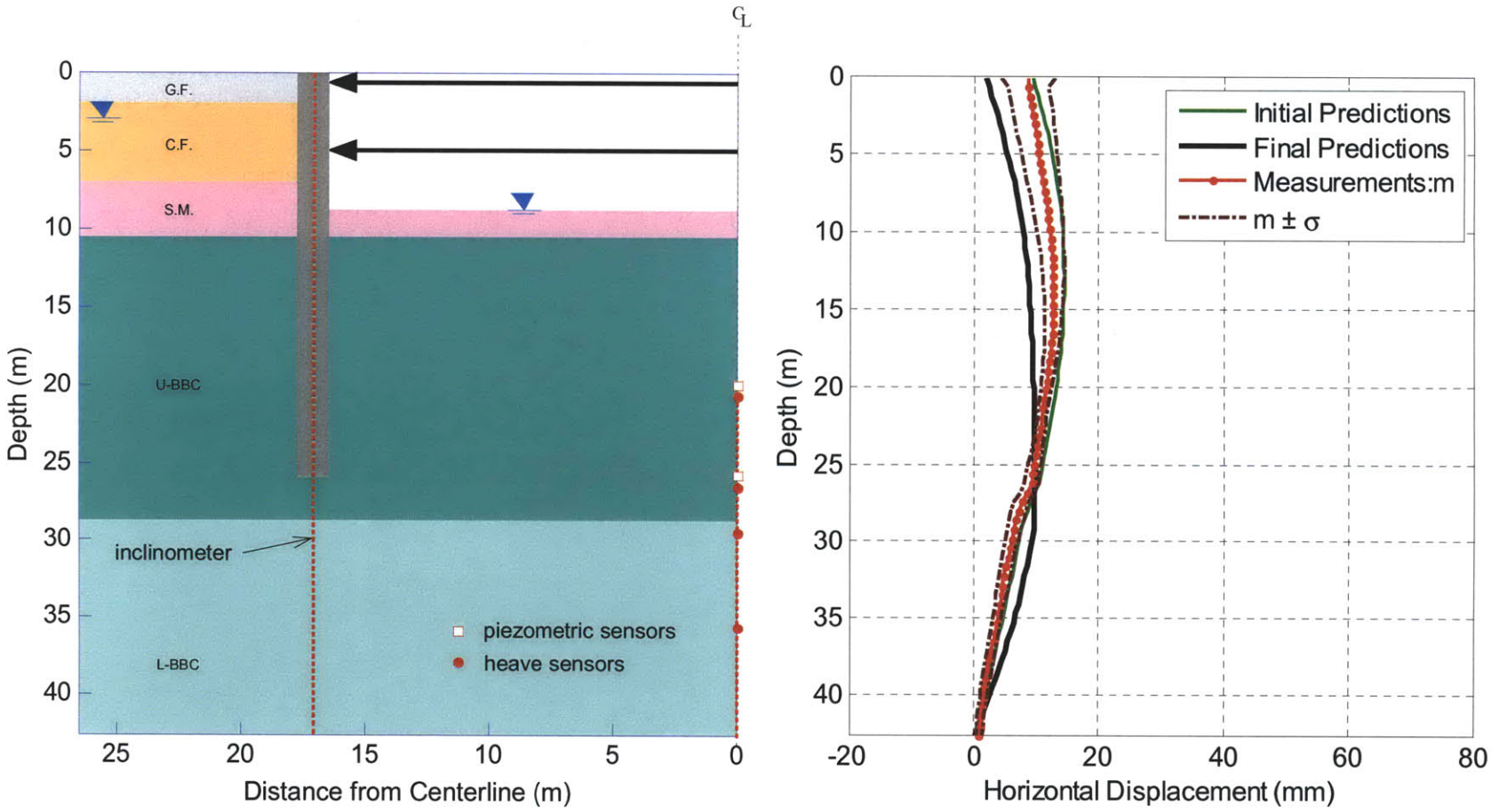

Figure B- 3: Measurements vs. Initial and Final Predictions of Lateral Wall/Soil Movement at Excavation Level 3

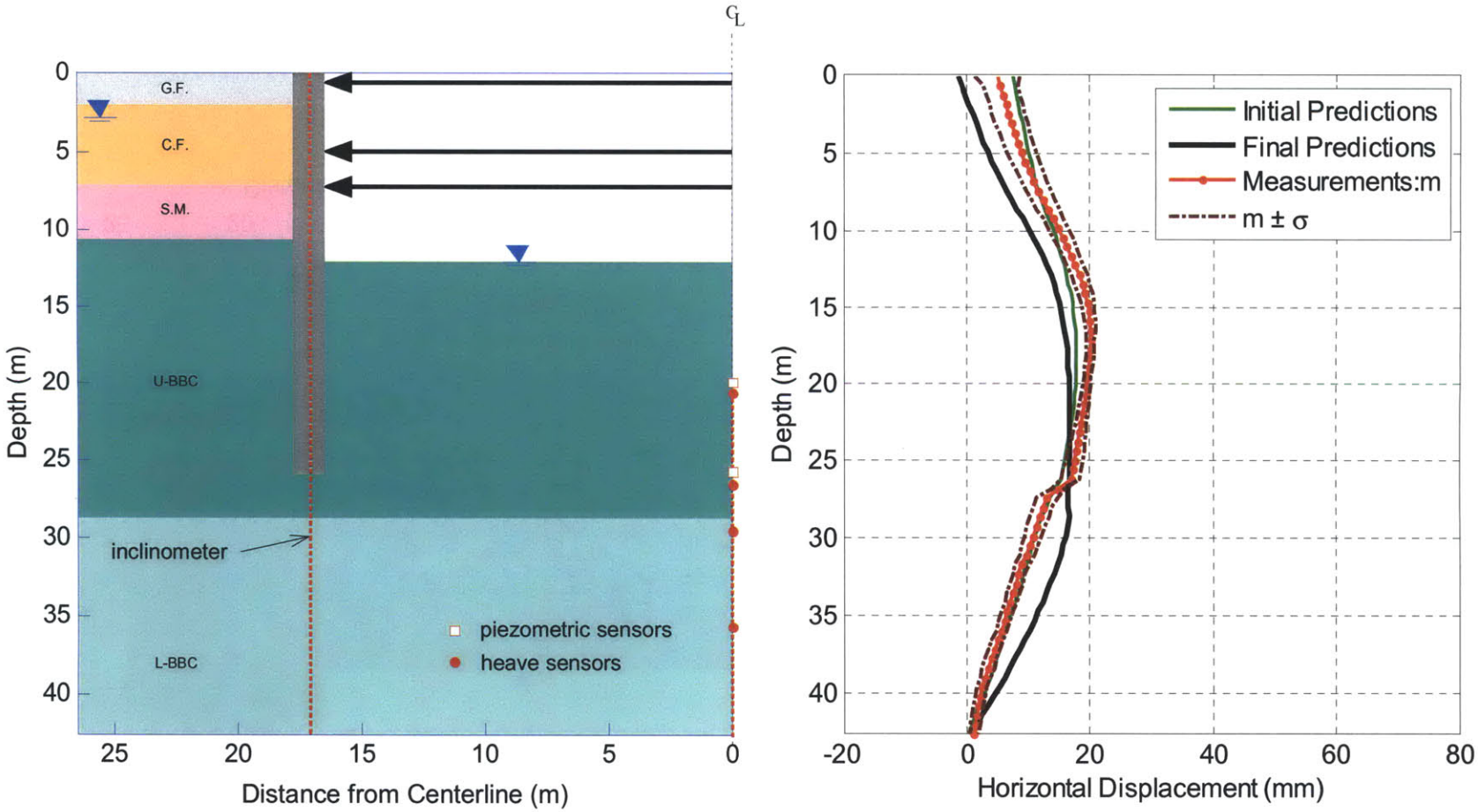

Figure B- 4: Measurements vs. Initial and Final Predictions of Lateral Wall/Soil Movement at Excavation Level 4

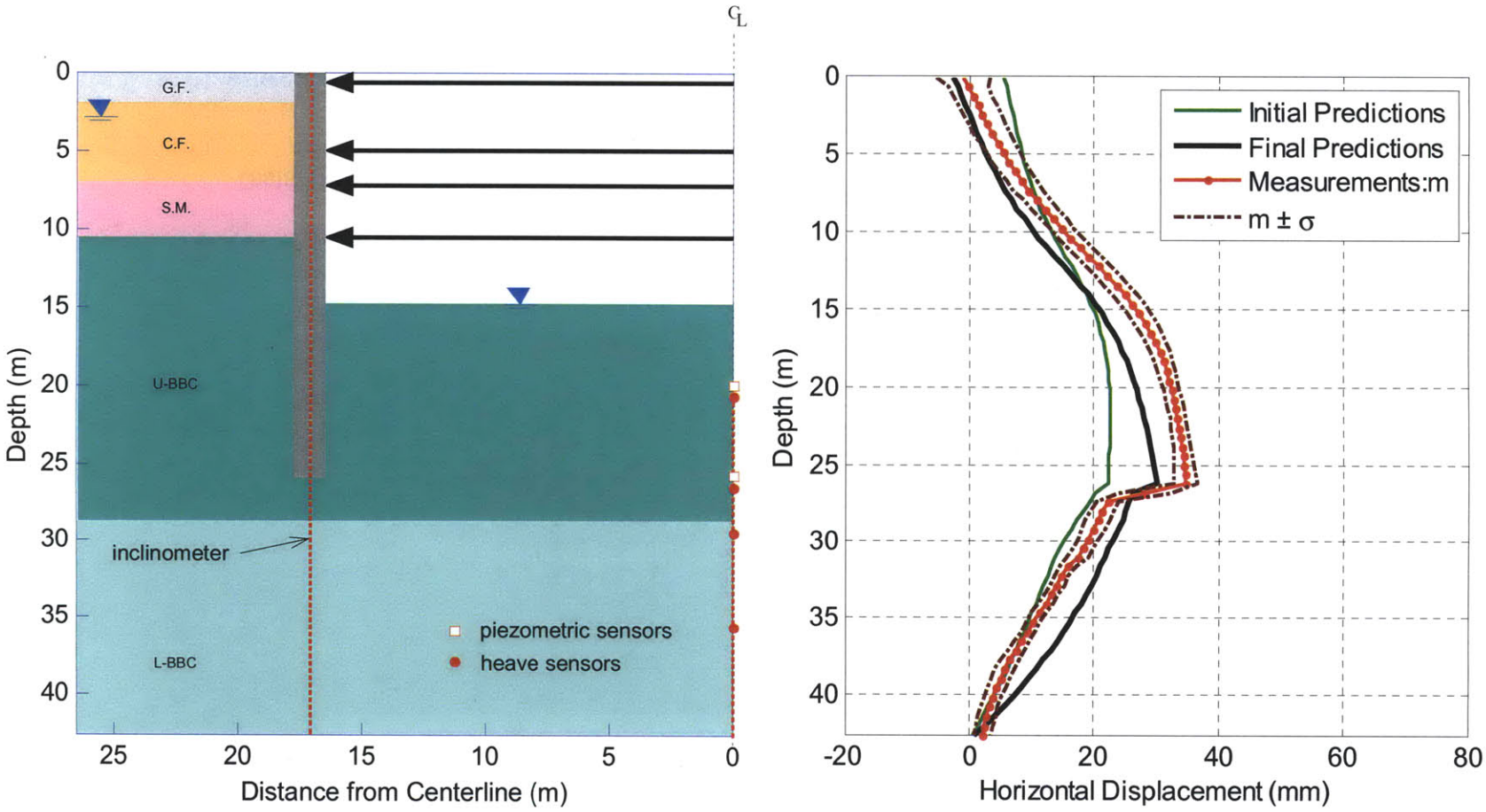

Figure B- 5: Measurements vs. Initial and Final Predictions of Lateral Wall/Soil Movement at Excavation Level 5

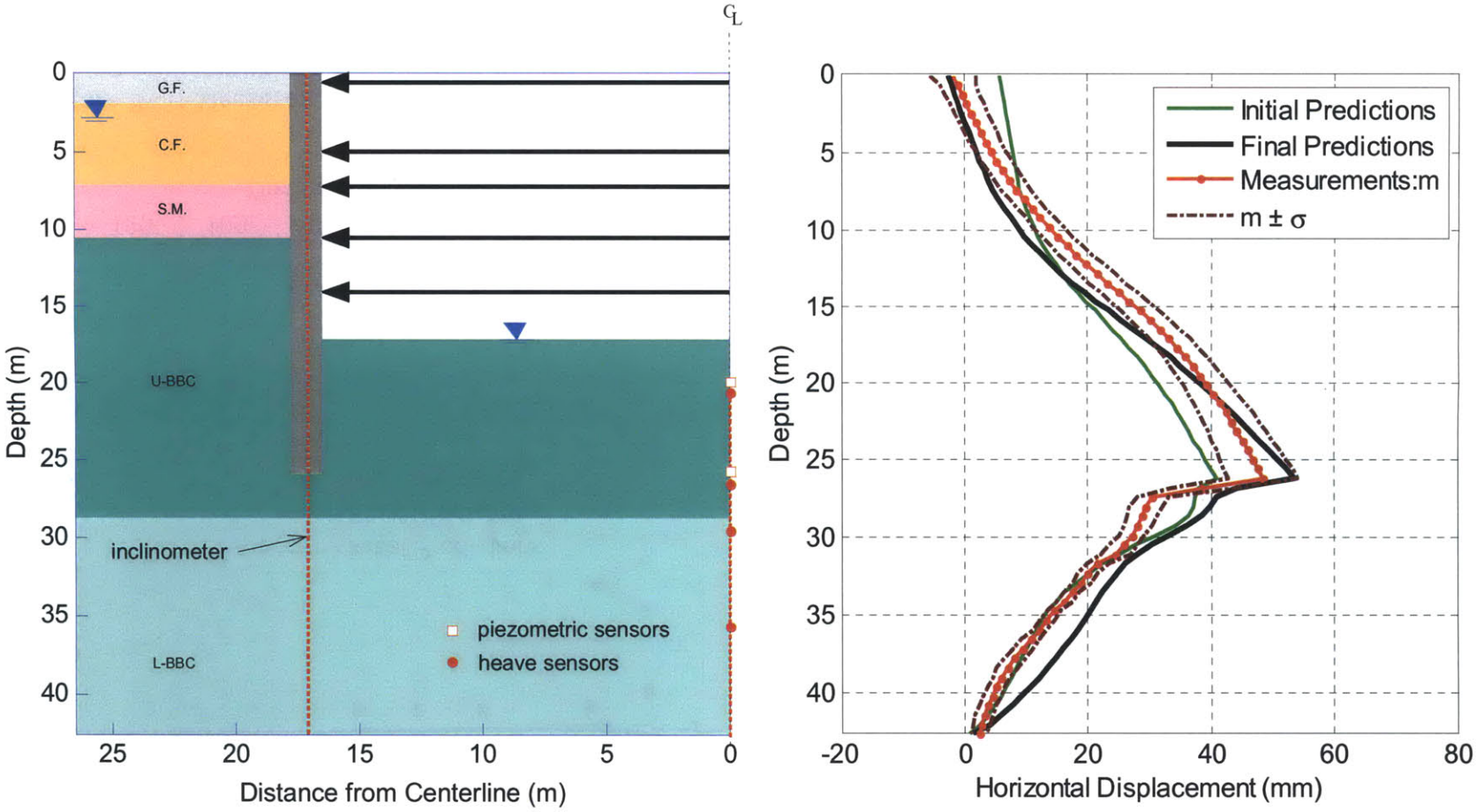

Figure B- 6: Measurements vs. Initial and Final Predictions of Lateral Wall/Soil Movement at Excavation Level 6

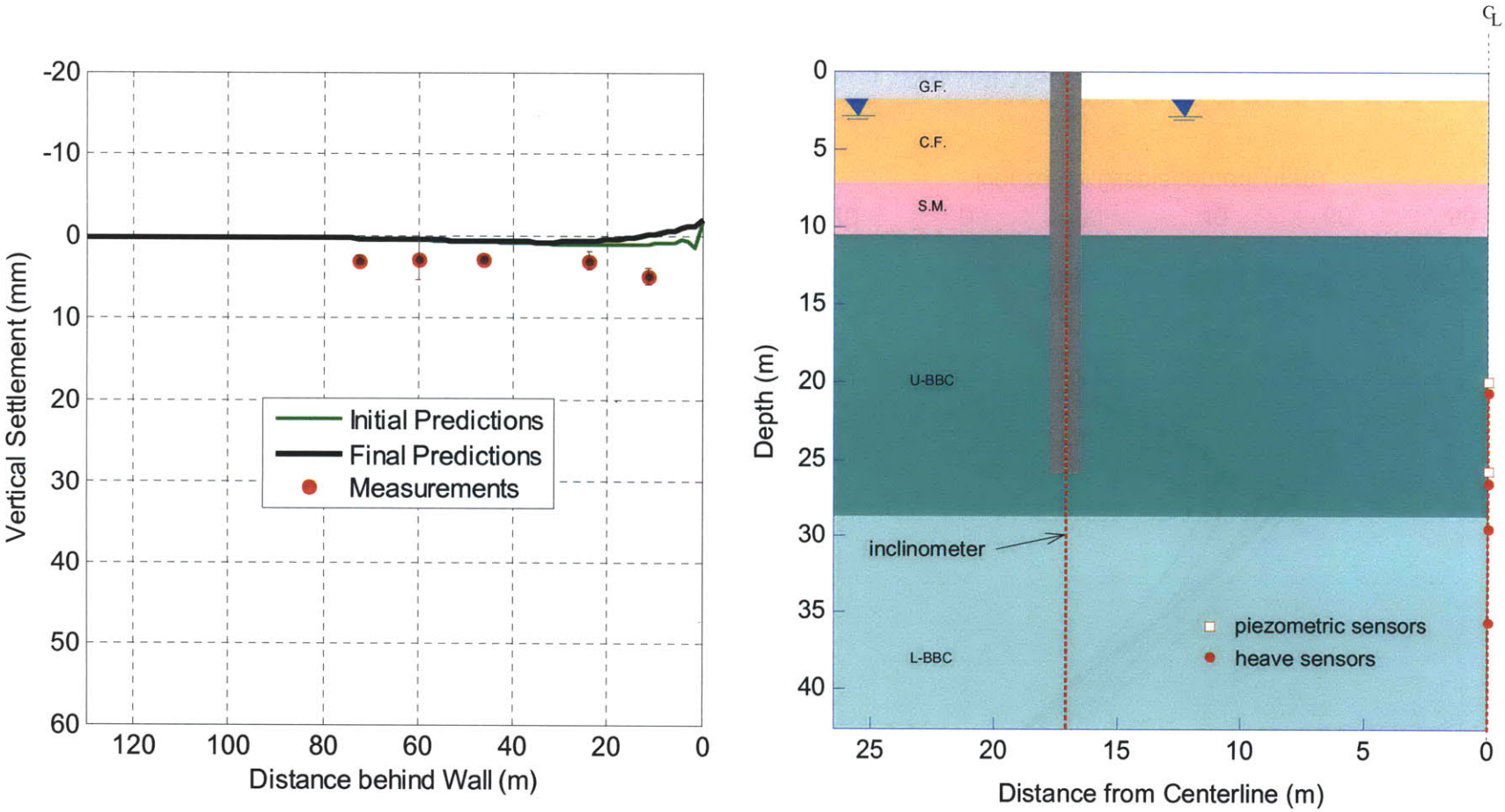

Figure B- 7: Measurements vs. Initial and Final Predictions of Surface Vertical Settlement at Excavation Level 1

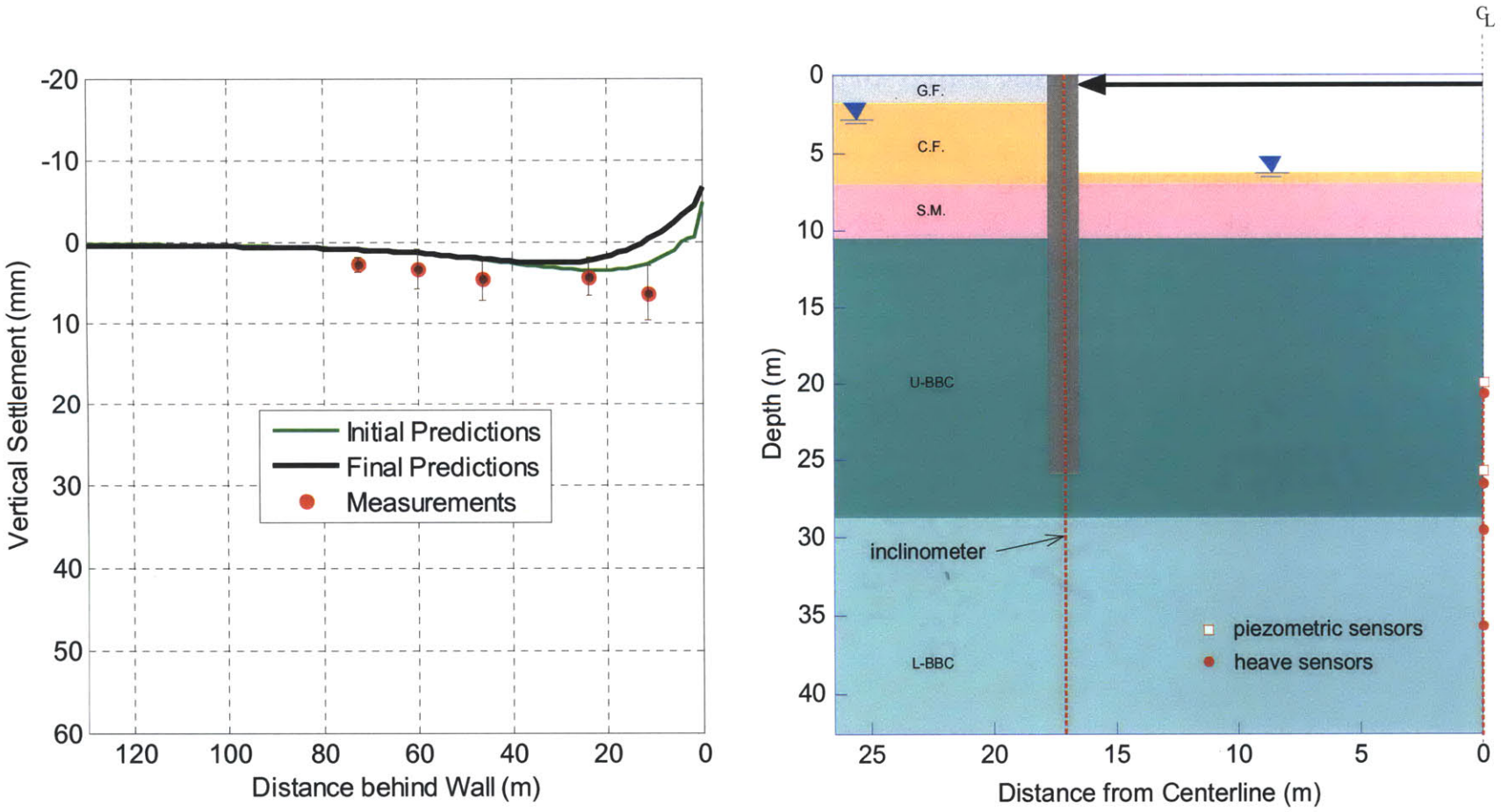

Figure B- 8: Measurements vs. Initial and Final Predictions of Surface Vertical Settlement at Excavation Level 2

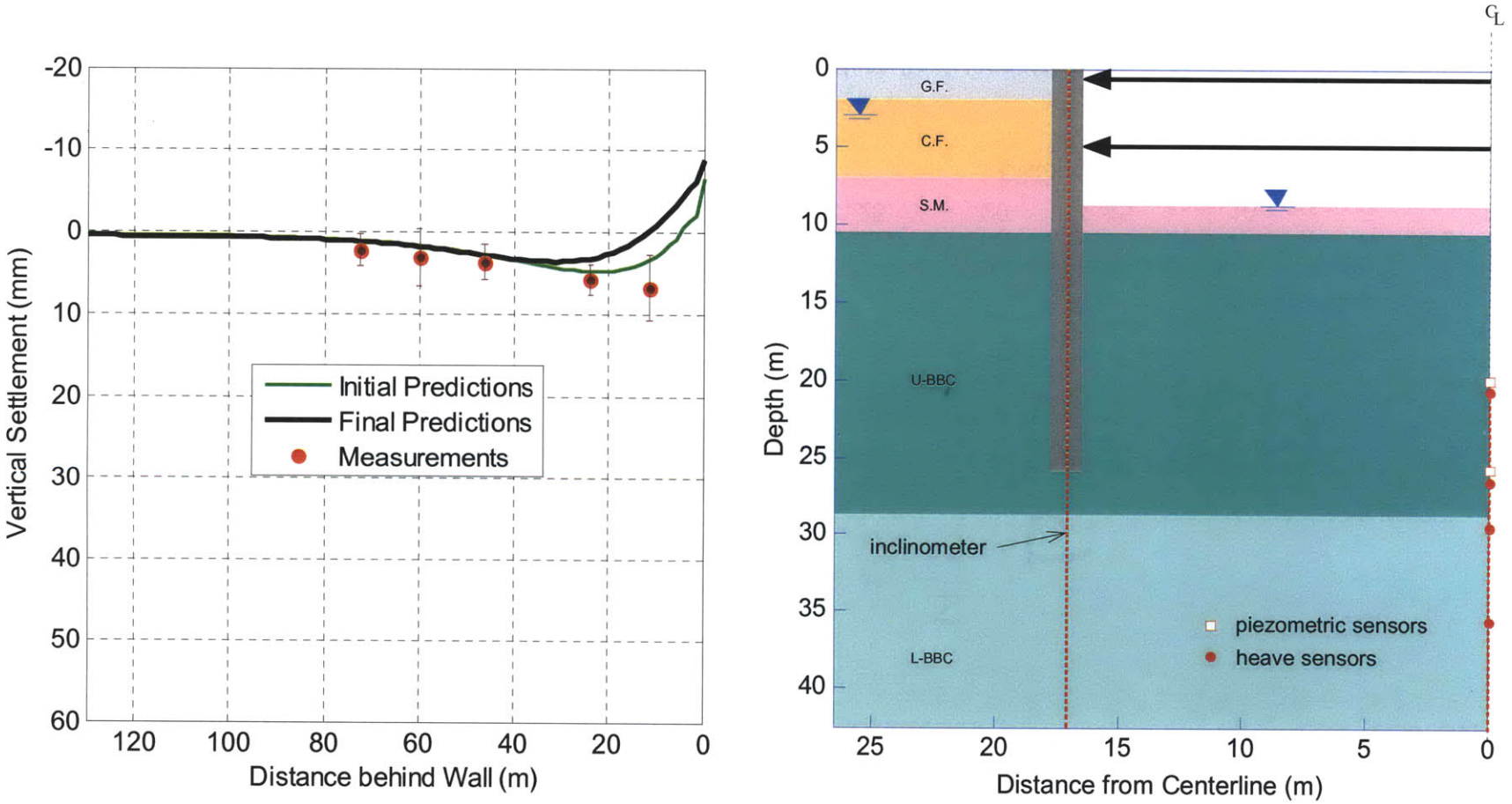

Figure B- 9: Measurements vs. Initial and Final Predictions of Surface Vertical Settlement at Excavation Level 3

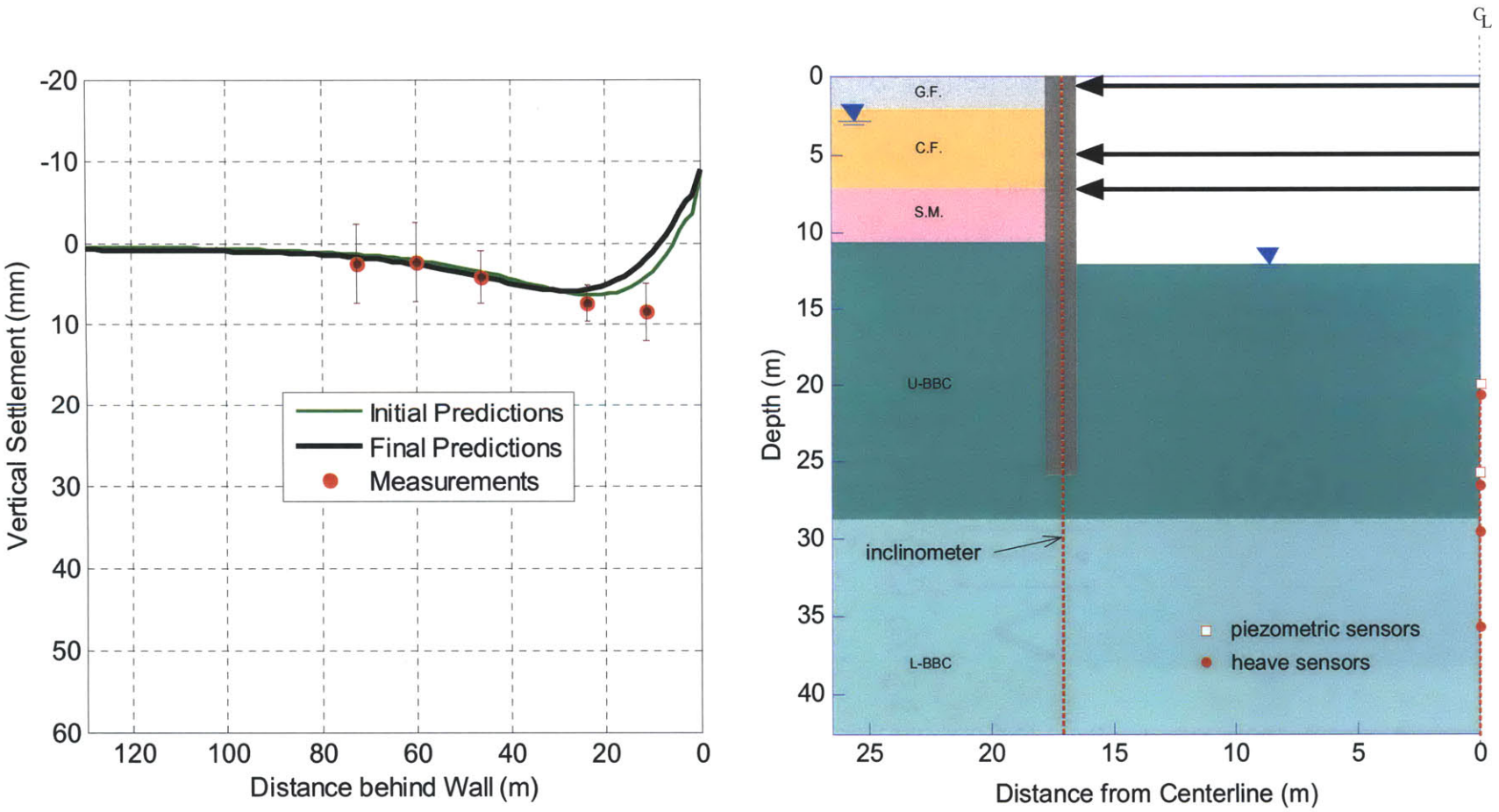

Figure B- 10: Measurements vs. Initial and Final Predictions of Surface Vertical Settlement at Excavation Level 4

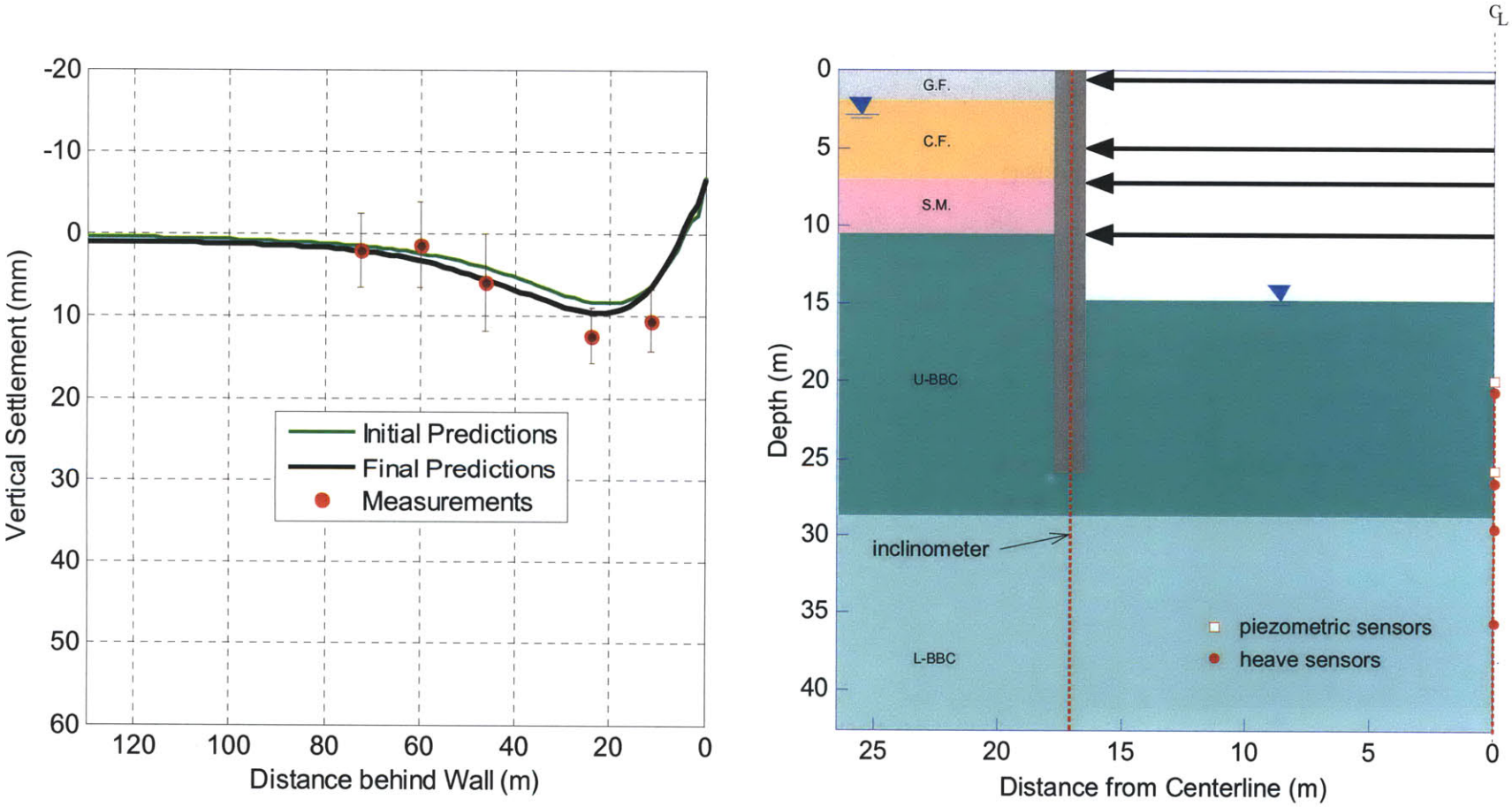

Figure B- 11: Measurements vs. Initial and Final Predictions of Surface Vertical Settlement at Excavation Level 5

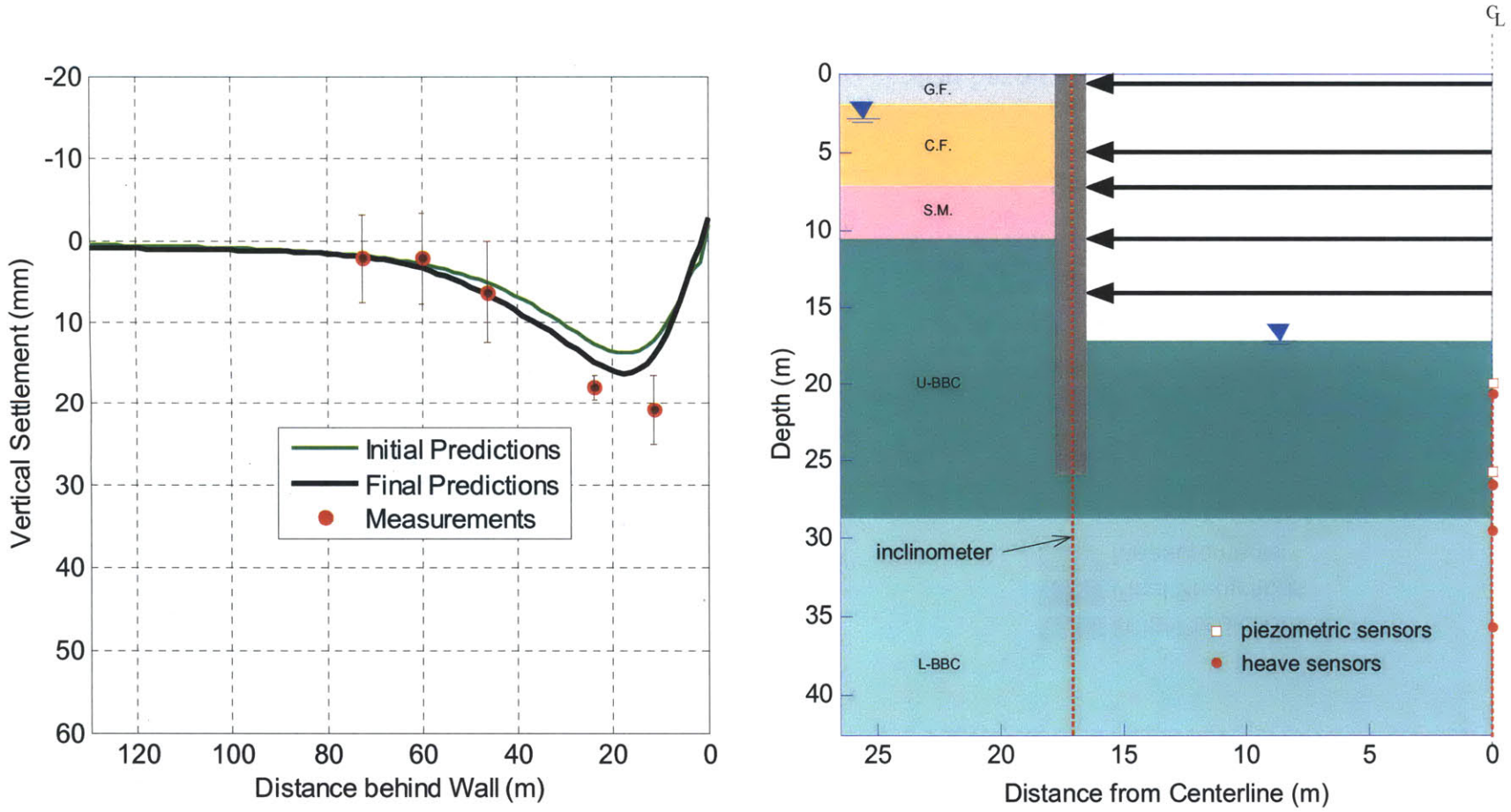

Figure B- 12: Measurements vs. Initial and Final Predictions of Surface Vertical Settlement at Excavation Level 6

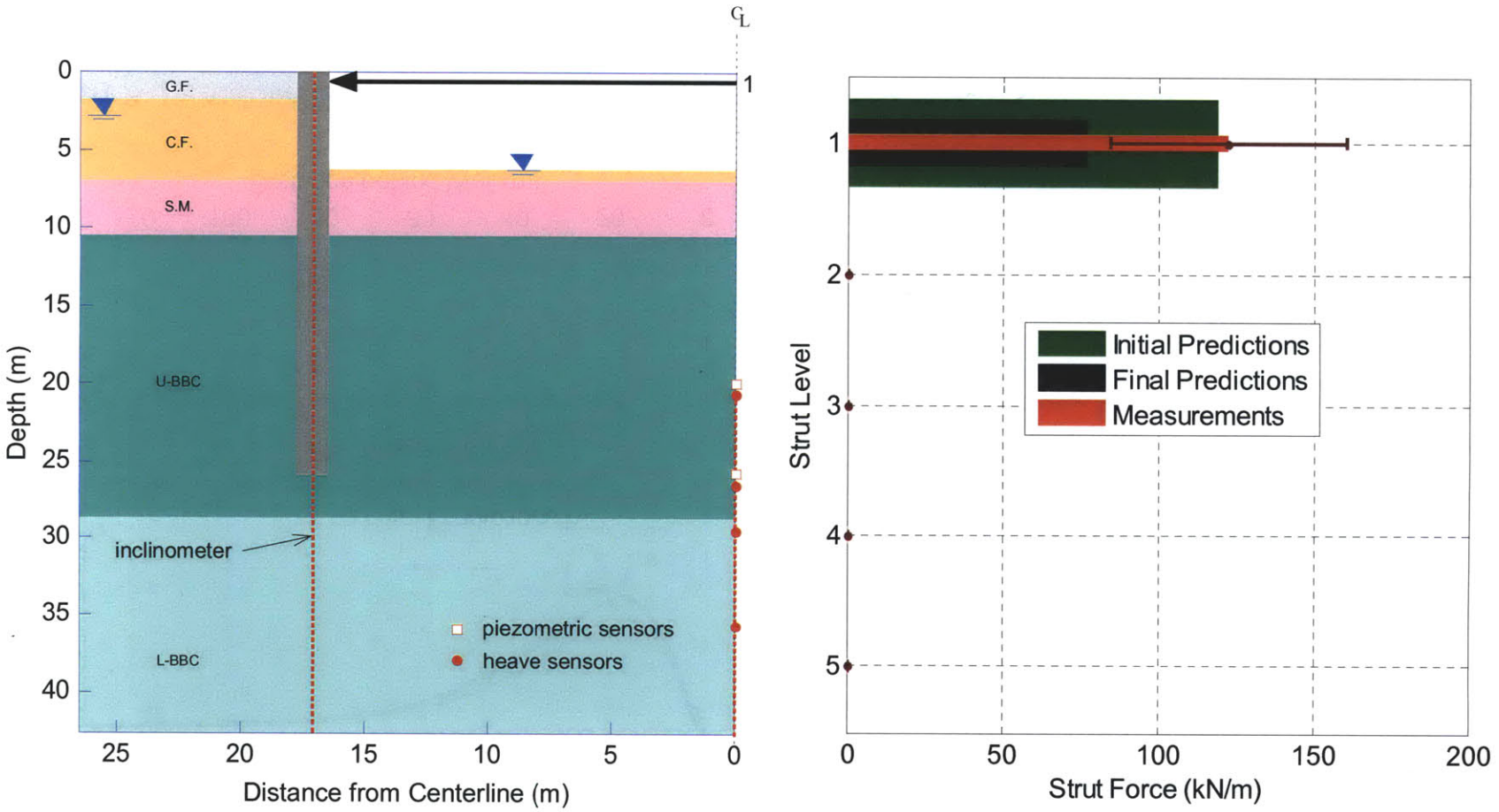

Figure B- 13: Measurements vs. Initial and Final Predictions of Strut Forces at Excavation Level 2

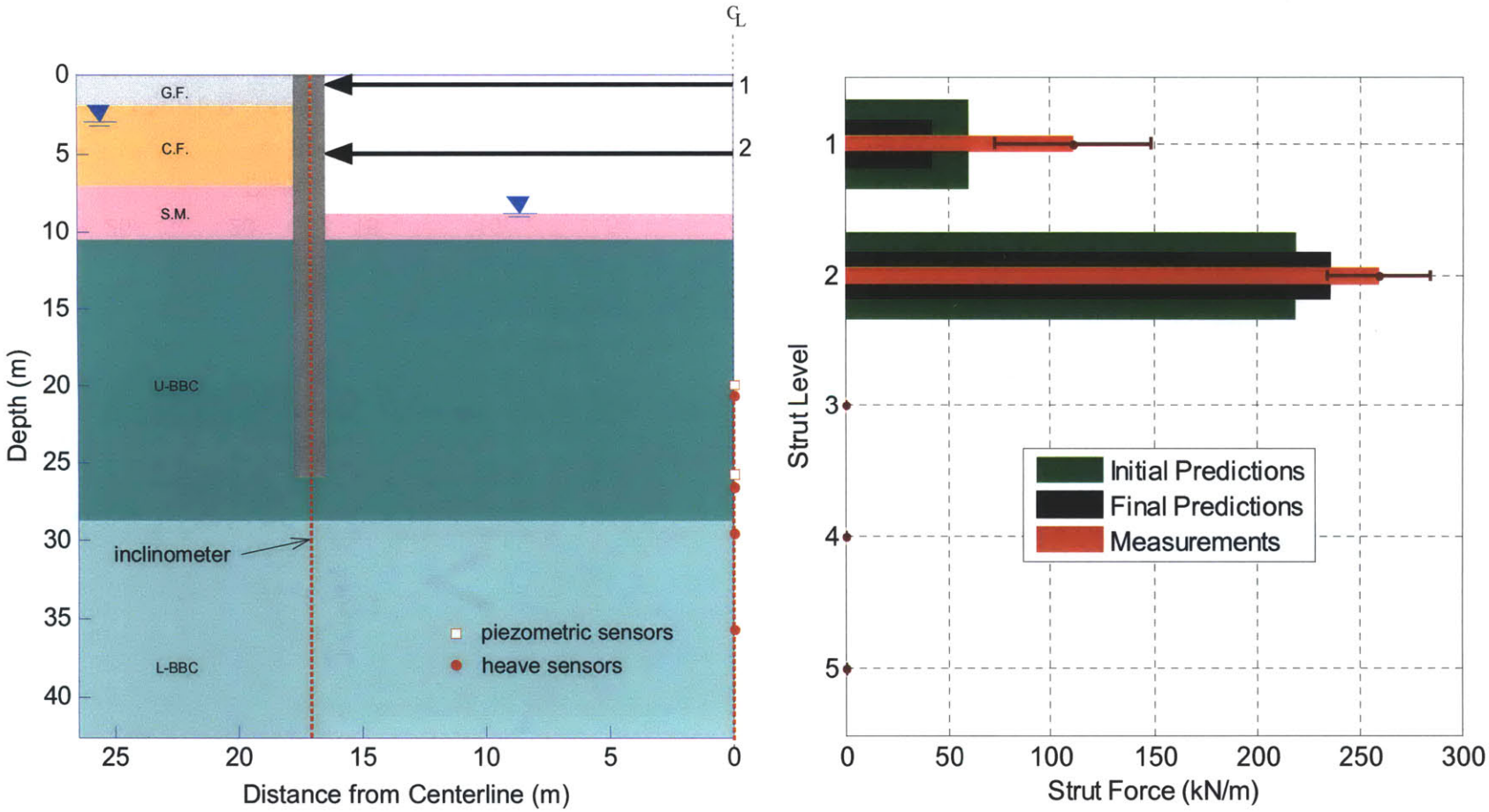

Figure B- 14: Measurements vs. Initial and Final Predictions of Strut Forces at Excavation Level 3

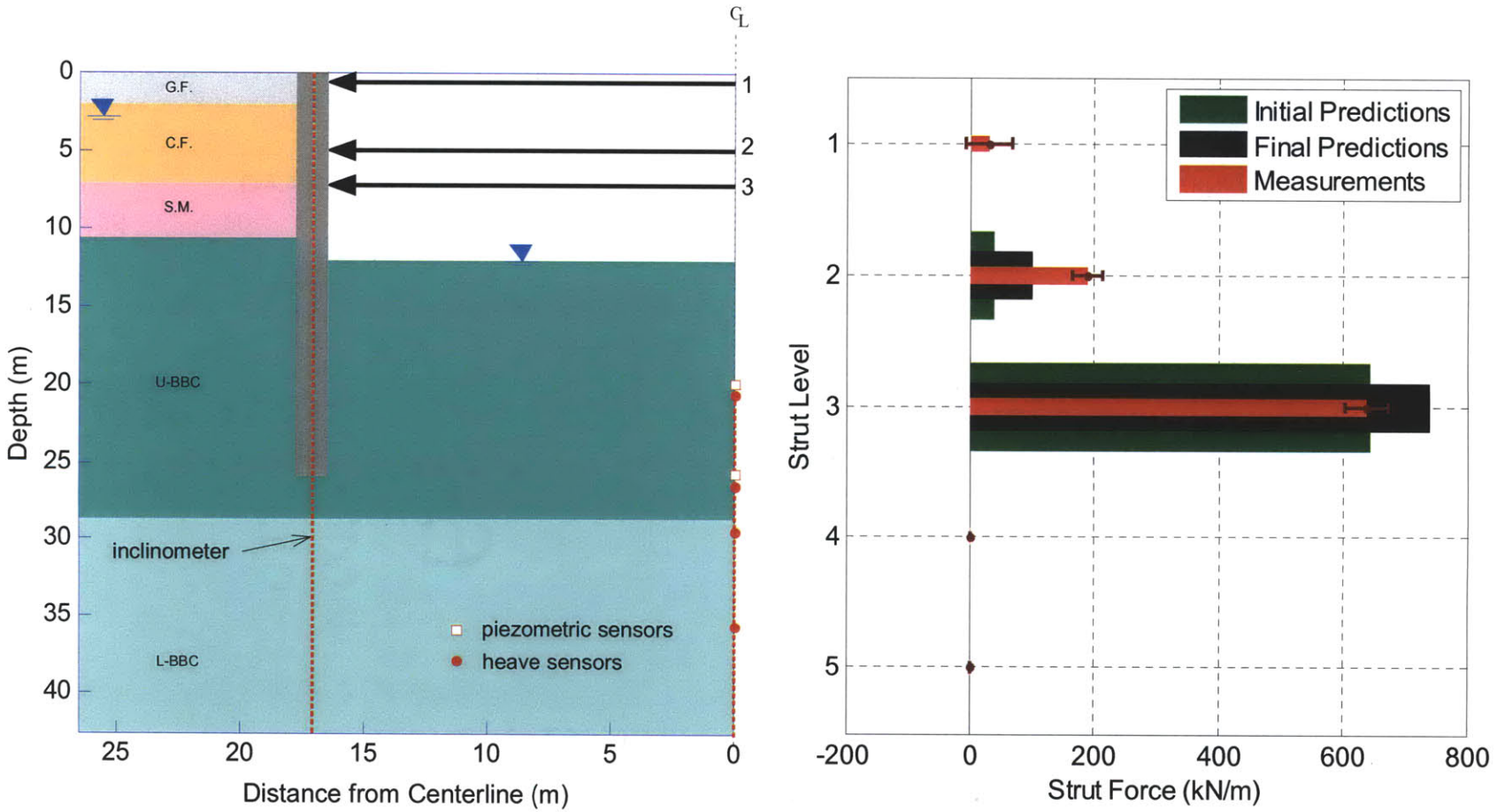

Figure B- 15: Measurements vs. Initial and Final Predictions of Strut Forces at Excavation Level 4

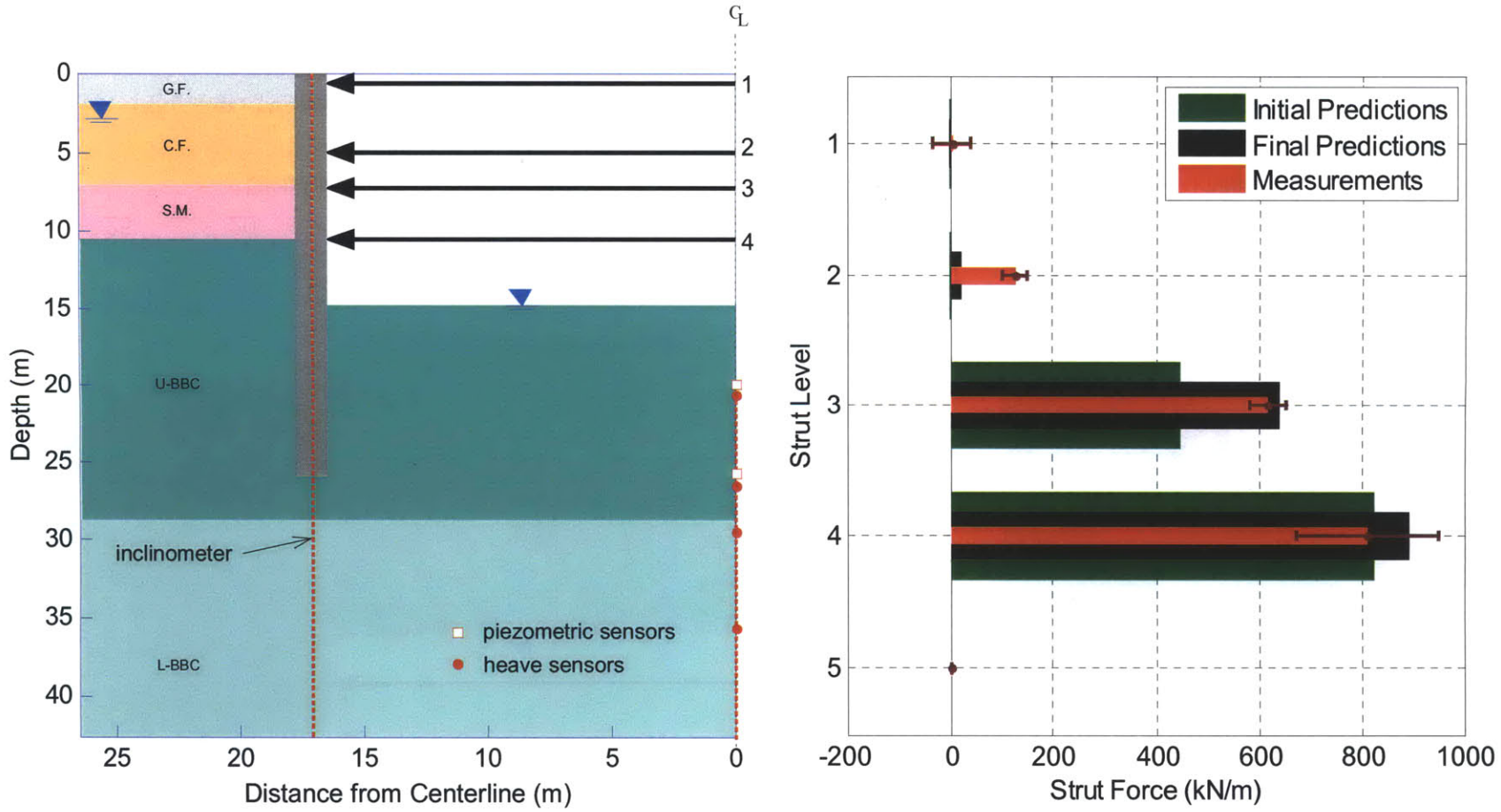

Figure B- 16: Measurements vs. Initial and Final Predictions of Strut Forces at Excavation Level 5

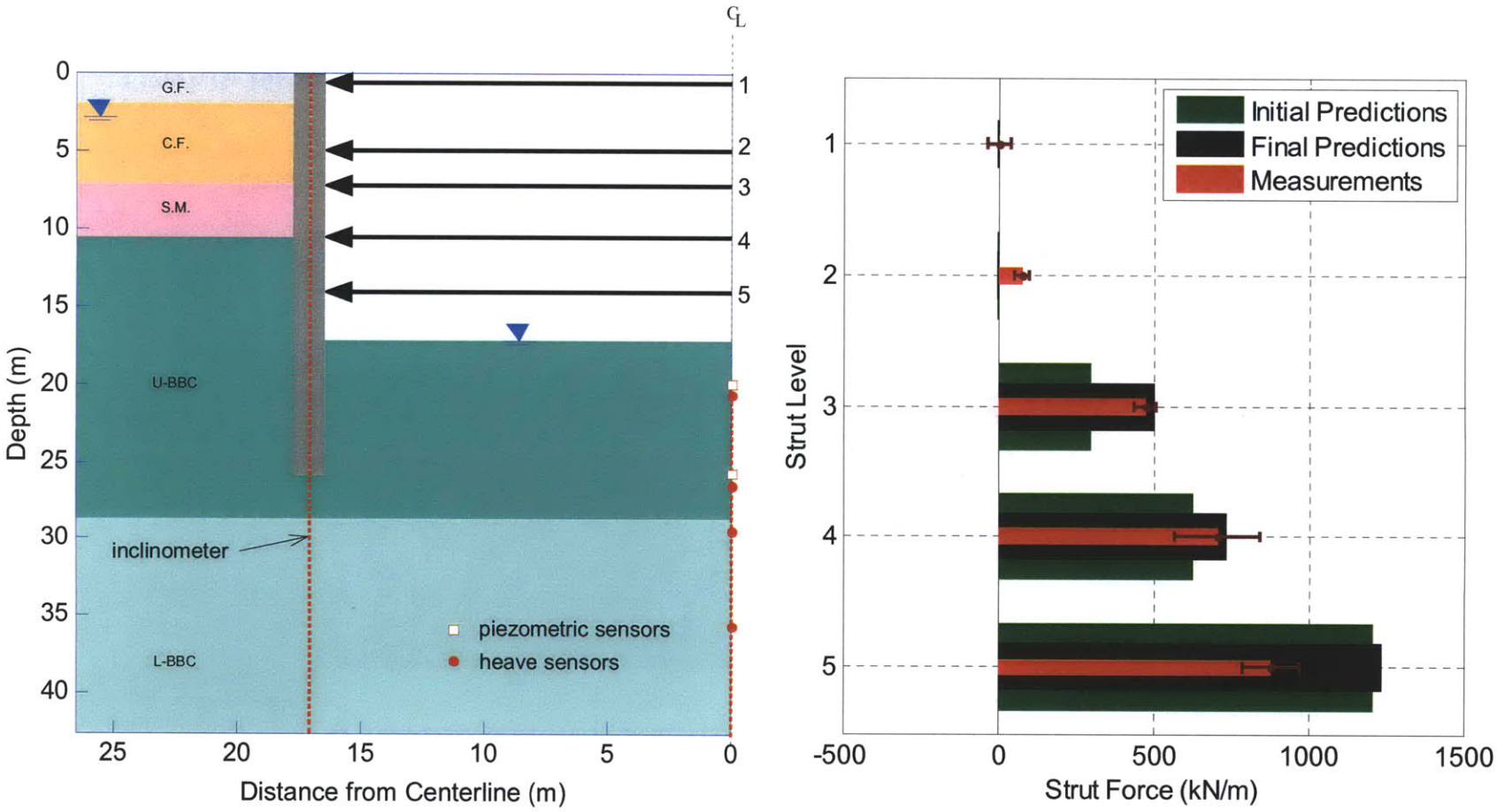

Figure B- 17: Measurements vs. Initial and Final Predictions of Strut Forces at Excavation Level 6

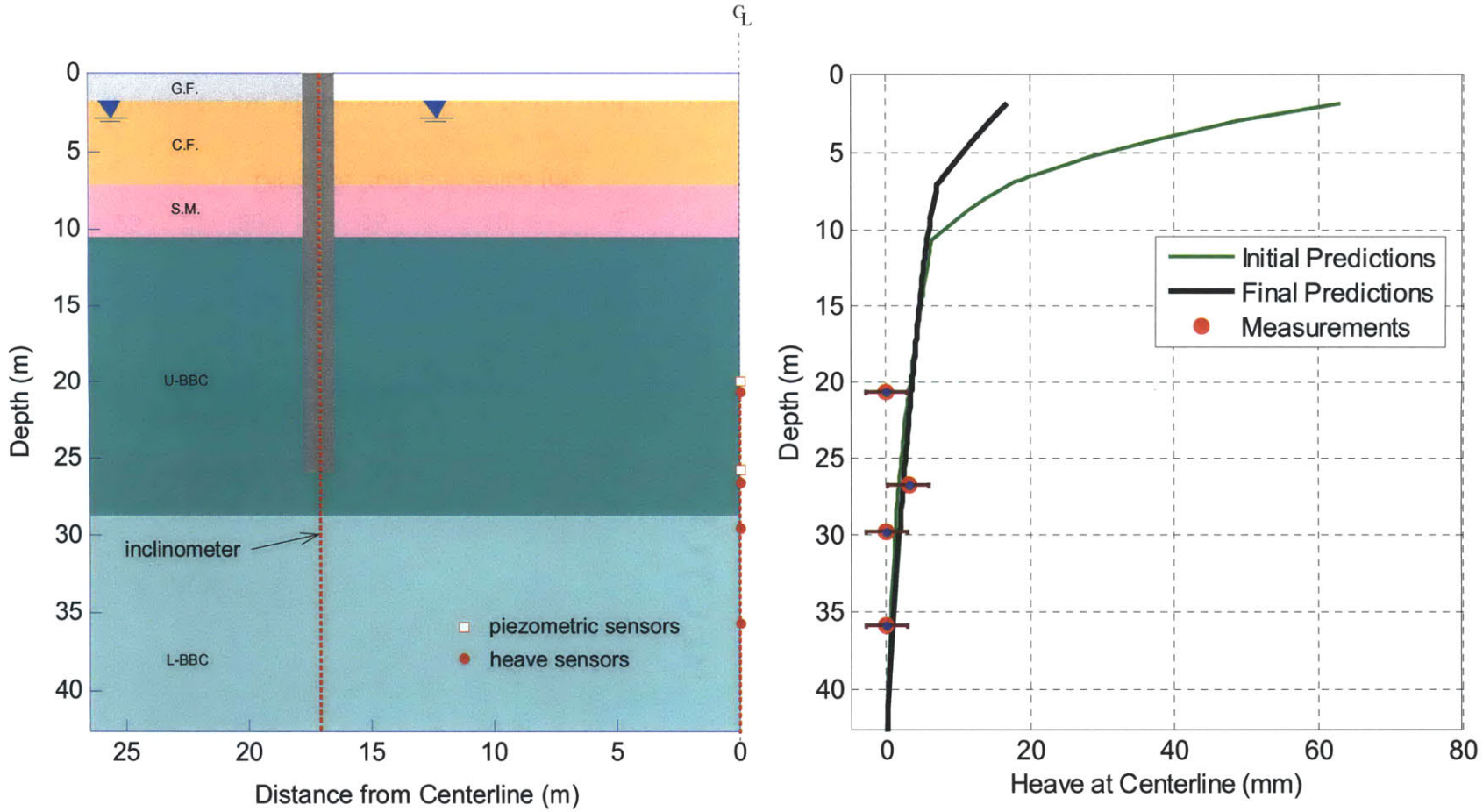

Figure B- 18: Measurements vs. Initial and Final Predictions of Centerline Heave at Excavation Level 1

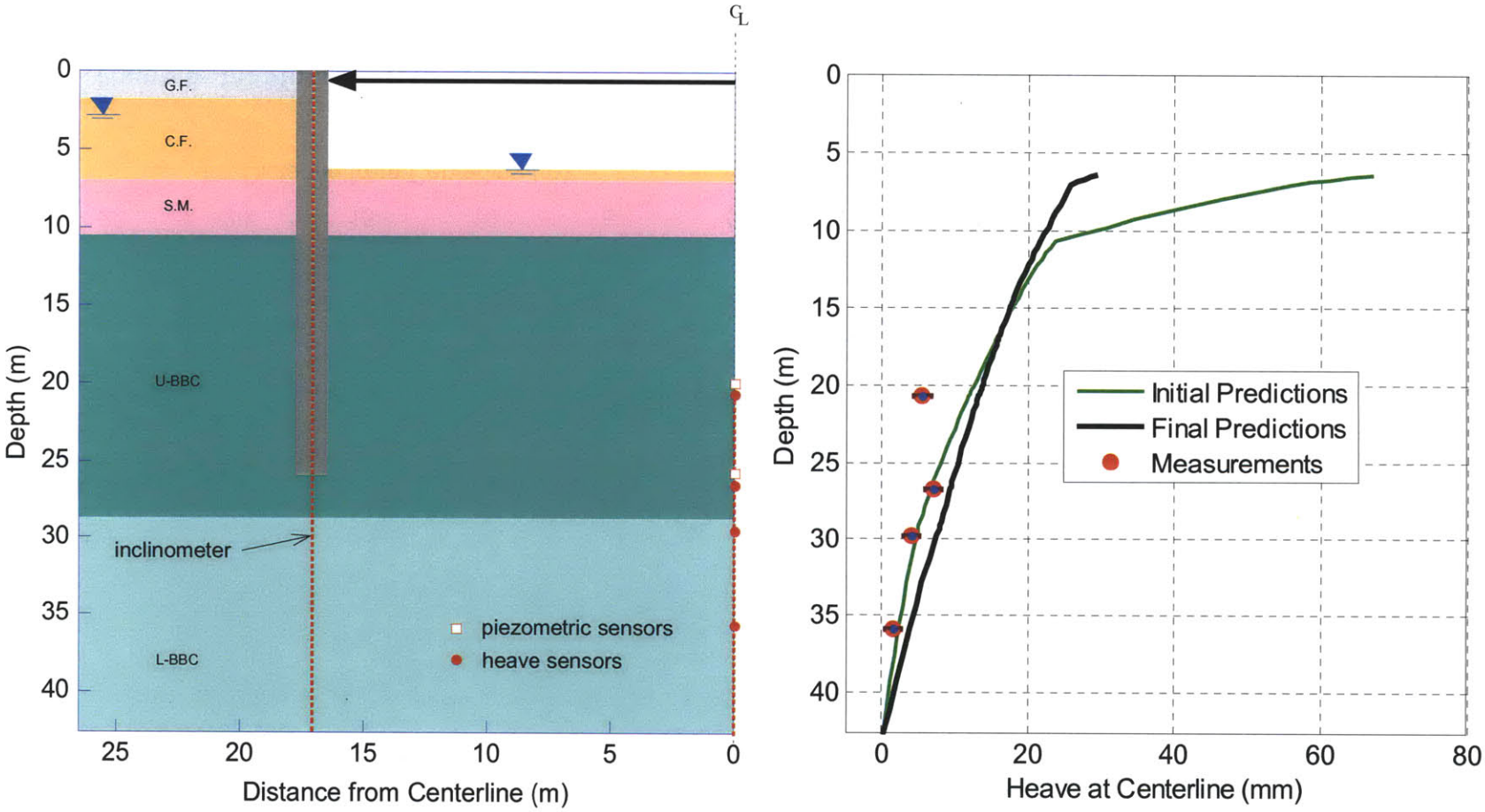

Figure B- 19: Measurements vs. Initial and Final Predictions of Centerline Heave at Excavation Level 2

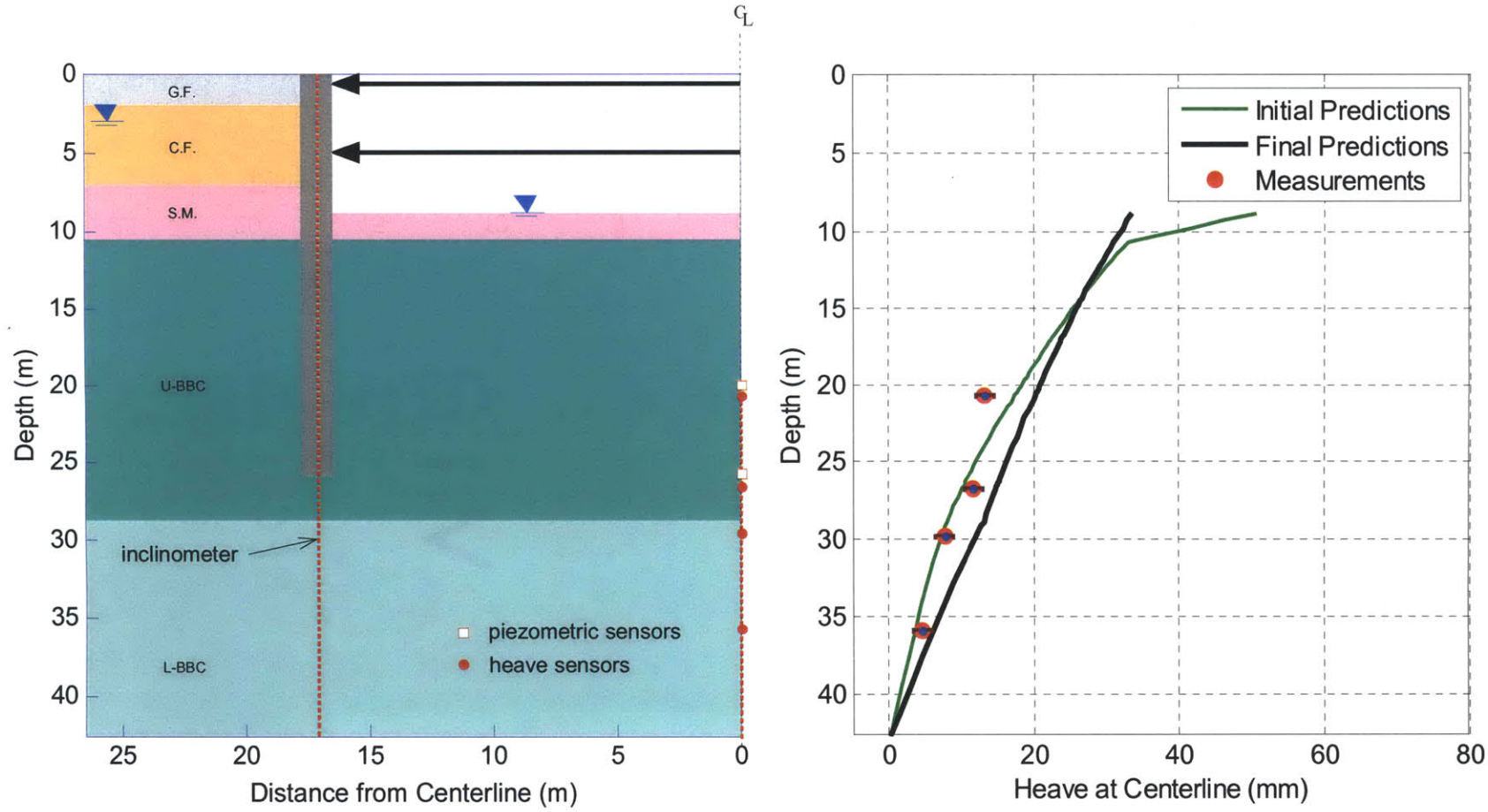

Figure B- 20: Measurements vs. Initial and Final Predictions of Centerline Heave at Excavation Level 3

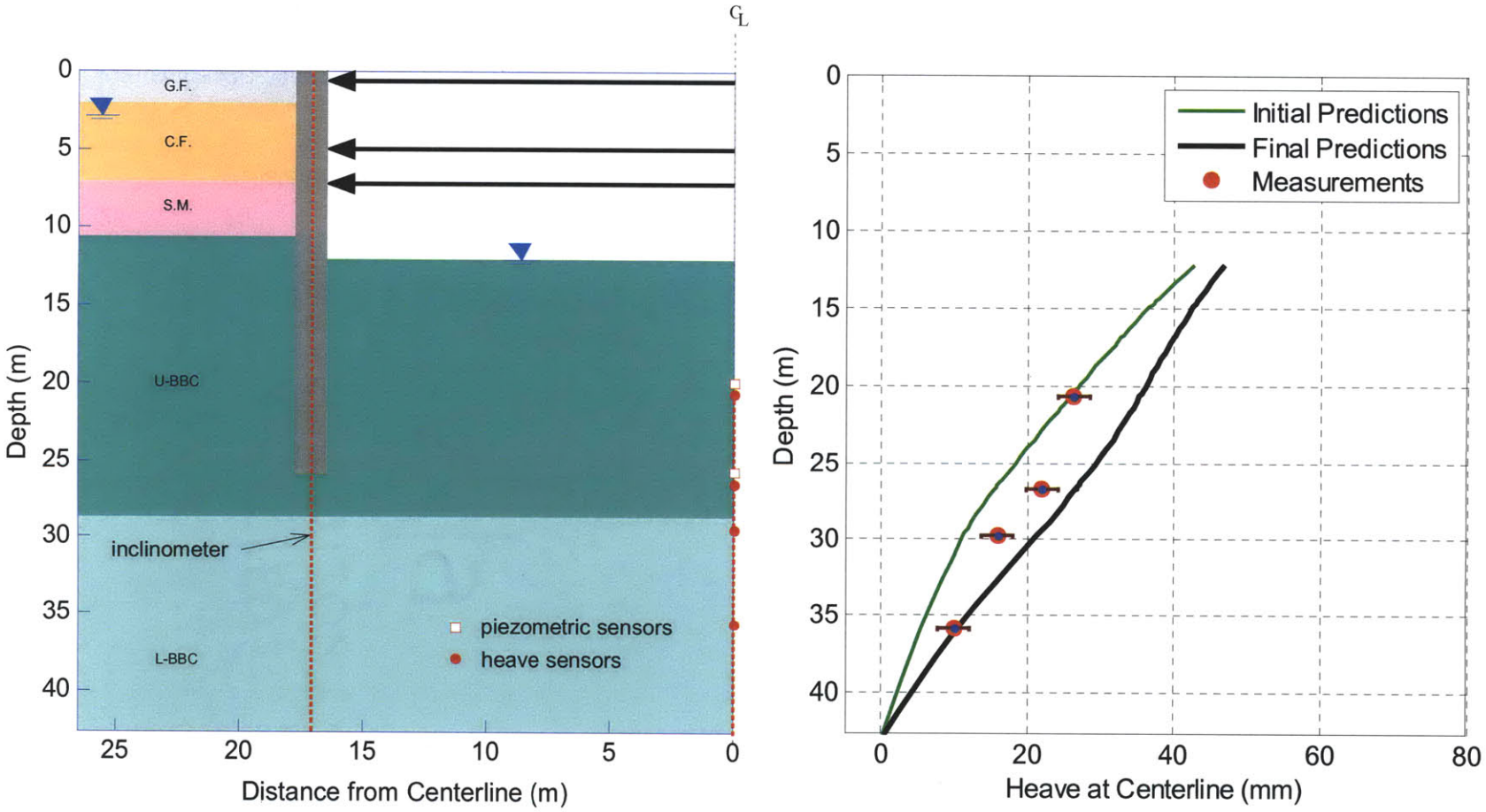

Figure B- 21: Measurements vs. Initial and Final Predictions of Centerline Heave at Excavation Level 4

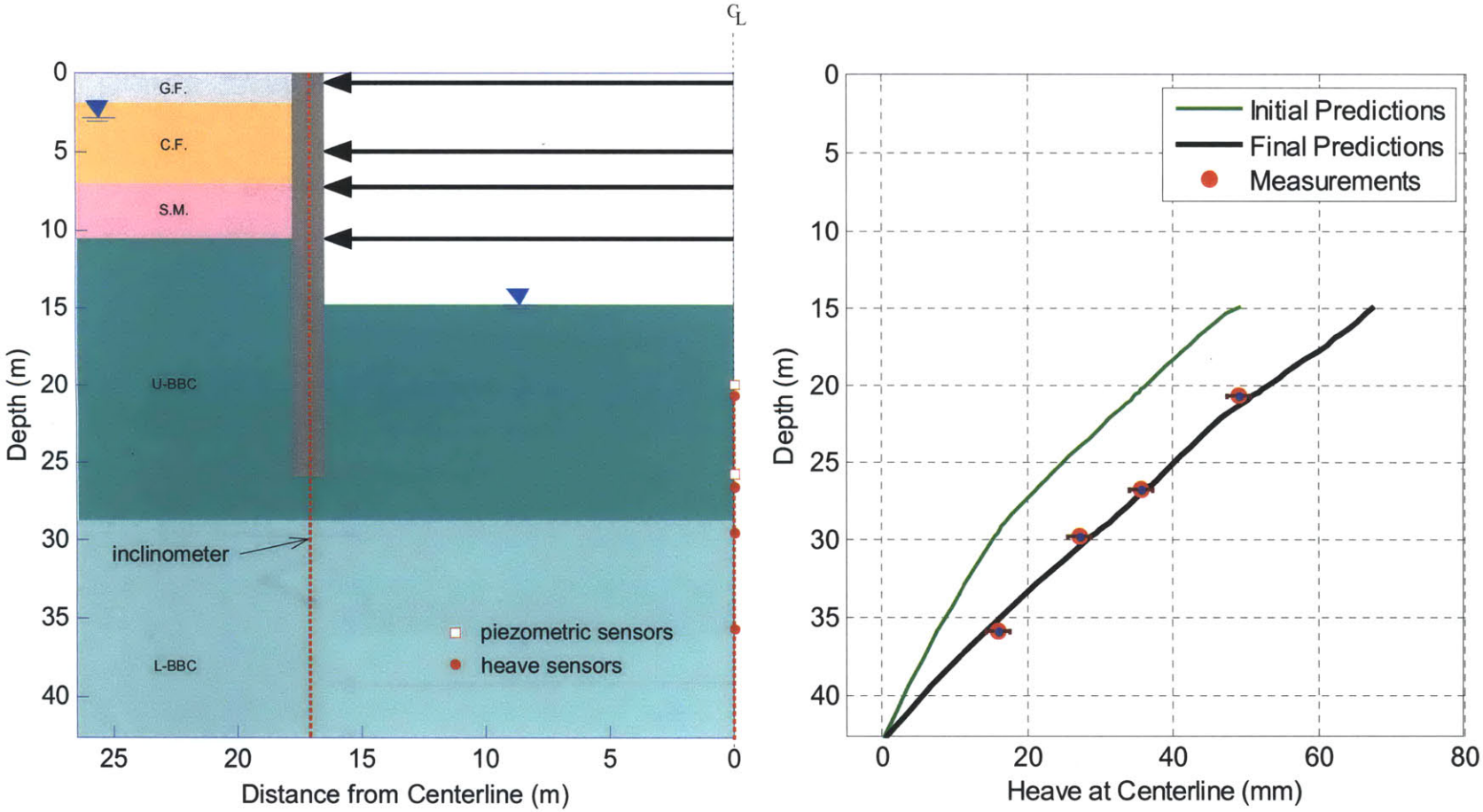

Figure B- 22: Measurements vs. Initial and Final Predictions of Centerline Heave at Excavation Level 5

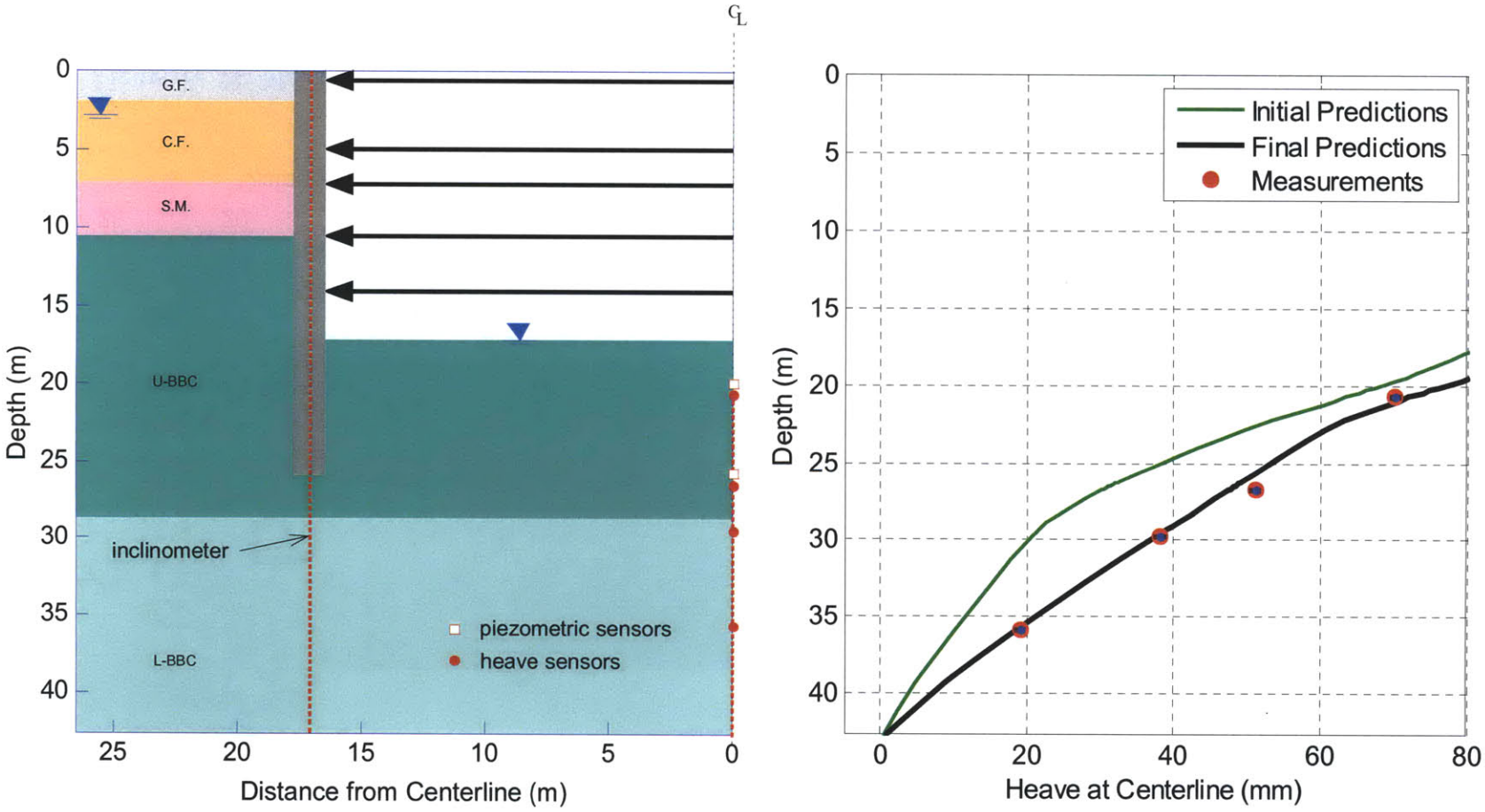

Figure B- 23: Measurements vs. Initial and Final Predictions of Centerline Heave at Excavation Level 6

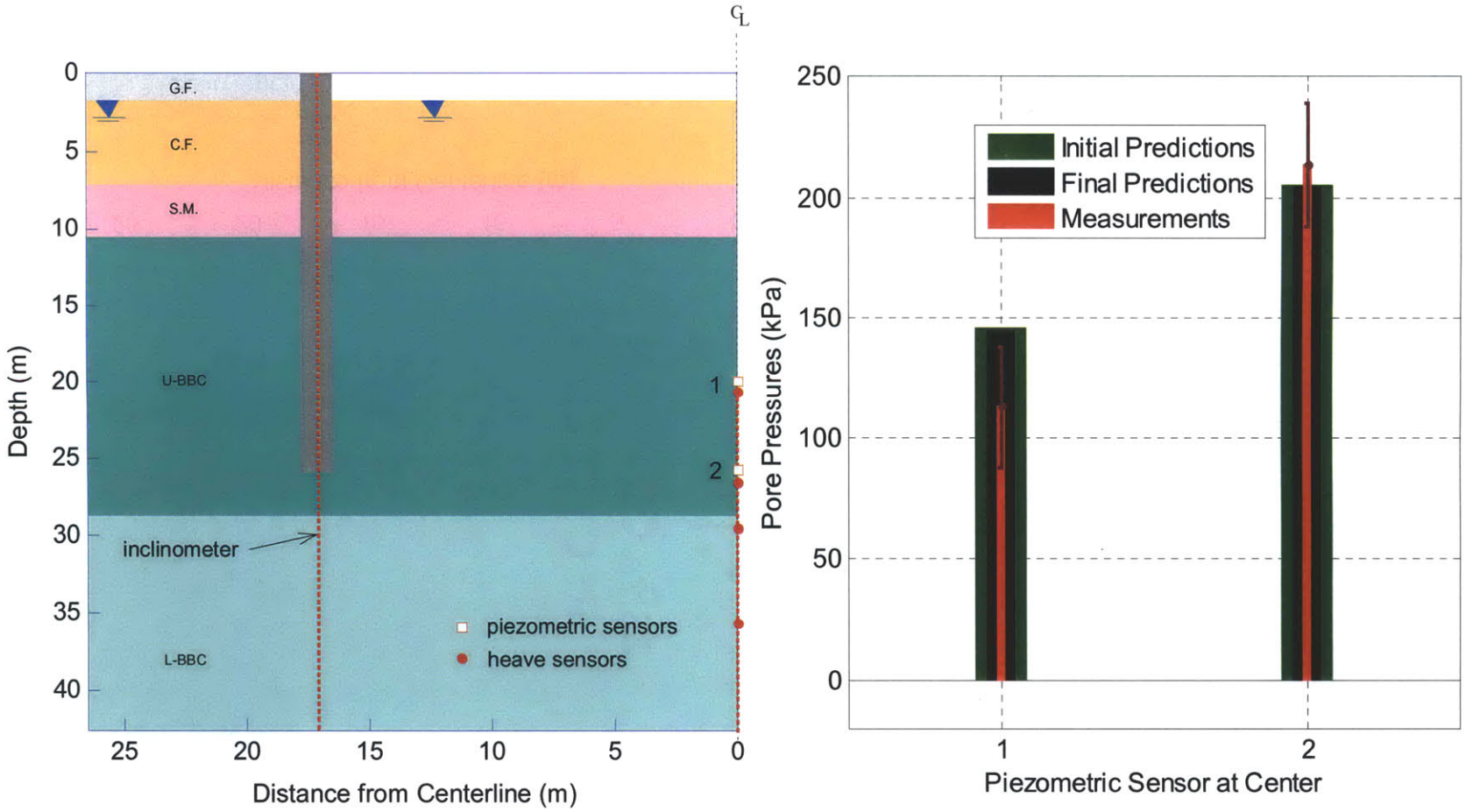

Figure B- 24: Measurements vs. Initial and Final Predictions of Pore Water Pressures (2 sensors at CL) at Excavation Level 1

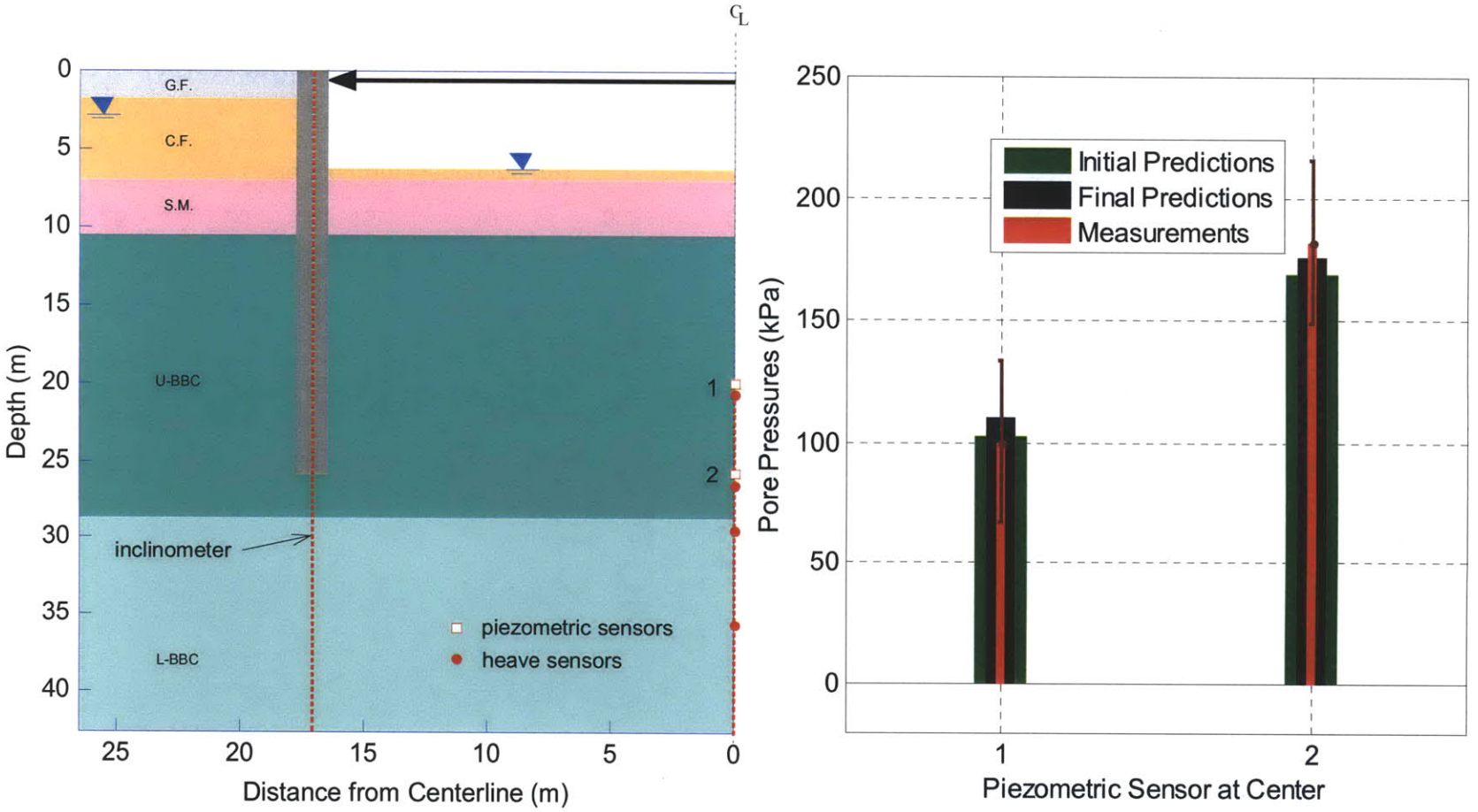

Figure B- 25: Measurements vs. Initial and Final Predictions of Pore Water Pressures (2 sensors at CL) at Excavation Level 2

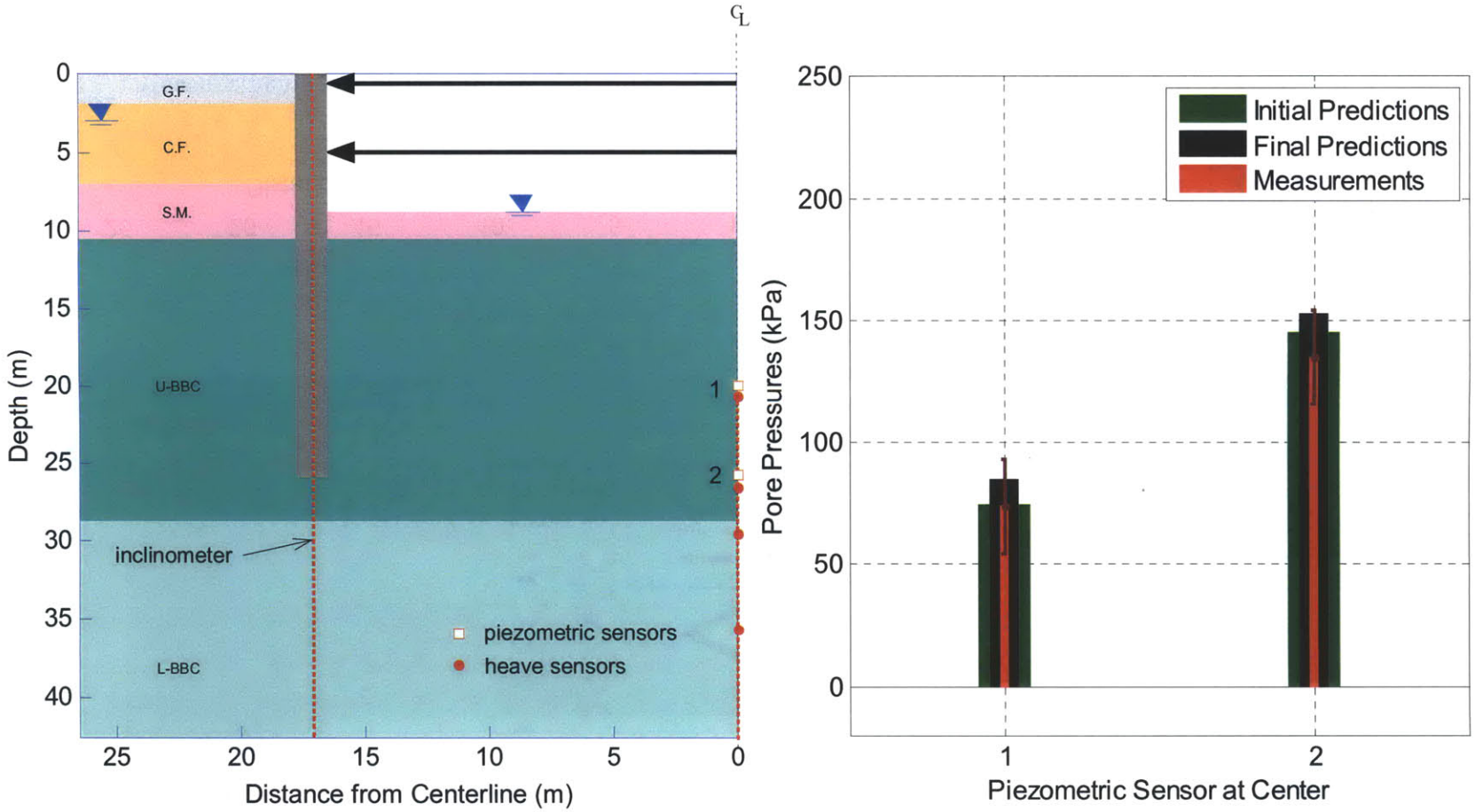

Figure B- 26: Measurements vs. Initial and Final Predictions of Pore Water Pressures (2 sensors at CL) at Excavation Level 3

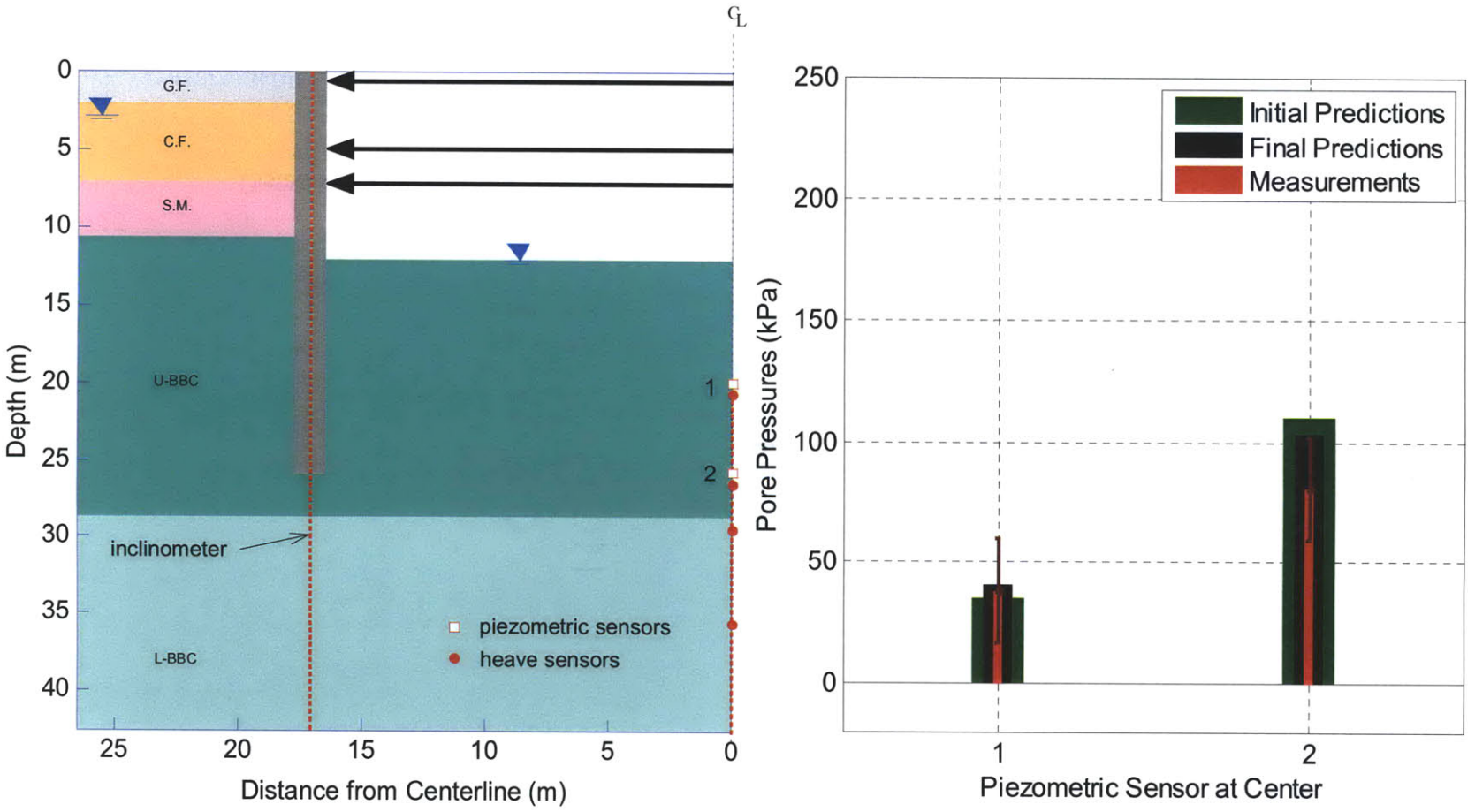

Figure B- 27: Measurements vs. Initial and Final Predictions of Pore Water Pressures (2 sensors at CL) at Excavation Level 4

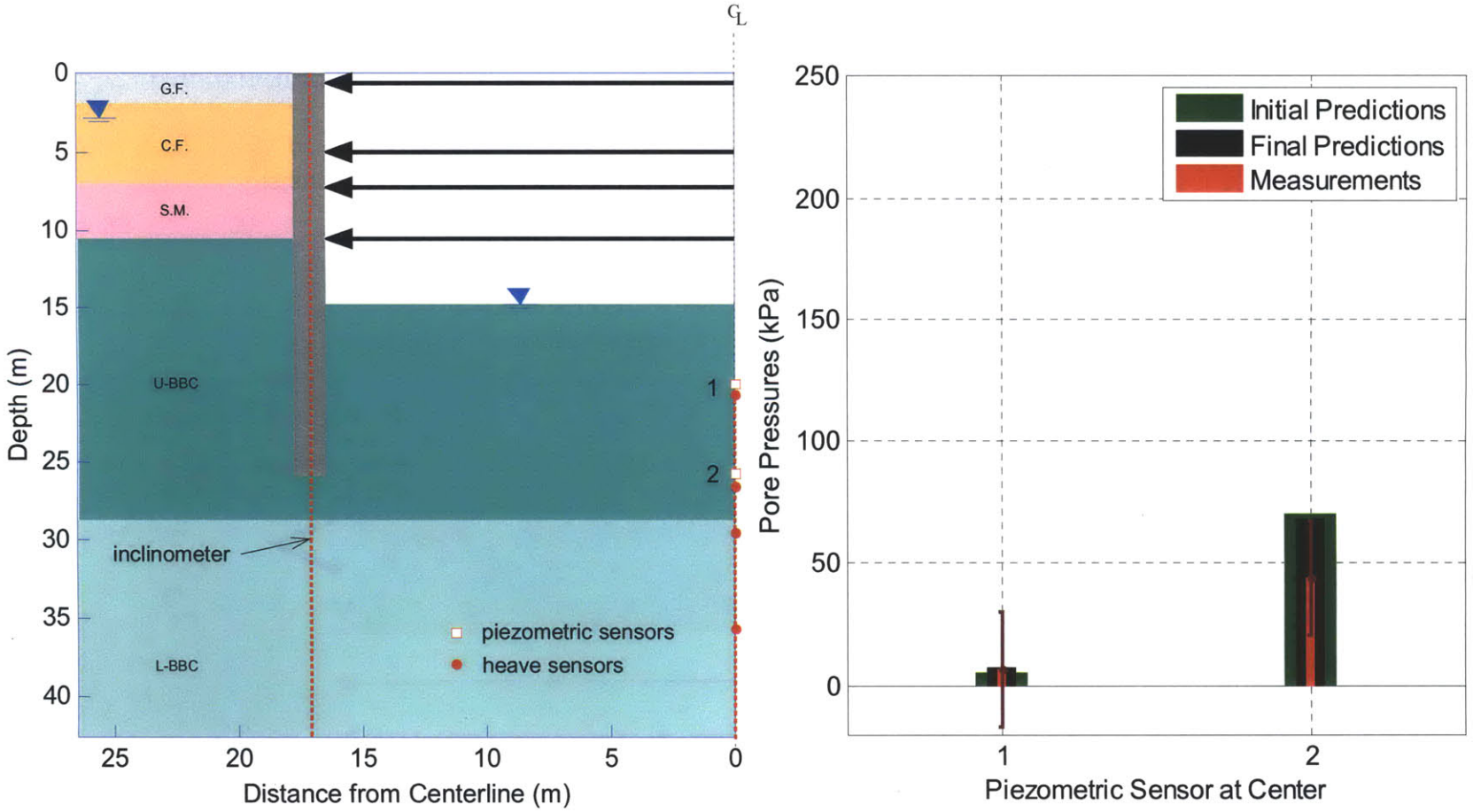

Figure B- 28: Measurements vs. Initial and Final Predictions of Pore Water Pressures (2 sensors at CL) at Excavation Level 5

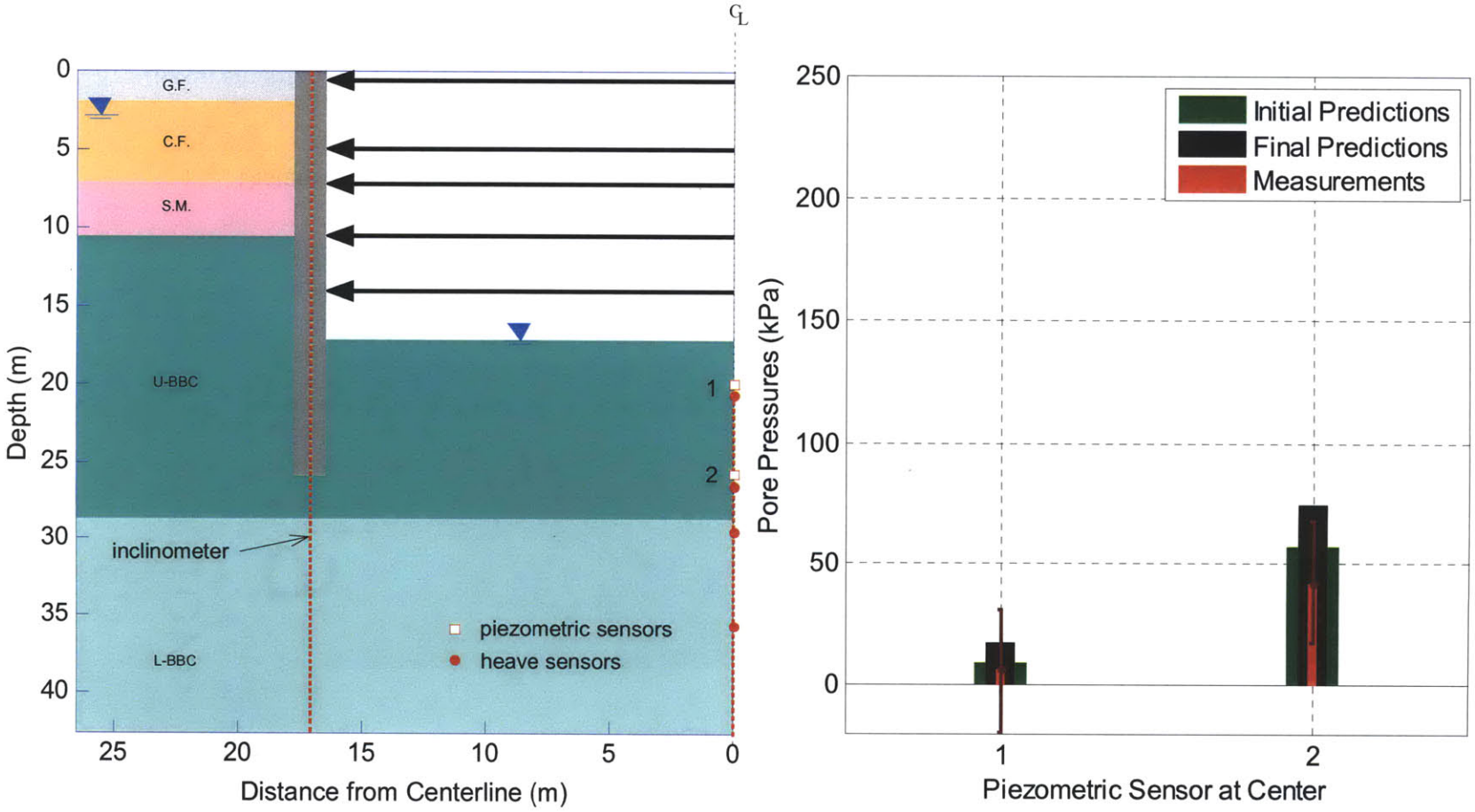

Figure B- 29: Measurements vs. Initial and Final Predictions of Pore Water Pressures (2 sensors at CL) at Excavation Level 6